SYMPOSIUM VOLUMES

ELSEVIER

JOURNAL

of

CHROMATOGRAPHY

SYMPOSIUM VOLUMES

*San Francisco street scene, 1851. Hulls
of abandoned ships were used as warehouses.*

SYMPOSIUM VOLUME

TENTH INTERNATIONAL SYMPOSIUM ON COLUMN LIQUID CHROMATOGRAPHY

PART II

San Francisco, CA (U.S.A.), May 18–23, 1986

Guest Editor

R. E. MAJORS

(Walnut Creek, CA)

The proceedings of the *Tenth International Symposium on Column Liquid Chromatography, San Francisco, CA, May 18–23, 1986*, are published in four volumes of the *Journal of Chromatography*: Vols. 371 (1986) and 384–386 (1987). The Foreword to the proceedings only appears in Vol. 371.

CONTENTS

10TH INTERNATIONAL SYMPOSIUM ON COLUMN LIQUID CHROMATOGRAPHY, SAN FRANCISCO, CA, MAY 18–23, 1986, PART II

CHROMSYMP. 1010

ZONE FORMATION IN ION-PAIR REVERSED-PHASE LIQUID CHROMATOGRAPHY

III. STEP-GRADIENT ELUTION OF OLIGODEOXYRIBONUCLEOTIDES

ANDERS SOKOLOWSKI

Department of Analytical Pharmaceutical Chemistry, Biomedical Center, University of Uppsala, Box 574, S-751 23 Uppsala (Sweden)

SUMMARY

Step-gradient elution by decrease of the counter-ion concentration or increase of the co-ion concentration was studied in an ion-pair reversed-phase system. As analytes, polyvalently negatively charged oligodeoxyribonucleotides were used. In the co-ion step-gradient technique, the retention volumes can be predicted by use of a simple equation. This technique gives a drastic decrease in peak width, which makes it possible to decrease the separation time by using an optimized composition of the two eluents used. Furthermore, the detectability of organic ions is considerably improved. The time for the introduction of the second eluent, containing the co-ion, into the column after the sample injection is critical.

INTRODUCTION

During the last decade, ion-pair reversed-phase chromatography has become a common technique for the separation of nucleotides and oligonucleotides[1–7]. When the nucleotides to be separated have different charges and/or hydrophobicities, the separation factors can be very high[1]. However, the last peaks eluted will be very broad and difficult to detect. To solve this so-called general elution problem[8], gradient elution is often used. Usually, the concentration of the organic modifier in the eluent is increased, either continuously[9,10] or stepwise[9,11]. In both cases, mathematical expressions describing the retention have been evaluated[9–11]. In the case of nucleotides, the continuous increase in organic modifier has chiefly been used[2,4–7].

In ion-pair chromatography the retention volume can be regulated by changing the concentration and/or the hydrophobicity of the counter ion or the co-ion, an ion with the same charge as the analyte[1,12–14]. It is possible to obtain a gradient effect by changing the concentration of the organic ionic species in the eluent during the chromatographic analysis, keeping the concentration of the organic modifier constant. It has been shown that the retention volume can be decreased by increasing the co-ion concentration in a single step[14].

In this work, the effect of gradient elution on oligodeoxyribonucleotides has

been studied by a stepwise change of one organic ionic species in the eluent, either by decreasing the counter-ion concentration or by increasing the co-ion concentration.

THEORETICAL

Retention model

The main quantitative expressions for ion-pair adsorption and retention are described elsewhere[12,13,15,16]. The same approach was used for the oligonucleotides, which are polyvalent anions in the eluents used. They are denoted as ON^{-p}.

If the counter ion, Q^+, and the buffer anion, Z^-, are present in the mobile phase, the net retention volume of ON^{-p} is given, *cf.*, refs. 1 and 17, by

$$V_{N,ON} = \frac{w_s K_0 K_{ONQp}[Q^+]_m^p}{1 + K_{QZ}[Q^+]_m[Z^-]_m} \tag{1}$$

where K_0 is the limited adsorption capacity of the surface, K_{ONQp} is the equilibrium constant for the adsorption of the ion pair ONQp, w_s is the amount of solid phase in the column (g), $[Q^+]_m$ and $[Z^-]_m$ are the concentrations (mol/l) of Q^+ and Z^-, respectively, in the mobile phase. Eqn. 1 is valid if the sample amounts are small and the peaks are symmetrical. It shows that a decrease in the counter-ion concentration results in a decrease in the net retention volume. The higher the charge of the oligonucleotide, the greater will be the decrease in retention volume[1].

If an organic anion, S^-, is also present in the mobile phase, it will compete with ON^{-p} for the limited adsorption sites on the surface of the solid phase[13-15]. The net retention volume will then be

$$V_{N,ON} = \frac{w_s K_0 K_{ONQp}[Q^+]_m^p}{1 + K_{QZ}[Q^+]_m[Z^-]_m + K_{QS}[Q^+]_m[S^-]_m} \tag{2}$$

If $[Q^+]$ and $[Z^-]$ are kept constant and $[S^-]$ is increased the net retention volume of the oligonucleotide will decrease.

Stepwise gradient elution

The migration distance of an analyte zone in a column equilibrated with the eluent can be calculated by the expression

$$s = vL/V_R \tag{3}$$

where L is the length of the column, s is the migration distance of the analyte zone when v ml of eluent have been eluted and V_R is the retention volume (ml) of the analyte, *i.e.*, the volume of eluate that is needed to obtain a migration distance equal to L.

In a single-step gradient process, an analyte migrates part of the distance, s_1, along the column with an elution volume, v_1, of eluent 1 and migrates the remaining distance, s_2, with an elution volume, v_2, of eluent 2. The retention volumes of the analyte in the two eluents are V_{R1} and V_{R2}, respectively. The following expressions are valid

$$L = s_1 + s_2 \tag{4}$$

$$V_{R,tot} = v_1 + v_2 \tag{5}$$

where $V_{R,tot}$ is the total retention volume of the analyte. Expressions for v_1 and v_2 can be obtained by combining eqns. 3–5:

$$V_{R,tot} = V_{R2} + \frac{s_1(V_{R1} - V_{R2})}{L} \tag{6}$$

It is assumed that, after introduction, eluent 2, migrates with a constant velocity along the column with a distinct front and reaches the end of the column with a breakthrough volume, V_{RA}. Eluent 2 will affect the retention of the analyte only if its front migrates faster than the analyte zone. The effect will depend not only on the composition of the eluents, but also on how far the analyte has migrated after the introduction of eluent 2.

The front has migrated the distance s_1 and overtakes the sample zone when the elution volume is v_A. The following relationship is valid (*cf.*, eqn. 3):

$$s_1 = \frac{v_A L}{V_{RA}} = \frac{v_1 L}{V_{R1}} \tag{7}$$

The volume, v_D, eluted between the injection of the sample and the introduction of eluent 2 is

$$v_D = v_1 - v_A \tag{8}$$

Combination of eqns. 6–8 then gives

$$V_{R,tot} = V_{R2} + \frac{v_D(V_{R1} - V_{R2})}{(V_{R1} - V_{RA})} \tag{9}$$

This expression is based on the assumption that the concentration changes at the front of eluent 2 are insignificant.

Eqn. 9 shows that $V_{R,tot}$ can be calculated for different values of v_D if V_{R1}, V_{R2} and V_{RA} are known and if the values are constant. If $v_D \leq 0$, which means that the sample is injected at the same time or after the introduction of eluent 2, $V_{R,tot}$ will be equal to V_{R2}. This is only valid if $V_{R2} \geq V_{RA}$, *i.e.*, the analyte zone migrates with a lower velocity than that of the front; thus, the column behaves as if equilibrated with eluent 2. If $v_D \geq (V_{R1} - V_{RA})$ and the analyte is injected before eluent 2 is introduced, the column behaves as if equilibrated with eluent 1, since the front does not reach the sample zone before it emerges from the column. Then $V_{R,tot}$ will be equal to V_{R1}.

EXPERIMENTAL

Apparatus

The pumps were an LDC Model 711-42 solvent-delivery system (Milton-Roy Minipump; Laboratory Data Control, Riviera Beach, FL, U.S.A.) and an Altex Model 100 (Berkeley, CA, U.S.A.). The detectors were an LDC SpectroMonitor III and a Beckman 156 refractive index detector (Berkeley, CA, U.S.A.). A Rheodyne

7125 sample injector (Berkeley, CA, U.S.A.) with a 20-μl loop was used for the sample injections and a Valco (Houston, TX, U.S.A.) CV-6-HPax injector, was used for switching eluent from one pump to the other in the breakthrough experiments. A Labotron eight-way selector valve SS (Kontron AB, Bromma, Sweden) was used at the low-pressure side of the pump in the gradient-elution studies. It is denoted as the "eluent selector".

The columns, 100 mm $\times$ 4.6 mm I.D., were equipped with modified Swagelok connectors and Altex 250-21 filters and were packed with LiChrosorb RP-18, 5 μm (Merck, Darmstadt, F.R.G.). A water-bath, HETO Type 02 PT 923 (Birkerød, Denmark), was used to thermostat the chromatograph. The pH was measured with a Model 801 A/digital pH meter (Orion Research, MA, U.S.A.), equipped with a Type 401 combined electrode (W. Ingold, Urdorf, Switzerland). The spectrophotometric measurements were made with a Zeiss PMQ II Spektralphotometer (Carl Zeiss, F.R.G.).

Chemicals

Methanol was of Merck p.a. quality. Tetrapentylammonium (TPeA) iodide (Eastman-Kodak, Rochester, NY, U.S.A.) was converted into the hydroxide by shaking the aqueous solution with silver oxide[18] before use in the eluents. Sodium octanesulphonate was also from Eastman-Kodak. All other substances and solvents were of analytical or reagent grade used without further purification.

The oligodeoxyribonucleotides were kindly supplied by J. B. Chattopadhyaya. They had been synthesized by a phosphotriester method[19]. The abbreviations used are as follows: A = 2'-deoxyadenosine and T = thymidine. In ApTp, A is the 5'-end and Tp the 3'-end of the oligonucleotide. An internucleotidyl phosphodiester linkage is denoted as p ($pK_a \approx 3$) and 3'-terminal p denotes a phosphomonoester ($pK_1 \approx 3.8$ and $pK_2 \approx 6\text{–}7$)[20,21].

Preparation of the eluent

The eluent was prepared by mixing equal volumes of methanol and phosphate buffer (pH 7.0) of ionic strength $I = 0.032$ (mol/l) and a total phosphate concentration of $1.51 \cdot 10^{-2}$ M. The phosphate buffer was prepared by mixing 1 M phosphoric acid and 1 M sodium hydroxide. When the eluent contained TPeA, an equivalent amount of sodium hydroxide was replaced by TPeA hydroxide to keep the ionic strength constant. Because octanesulphonate was added as the sodium salt, an increase of the ionic strength was expected.

The concentration of TPeA in the eluent was measured by the picrate method[22], using 1- or 5-cm cuvettes. The eluents were diluted at least 20 times in phosphate buffer (pH 6.5, $I = 0.1$) before the picrate extraction, in order to minimize phase-volume changes due to extraction of methanol.

Chromatographic technique

The chromatograph was thermostatted by circulating water from a water-bath kept at 25.00 $\pm$ 0.01°C. The eluent reservoir was kept in the thermostatted water-bath, which also thermostatted the analytical column by pumping water through a glass jacket, mounted on the column.

The flow-rate of the mobile phase was in the range of 0.5–0.8 ml/min. The

eluent was not recirculated. The oligonucleotides injected were dissolved in the eluent but their exact concentration in the injected sample was not known.

The hold-up volume of the column, V_m, was determined from the peak obtained when sodium nitrate was injected. When TPeA was present in the eluent the nitrate ion was retained. In those cases, the value of V_m used was that from the preceding or succeeding experiment without TPeA present in the eluent.

In the gradient-elution studies the eluent selector was used in combination with the LDC pump. The volume from the eluent selector to the top of the analytical column was measured as 1.74 ml, including the volume of the pump and of the injector loop. This volume was included in all calculations of volumes.

The adsorption and desorption studies were performed according to the breakthrough technique described in ref. 15, using the same equipment.

Peak efficiency and resolution determination

The number of theoretical plates was measured by use of the retention time, t_R, of the peak maximum and the width of the peak, w_t, measured at the base between the tangents to the inflexion points, in time units.

In gradient elution it is not correct to use the parameters N and H. In this study, the parameters of the gradient-elution peaks were measured in the ordinary way, but are indicated as *"N"* or *"H"* to indicate the peak-compression effect. The resolution, R_S, of two analytes was measured as the difference between the peak maxima, divided by the mean peak width. In gradient elution the resolution was also measured in this way.

RESULTS AND DISCUSSION

In the adsorption and desorption as well as in the gradient-elution studies two different eluents were used. The column was initially equilibrated with the first eluent, which may contain adsorbable organic ions, *e.g.*, the counter ion. A second eluent, which differed from the first eluent in the content of one organic ion, was then in-
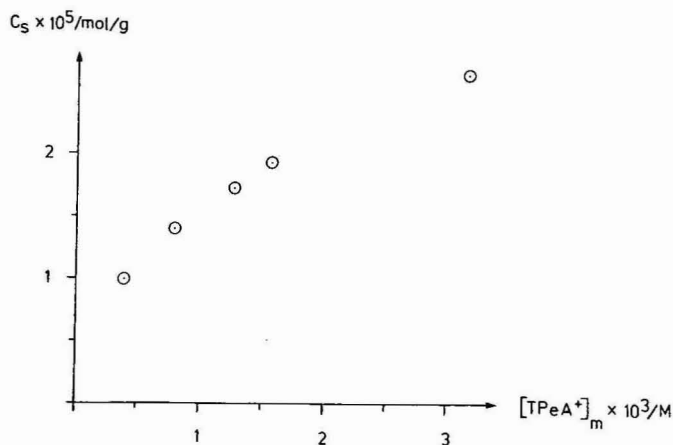
Fig. 1. Adsorption isotherm of TPeA as a phosphate ion pair.
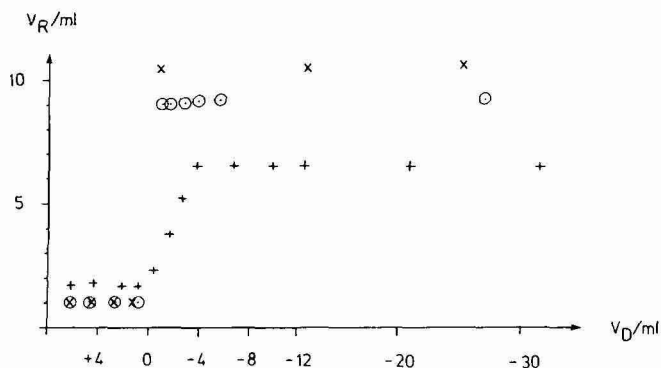
Fig. 2. Dependence of the retention volumes of nucleotides, injected at different times in relation to the introduction of the TPeA-containing eluent. See text for definition of v_D. Analytes: Ap ($+$); TpTp ($\times$); ApAp ($\bigcirc$). Eluents: 1, phosphate buffer (pH 7.0, $I = 0.032$)–methanol (1:1); 2, $1.57 \cdot 10^{-3}$ M TPeA in the eluent 1.

troduced into the column. The volume eluted between the sample injection and the introduction of eluent 2 is denoted as v_D (ml). Positive values of v_D mean that the injection was made before the introduction of eluent 2, negative values that the injection was made after the introduction.

Adsorption of TPeA as a phosphate ion pair

The adsorption of TPeA on the solid phase as a phosphate ion pair was studied by use of the breakthrough technique (Fig. 1). No fitting of the adsorbed amounts by the adsorption model was attempted, *cf.*, ref. 15, because there were too few data. A plot of $1/[QPA]_s$ *versus* $1/[Q^+]_m$ (ref. 12) gave a curved line for TPeA, indicating a heterogeneous surface.

To investigate the effect on the retention volume when TPeA was introduced into the column, some oligonucleotides were injected at different v_D values (Fig. 2). TpTp and ApAp were not separated and had very low retention volumes in the TPeA-lacking eluent. In the second eluent, TpTp and ApAp were strongly retained and were separated. For Ap, a gradual increase in the retention volume was observed when $v_D < 0$, until a constant value of 6.5 ml was obtained at $v_D \leqslant -3.7$ ml. The reason for this is that Ap will migrate through only part of the column in the TPeA-containing eluent. With the actual TPeA concentration and column used, the retention volume of the front was 9.9 ml and, consequently, Ap, when injected with $v_D > -3.7$ ml, will be eluted from a column only partly equilibrated with the TPeA-containing eluent. TpTp and ApAp have about the same retention as the TPeA front; thus, they will migrate in the column as if it were equilibrated with TPeA (for negative v_D values).

Desorption of TPeA

When an eluent lacking TPeA was introduced into the column equilibrated with TPeA, the quaternary ammonium compound was desorbed from the surface of the solid phase (Fig. 3). The retention volume to the point P, V_{RP}, where the concentration of TPeA starts to decrease, was dependent on the initial TPeA concentra-
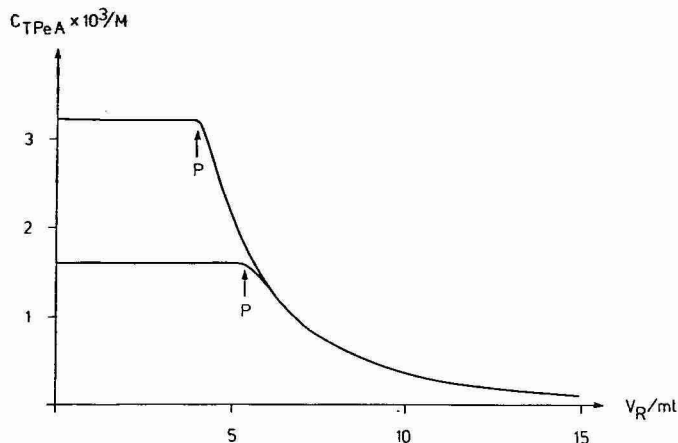
Fig. 3. Desorption profiles of TPeA. The column was equilibrated with $1.60 \cdot 10^{-3}$ and $3.21 \cdot 10^{-3}$ M TPeA, respectively, prior to introduction of the TPeA-lacking-eluent. P denotes the point where the TPeA concentration starts to decrease.

tion in the column; the higher its concentration, the smaller was V_{RP} (cf.,ref. 14). This behaviour is similar to that discussed by Helfferich[23] concerning the equilibrium changes in the system. It is of interest that when about 6 ml of the TPeA-lacking eluent had been pumped into the column the two different initial concentrations of TPeA gave the same desorption profile.

The desorption profile was similar to that for the desorption of N,N-dimethylprotryptiline (DMPT) from μBondapak Phenyl[14], but showed more tailing. The DMPT adsorption studies indicated an homogeneous surface of μBondapak Phenyl[15], while the TPeA adsorption indicated an heterogeneous surface of LiChrosorb RP-18.

The tailing of the TPeA desorption profile was very extensive, as demonstrated by continuously collecting 100-μl fractions of the eluate, which were then measured by the picrate method (see Experimental). Still, after 36 ml there was a detectable amount of TPeA, $4 \cdot 10^{-5}$ M. However, after collection and measurement of 100 ml of the eluate, it was demonstrated that the amounts adsorbed and desorbed were equal.

During the desorption studies, nucleotides were injected after the introduction of the TPeA-lacking eluent. When injected just after the introduction, there was a drastic decrease in the retention volumes, but when injected later the effect levelled off. As a further reflection of the slow desorption, after 50 ml the retention volumes had still not reached the values obtained with the TPeA-lacking eluent.

Step-gradient elution

Stepwise concentration changes of the counter ion (decrease) or the co-ion (increase) will decrease the analyte retention volumes, cf., eqns. 1 and 2, and in favourable cases improve the apparent chromatographic efficiency.

Counter-ion desorption. Fig. 4 shows the effect of the TPeA desorption on the retention volumes and the resolution of TpTp and ApAp for different v_D values. The retention volumes and the resolution decreased with decreasing v_D.
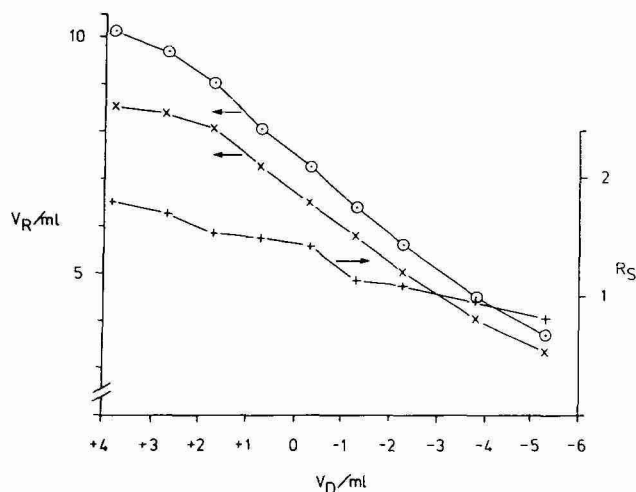
Fig. 4. Effect on the retention volumes and resolution, R_S (+), of using step-gradient elution after introduction of a TPeA-lacking eluent. Analytes: TpTp (O); ApAp (×). Eluents: 1, $1.57 \cdot 10^{-3}$ M TPeA in phosphate buffer (pH 7.0, I = 0.032)–methanol (1:1); 2, eluent 1 lacking TPeA.

On introduction of the second eluent, lacking TPeA (positive v_D value), the analyte initially migrates with a constant retention volume, which is dependent on the TPeA concentration in the first eluent. If the retention volume of P, V_{RP} (see Fig. 3), is smaller than for the analyte, P can reach and pass the analyte zone before it is eluted from the column. Behind P, the TPeA concentration continuously decreases, giving a continuous counter-ion gradient. The value of the total retention volume of the analyte will depend on the equilibration concentration of TPeA, and on the v_D value.

Since TpTp had the largest retention volume in the TPeA-containing eluent, it was affected by the point P earlier than was ApAp. This gives the resolution decrease shown in Fig. 4. Under isocratic conditions, R_S is 1.83 in the TPeA-containing eluent and 0.1 in the TPeA-lacking eluent.

Between v_D = +3.8 and −3.8 ml, peak compression was obtained. The effect
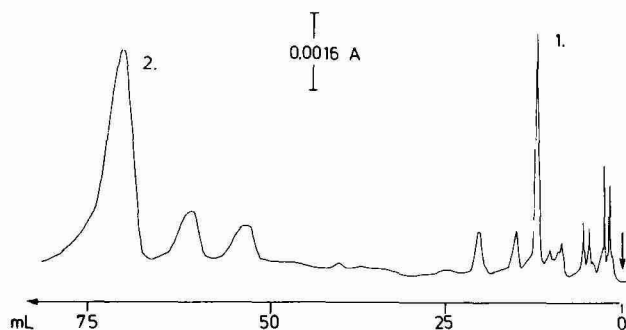
Fig. 5. Isocratic separation of oligonucleotides. Eluent: $1.63 \cdot 10^{-3}$ M TPeA in phosphate buffer (pH 7.0, I = 0.032)–methanol (1:1), flow-rate, 0.49 ml/min. Peaks: 1 = TpTp; 2 = TpTpTpTp.

was greatest in the range $v_D = +1.7$ to -0.4 ml. The value of "H" for ApAp was 0.05 and for TpTp it was 0.03, which is about three times lower than in the isocratic experiment with the TPeA-containing eluent. The peak compression is a consequence of the continuous decrease of the TPeA concentration in the mobile phase. The concentration is lower at the rear of the peak than at the front; thus, the rear migrates under conditions which increase the elution velocity compared to that of the front, *cf.*, eqn. 1.

Since the resolution between TpTp and ApAp was relatively small, there is no great advantage in using the step-gradient technique to improve the separation time for this sample mixture. By using two analytes with a very large resolution in the TPeA-containing eluent, the gradient effect will be more pronounced.

Fig. 5 shows an isocratic separation of a mixture of TpTp and TpTpTpTp in a TPeA-containing eluent. The retention volumes were 12.5 and 74.3 ml respectively. The TpTpTpTp peak showed high asymmetry, and the efficiency was very low (*cf.*, ref. 10). In a TPeA-lacking eluent there was no resolution at all, and the retention volumes were very small (*ca.* 1 ml).

When the step-gradient technique was used for this nucleotide mixture, TpTpTpTp was affected most (Fig. 6). The retention volume was 15.8 ml, and the peak was symmetrical. Due to the narrower peak obtained, the injected TpTpTpTp was diluted ten times, compared to the concentration in Fig. 5. The dilution may also decrease the asymmetry of the peak[13]. TpTp was affected only to a minor degree ($V_R = 10.1$ ml). When the v_D value was decreased, the retention volumes of both nucleotides were decreased and so was the resolution. When v_D was less than $+2.4$ ml, no resolution was obtained.

Co-ion adsorption. If the column is first equilibrated with TPeA (counter ion) and then a second eluent, also containing octanesulphonate (co-ion), is introduced,
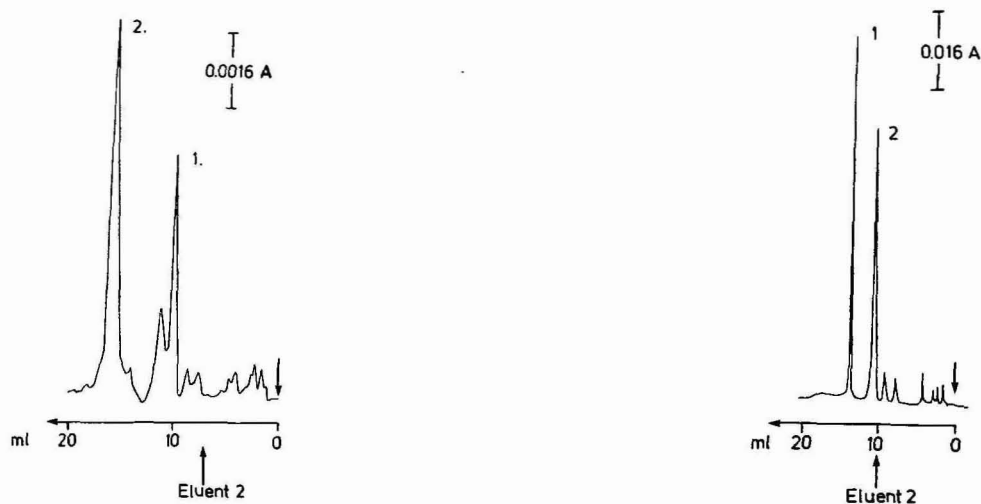
Fig. 6. Step-gradient elution, utilizing the TPeA desorption effect; $v_D = +7.6$ ml. Eluents: 1, as in Fig. 5; 2, eluent 1 lacking TPeA. Peaks as in Fig. 5. Flow-rate: 0.59 ml/min.

Fig. 7. Step-gradient technique with introduction of a co-ion; $v_D = +10.6$ ml. Eluents: 1, as in Fig. 5; 2, eluent 1 plus $1.00 \cdot 10^{-2}$ M octanesulphonate. Peaks as in Fig. 5. Flow-rate: 0.48 ml/min.

the octanesulphonate will give a distinct breakthrough front as it is eluted from the column[15]. When the column was equilibrated with respect to both TPeA and octanesulphonate, the retention volumes of TpTp and TpTpTpTp were smaller (*cf.*, eqn. 2) than when only TPeA was present, and no resolution was obtained between the nucleotides.

When the octanesulphonate eluent was introduced after the injection of the nucleotide sample (Fig. 7), the retention volume of TpTpTpTp was drastically decreased and a very narrow peak was obtained, compared to that obtained by isocratic elution (Fig. 5). TpTp was unaffected, which means that it was eluted from the column before the octanesulphonate front reached it. Due to the extremely narrow peak of TpTpTpTp, the peak width was three times smaller than for TpTp, and the chromatographic resolution was still very high (R_S = 5.2). "*N*" was 50000 plates for TpTpTpTp, while it was only 2700 for TpTp. The injected solution of TpTpTpTp was diluted 100 times, compared to the concentration in Fig. 5, while the TpTp concentration was unchanged. This shows that this gradient technique may have great potential for the analysis of low concentrations of an ionic organic analyte in the sample.

When v_D was less than + 6.0 ml, no resolution was obtained, and for values less than + 3.0 ml only one peak appeared. Not only the retention volume of the TpTpTpTp peak was affected. When the two eluents from Fig. 7 were used, TpTp was also affected, but to a much smaller degree. The total separation time was decreased by the use of a lower initial concentration of TPeA in the eluent. The analytes were then retained to a smaller extent (eqn. 1) and lower v_D values could be used while resolution was maintained.

When the TPeA concentration was kept constant and the octanesulphonate concentration in the second eluent was decreased, the retention decrease of TpTpTpTp was smaller (Fig. 8). This is probably due to the increased retention volume of the front[15]. The analyte thus migrated a longer distance through the col-
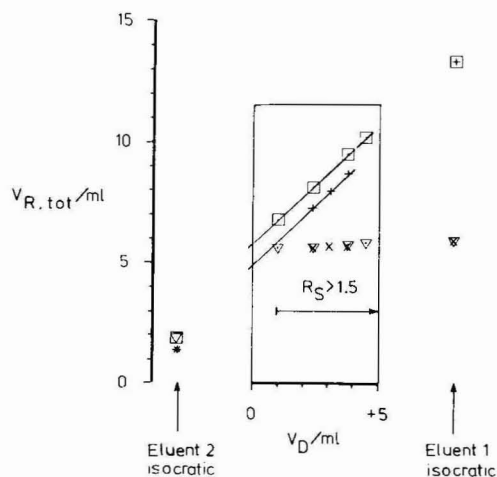
Fig. 8. Plot of $V_{R,tot}$ *versus* v_D. Eluents: 1, 7.76 · 10^{-4} *M* TPeA in phosphate buffer (pH 7.0, I = 0.032)–methanol (1:1); eluent 1 with addition of octanesulphonate [2.51 · 10^{-4} *M* for TpTp (∇), TpTpTpTp ($\square$); 3.80 · 10^{-4} *M* for TpTp ($\times$), TpTpTpTp (+)].

umn (higher s_1) before the front reached the analyte zone. In the v_D range investigated, the TpTp retention volume was unchanged at both concentrations of octanesulphonate.

A plot of $V_{R,tot}$ versus v_D should give a straight line with slope $(V_{R1} - V_{R2})/(V_{R1} - V_{RA})$ (eqn. 9), but only if the analyte is affected by the second eluent. TpTpTpTp gives straight lines at both concentrations of octanesulphonate (Fig. 8). The slopes of the lines are very close to $+1$, indicating that $V_{R2} = V_{RA}$. However, the intercepts are much higher than the V_{R2} values.

If it is assumed that the analyte retention volume is smaller in the second eluent, V_{R2}, then the retention volume of the front, V_{RA}, the analyte will be concentrated in the front. This means that the analyte retention volume is the same as that of the front and migrates through the rest of the column (s_2) with the front. V_{R2} in eqn. 9 can thus be exchanged for V_{RA}, resulting in the simple expression:

$$V_{R,tot} = V_{RA} + v_D \tag{10}$$

A plot of $V_{R,tot}$ versus v_D should now give a straight line with the slope $+1$ and the intercept V_{RA}.

The validity of eqn. 10 was tested by measurement of the retention volumes for the TpTpTpTp peak from the point where eluent 2 was introduced (v_D) in the two cases. Constant values were obtained, 5.7 and 4.8 ml (see intercepts in Fig. 8), at octanesulphonate concentrations of $2.5 \cdot 10^{-3}$ and $3.1 \cdot 10^{-3}$ M, respectively, indicating that V_{R2}, in fact, equals V_{RA} for this compound.

Higher concentrations of TPeA in the eluents also gave straight lines for TpTpTpTp, but the slopes were less than $+1$, indicating that the retention volume of TpTpTpTp in the second eluent was larger than that of the octanesulphonate front. In this case, eqn. 9 may be valid.

CONCLUSIONS

Two main principles can be used for the step-gradient technique introduced in this paper:

(1) decreasing the counter-ion concentration by desorption, and
(2) increasing the co-ion concentration.

The first principle, resulting in decreased retention by a gradual decrease of the counter-ion concentration, suffers from the drawback of slow desorption. The second principle, based on the competition for adsorption sites by the introduction of a co-ion, seems to be most fruitful for further development. Strong effects on the retention volumes and on the peak efficiencies were obtained, indicating possibilities for considerable improvements in analysis time, selectivity and detectability.

The equations developed permit the total retention volume for the analyte eluted last to be calculated.

REFERENCES

1 A. Sokolowski, N. Balgobin, S. Josephson, J. B. Chattopadhyaya and G. Schill, *Chem. Scr.*, 18 (1981) 189.
2 W. Haupt and A. Pingoud, *J. Chromatogr.*, 260 (1983) 419.
3 P. A. Perrone and P. R. Brown, *J. Chromatogr.*, 317 (1984) 301.
4 M. Kwiatkowski, A. Sandström, N. Balgobin and J. B. Chattopadhyaya, *Acta Chem. Scand. Ser. B*, 38 (1984) 721.
5 B. Allinquant, C. Musenger and E. Schuller, *J. Chromatogr.*, 326 (1985) 281.
6 C. R. Becker, J. W. Efcavitch, C. R. Heiner and N. F. Kaiser, *J. Chromatogr.*, 326 (1985) 293.
7 D. R. Webster, G. D. Boston and D. M. Paton, *J. Liq. Chromatogr.*, 8 (1985) 603.
8 L. R. Snyder, in J. J. Kirkland (Editor), *Modern Practice of Liquid Chromatography*, Wiley-Interscience, New York, 1971, p. 149.
9 P. Jandera and J. Churáček, *J. Chromatogr.*, 91 (1974) 223.
10 L. R. Snyder, in Cs. Horváth (Editor), *High-performance Liquid Chromatography, Advances and Perspectives*, Vol. 1, Academic Press, New York, 1980, p. 207.
11 P. Jandera and J. Churáček, *J. Chromatogr.*, 170 (1979) 1.
12 A. Tilly-Melin, Y. Askemark, K.-G. Wahlund and G. Schill, *Anal. Chem.*, 51 (1979) 976.
13 A. Sokolowski and K.-G. Wahlund, *J. Chromatogr.*, 189 (1980) 299.
14 A. Sokolowski, *Chromatographia*, 22 (1986) 177.
15 A. Sokolowski, *Chromatographia*, 22 (1986) 168.
16 S. O. Jansson, I. Andersson and B. A. Persson, *J. Chromatogr.*, 203 (1981) 93.
17 W. Jost, K. Unger and G. Schill, *Anal. Biochem.*, 119 (1982) 214.
18 K Gustavii and G. Schill, *Acta Pharm. Suec.*, 3 (1966) 259.
19 N. Balgobin, S. Josephson and J. B. Chattopadhyaya, *Acta Chem. Scand., Ser. B*, 35 (1981) 201.
20 N. K. Kochetkov and E. L. Budovskii, *Organic Chemistry of Nucleic Acids*, Part A, Plenum, New York, 1971.
21 R. Philips, P. Eisenberg, P. George and R. Rutman, *J. Biol. Chem.*, 240 (1965) 4393.
22 K. Gustavii and G. Schill, *Acta Pharm. Suec.*, 3 (1966) 241.
23 F. Helfferich, *J. Chem. Educ.*, 41 (1964) 410.

CHROMSYMP. 1011

ZONE FORMATION IN ION-PAIR REVERSED-PHASE LIQUID CHROMATOGRAPHY

IV. OPTIMIZATION OF PEAK RETENTION IN STEP-GRADIENT ELUTION WITH INTRODUCTION OF COMPETING IONS

ANDERS SOKOLOWSKI

Department of Analytical Pharmaceutical Chemistry, Biomedical Center, University of Uppsala, Box 574, S-751 23 Uppsala (Sweden)

SUMMARY

Step-gradient elution by introduction of a co-ion into an ion-pair reversed-phase system was studied. The analytes were organic acids and amines and were used as counter ions in eluents also containing phosphate buffer (pH 4 or 6)–methanol (1:1). The magnitude of the retention decrease obtained for the analytes was dependent on the hydrophobicity and concentration of the co-ion and on a temporary decrease in the counter-ion concentration on introduction of the co-ion. When some prerequisites were fulfilled, a simple equation could be used to predict the retention volume, and then the separation time could be optimized. Extremely narrow peaks were obtained. The peak width was dependent on the co-ion concentration in the second eluent and also on the efficiency of the column, which is responsible for the bandbroadening of the breakthrough front of the co-ion.

INTRODUCTION

Gradient elution is a powerful technique for decreasing the separation time of analytes having large differences in retention times. The most common technique in reversed-phase liquid chromatography (RPLC)[1,2] is based on a continuous increase of the organic solvent content in the eluent, but a stepwise increase is also used[1,3]. Although the mathematical expressions describing the retention times are rather complicated[1–3], the ion-pair step-gradient technique can be handled by rather simple expressions of the retention[4]. When a co-ion is introduced into the column, equilibrated with the counter ion, the existing equilibria are disturbed. As a result, a co-ion front and a zone containing a lower concentration of the counter ion than in the bulk mobile phase are obained[5]. Both the front and the zone migrate along the column and can increase the migration speed of an analyte, *cf.*, refs. 6–8.

In this work the optimization of the ion-pair step-gradient technique for some organic anions was studied with regard to both peak retention and compression. Quaternary ammonium ions are often used as cationic counter ions but they have

the drawback that they decrease the column stability[8,9]. Amines are preferable in this respect[8]. In this study, symmetrical amines, differing in their carbon contents, have been used as counter ions.

THEORETICAL

The main quantitative expressions for ion-pair retention are described elsewhere[5,7,8,10].

In the single-step gradient elution process used in this study the analyte migrates part of the column distance with an eluent containing the counter ion (eluent 1) and the remaining distance with an eluent containing both the counter- and the co-ion (eluent 2). The retention volume of the analyte is high in eluent 1 but low in eluent 2. The total retention volume of the analyte can be described by the expression[4]

$$V_{R,\text{tot}} = V_{R2} + \frac{v_D(V_{R1} - V_{R2})}{(V_{R1} - V_{RA})} \tag{1}$$

where V_{R1} is the retention volume in the eluent containing only the counter ion (eluent 1), V_{R2} that in the eluent containing both the counter- and the co-ion (eluent 2) in isocratic development, V_{RA} is the retention volume of the co-ion front (breakthrough front), cf., ref. 5, and v_D is the volume eluted between the injection of the analyte and the introduction of eluent 2. Positive v_D values mean that the injection was made before the introduction of eluent 2, negative values that the injection was made after the introduction.

If $V_{R2} < V_{RA}$, the analyte will be concentrated in the co-ion front and will migrate with the front through the rest of the column. Then, eqn. 1 can be simplified[4] to

$$V_{R,\text{tot}} = V_{RA} + v_D \tag{2}$$

This expression is valid if eluent 2 affects the analyte before it is eluted from the column.

EXPERIMENTAL

Apparatus and chemicals

The apparatus and chemicals were the same as in the Part III[4], with the following exceptions. The columns were packed with μBondapak Phenyl, 10 μm, Batch No. 15 (Waters Assoc., Milford, MA, U.S.A.).

Tripentylamine (TrPeA), trihexylamine (TrHexA) and the sodium salts of hexanesulphonic acid and 2-naphthalenesulphonic acid were from Eastman-Kodak (Rochester, NY, U.S.A.). Tributylamine (TrBA), 1-naphthoic acid, 1-naphthylacetic acid and sodium decanesulphonate were from Fluka (Buchs, Switzerland). Sodium 2-anthracenesulphonate was kindly supplied by D. Westerlund. It had been synthesized from sodium 2-anthraquinonesulphonate[11]. TrBA, TrPeA and TrHexA were distilled prior to use. All other substances were of analytical or reagent grade used without further purification.

Preparation of the eluents

The eluents were prepared by mixing equal volumes of methanol and phosphate buffer [pH 4.0 or 6.0, ionic strength, $I = 0.032$ (mol/l)]. The pH 4.0 phosphate buffer has a low buffer capacity, but because only the sodium salts of the sulphonates were used as samples, no change of pH occurred. The phosphate buffers were prepared by mixing 1 M phosphoric acid and 1 M sodium hydroxide. When the eluent contained an amine, an equivalent amount of sodium hydroxide was replaced by the amine to keep the pH and ionic strength constant. When sulphonate was present in the eluent the ionic strength was increased by the corresponding equivalents of sodium sulphonate.

The amines were distilled prior to use in the eluents. They were stored under nitrogen in a refrigerator since it was observed that on storage at ambient temperature they became pale yellow. For TPeA this happened after a few days storage. Even when stored cold, the amines turned the top of the columns yellowish brown, and the column pressure increased when amine-containing eluents were used for several days.

To remove the coloured impurities in the amine-containing eluents, they were pumped through a column packed with μBondapak Phenyl, 10 μm (100 mm × 4.6 mm). The first 50 ml of eluate were discarded, then 200 ml were collected prior to use in the analytical system. If sulphonate were also to be present in the eluent, it was added after this treatment. Before the next 200 ml of eluent were purified, 2 mm of the solid phase at the top of this column were replaced with fresh sorbent, and then 50 ml of methanol were pumped through the column.

TPeA-containing eluents could be used for only 2 days after purification. If they were used later, the column pressure increased and the yellow-brown colour developed. TrBA- and TrHexA-containing eluents did not exhibit these problems after purification.

The concentration of the amines in the eluents was measured by the picrate method[12], using 1- or 5-cm cuvettes, *cf.*, ref. 4.

Chromatographic technique

The breakthrough and the step-gradient elution studies were performed according to the breakthrough technique described in ref. 5, using the same equipment. The chromatograph was maintained at 25.00 ± 0.01°C and the flow-rate of the mobile phase was in the range 0.5–0.8 ml/min. The eluent was not recirculated. The analytes were dissolved in the eluent.

RESULTS AND DISCUSSION

Amines as counter ions

The retention volumes of organic anions depend on the concentration and hydrophobicity of the amines used as counter ions (Fig. 1) according to general ion-pair retention principles[7]. The highest concentration of amine in the eluent that could be used without increasing the ionic strength was $1.5 \cdot 10^{-2}$ M at pH 6. However, TrHexA could not be used at concentrations higher than $1.0 \cdot 10^{-3}$ M, due to its limited solubility.

The presence of co-ions in the amine-containing eluents resulted in decreased
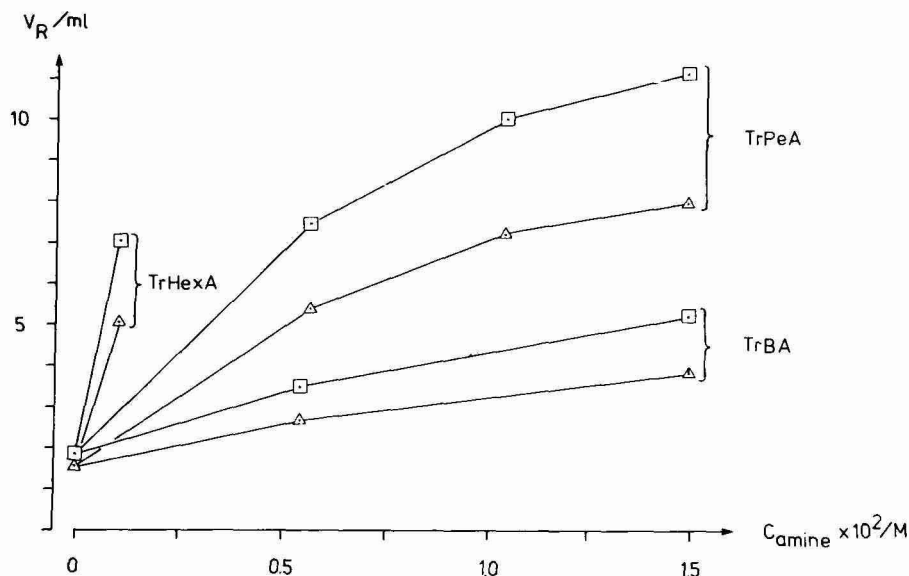
Fig. 1. Retention volumes of carboxylic acids as ion pairs with different amines. Eluents: phosphate buffer (pH 6.0)–methanol (1:1) containing different amines. Analytes: □ = 1-naphthylacetic acid; △ = 1-naphthoic acid.

retention volumes for the analytes, *cf.*, refs. 6 and 8. Hexane-, octane- and decane-sulphonate were tested with TrPeA or TrHexA as counter ions. Decanesulphonate, the most hydrophobic sulphonate, decreased the retention volumes most effectively. Fig. 2 shows the effect on some carboxylic acids when TrPeA was used as the counter ion and octanesulphonate as the co-ion.

Since TrPeA showed a rapid degradation when used as the counter ion in the eluents (see Experimental). TrHexA was preferred. When the pH of the phosphate buffer was decreased, the retention volume of anionic analytes increased for the same concentrations of TrHexA, *cf.*, ref. 7. This is shown in Table I. Although the reason for this is not known, the ratio $[H_2PO_4^-]/[HPO_4^{2-}]$ increases and could increase the ion-pair distribution. Furthermore, the protolysis of free silanol groups is suppressed, and this may change the character of the solid phase. Since the highest concentration of TrHexA that could be used was $1.0 \cdot 10^{-3}$ M, a pH of 4 was used to obtain sufficiently high retention volumes of the most retained analyte in the step-gradient elution studies.

Breakthrough retention volume of the co-ion

When an eluent containing $1.0 \cdot 10^{-3}$ M TrHexA was introduced into a column equilibrated with phosphate buffer (pH 4.0)–methanol (1:1) a breakthrough curve was obtained, which was detected by a refractive index detector. The retention volume was 11.5 ml[5]. If a second eluent, also containing decanesulphonate, was then introduced, two breakthrough curves were obtained. Increased concentrations of de-canesulphonate resulted in decreased retention volumes of the first breakthrough,
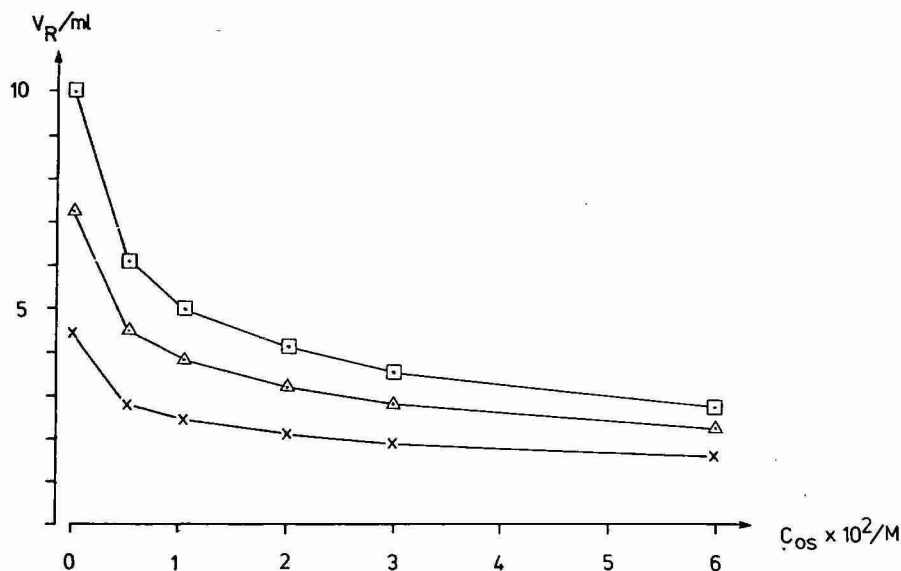
Fig. 2. Retention volumes of carboxylic acids in the presence of TrPeA and octanesulphonate (OS). Eluent: $1.04 \cdot 10^{-2}$ M TrPeA and OS in phosphate buffer (pH 6.0)–methanol (1:1). Analytes: □ = 1-naphthyl-acetic acid; △ = 1-naphthoic acid; × = 2,4-dinitrobenzoic acid.

V_1, while those of the second, V_2, increased (Table II). The results indicate that the first breakthrough represents the retention of decanesulphonate and the second the retention of TrHexA[5].

      The refractive index (RI) detector only registers the total change in the refractive index of the eluate. It is assumed that the breakthrough of decanesulphonate creates a negative TrHexA zone[5], and the sum of the decanesulphonate and TrHexA signals results in an elution profile containing two breakthrough curves (Fig. 3). This means that there are three different regions of mobile phase composition migrating along the column. The first region contains the bulk concentration of TrHexA, the second contains the bulk concentration of decanesulphonate, but at a smaller concentration than the bulk of TrHexA, and the third contains decanesulphonate and TrHexA at the bulk concentrations of both. The phase composition of these three regions forms the basis for the understanding and utilization of the ion-pair step-gradient elution technique.

TABLE I

DEPENDENCE OF RETENTION VOLUME ON pH

Eluent: $1.03 \cdot 10^{-3}$ M TrHexA in phosphate buffer–methanol (1:1).

Analyte	V_R (ml)	
	pH 4.0	pH 6.0
2,4-Dinitrobenzoic acid	3.85	3.21
2-Naphthalenesulphonate	5.93	4.90

TABLE II

RETENTION VOLUMES OF THE BREAKTHROUGH CURVES ON INTRODUCTION OF DE-
CANESULFONATE (DS) AND TrHexA INTO A COLUMN EQUILIBRATED WITH $1.00 \cdot 10^{-3}$ M
TrHexA

C_{DS} (M)	V_1 (ml)	V_2 (ml)
$2.40 \cdot 10^{-3}$	6.8	33
$5.00 \cdot 10^{-3}$	5.1	49
$1.00 \cdot 10^{-2}$	4.0	60

Step-gradient elution

When a mixture of 2,4-dinitrobenzoic acid (DNBA) and 2-anthracenesul-
phonate (AS) was injected into a column equilibrated with TrHexA (eluent 1) and
then an eluent, also containing decanesulphonate (eluent 2), was introduced into the
column (positive v_D values), only the retention volume of AS was affected (Fig. 4).
The separation was complete ($R_S > 1.5$) for all v_D values tested. A plot of $V_{R,tot}$
versus v_D gives a straight line with slope $+0.98$ and intercept 4.1, and indicating that
the retention of AS is in accord with eqn. 2. The intercept is in good agreement with
the retention volume of the decanesulphonate breakthrough front, V_{RA} (Table II).
This means, further, that AS is concentrated in the decanesulphonate front ($V_{R2} <
V_{RA}$).
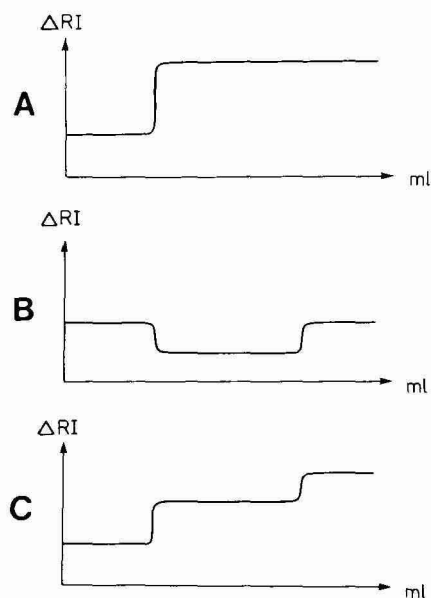
Fig. 3. Hypothetical and observed elution profiles after introduction of decanesulphonate into a column equili-
brated with TrHexA. For compositions of the eluents see Table II. (A) Hypothetical breakthrough of decanesul-
phonate; (B) hypothetical negative TrHexA zone; (C) observed elution profile.
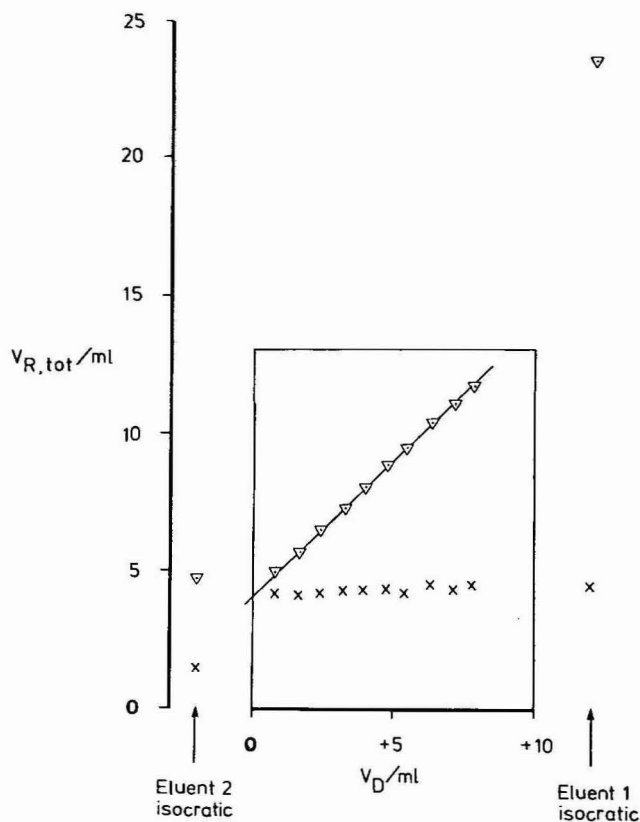
Fig. 4. Dependence of the total retention volume, $V_{R,tot}$, on time for step-gradient elution. Positive v_D values; see text for definition of v_D. Eluents: 1, $1.00 \cdot 10^{-3}$ M TrHexA in phosphate buffer (pH 4.0)–methanol (1:1); 2, $9.99 \cdot 10^{-3}$ M sodium decanesulphonate in eluent 1. Analytes: ∇, 2-anthracenesulphonate; $\times$, 2,4-dinitrobenzoic acid.

A drastic decrease in peak width, 4σ, was obtained when AS was affected by eluent 2. When the AS zone is concentrated in the front, the peak will be very narrow, since the rear of the AS zone migrates under conditions creating a greater velocity than that of the front. The difference in co-ion concentration between the front and rear depends on the steepness of the front, which is dependent on the column efficiency[13]. By using a very efficient column very narrow peaks can be obtained. The peak width of AS was 0.13 ml for all v_D values, while in isocratic elution with eluent 1 the peak width was 2.4 ml and with eluent 2 it was 0.53 ml. As a consequence, the higher $V_{R,tot}$ is for AS (high v_D), the higher will be the measured efficiency, "N"[4]. For $v_D = +7.79$ ml, "N" was calculated to be $1.3 \cdot 10^6$ plates per m.

The measured efficiency cannot be compared with those of isocratic systems, since the peak width was unchanged independent of $V_{R,tot}$. It is of greater interest that the peak was 16 times higher than in an isocratic elution with eluent 1 and 4 times higher than with eluent 2.
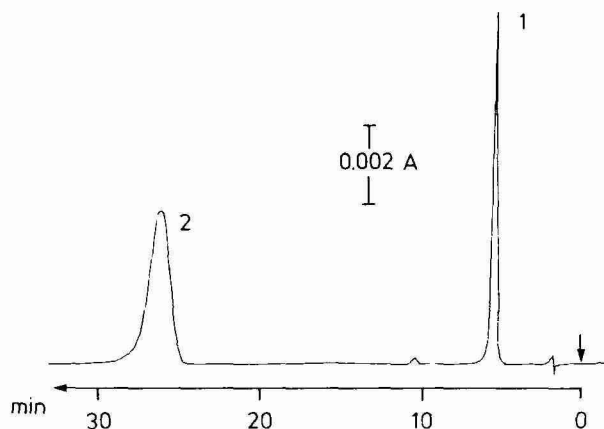
Fig. 5. Isocratic separation of anions. Eluent: $1.00 \cdot 10^{-3}$ M TrHexA in phosphate buffer (pH 4.0)–methanol (1:1). Peaks: 1 = 2,4-dinitrobenzoic acid ($C^0 = 2.0 \cdot 10^{-4}$ M), 2 = 2-anthracenesulphonate ($C^0 = 5.0 \cdot 10^{-5}$ M). Flow-rate: 0.71 ml/min.

The peak width of DNBA was unchanged for all v_D values and had the same value as in isocratic elution with eluent 1, 0.46 ml, while with eluent 2 it was half as wide, 0.22 ml.

The features of the step-gradient technique are most easily demonstrated by a comparison of isocratic elution (Fig. 5) with step-gradient elution (Fig. 6), where $v_D = 3.7$ ml. In gradient elution the retention volume of the peak eluted was reduced 2.5 times and the detectability considerably improved.

When decanesulphonate was replaced by hexanesulphonate, keeping the concentration at $1.0 \cdot 10^{-2}$ M, the retention (Fig. 7) and "N" of both DNBA and AS were affected. On increasing v_D (positive) the total retention increased. For DNBA a straight line with a slope of $+1$ was obtained when $V_{R,tot}$ was plotted against v_D.
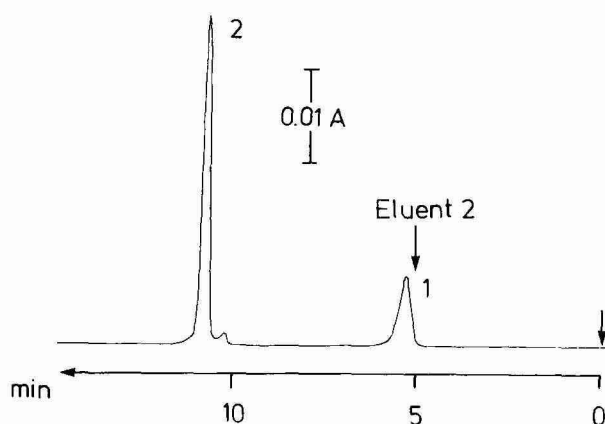
Fig. 6. Step-gradient elution by introduction of a co-ion; $v_D = +3.73$ ml. For eluents 1 and 2 see Fig. 4; peaks, see Fig. 5; Flow-rate: 0.74 ml/min.
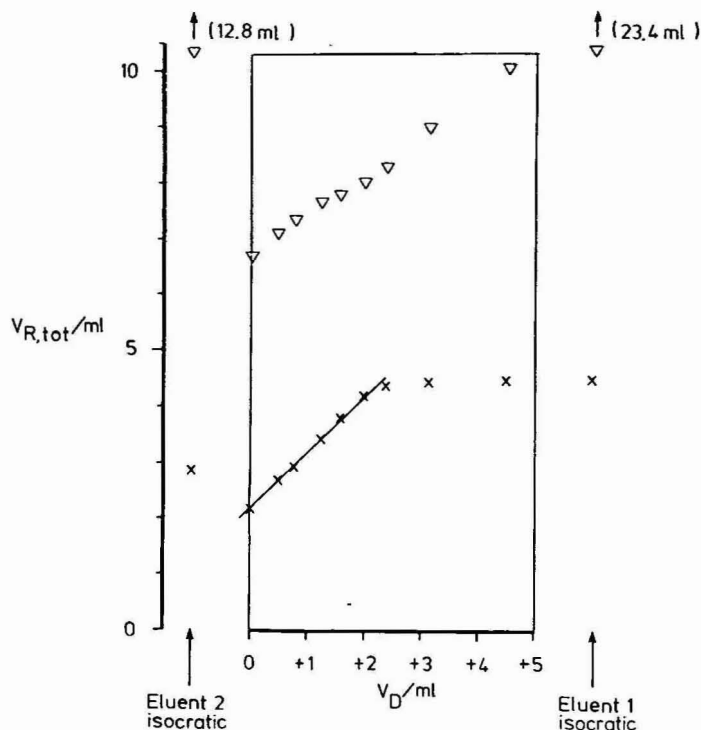
Fig. 7. Dependence of the total retention volume, $V_{R,tot}$, on time for step-gradient elution. Positive v_D values. Details as in Fig. 4 except eluent 2, $1.00 \cdot 10^{-3}$ M sodium hexanesulphonate in eluent 1.

At v_D values higher than $+2.4$ ml, the retention was unchanged and equal to that in isocratic elution with eluent 1. Eqn. 2 is valid for DNBA in the region $v_D = 0$ to $+2.0$ ml. The intercept of the line was in good agreement with the retention volume of the breakthrough front for $1.00 \cdot 10^{-2}$ M hexanesulphonate (2.0 ml). The peak width of DNBA was 0.13 ml in the region where it was affected by hexanesulphonate. In this region "N" also increased to a maximum of 150000 plates per m. At higher v_D values the peak width continuously increased and "N" decreased to the values obtained with eluent 1, 0.47 ml and 16000 plates per m, respectively. With eluent 2 the peak width was 0.28 ml.

The AS peak was also affected, but to a lesser extent, compared to the effect of decanesulphonate. With increasing v_D the retention volume of AS increased, but there was no linear relationship. With eluent 1 the retention volume of AS was very high, and thus, when eluent 2 was introduced, AS was very quickly reached by the hexanesulphonate front. The actual concentration of hexanesulphonate does not have enough competing effect to concentrate AS in the front. This means that the front will pass the AS zone, but the migration velocity of AS will be increased. Fig. 3B shows that the concentration of TrHexA, the counter ion, was decreased on introduction of decanesulphonate; a negative TrHexA zone was obtained. Also, this decrease in the TrHexA concentration will increase the migration velocity of AS.

TABLE III

EFFECT ON RETENTION VOLUME AND EFFICIENCY OF THE INTRODUCTION OF HEXANE-
SULPHONATE BY THE STEP-GRADIENT TECHNIQUE, COMPARED TO AN ISOCRATIC ELU-
TION

Eluents: 1, $1.00 \cdot 10^{-3}$ M TrHexA in phosphate buffer (pH 4.0)–methanol (1:1); 2, $1.00 \cdot 10^{-2}$ M sodium hexanesulphonate in eluent 1.

Analyte	Eluent 2 (isocratic)		Step gradient, $v_D = +1.6$ ml		Eluent 1 (isocratic)	
	V_R (ml)	N (per m)	$V_{R,tot}$ (ml)	"N" (per m)	V_R (ml)	N (per m)
DNBA	2.9	15 000	3.8	133 000	4.5	16 000
AS	12.8	17 000	7.8	25 000	23.4	17 000

When TrHexA is returned to its original bulk concentration (end of the negative TrHexA zone) the migration velocity of AS will decrease. The migration velocity of AS will be changed twice in different directions, and thus, no linear relationship between $V_{R,tot}$ and v_D is expected.

With increasing positive v_D values, the peak width of AS first decreased to 0.62 ml at v_D +2.4 ml and then increased. At higher v_D values, "N" increased, but the effect was not so pronounced as for DNBA.

For small positive v_D values it was observed that $V_{R,tot}$ for both DNBA and AS was smaller than in isocratic development with eluent 2 (Fig. 7). This indicates the effect on the retention of the negative TrHexA zone (Fig. 3B), in combination with the hexanesulphonate. For $v_D = +1.6$ ml the separation time was smaller and "N" was higher for the two analytes than in isocratic elution with eluent 2 (Table III).

Step-gradient elution with negative v_D values

When AS was injected after the introduction of decanesulphonate (negative v_D values), $V_{R,tot}$ was larger the later the injection was made (Fig. 8), but at larger
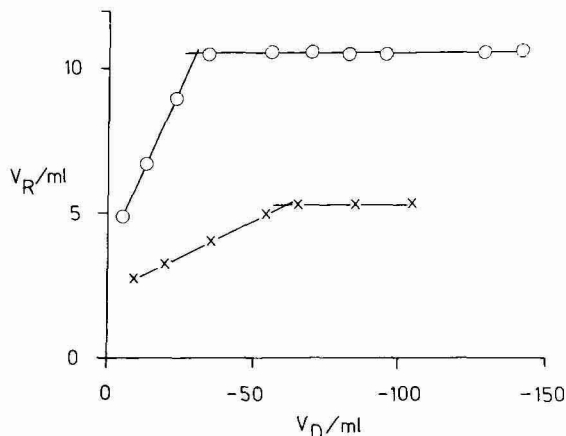
Fig. 8. Dependence of the total retention volume, $V_{R,tot}$, on time for step-gradient elution. Negative v_D values. Eluents: 1, $1.00 \cdot 10^{-3}$ M TrHexA in phosphate buffer (pH 4.0)–methanol (1:1); 2, $2.42 \cdot 10^{-3}$ (○) or $1.01 \cdot 10^{-2}$ M (×) decanesulphonate in eluent 1. Analyte: 2-anthracenesulphonate.

negative v_D values the retention volume was constant. The latter value is assumed to be the retention volume in eluent 2 when the column is equilibrated.

The increase in the retention volume shows the effect from the end of the negative TrHexA zone, *i.e.*, when the TrHexA concentration returns to the bulk concentration (Fig. 3B). AS migrates partly in the zone where the TrHexA concentration is lower and partly with the bulk concentration. The later AS was injected after the introduction of decanesulphonate the longer was the distance it migrated with the bulk concentration of TrHexA, and thus, the retention volume was increased. The position (v_D values) where the retention volume of AS starts to be constant is in good agreement with the second breakthrough retention volumes given earlier (Table II).

The effect of the negative TrHexA zone on the retention of AS demonstrates further that eqn. 1 can be used only if the retention in the negative zone is known and if the analyte is not affected by the end of this zone (the TrHexA concentration increases).

Reequilibration of the system

When the column was equilibrated with an eluent containing both TrHexA and decanesulphonate (eluent 2 in the step-gradient elution) the decanesulphonate had to be desorbed prior to the next experiment. This could be performed by introduction of an eluent containing only TrHexA (eluent 1). However, the desorption of the anion and the reequilibration would then have been a lengthy process. To speed up the reequilibration, a large volume of methanol was injected, just after the TrHexA-containing eluent was introduced into the column. When 1.0 ml of methanol was injected, both TrHexA and decanesulphonate were completely desorbed. This was confirmed by use of the refractive index detector and continuous injections of DNBA. TrHexA must then be adsorbed before the column is equilibrated. This was achieved when 12 ml (the breakthrough retention volume) of the TrHexA-containing eluent were pumped through the column. When only 0.5 ml of methanol were injected the desorption was incomplete, and a larger volume (25 ml) of eluent 1 had to be pumped through the column before it was equilibrated. The injection of methanol, in combination with the introduction of the TrHexA-containing eluent, seems to be the most rapid way of reequilibrating the column. At the actual concentrations of TrHexA and decanesulphonate, this technique is three times as fast as the introduction of eluent 1 alone.

CONCLUSIONS

Ion-pair step-gradient elution provides excellent possibilities for decreasing the analysis times and the detection limits of ionic analytes. By using suitable conditions, the separation times are decreased, while complete resolution is maintained. The total retention volume can in most cases be calculated by use of a simple equation. The peak width of late eluted peaks can be reduced to a large extent by increasing the hydrophobicity and/or the concentration of the co-ion in the second eluent. Early eluted peaks can also be affected by using more hydrophilic co-ions. In this case, late eluted peaks will also be affected but to a lesser extent. The system can be reequilibrated quickly by injection of a large volume of methanol in combination with the introduction of an eluent containing only the counter ion.

REFERENCES

1 P. Jandera and J. Churáček, *J. Chromatogr.*, 91 (1974) 223.
2 L. R. Snyder, in Cs. Horváth (Editor), *High-Performance Liquid Chromatography, Advances and Perspectives*, Vol. 1, Academic Press, New York, 1980, p. 207.
3 P. Jandera and J. Churáček, *J. Chromatogr.*, 170 (1979) 1.
4 A. Sokolowski, *J. Chromatogr.*, 384 (1987) 1–12.
5 A. Sokolowski, *Chromatographia*, 22 (1986) 168.
6 A. Sokolowski, *Chromatographia*, 22 (1986) 177.
7 A. Tilly-Melin, Y. Askemark, K.-G. Wahlund and G. Schill, *Anal. Chem.*, 51 (1979) 976.
8 A. Sokolowski and K.-G. Wahlund, *J. Chromatogr.*, 189 (1980) 299.
9 A. Sokolowski, N. Balgobin, S. Josephson, J. B. Chattopadhyaya and G. Schill, *Chem. Scr.*, 18 (1981) 189.
10 S. O. Jansson, I. Andersson and B. A. Persson, *J. Chromatogr.*, 203 (1981) 93.
11 D. Westerlund and K. O. Borg, *Acta Pharm. Suec.*, 7 (1970) 267.
12 K. Gustavii and G. Schill, *Acta Pharm. Suec.*, 3 (1966) 241.
13 C. N. Reilley, G. P. Hildebrand and J. W. Ashley, Jr., *Anal. Chem.*, 34 (1962) 1198.

CHROMSYMP. 969

SIMPLIFIED DESCRIPTION OF HIGH-PERFORMANCE LIQUID CHROMATOGRAPHIC SEPARATION UNDER OVERLOAD CONDITIONS, BASED ON THE CRAIG DISTRIBUTION MODEL

I. COMPUTER SIMULATIONS FOR A SINGLE ELUTION BAND ASSUMING A LANGMUIR ISOTHERM

J. E. EBLE and R. L. GROB

Chemistry Department, Villanova University, Villanova, PA 19085 (U.S.A.)

P. E. ANTLE

Biomedical Products Department, E. I. Du Pont de Nemours & Co., Concord Plaza, Wilmington, DE 19898 (U.S.A.)

and

L. R. SNYDER*

LC Resources, Inc., 26 Silverwood Court, Orinda, CA 94563 (U.S.A.)

SUMMARY

High-performance liquid chromatographic separation in an overload mode has been studied using the Craig-distribution scheme, assuming a Langmuir isotherm. Elution curves were determined as a function of sample mass by computer simulation, for different values of both capacity factor (k') and column plate number (N) at low loading (k_0 and N_0). It was possible to generalize these data so as to correlate Craig elution curves with sample mass and other experimental conditions, through the definition of certain "loading functions": w_{xk} and w_{xN}. This led to a more rapid ("second generation") computer program for the prediction of elution curves for single compounds, as a function of sample mass, retention, and any plate number. Predictions by the latter approach agree well with the more time-consuming Craig simulations. This work provides a starting basis for studying overload high-performance liquid chromatographic separation as a function of sample size and experimental conditions. Later papers will show that (a) experimental data under overload conditions correlate well with the present model, and (b) the model can be extended to the case of two co-eluting solutes.

INTRODUCTION

Preparative separations by high-performance liquid chromatography (HPLC) are of increasing interest. Today this technique is often used to purify multi-gram quantities of various compounds, and some groups are carrying out separations at the kilogram and higher scale[1,2]. For such applications, the column will usually be

operated in a "mass-overload" mode, such that sample retention and band-width are changed from what is observed under "analytical" (*i.e.*, small-sample) conditions[3]. Separation in an overload mode is usually much more complex than for the case of small-sample HPLC. A good deal of attention has been given to overload separations[4-20], but a comprehensive and convenient description of such procedures is not yet available. There is even considerable debate among experts as to whether analytical-scale separations can provide useful information for the design of corresponding overload separations.

There is a pressing need for a practical theory of overload HPLC that can be used for most separations, with a minimum of additional measurements, *e.g.*, no determination of sorption isotherms. The present two papers[21] plus reports to follow describe a new approach for understanding preparative HPLC under mass-overload conditions. We begin by using a model of chromatographic separation based on Craig-distribution[22] plus the assumption of Langmuir-isotherm retention[23]. This allows us to carry out computer-simulated HPLC separations under mass-overload conditions, for a single-solute sample. We then generalize the results of these computer simulations to arrive at simple relationships which give insight into overload-HPLC. These relationships also allow us to replace the time-consuming Craig simulations with second-generation computer simulations that require only a few minutes per run, regardless of column plate number. These results are described in the present paper.

In the following paper[21] we describe the extension of the above model to the case of non-Langmuir retention. We will show that a change in isotherm shape or type leads to an apparent reduction in the saturation capacity of the column, but often does not otherwise affect preparative separation. We will further show that an apparent column capacity (for a given HPLC system) is easily determined from a few overload experiments with small columns. This allows computer simulation of further runs under overload conditions. We will also show that experimental runs with a single solute (mass-overload conditions) are in reasonable agreement with our model. With minor, empirical adjustments in the starting Craig model, computer simulation can now be used to predict the effects of overload on the HPLC separation of a single band. Later papers will extend this treatment to the case of two co-eluting solutes.

COMPUTER SIMULATIONS

The Craig simulations were written in BASIC and executed on an IBM-XT (IBM, Boca Raton, FL, U.S.A.) with the use of a Microsoft BASIC compiler (Microsoft, Bellevue, WA, U.S.A.). Using the equations for a Langmuir isotherm (see Appendix I) and assigning the phase ratio $\psi = 0.1$, the fraction of solute in the mobile phase (r) was calculated as a function of total solute mass in both phases (for $k_0 = 1$, 3, and 10). Values of r *vs.* solute mass for each value of k_0 were then fit to an 8-term polynomial, using the General Statistics Pac (Hewlett-Packard, Palo Alto, CA, U.S.A.) on an HP-85 computer (Hewlett-Packard).

In our simulation algorithm, the sample is initially transferred to the mobile phase of the first cell. After equilibrating the two phases in the first cell, the fraction of solute in the mobile phase is calculated from the appropriate polynomial for r. The mobile phase is passed to the second cell, and fresh mobile phase is added to the

first cell. The two cells are again equilibrated, and the fraction of solute in the mobile phase of each cell is calculated as before. This process is repeated until 99.999% of the solute has left the last cell. Likewise, when the solute concentration in any cell decreases to 0.001% of the total injected sample-mass, that cell is ignored in further calculations. When the last cell is filled with mobile phase (after n transfers when the total number of cells, $n_c = n$), the solute mass in the mobile phase for this cell is transferred to an open file, as are subsequent transfers from the last cell. These data are equivalent to the calculated elution band. Calculations of k' and N were accomplished on the basis of both "band" and "cumulative" measurements (see Fig. 1 and below).

THEORY AND RESULTS

HPLC separations under analytical conditions generally approximate Gaussian elution bands with values of k' and N that do not vary with sample mass w_x (when w_x does not exceed a certain maximum value). Thus the shape and position of the band within the chromatogram remain fixed. When w_x is increased beyond some limit, values of the capacity factor k' and plate number N generally decrease with further increase in w_x, and the band becomes non-Gaussian (as measured by the peak asymmetry factor A_s)[*]. This is illustrated by reversed-phase HPLC runs for benzyl alcohol under analytical *vs.* overload conditions (0.94 mg injection, 5 × 0.46 cm column of Zorbax[**] C_8):

	Small sample	0.94 mg
k'	2.86	2.40
N	1836	241
A_s	1.0	3.3

Fig. 1a shows the benzyl alcohol band for this 0.94-mg sample.

Values of k' and N (in combination with derived overload parameters) determine the final separation under overload conditions. This is illustrated for Craig-simulated data in Fig. 8 of the present paper, and for experimental data in Figs. 26 and 27 of the following paper[21]. The following discussion is based on values of k' and N, and how these parameters vary with experimental conditions in overload separations. Overload values of k' and N can be measured in various ways. In Fig. 1a, k' is calculated from the retention time t_R (peak maximum, 95.7 s) and column dead time t_0 (28.2 s) in the usual way: $k' = 2.40$. Likewise, N is calculated from the bandwidth W_2 at 0.61 × band height (2σ, see p. 834 of ref. 3) and the retention time of 95.7 s: $N = (t_R/\sigma)^2$, or a value of $N = 241$ for the band of Fig. 1a.

Values of k' and N can also be determined from the derived cumulative elution (integral) plot of Fig. 1b. Here retention time is defined as the time when 50% of the solute has eluted from the column. Bandwidth is measured as the time difference between 15.9% and 84.1% elution, corresponding to $\pm 1\sigma$. Values of k' and N calculated in these two ways are slightly different for this overload separation (Fig. 1b *vs.* 1a). These differences become greater for increased sample size.

---

[*] For definitions of symbols used in these two papers, see the Glossary of symbols at the end of this paper. We define A_s in terms of the usual bandwidth measurements at 10% of peak maximum.

[**] Zorbax is a trademark of the Du Pont Company.
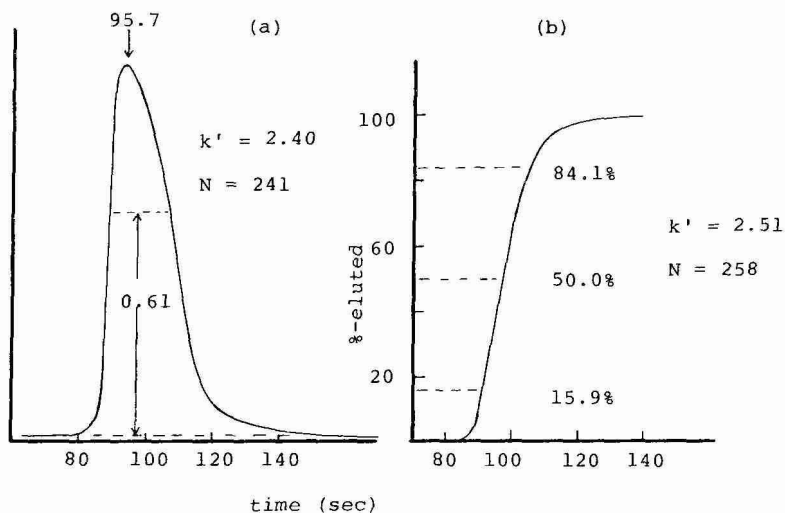
Fig. 1. Elution curves for a typical overloaded separation. Sample, benzyl alcohol, 0.94 mg injected; column 5 × 0.46 cm of C_{18} silica; mobile phase, methanol–water (40:60); flow-rate, 0.9 ml/min; temperature, 35°C (see ref. 21 for details). (a) elution curve from chromatogram; (b) cumulative elution calculated from (a) as described in ref. 21.

Sometimes we will find that the procedure of Fig. 1a is preferable for measurement of k' or N. More often we will use values of k' and N based on the cumulative elution curve (Fig. 1b). Fig. 2 shows two superimposed bands, separated under overload conditions, with an arbitrary cutpoint indicated by an arrow. In
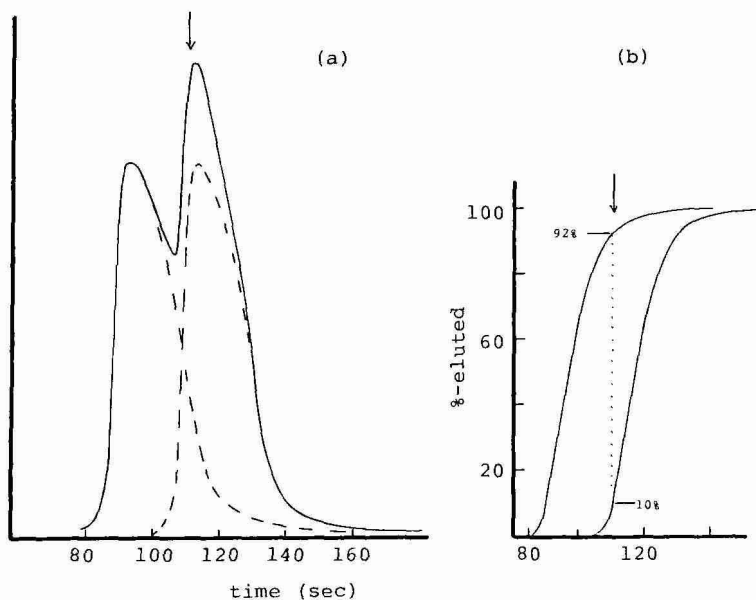
Fig. 2. Hypothetical elution curves for two overlapping bands under overload conditions. (a) From the chromatogram; (b) cumulative elution plots.

preparative HPLC, we are primarily interested in the yield and purity of fractions collected as illustrated in Fig. 2 (arrows). This information is more readily derivable from cumulative elution curves, as in Fig. 2b (92% yield of A in fraction 1, with a purity of 90%; assumes equal values of w_x for each band). We will refer to values of k' and N determined as in Fig. 1a as "band" values. Values of k' and N determined as in Fig. 1b will be referred to as "cumulative" values.

The Craig model

Attempts at creating a fundamental theory for overload HPLC have been reported by several workers. One of the more successful of these approaches is a perturbation model based on the mass balance equations that describe the concentrations of sample and mobile phase during separation (refs. 4, 5, 14, 16, 17 and related discussion in ref. 24). A Langmuir isotherm is assumed, and the model is limited to the case of moderate overloading of the column. Other approaches to predicting overload separation have also been described[10,11,15], but these appear less well developed, as well as more empirical. The major limitation of these treatments at the present time is that they apply only to the case of a single solute band. They are therefore unable to predict what will happen in the case of "real" separations, where two or more bands co-elute. We have therefore examined an alternative approach that will be shown applicable to the case of samples containing two or more components*.

The Craig distribution model, based on counter-current migration of a sample band in a train of equilibrated stages or "plates"[22], has often been used for illustrating or modeling chromatographic separation under non-overload conditions. The sample is placed in the first stage, and after equilibration of mobile and stationary phases, the mobile phase is then moved to the second stage; fresh mobile phase is added to the first stage, and the process is repeated. The process adequately describes the retention or equilibrium properties of the separation; the kinetic or band broadening characteristics can be represented by varying the number of stages in the system. The plate number N_0 (small sample) is related to the number of Craig stages n_c and capacity factor k_0 (small sample) as

$$N_0 = (n_c + 1)(k_0 + 1)/k_0 \tag{1}$$

Early attempts at modeling overload separation in liquid–solid chromatography[25] via the Craig model showed promising results, but the speed of pre-1960 computers made simulations for large values of N impractical. More recently, the Craig model has been used to simulate band shapes for HPLC systems that exhibit tailing[26]. Using an IBM XT computer, we have been able to extend this approach to separations under overload conditions, for reasonably large values of both N (2000) and k'(10). These data suggest a simplified model of overload separation that allows the fast prediction of elution curves for any values of N and k'.

---

* In later papers we will show that the present model for mass overloaded separation of single-component samples can be adapted to the case of samples containing more than one component. The latter approach makes use of the concept of "column blockage", where one solute is regarded as effectively saturating some fraction of the stationary phase, thereby reducing the stationary phase or column length available for sorption of the second solute.

The Craig model is deficient in that no band broadening is predicted for the case of $k_0 = 0$. While this result is physically unrealistic, bands eluted at $k' = 0$ are of minimal interest. For $k_0 > 0$ the value of n_c can be adjusted to match the desired value of N_0; in the second paper[21] we will see that Craig-derived values of N (large samples) correlate well with experimental data as a function of sample size. In the following discussion, values of N or N_0 correspond to plate number measurements as in Fig. 1; values of n_c from the Craig simulations are also noted, but are not considered to be significant, except as they define values of N_0 (eqn. 1).

Langmuir isotherm simulations
    Plate number N vs. sample mass. Initial simulations with the Craig model were carried out using classical Langmuir isotherms, which can be represented (Appendix I) as

$$1/w_{xs} = a + b/C_x \tag{2}$$

Here w_{xs} is the mass of solute in the stationary phase (g, for total column), and C_x is the concentration in the mobile phase (g/ml) at equilibrium. The constants a and b in eqn. 2 are given as

$$a = 1/w_s \tag{3}$$

and

$$b = 1/(V_m k_0) \tag{4}$$

The quantities k_0 and V_m refer, respectively, to the value of the capacity factor k' for small samples, and the column dead volume (equal to $[t_0 F]$; where F is the flow-rate). The saturation capacity w_s corresponds to the maximum solute uptake by the column when C_x is very large; it has also been referred to[27] as the "maximum loading capacity". A further discussion of the Langmuir isotherm is given in the following paper[21].

    Computer simulations based on the Craig model ("Craig simulations") were next carried out for a broad range of conditions. Values of the Craig stage-number n_c were varied from 50 to 1000, the capacity factor (small samples) k_0 was varied from 1 to 10, and sample size was varied from the linear-isotherm region to heavily-overloaded separations. Values of k' and N were determined for each run, and the ratios k'/k_0 and N/N_0 were used to assess the effect of column overload on the separation. These results are reported in Table I and summarized in the plots of Figs. 3 and 4 (n_c values of 50–1000; $k_0 = 1$, 3, and 10) as a function of w_x/w_s, the fractional loading of the column by sample. The quantity w_x is the mass of sample injected into the column; $w_s = 0.1$ g in these examples. Values of N_0 ranged from 53 to 1965. It is seen (Figs. 3 and 4) that the relative overloading of the column, as measured by values of k'/k_0 or N/N_0, can occur at quite different sample sizes (w_x/w_s), depending on k_0 and N_0.

    We next considered whether the data of Figs. 3 and 4 could be reduced to some simple relationships. The treatment of Poppe and Kraak[14] suggests for (a)

TABLE I

DATA FROM CRAIG SIMULATIONS OF OVERLOAD SEPARATION

Langmuir isotherms from eqns. 2–4 with $\psi = 100$ mg/ml, $w_s = 100$ mg, and $V_m = 1$.

n_c	N_0	k_0	w_x/w_s	w_{xk}	w_{xN}	k'/k_0		N/N_0	
						cum*	band*	cum*	band*
50	100	1	0.0001	0.0005	0.0025	1.00	1.00	1.00	1.00
			0.01	0.05	0.25	0.96	0.96	0.99	0.98
			0.03	0.15	0.75	0.90	0.88	0.95	0.93
			0.10	0.50	2.5	0.72	0.66	0.75	0.70
			0.30	1.5	7.5	0.46	0.32	0.43	0.36
			0.60	3.0	15	0.26	0.14	0.31	0.26
	65	3	0.001	0.006	0.036	1.00	1.00	1.00	1.00
			0.01	0.06	0.36	0.96	0.95	0.97	0.96
			0.03	0.18	0.11	0.88	0.85	0.87	0.82
			0.10	0.65	3.5	0.67	0.59	0.49	0.41
			0.20	1.2	7.3	0.51	0.38	0.27	0.20
			0.40	2.4	15.6	0.33	0.18	0.15	0.09
	53	10	0.0001	0.00066	0.0040	1.00	1.00	1.00	1.00
			0.003	0.02	0.13	0.99	0.99	0.99	0.99
			0.03	0.20	1.3	0.90	0.87	0.83	0.78
			0.06	0.4	2.6	0.78	0.71	0.55	0.47
			0.10	0.66	4.4	0.67	0.56	0.33	0.24
			0.20	1.3	8.8	0.49	0.33	0.14	0.07
			0.35	2.3	15	0.33	0.17	0.07	0.03
200	398	1	0.0005	0.005	0.050	1.00	1.00	1.00	1.00
			0.005	0.05	0.50	0.97	0.96	0.98	1.97
			0.02	0.20	2.0	0.88	0.84	0.80	0.77
			0.05	0.50	5.0	0.76	0.69	0.50	0.46
			0.10	1.5	15	0.56	0.43	0.22	0.19
	264	3	0.0002	0.0025	0.030	1.00	1.00	1.00	1.00
			0.005	0.061	0.74	0.96	0.95	0.94	0.93
			0.02	0.245	3.0	0.85	0.81	0.62	0.58
			0.05	0.61	7.4	0.73	0.65	0.30	0.25
			0.10	1.2	15	0.61	0.49	0.15	0.12
	216	10	0.0001	0.0013	0.018	1.00	1.00	1.00	1.00
			0.004	0.053	0.72	0.98	0.98	0.98	0.97
			0.01	0.13	1.8	0.94	0.94	0.86	0.83
			0.02	0.27	3.6	0.88	0.84	0.59	0.54
			0.03	0.40	5.4	0.83	0.77	0.40	0.35
			0.05	0.67	8.9	0.76	0.66	0.23	0.18
			0.08	1.1	14	0.67	0.54	0.13	0.09
			0.095	1.3	17	0.64	0.50	0.10	0.07
600	1193	1	0.0001	0.0017	0.030	1.00	1.00	1.00	1.00
			0.003	0.052	0.89	0.96	0.95	0.94	0.93
			0.01	0.17	3.0	0.90	0.87	0.67	0.65
			0.02	0.35	6.0	0.83	0.78	0.43	0.40
			0.03	0.52	8.9	0.79	0.72	0.31	0.29
			0.051	0.88	15	0.72	0.62	0.20	0.18

TABLE 1 (continued)

n_c	N_0	k_0	w_x/w_s	w_{xk}	w_{xN}	k'/k_0 cum*	k'/k_0 band*	N/N_0 cum*	N/N_0 band*
	790	3	0.0001	0.002	0.04	1.00	1.00	1.00	1.00
			0.001	0.021	0.44	0.99	0.98	0.98	0.97
			0.004	0.084	1.8	0.94	0.93	0.81	0.79
			0.01	0.21	4.5	0.89	0.85	0.49	0.46
			0.02	0.42	8.9	0.82	0.76	0.27	0.25
			0.034	0.72	15	0.76	0.68	0.16	0.14
	627	10	0.0001	0.0023	0.053	1.00	1.00	1.00	1.00
			0.01	0.23	5.3	0.91	0.88	0.52	0.49
			0.03	0.69	16	0.81	0.73	0.16	0.13
1000	1965	1	10-5	0.00022	0.0049	1.00	1.00	1.00	1.00
			0.005	0.11	2.5	0.93	0.92	0.73	0.72
			0.01	0.22	4.9	0.88	0.86	0.48	0.47
			0.02	0.44	9.9	0.82	0.77	0.28	0.26
			0.03	0.67	15	0.78	0.71	0.20	0.18
	1300	3	10-5	0.00003	0.0008	1.00	1.00	1.00	1.00
			0.0025	0.067	1.8	0.95	0.94	0.81	0.79
			0.005	0.14	3.6	0.92	0.90	0.56	0.55
			0.015	0.41	11	0.84	0.78	0.23	0.21

* Cum values calculated from cumulative elution curve as in Fig. 1b; band values from elution curve as in Fig. 1a.
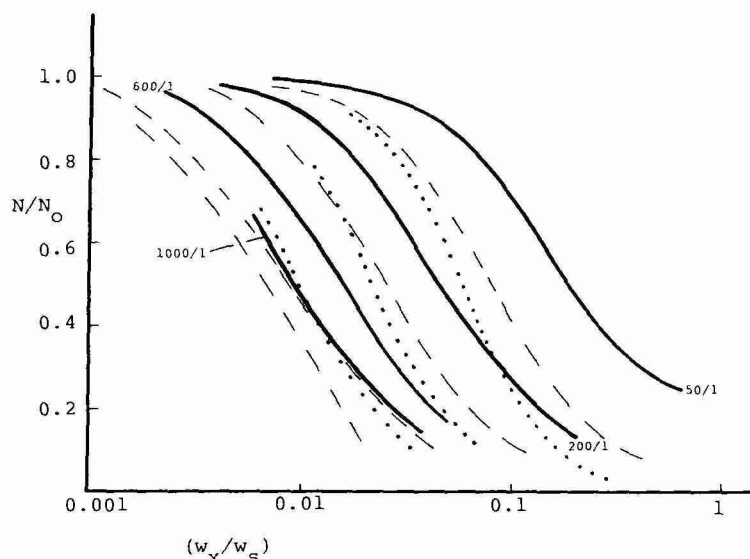
Fig. 3. Craig simulation data for plate number N as a function of sample size (w_x/w_s) and non-overload values of k' (k_0) and N (N_0). Numbers on curves, 100/1 indicates $N_0 = 100$ and $k_0 = 1$ (see Table 1 and text). Values of N_0 are "band" values, calculated as in Fig. 1a (not 1b). (– – –) $k_0 = 3$; (· · · ·) $k_0 = 10$.
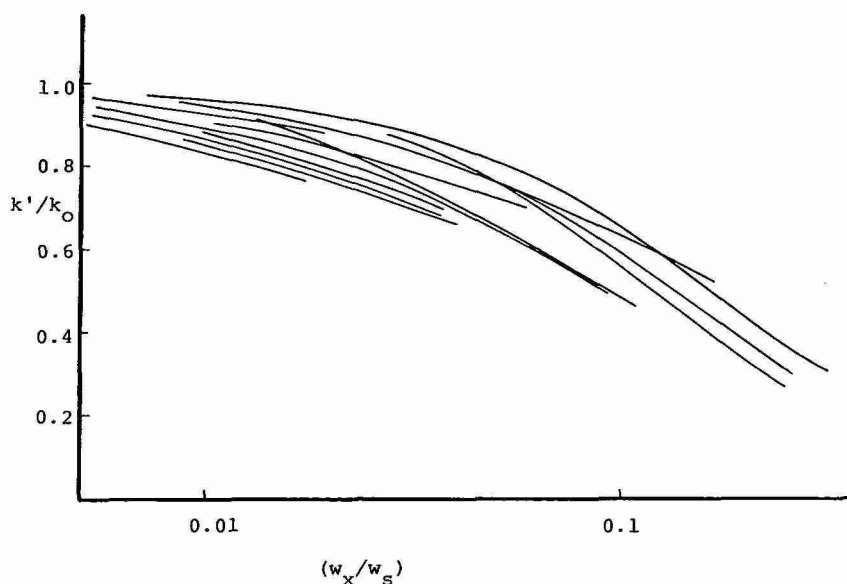
Fig. 4. Craig simulation data for capacity factor k' as a function of sample size (w_x/w_s) and non-overload values of k' (k_0) and N (N_0). See data of Table I. Values of k' are "band" values, calculated as in Fig. 1a (not 1b).

moderate overloading of the column, and (b) a Langmuir isotherm, that N/N_0 will be defined by some function of N_0, k_0, and w_x/w_s

$$N/N_0 = f\{N_0[k_0/(1+k_0)]^2 \, w_x/w_s\}$$

$$= f\{w_{xN}\}$$

(5)

Here we define $w_{xN} = N_0[k_0/(1+k_0)]^2 \, w_x/w_s$: w_{xN} is the "loading function" for N/N_0 as a function of sample size. The data of Fig. 3 are replotted against w_{xN} in Fig. 5; as expected from ref. 14, the values of N/N_0 now cluster about a single curve. That is, use of the loading function w_{xN} allows us to predict values of N/N_0 for any combination of values of N_0, k_0 and w_x/w_s, using the master curve (solid line) of Fig. 5. This master curve is the best fit to data for large N_0 (see below). Note that w_{xN} can be regarded as the mass of sample X contained in the stationary phase of the first Craig stage.

While the treatment of Poppe and Kraak[14] and eqn. 5 have been derived for the case of moderate column overloading, we will show that this relationship (eqn. 5) is reasonably accurate for samples large enough to effect a 90% reduction in values of N.

Capacity factor k' vs. sample mass. The effect of sample overload on k' is related to the average sample concentration in the stationary phase during migration of the band through the column. That is, the instantaneous value of k' during migration of the band through the column will vary (approaching k_0 as the sample becomes more dilute), depending on the mass of sample in a given plate (*i.e.*, sample
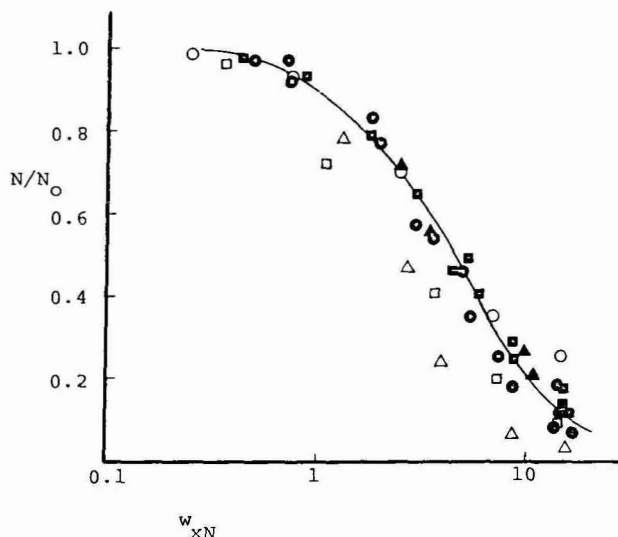
Fig. 5. Correlation of values of N/N_0 with column loading function w_{xN}.

n_c	k_0		
	1	*3*	*10*
50	○	□	△
200	●	●	●
600	■	■	■
1000	▲	▲	

Values of N are "band" values, calculated as in Fig. 1a (not 1b). The solid curve is drawn through data-points for $N_0 \geqslant 200$.

concentration at each point within the column). The resulting k' value at elution will then be (roughly) the average of k' values for the band maximum at every point along the column, which is in turn related to the average concentration of solute in the stationary phase (w_{xs}; *cf.* eqn. 4-1 of ref. 23). We can obtain an inferential relationship between the average k' value and experimental conditions (including sample size) as follows. The band-maximum concentration of sample in the stationary phase will be proportional to the fraction of total solute in the stationary phase, equal to $k'/(1+k')$. This solute concentration will also be inversely proportional to band width; *i.e.*, proportional to $N^{0.5}$. This suggests, by analogy with eqn. 5, that

$$k'/k_0 = f\{N_0^{0.5} [k_0/(1+k_0)] w_x/w_s\}$$

$$= f(w_{xk})$$

(6)

Here the loading function w_{xk} equals $[k_0/(1+k_0)] N_0^{0.5}$. Eqn. 6 suggests that column overload, as measured by values of k'/k_0, is determined by the value of the loading factor w_{xk}; *i.e.*, plots of k'/k_0 *vs.* w_{xk} should fall on a single curve for various values of k_0, N_0 or w_x/w_s. Fig. 6 replots the data of Fig. 4 as k'/k_0 *vs.* w_{xk}, and shows (as
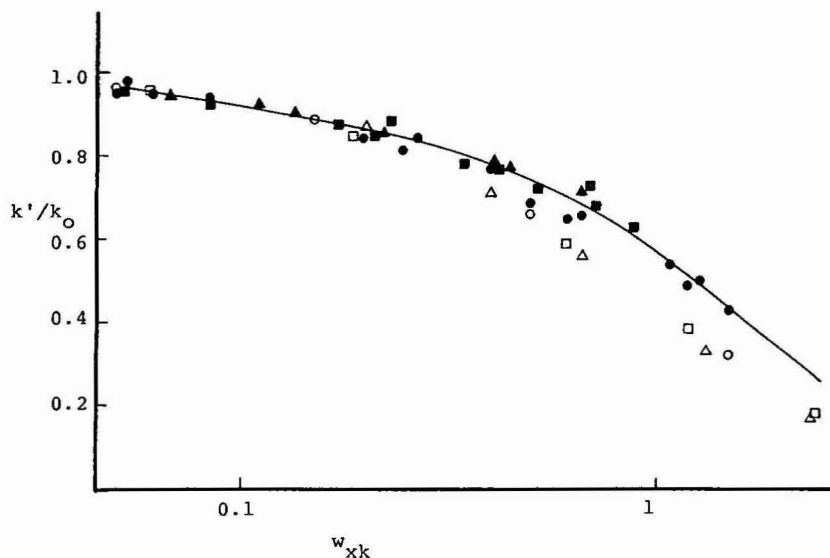
Fig. 6. Correlation of values of k'/k_0 with column loading function w_{xk}. Same symbols as in Fig. 5. Values of k' are "band" values, calculated as in Fig. 1a (not 1b). the solid curve is drawn through data points for $N_0 \geqslant 200$.

in Fig. 5) that all the data cluster about a single curve that can be used to predict k'/k_0 as a function of experimental conditions.

It appears that eqns. 5 and 6 become progressively more reliable for larger values of N_0, as summarized below:

Variable	x-axis scatter in plotted values		
	vs. w_x	vs. w_{xk}, w_{xN}	
		All data	$N_0 \geqslant 200$
N	40×	4×	1.2×
k'	4×	2×	1.3×

That is, for $N_0 \geqslant 200$, the scatter in the data is equivalent to an uncertainty of only 20–30% in sample size (or values of the loading factor)*. Values of N_0 in preparative HPLC will usually exceed 200; we have therefore drawn the curves of Figs. 5 and 6 through data points for $N_0 \geqslant 200$. The reduced accuracy of eqns. 5 and 6 for small N_0 ($n_c < 200$) is probably the result of increasing differences in Craig distribution vs. continuous chromatography as a stage or plate occupies a larger fraction of the total column.

For the case of systems following the Langmuir isotherm (eqn. 2), Figs. 5 and

---

* That is, when the solid curves of Figs. 5 or 6 are shifted horizontally by ca. 20–30%, they overlap most of the data points for $N_0 \geqslant 200$. This reflects the error in values of k'/k_0 or N/N_0 that are predicted from the solid curve.
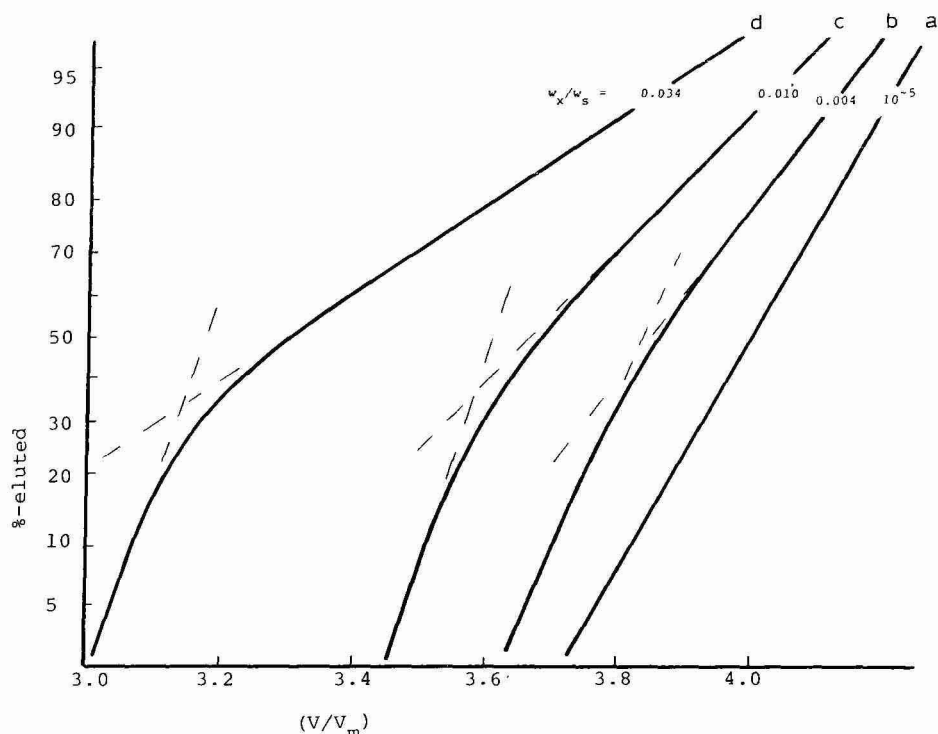
Fig. 7. Shape of cumulative elution band as a function of column overloading (see text). $n_c = 600$, $k_0 = 3$ (Table I).

6 suggest that we can predict k' and N in preparative HPLC as a function of k_0, N_0 and w_x/w_s. So far, we have only considered computer simulation (Craig model) data, but in the following paper we will see that this is true for experimental data as well. Thus, we can determine k_0 and N_0 from an initial analytical-scale run, and values of w_s can then be determined in various ways, as described in the following paper[21].

Band shape vs. sample size. We desire to predict the cumulative elution curve (as in Fig. 1b) as a function of sample size and other experimental conditions. This curve is related to values of k' and N, which can be predicted as above for overload separations. However, band shape also changes with overload, and we must take this into account. We have found that various measures of band shape (*e.g.*, band asymmetry) correlate well with the loading function w_{xN}, suggesting a simple approach for predicting band shape as a function of sample size (Appendix II).

Fig. 7 shows some representative examples of cumulative-elution curves* for varying sample size, taken from a series of Craig simulations where only sample size was varied. Curve a shows a non-overloaded run, with the data falling on a single straight line. This is expected for a Gaussian band, when plotted on "probability

---

* These plots of Fig. 7 are on "probability paper". The y-axis is labeled "cumulative %", but is linear in units of σ (standard deviation) of the Gaussian curve. Thus, 50% corresponds to $\sigma = 0$, 16% to $\sigma = -1$, 84% to $\sigma = +1$, etc. Any "true" Gaussian distribution will therefore plot as a straight line on probability paper.
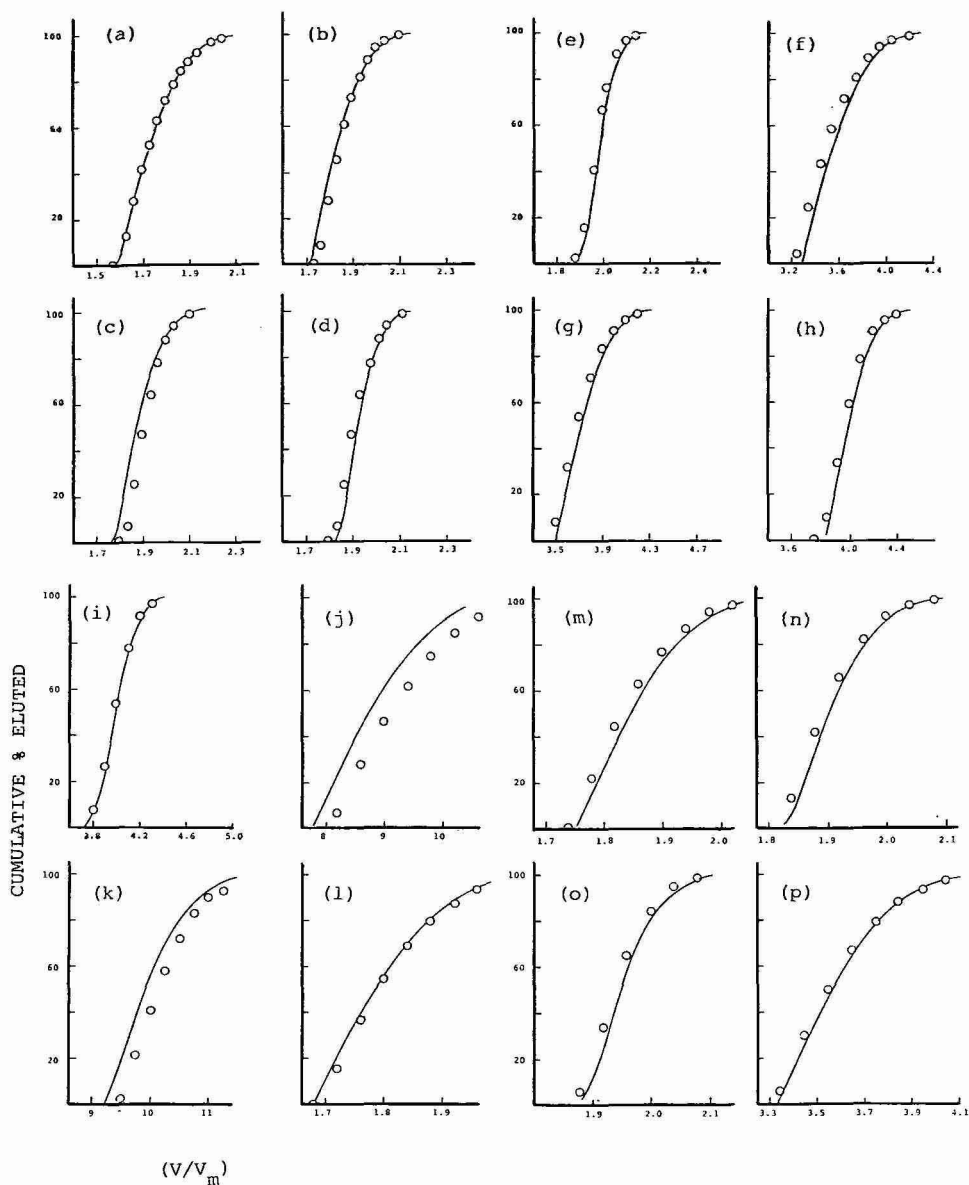
Fig. 8. Prediction of elution curves (Craig simulation, Langmuir isotherm, data of Table I) based on relationships of Table II (cumulative values) and procedure of Appendix I (see text). ○, Craig simulations; ——, model simulations.

Curve	n_c	k_0	w_x/w_s	Curve	n_c	k_0	w_x/w_s
a	600	1	0.051	j	600	10	0.030
b			0.030	k			0.010
c			0.020	l	1000	1	0.030
d			0.010	m			0.020
e			0.003	n			0.010
f		3	0.020	o			0.005
g			0.010	p		3	0.015
h			0.004				
i			0.001				

paper". Curves b-d show that, as overloading of the column increases, there is increasing deviation of the cumulative elution curve from a Gaussian distribution.

Cumulative elution curves as in Fig. 7 characteristically exhibit two distinct parts, where the initial part of the elution curve follows a steeper, roughly linear plot and the final part of the curve follows a shallower, roughly linear plot. That is, such elution curves appear to be a composite of parts from two separate Gaussian curves: one describing the first part of the elution band, and one describing the last part. The slopes and points of intersection of these two straight-line curves correlate well with the loading function w_{xN}, over a broad range of choices of k_0, N_0 and w_x/w_s. That is, the overall shape of the elution band appears to be defined by the value of w_{xN}.

It is possible to generalize these observations relating to Fig. 7, and to predict the shape of the elution band as a function of experimental conditions (k_0, N_0, w_x and w_s). These relationships are summarized in Appendix II. Combining these equations with the correlations of Figs. 5 and 6 then allows prediction by computer of the entire elution curve (Craig model, Langmuir isotherm) for any experimental conditions (any values of k_0, N_0, w_x and w_s), but without repeating an actual Craig simulation. We will refer to such simplified calculations as "model simulations". Several examples of model simulations are compared with Craig simulations in Fig. 8, with good agreement between the two simulations. The advantages of bypassing the actual Craig simulations include:

(1) Craig simulations for N_0 values > 1000 require a prohibitive amount of

TABLE II

BEST-FIT VALUES OF N/N_0 AND k'/k_0 *vs.* THE VARIOUS LOADING FUNCTIONS

Data from Figs. 5 and 6 and Table I

w_{xN} or w_{xk}	N/N_0 Cum[*]	k'/k_0	
		Band	*Cum*[**]
0.01	1.00	1.00	1.00
0.02	1.00	0.99	0.99
0.05	1.00	0.97	0.97
0.10	1.00	0.93	0.95
0.20	1.00	0.86	0.90
0.50	0.98	0.74	0.81
1.0	0.93	0.57	0.70
2.0	0.80	0.33	0.45
5.0	0.48		0.18
10	0.26		0.07
20	0.14		
50	0.06		
100	0.03		

[*] Data can be fit by the following polynomial in $x = \log w_{xN}$, within the limits of $0.5 < w_{xN} < 20$: $N/N_0 = 0.9308 - 0.2779 x - 0.5098 x^2 - 0.3252 x^3 + 0.3127 x^4 + 0.3275 x^5 - 0.1434 x^6 - 0.0946 x^7 + 0.0394 x^8$.

[**] Data can be fit by the following polynomial in $x = \log w_{xk}$, within the limits of $0.02 < w_{xk} < 5$: $0.6857 - 0.6427 x - 0.6453 x^2 + 0.1303 x^3 + 0.8568 x^4 + 0.3653 x^5 - 0.3270 x^6 - 0.2867 x^7 - 0.0591 x^8$.

time for small computers (*e.g.*, the **IBM XT**); model simulations (Appendix II) require less than 1 min per run for any value of N_0.

(2) The value of N_0 for each solute in a model simulation can be assigned, whereas these values are fixed in Craig simulations according to eqn. 1.

(3) The generalized correlations of Figs. 5, 6 and Appendix II allow better insight into the effects of different variables on preparative separation; we will show this in later papers.

Table II summarizes values of N/N_0 vs. w_{xN} and k'/k_0 vs. w_{xk} (solid curves of Figs. 5 and 6) for use in model simulations, as described in Appendix II.

DISCUSSION AND CONCLUSIONS

Considerable simplification has been achieved so far in describing how an elution band changes with column overload. For the case of Langmuir-isotherm Craig-simulation runs, we have shown that the resulting changes in the elution curve can be predicted from a knowledge of (a) the elution band under non-overload conditions (values of k_0 and N_0) and (b) sample size in relation to column saturation capacity (w_x/w_s). The comparisons in Fig. 8 show our ability to predict the final elution band (as obtained by Craig simulation), using the much faster "model simulations". The expanded scale of the x axis of Fig. 8 should be noted, as it exaggerates errors in predicted data points.

Previous workers[8,26] have noted that columns can be overloaded with respect to plate number N, while the capacity factor k' remains unchanged. This becomes more noticeable with decrease in size of the column packing particles[8,12]. The present analysis confirms (as noted in ref. 12) that particle size *per se* is not the critical factor in these obervations; rather it is the actual value of N under non-overload conditions (N is usually larger for small-particle columns).

We can calculate the value of (w_x/w_s) equal to the fractional saturation of column capacity required to reduce both N and k' by some arbitrary amount (*e.g.*, 20%), as a function of N_0 (value of N for non-overload separation). These results are shown in Table III. Also shown are approximate weights for a typical preparative

TABLE III

SAMPLE SIZE REQUIRED TO REDUCE k' or N BY 20% (*VS.* VALUES OF k_0 AND N_0 — NON-OVERLOAD SEPARATION)

$k_0 = 3$. Data of Figs. 5 and 6.

N_0	w_x/w_s for 20% reduction in k'	w_x/w_s for 20% reduction in N	mg sample*	
			k'	N
100	0.07	0.04	730	420
300	0.04	0.01	450	105
1000	0.02	0.004	210	42
10 000	0.007	0.0004	70	4
100 000	0.002	0.00004	21	0.4

* For 20% reduction in k' or N; assumes 10.5 g for w_s; *e.g.*, 25 × 2.1 cm column, 300 m²/g surface area.

column (25×2.1 cm, $w_s \approx 10.5$ g). For small-N columns ($N < 1000$) we see that both k' and N will decrease when the sample size exceeds some maximum value. However, for more efficient columns ($N \geqslant 10\,000$), larger samples will result in a decrease in N long before any change in k' is apparent (*cf.* also Figs. 3 and 4).

APPENDIX I

Derivation of Langmuir isotherm
       The Langmuir isotherm assumes an adsorbed monolayer for the stationary phase, with one molecule of solute (X) replacing one adsorbed molecule of mobile phase (M) during retention of the solute. This leads to the general equation (*e.g.*, 23)

$$\theta_x = K N_x/(1 + K N_x) \tag{A1}$$

where θ_x is the mole fraction of solute in the adsorbed monolayer and N_x is the mole fraction of X in the mobile phase; K_x is the thermodynamic distribution coefficient for X. Eqn. A1 assumes that $N_x \ll 1$. If we further assume that the density and molecular weight of molecules of M and X are the same for each compound, then

$$\theta_x = w_{xs}/w_s \tag{A2}$$

and

$$N_x = w_{xm}/V_m = C_x \text{ (g/ml)} \tag{A3}$$

Here w_{xs} and w_{xm} are the weights of X in the stationary and mobile phases, respectively, w_s is the weight of an adsorbed monolayer of X, V_m is the volume of mobile phase within the column (column dead-volume), and C_x is the concentration of X in the mobile phase (g/ml).
       Eqns. A1–A3 combine to give

$$1/w_{xs} = 1/w_s + (1/w_s) [1/(K C_x)] \tag{A4}$$

For small values of θ_x and N_x, we have (eqns. A1–A3).

$$K = (w_{xs}/w_s) (1/C_x) \tag{A5}$$

and

$$k_0 = w_{xs}/(V_m C_x) \tag{A6}$$

We can define the phase ratio

$$\psi = w_s/V_m \tag{A7}$$

and eqns. A5 and A6 then give

$$K = k_0/\psi \tag{A8}$$

Now eqns. A4 and A8 yield

$$1/w_{xs} = 1/w_s + [1/V_m k_0)] (1/C_x)$$

$$= a \quad + b \qquad (1/C_x) \qquad\qquad (A9)$$

The parameters a and b are fixed for a given HPLC system, with

$$a = 1/w_s \qquad\qquad (A10)$$

and

$$b = 1/V_m k_0 \qquad\qquad (A11)$$

The units for the various quantities above may appear confusing, until it is recalled that our derivation assumes that the densities of solute and mobile phase are the same. Therefore concentration C_x (g/ml) is equivalent to (g/g). See the Glossary of symbols for preferred units for each quantity.
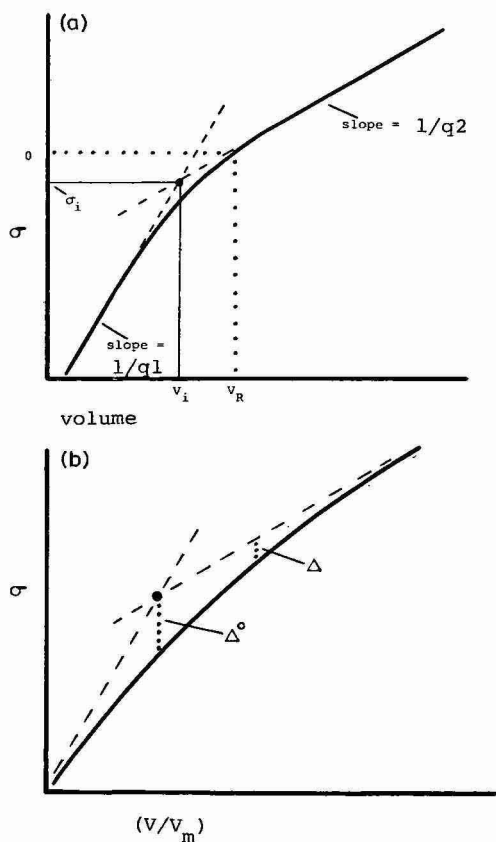
Fig. A1. Illustration of cumulative elution curve under overload conditions and empirical parameters used to predict the elution curve (cf. Fig. 7 and Appendix II). (a) Full elution curve; (b) magnified portion of (a).

APPENDIX II

Empirical description of overload elution curves

The characteristic cumulative elution curves of Fig. 7 can be represented generally by the diagram of Fig. A1. The two linear parts of the elution curve are shown, along with the volume corresponding to intersection of the two linear curves (V_i), the corresponding Gaussian standard deviation σ_i, and the retention volume V_R (either "band" or "cumulative"). The slopes of the two curves as measured from $\sigma = 0$ to $\sigma = -1$ and $+1$ are defined as $1/q_1$ and $1/q_2$, respectively. In each case, the slopes are equal to $d\sigma/dV_R$, where V_R is elution volume. We can regard the total elution curve as the sum of two separate elution curves; one with a larger N-value and smaller bandwidth (q_1, volume units/σ), and the other with a smaller N value and a larger bandwidth (q_2).

Fig. A1b shows an expanded view of Fig. A1a; here we further define the deviation of the actual (solid) elution curve from the dashed linear curves by the quantity Δ, and likewise the maximum value of Δ at V_i can be defined: Δ^0.

We have studied the dependence of each of the parameters of Fig. A1 (Δ, q_1, q_2, etc.) on separation conditions (runs of Table I), and found that these parameters can be empirically correlated with known properties of the system as follows:

$$\sigma_i = 0.14 \, w_{xN}^{0.55} \tag{A12}$$

$$q_2/q_1 = 1 + 0.72 \, w_{xN}^{0.70} \tag{A13}$$

$$\Delta^0 = 0.16 \, w_{xN}/(1 + 0.4 \, w_{xN}) \tag{A14}$$

$$\Delta = \Delta^0 \, 10^{-1.2(\sigma - \sigma_i)} \tag{A15}$$

The average band width (σ_v, volume units) can be calculated from the plate number N (assumes a Gaussian):

$$\sigma_v = V_R \, N^{0.5} \tag{A16}$$

The inverse slopes of the linear plots in Fig. A1 are equal to q_1 and q_2, respectively. Since values of N are measured from bandwidth as defined for ± 1 standard deviation around the 50% elution point (cumulative values), we then have

$$2 \, \sigma_v = (1 - \sigma_i)q_1 + (1 + \sigma_i)q_2 \tag{A17}$$

Values of q_1 and q_2 are then obtainable from eqns. A16 and A17 and previously determined values of N and (q_2/q_1).

Knowing the value of V_R at $\sigma = 0$ from the w_{xk} function and knowing the slope, $1/q_2$, the retention volumes at points greater than $\sigma = 0$ are calculated. The volume corresponding to σ_i is calculated from $V_i = V_R$ (at $\sigma = 0$) $+ \sigma_i q_2$. Volumes at smaller σ are calculated using the slope q_1. The two resulting straight lines are then curved by subtracting the corresponding value from each σ.

Once the elution curve is calculated, the value of V_R is checked against the original value determined from k':

$$V_R = V_m (1 + k')$$ (A18)

Generally the calculational procedure will have introduced a small shift in the curve along the x-axis, so that the final value of V_R is slightly in error. The final step is then to shift the elution curve to correct for this effect and generate a final curve with a value of V_R that matches that calculated from the input value of k' (eqn. A18).

GLOSSARY OF SYMBOLS

For both this and the following papers; I- or II- is used for reference to specific equations; thus, I-6 refers to eqn. 6 of Part I)

a	constant in eqn. I-2; equal to $1/w_s$ (g^{-1})
a_1, a_2	value of a for sites of Type 1 or 2; eqns. II-3 and 4
A_s	band asymmetry factor[3]
b	constant in eqn. I-2 (ml^{-1}); equal to $1/(V_m k_0)$
b_1, b_2	value of b for sites of Type 1 or 2; eqns. II-3 and 4
"band"	refers to values of k' or N measured as in Fig. I-1a
Craig simulation	refers to predictions of k', N or band shape by carrying out computer simulations based on Craig distribution
C_x	solute concentration in the mobile phase (mg/ml)
"cumulative"	refers to values of k' or N measured as in Fig. I-1b
f( )	a function of ( )
k'	capacity factor[3]; "band" values of k' measured as in Fig. I-1a; "cumulative" values measured as in Fig. I-1b
k_0	value of k' for a small solute mass; constant as solute size is varied within a certain range
K	thermodynamic distribution constant for retention of solute; eqn. I-A1
L	column length (cm)
M	a molecule of mobile phase; eqn. II-1
model simulation	refers to prediction of k', N or band shape using the simplified model of Appendix II
n	stoichiometry factor for retention process; eqn. II-2
n_c	number of stages in a Craig simulation; eqn. I-1
N	column plate number[3]; "band" values of N, measured as in Fig. I-1a; "cumulative" values measured as in Fig. I-1b
N_x	mole fraction of solute in the mobile phase; eqn. I-A3
N_0	value of N for a small solute mass; constant within a certain range of sample size
SA	surface area (m^2/g) of column
V_m	column dead-volume (ml) (ref. 3)
V_s	column saturation capacity, measured as solute volume; eqn. II-6
V_R	retention volume (ml), measured as "cumulative" value
w_s	column saturation capacity (mg); maximum column loading at large values of C_x

w'_{xk}	loading function for a given capacity factor as a function of sample size and conditions; equal to $N_0^{0.5}$ $[k_0/(1+k_0)]$ (w_x/w_s)
w'_{xm}	mass of solute in the mobile phase (mg)
w'_{xN}	loading function for a given plate number as a function of sample size and conditions; equal to $N_0[k_0/(1+k_0)]^2$ (w_x/w_s)
w_x	total mass of solute injected into the column (mg)
w_{xs}	mass of solute in the stationary phase (mg); eqn. I-2
w_1, w_2	value of w_{xs} for sites of Type 1 of 2; eqn. II-3
X	a molecule of solute; eqn. II-1
θ_x	mole fraction of solute in the stationary phase; eqn. I-A1
Δ, Δ^0	quantities defined in Fig. I-9b
σ	one standard deviation of a Gaussian-shaped band
σ_i	defined from the intersection of two lines as in Fig. I-9a
σ_v	one standard deviation of a Gaussian-shaped band; measured in ml in Appendix I-II
q_1, q_2	reciprocal slopes of initial and final plot, as in Fig. I-9a; values of σ for the two parts of the band
ψ	phase ratio (mg/ml); eqn. I-A7

REFERENCES

1 A. M. Cantwell, R. Calderone and M. Sienko, *J. Chromatogr.*, 316 (1984) 133.
2 H. Colin, G. Lowy and J. Cazes, *Am. Lab.*, 17 (1985) 139.
3 L. R. Snyder and J. J. Kirkland, *Introduction to Modern Liquid Chromatography*, Wiley-Interscience, New York, 2nd ed., 1979, Ch. 15.
4 G. Houghton, *J. Phys. Chem.*, 67 (1963) 84.
5 P. C. Haarhoff and H. J. van der Linde, *Anal. Chem.*, 38 (1966) 573.
6 J. J. De Stefano and H. C. Beachell, *J. Chromatogr. Sci.*, 10 (1972) 654.
7 K. J. Bombaugh and P. W. Almquist, *Chromatographia*, 8 (1975) 109.
8 J. N. Done, *J. Chromatogr.*, 125 (1976) 43.
9 A. Wehrli, U. Hermann and J. F. K. Huber, *J. Chromatogr.*, 125 (1976) 59.
10 H. Brusset, D. Depeyre and J. P. Pewtit, *Chromatographia*, 11 (1978) 287.
11 P. Gareil, L. Personnaz, J. P. Feraud and M. Caude, *J. Chromatogr.*, 192 (1980) 53.
12 A. W. J. de Jong, H. Poppe and J. C. Kraak, *J. Chromatogr.*, 209 (1981) 432.
13 B. Coq, G. Cretier and J. L. Rocca, *Anal. Chem.*, 54 (1982) 2271.
14 H. Poppe and J. C. Kraak, *J. Chromatogr.*, 255 (1983) 395.
15 P. Gareil, C. Durieux and R. Rosset, *Sep. Sci. Technol.*, 18 (1983) 441.
16 G. Cretier and J. L. Rocca, *Chromatographia*, 18 (1984) 623.
17 G. Cretier and J. L. Rocca, *Chromatographia*, 20 (1985) 461.
18 A. Jaulmes, C. Vidal-Madjar, H. Colin and G. Guiochon, presented at the *8th International Symposium on Column Liquid Chromatography, New York, May 20–25, 1984*.
19 J. Frenz and Cs. Horváth, *AIChE J.*, 31 (1985) 400.
20 M. Verzele and C. Dewaele, *LC Liq. Chromatogr. HPLC Mag.*, 3 (1985) 22.
21 J. E. Eble, P. E. Antle, R. L. Grob and L. R. Snyder, *J. Chromatogr.*, 384 (1986) 45.
22 B. L. Karger, L. R. Snyder and Cs. Horváth, *An Introduction to Separation Science*, Wiley-Interscience, New York, 2nd ed., 1979, pp. 110–116.
23 L. R. Snyder, *Principles of Adsorption Chromatography*, Marcel Dekker, New York, 1968, pp. 55–58.
24 A. Jaulmes, C. Vidal-Madjar, A. Ladurelli and G. Guiochon, *J. Phys. Chem.*, 88 (1984) 5378.
25 L. R. Snyder, in C. N. Reilley (Editor), *Advances in Analytical Chemistry and Instrumentation*, Vol. 3, Wiley-Interscience, New Yorki, 1964, p. 251 (see Fig. 14, p. 295).
26 S. Seshadri and S. N. Deming, *Anal. Chem.*, 56 (1984) 1567.
27 P. Gareil, L. Semerdjian, M. Caude and R. Rosset, *J. High Resolut. Chromatogr. Chromatogr. Commun.*, 7 (1984) 123.

SIMPLIFIED DESCRIPTION OF HIGH-PERFORMANCE LIQUID CHROMATOGRAPHIC SEPARATION UNDER OVERLOAD CONDITIONS, BASED ON THE CRAIG DISTRIBUTION MODEL

II. EFFECT OF ISOTHERM TYPE, AND EXPERIMENTAL VERIFICATION OF COMPUTER SIMULATIONS FOR A SINGLE BAND

J. E. EBLE and R. L. GROB

Chemistry Department, Villanova University, Villanova, PA 19085 (U.S.A.)

P. E. ANTLE

Biomedical Products Department, E. I. Du Pont de Nemours & Co., Concord Plaza, Wilmington, DE 19898 (U.S.A.)

and

L. R. SNŸDER*

LC Resources, Inc., 26 Silverwood Court, Orinda, CA 94563 (U.S.A.)

SUMMARY

The preparative high-performance liquid chromatography (HPLC) model described in the preceding paper has been tested for nine different solute–column combinations under reversed-phase overload conditions. Following certain empirical adjustments of the model, good agreement between experimental and predicted elution curves was observed. One such adjustment relates to the value of the column saturation capacity w_s. This value can be obtained either from isotherm data or from separations under overload conditions. In some cases these two w_s values agree, but in other cases they differ by factors of almost 100. The latter situation appears due to strong retention of solute molecules on silanol sites, rather than on the non-polar bonded phase. Use of chromatographically derived values of w_s leads to accurate predictions of the elution band as a function of sample size.

Minor adjustments were also required in the shapes of the k'/k_0 vs. w_{xk} and N/N_0 vs. w_{xN} plots predicted by Craig simulations. Finally, it was found that in every case "real" columns are more quickly overloaded with respect to N than is predicted by Craig simulation. The value of w_s that can be inferred from k' overloading must be decreased by a factor of about 2.5 to account for the dependence of N on sample size. With these modifications of the model, it appears possible to accurately predict the elution curves for most HPLC systems as a function of sample size.

INTRODUCTION

In the preceding paper[1] a simple approach for understanding high-perform-

ance liquid chromatographic (HPLC) separations under overload conditions was described. That study began with Craig simulations of HPLC separations as a function of (a) sample size w_x, (b) the maximum ("saturation") capacity of the column for sample w_s, and (c) the plate number N_0 and capacity factor k_0 measured for a small sample. It was then shown that the concentration-time profile of a single elution band (from Craig simulations) can be predicted as a function of w_x/w_s, k_0 and N_0, using a simplified (faster) computer simulation. The latter was referred to as a "model simulation", in contrast to the original approach ("Craig simulation"). These Craig simulations and derived correlations for the model simulations are so far based on Langmuir isotherms.

"Real" HPLC systems do not often meet all the requirements of Langmuir-isotherm sorption. It is therefore of interest to examine how our model will be affected in practice by such deviations from "ideal" behavior. The present paper addresses this question. We also report experimental data that verify our model for HPLC systems that involve the overload separation of a single solute. The present studies provide a basis for the corresponding interpretation and prediction of separations involving two or more co-eluting solutes. We will report on this in following papers.

THEORY

Non-Langmuir isotherms

The Langmuir isotherm is a good starting point for an understanding of the general characteristics of HPLC separation under overload conditions. Many experimental systems appear to exhibit Langmuir sorption, and most HPLC separations show a decrease in retention and plate number plus increase in band-tailing with increasing sample size, as predicted by the Langmuir isotherm. However in most cases the Langmuir isotherm is only an approximation of actual sorption data. Three separate effects can contribute to non-Langmuir behavior:

(i) Heterogeneity of the sorption surface and/or "localization" effects, such that the sorption of solute at low surface coverages is more favorable than at high coverages; a simple case is a two-site stationary phase, where sample molecules are retained strongly by one kind of site and weakly by the other;

(ii) non-unity stoichiometry of the retention process; the Langmuir isotherm assumes a one-to-one displacement process of the form

$$X_m + M_s \rightleftharpoons X_s + M_m \tag{1}$$

for a solute molecule X and mobile phase molecule M, in stationary (s) or mobile (m) phases. However, a more general possibility is

$$X_m + nM_s \rightleftharpoons X_s + nM_m \tag{2}$$

where $n > 1$. This might correspond to the displacement of n small molecules of mobile phase by a single large solute molecule;

(iii) solute–solute interactions that alter the free energy of sorption for high solute concentrations in the mobile or stationary phase.

A discussion of these effects for the case of liquid–solid (adsorption) chro-

matography is given in refs. 2–4. For the general case, a complete theoretical description of real isotherms will be quite complex; such a treatment is not readily adaptable to practical application in preparative separations. Here, we will examine certain general features of non-Langmuir adsorption with reference to our model for overload HPLC. We will see that many non-Langmuir systems yield isotherms that closely resemble the Langmuir isotherm over a certain range of solute concentrations. This means that our present model[1] can still provide a good description of the resulting elution band.

Heterogeneous stationary phases and solute localization

These effects have been discussed by several workers[2-6] for silica or alumina as adsorbents (liquid–solid chromatography). Stationary phase heterogeneity refers to the presence on the adsorbent surface of different kinds of adsorption sites or sites of differing energy. As a result, solute molecules will adsorb onto the stronger sites first, before filling the weaker sites. Solute localization refers to the attachment of solute molecules to specific sites, so that the solute occupies a narrowly defined position on the adsorbent surface. When a certain fraction of the surface is covered by adsorbed (and localized) solute molecules, further filling of the adsorbed monolayer is energetically less favorable. Either access to the surface is restricted by steric crowding of already adsorbed molecules, or proper positioning of the adsorbate for localized adsorption becomes impossible. These two effects, site heterogeneity and solute localization, have often been confused or lumped together.

Site heterogeneity. Consider the simplest such case, an adsorbent with sites of two different kinds. This frequently arises in the reversed-phase HPLC of polar or ionic solutes, which can interact either with the non-polar bonded phase or with unreacted silanol groups. We can describe the resulting isotherm as the sum of two separate isotherms, one for each set of sites. Let the column capacity w_s for adsorption onto sites of the first kind (i) be w_{s1}, and let the column capacity for the second set of sites (2) be w_{s2}. Similarly, let the solute mass w_{xs} in the stationary phase be w_1 for sites of the first type, and w_2 for sites of the second type. Let the value of k_0 for the first group of sites be k_1, and for the second group k_2. From eqn. 2 of the preceding paper[1] we know that the equilibrium uptake of solute (w_1 or w_2) by the adsorbent is equal to

$$\text{(sites 1)} \quad 1/w_1 = a_1 + b_1/C_x \tag{3}$$

and

$$\text{(sites 2)} \quad 1/w_2 = a_2 + b_2/C_x \tag{4}$$

The quantities a_1 and a_2 are equal to $1/w_{s1}$ and $1/w_{s2}$, respectively. Similarly, b_1 and b_2 are equal to $1/(V_m k_1)$ and $1/(V_m k_2)$, respectively. The combined uptake of solute by the column is

$$w_{xs} = w_1 + w_2 \tag{5}$$

Consequently we can calculate the composite isotherm from a knowledge of the individual isotherms.
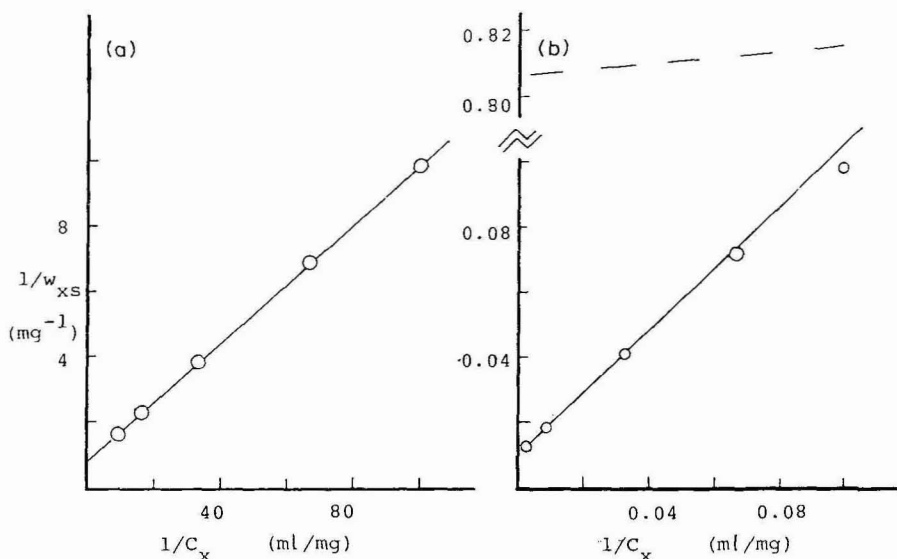
Fig. 1. Calculated isotherm for a two-site surface (site heterogeneity). w_{s1} = 1 mg, w_{s2} = 100 mg, $V_m k_1$ = 10, $V_m k_2$ = 1. (a) Data for low values of C_x; (b) data for high values of C_x.

When the values of k_0 for the two kinds of sites (k_1 and k_2) are sufficiently different, plots of $1/w_{xs}$ vs. $1/C_x$ become bimodal, each part corresponding roughly to the isotherm for a given set of sites. This is illustrated in Fig. 1, for a hypothetical case that is representative of many real HPLC systems: sites 1 are quite strong, but present in small concentration; sites 2 are much weaker, but constitute most of the available sites*. In Fig. 1a the isotherm is shown for $0.01 < C_x < 0.10$ mg/ml (or $100 > (1/C_x) > 10$ ml/mg), plotted as $1/w_{xs}$ vs. $1/C_x$ (which will linearize a Langmuir isotherm; *cf.* eqn. 2 of ref. 1). It is seen that this plot (based on calculated isotherm data) is indistinguishable from a Langmuir isotherm.

If a different range of mobile-phase concentrations is examined ($10 < C_x < 300$ mg/ml, or $0.1 > 1/C_x > 0.003$), as in Fig. 1b, the plot of $1/w_{xs}$ vs. $1/C_x$ is again linear, but with a different slope (the dashed curve in Fig. 1b corresponds to the solid curve in Fig. 1a). Note that the plot of Fig. 1a can be extrapolated to a value of w_s ≈ 1 mg**, while the plot of Fig. 1b gives a value of w_s ≈ 100 mg. That is, the plot of Fig. 1a is determined mainly by the lower-concentration, stronger sites (w_s = 1), while the plot of Fig. 1b reflects mainly the higher-concentration, weaker sites (w_s = 100). We will see that it is the stronger sites and smaller values of C_x that mainly determine chromatographic behavior during column overload.

Thus, within a certain range of solute concentration C_x, the system of Fig. 1 closely resembles a Langmuir isotherm. This has practical consequences for the effects of site heterogeneity on HPLC separations in the overload mode. In reversed-

---

* w_{s1} = 1 mg, k_1 = 10, w_{s2} = 100 mg, k_2 = 1, V_m = 1 ml.
** The y axis intercepts in Fig. 1 give the maximum column capacity ($1/w_s$); *e.g.*, w_s = 1.2 mg in Fig. 1a (*cf.* eqns. 3 and 4).

phase HPLC, silanol sites are usually present in small concentrations (for fully bond-ed packings), and their interaction with solute molecules can be much stronger than in the case of solvophobic interactions. In these cases, Langmuir retention may ap-pear to be observed, as in Fig. 1a. However, the apparent column capacity w_s (ex-trapolated value from Fig. 1a), will then be much smaller than the maximum column capacity.

Localized adsorption. A detailed discussion of this phenomenon as it affects the adsorption isotherm is given in ref. 4 (where it is referred to as "restricted-access solvent delocalization"). While that discussion is specifically for the case of two-component mobile phases, the basic arguments are similar both for that case and for the case of solutions of a solute in a mobile phase (which are of interest here). When the adsorbent surface is covered with a high concentration of equivalent strong sites that occupy fixed positions on the adsorbent surface (*e.g.*, silanols on silica), and the adsorbate (solute) prefers to attach itself (localize) to these sites, all adsorbed solute molecules will be localized for lower coverages of the surface (values of θ_x). However, when θ_x exceeds about 0.7, the remaining surface is not favorable for localization, and further adsorption of solute will occur without localization. This means that the apparent retention (value of k' for delocalized molecules) will be much weaker than for localized solute molecules. The net effect is similar to that for a two-site surface (site heterogeneity as above). Thus, Langmuir plots ($1/w_{xs}$ *vs.* $1/C_x$) are found to be bimodal[3], just as in Fig. 1b for the case of a heterogeneous surface.

The theory developed[2-4] appears to give reliable predictions of the adsorption isotherm for cases involving both localizing and non-localizing solutes[4]. Elsewhere, we will explore its application to an understanding of the adsorption isotherm for silica and other polar adsorbents. Here, we are concerned mainly with overload sep-aration in reversed-phase HPLC, and for these systems localized adsorption effects are generally unimportant. That is, reversed-phase packings do not normally have a high concentration of accessible strong sites (silanols). The Langmuir isotherm is actually a useful approximation for both cases, within a certain range of sample concentrations. This means that our model[1] for HPLC in the overload mode will be applicable over the same range of solute concentrations C_x.

A final comment can be made concerning site heterogeneity in reversed-phase HPLC *vs.* solute localization in normal-phase separations. In each case, the apparent value of w_s inferred from lower sample concentrations will be less than the maximum saturation capacity of the column. However, solute localization typically involves *ca.* 3/4 of the surface, so that the apparent w_s value at low values of C_x will then be *ca.* 3/4 of the maximum value. We will see in a following section that site heterogeneity in reversed-phase HPLC involves much smaller values of w_s for the low C_x part of the isotherm. Thus, the practical consequences (lower effective column loadability) are much more serious in the case of reversed-phase systems.

Non-unity stoichiometry of the sorption process

Extensive data, reviewed in refs. 2 and 4), show for adsorption chromato-graphy with alumina or silica as column packing that large solute molecules displace more than one solvent molecule during retention of the solute. That is, eqn. 2 applies, n being determined by the molecular sizes of the solute X and mobile phase M mole-cules. Other studies[7,8] suggest that retention in reversed-phase HPLC is also governed
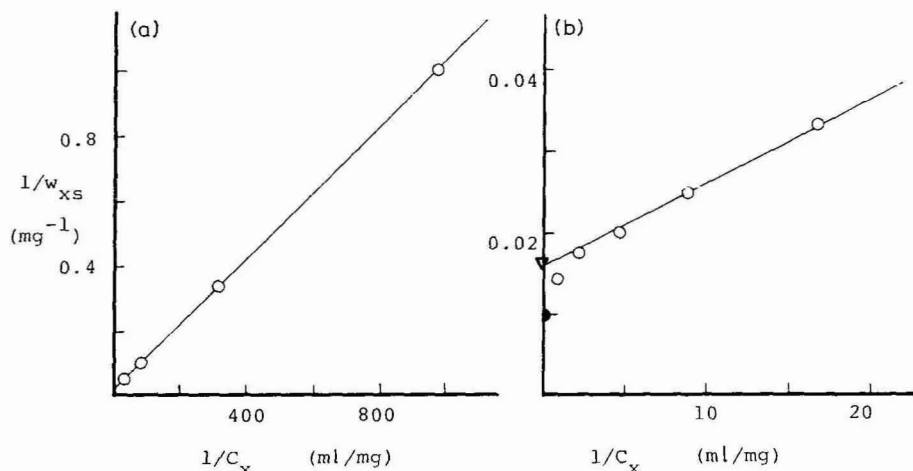
Fig. 2. Calculated isotherm for non-unity stoichiometry for a Langmuir-type isotherm (eqn. 2). Stoichiometry factor $n = 6$; $w_s = 100$ mg. See text for details. (a) Data for low values of C_x; (b) data for high values of C_x. $\triangledown$, $\ominus$, extrapolated values of $1/w_s$.

by a displacement process, so that eqn. 2 applies to these systems as well. For typical separations, values of n can vary widely[7,8].

The isotherm resulting from retention as described by eqn. 2 is derived in Appendix I. Fig. 2 shows a resulting isotherm for the case where $k_0 = 1$, stoichiometry factor $n = 6$, $w_s = 100$ mg and phase ratio $\varphi = 0.1$. Two different concentration ranges are plotted: $0.001 < C_x < 0.03$ in Fig. 2a, and $0.2 < C_x < 1$ mg/l in Fig. 2b. The solid line in Fig. 2b is an extension of the solid line from Fig. 2a, showing that the data appear to follow a Langmuir isotherm over almost the entire range of solute concentrations. The y-axis intercept ($\triangledown$ in Fig. 2b) suggests a value of w_s equal to 67 mg, as compared to the maximum column capacity of 100 mg ($\ominus$ in Fig. 2b). We can conclude that systems with non-unity stoichiometry ($n \neq 1$) will not affect the application of our model[1] to the prediction of elution bands in the overload mode. However, apparent column capacities w_s will be lower than "true" values of w_s^*.

Solute–solute interactions

As the concentration of solute in an HPLC system increases, interactions between solute molecules in both the mobile phase and stationary phase become more likely. In principle this might affect the thermodynamic activities of solute molecules in the two phases, resulting in deviations from Langmuir behavior. Other data[3] suggest that solute–solute and solvent–solute interactions frequently cancel in adsorption systems, for a variety of reasons. One exception to this would be the case of an ionized solute that does not exhibit ionic attraction to the stationary phase. An example is that of ionized carboxylic acids separated by reversed-phase chromato-

---

* A physical explanation for lower values of w_s when $n \neq 1$ is as follows. As the surface is progressively filled with adsorbed molecules of X, it becomes more difficult for an adsorbing molecule of X to locate two adjacent molecules of adsorbed M to replace.

graphy. As will be discussed later in this paper, these compounds appear to obey Langmuir sorption (eqn. 2 of ref. 1) but have much smaller (apparent) values of w_s, as a result of ionic repulsion between sorbed solute molecules.

Maximum column capacity w_s

First consider column packings with rigid surfaces, such as silica or alumina, and assume that the adsorbent surface is covered by a monolayer of solute (Langmuir adsorption). For this case, the maximum column capacity w_s can be estimated from the surface area (SA, m²/g) of the column packing (see ref. 2 and Table III of ref. 3). The volume of the adsorbed monolayer per m² of surface is

$$\text{(silica)} \quad (V_s/SA) \approx 0.35 \; \mu l/m^2 \tag{6}$$

and assuming a density of about 0.9 for the retained solute,

$$\text{(silica)} \quad (w_s/SA) \approx 0.3 \; mg/m^2 \tag{7}$$

In the case of reversed-phase packings, the situation is more complex. First, the surface area of the starting silica is usually known, but this differs from the surface area of the resulting bonded-phase packing. In the case of small-pore silicas bonded with long alkyl groups (*e.g.*, C_{18}), a considerable reduction in apparent surface area can result (ref. 9 and Table VIII of ref. 10). We can estimate this surface-area reduction by assuming that (a) the bonded phase is equivalent to a liquid that coats the silica surface, thereby reducing the pore radius and the area of the surface of the bonded phase, and (b) all pores are cylinders of fixed diameter. Table I summarizes the resulting reduction in surface area as a function of the pore diameter of the silica and the chain length of the alkyl-bonded phase.

Another complication concerns the nature of the monolayer. In the case of inorganic adsorbents, it appears that molecules are generally adsorbed in a flat configuration, and this allows us to estimate the monolayer volume from eqn. 7. If some penetration of the bonded-phase surface occurs during reversed-phase retention (corresponding, to *e.g.*, vertical or "sideways" sorption, *cf.* ref. 11), we might expect values of w_s to be larger than those predicted by eqn. 7. Data from the present study provide further insight into this question.

TABLE I

EFFECTIVE SURFACE AREA (SA) OF BONDED-PHASE PACKINGS AS A FUNCTION OF PORE DIAMETER

Pore diameter (nm)	Surface area of bonded-phase divided by surface area of silica	
	C_8	C_{18}
6	0.80	0.55
8	0.86	0.69
10	0.89	0.76
15	0.93	0.85

EXPERIMENTAL

Chemical and reagents

Benzyl alcohol (> 99% purity) was purchased from Aldrich (Milwaukee, WI, U.S.A.). Angiotensin II, human sequence, acetate salt (99% purity), insulin chain A, oxidized form from bovine insulin, caffeine, and 7β-hydroxypropyltheophyline were purchased from Sigma (St. Louis, MO, U.S.A.). Methanol and acetonitrile were HPLC grade, purchased from Fisher Scientific (Fair Lawn, NJ, U.S.A.). Water was purified and deionized with a Milli-Q water purification unit (Millipore, Bedford, MA, U.S.A.). Buffer salts were purchased from Fisher Scientific and from J. T. Baker (Phillipsburg, NJ, U.S.A.).

Columns

The isotherm measurements and the experimental loading studies were performed on Zorbax* ODS, C_8 and 150-C_8 5-μm and C_8 10-μm packing materials in either 5 cm × 4.6 mm I.D. or 15 cm × 4.6 mm I.D. columns.

Equipment

The instrumentation for the isotherm measurements and the experimental loading studies consisted of a Du Pont Model 8800 liquid chromatograph with a gradient controller, a Model 870 pump, a Model 864 variable-wavelength detector, a thermostatted column compartment and a Valco sampling valve Model CV-6UHPa-N60 (Du Pont, Wilmington, DE, U.S.A.). The analog data were digitized and stored by means of a Nelson analytical series interface (Nelson, Cupertino, CA, U.S.A.) and by means of a modified version of Nelson analytical chromatography software on an HP Series 220 microcomputer (Hewlett-Packard, Palo Alto, CA, U.S.A.). All polynomials were generated with the General Statistics Pàc (Hewlett-Packard) and an HP-85 computer.

Procedures

Isotherm measurements. These measurements were performed by the breakthrough or frontal analysis method[12–14]. A relatively large volume, typically 1 or 2 ml of a mobile phase solution containing a known concentration of the solute was injected into the column. The volume of the injection was adjusted so that flat-topped peaks resulted. The concentration of the injected sample was varied over several orders of magnitude. The dead volume of the column was measured by an injection of concentrated sodium nitrate. In the case of angiotensin II as solute, it was observed that flat-topped peaks could be obtained only at lower flow-rates (which were used in these studies).

The uptake of solute by the stationary phase was calculated from the concentration of solute in the mobile phase plus the difference between the breakthrough volume and the dead volume of the column. The breakthrough volume was taken as the volume corresponding to the inflection point in the leading edge of the solute peak[14]. Table II summarizes these isotherm studies.

---

* Zorbax is Du Pont's registered trademark for its LC columns and packings.

TABLE II

SUMMARY OF ISOTHERM MEASUREMENTS

Column: 5 × 0.46 cm Zorbax C_{18}. See Figs. 3 and 4 and Experimental section for additional details. k_0 was calculated from the $V_m k_0$ value, assuming $V_m = 0.47$ ml.

Solute	Mobile phase*	Flow-rate (ml/min)	w_s	$V_m k_0$	k_0
Benzyl alcohol	40% (v/v) M	0.9	67 ± 3	1.03 ± 0.01	2.2
	30% (v/v) M	0.9	63 ± 8	2.81 ± 0.01	6.0
		6.8	72 ± 20	2.80 ± 0.10	
	20% (v/v) M	0.9	62 ± 5	3.98 ± 0.06	8.5
Angiotensin II	15% (v/v) A	1.0	1**	5.9**	12.5
			60***	2.2***	4.7

* Mobile phase (see Experimental), M refers to concentration of methanol in water; A refers to acetonitrile concentration in aq. 0.1 M phosphate (pH 2.3).
** Values for adsorption onto strong sites (Fig. 4a).
*** Values for adsorption onto weak sites (Fig. 4b).

Chromatographic measurements. These measurements were performed by using small-volume injections (unless otherwise noted, sample volume = 15 μl) of various concentrations of a single solute, dissolved in the mobile phase. Values of k_0 and N_0 were calculated from injections of dilute solutions. Repeat measurements of k_0 and N_0 were performed periodically throughout each study; this allowed correction for any changes in column performance (values of k_0 and N_0).

The retention volume V_R ("cumulative" value in ref. 1) of each peak was determined as the volume at which 50% of the sample was eluted. Values of bandwidth σ_v were calculated as 1/2 the difference between the volumes at which 15.9% and 84.1% of the sample was eluted from the column.

The detection wavelength was chosen so that an absorbance value of 1.0 was not exceeded; however, Beer's law non-linearities were still observed in the benzyl alcohol studies. For this case, calibration curves were obtained from the steady-state absorbance values for large-volume injections of known solute concentrations. Calibration curves fit by a polynomial were used to correct for non-linearity within short intervals across the solute elution band. Values of V_R (and k') and σ_v (and N) were calculated from the resulting (corrected for non-linearity) cumulative elution band, as described above.

Chromatographic data with small sample sizes are given in Table III, while a complete tabulation of individual data points for both isotherm measurements and loading studies is given in ref. 15.

RESULTS AND DISCUSSION

Isotherm measurements

Isotherms were measured experimentally for a 5-cm reversed-phase column (Zorbax ODS, a 6-nm-pore C_{18} packing) and two solutes: benzyl alcohol and angiotensin II. Three different mobile phase compositions were used for benzyl alcohol.

TABLE III

SUMMARY OF EXPERIMENTAL HPLC RUNS UNDER OVERLOAD CONDITIONS
Columns used are 5 × 0.46 cm, except for caffeine and 7β-hydroxypropyltheophyline (15 × 0.46 cm).

Solute	Column	Mobile phase*	Flow-rate (ml/min)	k_0**	N_0**	A_s
Benzyl alcohol	ODS	20% M	0.9	7.6	2280	1.1
			6.8	11.2	1440	1.2
		30% M	0.9	5.8	3060	1.1
			6.8	5.8	1100	1.2
		40% M	0.9	2.9	1810	1.2
			6.8	3.5	990	1.2
	C_8	30% M	1.0	5.9	3550	1.0
	150-C_8	30% M	1.0	3.3	2900	1.1
Angiotensin II	ODS	15% A in B	1.0	12.8	1880	1.3
	C_8	18% A in B	0.5	4.1	485	2.4
	150-C_8	18% A in B	0.5	9.7	1690	1.7
Insulin A chain	C_8	17% A in B'	0.4	9.0	550	1.6
Caffeine	C_8	5% A, 20% M in B''	1.0	2.9	5600	1.5
7β-Hydroxypropyl-theophyline	C_8	5% A, 20% M in B''	1.0	2.6	6500	1.1

* Percentages refer to % (v/v) organic in water or buffer mobile phase; M refers to methanol, A refers to acetonitrile, B refers to 0.1 M phosphate buffer (pH 2.3), B' refers to 0.1 M phosphoric acid plus triethylamine (pH 2.2), and B'' refers to 0.1 M monobasic sodium phosphate.

** Different columns were used, resulting in some variation in k_0 and N_0.

The procedure followed is described in the Experimental section; it consisted of measurements on the same (or a similar) column later used for HPLC studies, as a function of sample size and experimental conditions (following section).

Benzyl alcohol. Results for benzyl alcohol and methanol–water (40:60) are shown in Fig. 3. In Fig. 3a the data points cover the range $0.2 < C_x < 20$ mg/ml, and the resulting plot is seen to be linear within experimental error (Langmuir behavior). Fig. 3b shows a similar plot, covering the range $40 < C_x < 200$ mg/ml, with the solid curve from Fig. 3a superimposed onto that in Fig. 3b. This system appears to exhibit Langmuir behavior over the entire range of concentrations studied ($0.2 < C_x < 200$ mg/ml). Pair-wise calculations (values of w_s *vs.* C_x) yield values of both the intercept ($1/w_{xs}$) and slope ($1/V_m k_0$) for this system, as summarized in Table II*.

Similar measurements were performed by using mobile phases of varying composition (20–40% (v/v) methanol in water), as well as at different flow-rates. The

* Note that fitting the data in Fig. 3 on a single plot with a least-squares line is insensitive to isotherm non-linearity, as in Fig. 1. The reason is that deviant data points at large values of C_x show negligible deviations in $1/w_s$; correlation coefficients are therefore close to 1, even for plots as in Fig. 1 and 2. For this reason we have presented all isotherm data in the form of complementary plots (Figs. 1–4).
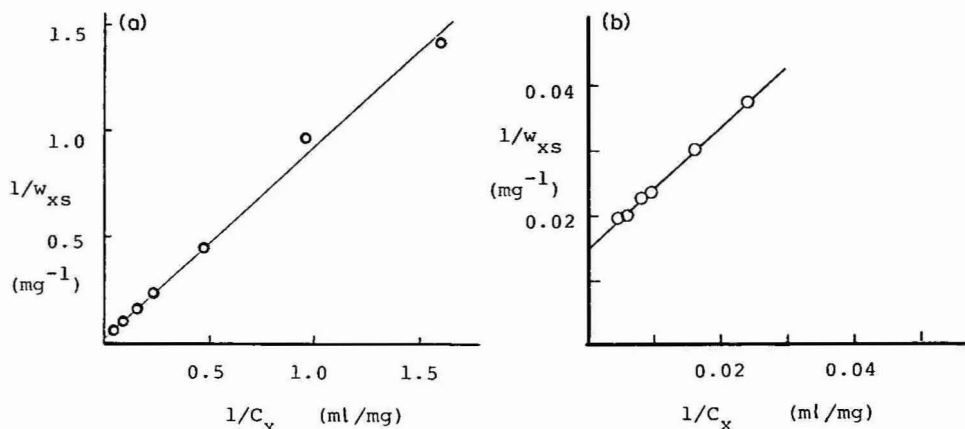
Fig. 3. Experimental isotherm data for benzyl alcohol as solute. Mobile phase, methanol–water (40:60); column, 5 × 0.46 cm Zorbax ODS. (a) Data for low solute concentrations, $0.2 \leqslant C_x \leqslant 20$ mg/ml; (b) data for high solute concentrations, $40 \leqslant C_x \leqslant 200$ mg/ml.

resulting isotherm plots resembled those of Fig. 3, showing Langmuir-isotherm behavior over wide ranges in C_x: methanol–water (30:70), $0.1 < C_x < 30$ mg/ml; methanol–water (20:80), $0.1 < C_x < 40$ mg/ml. Resulting values of w_s from these different isotherm measurements are summarized in Table II, and are seen to be constant within experimental error: 64 ± 6 (1 S.D.) mg for a flow-rate of 0.9 ml/min. These results, together with the Langmuir plots as in Fig. 3, confirm that this system follows Langmuir behavior; *i.e.*, true Langmuir adsorption must yield a constant value of w_s for a given solute/column combination.

Angiotensin II. Fig. 4 presents Langmuir plots for angiotensin II as solute and the same column as for benzyl alcohol. Fig. 4a shows the isotherm for the concentration range $0.07 < C_x < 0.35$ mg/ml, with good adherence of the data to a linear plot (apparent Langmuir behavior). However, the extrapolated value of w_s is quite small (only 2 mg). This suggests site heterogeneity, and this is confirmed by isotherm measurements at higher values of C_x: $0.3 < C_x < 7$ mg/ml, as summarized in Fig. 4b. The dashed curve in Fig. 4b is taken from Fig. 4a, and the data for large C_x are seen to deviate markedly from that curve. The latter points can be extrapolated to a value of $w_s \approx 60$ mg, which is much larger than for the case of Fig. 4a, but close to the result for benzyl alcohol ($w_s = 64$) in Fig. 3.

We can use adjacent points in the plots of Figs. 4a and b to solve eqn. 2 of ref. 1 for values of w_s and $V_m k_o$, as a function of the total uptake of angiotensin II by the column (w_{xs}). Resulting values of the apparent column capacity w_s are plotted against w_{xs} in Fig. 4c. It is seen that these change regularly as w_{xs} increases, tending to a value of about 1 mg at low value of w_{xs}, and tending to a value of about 60 mg at high values of w_{xs}. The dashed line at $w_s = 64$ mg in Fig. 4c corresponds to the expected value from the benzyl alcohol data, assuming that the maximum uptake of either solute by the column will be the same (as expected, approximately, for a simple Langmuir system; eqn. 7).

These observations suggest that two types of sites contribute to the retention of angiotensin II in this system. Presumably residual silanols comprise the strong
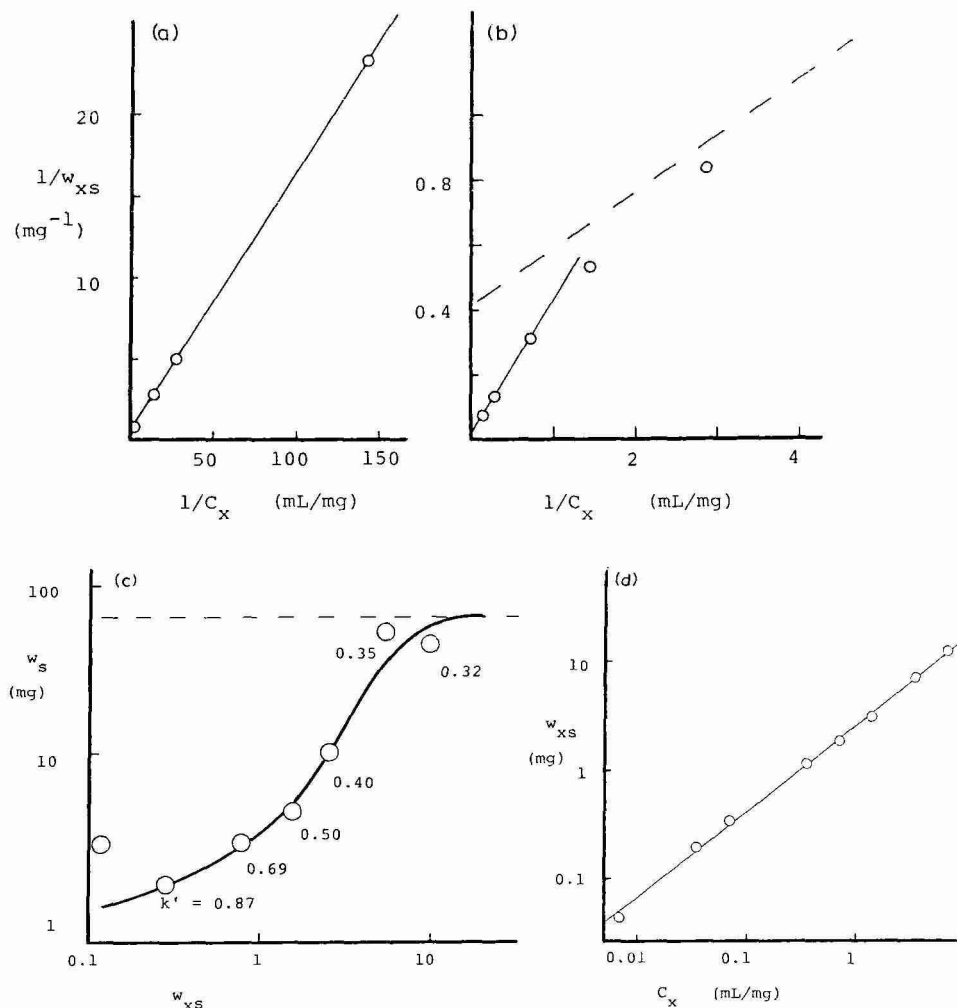
Fig. 4. Experimental isotherm data for angiotensin II as solute. Mobile phase, acetonitrile–0.1 M aqueous phosphate (pH 2.3) (15:85); column, 5 × 0.46 cm Zorbax ODS. (a) Data for low solute concentrations, $0.07 \leqslant C_x \leqslant 0.35$ mg/ml; (b) data for high solute concentrations, $0.3 \leqslant C_x \leqslant 7$ mg/ml; (c) apparent w_s values *vs.* weight of solute in stationary phase (w_{xs}); (d) log w_{xs} *vs.* log C_x plot (Freundlich isotherm plot).

sites, and constitute about 2% of the available surface of the packing. Values of k_0, derived from these data and summarized in Table I, suggest that the strong sites have a k_0-value about 3-times greater than for the weak sites (small sample sizes). Together with the site–concentration ratio ($\approx 1/60$ for silanols), this suggests that the equilibrium distribution constant K for the silanols is about 200 times larger than for binding of angiotensin II to the hydrophobic surface.

It should be noted that the isotherm data of Fig. 4a and b can be described by the Freundlich isotherm[4]:

$$w_{xs} = g\ C_x^h \tag{8}$$

Here, g and h are constants for a given system. Eqn. 8 predicts linear plots of log w_{xs} vs. log C_x, and this is observed for the angiotensin II data in Fig. 4d. The Freundlich isotherm is a purely empirical fitting function, so that the correlation of Fig. 4d has no fundamental significance. However, it should be noted that the Freundlich isotherm is often a good approximation for isotherms that are non-Langmuir (as in this case, for a wide range of C_x values). Later, we will see that our model in ref. 1 (which assumes Langmuir behavior) fits the angiotensin II system rather well. This suggests its similar utility for other non-Langmuir-isotherm systems that follow the Freundlich isotherm.

Chromatographic data under overload conditions

Single-solute samples were chromatographed under the same conditions (and on the same columns) as those used for the isotherm studies. This alowed a direct correlation of experimental values of k', N and band shape with values predicted by the model in ref. 1. Additional chromatographic data were obtained for other solutes and experimental conditions (different column types), but without measuring isotherms. These runs allow a further check of experimental data against the model.

Table III summarizes the various HPLC systems studied in an overload chromatographic mode. Values of k_0 and N_0 are given for each series of runs, as well as band asymmetry A_s for small sample injections. Data for the various runs at higher sample size are summarized in the following figures and tables. A complete tabulation of these results can be obtained from ref. 15.

The model presented in ref. 1 predicts that experimental values of k'/k_0 and N/N_0 should be correlated with values of the loading functions w_{xk} and w_{xN}, respectively. These functional dependencies were defined from Craig simulations, as summarized in Table II of ref. 1. These "master curves" are shown in Fig. 5a–c as dashed lines. Fig. 5a and b are for "cumulative" values of k' and N; we will be
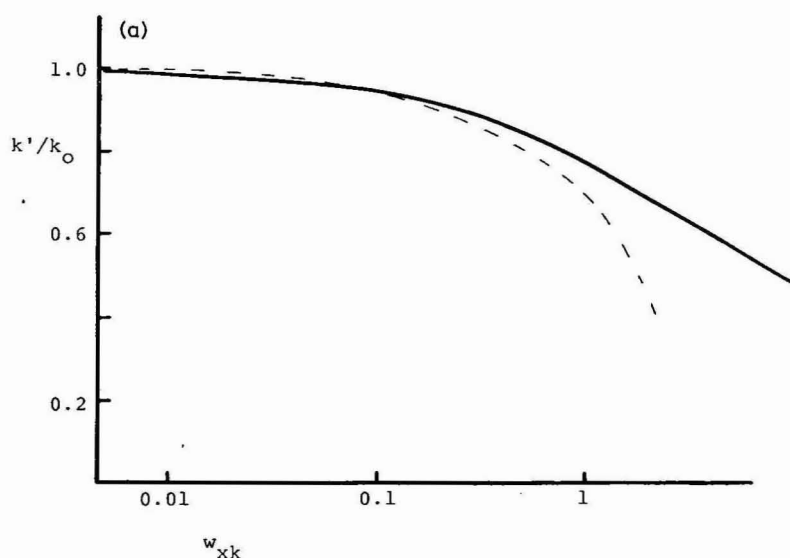
Fig. 5.
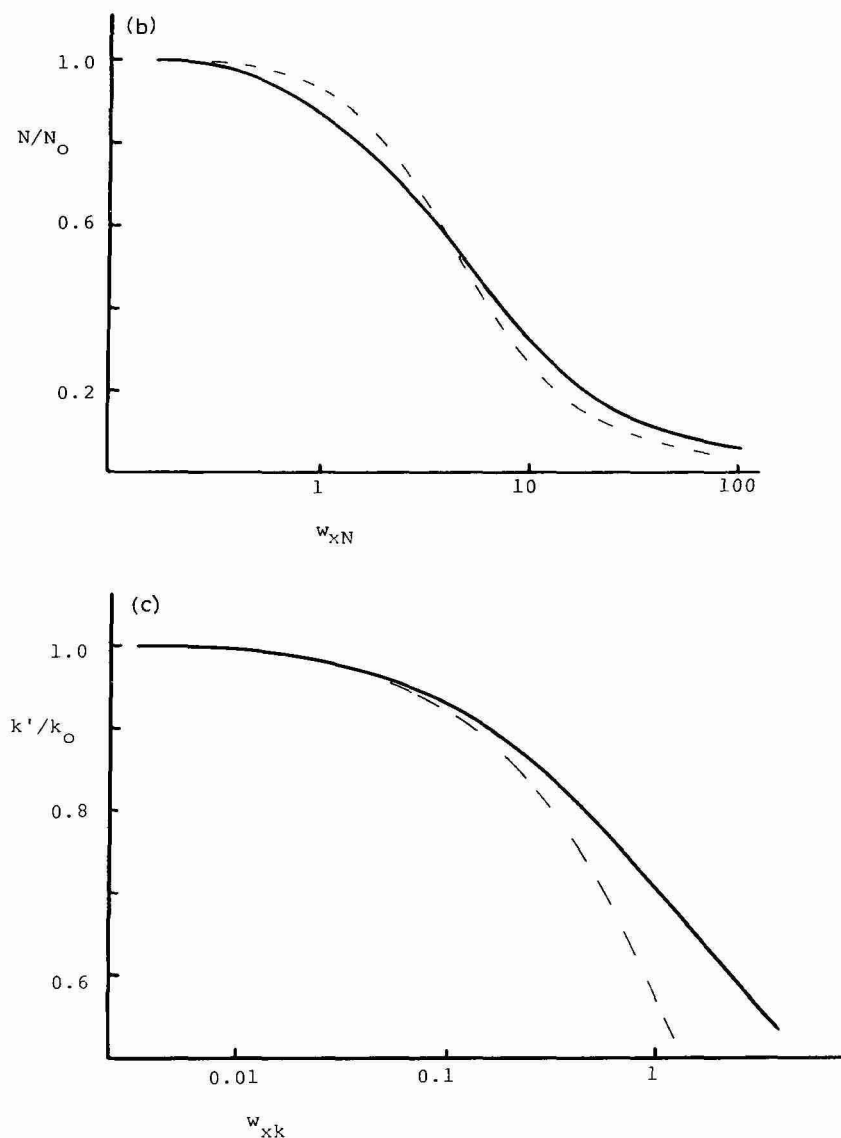
Fig. 5. Dependence of k'/k_0 and N/N_0 on w_{xk} and w_{xn}, respectively. (a) "Cumulative" values of k'; (b) "cumulative" values of N; (c) "band" values of k'. (— — —) Craig-model values from Table II of ref. 1; (———) empirical, best-fit values from present study.

concerned with these correlations for the most part. When experimental values of k'/k_0 and N/N_0 were compared with Fig. 5a and b, it was found that an approximate superimposition of experimental data and master curves could be obtained. However, a slight adjustment in the shape of the master curves (solid curves in Fig. 5a and b) was found to give a better overall fit to the experimental data. Presumably, this reflects subtle differences between the Craig model and "real" HPLC separations.

TABLE IV

EMPIRICAL BEST-FIT DEPENDENCE OF k'/k_0 AND N/N_0 vs. THE LOADING FUNCTIONS w_{xk} AND w_{xN} (FIG. 5)

Cumulative values of k'/k_0 vs. w_{xk} and N/N_0 vs. w_{xN} can also be expressed mathematically. Appropriate fitting functions are available from the authors.

w_{xk} or w_{xN}	k'/k_0	N/N_0	w_{xk} or w_{xN}	k'/k_0	N/N_0
"Cumulative" values (Fig. 5a,b)*					
0.01	0.99	1.00	2	0.69	0.74
0.02	0.98	1.00	5	0.57	0.51
0.05	0.97	1.00	10	0.48	0.32
0.10	0.95	1.00	20	(0.39)	0.19
0.20	0.92	1.00	50	(0.27)	0.10
0.50	0.85	0.95	100	(0.18)	0.06
1.00	0.77	0.87	200		0.04
w_{xk}	(k'/k_0)	w_{xk}	(k'/k_0)		
"Band" values (Fig. 5c)**					
0.01	0.99	0.5	0.79		
0.02	0.98	1	0.71		
0.05	0.96	2	0.62		
0.10	0.93	5	0.50		
0.20	0.88	10	0.41		

* As in Fig. 1b of ref. 1.
** As in Fig. 1a of ref. 1.

We therefore used the solid curves in Fig. 5a and b in further correlations of experimental data. These latter loading function curves are listed in Table IV.

Benzyl alcohol, Zorbax ODS column. Sample sizes of 0.003–5 mg were injected, the data for the elution band were expressed as cumulative percent vs. time curves (e.g., as in Fig. 1b of ref. 1), and values of k' and N ("cumulative" values) were obtained. The loading functions w_{xk} and w_{xN} were then calculated for each sample mass, and values of k'/k_0 were plotted against $w_{xk} w_s$ (Fig. 6). Similarly, N/N_0 was plotted against $w_{xN} w_s$ in Fig. 7*. For a particular solute and column (where w_s is constant), the resulting data should describe a plot that can be superimposed onto one of the master curves of Fig. 5a and b. This is seen to be the case for both Figs. 6 and 7.

The best curve through the data of Figs. 6 or 7 corresponds to some value of w_s in each case. This w_s value is obtained by simply overlaying plots as in Figs. 6 and 7, onto the corresponding curves from Fig. 5a or b. The value of the x axis from the experimental-data plots that corresponds to $x = 1$ from the plots of Fig. 5 then equals the best-fit value of w_s. For the k' data of Fig. 6, the best-fit value of w_s is found to be about 90 mg. Similarly, the best-fit value of w_s for the data of Fig. 7 is 30 mg. Note that the isotherm value of 64 mg lies midway between these two values (30 and 90 mg). At this point, we see that the predicted curves for k' and N as a

---

* At this point, we assume that w_s is not known; $w_{xk} w_s$ is then equal to $[k_0/(1 + k_0)] N_0^{0.5} w_x$, and $w_{xN} w_s = [k_0/(k_0 + 1)]^2 N_0 w_x$.
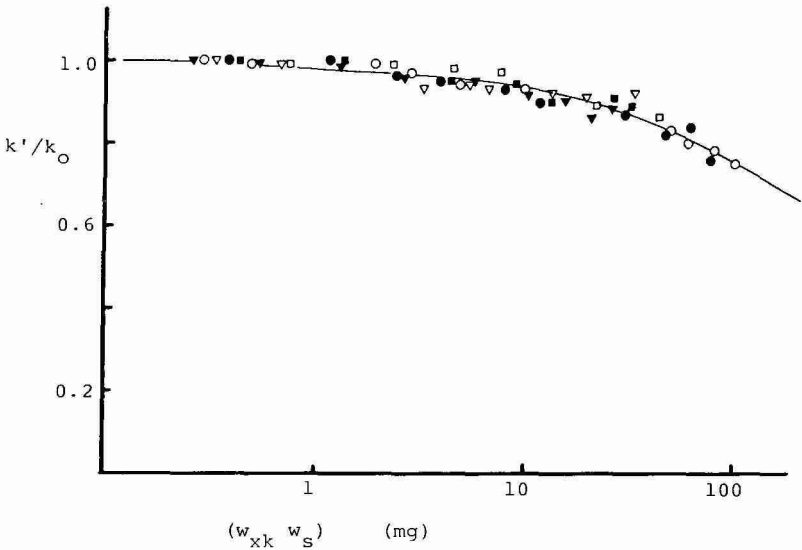
Fig. 6. Chromatographic data for benzyl alcohol and Zorbax ODS column: dependence of k'/k_0 on w_{xk} w_s. (——————) Superimposed master curve of Fig. 5a, best-fit value of w_s = 90 mg. Experimental data points:

Methanol–water (v/v)	0.89 ml/min	6.8 ml/nmin
20:80	▽	▼
30:70	☐	▣
40:60	○	●

Other conditions described in Experimental section.
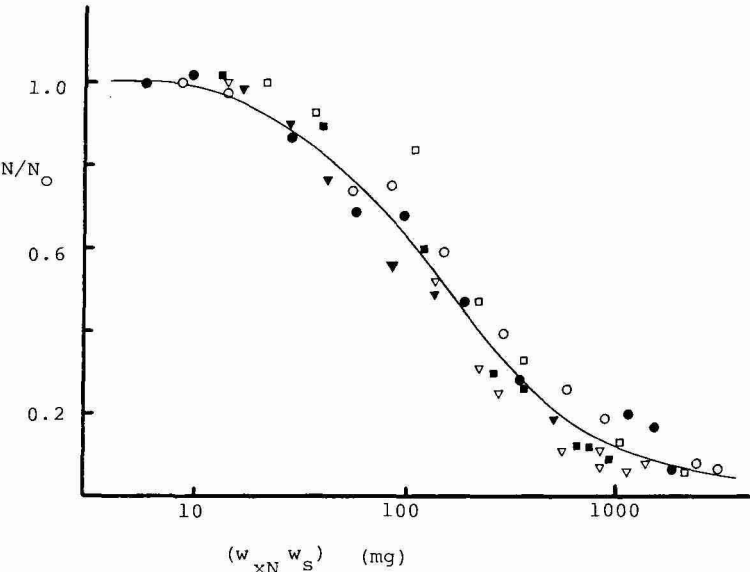
Fig. 7. Chromatographic data for benzyl alcohol and Zorbax ODS column: dependence of N/N_0 on $w_{xN}w_s$. (——————) Superimposed master curve of Fig. 5b, best-fit value of w_s = 30 mg. Symbols for data points as in Fig. 5.
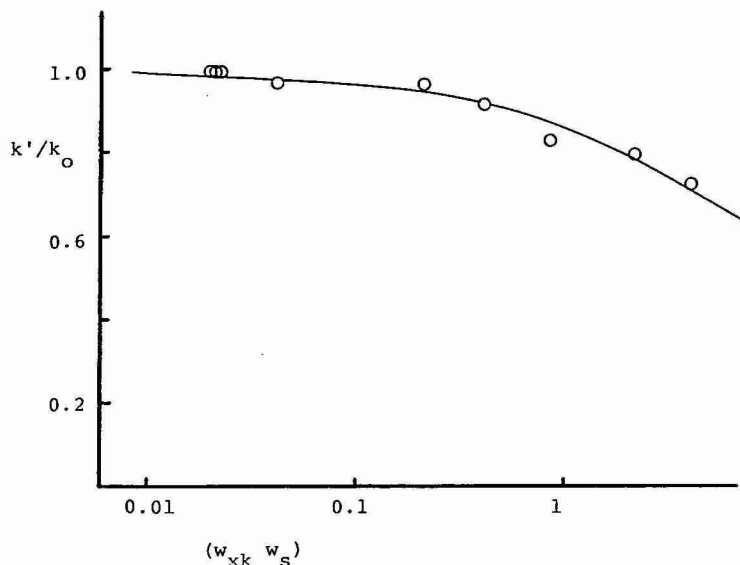
Fig. 8. Chromtographic data for angiotensin II and Zorbax ODS column: dependence of k'/k_0 on w_{xk} w_s. Mobile phase, acetonitrile–0.1 M phosphate (pH 2.3) (15:85); flow-rate, 1 ml/min. (———) Superimposed master curve of Fig. 5a, best-fit value of w_s = 2.5 mg. (O) Experimental data points. Other conditions in Experimental section.
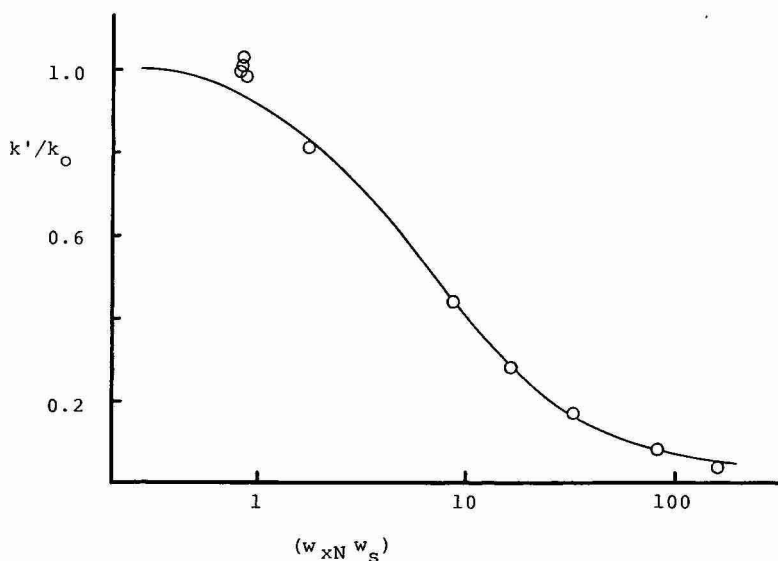
Fig. 9. Chromatographic data for angiotensin II and Zorbax ODS column: dependence of N/N_0 on w_{xk} w_s. Conditions as in Fig. 8. (———) Superimposed master curve of Fig. 5b, best-fit value of w_s = 1.4 mg; (O) Experimental data points.

function of sample size (using the isotherm value of 64 mg) give an approximate prediction of the two experimental curves of Figs. 6 and 7. We will discuss these different values of w_s, obtained from k'/k_0 *vs.* N/N_0 plots, later, after reviewing additional data for other solutes and columns (however at the present time we do not have an explanation for this effect).

Angiotensin II, Zorbax ODS column. Sample sizes of 0.5–105 μg angiotensin II were injected in this series of runs, and the same conditions were used as for the isotherm studies of Fig. 4 and Table II. The results are plotted in Figs. 8 and 9 in the same way as for benzyl alcohol in Figs. 6 and 7. Again, a reasonable adherence of the experimental values of k'/k_0 and N/N_0 to the predicted curves (Fig. 5) is seen. The best-fit values of w_s are 2.5 mg for the k'/k_0 data, and 1.4 mg for the N/N_0 data. These values are in rough agreement with the small-sample w_s value from the isotherm measurements (1 mg), suggesting that the strong sites largely determine the effective value of w_s — as far as values of k'/k_0 and N/N_0 are concerned. Reference to Fig. 4d is also helpful in this connection. From Fig. 8. we see that the average value of k'/k_0 is about 0.85, for values of k'/k_0 significantly different from unity. Fig. 4d suggests a value of w_s for this average sample size (or value of w_{xs}) equal to about 2 mg (a value that is midway between the above values of 1.4 and 2.5 mg, from chromatographic runs). These comparisons are summarized in Table II.

The following discussion emphasizes values of w_s obtained as in the preceding example, for other HPLC systems. We will see that values of w_s vary with both the solute and the column, and that larger values of w_s are consistently observed for plots of k'/k_0 as compared with plots of N/N_0. Later we will show that values of w_s for predicting values of k'/k_0 and N/N_0 —and therefore the elution curve as a function of sample loading— can be obtained from a few experiments under overload con-
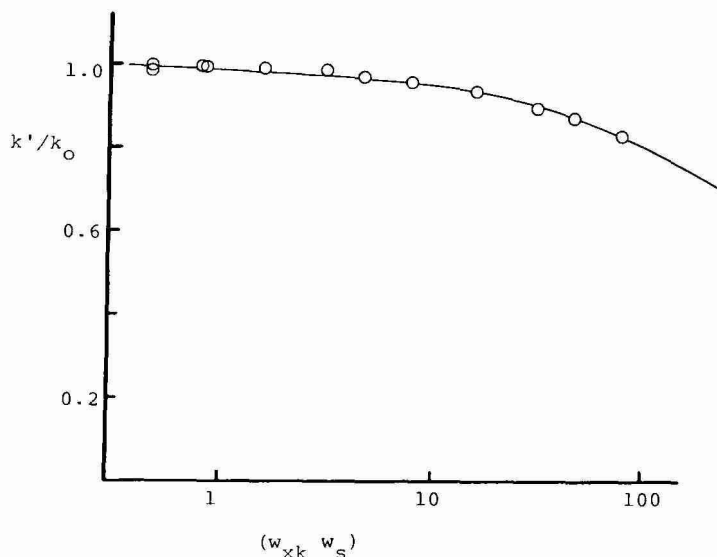
Fig. 10. Chromatographic data for benzyl alcohol and Zorbax C_8 column: dependence of k'/k_0 on $w_{xk} w_s$. Mobile phase methanol–water (30:70); flow-rate, 1 ml/min. (———) Superimposed master curve of Fig. 5a, best-fit value of w_s = 140 mg. (○) Experimental data points.
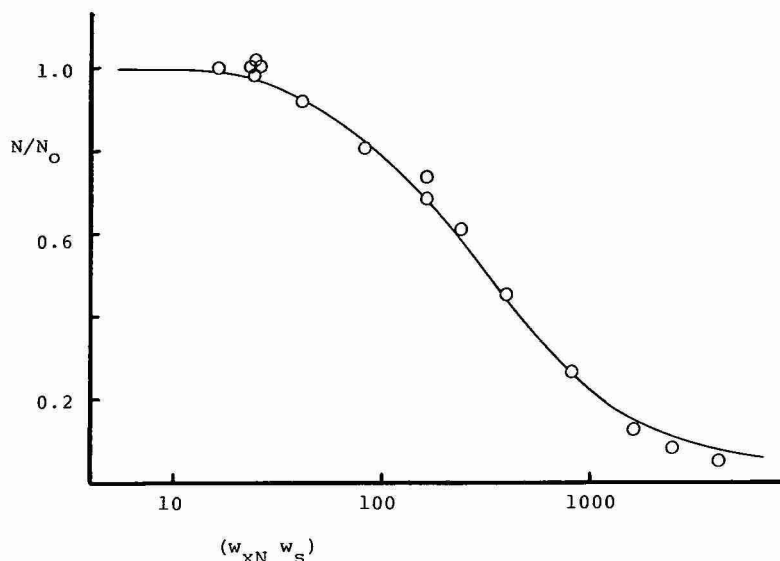
Fig. 11. Chromatographic data for benzyl alcohol and Zorbax C_8 column: dependence of N/N_0 on w_{xN} w_s. Conditions as in Fig. 10. (————) Superimposed master curve of Fig. 5b, best-fit value of $w_s = 60$ mg. (O) Experimental data points.

ditions. This allows the easy application of the present approach (model simulations) to actual HPLC separation in an overload mode.

Other overload HPLC studies

Several other systems were investigated, involving different solutes and col-
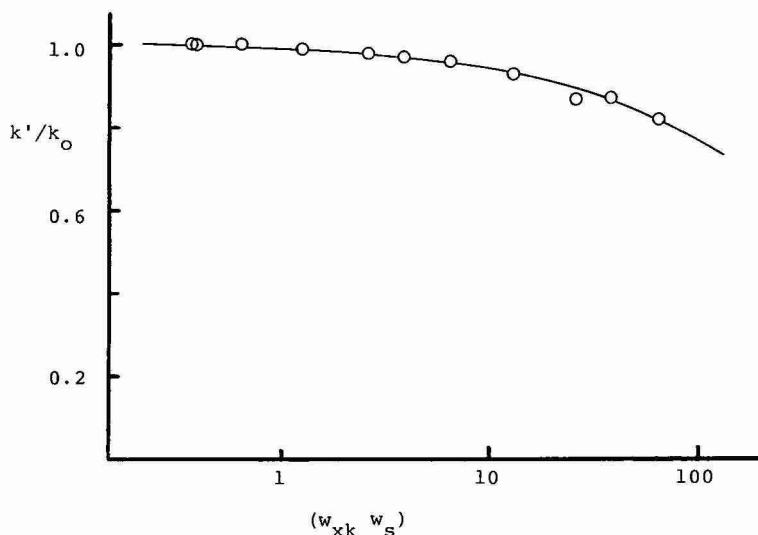
Fig. 12. Chromatographic data for benzyl alcohol and Zorbax 150-C_8 column: dependence of k'/k_0 on w_{xk} w_s. Mobile phase, methanol–water (30:70); flow-rate, 1 ml/min. (————). Superimposed master curve of Fig. 5a, best-fit value of $w_s = 100$ mg. (O) Experimental data points.
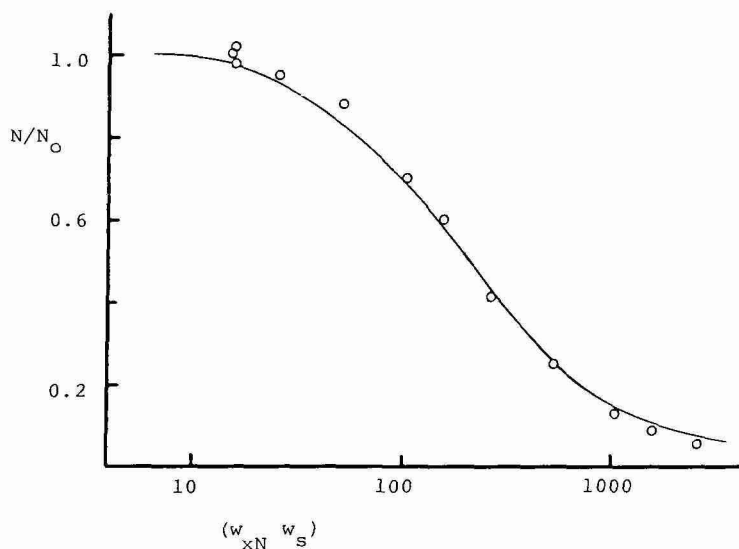
Fig. 13. Chromatographic data for benzyl alcohol and Zorbax 150-C$_8$ column: dependence of k'/k_0 on w_{xk} w_s. Conditions as in Fig. 12. (————) Superimposed master curve of Fig. 5b, best-fit value of w_s = 40 mg. (○) Experimental data points.

umns. These data are summarized in Figs. 10–23 and Table V. The correlations of Figs. 10–23 with the (solid) master curves of Fig. 5a and b are seen to be generally satisfactory. The best-fit values of w_s for these various correlations are summarized in Table V, although isotherm data for comparison were not collected. In the resulting data of Table V, certain general trends are apparent, which we will examine.
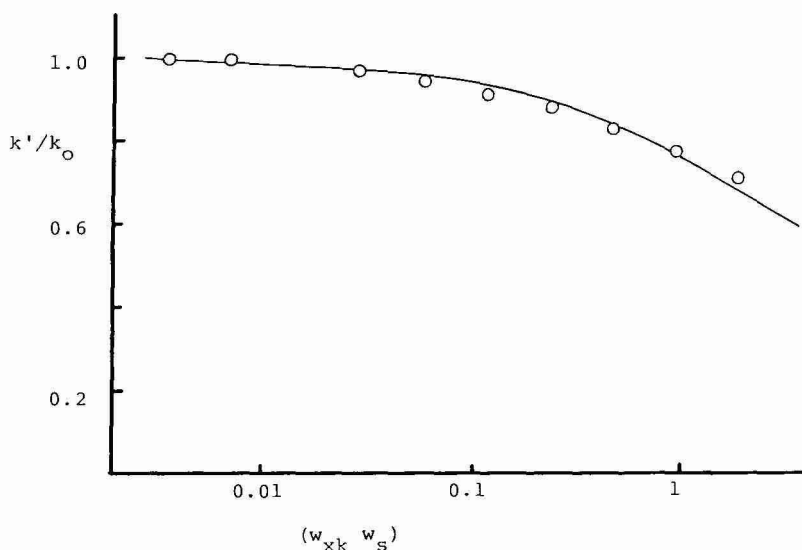
Fig. 14. Chromatographic data for angiotensin II and Zorbax C$_8$ column: dependence of k'/k_0 on w_{xk} w_s. Mobile phase, acetonitrile–0.1 M phosphate buffer (pH = 2.3) (18:72); flow-rate, 0.5 ml/min. (————) Superimposed master curve of Fig. 5a, best-fit value of w_s = 0.9 mg. (○) Experimental data points.
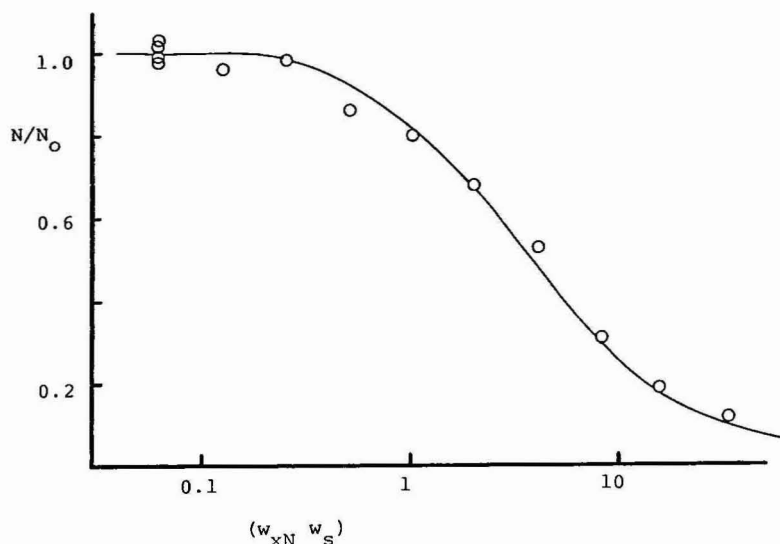
Fig. 15. Chromatographic data for angiotensin II and Zorbax C_8 column: dependence of N/N_0 on w_{xN} w_s. Conditions as in Fig. 14. (————) Superimposed master curve of Fig. 5b, best-fit value of $w_s = 0.7$ mg. (O) Experimental data points.

Effects of flow-rate and mobile phase composition on overload separation. The plots of Figs. 6 and 7 for benzyl alcohol and the ODS column show more scatter than later plots for other solute–column combinations. The data of Figs. 6 and 7 include runs where flow-rate (and N_0) and mobile phase composition (and k_0) were
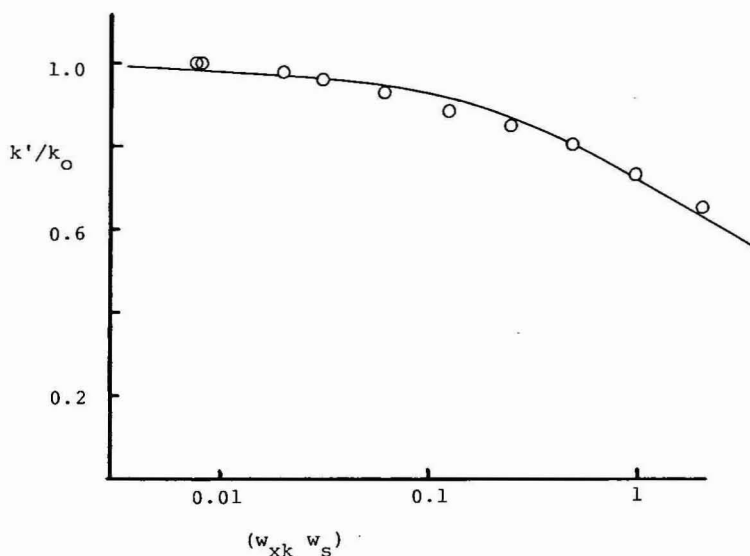
Fig. 16. Chromatographic data for angiotensin II and Zorbax 150-C_8 column: dependence of k'/k_0 on w_{xk} w_s. Mobile phase, acetonitrile–0.1 M phosphate buffer (pH $= 2.3$) (18:82); flow-rate, 0.5 ml/min. (————) Superimposed master curve of Fig. 5a, best-fit value of $w_s = 0.7$ mg. (O) Experimental data points.

TABLE V

COMPARISON OF VALUES OF COLUMN CAPACITY w_s OBTAINED FROM ISOTHERM AND CHROMATOGRAPHIC MEASUREMENTS

Solute	Column	w_s (mg)			
		Isotherm	HPLC		
			k'/k_0	N/N_0	Ratio*
Benzyl alcohol	Zorbax ODS	64	90	30	3.0
	Zorbax C_8		140	60	2.3
	Zorbax 150-C_8		100	40	2.5
Angiotensin II	Zorbax ODS	2**	2.5	1.4	1.8
	Zorbax C_8		0.9	0.7	1.3
	Zorbax 150-C_8		0.7	0.55	1.4
Insulin A chain	Zorbax C_8		1.3	0.5	2.3
Caffeine	Zorbax C_8		180	50	3.6
7β-Hydroxypropyl-theophyline	Zorbax C_8		300	70	4.5
				Average	2.5 ± 1.0

* Ratio of w_s value from k'/k_0 vs. w_s value from N/N_0.
** Value from Fig. 4d (see text).
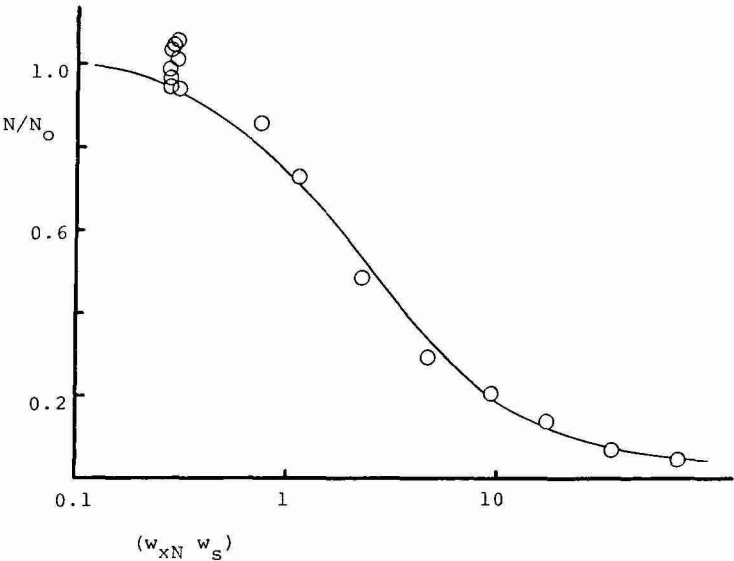
Fig. 17. Chromatographic data for angiotensin II and Zorbax 150-C_8 column: dependence of N/N_0 on $w_{xN} w_s$. Conditions as in Fig. 16. (————) Superimposed master curve of Fig. 5b, best-fit value of w_s = 0.5 mg. (○) Experimental data points.

Fig. 18. Chromatographic data for insulin A chain and Zorbax ODS column: dependence of k'/k_0 on w_{xk} w_s. Mobile phase, acetonitrile–0.1 M phosphate (pH = 2.3) (27:73); flow-rate, 0.4 ml/min. (———) Superimposed master curve of Fig. 5a, best-fit value of w_s = 1.3 mg. (O) Experimental data points.

varied; in later studies (Figs. 8–23) the flow-rate or the mobile phase was not varied. It is therefore possible that the greater scatter in Figs. 6 and 7 reflects systematic effects due to N_0 and k_0 that have not been adequately corrected for. To answer this question, the runs in Figs. 6 and 7 were segregated according to flow-rate and solvent composition, and were replotted (Fig. 24).
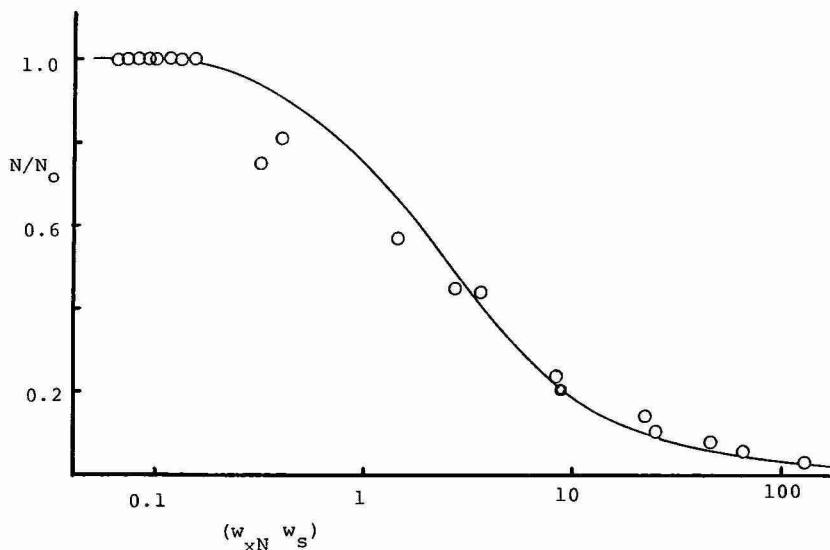
Fig. 19. Chromatographic data for insulin A chain and Zorbax ODS column: dependence of N/N_0 on w_{xN} w_s. Conditions as in Fig. 18. (———) Superimposed master curve of Fig. 5b, best-fit value of w_s = 0.5 mg. (O) Experimental data points.
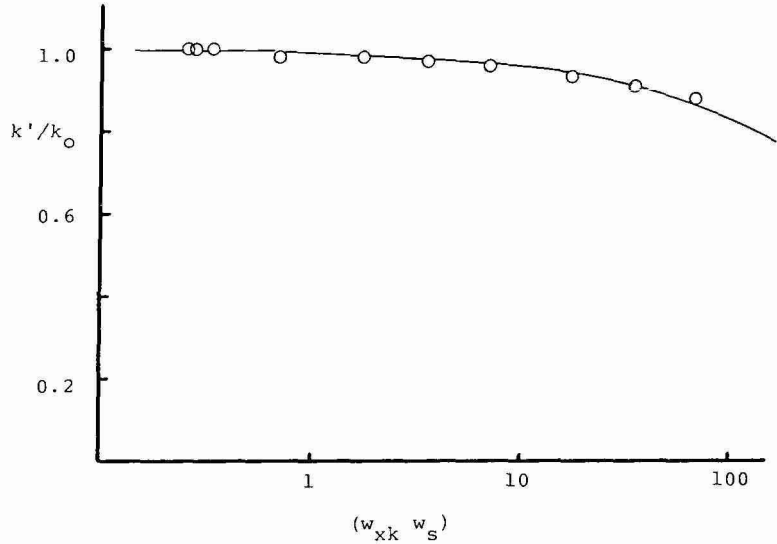
Fig. 20. Chromatographic data for caffeine and 15-cm Zorbax C_8 column: dependence of k'/k_0 on $w_{xk}\, w_s$. Mobile phase, methanol–acetonitrile–0.01 M phosphate buffer (pH = 4.0) (20:5:75); flow-rate, 1 ml/min. (———) Superimposed master curve of Fig. 5a, best-fit value of w_s = 180 mg. (O) Experimental data points.
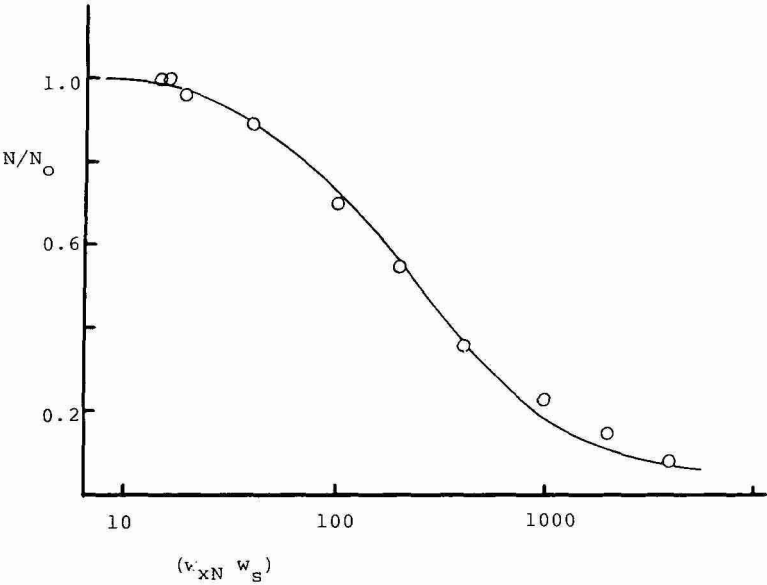
Fig. 21. Chromatographic data for caffeine and 15-cm Zorbax C_8 column: dependence of N/N_0 on $w_{xN}\, w_s$. Conditions as in Fig. 20. (———) Superimposed master curve of Fig. 5b, best-fit value of w_s = 50 mg. (O) Experimental data points.
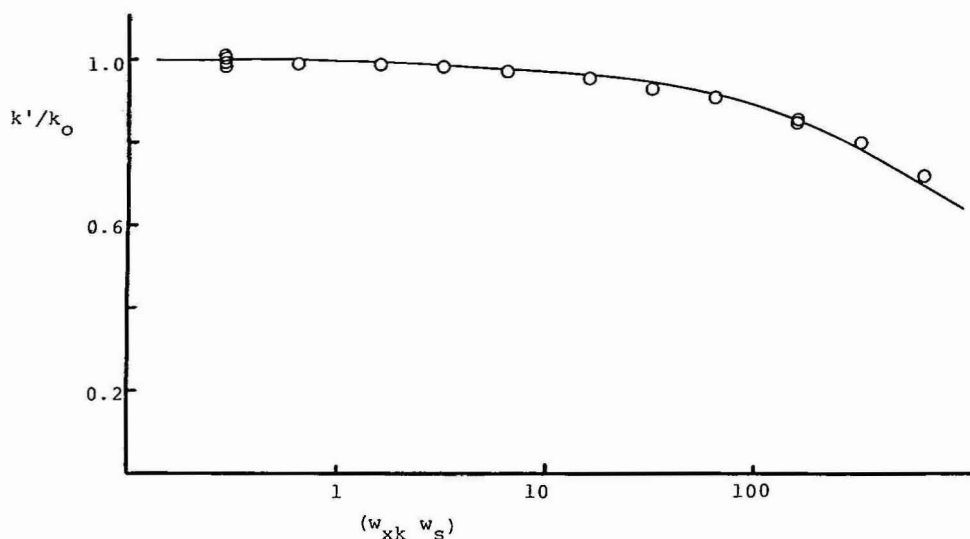
Fig. 22. Chromatographic data for 7β-hydroxypropyltheophyline and 15-cm Zorbax C_8 column: dependence of k'/k_0 on $w_{xk}\ w_s$. Conditions as in Fig. 20. (————) Superimposed master curve of Fig. 5a, best-fit value of $w_s = 300$ mg. (O) Experimental data points.

Fig. 24 shows that the experimental scatter in these plots is reduced (*cf.* Figs. 6 and 7), suggesting additional (unrecognized) contributions from flow-rate or mobile phase composition. Values of w_s were derived for each of the plots of Fig. 24 and are summarized in Table VI.

Our conclusion is that values of the effective column capacity w_s vary in minor
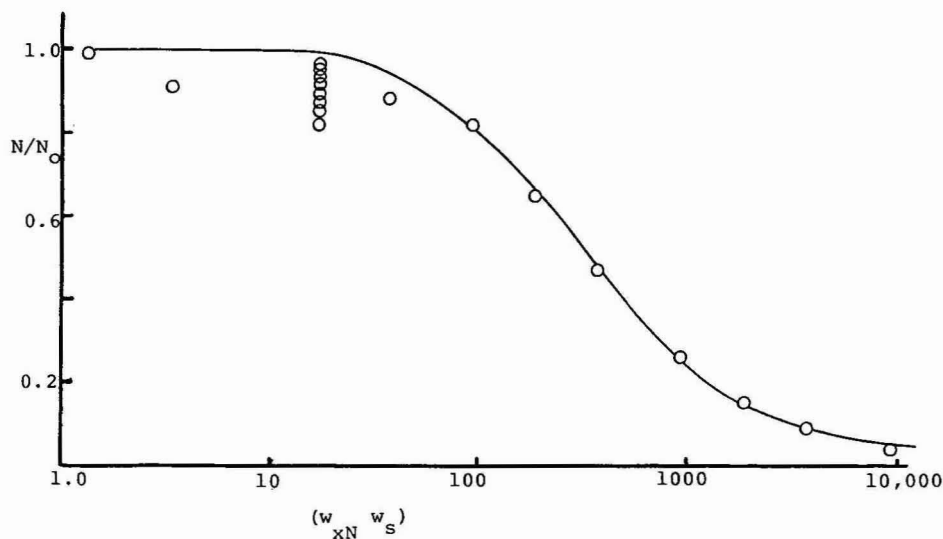
Fig. 23. Chromatographic data for 7β-hydroxypropyltheophyline and 15-cm Zorbax C_8 column: dependence of N/N_0 on $w_{xN}\ w_s$. Conditions as in Fig. 20. (————) Superimposed master curve of Fig. 5b, best-fit value of $w_s = 70$ mg. (O) Experimental data points.
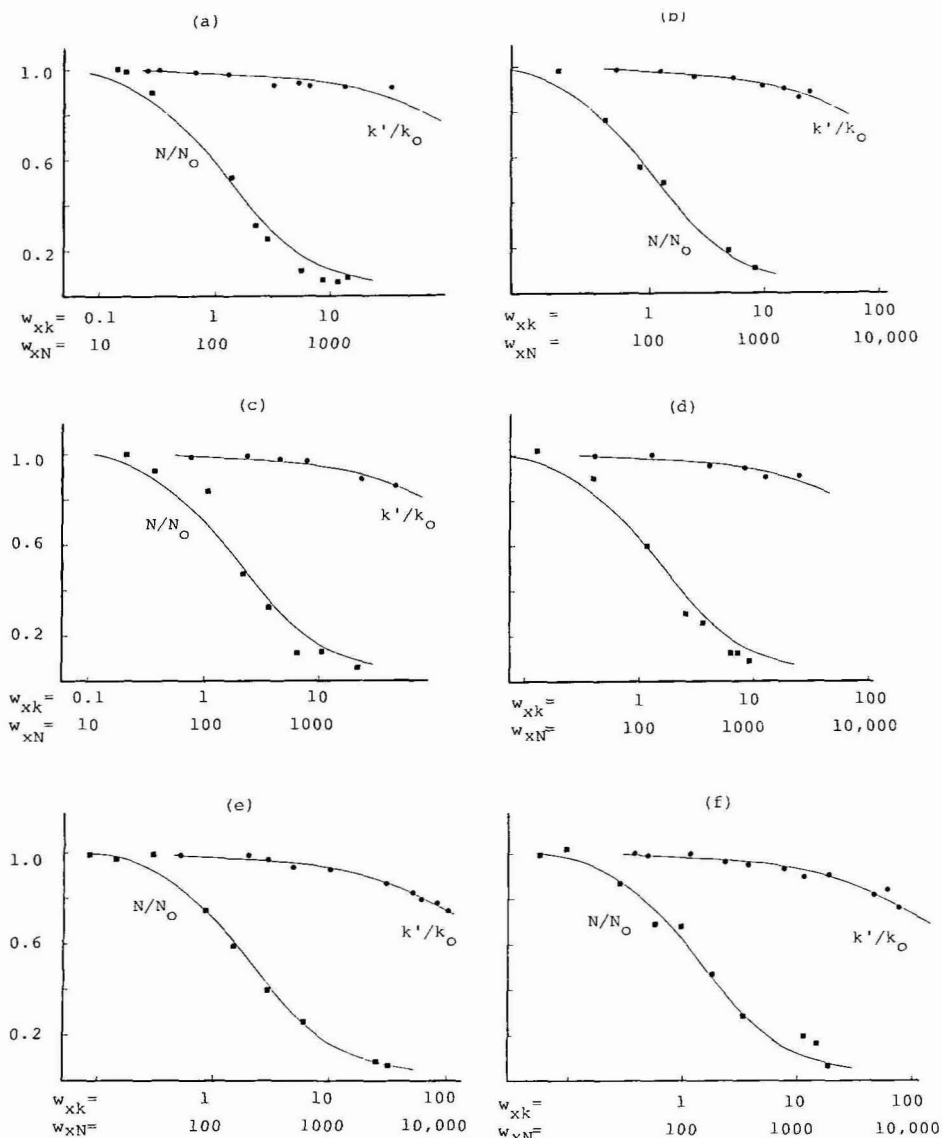
Fig. 24. Data of Figs. 6 and 7 replotted for particular values of flow-rate and mobile phase composition. (a) 20% (v/v) methanol, 0.89 ml/min; (b) 20%, 6.8 ml/min; (c) 30%, 0.89 ml/min; (d) 30%, 6.8 ml/min; (e) 40%, 0.89 ml/min; (f) 40%, 6.8 ml/min. (●) Data for k'/k_0; (■) data for N/N_0.

degree with flow-rate and mobile phase composition, but it is possible that these apparent differences are within experimental error.

Differences in chromatographic w_s values: k'/k_0 vs. N/N_0. The data in Table V show a consistent bias toward higher values of w_s from the k'/k_0 plots, compared to the corresponding N/N_0 plots: average ratio, 2.5; range, 1.3–4.5. We initially considered some possible causes for this discrepancy:

TABLE VI

EFFECT OF FLOW-RATE AND SOLVENT STRENGTH ON w_s VALUES FOR BENZYL ALCO-HOL AND THE ZORBAX ODS COLUMN.

Data from Fig. 24.

Mobile phase (methanol–water)	w_s (mg)				
	0.89 ml/min		6.8 ml/min		Average*
	k'/k_0	N/N_0	k'/k_0	N/N_0	
20:80	75	25	60	25	46
30:70	105	40	75	30	62
40:60	80	45	74	30	57
Average**:	62		49		

  * Average value for each mobile phase.
 ** Average value for each flow-rate.

(i) transient overloading of the particle surface, with a greater effect on N than on k',

(ii) poor mass distribution of the sample at the column inlet,

(iii) viscosity effects from concentrated sample solutions.

"Transient overloading" refers to the fact that as a band passes a sorbent particle, the concentration (and stationary phase load) will be higher at the outside of the particle. The Craig model does not take such an effect into account. We would expect this to be more important at higher flow-rates, where the sample has less time to come to equilibrium with the interior of the particle. In this case, plots as in Figs. 6 and 7 should show that high-flow-rate data (solid points, 6.8 ml/min) are biased toward higher values of x in Fig. 6, and toward lower values of x in Fig. 7. That is, the discrepancy in apparent w_s values should increase for higher flow-rates, if this effect is responsible for the different w_s values from k' vs. N plots. However, no such tendencies are to be found in these data. This is confirmed by the data of Table VI, which show that the ratio of w_s values from k' vs. N plots is constant (2.4 ± 0.4) as the flow-rate is varied. We therefore consider transient overloading effects as unlikely.

Poor mass distribution of the sample across the column (in a radial direction) could occur during sample injection. Again, this is not anticipated by the Craig model, and might explain the discrepancy in w_s values. This possibility was investigated by repeating one of the above studies, but with a distributor plate installed at the column inlet to improve the sample distribution during injection. The system chosen was benzyl alcohol as solute, the Zorbax ODS column, and methanol–water (40:60) at 0.89 ml/min. Resulting plots of k'/k_0 and N/N_0, as in Figs. 6 and 7 showed no difference, with or without a distributor plate.

Finally, sample viscosity as a variable was investigated by comparing 15-μl injections of highly viscous benzyl alcohol solutions with 50-μl injections of a less concentrated (therefore less viscous) solution. The volumes of both injections were such as to have no effect on N_0. Again, no effect on derived values of w_s could be seen.

At the moment, we do not have an explanation for the larger w_s values in the case of k'/k_0 plots. However, we believe that the effect is real and consistent (for data in Tables V and VI, ratio = 2.5 ± 0.8, 1 S.D.; 14 systems). Meanwhile we will simply use this ratio as an empirical constant in further applications of our model for predictive purposes.

Measuring values of w_s

The present study is intended to facilitate the design of preparative HPLC separations, by allowing predictions of separation as a function of sample size and other conditions. This approach requires an estimate of the effective column capacity w_s. We have seen that values of w_s can be obtained, either from isotherm measurements (Table II), or from chromatographic runs (Table V) plus measurement of "cumulative"* values of k' and N. Practical workers will prefer to avoid either of these alternatives, since they involve additional work and tedious procedures. Therefore, in applying our model in practice, another approach to determining "effective" values of w_s would be advantageous. This is possible, simply by measuring "band" values of k' in the usual way, for sample injections in the overload region (*e.g.*, using a small-scale column). The resulting plots of k'/k_0 *vs.* w_{xk} w_s can be used to estimate w_s, in the same way as in Fig. 6 for "cumulative" values of k'/k_0. The corresponding master curve is shown in Fig. 5c and tabulated in Table III.

Fig. 25 shows four representative plots of "band" values of k'/k_0 *vs.* w_{xk}. The curves through each data set are predicted from w_{xk} values in Fig. 5c along with the w_s values in Table V (chromatographic values from k' plots). Good agreement is seen in all four cases. For all 9 sample–column systems tested, the values of w_s obtained from fitting the k'/k_0 "band" data to the master plot in Fig. 5c showed good agreement with the values in Table V. We therefore assume that w_s values obtained from "band" elution data can be related to values obtained from "cumulative" data. Consequently, values of w_s (for k'/k_0 predictions) can be obtained for any HPLC system, using the procedure of Fig. 25.

The theoretical approach of Poppe and Kraak[16] yields a prediction of N/N_0 *vs.* w_{xN} for columns that are not too severely overloaded:

$$w_x \text{ (for } N/N_0 = 0.9) = 2(1+k_0)^2 w_s/N_0 \, k_0^2 \tag{9}$$

For a typical case from Tables III and V, we have for the benzyl alcohol–Zorbax ODS system: $w_s = 60$ mg, $N_0 = 1800$, $k_0 = 2.9$. Eqn. 9 predicts for this example that $w_x = 120$ μg should lead to a 10% decrease in N/N_0, whereas the experimental value is 35 μg. That is, the column overloads 3.5-fold faster than predicted. We have no explanation for this discrepancy, although it might be noted that this factor of 3.5 is similar to that found for experimental w_s values from N/N_0 *vs.* k'/k_0 plots (2.5-fold).

The preceding observation means that eqn. 9 appears to yield a 3.5-fold discrepancy when applied to the present experimental system (benzyl alcohol–Zorbax ODS). However the form of eqn. 9 correctly correlates values of N/N_0 *vs.* w_{xN}, as in

---

* "Cumulative" and "band" measurements of k' and N were discussed in ref. 1; (*cf.* Fig. 1 of ref. 1).
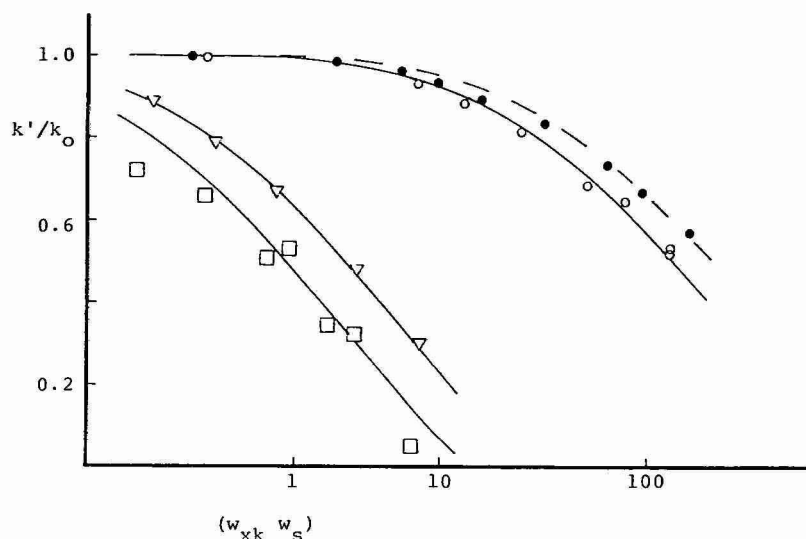
Fig. 25. Plots of "band" values of k'/k_0 vs. $w_{xk} w_s$ for different solute–column conditions. (————) Calculated curves based on w_s values from "cumulative" k'/k_0 plots of Table V plus master curve of Fig. 5c. (●) Data for benzyl alcohol and Zorbax C_8 column; (○) data for benzyl alcohol and Zorbax 150-C_8 column; (▽) data for angiotensin II and ODS column; (□) data for insulin A chain and C_8 column.

TABLE VII

COLUMN CAPACITIES w_s (TOTAL COVERAGE) ON A mg/m² BASIS

Solute–column	Pore diameter (nm)	Surface area (m²)*		w_s/SA** (mg/m²)
		Silica	Bonded-phase	
Benzyl alcohol–Zorbax ODS	6–7	200 m	110 m	0.55
Angiotensin II–Zorbax ODS	6–7	200	110	0.55
Caffeine–Zorbax C_8	10	600	530	0.22
7β-Hydroxypropyl-theophyline–Zorbax C_8	10	600	530	0.35
Benzyl alcohol–Zorbax C_8	10	200	178	0.56
Benzyl alcohol–Zorbax 150-C_8	15–17	84	78	0.91

* m²/column; silica values are experimentally determined; bonded-phase values calculated as described in text.

** Maximum w_s values for solute at large values of C_x; average of values of Table V from k'/k_0 and N/N_0 plots.

Fig. 7. Therefore any error in eqn. 9 has no effect on our present treatment (model simulation).

Column capacity values w_s as a function of pore diameter and surface area

Table VII summarizes (maximum) values of column capacity per unit surface (w_s/SA, mg/m^2) for the various systems of Table V. Eqn. 7 suggests that w_s/SA $\approx$ 0.3 mg/m^2, if the solute molecules are adsorbed in a flat configuration. It is seen (Table VII) that in all cases except for caffeine, this value is exceeded. This is expected, in that the adsorption of one monolayer of solute in a flat configuration yields a minimum surface capacity. For larger-pore-size packings (15–17 nm), w_s/SA $\approx$ 0.9 mg/m^2. That is, in this larger pore, the concentration of solute molecules sorbed on the stationary phase surface is 3-times greater than predicted by eqn. 7. Apparently, flat adsorption is not preferred in this case*. The uptake of organic solvent from reversed-phase solvent–water mobile phases has been reported equal to 2–4 monolayers[17], corresponding to w_s/SA values of 0.6–1.2 mg/m^2 (for wide-pore packings). This figure is reduced by 40% in 6-nm-pore packings[10], in agreement with the smaller w_s/SA values of Table VII for 6- to 10-nm-pore packings (0.2–0.6 mg/m^2) *vs.* 15- to 17-nm-pores (0.9 mg/m^2).

Jacobson *et al.*[13] have measured isotherms for several phenol and benzoic acid derivatives in a reversed-phase HPLC system (water as mobile phase). They found that these data follow the Langmuir isotherm over the range of C_x values studied (10 to 20-fold variation in C_x, *vs.* 100- to 1000-fold variation of C_x in our present studies). Values of w_s for this system can be determined[18], as summarized in Table VIII. These values of w_s/SA are generally lower than would be expected from Table VI for a 9-nm-pore packing (about 0.4 mg/m^2), and are quite variable. With water as mobile phase in this system, it is possible that the bonded-phase surface is sufficiently collapsed to prevent any penetration of solute molecules into the bonded phase. If so, the maximum column capacity should be given by eqn. 7; *i.e.*, 0.3 mg/m^2. The monofunctional phenols and anilines in fact have w_s/SA values in this range; *i.e.* 0.21–0.65 mg/m^2. The data in Table VI further support the proposal that values of w_s may be lower for water as mobile phase, in that a 20% reduction in w_s was observed for 20% (v/v) methanol compared to 30 or 40% methanol mobile phases (Table VI).

The much lower w_s/SA values for the benzoic acids of Table VIII probably arise from competitive adsorption of the ionized solute. That is, initially adsorbed solute molecules (carrying a negative charge) create a negative charge on the column-packing surface, and this discourages further sorption of negatively-charged sample molecules (note similar effects in ion-pairing; Fig. 4 of ref. 19). The solute *p*-aminobenzoic acid has a very low value of w_s/SA, similar to that for angiotensin II or insulin A chain in Table V. *p*-Aminobenzoic acid probably exists as the zwitterion, and it may be retained on silanols by cation exchange. If this is the case, w_s for this compound should be lower by about 2 orders of magnitude (*cf.* values of w_s in Table V), and this is roughly the case.

Resorcinol and hydroquinone have intermediate values of w_s/SA, which may reflect the presence of two strongly hydrogen-bonding groups in the molecule. These

---

* Alternatives to flat adsorption include vertical adsorption, which may involve partial penetration into the bonded phase, as well as an actual partitioning into the stationary phase.

TABLE VIII

VALUES OF w_s/SA FROM THE STUDY OF JACOBSON et al.[13]

C_{18}, 9-nm-pore column; water as mobile phase, buffered at pH = 6.3 for benzoic acid derivatives only.

Solute	w_s/SA $(mg/m^2)^*$
Phenol	0.21
Resorcinol	0.09
Hydroquinone	0.03
m-Cresol	0.33
p-cresol	0.47
o-Toluidine	0.46
p-Toluidine	0.65
Benzoic acid	0.04
p-Aminobenzoic acid	0.004
m-Nitrobenzoic acid	0.05
2-Amino-4-nitrophenol	0.21

* Calculated from the bonded-phase surface area, assuming that this equals 0.72 times the silica surface area (220 m²/g) (Table III).

probably prevent the molecule from penetrating the non-polar hydrocarbon phase, forcing flat-wise adsorption which then requires more surface area per molecule.

From the foregoing discussion it may be concluded that predicting values of w_s for a given reversed-phase system is at best uncertain. However, for uncharged molecules it appears that w_s will vary from 0.2 to 1.0 mg/m² of silica surface, being larger for wider-pore packings. Much lower values of w_s are possible, whenever silanols play a major role in sample retention and/or the solute molecule carries a charge.

Using the present model to predict the elution band

The data in Figs. 6–24 suggest that values of k' and N should be accurately predictable as a function of sample size, once values of k_0, N_0 and w_s have been determined. Since this is somewhat complicated, it is useful to summarize our predictive scheme in detail:

(i) Run initial chromatograms to obtain values of k_0 and N_0 (small sample, analytical-scale column).

(ii) Run 3–5 additional chromatograms (same column) with larger samples, such that k'/k_0 is decreased to about 0.9 or less.

(iii) Plot "band" values of k'/k_0 vs. $\{[k_0/(1 + k_0)] N^{\frac{1}{2}} w_x\}$ and superimpose these data onto Fig. 5c (or values of Table IV) in order to determine w_s (band).

(iv) Cumulative values of w_s are given as 1.0 w_s (band) for k'/k_0; 0.4 w_s (band) for N/N_0.

(v) Use the values (iv) of w_s (cumulative) plus k_0 and N_0 to obtain values of k' and N from Fig. 5 (or Table IV).

(vi) With these values of k', N and w_s, predict the elution curve (as described in Appendix II of ref. 1) for the scaled-up separation (same packing), assuming that w_s is proportional to the column volume.

Examples of the prediction of actual elution curves are shown in Fig. 26 for benzyl alcohol and the 150-C_8 column. Sample sizes of 0.01–1.6 mg are used, resulting in large changes in the elution band. The experimental data points are seen to track the predicted elution curves closely, except for the 1.6-mg-run. N/N_0 for this run was predicted by our model to be about 0.08, while the actual experimental value was $N/N_0 = 0.05$. The present model appears to be less accurate for heavily overloaded columns.

A similar comparison for insulin A chain as solute and a C_8 column is shown in Fig. 27. The agreement between experimental and predicted elution curves is similar to that seen in Fig. 26.

CONCLUSION

The preceding paper presented a model for predicting elution bands under overload conditions. This model is based on a Craig-distribution process, with assumption of a Langmuir isotherm. In the present study we examined other isotherm types, both theoretically and experimentally. It appears that many HPLC isotherms fail to meet all the requirements for Langmuir sorption. For example, sorption sites of different types (or energy) can be present in the stationary phase, ionized solutes may exhibit competitive adsorption, etc.
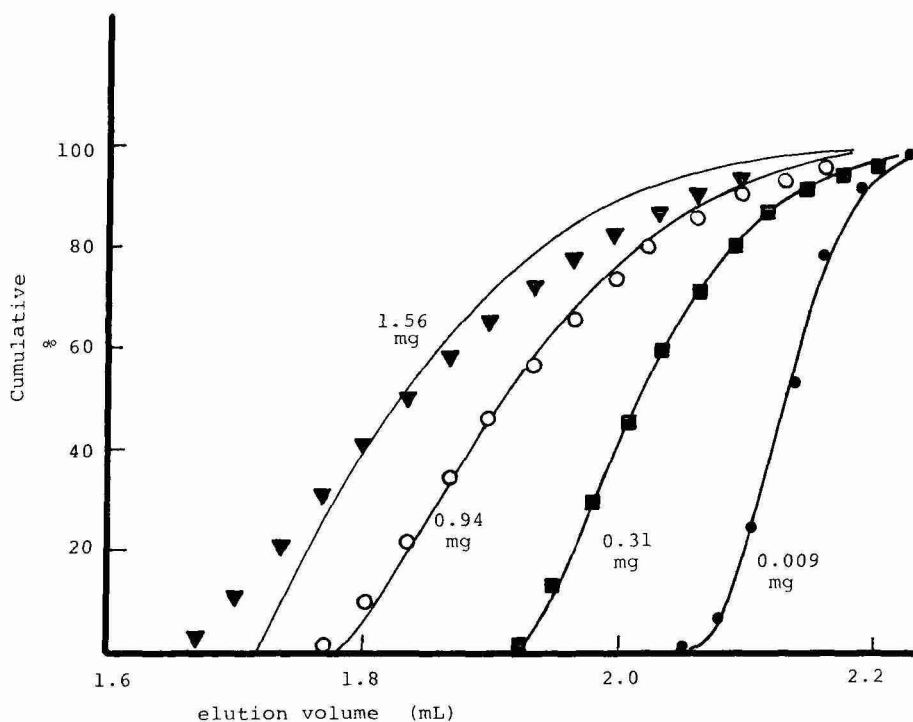
Fig. 26. Experimental *vs.* predicted elution curves for benzyl alcohol and Zorbax 150-C_8 column as a function of sample size. (———) Predicted curves as described in text. (●) Data points for 9.4 μg; (■) 314 μg; (○) 940 μg; (▼) 1560 μg.
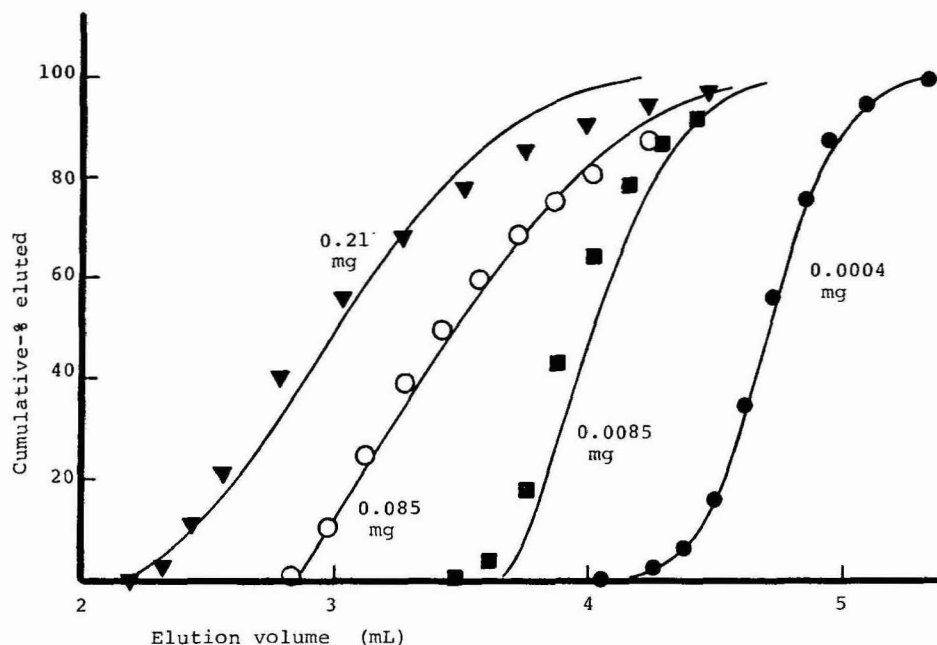
Fig. 27. Experimental *vs.* predicted elution curves for insulin A chain and Zorbax C_8 column as a function of sample size. (————) Predicted curves, as described in text. (●) Data points for 0.42 μg; (■) 8.5 μg; (○) 84.6 μg; (▼) 212 μg.

In many cases (including the Freundlich isotherm), these non-Langmuir isotherms closely resemble the Langmuir isotherm within a certain range of sample concentrations. Our model is then able to predict separation under overload conditions with reasonable accuracy. A general characteristic of these non-Langmuir systems is that the "apparent" column-saturation capacity w_s (as reflected in chromatographic performance at overload) is lower than the actual capacity of the column (as determined at high solute concentrations). We describe how the "apparent" w_s value for a given sample and column can be measured conveniently. Maximum values of the column capacity w_s occur for non-ionic samples (or for systems where silanol-retention effects are minimized).

Nine different reversed-phase systems were studied experimentally in an overload mode (5 solutes, 4 columns). Elution curves could be accurately predicted for these various experiments, using the present model. This provides a basis for extending our approach to the prediction of separations that involve two or more co-eluting solutes. This work is near completion and will be described within the near future.

APPENDIX I

Calculating the isotherm for the case of a large solute molecule displacing several small solvent molecules

The equilibrium constant K is related to mole fractions of X and M in the adsorbed (a) and liquid (m) phases as

$$K = N_{xa} N_{mm}^n / N_{xm} N_{ma}^n \tag{A1}$$
$$\approx N_{xa} / N_x N_{ma}^n$$

Here N_{xa} refers to the mole fraction of solute X in the adsorbed phase (a), N_x is the mole fraction of X in the mobile phase, and N_{ma} is the mole fraction of mobile phase in the adsorbed phase. Eqn. A1 assumes that the mole fraction of solute in the mobile phase (N_x) is always small, which is a good approximation for most cases. If the densities of X and M are assumed equal, then the capacity factor k' can be expressed as

$$k' = \varphi \theta_x / C_x \tag{A2}$$

θ_x is the fraction of the surface covered by molecule X, C_x is the concentration (g/ml) of sample in the mobile phase, and φ is the phase ratio — equal to the weight of a monolayer of sample or mobile phase (assumed equal here) divided by the column dead volume V_m.

The mole fraction of X in the mobile phase N is given by

$$N = (\text{moles X})/(\text{total moles})$$
$$= (C_x/M_x)/[C_x/M_x) + (C_s/M_s)]$$
$$\approx C_x(M_s/M_x) = C_x/n \tag{A3}$$

Eqn. A3 assumes that N_x (and C_x) is small, and that (M_x/M_m) is equal to n. In similar fashion we have

$$N_{xa} = (\theta_x/n)/[(\theta_x/n) + \theta_s] \tag{A4}$$

and

$$N_{sa} = \theta/[(\theta_x/n) + \theta_s] \tag{A5}$$

Beginning with values of θ_x, K, n and φ, a value of k' can be determined from the above relationships: $\theta_s = (1 - \theta_x)$, and N_{xa} and N_{sa} are determined from eqns. A4 and A5. These quantities are next substituted into eqn. A1 to obtain N_x. C_x is then calculated from N_x and eqn. A3.

REFERENCES

1 J. E. Eble, P. E. Antle, R. L. Grob and L. R. Snyder, *J. Chromatogr.*, 384 (1987) 25.
2 L. R. Snyder, *Principles of Adsorption Chromatography*, Marcel Dekker, New York, 1968.
3 L. R. Snyder and H. Poppe, *J. Chromatogr.*, 184 (1980) 363.
4 L. R. Snyder, in Cs. Horváth (Editor), *High-performance Liquid Chromatography. Advances and Perspectives*, Vol. 3, Academic Press, New York, 1983, p. 157.
5 M. Jaroniec, J. K. Różylo and W. Gołkiewicz, *J. Chromatogr.*, 178 (1979) 27.
6 W. Rudzinski and J. N-Michalek, *J. Chem. Soc., Faraday Trans. 1*, 81 (1985) 553.
7 X. Geng and F. E. Regnier, *J. Chromatogr.*, 296 (1984) 15.
8 X. Geng and F. E. Regnier, *J. Chromatogr.*, 332 (1985) 147.

9 J. P. Larman, J. J. DeStefano, A. P. Goldberg, R. W. Stout, L. R. Snyder and M. A. Stadalius, *J. Chromatogr.*, 255 (1983) 163.
10 M. A. Quarry, R. L. Grob and L. R. Snyder, *J. Chromatogr.*, 285 (1984) 19.
11 A. Tchapla, H. Colin and G. Guiochon, *Anal. Chem.*, 56 (1984) 621.
12 A. W. J. de Jong, J. C. Kraak, H. Poppe and F. Nooitgedacht, *J. Chromatogr.*, 193 (1980) 181.
13 J. Jacobson, J. Frenz and Cs. Horváth, *J. Chromatogr.*, 316 (1984) 53.
14 U. Lund, *J. Liq. Chromatogr.*, 4 (1981) 1933.
15 J. E. Eble, *Thesis*, Villanova University, Villanova, PA, 1986.
16 H. Poppe and J. C. Kraak, *J. Chromatogr.*, 255 (1983) 395.
17 N. Le Ha, J. Ungvaral and E. sz. Kovats, *Anal. Chem.*, 54 (1982) 2410.
18 Cs. Horváth, personal communication.
19 J. H. Knox and R. A. Hartwick, *J. Chromatogr.*, 204 (1981) 3.

CHROMSYMP. 1027

EFFECT OF COLUMN DEGRADATION ON THE REVERSED-PHASE HIGH-PERFORMANCE LIQUID CHROMATOGRAPHIC SEPARATION OF PEPTIDES AND PROTEINS

J. L. GLAJCH*, J. J. KIRKLAND and J. KÖHLER*

Central Research and Development Department, E. I. du Pont de Nemours and Company, Experimental Station, Wilmington, DE 19898 (U.S.A.)

SUMMARY

Many reversed-phase separations of proteins and peptides are currently performed in acidic mobile phases, *e.g.*, 0.1% trifluoroacteic acid in water (pH 2) with organic modifiers. Such conditions are known to promote the cleavage of the silane from the silica in bonded-phase columns, especially for monomeric stationary phases. The stability of some columns commonly used for proteins and peptides has been examined, and it has been shown by both chromatographic and elemental analysis that degradation occurs very rapidly with fresh, "totally covered" column materials. Despite the loss of over half of the bonded phase in some cases, certain columns still exhibit adequate chromatographic performance, although reproducibility can be affected. The implications of these results with respect to both bonded-phase synthesis and mechanistic interpretation of chromatographic data is discussed.

INTRODUCTION

The use of high-performance liquid chromatography (HPLC) for the separation and purification of unmodified or unprotected peptides and proteins has increased dramatically in the past ten years. Although a number of different modes of chromatography have been used, such as size-exclusion, ion-exchange, and affinity chromatography, the focus has been on reversed-phase separations. The introduction of trifluoroacetic acid or heptafluorobutyric acid[1,2] into aqueous–organic solvent systems was the main reason for the explosive growth in the reversed-phase separations of proteins and peptides. These reagents have been important in minimizing mixed-mode effects in HPLC, *i.e.*, avoiding secondary equilibrium effects due to the partial ionization of amine or carboxylic acid groups prevalent in peptides and proteins. The more common mobile phase systems for separating peptides and proteins have a relatively low pH of 2–3. These systems generally are preferred, because of

---

* Permanent address: Max-Planck-Institut für Kohlenforschung, Kaiser-Wilhelm-Platz 1, 4330 Mulheim/Ruhr, F.R.G.

(1) increased solubility of the peptides/proteins at low pH, (2) complete ionization of the amino groups, and (3) easy removal of the reagents for subsequent analysis.

Reversed-phase packings fall into two general classes: fully polymeric materials and silica with alkyl modifiers. Although most polymeric column packings have the advantage of wide pH stability, silica-based columns are still more widely employed, since they can be prepared with a variety of alkyl groups, e.g., trimethylsilyl, C_3, C_4, C_8, C_{18}, CN, phenyl. In addition, silica-based particles are stronger than polymeric beads, and this increased strength is critical in preparative and process separations. Most importantly, silica-based packings exhibit higher column efficiencies because of their superior mass transfer characteristics.

Bonded-phase columns are a preferred media for HPLC separations because of their convenience and relatively high stability. If operated properly, bonded-phase columns provide reproducible separations under a variety of mobile phase conditions. Especially convenient is the rapid re-equilibration of the bonded stationary phase with the mobile phase, which is a great advantage in gradient elution separations. However, covalently bonded alkyl groups, formed by the reaction of chloro- or alkoxysilanes with hydroxylated silica, are not completely stable. The siloxane bond connecting the silane to the silica support is relatively easily hydrolyzed at low pH in aqueous solutions.

During optimization studies on the separation of the phenylthiohydantoin (PTH)-amino acids, we noted that C_8 reversed-phase columns rapidly deteriorated in phosphoric acid (pH 2.1)–methanol solutions[3]. Qualitatively, the same effect was observed for other acids in the same study. These results were obtained on alkyl reversed-phase columns similar to those that are widely used for peptide and protein separations at low pH. Since this is an important application, we decided to investigate this effect systematically. In particular, we were interested in (1) the rate of column deterioration under usual operating conditions, (2) possible effect of this deterioration on separations, and (3) ways to develop more stable bonded-phase columns.

EXPERIMENTAL

All measurements were carried out with a Model 8800 liquid chromatograph with a four-solvent pumping system, a heated column compartment, maintained at either 35 or 50°C, and a Model 860 variable-wavelength detector (Du Pont Biomedical Products Department, Wilmington, DE, U.S.A.). Samples were injected with either a 6-port sampling valve (Valco Instruments, Houston, TX, U.S.A.) or a WISP autoinjector (Millipore, Waters Chromatography Division, Milford, MA, U.S.A.).

Vydac 214TP5 (Separations Group, Hesperia, CA, U.S.A.) and Ultrapore RPSC (Beckman Instruments, Berkeley, CA, U.S.A.) columns were used as received. The Vydac columns and Ultrapore columns were 15 × 0.46 cm I.D. and 7.5 × 0.46 cm I.D., respectively. The physical characterization of packings from fresh columns was performed after unpacking an unused column from the same lot as the column used for chromatographic testing. Nucleosil columns with polymerized stationary phases were prepared by procedures detailed elsewhere[4,5]. Zorbax silica was hydroxylated by procedures described by Köhler and Kirkland[6,7] and allowed to react with silanes as described in ref. 8. All column materials were packed into 15 × 0.46

cm I.D. tubes (Alltech Associates, Deerfield, IL, U.S.A.) by conventional proce-
dures[9].

LC-grade methanol, acetonitrile, and water (J. T. Baker, Phillipsburg, NJ,
U.S.A.) were used for all studies. Trifluoroacetic acid (TFA) (Ionate grade, Pierce,
Rockford, IL, U.S.A.) was used to prepare 0.1% (v/v) solutions in both water and
acetonitrile. Lysozyme, ovalbumin (Sigma, St. Louis, MO, U.S.A.), and melittin
(United States Biochemicals, Cleveland, OH, U.S.A.) were used as test solutes. So-
lutions of 0.5–1.0 mg/ml were prepared for the gradient elution studies. N,N-diethy-
laniline, 1-phenylpentanol, 1-phenylhexane, and 1-phenylheptane were obtained
from Aldrich (Milwaukee, WI, U.S.A.) and dissolved to make solutions of 0.05–1.7
mg/ml in methanol–water (50:50) for testing. Trimethylchlorosilane was obtained
from Petrarch Systems (Bristol, PA, U.S.A.).

Initial isocratic measurements were performed with methanol–water mobile
phase systems ranging from 50:50 to 70:30 to obtain reasonable k' values for a spe-
cific column. Measurements of k' for the neutral 1-phenylheptane solute under iso-
cratic conditions were used as a measure of the level of alkyl ligand remaining on
the column packing during the deterioration of the stationary phase. Measurements
were repeated under the same conditions after subjecting the columns to water–
acetonitrile–TFA gradient elution conditions. Thus, isocratic measurements were
performed on most columns with water–TFA and acetonitrile–TFA under isocratic
conditions which were then alternated with the gradient elution conditions for col-
umn deterioration measurements.

Data were collected and analyzed on a Hewlett-Packard 3357 Laboratory Au-
tomation System (LAS). Chromatograms were plotted using CPLOT software and
other data analysis were performed using RS/1 (BBN Research Systems, Cambridge,
MA, U.S.A.) software on a VAX-11/780 computer (Digital, Maynard, MA, U.S.A.).

RESULTS AND DISCUSSION

Literature reports[10,11] indicate that certain reversed-phase columns produce
better results than others in the separation of some biomolecules and basic solutes.
Our work[11] confirmed this effect, and we concluded that the less active Type B
silicas[11] are to be preferred for best separations and highest recoveries. All of the
silicas used in this study were of Type B. These were chosen for study on the basis
our experience and the experience of others that suggested that columns produced
from these silicas were among the most useful for reversed-phase separations of pep-
tides and proteins.

In order to compare various columns materials systematically, we subjected
each silica and bonded-phase packing to several analyses prior to actual chromato-
graphic testing. Ultrapore RPSC and Vydac 214TP5 were available only in prepacked
columns; therefore, characterizations were performed on material from columns of
the same lot to insure representative results.

The surface area for each column packing was measured by the Brunauer-
Emmett-Teller (BET) method, using nitrogen adsorption. Pore-size-distributions
were determined by mercury porosimetry. Bonded-phase materials were analyzed for
carbon, hydrogen and nitrogen by elemental analyses both prior to use and after
gradient elution testing with the TFA–water–acetonitrile mobile phases. These data
are summarized in Table I.

TABLE I

COLUMN PACKING CHARACTERIZATION

Nominal particle size, 7–8 μm; k' measured in acetonitrile–water (50:50) with 0.1% TFA in both solvents except as noted.

Column packing	Surface area (m^2/g)	Average pore size $(\mathring{A})$	Organic ligand	Carbon analysis		k' of 1-phenyl heptane		Purge column volumes
				%C initial	%C final	Initial	Final	
Nucleosil®-Cl	86	248	C_1	1.3	0.3	7.95*	<0.1*	3663
Nucleosil®-PMSCl	86	248	C_1 (polymer)	9.0	1.7	7.42**	2.82**	3639
Ultrapore® RPSC	81	228	C_3	1.7	1.4	3.58	1.06	7906
Vydac® 214TP5	78	312***	C_4	3.3	2.6	5.62	3.55	3459
Zorbax®-Cl	58	280	C_1	1.0	0.4	15.51	0.80	785

* k' measured in methanol–water (50:50).
** k' measured in methanol–water (70:30).
*** Pore size is actually bimodal (150 Å, 435 Å).

Scanning electron micrographs were obtained on each of the silicas to deter-
mine an approximate particle size and shape. Micrographs of various particles are
shown in Fig. 1. It appears that these four column packings represent at least three
different silica types. Nucleosil is spherical and appears to have an outer shell around
each particle. Zorbax is also spherical and shows the characteristic appearance of a
particle made by the coascervation of collodial silica. Ultrapore and Vydac materials
are both more irregular in shape; each encompasses a wider particle size and shape
distribution than the Nucleosil and Zorbax packings. In our experience, columns of
Nucleosil and Vydac are less stable to high pressure, and columns made of these
materials exhibit higher back-pressures than Zorbax columns.

Before using each column for the gradient elution separation of peptides and
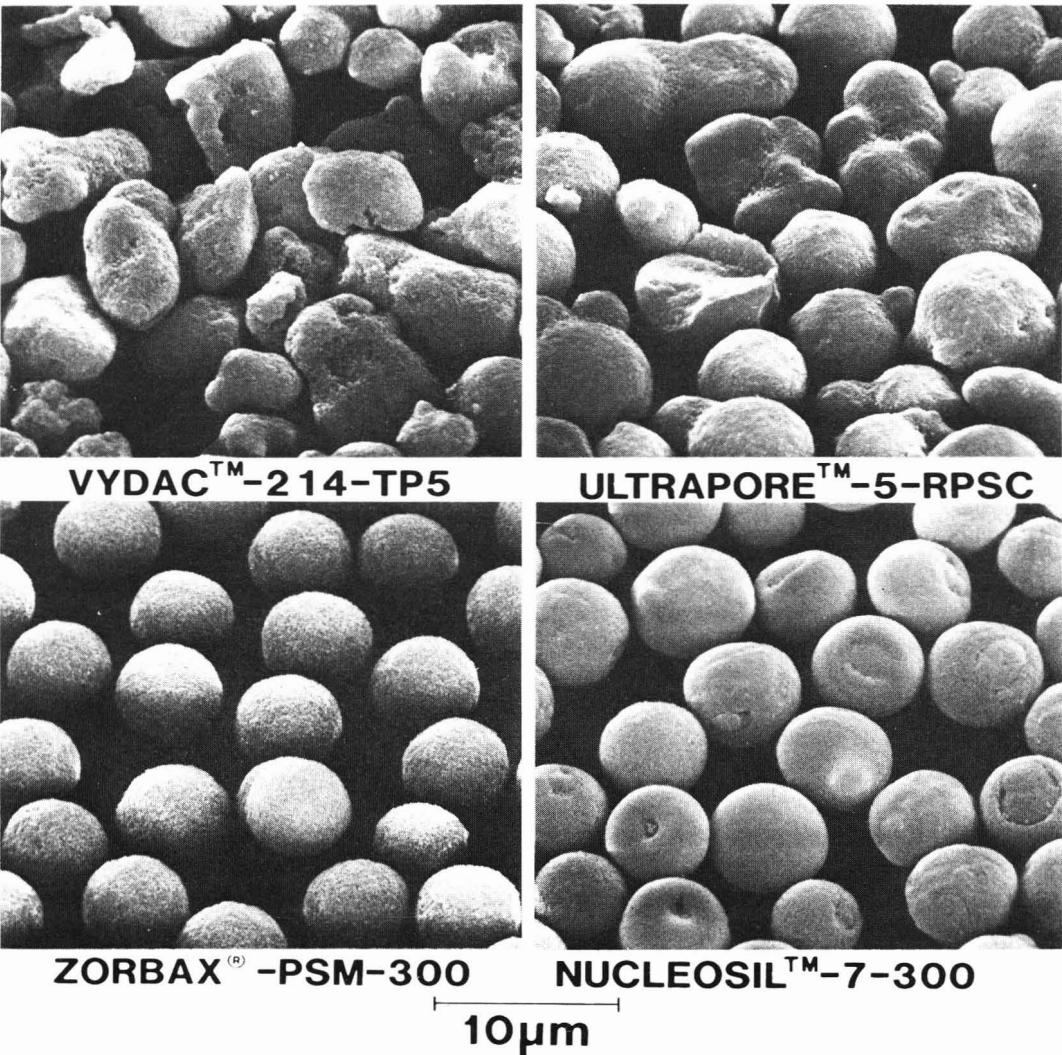
Fig. 1. Scanning electron micrographs of silica particles used in this study.

proteins, we measured the isocratic retention of a mixture of 1-phenylpentanol (unretained), 1-phenylhexane, 1-phenylheptane, and N,N-diethylaniline (N,N-DEA) using methanol–water mobile phases ranging in composition from 50:50 to 70:30, depending on the bonded phase being examined. N,N-DEA has previously been shown to be a useful indicator of undesirable acidic sites on adsorptive silica packings[11]; however, none of the Type B silica columns in this work exhibited any adsorptive properties toward this basic solute. 1-Phenylheptane was used to ascertain the amount of bonded phase on the silica after exposure to the gradient elution process, as a measure of bonded-phase loss. Values obtained in the column deterioration study are shown in Table I. Similar information might have been obtained from elemental carbon analysis, but unfortunately, this method is imprecise at the low carbon levels on the packings of interest.

In the column deterioration studies, each column was kept in contact with solution for a total of 96 h at a flow-rate of 1.0 ml/min, with 0.1% TFA in water (A) and 0.1% TFA in acetonitrile (B) mobile phases at 50°C. The gradient used was generally 0 to 100% B in 80 min with isocratic steps at 100% B and 0% B for equilibration. Measurements of the retention time of 1-phenylheptane under isocratic conditions were performed at 50% B so that the average mobile phase composition contacting any column during the entire 96 h testing period was always 50% B.

Capacity factor (k') data for 1-phenylheptane in these tests are shown in Fig. 2 for three of the columns studied. These data show that each column significantly loses retention for the neutral test sample during the relatively short study period. The three complete plots in Fig. 2 are for Zorbax-C_1. Ultrapore RPSC, and Vydac 214TP5 columns, and represent retentions measured with the TFA–water–acetonitrile system. The two-point (start/final) measurements in methanol–water (in Table I but not shown in Fig. 2) on the covalently bonded and polymer-coated Nucleosil columns are in general agreement with the full curves for the other columns.

The full deterioration curves of Fig. 2 suggest an exponential retention time decay or a first-order rate loss of the bonded phase under these conditions. However,
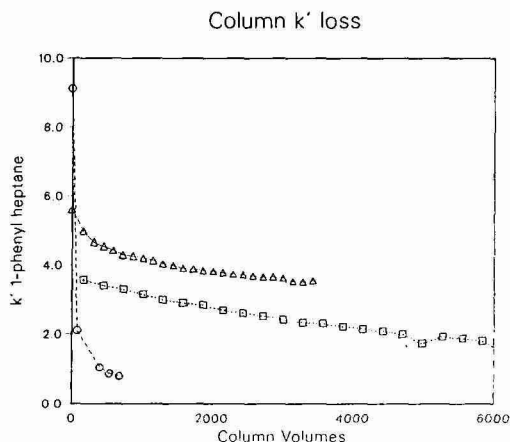
Fig. 2. Capacity factor (k') of 1-phenylheptane as a function of volume of mobile phase passed through the column in the gradient elution testing. Conditions given in the text. △ = Vydac C_4, □ = Ultrapore C_3, ○ = Zorbax C_1.

simple analysis of the data is not possible. Both the Vydac (C_4) and Ultrapore (C_3) columns are known to be endcapped with trimethylchlorosilane. It is well known that trimethylsilyl groups are most easily hydrolyzed and lost from silica surfaces[11]. Thus, it is likely that two species (trimethyl, and C_3 or C_4) are being lost from these columns simultaneously at different rates. Further studies are underway in our laboratories to clarify this point.

Further evidence that bonded phase is being lost from these columns can be seen by the %C data in Table I. In all cases, a significant fraction of the bonded phase is lost as a result of the gradient elution with acetonitrile–water–TFA. As anticipated from a previous study[11], the Nucleosil- and Zorbax-TMS columns lost organic ligand more rapidly than Ultrapore or Vydac. However, the data in Table I show that a significant loss of organic ligand also takes place from the latter materials. It is obvious that none of these packings remained fully covered after four days of gradient elution under typical conditions for the separation of peptides and proteins. Nucleosil-PMSCl, having a polymer coating prepared by cross-linking polysiloxane[4,5] appears somewhat more stable than Nucleosil-Cl. From the data in Fig. 2 and Table I, one would expect that the TMS columns have no practical utility, but the discussion below indicates otherwise.

An important consequence of the loss of bonded phase during use is that significant organic material must be eluted from the column during gradient elution. Estimations of ligand loss for each of the columns during the 96 h period show that 8–38 μmol of silane are lost (depending on the ligand) in the 1300–6700 ml of mobile phase used in the tests. It is unlikely that the loss is evenly distributed. We speculate that ligand degradation (hydrolysis) occurs preferentially in mobile phases with a low organic solvent content, while the organic ligand is eluted from the column preferentially at higher organic solvent concentrations. We estimate the average ligand loss during the experiments to be 1–25 nmol/ml of mobile phase. Obviously, elution of such contaminating organic ligand material at this level would have serious consequences for both analytical and preparative or process separations. The level of contaminating silane in the mobile phase could actually be higher than the level of the peptide or protein being chromatographed. This fact can make the identification of isolates by mass spectrometry and other techniques very difficult. We speculate that some problems regarding recovery and reproducibility of peptide and protein separations could actually be due to column degradation and contamination of the eluent with silane; however this point requires further study.

It is instructive to look at the retention of a peptide–protein mixture on both "fresh" and "used" columns, *i.e.*, when a significant amount of bonded phase has been stripped from the column. Lysozyme, melittin, and ovalbumin were chosen as test solutes because these compounds represent "easy" (lysozyme), strongly basic (melittin, 2 peaks), and "difficult" (ovalbumin) compounds for reversed-phase HPLC, based on experiences in our laboratories and outside reports. Fig. 3 show the generally satisfactory separations after the first and last (24th) injection for gradient elution separations of these three solutes with an Ultrapore RPSC column. Clearly, retention for all of the peaks has decreased during column use, and there is some loss in resolution, especially for the second melittin peak and ovalbumin peak. However, this resolution loss is not as great as anticipated from the isocratic retention data, which showed that *ca.* 40% of the organic bonded phase had been removed from the column.
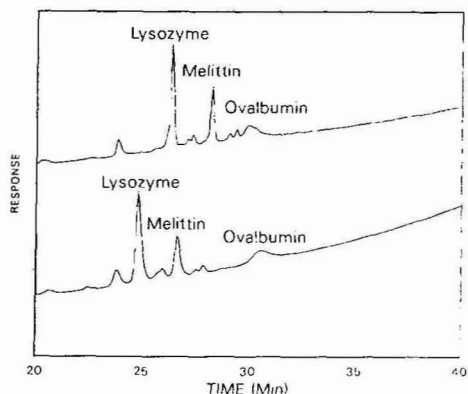
Fig. 3. Separation of lysozyme, melittin and ovalbumin on Ultrapore C_3 column. Top chromatogram is first gradient injection; bottom chromatogram is after 6000 column volumes of gradient use.

Data from the other columns were similar to that for Ultrapore-C_3, although the absolute rate of bonded phase loss was dependent on the substituent ligand. These results confirm our general hypothesis that aqueous–organic solvent systems at low pH gradients are deleterious to bonded-phase stability. Note, however, that full coverage of the surface apparently is not required for good peak shape and convenient separation of biomolecules, provided columns are based on the less adsorptive Type B silicas. Bonded-phase loss in TFA-containing mobile phases occurs fairly rapidly with fresh columns (see results for the first 1000 ml of mobile phase for each column in Fig. 2). Thus, it appears that most reversed-phse protein separations are now probably performed on silicas that are only partially covered with ligand. This result is in contrast to the frequently-held position that a fully bonded packing is required to prevent deleterious interaction of proteins and other macromolecules with residual silanols on the packing surface.

To further demonstrate the effectiveness of protein reversed-phase separations on partially covered bonded-phase silicas, we prepared two additional columns of silica, modified with trimethylchlorosilane (C_1 phase). The first column contained a silica which had been totally rehydroxylated[6,7]. The second column contained the same silica which was incompletely rehydroxylated and this silica was subjected to the identical reaction with trimethylchlorosilane. Isocratic retention and subsequent %C data showed that the columns were similar in retention for a non-polar solute. However, the initial peptide/protein chromatograms in Fig. 4 clearly demonstrate that the column made from completely rehydroxylated silica gave an adequate separation, while the column made from incompletely rehydroxylated silica became totally unusable after the first injection. The latter column was immediately retested with 1-phenylheptane in the isocratic test. It showed that only 5–10% of the bonded phase had been lost from the original column. This level of degradation was subsequently confirmed by %C analysis.

Finally, a third C_1 column, prepared from completely rehydroxylated silica, was tested initially with a melittin mixture and used intermittently for one month for both synthetic test mixtures and unknown samples for protein sequencing. Although C_1 phases are known to be relatively unstable, this column, nonetheless, was useful,
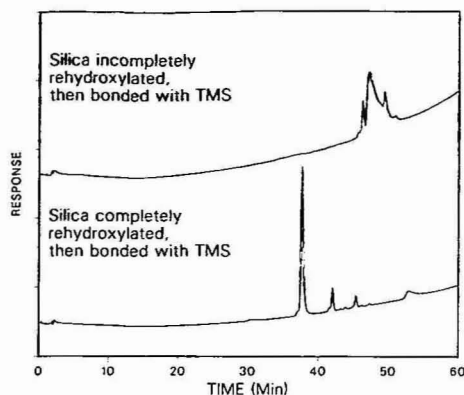
Fig. 4. Effect of silica support treatment on separation of lysozyme, melittin, and ovalbumin. Top chromatogram is silica which was incompletely rehydroxylated and then modified with trimethylchlorosilane. Bottom chromatogram is silica which had been completely rehydroxylated and then modified with trimethylchlorosilane.

especially for very hydrophobic proteins that are difficult to separate on other column types[12]. During this period of application, the column was retested with a melittin mixture and, as shown in Fig. 5, it exhibited retention and separation characteristics similar to those measured when the column was initially prepared. Isocratic measurements performed with 1-phenylheptane showed a significant loss of retention ($>50\%$) when the second melittin sample was run. Subsequent elemental analysis confirmed that the column had only *ca.* 50% of the initial carbon content remaining on the surface; despite this, the separation was still satisfactory.
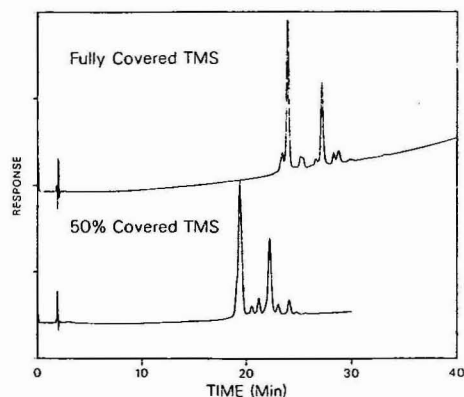
Fig. 5. Effect of bonded-phase loss on the separation of an impure melittin sample. Top chromatogram is a fresh, fully-reacted TMS column. Bottom chromatogram is a used column which has lost *ca.* 50% of the TMS bonded-phase.

CONCLUSIONS

From the data in this study, we can draw some important conclusions about reversed-phase columns as applied to protein separations. First, the type and state of silica support for the packing is important to insure a satisfactory initial separation and repeatable results. This effect has been previously described[10,11]. However, we now know the factors that are necessary to insure the desired results: complete re-hydroxylation of the silica support surface and generation of a homogeneous population of silanol groups prior to bonding.

Second, all of the columns examined lost significant amounts of bonded phase during use with TFA–water–acetonitrile gradients. However, all columns performed well in the separation of certain proteins, even when 50% of the original covalently bonded stationary phase was lost from the packing. This result implies that complete coverage of the proper silica support is not required for protein separations. However, it may be concluded, that a stable, full coverage of the support could be more desirable for reproducible separations by true reversed-partition.

Finally, although longer chain-length bonded-phase materials appear to be more stable than short-chain length ligands, e.g., $C_4 > C_3 > C_1$, C_1 columns exhibit significant utility despite relative instability of the organic ligand. Certainly, improved column stability would be desirable, and we are currently working on this aspect of reversed-phase columns.

ACKNOWLEDGEMENTS

REFERENCES

1 H. J. P. Bennett, A. M. Hudson, C. McMartin and G. E. Purdon, *Biochem. J.*, 168 (1977) 9.
2 H. J. P. Bennett, C. A. Browne and S. Solomon, *J. Liq. Chromatogr.*, 3 (1980) 1353.
3 J. L. Glajch, J. C. Gluckman, J. G. Charikofsky, J. M. Minor and J. J. Kirkland, *J. Chromatogr.*, 318 (1985) 23.
4 U. Bien-Vogelsang, A. Deege, H. Figge, J. Köhler and G. Schomburg, *Chromatographia*, 19 (1984) 170.
5 H. Figge, A. Deege, J. Köhler and G. Schomburg, *J. Chromatogr.*, 351 (1986) 393.
6 J. Kohler and J. J. Kirkland, *U.S. Pat. Appl. No. 798,332* (1985).
7 J. Kohler and J. J. Kirkland, 385 (1987) 125.
8 L. R. Snyder and J. J. Kirkland, *An Introduction to Modern Liquid Chromatography*, Wiley-Interscience, New York, 2nd ed., 1979, Ch. 7.
9 L. R. Snyder and J. J. Kirkland, *An Introduction to Modern Liquid Chromatography*, Wiley-Interscience, New York, 2nd ed., 1979, Ch. 5.
10 J. D. Pearson, N. T. Lin and F. E. Regnier, *Anal. Biochem.*, 124 (1982) 217.
11 J. Köhler, D. B. Chase, R. D. Farlee, A. J. Vega and J. J. Kirkland, *J. Chromatogr.*, 352 (1986) 275.
12 J. L. Glajch, R. M. Kutny and J. E. Shively, in preparation.

CHROMSYMP. 1021

PEAK-DECAY METHOD FOR THE MEASUREMENT OF DISSOCIATION RATE CONSTANTS BY HIGH-PERFORMANCE AFFINITY CHROMATOGRAPHY

ROBERT M. MOORE and RODNEY R. WALTERS*,*

Department of Chemistry, Iowa State University, Ames, IA 50011 (U.S.A.)

SUMMARY

A new method was described for the measurement of dissociation rate constants of biological complexes by affinity chromatography. Theory and computer modeling were used to establish conditions such that each solute molecule would undergo only a single dissociation step during its passage through the column. As a result, the dissociation rate constant could easily be determined from the slope of the logarithm of the tailing portion of the peak. An experimental system, consisting of immobilized concanavalin A and a fluorescent sugar, was used to test the theory and to compare the peak-decay method with the conventional isocratic method.

INTRODUCTION

Affinity chromatography can be used to estimate the association and dissociation rate constants of biological complexes. Several experimental modes may be used for such measurements.

The broadening of a band of solute, applied to a column containing immobilized affinity ligand, is measured in the isocratic, competitive elution, zonal mode by using one or more competing inhibitor concentrations[1,2]. Although this method has been applied several times, the measured rate constants have generally been one or more orders of magnitude lower than expected from free solution studies[3–6]. A recent paper has suggested that these apparent low values may have been due to inadequacies in the band-broadening theories used for the calculations and/or the dominance of mass transport-caused band-broadening over slow adsorption–desorption kinetic band-broadening[7].

Rate and equilibrium constants may also be measured in the frontal mode by utilizing the shapes and positions of the break-through curves for several concentrations of solute applied to the column[8]. This method has not yet been examined with biological complexes having known rate constants.

In the split-peak zonal mode, the association rate constant can be determined

---

using data from several flow-rates under conditions where some of the solute does not have time to become adsorbed on immobilized ligand during its passage through the column and is thus eluted in the column void volume[9]. This method has also not yet been tested with complexes of known rate constants.

This paper describes a new method for determining dissociation rate constants. This method, called the "peak-decay" method, eliminates certain disadvantages of the isocratic method; specifically, the need to measure peak variances, the need to perform calculations as a function of capacity factor (k'), and the need to use linear elution conditions. The peak-decay method does require the use of a competitive inhibitor; however, the kinetic effects of non-competitive eluents can also be studied.

THEORY

The theory for the peak-decay method is based on the model utilized by Hethcote and DeLisi[1] for isocratic affinity chromatography. The model assumes that there are two reversible rate processes occurring in the column, a diffusional mass transport step and an adsorption–desorption step:

$$E_e \underset{k_{-1}}{\overset{k_1}{\rightleftharpoons}} E_p \tag{1}$$

$$E_p + L \underset{k_{-3}}{\overset{k_3}{\rightleftharpoons}} E_p\text{-}L \tag{2}$$

The symbol E represents the solute applied to the column and present in the flowing mobile phase (or excluded volume, e), stagnant mobile phase (or pore volume, p), or bound to immobilized ligand (L). The diffusional rate constants (k_1, k_{-1}) are related to the excluded volume and pore volume accessible to the solute[1]:

$$\frac{k_1}{k_{-1}} = \frac{V_p}{V_e} \tag{3}$$

The adsorption and desorption rate constants (k_3, k_{-3}) are related to K_3, the equilibrium binding constant[3]:

$$\frac{k_3}{k_{-3}} = K_3 \tag{4}$$

In an isocratic experiment, a competing inhibitor (I) is usually present in the mobile phase to control retention. If the inhibitor binds to L rather than to E, i.e., reversed-role affinity chromatography[2], then the band-broadening due to the two kinetic processes is given by[7]

$$H_{sm} = \frac{2u V_p (1 + V_m k'/V_p)^2}{V_m k_{-1} (1 + k')^2} \tag{5}$$

$$H_k = \frac{2 \, uk'}{k_{-3}(1 + k')^2} \tag{6}$$

where H_{sm} is the plate height due to slow mass transfer between the moving and stagnant mobile phase, H_k is the plate height due to slow adsorption–desorption kinetics, u is the linear velocity of the mobile phase, and V_m is the void volume ($V_p + V_e$). We have previously shown[7] that these equations are identical in form to the well known equations derived by Horváth and Lin[10]. However, the equations above do not include interparticle band-broadening processes, such as eddy diffusion.

Consider a modification of the isocratic experiment in which the adsorption sites are first saturated with solute (by means of frontal rather than zonal application of E), then the column is washed to remove excess E. A high concentration of competing inhibitor is next applied to the column in a frontal mode so that retention of E is suddenly reduced nearly to zero. The solute is then eluted under isocratic conditions. Since the inhibitor does not itself cause dissociation of the E–L complex, but instead functions to prevent readsorption by filling any empty adsorption sites, the value of k_{-3} is not altered.

The elution profile of the solute leaving the column cannot, in general, be easily used to extract kinetic data. However, if extreme conditions are utilized, useful information may be obtained. In particular, if readsorption and diffusion back into stagnant mobile phase are prevented, then only a single dissociation will take place for each solute–ligand complex. Then the peak profile should resemble an exponential decay with rate constant k_{-1} or k_{-3}, whichever is smaller.

Mathematically, the peak-decay method is described by the reactions

$$E_p\text{-}L \xrightarrow{k_{-3}} E_p + L \tag{7}$$

$$E_p \xrightarrow{k_{-1}} E_e \tag{8}$$

which are just the irreversible equivalents of equilibria 1 and 2. To prevent reversibility completely requires infinitely large competing inhibitor concentrations (so that $k' = 0$) and a column length of zero (so that diffusion back into the stagnant mobile phase is prevented). Under such conditions, the differential equations describing reactions 7 and 8 are as follows:

$$\frac{dm_{E_p\text{-}L}}{dt} = -k_{-3}m_{E_p\text{-}L} \tag{9}$$

$$\frac{dm_{E_p}}{dt} = k_{-3}m_{E_p\text{-}L} - k_{-1}m_{E_p} \tag{10}$$

where m is the number of moles of solute. Assuming that all of the solute is initially adsorbed and of total amount m_{E_0}, and that $k_{-3} < k_{-1}$, the equations can be solved[11] in terms of the amount eluted up to time t:

$$m_{E_e} = \frac{m_{E_0}}{k_{-1} - k_{-3}} \{k_{-1}[1 - \exp(-k_{-3}t)] - k_{-3}[1 - \exp(-k_{-1}t)]\} \qquad (11)$$

The elution profile is the derivative of eqn. 11:

$$\frac{dm_{E_e}}{dt} = \frac{k_{-1}k_{-3}m_{E_0}}{k_{-1} - k_{-3}} [\exp(-k_{-3}t) - \exp(-k_{-1}t)] \qquad (12)$$

If $k_{-3} \ll k_{-1}$, then eqn. 12 reduces to a simple exponential decay. The rate constant k_{-3} is obtained from the slope of a plot of the natural logarithm of the elution profile:

$$\ln \frac{dm_{E_e}}{dt} = \ln(m_{E_0}k_{-3}) - k_{-3}t \qquad (13)$$

An analogous derivation can be made for the case where $k_{-1} < k_{-3}$.

The use of a finite inhibitor concentration and column length will result in some readsorption of solute onto the stationary phase and some diffusion of solute back into the stagnant mobile phase. This will cause further band-broadening, a shallower elution profile, and an apparent low value for the rate constant determined from the slope of the logarithm of the profile. However, it is possible to find useful conditions under which eqn. 13 provides a reasonably accurate description of the elution profile. These conditions are most easily obtained by means of computer simulations.

The computer model used here is based on the first-order reactions equivalent to reactions 1 and 2:

$$E_e \underset{k_{-1}}{\overset{k_1}{\rightleftharpoons}} E_p \underset{k_{-3}}{\overset{k_3^*}{\rightleftharpoons}} E_p\text{-L} \qquad (14)$$

The first-order adsorption rate constant, k_3^*, is equal to $k_3 m_L/V_p$, where m_L is the number of moles of ligand in the column. The general solution to this reaction was derived by Rakowski[12] and can be easily recast in terms of k', V_p, and V_e.

To utilize reaction 14 for column chromatography, the convective mass transport of E in the excluded volume must also be taken into account. This can be done by dividing an imaginary column longitudinally into a large number of slices and radially into three regions (flowing and stagnant mobile phase, and stationary phase). Each iteration of the computer consists of equilibrating the solute between the three radial regions according to the solution of reaction 14, then moving the solute in the excluded volume of one slice into the excluded volume of the next slice (the excluded linear velocity, u_e, is one slice per iteration). The solute leaving the last slice is monitored.

The time between recalculation of the amounts of solute in each slice and phase is one iteration. If the rate constants are approximately one iteration^{-1} or larger, then the system is close to equilibrium and the elution profile can be predicted from the Craig distribution[13]. This undesirable characteristic can be avoided by using smaller values for the rate constants (≤ 0.1 iteration^{-1}). By decreasing the rate

constants and proportionally increasing the number of slices of column length, one can easily ensure that the results have converged to a single value. This model was previously used for isocratic studies and it was shown that the band-broadening obtained was identical to that predicted by eqns. 5 and 6[7].

For use in the peak-decay mode, the program is modified so that solute is initially distributed throughout the column. At time zero, a plug of mobile phase containing inhibitor begins to move down the column, k' decreases to some predetermined value behind the mobile-phase front, and the solute begins to undergo dissociation, readsorption, and diffusion, just as in the isocratic method.

The simulation does not take into account broadening and dilution of the competing inhibitor front, nor does it take into account the finite number of ligand sites. Inclusion of the former process in the model would probably cause the elution profile to be broader, while the latter would cause it to be narrower.

EXPERIMENTAL

Reagents

Concanavalin A (Con A), type IV, 4-methylumbelliferyl α-D-mannopyranoside (MUM), and 4-methylumbelliferyl α-D-galactopyranoside (MUGA) were purchased from Sigma (St. Louis, MO, U.S.A.). The Hypersil WP-300, 5-μm particle diameter, was purchased from Alltech (Deerfield, IL, U.S.A.). Mannose and 1,1'-carbonyldiimidazole were from Aldrich (Milwaukee, WI, U.S.A.).

Apparatus

A Model 334 liquid chromatograph (Beckman, Berkeley, CA, U.S.A.) was modified by replacing the mixing chamber with a tee. A Model 757 UV–VIS detector (Kratos, Ramsey, NJ, U.S.A.) with a 12-μl flowcell was used for detection at 316 nm. An Apple IIe computer (Cupertino, CA, U.S.A.) with an Interactive Microware interface (State College, PA, U.S.A.) was used for data acquisition. A refrigerated circulating bath (Fisher, Chicago, IL, U.S.A.) was used to maintain the temperature of the column.

Computer simulations were performed on a National Advanced Systems 9160 computer (Mountain View, CA, U.S.A.).

Procedure

Diol-bonded Hypersil WP-300 was prepared according to a published procedure[14]. A 2-ml volume of a solution containing 9.8 mg/ml purified[15] Con A in 0.50 M sodium acetate buffer (pH 5.00), containing 1.0 mM calcium chloride and 1.0 mM manganese chloride, was immobilized at 4°C for seven days using the 1,1'-carbonyldiimidazole procedure[16,17] and 0.1 g diol-bonded silica. The immobilized Con A concentration was found to be 38 mg/g silica on the basis of the bicinchoninic protein assay (Pierce, Rockford, IL, U.S.A.). The silica was packed into a 6.3 mm × 2.1 mm I.D. column of published design[18] using the vacuum slurry packing method[19].

The weak mobile phase used for chromatographic experiments was the buffer described above. The strong mobile phase contained, in addition, 0.1 M mannose.

In a typical experiment, the column was first equilibrated with weak mobile phase at 1 ml/min and 25°C. A 2.4-ml injection of $1 \cdot 10^{-5}$ M MUM in weak mobile

phase was then made, and the excess MUM was removed by washing the column for 3.5 min. A step change to a flow-rate of 10 ml/min and the strong mobile phase was then made, and MUM elution data were acquired for 15 s at a rate of 10 points per second.

The slope of the natural logarithms of the tailing portion of the peak was calculated using the method of Guggenheim[20]. Baseline correction using a blank run was found to be unnecessary because the baseline disturbance due to the mobile phase change did not overlap with the tail of the MUM peak.

RESULTS AND DISCUSSION

Computer simulations

Fig. 1 shows two peak-decay profiles, calculated from eqn. 12 by using different values of k_{-1}/k_{-3}. Note that when k_{-1} and k_{-3} were similar in magnitude, the peak was broader and the logarithm of the profile was somewhat curved, as expected from the theoretical equation. In such a situation, an arbitrary choice of the portion of the profile to use in determining the slope had to be made. All of the slopes from computer simulations were measured in the following way: the times corresponding to the top of the peak profile and the point where 99% of the solute was eluted were determined. The time between these points was divided into five equal segments. The slope of the second segment (from the peak) was determined by linear least squares fitting of the points. The segment used is marked in Fig. 1. This particular segment was chosen because it most closely duplicated the region used in the experimental data.

Plots identical to Fig. 1 were obtained from the two-step reversible computer model when the column length and k' were both very small. This observation plus the previous isocratic experiments[7] support the accuracy of the computer model with respect to the mathematical model of Hethcote and DeLisi[1,2].
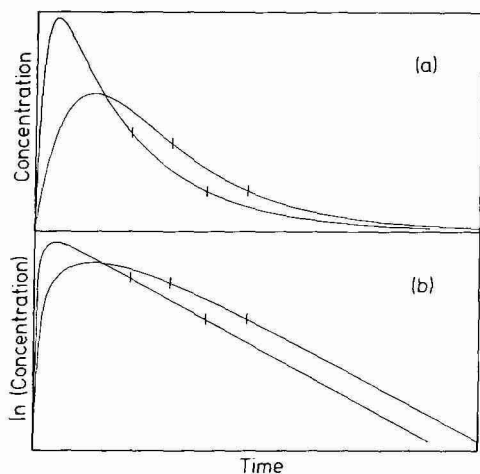
Fig. 1. Peak-decay profiles (a) and the natural logarithm of the profiles (b) calculated from eqn. 12 for the conditions $k_{-1}/k_{-3} = 10$ (taller peak) and $k_{-1}/k_{-3} = 2$ (shorter peak). The vertical marks indicate the region used for slope measurements.

The computer model was first used to examine the case in which retention was large enough that significant readsorption could occur but the column length was still insignificantly small. Rate constants were measured from simulated peak-decay profiles as a function of k' and k_{-1}/k_{-3} (Fig. 2). The slopes of the logarithm plots were normalized by dividing by the smaller of k_{-1} or k_{-3}. Thus, a normalized slope of 1.0 indicated that the rate constant of the slowest step could be accurately measured. Note that the slopes were always low when k_{-1} was similar in magnitude to k_{-3}. However, if k_{-1} was at least 10-fold larger or smaller than k_{-3}, then the smaller of the two rate constants could be measured with good accuracy when k' was small.

Fig. 2 also shows that the accuracy of the apparent rate constants declined as k' increased. This is because multiple adsorption and desorption steps began to take place and caused additional band-broadening. Interestingly, at high k', the plot was very asymmetric and indicated that when $k_{-1}/k_{-3} > 100$, k_{-3} could still be determined accurately, but when $k_{-1}/k_{-3} < 0.01$, k_{-1} could not be determined accurately. This difference was due to the fact that in the former case, as soon as the adsorbed complex dissociated, the solute immediately diffused out of the pore and was washed from the column. In the latter case, adsorbed solute and free solute in the pore volume were essentially in equilibrium, and so the solute diffused out of the pore more slowly than if all the solute were free.

Plots drawn with different values of V_p/V_e were similar to Fig. 2 but shifted vertically. Examination of the data indicated that plotting the data as a function of $k'V_m/V_p$ caused the data generated at different V_p/V_e values to merge into a single family of curves. From such a plot it was possible to determine the maximum allowable value of $k'V_m/V_p$ such that k_{-1} or k_{-3} could be determined accurately.

As the column length increased to significant values (Fig. 3), there was a greater likelihood of multiple adsorption–desorption steps with the result that the elution profiles became less steep. This was not really a function of the column length itself,
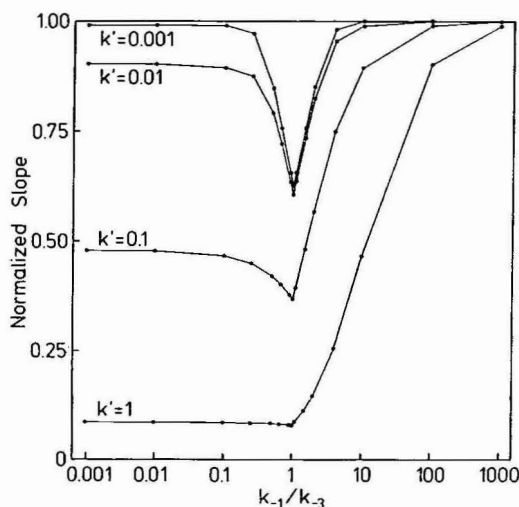
Fig. 2. Plot of normalized slope from computer simulations of peak-decay profiles as a function of k_{-1}/k_{-3} and k' for $V_p/V_e = 0.1$ and zero column length.
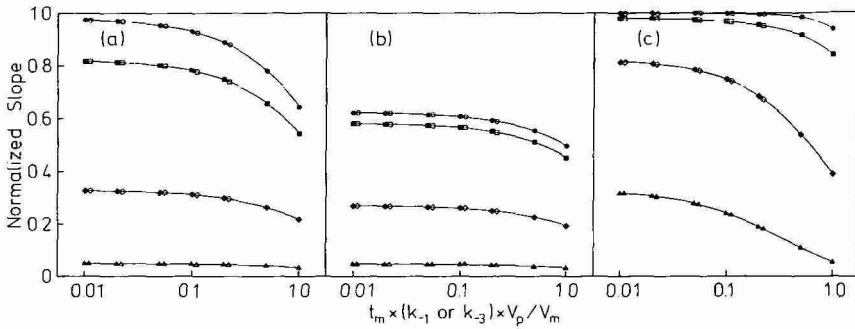
Fig. 3. Plots of normalized slope from computer simulations of peak-decay profiles as a function of void time for $k_{-1}/k_{-3} = 0.1$ (a), 1.0 (b), and 10.0 (c). From top to bottom, the curves represent 10-fold increases in $k'V_m/V_p$ beginning at a value of 0.02 for $V_m/V_p = 2$ (solid symbols) and $V_m/V_p = 10$ (open symbols).

but rather of the residence time of solute in the column (*i.e.* the void time, t_m) relative to the rate constants. The factor V_m/V_p also was important here; hence, the normalized slope is plotted in Fig. 3 *vs.* the product of t_m, V_p/V_m, and the smaller of k_{-1} or k_{-3}. From this plot, the maximum allowable void time could be determined.

By examination of the data used to prepare Figs. 2 and 3, conditions were found such that the smaller of k_{-1} or k_{-3} could be measured with less than a 5% error. The conditions for accurate determination of k_{-1} were:

$$k_{-1}/k_{-3} \leq 0.1 \tag{15}$$
$$t_m k_{-1} V_p/V_m \leq 0.05 \tag{16}$$
$$k' V_m/V_p \leq 0.02 \tag{17}$$
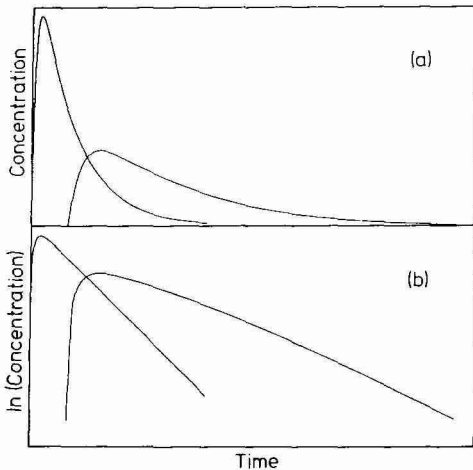
Fig. 4. Computer-simulated peak-decay profiles (a) and the natural logarithms of the profiles (b) for $k_{-1}/k_{-3} = 10$ and $V_p/V_e = 1$. For the taller peak, $t_m k_{-3} V_p/V_m = 0.01$ and $k'V_m/V_p = 0.02$. For the shorter peak, the quantities are 1.0 and 2.0, respectively.

The conditions for accurate determination of k_{-3} were:

$$k_{-1}/k_{-3} \geq 10 \tag{18}$$
$$t_m k_{-3} V_p/V_m \leq 0.2 \tag{19}$$
$$k' V_m/V_p \leq 0.2 \tag{20}$$

Other conditions may also be acceptable. For example, if $k_{-1}/k_{-3} \geq 100$, then Fig. 2 shows that the requirement for k' could be relaxed somewhat.

Fig. 4 shows two peak profiles generated from the computer model. One was a nearly ideal case in which $k_{-1}/k_{-3} = 1.0$, $V_p/V_e = 1$, $t_m k_{-3} = 0.02$, and $k' = 0.01$. The normalized slope was 0.998, i.e. only 0.2% less than the expected value. The other curve was for a case where $t_m k_{-3} = 2$ and $k' = 1$. The normalized slope decreased to 0.386 and thus the apparent rate constant was significantly less than the expected value.

Effect of heterogeneity

If there were heterogeneity in the values of k_{-1} or k_{-3}, then eqn. 12 could be expanded to include more terms, each with its own m_{E_0}, k_{-1}, and k_{-3}. The logarithm plots would then be the sum of several exponential terms, leading to a plot which flattens as time increased (just the opposite of Fig. 1b, where the plot became steeper with time).

If the slope were measured late in the tail of the peak, it always approached the smallest of the individual rate constants because the faster-decaying solute molecules had already left the column. If the slope were measured as described earlier, the apparent rate constant turned out to be quite close to the apparent value that would have been obtained from an isocratic experiment, i.e. weighted toward the smallest rate constant.

Comparison with isocratic methods

Since both the peak-decay and isocratic methods utilize competing inhibitors, it is useful to compare the potential advantages of one method over the other.

In the isocratic method, one must generally correct the total plate height for the contributions due to H_{sm} and the eddy diffusion/mobile-phase mass transfer plate height. This involves mesurement of u, V_p, V_e, and k_{-1} and recalculation of the plate heights as a function of k', all of which introduce significant uncertainty in the final results[7]. In contrast, the rate constant is obtained directly from the slope of the logarithm of the detector response in the peak-decay method.

Some of the calculation problems of the isocratic method can be avoided if the entire measured plate height is attributed to H_k. Then only u and k' need to be measured (eqn. 6). Consider the case where $k_{-1}/k_{-3} = 10$ and $V_p/V_e = 1$. Since at $k' = 10$, $H_{sm}/H_k = 2.2$ from eqns. 5 and 6, the apparent value of k_{-3} would be only 31% of its true value if H_{sm} were not subtracted from the total plate height. A more favorable case is at $k' = 1$, since H_k reaches a maximum at that point but H_{sm} has not increased to its maximum value. The apparent rate constant would still be only 69% of its true value at this point. In contrast, for the same system but with k' and t_m adjusted in accordance with eqns. 19 and 20, the apparent value of k_{-3} would be at least 95% of its true value. Thus, with the peak-decay method, one can measure

k_{-3} accurately when $k_{-1}/k_{-3} \geq 10$. With the isocratic method, similar accuracy requires $k_{-1}/k_{-3} \geq 100$.

Other practical advantages of the peak-decay method over the isocratic method include (a) better precision, since slopes rather than variances of the peak profiles are measured, (b) shorter analysis times, since dissociation only needs to take place once rather than many times, (c) reasonable analysis times, even in cases where k_{-3} is quite small, and (d) improved detectability, because the column can be saturated with solute.

Potentially offsetting these advantages are the need to use very high inhibitor concentrations to reduce k', and high flow-rates or short columns to minimize t_m in cases where k_{-3} is moderately large. Since there is a step change in mobile phase at time zero, detectability may also be adversely affected by refractive-index effects.

Preliminary calculations taking into account analysis time, inhibitor concentration, flow-rate, column size, and detectability are described in ref. 21 and may be useful in determining whether isocratic or peak-decay experiments are feasible in particular situations.

Experimental data

A system consisting of an immobilized protein, Con A, as the ligand, and the sugars MUM and mannose as solute and inhibitor, respectively, were utilized for the experimental studies. From previous isocratic measurements, approximate values of the rate constants were known: $k_{-1} \approx 120 \text{ s}^{-1}$; $k_{-3} \approx 2 \text{ s}^{-1}$ (ref. 7). The ratio of the rate constants easily met the criterion of eqn. 18. For the Hypersil column used, $V_p/V_m \approx 0.44$. Thus, eqn. 19 required $t_m \leq 0.23$ s. This was a severe requirement, and therefore high flow-rates and/or small columns were needed to measure a dissociation rate this fast. A 6.3 mm $\times$ 2.1 mm I.D. column was chosen. With a void volume of approximately 14 μl, the flow-rate needed was 3.7 ml/min. To meet the criterion of eqn. 20 required $k' \leq 0.088$. From isocratic studies, the binding constants for the sugars were determined: K_3 (MUM) = 45 000 M^{-1}; K_2 (mannose) = 1500 M^{-1}. From break-through curve and protein assay data, the number of moles of active Con A in the column was estimated to be 18 nmol. From eqn. 3 of ref. 7, the minimum inhibitor concentration was calculated to be 0.44 M.

Fig. 5 shows the data from a typical experimental run at a flow-rate of 10 ml/min and 0.1 M mannose concentration. The logarithmic plots (Fig. 5b) typically were somewhat concave, but the slope could be determined with excellent precision [$\pm 3\%$ relative standard deviation (R.S.D.) from the slope of a single run, $\pm 5\%$ R.S.D. for replicate runs]. As pointed out earlier, one possible cause of the concave plot could be heterogeneity in the immobilized Con A.

Experiments were performed at several flow-rates (Fig. 6) and mannose concentrations (Fig. 7) to determine whether the data obeyed eqns. 19 and 20. Both experiments exhibited the expected trends, with the apparent rate constants reaching a plateau value of approximately 1.78 s^{-1} at high flow-rate (small t_m) and high inhibitor concentration (small k').

The flow-rate and inhibitor concentration needed to reach the plateau value of k_{-3} were somewhat different than those predicted above. To examine this further, the experimental system was modeled with the parameters listed above and a value of 1.82 s^{-1} for k_{-3}. The simulated data are also shown in Figs. 6 and 7. From Fig.
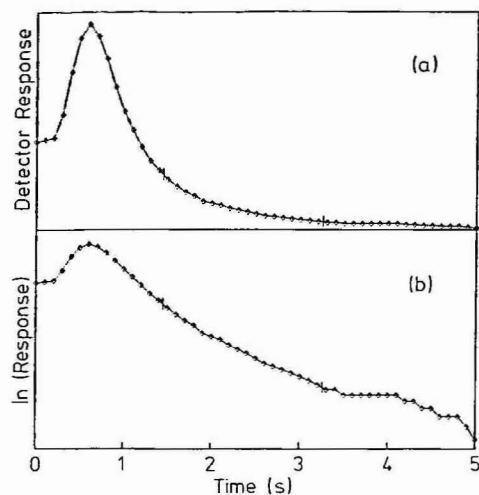
Fig. 5. An experimental peak-decay profile (a) and natural logarithm of the profile (b) for MUM eluted from an immobilized Con A column at a flow-rate of 10 ml/min with a mannose concentration of 0.1 M. The vertical marks indicate the region used for slope measurements.

6, it is apparent that the model predicted only a small change in the apparent rate constants over the flow-rate range used, whereas the actual change was much greater. The difference was probably caused by factors not taken into account in the model, such as dispersion of the inhibitor front as it passed through the column, or eddy diffusion/mobile-phase mass-transfer effects on the solute band-broadening. On the other hand, Fig. 7 shows better agreement between experimental and predicted values of k_{-3} as a function of inhibitor concentration. Some of the discrepancies between theory and experiment in both Figs. 6 and 7 could be due to inaccuracies in the values of m_L, V_m, etc. used in the simulations.
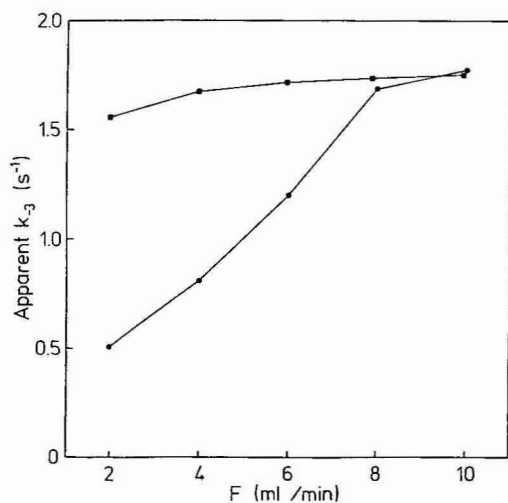
Fig. 6. Experimental ($\bullet$) and theoretical ($\blacksquare$) plots of the apparent value of k_{-3} vs. flow-rate for the Con A–sugar system with 0.1 M mannose as inhibitor.
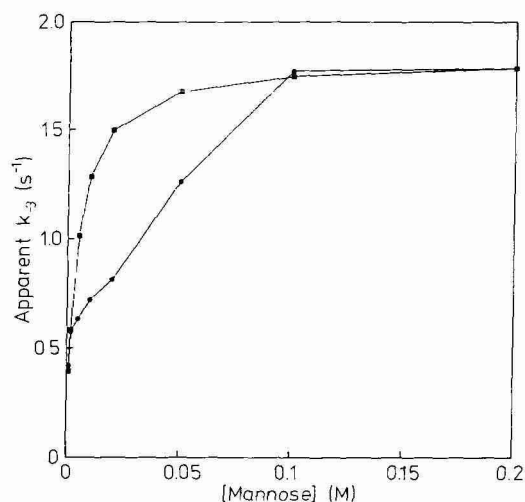
Fig. 7. Experimental ($\bullet$) and theoretical ($\blacksquare$) plots of the apparent value of k_{-3} vs. inhibitor concentration for the Con A–sugar system at a flow-rate of 10 ml/min.

Another factor examined was the effect of washing the column with buffer to remove excess MUM prior to the step change in mobile phase. The calculated k' for MUM in the absence of inhibitor was 58. It is apparent that with the small void volume of the column, all the MUM would be eluted isocratically in a relatively short time period. To examine this, the length of the wash time was varied from 2 to 5 min at 1 ml/min. The rate constants were measured using a flow-rate of 10 ml/min and 0.1 M mannose. Table I shows the results of this study. No change in the rate constant was observed at wash times of less than 4 min. The apparent change at longer wash times may have been due to experimental error in the data, as the amount of MUM remaining in the column declined.

Taking into account column-to-column reproducibility, the dissociation rate constant for the MUM–immobilized Con A complex was $1.8 \pm 0.1 \text{ s}^{-1}$ at 25°C. This is in excellent agreement with a value of $2.0 \pm 0.6 \text{ s}^{-1}$ from the best of our previous isocratic studies[7] and in fair agreement with a value of 3.4 s^{-1} from free solution studies[22]. Since the equilibrium binding constant appears to be larger for

TABLE I

EFFECT OF COLUMN WASHING PRIOR TO ELUTION OF MUM

Wash time (min)	Apparent k_{-3} (s^{-1})	Relative peak area
2.0	1.54	1.00
2.5	1.79	0.40
3.0	1.77	0.31
3.5	1.75	0.21
4.0	1.76	0.13
4.5	1.10	0.09
5.0	1.18	0.06

immobilized Con A[7], the values of k_3 calculated from eqn. 4 for immobilized Con A ($8.1 \cdot 10^4 \ M^{-1} \ s^{-1}$) and free Con A ($11.2 \cdot 10^4 \ M^{-1} \ s^{-1}$) are in good agreement. Further work is underway to determine the effect of temperature on the rate and equilibrium constants.

CONCLUSIONS

Since there were some discrepancies between the model used to obtain eqns. 15–20 and the experimental data from the Con A–sugar system, particularly in the case of flow-rate effects, it is suggested that eqns. 15–20 be used only to establish initial conditions for peak-decay measurements. Flow-rate and inhibitor concentration studies should be performed to ensure that the "plateau" value of the dissociation rate has been reached.

The superior precision of the rate constants obtained from peak-decay measurements compared to isocratic measurements suggest that the peak-decay method should be the method of choice for affinity chromatographic estimation of dissociation rate constants. The method should be useful for rate constants of monovalent interactions ranging from about $10 \ s^{-1}$ to less than $10^{-3} \ s^{-1}$.

ACKNOWLEDGEMENT

REFERENCES

1 H. W. Hethcote and C. DeLisi, *J. Chromatogr.*, 248 (1982) 183.
2 H. W. Hethcote and C. DeLisi, in I. M. Chaiken, M. Wilchek and I. Parikh (Editors), *Affinity Chromatography and Biological Recognition*, Academic Press, New York, 1983, p. 119.
3 I. M. Chaiken, *Anal. Biochem.*, 97 (1979) 1.
4 V. Kasche, K. Buchholz and B. Galunsky, *J. Chromatogr.*, 216 (1981) 169.
5 K. Nilsson and P.-O. Larsson, *Anal. Biochem.*, 134 (1983) 60.
6 A. J. Muller and P. W. Carr, *J. Chromatogr.*, 284 (1984) 33.
7 D. J. Anderson and R. R. Walters, *J. Chromatogr.*, 376 (1986) 69.
8 H. A. Chase, *J. Chromatogr.*, 297 (1984) 179.
9 D. S. Hage, R. R. Walters and H. W. Hethcote, *Anal. Chem.*, 58 (1986) 274.
10 C. Horváth and H.-J. Lin, *J. Chromatogr.*, 149 (1978) 43.
11 J. H. Espenson, *Chemical Kinetics and Reaction Mechanisms*, McGraw-Hill, New York, 1981, p. 65.
12 A. Rakowski, *Z. Phys. Chem.*, 57 (1906) 321.
13 B. L. Karger, L. R. Snyder and C. Horvath, *An Introduction to Separation Science*, Wiley, New York, 1973, p. 110.
14 R. R. Walters, in P. D. G. Dean, W. S. Johnson and F. A. Middle (Editors), *Affinity Chromatography: A Practical Approach*, IRL Press, Oxford, 1985, p. 25.
15 B. A. Cunningham, J. L. Wang, M. N. Pflumm and G. M. Edelman, *Biochemistry*, 11 (1972) 3233.
16 G. S. Bethell, J. S. Ayers, W. S. Hancock and M. T. W. Hearn, *J. Biol. Chem.*, 254 (1979) 2572.
17 S. C. Crowley, K. C. Chan and R. R. Walters, *J. Chromatogr.*, 359 (1986) 359.
18 R. R. Walters, *Anal. Chem.*, 55 (1983) 591.
19 R. M. Moore and R. R. Walters, *J. Chromatogr.*, 317 (1984) 119.
20 E. A. Guggenheim, *Philos. Mag.*, 2 (1926) 538.
21 R. R. Walters, in I. M. Chaiken (Editor), *Analytical Affinity Chromatography*, CRC Uniscience, Boca Raton, in press.
22 R. M. Clegg, F. G. Loontiens, A. Van Landschoot and T. M. Jovin, *Biochemistry*, 20 (1981) 4687.

CHROMSYMP. 937

SYNTHESIS OF THREE ALKYLDIHYDROCHLOROSILANES AND THEIR APPLICATION IN STUDIES OF STERIC FACTORS IN THE SURFACE DEACTIVATION OF POROUS SILICA

RANDY D. GOLDING, ARTHUR J. BARRY and MICHAEL F. BURKE*

Department of Chemistry, University of Arizona, Tucson, AZ 85721 (U.S.A.)

SUMMARY

The synthesis and bonding to silica of ethyl-, octyl-, and octadecyldihydrochlorosilane are reported. These silanes are shown to react to a greater extent with surface hydroxyls than analogous alkyldimethylchlorosilanes, and this results in chromatographic stationary phases with reduced residual silanol activity.

INTRODUCTION

Since workers began to bond alkylsilyl groups to the surface of porous silica the understanding of the structure of the solvated bonded phase and its impact on mechanisms of separations in reversed-phase liquid chromatography has grown in detail[1]. These stationary phases are now described as pseudo liquids[2-4], which are mixtures of the bonded moieties and the various mobile phase components which partition themselves into the stationary phase to a degree controlled by their concentrations in the bulk mobile phase and their reversed-phase solvent strengths[5-7]. The selectivities of these bonded phases arise from solvation interactions between the solutes and the various components of the stationary phases, namely the bonded moieties[8,9], the imbibed solvent molecules[6,7], and the residual surface hydroxyls that remain after the bonding process[10-12]. In recent work, it has been shown that various solutes find their most favorable interactions in different regions of the stationary phase, and it has been proposed that a polarity excursion is experienced by the sorbed solute molecule that is greatest in the near-surface region of silanols and adsorbed water reaches a minimum near the center region of the stationary phase, and increases to that of the bulk mobile phase as the solute molecule moves up through the solvated layer from the silica surface[13]. Thus, the apparent polarity of bonded phases is both a function of the alkyl group(s) of the bonding silane and the extent to which the bonding has proceeded[12-16]. Researchers have long studied the role of residual surface hydroxyls in yielding the particular properties of silica-based adsorbents, and the question how bonded phases would behave if the activity of these residual sites was completely removed is still unanswered[12].

Two families of alkylsilanes have traditionally been used to modify the surface of porous silica. They have been called monomeric and polymeric modifiers, respec-

tively. Each class has advantages and, depending on the application of the adsorbent in question, one type or the other can be the modifier of choice[15]. Monomeric modifiers of the general formula $R(CH_3)_2SiX$ (where X is some easily hydrolyzed group) have the advantages of greater reproducibility, reduced activity, and conformation to the original topography of the silica, because the bonding molecule deactivates surface sites without the possibility of creating new ones[15,17]. Polymeric modifiers of the general formula $RSiX_3$ have the advantages of higher carbon load, shorter reaction time, and increased stability towards hydrolysis[15,18]. One of the causes of the variable features of polymeric phases is the tendency of these reagents to react with trace amounts of water present in the solvent or extracted from the silica and then to polymerize in solution before bonding to the surface hydroxyls in ways that may or may not conform to the original surface[18,19]. It is for this reason that researchers investigating mechanisms have preferred monomeric modifiers. The goal of this research has been to develop a new family of surface modifiers that would combine the reproducibility and reduced polarity attainable with monomeric modifiers with the stability and higher carbon load attainable with polymeric modifiers.

This paper describes the synthesis of a family of surface modifiers of the general structure RH_2SiCl that may afford higher carbon load and yet conform to the original surface structure of the substrate. This new family of surface modifiers reacts with surface hydroxyls as monomers and leads to higher surface coverages because of the reduced size of the bonding silane which has had the bulky methyl groups replaced with hydrogens. After bonding, the silylhydrides can be oxidized to Si–OH groups, possibly allowing these materials to take on the properties of and serve as models for polymeric systems. The bonding of these new modifiers to porous silica is described, along with spectroscopic and chromatographic characterization of the resulting materials. Also, the properties of these new adsorbents are compared to those of the same type of silica that has reacted with the analogous alkyldimethylchlorosilanes.

EXPERIMENTAL

Reagents
Methanol, toluene, hexane (isomeric mixture), benzene, and mercuric chloride, all analytical-reagent grade, were obtained from Fisher Scientific (Fair Lawn, NJ, U.S.A.); ethyldimethylchlorosilane, ethyltrichlorosilane, octyldimethylchlorosilane, octadecyldimethylchlorosilane, and dichlorosilane from Petrarch (Bristol, PA, U.S.A.); 1-chlorooctadecane, trimethylchlorosilane, dibromomethane, glyme, phenol, phenethyl alcohol, 3-phenyl-1-propanol, 4-phenyl-1-butanol, 5-phenyl-1-pentanol, and lithium aluminum hydride from Aldrich (Milwaukee, WI, U.S.A.); Grignard-grade magnesium turnings, acetophenone, 30% hydrogen peroxide, methylbenzoate, anisole, and aniline from Mallinckrodt (Paris, KY, U.S.A.); anhydrous diethyl ether and benzylamine from J. T. Baker (Phillipsburg, NJ, U.S.A.); 1-chlorooctane from Eastman (Rochester, NY, U.S.A.); and dibutyltin diacetate from Alpha Products (Danvers, MA, U.S.A.). All solvents brought into contact with silica particles were filtered using 0.45-μm membrane filters, obtained from Millipore (Bedford, MA, U.S.A.). Glyme was distilled from lithium aluminum hydride before use, and distilled water was redistilled from a solution of potassium permanganate and potassium hydroxide. All other chemicals were used without further purification.

Synthesis of octyldihydrochlorosilane (ODHCS) and octadecyldihydrochlorosilane (ODDHCS)

Octyl magnesium chloride or octadecyl magnesium chloride, prepared from the corresponding alkyl chloride, was added while refluxing to a 1.3-fold excess of dichlorosilane in diethyl ether. The resultant solution was decanted and fractionally distilled at reduced pressure through a 15-cm Vigreux column: ODHCS distilled at 60.5°C and 4 Torr; ODDHCS distilled at 142°C and 0.3 Torr. The yield of purified product in both instances was about 40%, based on the initial amount of the alkyl chloride. Both structures were verified by transmission infrared spectrophotometry with a Perkin-Elmer (Norwalk, CT, U.S.A.) Model 983 IR spectrophotometer, by proton NMR spectrometry with a Varian (Sunnyvale, CA, U.S.A.) Model T-60 NMR spectrometer, and by mass spectrometry with a Hewlett-Packard (Palo Alto, CA, U.S.A.) Model 5990A gas chromatograph–mass spectrometer.

Synthesis of ethyldihydrochlorosilane (EDHCS)

The method used was similar to that used by Anderson and Hendifar[20] in the synthesis of heptyldihydrochlorosilane. Ethyltrichlorosilane was reduced by addition to a slurry of lithium aluminum hydride in glyme. The resulting ethylsilane (b.p. −59°C) was condensed and dissolved in glyme, cooled by a dry ice–methanol slurry. An equimolar amount of mercuric chloride was added to the cooled solution over the course of 3 h. The formation of metallic mercury indicated the progress of the reaction. The mixture was then heated over a period of 3 h until the reflux temperature reached 40°C. The product was recovered by fractional distillation. The yield of purified product was 55%, based on the initial amount of ethyltrichlorosilane. The identity of EDHCS (b.p.$_{760}$ 43°C) was confirmed by gas chromatography–mass spectrometry.

Silica modification

The silica used in this study was obtained from Lochmuller (Duke University, Durham, NC, U.S.A.) and is part of a single batch (Id. No. RR-129-7A), donated by Whatman Chemical Separation (Clifton, NJ, U.S.A.) that has been used by Lochmuller and others in surface modification studies. This silica had been acid-washed and was used here without further treatment. The manufacturer reports a mean particle size of 7.53 μm, an average pore diameter of 96 Å, and a nitrogen BET surface area of 323 m^2/g. The bonding of all silica samples was accomplished by refluxing the sample in a 10% (v/v) solution of the silylating agent in toluene, in a volume calculated to contain at least a five-fold excess of the silylating agent for the number of surface hydroxyls present (based on the weight of the sample, the reported surface area, and the assumption of 4–5 silanols per nm^2). The silica samples were refluxed under dry nitrogen purge for the indicated amount of time, which varied from 2 to 72 h. Each sample was then filtered through a 5-μm membrane filter and washed at least ten times with 30 ml of fresh toluene and then ten times with 30 ml of methanol. The samples were dried overnight at 120°C under reduced pressure (*ca.* 0.1 Torr). The percentage carbon atoms of each sample was determined by combustion analysis, using a Perkin-Elmer Model 240C elemental analyzer.

Spectroscopic characterization

Transmission infrared spectra of bonded silicas were obtained as mulls with carbon tetrachloride in capillary cells with sodium chloride windows. The cross-polarization magic-angle spinning (CPMAS) ^{29}Si NMR spectrum of silica bonded with ODDHCS was graciously provided by the Regional NMR Facility (Boulder, CO. U.S.A.).

Chromatographic characterization

Samples of bonded silica were packed as a density-balanced slurry of dibromomethane and methanol or of dibromomethane and hexane. Approximately 0.3 g of silica were slurried in 4.5 ml of density-balanced solvent and sonicated for 10 min. The slurry was then added to a 250 × 4.6 mm stainless-steel packing bomb, coupled to a 100 × 2.1 mm stainless-steel column with a 2-μm stainless-steel frit in the outlet end. The packing bomb was then connected to a pneumatically driven pump, and methanol or hexane was pumped for 10 min at 6000 p.s.i. Chromatographic experiments were carried out with an IBM Instruments (Danbury, CT, U.S.A.) Model 9533 ternary solvent gradient liquid chromatograph. The elution of UV-absorbing solutes was monitored with an IBM Instruments Model 9522 fixed-wavelength UV absorbance detector at 254 nm. The elution of non-absorbing solutes was monitored with a Micromeritics (Norcross, GA, U.S.A.) Model 771 refractive-index detector. The retention times of solutes were measured with a Linear Instruments (Irvine, CA, U.S.A.) Model 261/MM strip-chart recorder. Flow-rates were measured by noting the time required to collect a given volume in a precision buret. Extra-column volumes were measured by replacing the column with a zero-dead-volume union. Maximum void volumes were measured as the elution volume of pentane or heptane with hexane as the mobile phase. Capacity factors were calculated using the maximum void volume thus measured and corrected for extra-column volume.

RESULTS AND DISCUSSION

The synthesis of several alkyldihydrochlorosilanes, including methyl-[21], ethyl-[22], propyl-, butyl-[23], and heptyl-[20], by various methods has been reported, but these compounds are not widely used and are therefore not commercially available. The synthetic methods used fall into two classes: (1) the chlorination of the alkylsilane with[21] or without[20] a catalyst, and (2) the disproportionation of the alkyldichlorosilane with the help of some catalysts. As catalysts aluminium chloride[22] or some mild organic base such as a nitrile[23] have usually been used. The synthetic method used for ODHCS and ODDHCS, both previously unreported compounds, was chosen because of the ready availability of dichlorosilane, and because the most likely impurity to be produced in each case was the disubstituted alkylsilane, which would be easy to separate from the desired product due to the large difference in boiling point. This method was not used for EDHCS because of the difficulty of separating it from dichlorosilane.

Many researchers have bonded $R(CH_3)_2Si-$ groups to silica with the result that the number of groups bonded was always less than the calculated number of silanols present, the calculation being based on the surface area, as measured by the nitrogen BET isotherm method and by assuming 4–5 silanols per nm^2. The best
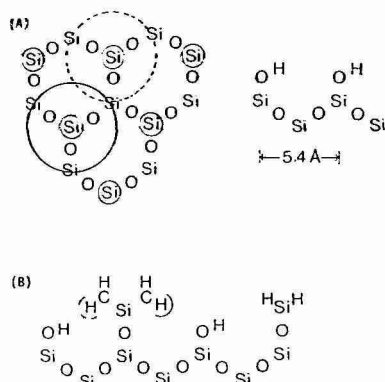
Fig. 1. (A) Two-dimensional schematic representation of an idealized silica surface, showing the approximate size of bonded trimethylsilyl groups and the maximum distance between neighboring silanols. Bonded trimethylsilyl groups are represented by large solid circle. The large broken circle represents the location of a trimethylsilyl group reacting with a neighboring silanol. $\widehat{Si}$ shows the original location of silanol. (B) Two-dimensional schematic representation of an idealized silica surface, showing the approximate size of bonded silanes $R(CH_3)_2Si-$ $vs.$ RH_2Si-.

coverage is attained with trimethylchlorosilane (TMCS), which implies that the limitation is steric hindrance. Calculation of the surface required for each TMCS group, based on its density or the density of tetramethylsilane, yields a value of about 35 Å², in agreement with the usually reported values of coverage by TMCS which lie between 60 and 70% of the predicted number of silanols present[12,24,25]. It was assumed that, if the size of the groups filling the valencies of the bonding silicon atom could be reduced, the coverage attainable by such a molecule would increase relative to its predecessors.

Fig. 1A is a two-dimensional view of silica, approximately to scale, where the fourth bond to each silicon atom is directed into or out of the page. The large, solid circle shows the projected surface area (35 Å²) occupied by a bound trimethylsilyl
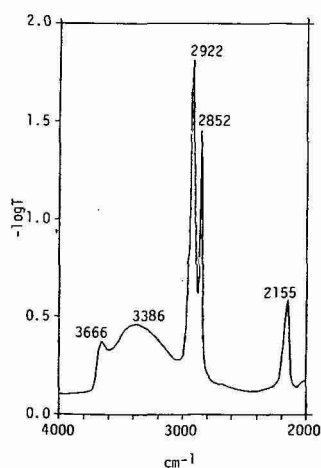
Fig. 2. Transmission IR spectrum of ODDHS-bonded silica after six months' exposure to air.

group. The distance between neighboring silanol groups of 5.4 Å is certainly an upper limit, but, as can be seen in the diagram, the bound $R(CH_3)_2Si-$ group is large enough to hinder sterically the bonding of another silane (represented by the broken circle) to either of the neighboring silanols. Shown in Fig. 1B is the increased freedom obtained by replacing the bulky methyl groups with hydrogens. In order to investigate this idea, the three new modifiers were applied to the surface of silica by the method outlined. To verify that the potentially unstable Si–H groups had remained intact during the bonding process, the IR spectrum of each sample was taken between 4000 and 2000 cm^{-1}, and the intensity of the Si–H stretch at 2155 cm^{-1} was compared to that of the C–H stretches between 3000 and 2750 cm^{-1}. For fresh samples, the relative intensities of these two bands were within the precision of measurement of the expected value, assuming that no change in absorptivity occurred upon bonding to the surface.

Fig. 2 is the IR spectrum from 4000 to 2000 cm^{-1} of an octadecyldihydrosilyl (ODDHS)-bonded silica which had been exposed to air for six months. The integrated area of the absorption peak at 2155 cm^{-1} due to the Si–H stretching vibration is approximately 22% of the combined area of the peaks at 2920 and 2850 cm^{-1} due to the C–H stretching vibrations. The area of the peak due to the Si–H stretches in a neat sample of ODDHCS is 32% of the area of the C–H stretches. Assuming that the absorptivities of the respective vibrations have not changed, this would indicate that 31% of the Si–H groups originally present had been oxidized to Si–OH groups.

Fig. 3 is the CPMAS ^{29}Si NMR spectrum of the same sample. The peaks at -15 and -30 ppm have tentatively been assigned to the signals arising from $-OSiH_2R$ and $-OSiHOHR$ groups, respectively. If it can be assumed that the area measurements of these peaks are quantitative, this spectrum indicates that 29% of the Si–H groups originally present had been oxidized, which is in good agreement with the IR results. The fact that this sample was exposed to air for six months illustrates the stability of these bound Si–H moieties. It is just this stability which allowed us to characterize these bonded phases in their reduced form. IR spectra of
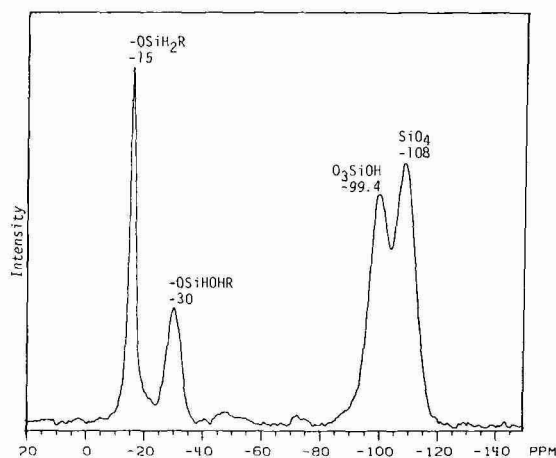
Fig. 3. CPMAS ^{29}Si NMR spectrum of ODDHS-bonded silica after six months' exposure to air.
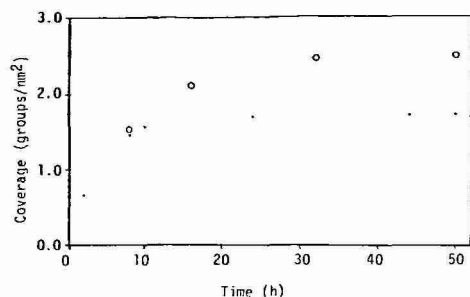
Fig. 4. Plot of coverage of silica by octadecylchlorosilanes vs. reaction time. (O) –ODDHCS; (●) – ODDMCS.

ODDHS-bonded silica samples, removed from the column after the completion of chromatographic experiments, indicated that most of the Si–H groups were still present, although no rigorous quantitation was attempted.

The first comparison to be made between $R(CH_3)_2SiCl$ and RH_2SiCl modifiers was the extent to which they could be bonded to a given silica surface. Each coverage is reported as groups per $R(CH_3)_2SiCl$ and is calculated from the percentage carbon atoms obtained from combustion analysis. The manufacturer's reported surface of 323 m^2/g was used in the following formula:

$$\frac{X_0(12.01/n_0)N}{\{1 - [X_0(12.01/n_0) (MW - 1.008)]\}323 \cdot 10^{10}}$$

in which X_0 is the measured mass fraction of carbon, n_0 is the number of carbons in each bonded group, N is Avagodro's number, and MW is the calculated formula weight of the alkylsilyl radical.

Fig. 4 shows the coverage of octadecyldimethylchlorosilane (ODDMCS) and ODDHCS vs. reaction time under the conditions described. As is indicated by the plot, the extent of bonding by each type of modifier seems to be roughly equivalent at short reaction times, but the reaction between silica and ODDMCS levels off faster
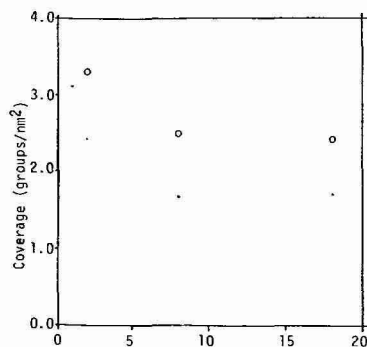
Fig. 5. Plot of maximum coverage attained by alkylchlorosilanes vs. chain length. (O) –RH₂SiCl; (●) R(CH₃)₂SiCl.

TABLE I

INCREASE IN SURFACE COVERAGE AVAILABLE BY REPLACING PENDANT METHYL GROUPS WITH HYDROGENS

H = Maximum coverage attained by RH_2SiCl; M = maximum coverage attained by $R(CH_3)_2SiCl$.

R	H–M (groups per nm^2)
Ethyl	0.87
Octyl	0.85
Octadecyl	0.71

than the reaction between ODDHCS and silica after about 10 h. The latter does not reach a plateau until at least 32 h of reaction time. In order to compare the full extent to which each modifier could be bonded, reaction times of at least 32 h were always employed. It is also worth noting that the shape of the kinetic curves shown did not change if the sample was periodically removed and washed, and the reaction was continued after the addition of fresh reagent.

Fig. 5 shows the maximum coverage attainable with chlorosilanes as a function of chain length of the alkyl group R– for the two types of modifiers, $R(CH_3)_2SiCl$ and RH_2SiCl. In all cases, the RH_2SiCl modifier yielded higher coverages than the dimethyl analogue. However, it is interesting to note that the two curves generated by the respective classes of modifiers seem to be parallel, indicating that, regardless of the length of the hydrocarbon chain filling the fourth valency of the bonding silicon atom, the increase in coverage available by replacing the two methyl groups with hydrogens is constant. Table I is a list of the differences in coverages given by each pair of the different types of modifiers of equal chain length. Although methyldihydrochlorosilane has not yet been successfully synthesized and bonded to silica in our laboratory, the above plot indicates that it should yield a coverage around 4 groups per nm^2. Experiments are currently underway in our laboratory to test this hypothesis and will be reported in the near future.

To determine which type of modifier would leave silica with the least amount of residual activity, a chromatographic comparison was made between silica samples that had been reacted with either ODHCS or octyldimethylchlorosilane (ODMCS) for 50 h so that in each case maximum coverage had been reached. This coverage was 2.53 groups per nm^2 for ODHCS and 1.68 groups per nm^2 in the case of ODMCS. Each sample of bonded silica was packed into stainless-steel columns, as described, using hexane as the packing solvent and subsequently as the mobile phase.

TABLE II

RETENTION OF SOLUTES USING HEXANE AS MOBILE PHASE

Silica modifier	Groups per nm^2	Capacity factor, k'		
		Anisole	Methylbenzoate	Acetophenone
Octyldihydrochlorosilane	2.53	1.6	6.3	19
Octyldimethylchlorosilane	1.68	2.4	12	34

Hexane was chosen as the mobile phase because of its structural similarity with the bonded hydrocarbon chains. Thus, any retention observed could be directly attributed to residual silanol activity. The particular solutes chosen were small molecules that could be conveniently detected by UV absorption at 254 nm, had functional groups that could interact with silanols to varying extents, and would be eluted in reasonable time. Anisole, methylbenzoate, and acetophenone fit this description. The capacity factors for these solutes are reported in Table II. The retention of all three solutes by silica, modified with ODMCS, is roughly twice that of silica modified with ODHCS. The ability of ODHCS to deactivate silica to a greater extent than ODMCS indicates promise for this new family of surface modifiers.

In order to investigate the extent to which the deactivation of silica by alkyldimethylchlorosilanes can be attributed to steric exclusion of solutes from existing silanols by the pendant methyl groups, a comparison was made between silica samples that had been modified by either ODDHCS or ODDMCS in such a way that the coverage by each modifier was approximately the same. This was accomplished by stopping the bonding process early (8 h for ODDHCS and 10 h for ODDMCS). The coverage on the ODDHS-bonded silica was 1.53 groups per nm^2 and the coverage on the octadecyldimethylsilyl (ODDMS)-bonded silica was 1.59 groups per nm^2. The retention of methoxybenzene and methyl benzoate in a mobile phase of hexane was used to measure the residual silanol activity. The resulting capacity factors are also listed in Table III. The capacity factors in Table III cannot be compared with those in Table II, because the hexane used for the former was drier. However, the comparisons within each table are valid, since the same batch of hexane was used throughout each set of experiments. The retention of both solutes by the ODDHS-bonded silica was roughly twice that of the ODDMS-bonded silica. This shows that even though essentially the same number of silanols was present after bonding, those next to a silicon atom with pendant hydrogens instead of methyl groups were much more available for adsorption by a solute or perhaps for further reaction with a silylating reagent.

It was possible to investigate the role of residual silanols in reversed-phase liquid chromatography in a novel manner, using the previously mentioned pair of octadecylsilyl-bonded columns, because both adsorbents contained approximately the same carbon load (14.41% C for ODDHS-bonded silica and 16.21% C for ODDMS-bonded silica) and very close to the same number of bound octadecyl chains per unit area, but the residual activity of the remaining silanols was very different. The retention of a variety of solutes by both bonded silicas was measured using methanol–water (40:60, v/v) as mobile phase. The solutes were chosen to represent

TABLE III

RETENTION OF SOLUTES USING HEXANE AS MOBILE PHASE

Surface modifier	Groups per nm^2	Capacity factor, k'	
		Anisole	Methylbenzoate
Octadecyldihydrochlorosilane	1.53	8.5	49
Octadecyldimethylchlorosilane	1.59	4.1	21

TABLE IV

COMPARISON OF RETENTION OF SOLUTES USING METHANOL–WATER (40:60) AS MO-BILE PHASE

Solute	Capacity factor, k'		Ratio k'_2, k'_1
	ODDHS-bonded silica (k'_1)	ODDMS-bonded silica (k'_2)	
Analine	2.80	2.36	0.84
Benzylamine	5.48	5.39	0.98
Phenol	2.66	2.63	1.01
Benzyl alcohol	2.86	2.88	1.01
Benzaldehyde	5.05	5.15	1.02
Phenethylalcohol	4.76	5.12	1.08
3-Phenyl-1-propanol	9.72	10.74	1.10
4-Phenyl-1-butanol	20.0	22.57	1.13
Benzene	9.61	12.21	1.27
Toluene	22.5	30.3	1.35
Ethylbenzene	48.3	69.0	1.43

a broad range of polarities and functional groups to investigate the range of inter-actions available with the solvated bonded phase. A phenyl group was also included in each solute for convenient and sensitive detection by UV absorption at 254 nm. The results are shown in Table IV along with the ratios obtained by dividing the capacity factor of each solute in the ODDMS column by the capacity factor of the same solute in the ODDHS column. In order to facilitate the interpretation of the results, the solutes in Table IV can be divided into three categories. Solutes which were more retained by the ODDHS column are basic solutes, solutes about equally retained by both stationary phases are hydrogen-bonding solutes of intermediate polarity, and solutes which were markedly more retained by the ODDMS-bonded silica are the solutes of lowest polarity.

These results can be explained by considering the polarity profile proposed to exist in bonded phases when they are used as reversed-phase sorbents with mixed solvents as the mobile phases[13]. It must be realized that the retention of each solute will be influenced most by changes in the region of the stationary phase where its interactions are energetically most favorable. As observed, solutes retained mostly in the upper regions of the stationary phase, such as the alcohols, should experience little difference between the two stationary phases. Also as observed, solutes inter-acting with the highest energy in the near-surface region of the stationary phase, such as the basic solutes, should experience a difference between the two stationary phases, reflecting the greater polarity of the ODDHS-bonded silica. Low-polarity solutes, such as the alkylbenzenes, interact most energetically with the central region of the stationary phase, where the polarity is a minimum. The decreased retention of these solutes by the ODDHS-bonded silica indicates that the absence of methyl groups on the bonding silicon atom or in the near-surface region allows silanol groups on the surface to have a greater influence on the polarity of the central region of the sta-tionary phase. Thus, residual silanols serve as high-energy adsorption sites for basic solutes and affect the retention of other solutes by influencing the polarity of other

regions in the stationary phase through hydrogen-bonding interactions with the polar components of mixed mobile phases.

Bonded phases of the type described in this paper would not be of practical use if it were difficult to oxidize the bound Si–H functionalities selectively. If they instead oxidized slowly with use, they would show transient chromatographic characteristics. Much has been written about the use of silyl hydrides as selective reducing agents for organic compounds. Dibutyltin diacetate is a commonly used catalyst for this purpose[26]. By refluxing silica modified with ODDHCS in a solution of dibutyltin diacetate and hydrogen peroxide in methanol for a few hours, 90% of the Si–H groups originally present were oxidized (judging from the intensity of the IR band at 2155 cm^{-1} relative to bands near 3000 cm^{-1}). This is a promising result. Silicon hydrides also readily add across C–C double bonds[27]. This implies that compounds with two double bonds might be used to cross-link neighboring Si–H groups. Experiments designed to oxidize bound silyl hydrides with the intent of cross-linking the newly oxidized surface sites in order to further alter the activity of the surface and to stablize it toward hydrolysis are underway and will soon be reported.

CONCLUSIONS

A group of new alkylchlorosilanes has been synthesized and successfully bound to the surface of silica. It has been shown that alkyldihydrochlorosilanes can be bound in a monomeric fashion to silica and that replacing bulky methyl groups on the bonding silicon atom with hydrogens reduces the steric hindrance of the bonding group and leads to higher surface coverage. It has also been shown that part of the surface deactivitation of silica by alkyldimethylchlorosilanes is due to steric factors. Finally, there is good evidence that surface-bound silyl hydrides can be selectively oxidized for future *in situ* cross-linking of neighboring groups.

ACKNOWLEDGEMENTS

REFERENCES

1 R. E. Majors, H. G. Barth and C. H. Lochmuller, *Anal. Chem.*, 56 (1984) 300R.
2 D. Morel and J. Serpinet, *J. Chromatogr.*, 248 (1982) 231.
3 R. C. Bogar, J. C. Thomas and J. B. Callis, *Anal. Chem.*, 56 (1984) 1080.
4 R. K. Gilpin and M. E. Gangoda, *J. Chromatogr. Sci.*, 21 (1983) 352.
5 R. M. McCormick and B. L. Karger, *Anal. Chem.*, 52 (1980) 2257.
6 C. R. Yonker, T. A. Zwier and M. F. Burke, *J. Chromatogr.*, 241 (1982) 257.
7 C. R. Yonker, T. A. Zwier and M. F. Burke, *J. Chromatogr.*, 241 (1982) 269.
8 K. Karch, I. Sebastion and I. Halász, *J. Chromatogr.*, 122 (1976) 3.
9 W. R. Melander, J. F. Erard and Cs. Horváth, *J. Chromatogr.*, 282 (1983) 211.
10 A. Nahum and Cs. Horváth, *J. Chromatogr.*, 203 (1981) 53.
11 K. E. Bij, Cs. Horváth, W. R. Melander and A. Nahum, *J. Chromatogr.*, 203 (1981) 65.
12 J. Köhler, D. B. Chase, R. D. Farlee, A. J. Vega and J. J. Kirkland, *J. Chromatogr.*, 352 (1986) 275.
13 T. C. Schunk and M. F. Burke, *J. Chromatogr.*, submited for publication.

14 G. E. Berendsen and L. De Galan, *J. Chromatogr.*, 196 (1980) 21.
15 S. A. Wise and W. E. May, *Anal. Chem.*, 55 (1983) 1479.
16 C. H. Lochmuller and D. R. Wilder, *J. Chromatogr. Sci.*, 17 (1979) 574.
17 G. E. Berendsen, K. A. Pikaart and L. De Galan, *J. Liq. Chromatogr.*, 3 (1980) 1437.
18 L. C. Sanders and S. A. Wise, *Anal. Chem.*, 56 (1984) 504.
19 R. K. Gilpin, D. J. Camillo and C. A. Janicki, *J. Chromatogr.*, 121 (1976) 13.
20 H. Anderson and A. Hendifar, *J. Am. Chem. Soc.*, 81 (1959) 1027.
21 A. Stock and C. Somieski, *Ber. Dtsch. Chem. Ges.*, 52 (1919) 695.
22 B. N. Dolgov, M. G. Voronkov and S. N. Borisov, *Zh. Obshch. Khim.*, 27 (1957) 709.
23 M. G. Voronkov and L. A. Abramas, *Izv. Akad. Nauk, S.S.S.R. Ser. Khim.*, 27 (1978) 1181.
24 L. Boksanyi, O. Liardon and E. Sz. Kovats, *Adv. Coll. Int. Sci.*, 6 (1976) 95.
25 R. K. Gilpin and M. F. Burke, *Anal. Chem.*, 45 (1973) 1383.
26 J. Lipowitz and S. Bowman, *J. Org. Chem.*, 38 (1973) 162.
27 T. H. Mourey and S. Siggia, *Anal. Chem.*, 51 (1979) 763.

CHROMSYMP. 965

EFFECT OF MODEL INACCURACY ON SELECTIVITY OPTIMIZATION PROCEDURES IN REVERSED-PHASE LIQUID CHROMATOGRAPHY

PETER J. SCHOENMAKERS*

Philips Research Laboratories, P.O. Box 80 000, 5600 JA Eindhoven (The Netherlands)

and

THOMAS BLAFFERT

Philips Research Laboratories, Vogt-Koelln Strasse 30, D-2000 Hamburg 54 (F.R.G.)

SUMMARY

Interpretive methods for the optimization of the selectivity in chromatography require the description of the retention surfaces of all individual solutes in a mixture by some kind of model. The requirements and availability of such models are discussed for the particular case of optimizing ternary and quaternary mobile phase compositions in reversed-phase liquid chromatography.

It is concluded that in order to allow an adequate prediction of the optimal conditions, a model equation should describe the experimental data to within 1% or less (in terms of the capacity factor k). Several suggested models from the literature were tried, but it appears that none of the currently available models provides a description of the data with the required accuracy. It is demonstrated that this situation does not improve when more experimental data become available.

The alternative of using piecewise (linear) interpolation is discussed, and it is demonstrated that this approach may provide a sufficiently accurate description of the data on the basis of a limited number of carefully selected experiments.

INTRODUCTION

Methods for the optimization of chromatographic selectivity can roughly be divided into simultaneous, sequential and interpretive procedures[1]. In simultaneous (or "grid search") procedures, a (large) number of chromatograms are recorded according to a pre-planned experimental design ("grid") and the optimum is identified as the best chromatogram obtained. In sequential procedures (*e.g.*, Simplex optimization), the optimum is approached in a stepwise manner. A minimum number of chromatograms is recorded and the resulting data are used to establish conditions for a subsequent experiment that is expected to be closer to the optimum.

Both categories of optimization procedures suffer from the large number of experiments that are required to locate the optimum (see Table I). Typically, a grid search optimization involving two parameters may require about 100 experiments, and a typical number for Simplex optimization is 25–40[2]. Such a large number of

experiments is unattractive for the optimization of the selectivity in reversed-phase liquid chromatography (RPLC) for two reasons: (1) the time required for equilibrating the system and recording a chromatogram is typically about 30 min; and (2) some of the most relevant parameters (*e.g.*, the mobile phase pH) are difficult to control automatically in small steps over a wide range.

The reason why so many experiments are required for the optimization of the selectivity in chromatography is the complexity of the response surface, which describes the variation of the quality of the chromatogram ("optimization criterion") as a function of the parameters considered. A typical response surface may contain a number of maxima (local optima). Only one of these represents the true (global) optimum. For several reasons[1], the global optimum should be the aim of optimization procedures. Because of the complexity of the response surface, the application of a simultaneous optimization method requires a fine grid and hence a large number of experiments to locate the global optimum. The result of a sequential optimization procedure is likely to be one of the local optima.

In order to locate the global optimum with a small number of experiments (typically between 5 and 15), a number of procedures have been developed specifically for the optimization of chromatographic selectivity. These methods can be classified as interpretive methods. By definition, interpretive methods are those which:

(1) interpret a chromatogram in terms of the retention times of the individual solutes;

(2) describe the retention surface of each individual solute with some kind of model;

(3) use this model for the retention surfaces and a suitable optimization criterion to calculate the response surface; and

(4) locate the optimum on the response surface.

The first of these steps greatly increases the complexity of the optimization procedure, as is indicated in Table I. Not only are the retention times of the peaks in each chromatogram required, but also the order in which the peaks appear is relevant for establishing the retention surfaces of the individual solutes. The peaks obtained for a particular solute need to be assigned the same label or number in each chromatogram, which implies that peaks need to be recognized (but not identified) in each chromatogram. This problem has recently received much attention, especially in connection with RPLC[3], and will not be discussed further in this paper.

TABLE I

SUMMARY OF METHODS FOR OPTIMIZING CHROMATOGRAPHIC SELECTIVITY

Characteristic	Procedure		
	Simultaneous	Sequential	Interpretive
Required number of experiments	Very large	Large	Small
Optimum found	Global	Local	Global
Complexity of method	Low	Moderate	High
Accuracy of optimum	Low	High	Variable*

* The accuracy of the predicted optimum is the subject of this paper. A high accuracy may be obtained with an iterative procedure (see below).

The second step in the above series is the most critical. Interpretive methods owe their existence to the observation that retention surfaces of individual solutes are much simpler than the response surface of the entire mixture and may therefore be described adequately by some kind of model. This model may be a (set of) mathematical equations or (for one-parameter optimization problems) a graphical relationship. Alternatively, the retention surface may be approximated by linear interpolation between the experimental data points.

If the model provides a perfect description of the true retention surface, then the calculation of the response surface (step 3 above) and the location of the true (global) optimum (step 4) are almost trivial. Unfortunately, such perfect models do not exist and therefore the reliability and the accuracy of the optimum that results from an interpretive optimization method is determined by the accuracy with which the true retention surfaces are described by the model.

One way to improve the accuracy of the predicted optimum is to use iterative methods. These are interpretive methods, in which the predicted optimum is verified by a new experiment (at or around the location of the predicted optimum) and the resulting data are used to improve the model and to calculate a new optimum.

In this work we investigated the description of the retention surface in RPLC using ternary and quaternary mobile phase mixtures. Several mathematical models were used in attempts to describe the retention surfaces within experimental error. The practical consequences of deviations between the models and the true retention surfaces are demonstrated using simulated chromatograms.

TERNARY MOBILE PHASE MIXTURES

Experimental data for ternary mobile phases were taken from the compilation in ref. 4. Practical optimization processes should focus on mobile phase mixtures that yield roughly optimal capacity factors (e.g., $1 < k < 10$). Hence, interest is limited to solvents within a small range of eluotropic strengths (see Table II), i.e., to a narrow band in the triangle representing all possible ternary mixtures. Fig. 1 illustrates the experimental locations that were considered for mixtures consisting of water, methanol and tetrahydrofuran (THF). The solvent compositions are given in Table II,

TABLE II

COMPOSITION AND ELUOTROPIC STRENGTH OF MOBILE PHASE MIXTURES CONSIDERED FOR THE SYSTEM WATER–METHANOL–THF

Data point No.	Water (%)	Methanol (%)	THF (%)	Eluotropic strength*
1	40	60	0	60
2	30	70	0	70
3	50	25	25	65
4	40	30	30	78
5	60	0	40	65
6	50	0	50	81
7	35	65	0	65
8	40	45	15	69

* Expressed as the corresponding percentage of methanol.

Fig. 1. Experimental data points considered for the system water–methanol–THF. Experimental data were taken from ref. 4. See also Table II. MeOH = methanol.

together with the eluotropic strength expressed as the corresponding percentage of methanol (see refs. 5 and 6). In Table II 1% of methanol was assumed to correspond to 0.62% of THF[6].

The experimental data for the logarithm of the capacity factor can be described by a quadratic equation[4]:

$$\ln k = A_m \varphi_m^2 + A_t \varphi_t^2 + B_m \varphi_m + B_t \varphi_t + C + D \varphi_m \varphi_t \qquad (1)$$

where φ_m is the volume fraction of methanol in the mobile phase and φ_t is the volume fraction of THF. A_m, A_t, B_m, B_t, C and D are the six coefficients of the quadratic expression, the values of which will be dependent on the solute. If six experimental capacity factors are available, then the coefficients can be determined and it is in principle possible to calculate the capacity factors at other compositions. For example, the first six data points in Table II may be used to calculate the coefficients of eqn. 1. This could be done for 30 solutes using the data in ref. 4. Using the coefficients thus obtained, the retention data at points 7 and 8 were calculated and compared with the experimental data. For point 7, which is located between and close to data points 1 and 2 (see Fig. 1), the average deviation between the calculated and experimental values for ln k was 0.031. This corresponds to an average error in the predicted capacity factors of about 3%. However, for point 8, which is not so close to the other experimental data points, the average deviation was 0.193, which corresponds to an average error in k between the model equation and the experimental data of about 20%.

The effect of the large deviations between the model equation and the experimental data at point 8 is illustrated in Fig. 2, which shows the (simulated) experimental chromatogram for five selected solutes (thin line) and the predicted chromatogram from the model (thick line). The simulated chromatogram is reconstructed by a computer program, using the experimentally observed capacity factors. Obviously, the two chromatograms are entirely different.

Fig. 3a shows the response surface for the separation of the five solutes in Fig. 2, calculated using the retention surfaces for the individual solutes, which were calculated from the retention data at the first six data points. The response surface shows the variation of a selected optimization criterion, representing the quality of the separation, as a function of the parameters in the parameter space. The criterion
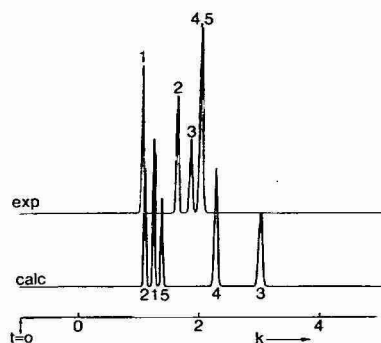
Fig. 2. Calculated (thick line) chromatogram at point 8 using the quadratic model of eqn. 1 fitted through the first six data points. The thin line shows a (simulated) experimental chromatogram. Solutes: 1 = anisole; 2 = *o*-cresol; 3 = N-methylaniline; 4 = *p*-nitroacetophenone; 5 = 3-phenylpropanol. Mobile phase: water–methanol–THF (40:45:15).
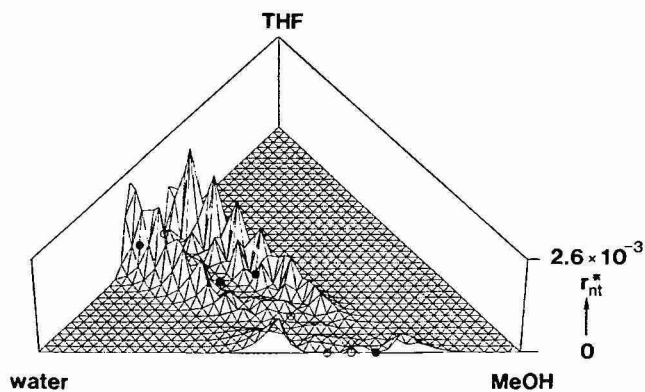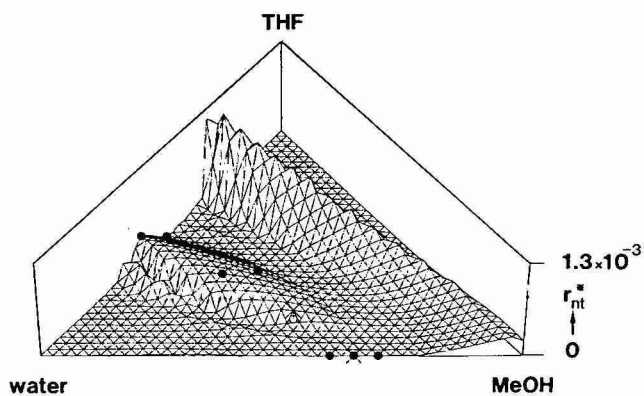
Fig. 3. (a) Response surface for the five solutes in Fig. 2 in the triangle shown in Fig. 1, calculated from the retention surfaces of the individual solutes using the quadratic model of eqn. 1 fitted trough the first six data points. Deviations between the experimental response and the calculated response are indicated for points 7 and 8. Crosses indicate data points not included in establishing the model. (b) As (a), but now with the quadratic model fitted through seven data points (1–6 and 8). Error bars may be observed for data point 7 (not included) and several other data points.

used in Fig. 3 is the time-corrected resolution product[1]. This criterion is based on the calibrated normalized resolution product (r^*) of Drouen et al.[7]:

$$r^* = \prod_{i=0}^{n} (R_s/\bar{R}_s) \tag{2}$$

where R_s is the resolution between two successive peaks in the chromatogram and $\bar{R}_s$ the average resolution for all pairs of successive peaks. Both the product and the average are taken from $i = 0$ (the zeroth peak being a hypothetical peak at $t = t_0$) to $i = n$ (where n is the number of peaks in the chromatogram). The time-corrected resolution product is

$$r^*_{\text{nt}} = \exp\left(\frac{\ln r^*}{n}\right)\bigg/ t_{\text{ne}} \tag{3}$$

where t_{ne} is a measure of the required analysis time and n is again the number of peaks.

In Fig. 3a, the actual response calculated from the experimental capacity factors is indicated at the locations of the six points in Fig. 1. The bold dots are located above the response surface (i.e., the predicted response is lower than the experimental response). Open circles represent response values below the predicted surface. A cross indicates the points that were not included in fitting the model. The difference between the actual (experimental) response at points 7 and 8 and the predicted response is indicated by vertical error bars. It is seen that a smooth response surface is predicted in the experimental range, but that extrapolation outside this area suggests that the location of the global optimum is at much higher concentrations of organic modifier.

It can be concluded from Figs. 2 and 3a that an optimization procedure in which (1) experimental data are obtained at the locations of the first six points in Table II (or Fig. 1) and (2) the retention surfaces are fitted by the quadratic model of eqn. 1 is not sufficient accurate to predict the location of the optimum. This conclusion is not only valid for the example involving five solutes, but may be extended to the entire set of 30 solutes of ref. 4 (see Table III). We also fitted the model equations to several other selections of six data points from Fig. 1, but the description of the two remaining data points was always much worse than in the situation described above. Therefore, in order to improve this situation, either the number of experiments needs to be increased or a better model should be used to describe the retention surfaces.

REGRESSION ANALYSIS

As point 8 appears to be badly described by the model if only six data points are available, it is logical to "obtain" additional experimental data at this location. The average deviation between the quadratic model and the experimental data using seven data points (1–6 and 8) to establish the six coefficients in eqn. 1 is illustrated in Table III (last column).

Table III shows that the large deviation for point 8 is reduced by a factor of about 3. However, the errors are now distributed more evenly over the entire parameter space and the first six data points, which were by definition described exactly by the model through six points, now show average deviations that are typically a few percent, but up to about 8% (in terms of k) for data point 3. Fig. 4 shows examples of (simulated) experimental and calculated chromatograms for the same solutes as in Fig. 2 at the compositions of data points 8, 3, 2 and 4 (Fig. 4a–d, respectively).

Fig. 4a shows that the prediction of the chromatogram at point 8, although better than in Fig. 2, is still unacceptable for optimization purposes. At point 3, where the average deviation between the model and the experimental data is about 8%, we see that the elution order is predicted correctly by the model and that the baseline separation predicted by the model can indeed be obtained for all solutes in practice (see Fig. 4b). Nevertheless, there are considerable differences in retention times (k values) between the predicted and the experimental chromatograms. In fact, Fig. 4b represents a fortuitous example, as is demonstrated in Fig. 4c. This figure, showing the calculated and experimental chromatograms at point 2, yields only minor deviations between the predicted and experimental capacity factors (the average deviation is 2.9% at point 2). However, the model predicts solutes 1 and 5 to be reasonably separated, whereas solutes 2 and 3 are expected to co-elute. In practice, solutes 1 and 5 overlap completely and solutes 2 and 3 are separated to the baseline. Finally, Fig. 4d shows that at point 4, where the average deviation is 0.3% in terms of k, the model yields a perfect prediction of the experimental chromatogram.

It appears from Fig. 4 that in order to use model equations for the retention surfaces for optimization purposes, deviations between the model and the experimental data of a few percent cannot be accepted (Fig. 4c). The accuracy of the model needs to be (much) greater than 1% to yield reliable predictions of the optimal chromatographic conditions (Fig. 4d). This conclusion should be seen in the perspective of possible experimental errors in the determination of capacity factors. A reasonable

TABLE III

AVERAGE DEVIATIONS (× 100) BETWEEN THE CALCULATED AND EXPERIMENTAL VALUES FOR ln k USING THE QUADRATIC MODEL OF EQN. 1 TO DESCRIBE THE RETENTION SURFACES

Thirty solutes for which data are available in ref. 4 were included in the calculations. Data points refer to Table II.

Data point No.	No. of data points included	
	6	7
1	—	1.3
2	—	2.9
3	—	8.2
4	—	0.3
5	—	2.9
6	—	0.6
7	3.1	7.3
8	19.3	7.2
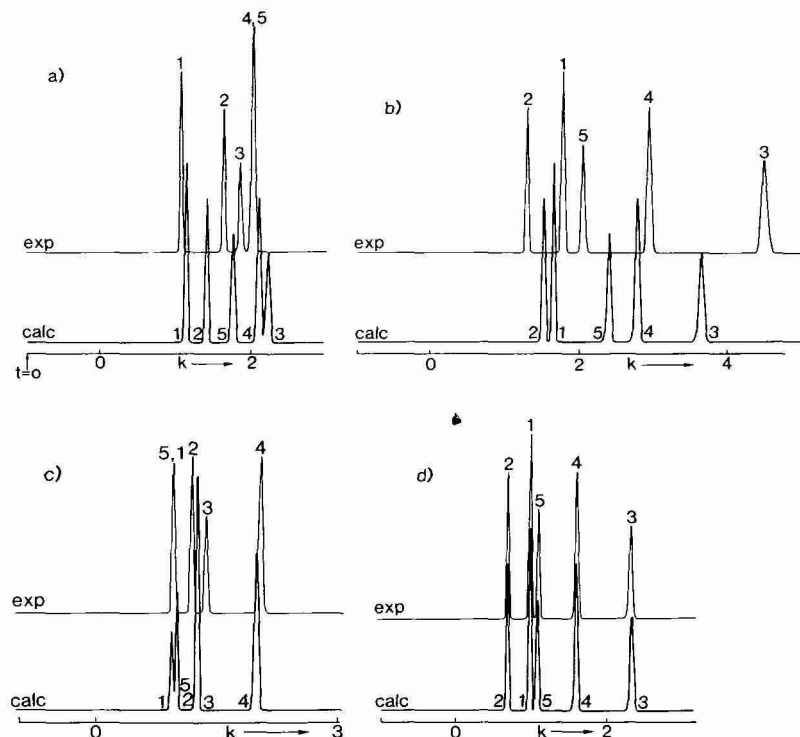
Fig. 4. Calculated (thick line) chromatogram at points 8, 3, 2 and 4 using the quadratic model of eqn. 1 fitted through seven data points (1–6 and 8). The thin lines show (simulated) experimental chromatograms. Solutes as in Fig. 2. Mobile phases: (a) water–methanol–THF (40:45:15) (point 8; average deviation for all solutes 7.2%); (b) water–methanol–THF (50:25:25) (point 3; average deviation 8.2%); (c) water–methanol (30:70) (point 2; average deviation 2.9%); (d) water–methanol–THF (40:30:30) (point 4; average deviation 0.3%).

estimate for the experimental error in terms of k is 1% (see also ref. 4). A more accurate determination of k would require considerable extra precautions. Therefore, we should aim to describe the data within experimental error.

Fig. 3b shows the response surface obtained for the five solutes in Fig. 2, now calculated using the retention surfaces fitted through seven data points (data point 7 was not included, as is indicated by a cross in the figure). Error bars may also be observed for other points in this figure, but the most striking feature is the vastly different overall appearance of the response surface. This underlines the sensitivity of interpretive optimization procedures to slight alterations in the model fitted through the retention surfaces. Moreover, the vast differences between Fig. 3a and b are indicative of the fact that whereas an accurate description of the response surface within the experimental parameter space is difficult, extrapolations outside the experimental range are tentative at best.

In order to investigate the effect of additonal data points on the accuracy of the description of the retention surfaces by a quadratic model, we referred to the ternary system water–methanol–acetonitrile. The locations of the available experi-
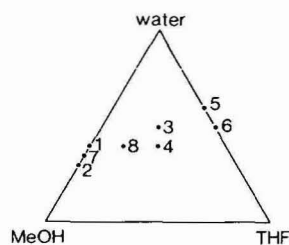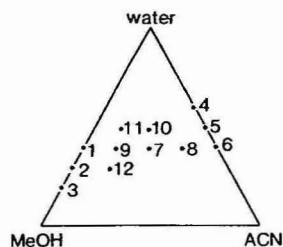
Fig. 5. Experimental data points considered for the system water–methanol–acetonitrile. Experimental data were taken from ref. 4. See also Table IV. ACN = acetonitrile.

mental data in a limited part of the triangle are illustrated in Fig. 5 and Table IV. In Table IV, 1% of methanol was assumed to correspond to 0.78% of acetonitrile[6].

Table V shows the average deviations observed between the quadratic model of eqn. 1 and the experimental data at the 12 data points shown in Fig. 5 and Table IV. The number of data points included in the regression analysis is increased progressively from 7 to 12 in the table. Again, the average deviations could not be reduced by selecting another set of seven data points. It is shown that the average deviations are generally larger for data points that are not included in the regression analysis (typically 10–30%) than for data points that are included (typically 10% or less). The observation in Table III that the errors are distributed more evenly over the entire parameter space when more experimental data points are added to the model is underlined in Table V. It is obvious from Table V that the addition of more data points does not lead to a description of the data that is sufficiently accurate in the light of the conclusions obtained from Fig. 4.

TABLE IV

COMPOSITION AND ELUOTROPIC STRENGTH OF MOBILE PHASE MIXTURES CON-SIDERED FOR THE SYSTEM WATER–METHANOL–ACETONITRILE

Data point No.	Water (%)	Methanol (%)	Acetonitrile (%)	Eluotropic strength[*]
1	40	60	0	60
2	30	70	0	70
3	20	80	0	80
4	60	0	40	51
5	50	0	50	64
6	40	0	60	77
7	40	30	30	68
8	40	15	45	73
9	40	45	15	64
10	50	25	25	57
11	50	37.5	12.5	54
12	30	52.5	17.5	75

* Expressed as the corresponding percentage of methanol.

TABLE V

OBSERVED AVERAGE DEVIATIONS ($\times$ 100) IN ln k BETWEEN THE QUADRATIC MODEL (EQN. 1) AND EXPERIMENTAL DATA FROM REF. 4 FOR THE SYSTEM WATER–METHANOL–ACETONITRILE FOR 49 SOLUTES

The number of data points included in the regression analysis increases in the table.

n^*	Data point No.											
	1	2	3	4	5	6	7	8	9	10	11	12
7	3.7	6.4	2.8	2.0	3.2	1.3	0.0	30.7	7.8	21.2	16.5	21.6
8	5.0	5.2	2.3	1.6	2.6	7.5	13.5	18.0	15.0	29.4	20.9	12.7
9	7.1	4.8	2.1	1.5	2.4	9.2	9.1	20.5	9.7	25.2	16.6	13.2
10	11.0	6.6	1.2	6.2	2.1	10.5	4.5	23.2	6.8	16.2	15.1	17.9
11	11.6	6.2	1.5	6.8	5.2	9.9	4.3	22.5	6.0	16.4	6.9	17.8
12	13.3	5.9	4.0	7.9	6.6	9.6	8.2	20.1	6.1	18.3	6.5	11.0

* First n data points in the table were included in the regression analysis.

ALTERNATIVE MODELS

We have concluded above that the prediction of the response surface using the quadratic model cannot be improved sufficiently by adding more experimental data points. The logical conclusion then is that a model is required which describes the experimental retention data more accurately, preferably within experimental error. Several different mathematical expressions have been fitted to the data for the water–methanol–THF system in order to try and find a more accurate description. All of these models are based on some kind of physical picture for the chromatographic process, as described in the original literature. To allow a fair comparison with eqn. 1, the different alternative models were all used in the form of equations with six coeficients.

Reciprocal model

Plotting $1/k$ instead of ln k against composition in RPLC has been suggested by McCann et al.[8]. The resulting plots yield slightly curved lines for binary mixtures. Therefore, a quadratic model analogous to that described by eqn. 1 has been fitted to the data in terms of $1/k$:

$$1/k = A_m \varphi_m^2 + A_t \varphi_t^2 + B_m \varphi_m + B_t \varphi_t + C + D \varphi_m \varphi_t \qquad (4)$$

Extended linear model

The retention *vs.* composition lines in binary mixtures over limited ranges of composition may be accurately described by a straight line[9,10]. Eqn. (1) reduces to a quadratic curve if either φ_m or φ_t is zero (binary mixtures) or if the ratio φ_m/φ_t is held constant (pseudo-binary mixtures). An equation that yields a straight line for both binary and pseudo-binary mixtures is

$$\ln k = A R^2 + B R + C + (D R^2 + E R + F)\psi \qquad (5)$$

where ψ is the total volume fraction of solvents ($\psi = \varphi_m + \varphi_t$) and R is a ratio defined as

$$R = \varphi_t/(\varphi_m + \varphi_t) = \varphi_t/\psi \tag{6}$$

Logarithmic model

An extended version of the logarithmic model of Lu and Lu[11] for ternary mixtures may be formulated as

$$\ln k = A + B \varphi_m + C \varphi_t + D \ln (1 + E \varphi_m + F \varphi_t) \tag{7}$$

We were not able to fit this model, nor various similar equations involving a logarithmic function, to our data. It appears that over limited ranges of eluotropic strength the linear and logarithmic contributions to $\ln k$ are not sufficiently different for the numerical process to converge.

Piecewise linear interpolation

The retention surfaces can be approximated by piecewise linear interpolation. For example, the retention data at point 7 can be estimated from those at points 1 and 2, and the retention data at point 8 from points 1 and 4 (see Fig. 1). An important aspect of linear interpolation is that the description of the retention data at the experimental locations remains exact if additional experiments become available. We have seen above that this is not the case if a model equation (*e.g.*, the quadratic eqn. 1) is used, as was demonstrated in Table V, We shall return to this aspect later.

Table VI summarizes the results obtained with the different models. It is seen that the average deviations between the model and the experimental data do not vary a great deal between the different models, and that in general none of the above models provides a description of the retention surfaces to within the required accuracy of 1% or better.

TABLE VI

AVERAGE DEVIATIONS ($\times$ 100) BETWEEN THE CALCULATED AND EXPERIMENTAL VALUES FOR $\ln k$ USING VARIOUS MODELS TO DESCRIBE THE DATA

All solutes for which data are available in ref. 4 have been included in the calculations. Data points refer to Table II.

Model	Eqn.	n^*	Data point No.							
			1	2	3	4	5	6	7	8
Quadratic	1	6	—	—	—	—	—	—	3.1	19.3
Quadratic	1	7	1.3	2.9	8.2	0.3	2.9	0.6	7.3	7.2
Reciprocal	4	6	—	—	—	—	—	—	4.9	17.9
Reciprocal	4	7	2.3	2.2	10.4	0.2	3.7	0.3	4.9	17.9
Extended linear	5	7	5.0	0.0	0.0	9.9	1.6	3.3	2.8	13.3
Linear interpolation**	—	—	—	—	—	—	—	—	2.8	23.7

  * Number of data points used to model the retention surfaces.
  ** Data at point 7 can be found from a linear interpolation between points 1 and 3. Point 8 can be found from points 1 and 4.

QUATERNARY MOBILE PHASE MIXTURES

A convenient way to create quaternary mobile phase mixtures for RPLC is to combine variable proportions of three isoeluotropic binary mixtures[12]. This has the effect that all resulting mixtures may also be expected to be isoelutropic, *i.e.*, give rise to roughly the same capacity factors. Such a strategy has been applied for optimization purposes by Glajch *et al.*[12]. The composition of isoeluotropic quaternary mixtures can again be represented by a triangle, in which the isoeluotropic binary mixtures are located at the corners and identified by bars above the abbreviations for the modifiers (*e.g.*, methanol). This design is illustrated in Fig. 6.
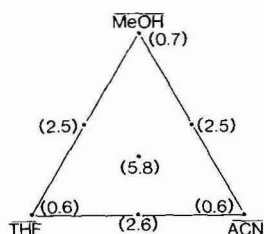
Fig. 6. Experimental design involving isoeluotropic binary (vertices), ternary (edges) and quaternary (centre) mobile phase mixtures for RPLC. The figures indicate the observed average deviation between the experimental data and the model of eqn. 8 in terms of ln *k*.

The data of Glajch *et al.*[12] may again be fitted to a quadratic expression, similar to eqn. 1:

$$\ln k = A_m \, \bar{\varphi}_m^2 + A_t \, \bar{\varphi}_t^2 + B_m \, \bar{\varphi}_m + B_t \, \bar{\varphi}_t + C + D \, \bar{\varphi}_m \, \bar{\varphi}_t \tag{8}$$

where $\bar{\varphi}_m$ and $\bar{\varphi}_t$ now represent the volume fractions of the isoeluotropic binary mixtures of methanol and water and THF and water, respectively. Data for nine substituted naphthalenes are available from ref. 12. The resulting average deviations are indicated in Fig. 6. The observed deviations are small for the binary mixtures on the vertices of the triangle, a few percent for the ternary mixtures along the sides and up to 6% for quaternary mixtures in the centre. A figure of 6% was also reported by D'Agostino *et al.*[13] for the description of retention data in (non-isoelutropic) quaternary mixtures. This implies that once again the accuracy of the description is insufficient for optimization purposes (see Fig. 4). However, the situation is slightly more favourable than is indicated by the data in Fig. 6. Fig. 7 shows the retention surfaces for two of the solutes. Clearly, these are smooth surfaces. The deviations between the model and the experimental data are indicated by vertical bars. For the two solutes shown in Fig. 7, and also for the other six solutes, the model predicts *k* values that are slightly too high for all three ternary mixtures and too low for the quaternary mixture. This implies that deviations from the model will be systematic and that small errors in the predicted absolute retention times (*k* values) will be levelled out to some extent when it comes to relative retentions (α values).

Fig. 8 shows the calculated chromatogram (predicted from the model) and the (simulated) experimental chromatogram for the quaternary mixture in the centre of
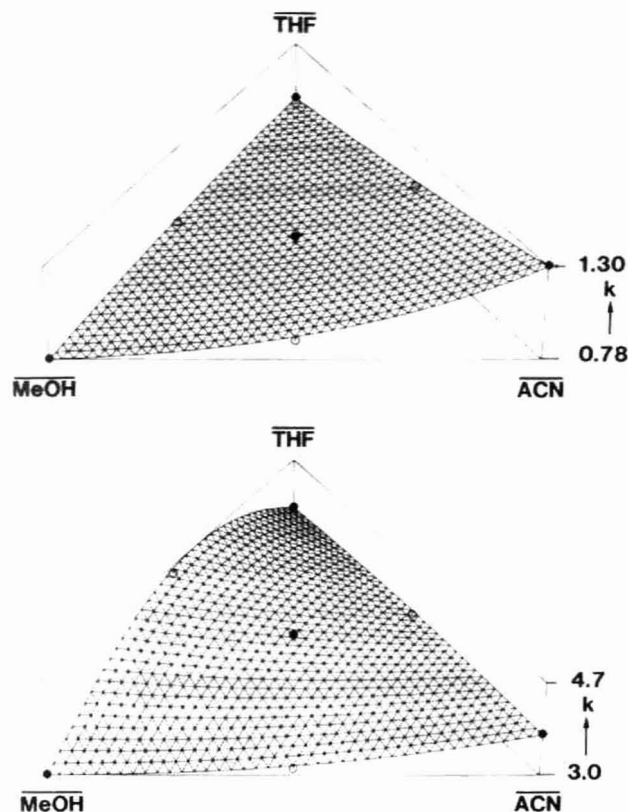
Fig. 7. Retention surfaces for 2-naphthyl methyl sulphone (solute 2) and 1-nitronaphthalene (solute 5) in the parameter space of Fig. 6 calculated using eqn. 8. Deviations between the model equation and the experimental data are indicated. Bold dots are located above the surface; open circles are located underneath.
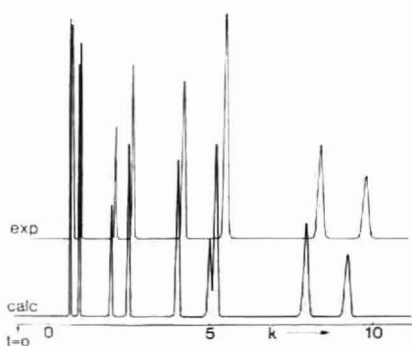
Fig. 8. Calculated (thick line) chromatogram at the quarternary mobile phase composition in the centre of Fig. 6 using the quadratic model of eqn. 8 fitted through all seven data points. The thin line shows a (simulated) experimental chromatogram. Solutes: 1 = 1-acetaminonaphthalene; 2 = 2-naphthyl methyl sulphone; 3 = 2-hydroxynaphthalene; 4 = 1-acetylnaphthalene; 5 = 1-nitronaphthalene; 6 = 2-methoxynaphthalene; 7 = naphthalene; 8 = 1-naphthyl methyl sulphide; 9 = 1-chloronaphthalene. Mobile phase: water–methanol–THF–acetonitrile (49:21:13:17).

$$\overline{THF}$$

$$-1.3 \cdot 10^{-4}$$
$$r_{nt}^{\bullet}$$
$$\downarrow$$
$$0$$

$$\overline{MeOH} \qquad\qquad\qquad \overline{ACN}$$
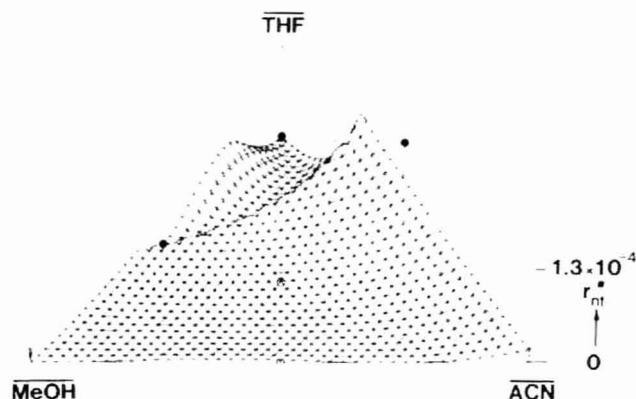
Fig. 9. Response surface calculated from the coefficients in Table VII for the solutes shown in Fig. 8. The deviations between the true (experimental) response and the calculated surface are indicated. Bold d. are located above the surface; open circles are located underneath.

the triangle. It can be seen that all components of the mixture elute slightly later in practice than predicted by the model. Again, these small differences in terms of k values may be significant in terms of resolution, as is evident in Fig. 8 for solutes 6 and 7.

Fig. 9 shows the response surface obtained for the nine solutes in Fig. 8. Considerable error bars are observed for the quaternary mixture and for the ternary mixture of THF, acetonitrile and water. The experimental response in the methanol water binary mixture is located just below the response surface. It is obvious that the accuracy of the quadratic model is again insufficient for optimization purposes.

Table VII lists the coefficients obtained for the nine solutes in Fig. 8 using eqn. 8 to model the retention surfaces.

TABLE VII

COEFFICIENTS OF EQN. 8 DESCRIBING THE RETENTION SURFACES OF THE SOLUTES IN FIG. 8

Solute No.*	Coefficient						$2A_m + 2A_t + D$	$\Delta\varphi^{**}$ (eqn. 11a)
	A_m	A_t	B_m	B_t	C	D		
1	0.84	-0.55	-0.90	0.36	-0.38	1.24	1.82	0.22
2	0.39	0.03	-0.88	-0.29	0.24	0.56	1.40	0.25
3	0.37	-0.55	0.47	1.15	0.29	1.51	1.15	0.28
4	0.34	0.04	-0.55	-0.16	1.02	0.79	1.93	0.22
5	0.22	-0.10	-0.44	0.12	1.33	1.39	1.63	0.23
6	0.22	-0.22	0.34	0.23	1.51	1.20	1.20	0.27
7	0.37	0.22	-0.52	0.31	1.55	1.34	1.64	0.23
8	0.13	-0.24	-0.17	0.21	1.93	1.26	1.04	0.29
9	0.14	-0.54	0.16	0.38	2.06	1.16	0.36	0.50

* For solute identification see Fig. 8.
** Eqn. 11a.

PIECEWISE LINEAR INTERPOLATION

We have seen above that neither the addition of extra data points nor the use of alternative model equations will lead to a description of the retention surfaces that is sufficiently accurate to allow the application of interpretive optimization procedures with fixed experimental designs. We also mentioned above that when the retention surface is approximated by linear interpolation between data points, the effect of additional data becoming available will be (1) to yield an exact description of the retention surfaces (and hence an exact prediction of the response value) at each experimental location (assuming the absence of experimental error) and (2) to increase the accuracy of interpolation.

It can easily be shown[7] that the error caused by linear interpolation of data points along a retention surface that is more accurately described by a quadratic equation (e.g., eqn. 1) is largest in the middle between two data points and amounts to

$$d = 1/4(A_m \, \Delta\varphi_m^2 + A_t \, \Delta\varphi_t^2 + D \, \Delta\varphi_m \, \Delta\varphi_t) \tag{9}$$

where d is the difference between the value of $\ln k$ obtained by linear interpolation and the value obtained using a quadratic equation that is exact for the existing data points. In eqn. 9 $\Delta\varphi_m$ and $\Delta\varphi_t$ are the distances between the existing data points in terms of the two composition parameters φ_m and φ_t.

We can use an equation similar to eqn. 9 to investigate the possibility of using piecewise linear interpolation for the description of the retention surfaces for quaternary mobile phases in Table VII. For example, if we were to approximate the complete triangle with a series of smaller equilateral triangles, the equivalent expression for the deviation between a quadratic expression and a planar triangle through three data points becomes for the centre of the triangle

$$d = 1/9(2A_m \, \Delta\varphi_m^2 + 2A_t \, \Delta\varphi_t^2 + D \, \Delta\varphi_m \, \Delta\varphi_t) \tag{10}$$

where $\Delta\varphi_m$ and $\Delta\varphi_t$ are now the lengths of the sides of the triangle in terms of φ_m and φ_t, and with $\Delta\varphi_m = \Delta\varphi_t = \Delta\varphi$ we find

$$\Delta\varphi = 3\sqrt{d} \, (2A_m + 2A_t + D)^{-1/2} \tag{11}$$

If we tolerate a deviation of 0.01 in terms of $\ln k$ (about a 1% variation in k), then

$$\Delta\varphi = 0.3(2A_m + 2A_t + D)^{-1/2} \tag{11a}$$

In Table VII the values for $\Delta\varphi$ calculated from eqn. 11a are listed for the nine retention surfaces. It can be seen that for solute 9 the entire retention surface can be described to within 1% if the triangle is divided into four smaller ones, each half the original size. This may be achieved with only six data points (Fig. 10a). For the eight remaining solutes the required size of the triangle is about one quarter of the initial size. This would require 15 data points for the entire triangle.
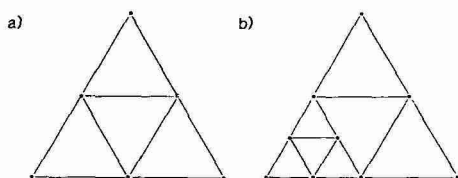
Fig. 10. (a) Possible six-point initial design for the optimization of quaternary mobile phase mixtures for RPLC. The parameter space (triangle) is divided into four parts. (b) As (a), but with three additional experiments to improve the accuracy of prediction.

A final remark concerning piecewise linear interpolation is that we have been discussing maximum errors, for instance the deviation between the model and the quadratic surface in the centre of a triangle. Anywhere else in the triangle the deviations will be smaller, so that the average deviation throughout the entire parameter space is much smaller.

ITERATIVE OPTIMIZATION PROCEDURES

Piecewise linear interpolation has been suggested by Schoenmakers et al.[14] and by Drouen and co-workers[7,15] as part of iterative optimization procedures. In such procedures, a minimum number of experimental data are collected. These data are used to make a first prediction of the location of the optimum. The next experiment is then performed at (or close to) the optimum. The additional data point is used to make a new prediction of the optimum and to establish the location of the next experiment, and so on. The main advantage of such a procedure is that the accuracy of the prediction is verified as part of the procedure and improved during each iteration cycle. Drouen et al.[15] described the application of an iterative procedure for optimization of a quaternary mobile phase composition in RPLC. We shall discuss below an example of a procedure that combines an initial fixed experimental design with an iterative approach to the optimum.

If piecewise linear interpolation is used for the optimization of quaternary mobile phase mixtures for RPLC, then an initial design of six data points may be used to divide the full triangle of Fig. 6 into four smaller ones (see Fig. 10a). According to eqn. 10, the maximum interpolation error is then (with $\Delta\varphi_m = \Delta\varphi_1 = 0.5$)

$$d = 1/36(2A_m + 2A_1 + D) \tag{10a}$$

Using the coefficients in Table VII, we expect the deviations between the calculated and experimental values of k to be of the order of 3–5% (in the centres of the four triangles). This is not sufficient to predict the optimum composition accurately (see Fig. 4). However, if it can be decided in which of the four triangles the optimum is located, then a further three experiments will allow this triangle in its turn to be divided into four smaller ones, and the accuracy of the prediction to be increased to within 1%. This is illustrated in Fig. 10b. The process may be repeated to increase further the accuracy of the predicted optimum.

As an alternative to piecewise linear interpolation, non-linear models may be used to describe parts of the parameter space with greater accuracy, as was suggested by Lankmayr and Wegscheider[16].

CONCLUSIONS

In order to make reliable predictions of optimum mobile phase compositions in interpretive optimization methods, the retention data for the individual solutes need to be known with an accuracy of greater than 1%.

Quadratic equations that describe the (logarithm of the) capacity factor as a function of composition do not provide the required accuracy. This situation cannot be improved by collecting more experimental data points, nor by using any of various alternative model equations.

A more accurate description of the retention surfaces may be obtained from a piecewise linear (or non-linear) interpolation between the available data points.

Piecewise interpolation in combination with iterative interpretive optimization procedures appears to be the most promising approach.

REFERENCES

1 P. J. Schoenmakers, *Optimization of Chromatographic Selectivity. A Guide to Method Development*, Elsevier, Amsterdam, 1986.
2 J. C. Berridge, *J. Chromatogr.*, 244 (1982) 1.
3 A. C. J. H. Drouen, H. A. H. Billiet and L. de Galan, *Anal. Chem.*, 57 (1985) 962.
4 P. J. Schoenmakers, H. A. H. Billiet and L. de Galan, *J. Chromatogr.*, 218 (1981) 261.
5 P. J. Schoenmakers, H. A. H. Billiet and L. de Galan, *J. Chromatogr.*, 205 (1981) 13.
6 P. J. Schoenmakers, H. A. H. Billiet and L. de Galan, *Chromatographia*, 15 (1982) 205.
7 A. C. J. H. Drouen, P. J. Schoenmakers, H. A. H. Billiet and L. de Galan, *Chromatographia*, 16 (1982) 48.
8 M. McCann, J. H. Purnell and C. A. Wellington, *Faraday Soc. Symp. Ser.*, 15 (1980) 82.
9 L. R. Snyder, J. W. Dolan and J. R. Gant, *J. Chromatogr.*, 165 (1979) 3.
10 P. J. Schoenmakers, H. A. H. Billiet and L. de Galan, *J. Chromatogr.*, 185 (1979) 179.
11 P. Lu and X. Lu, *J. Chromatogr.*, 292 (1984) 169.
12 J. L. Glajch, J. J. Kirkland, K. M. Squire and J. M. Minor, *J. Chromatogr.*, 199 (1980) 57.
13 G. D'Agostino, L. Castagnetta, F. Mitchell and M. J. O'Hare, *J. Chromatogr.*, 338 (1985) 1.
14 P. J. Schoenmakers, A. C. J. H. Drouen, H. A. H. Billiet and L. de Galan, *Chromatographia*, 15 (1982) 688.
15 A. C. J. H. Drouen, H. A. H. Billiet and L. de Galan, *J. Chromatogr.*, 352 (1986) 127.
16 E. P. Lankmayr and W. Wegscheider, *9th International Symposium on Column LC, Edinburgh, July 1–5, 1985*, paper L3.2.

CHROMSYMP. 1066

COPOLYMER FRACTIONATION BY GRADIENT HIGH-PERFORMANCE LIQUID CHROMATOGRAPHY

GOTTFRIED GLÖCKNER*

Dresden University of Technology, Department of Chemistry, Dresden (G.D.R.)

and

JO H. M. VAN DEN BERG*

DSM Research and Patents, FPO, Geleen (The Netherlands)

SUMMARY

The size distribution and composition of statistical copolymers has been investigated by size-exclusion chromatography (SEC) and off-line gradient high-performance liquid chromatography of the SEC fractions. The copolymers were poly(styrene–acrylonitrile) (SAN) and poly(styrene–methyl methacrylate) (SMMA) model mixtures. SAN copolymers were separated with a suitable gradient of increasing dissolution power on normal-phase columns as well as on reversed-phase columns. In contrast, SMMA copolymers were eluted from a reversed-phase column by a solubility gradient as broad bands, whereas the same gradient gave excellent resolution on a normal-phase column. The elution characteristics of SMMA samples roughly parallelled their solubility characteristics in the system investigated but there was an extra contribution to retention on active columns.

INTRODUCTION

Cross fractionation (CF) of copolymers is a combination of their separation according to molecular size with the analysis of the chemical composition of each fraction[1], *i.e.*, the two-dimensional analysis of the molar mass distribution (MMD) and chemical composition. With classical fractionating techniques, the investigation of a copolymer requires 10–20 g of sample material and 8–16 weeks of experimental work. There have been few reports on classical CF, which does not reflect the importance of this technique in fundamental polymer science and copolymer technology.

Chromatographic investigation of copolymers usually involves analysis by size-exclusion chromatography (SEC) with dual detection.

This paper deals with CF of synthetic copolymers by the combination of SEC and high-performance liquid chromatography (HPLC). The method is similar to

---

* Present address: Duphar B.V., Research Laboratories, Weesp, The Netherlands.

"coupled-column chromatography" for the investigation of complex mixtures[2]. Co-polymers have already been investigated by combinations of dry-column adsorption chromatography and SEC[3,4] or of SEC and thin-layer chromatography (TLC)[5,6]. SEC and turbidimetric titration of the fractions have also been employed[7-9]. Optimum results have been obtained by the combination of SEC and HPLC of the frac-tions[10,11].

EXPERIMENTAL

HPLC apparatus

System 1 comprised a liquid chromatograph 1090 A (Hewlett-Packard, Wald-bronn, F.R.G.) with a ternary solvent-delivery system, Model DR5, a temperature-controlled column compartment, an autosampler, an autoinjector, a diode-array de-tector, Model HP 1040 A, an integrator, Model 3392 A, and a system controller Model HP 85 with double disc drive, HP 9121 D, and a plotter, HP 7470. Addition-ally, an analog recording device was connected to the analog port of the HP 1090 A.

System 2 comprised a high-pressure pump Model 5200 with an UV detector Model 8100 (Knauer, Bad Homburg, F.R.G.) and a laboratory-built gradient device using a metering pump MMC (Mikrotechna, Prague, Czechoslovakia) with pump head 2c for the controlled addition of solvent B to the mixture at the eluent inlet of the high-pressure pump[12].

System 3 comprised a liquid chromatograph Model 5020 (Varian, Palo Alto, CA, U.S.A.), equipped with a sampling valve Model 7105 (Rheodyne, Berkeley, CA, U.S.A.) and a variable-wavelength flow-through UV photometer Model SF 770 (Schoeffel, Kratos, Westwood, NJ, U.S.A.).

Columns: 1, 150 mm × 4.6 mm, Nucleosil CN, $d_p = 5 \mu m$, spherical; 2, 150 mm × 4.6 mm, Polygosil 60-5, $d_p = 5 \mu m$; 3, 150 mm × 4.6 mm, Polygosil 60-5 C_{18}, $d_p = 5 \mu m$; 4, 300 mm × 4.0 mm, μBondagel, E-1000, $d_p = 10 \mu m$; 5, 150 mm × 4.6 mm, LiChrospher Si 1000 C_8, $d_p = 10 \mu m$; 6, 60 mm × 4.0 mm (Car-tridge), Nucleosil C_{18}, $d_p = 5 \mu m$; 7, 60 mm × 4.0 mm (Cartridge), Nucleosil 50, $d_p = 5 \mu m$; 8, 150 mm × 4.6 mm, LiChrosorb Si 4000 C_{18}, $d_p = 10 \mu m$.

Samples

The copolymers investigated had been prepared by radical polymerization under conditions ensuring a narrow range of chemical compositions. The specimens had been reprecipitated twice. For HPLC, they were dissolved in tetrahydrofuran (THF) stabilized with butylated hydroxytoluene. Some properties of the samples are listed in Table I.

Solvents

THF was distilled under nitrogen to remove the stabilizer and was kept under nitrogen to prevent peroxide formation. *n*-Hexane (pa quality) was obtained from VEB Berlinchemie (Berlin, G.D.R.) and isooctane (2,2,4-trimethylpentane, purum quality) from Fluka (Buchs, Switzerland). The solvents were filtered through a 0.45-μm filter and purged with nitrogen. Methanol was obtained from Fisons (Loughborough, U.K.) as HPLC quality. The gradients used are listed in Table II.

TABLE I

THE COPOLYMERS INVESTIGATED

	I	II	III	IV	V	VI	VII
(1) Poly(styrene–acrylonitrile) (SAN) samples							
Acrylonitrile (mol. %)	27.4	36.9	44.6	52.9	59.4		
(wt. %)	16.1	23.0	29.2	36.4	42.5		
Molar mass (kg/mol)							
by osmosis	325	480	510	380	340		
by light scattering		825					
Content in mixture A							
(in μg per 30 μl)	7.2	14.1	11.1	16.35	13.95		
(2) Poly(styrene–methyl methacrylate) (SMMA) samples							
Methyl methacrylate							
(mol. %)	88.9	76.9	64.9	50.5	37.9	24.5	11.8
Molar mass (kg/mol)							
by light scattering	220	220	235	185	150	250	160
Content in mixture B							
(wt. %)	18.5	17.2	12.7	12.7	12.1	14.0	12.7
Content in mixture C							
(in μg per 9 μl)	–	5.8	–	3.3	–	2.0	–

HPLC conditions

The flow-rate was 1 ml/min, unless stated otherwise. Column temperature: 50°C. Detection, UV at 259 nm.

RESULTS AND DISCUSSION

Chromatographic cross-fractionation (CCF) of SAN (model mixture A and commercial samples) had been performed by SEC fractionation with THF as an eluent. Without any additional preparation the fractions were subsequently analyzed by HPLC on column 1 using gradient program 37b/84 (see Table II)[11].

Fig. 1 shows a similar separation performed on a model mixture of SMMA specimens. Here, the mixture of seven copolymers with a methyl methacrylate (MMA) content ranging from 12 to 89 mol. % was investigated by SEC using THF as an eluent, and by HPLC on a silica column. The gradient elution was performed with isooctane and THF, the concentration of the latter increasing at 5%/min.

In both CCF experiments, individual peaks for the specimens in the model mixtures were obtained. The difference in the patterns of the different SEC fractions is mainly due to the amount of sample contained. A given sample volume injected into the gradient HPLC system will yield a higher signal when taken from an SEC fraction near to the maximum of the SEC curve than from a fraction at the edges. Although the influence of molar mass is only small, in both examples the HPLC peaks appear earlier for SEC fractions of a higher fraction number, *i.e.*, for lower solute molar masses.

The flattening of the peaks with increasing retention is more pronounced with

TABLE II

GRADIENT PROGRAMS

n-hex = n-hexane; i-oct = isooctane; THF = tetrahydrofuran.

1/83	t/min	0	3.5	5.5	8	9	18.5	
	n-hex (%)	90	90	70	70	65	20	
	THF* (%)	10	10	30	30	35	80	
	(smoothly shaped gradient, HPLC No. 2)							
2/83	t/min	0	8	9.9	10	11		
	i-oct (%)	90	50		20	0		
	THF* (%)	10	50		80	100		
	Flow-rate (ml/min)	1		1	0.3	0.3		
28/84	t/min	0	1	1.2	1.8	2	22	23
30/84	i-oct (%)	90	90	85	55	50	0	0
	THF* (%)	10	10	15	45	50	100	100
37b/84	t/min	0	10	15	17			
	i-oct (%)	50	0	0	0			
	THF (%)	50	100	50	50			
	Methanol (%)	0	0	50	50			
04/85	t/min	0	9.5	11.5	13			
	i-oct (%)	95	0	0	0			
	THF (%)	5	100	100	60			
	Methanol (%)	0	0	0	40			
58/85	t/min	0	14	16	17			
	i-oct (%)	90	20	0	0			
	THF (%)	10	80	100	0			
	Methanol (%)	0	0	0	100			

* With 10% (v/v) methanol added.
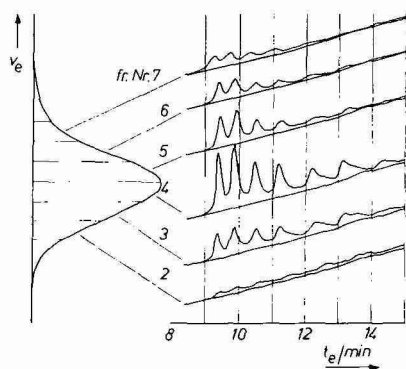
Fig. 1. Size-exclusion chromatography of 1.0 mg of SMMA mixture B (see Table I) and HPLC tracings of the SEC fractions on silica (column 7). Gradient No. 58/85 (see Table II).
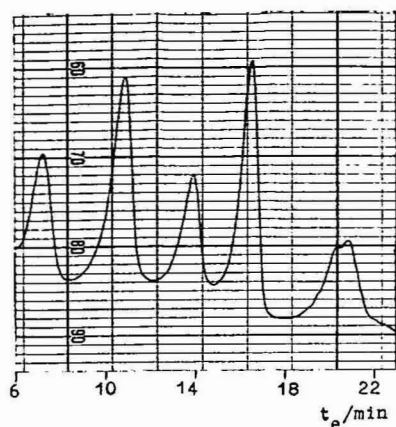
Fig. 2. Gradient chromatogram of SAN mixture A (see Table I) on silica (column 2): V_0 = 30 μl; m_0 = 62.7 μg; gradient No. 30/84. First peak is SAN I.
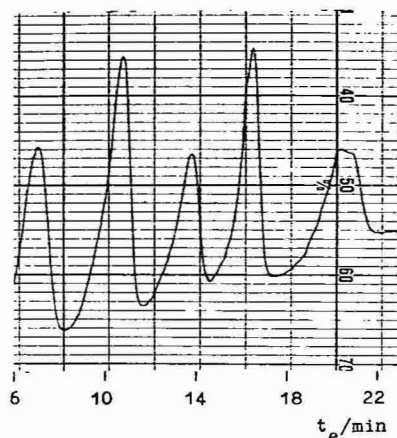
Fig. 3. Gradient chromatogram of SAN mixture A on reversed-phase C_{18} (column 3): V_0 = 30 μl; m_0 = 62.7 μg; gradient No. 30/84. First peak is SAN I.

the SMMA than with the SAN mixture. This might be simply due to the wider range of composition of mixture B in comparison with A (12–89 vs. 27–59%). On the other hand, there is a striking difference in the behaviour of SAN and SMMA in gradient HPLC, which also might be the reason for the flattening effect.

Fig. 2 shows the separation by composition of mixture A containing five SAN specimens on silica column 2 and Fig. 3 the corresponding results obtained on the reversed-phase C_{18} column 3. Fig. 4a and b show HPLC patterns obtained on repeated injections of the same mixture into the wide-pore reversed-phase C_{18} column 8.
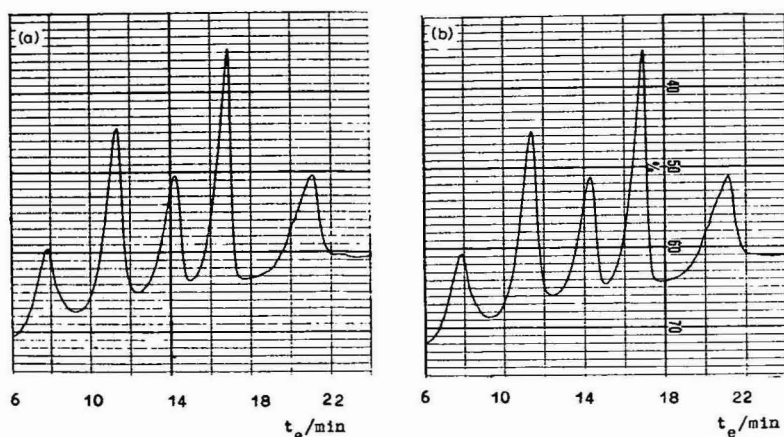
Fig. 4. Gradient chromatograms of repeated injections of SAN mixture A on reversed-phase C_{18} wide-pore material (column 8): V_0 = 30 μl; m_0 = 62.7 μg; gradient No. 30/84.
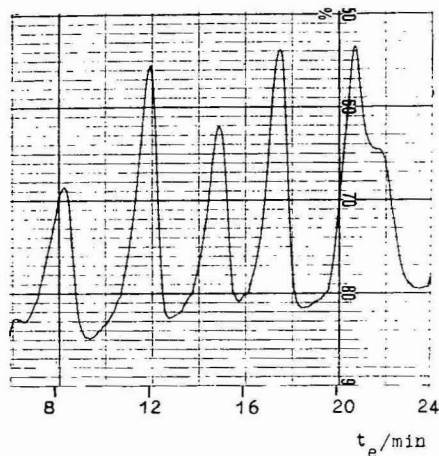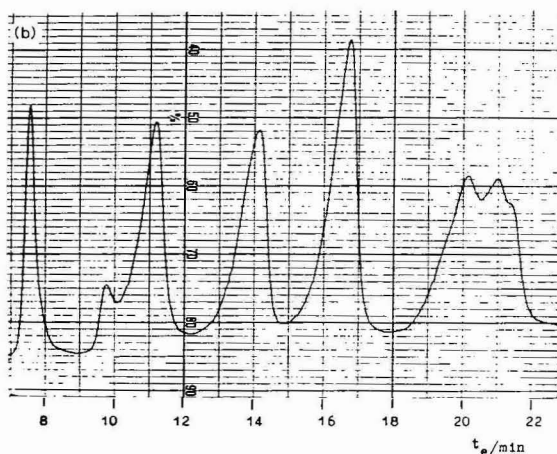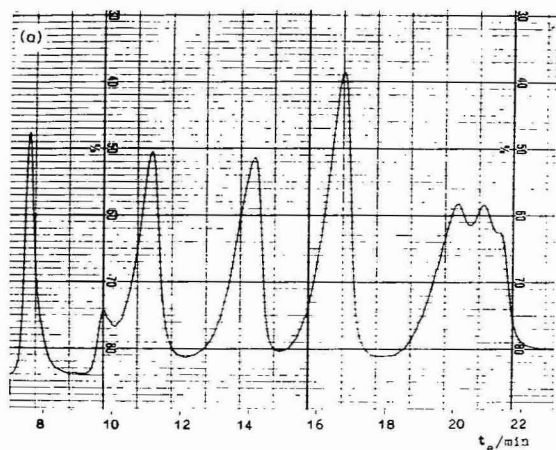
Fig. 5. Gradient chromatograms of repeated injections of SAN mixture A on CN bonded phase (column 1): $V_0 = 30$ μl; $m_0 = 62.7$ μg; gradient No. 28/84. First peak is SAN I. Paper feed rate: 10 mm/min.

Fig. 6. Gradient chromatogram of SAN mixture A on μBondagel (column 4): $V_0 = 30$ μl; $m_0 = 62.7$ μg; gradient No. 28/84. First peak is SAN I.

Fig. 5a and b present the chromatogram obtained by repeated injection of the test mixture A into the CN column 1, which had been also used for the cross fractionation of the SAN samples[11]. The separation of this mixture is also shown in Fig. 6 where the Bondagel column 4 was used.

The elution curves are reproduced without redrawing from the recordings of the analogue recorder in order to enable the patterns to be compared in detail.

In Table III the height/area ratios read from the chromatograms are compiled. The data for the peaks were taken from valley to valley.

Fig. 7 shows the elution behaviour of SMMA copolymers on the reversed-phase C_8 column 5. The tracings were obtained after separate injections of each copolymer. The gradient shape was determined experimentally with the help of an UV stained solvent B, which was tetrahydrofuran–methanol (9:1) in this case. The eluent composition was calculated from the first statistical moment of the peak position. The data are represented by triangles in Fig. 8.

TABLE III

HEIGHT/AREA RATIOS OF THE FIVE SAN PEAKS OBTAINED ON DIFFERENT COLUMNS

Peaks measured from valley to valley. Gradient program and all other conditions were identical.

	Peak number (= no. of SAN sample)				
	I	II	III	IV	V
Silica column (Fig. 2)	8.9	7.2	8.5	8.9	3.9
Reversed-phase C_{18} (Fig. 3)	6.7	6.5	6.8	8.6	3.9
RP C_{18} wide-pore column (Fig. 4a)	6.4	7.9	7.9	9.7	5.4
(Fig. 4b)	6.9	8.0	8.4	9.5	4.8
CN bonded phase, column 1 (Fig. 5a)	9.9	8.1	8.8	9.0	3.7
μBondagel column (Fig. 6)	7.4	7.4	7.6	7.9	4.8

Although no effort had been spared to prepare the copolymer samples as homogeneous as possible as regards both composition and molar mass, specimens of that kind are never chemical individuals in the sense of low-molecular-weight substances. Thus, a peak may be broader due either to the higher selectivity of a chromatographic system for certain sample properties or to a lower plate number. The former explanation is more likely if the peak exhibits additional features (see the shoulder on the last peak in Fig. 6 or on the second peak in Fig. 5a and b).
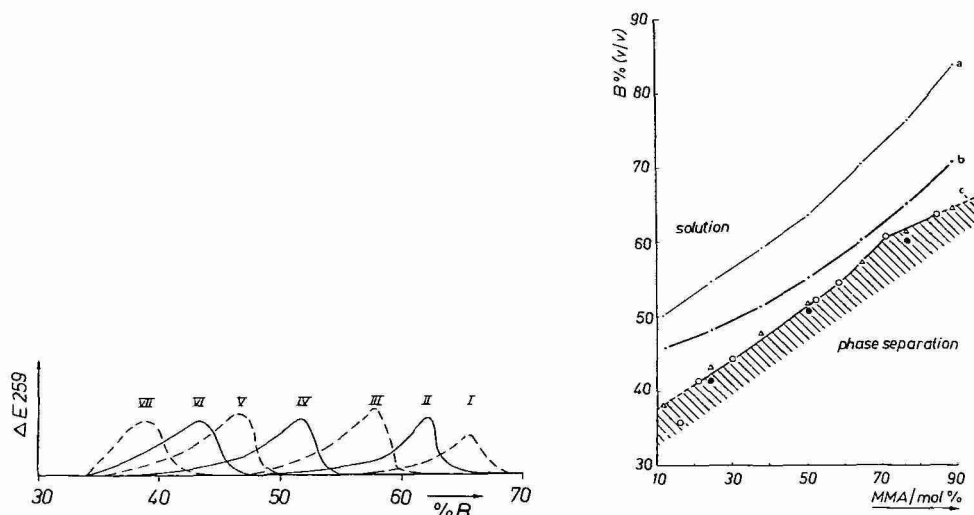
Fig. 7. Elution patterns of SMMA copolymers on reversed-phase C_8 (column 5). Separate injection of each copolymer; V_0 = 100 μl; m_0 = 20 μg; gradient No. 1/83[20]. First peak is SMMA VII.

Fig. 8. Elution characteristics and solubility boundary *vs.* composition of SMMA copolymers in alkane–THF systems. Curves: a, peak position (first moment) from an experiment 38/83 (ref. 17) with the mixture of samples I–VII on silica (column 2), gradient No. 2/83 (solvent A = isooctane, B = THF + 10% methanol); b, first moment of the peak position from Fig. 1 for the central SEC fractions on silica column 7 (solvent A = isooctane, B = THF); c, solubility boundary according to turbidimetric titration with *n*-hexane of copolymer solutions in THF[21] (O, experimental results). ●, First moment of the broad elution patterns of individually injected SMMA samples II, IV and VI; △, first moment of the elution patterns shown in Fig. 7 (solvent A = *n*-hexane, B = THF + 10% methanol).

A prerequisite for peak comparison in gradient HPLC is the equivalence of the gradients used. All gradients employed in the experiments shown in Figs. 2–6 were based on a linear increase in the THF content at 2.5%/min. The chromatograms showing the separation of the five copolymers in mixture A differ only slightly. The solvent composition at the SAN peak positions was almost independent of the chemical nature of the packings[13].

The most surprising result in the separation of SAN copolymers according to their acrylonitrile content was the equivalence of silica and reversed-phase columns (see Figs. 2 and 3, and also the results presented in refs. 14 and 15).

The gradients used in these experiments changed from a low to an high content of THF in alkanes (n-hexane or isooctane). In terms of polarity, they are normal-phase gradients. Applied to a normal-phase column, they should result in separations according to the polarity of the sample, as shown in Fig. 2 for the silica column. What is strange is the similarity of the results obtained when the same normal-phase gradient is used with a reversed-phase column (Fig. 3).

The alkanes n-hexane or isooctane are non-solvents for the SAN copolymers investigated. Since the elution of the specimens always occurred in mixtures containing the same amount of THF as that required for the dissolution of the samples, we have discussed these separations using the term high-performance precipitation LC (HPPLC)[14–16]. The column packing material had only a minor influence in these separations but a pronounced effect on the chromatography of SMMA copolymers.

Alkanes are also non-solvents for SMMA specimens, while THF is a solvent. The solubility of the copolymers decreases with increasing content of MMA units and can be measured by titrating dilute solutions in THF with a hydrocarbon non-solvent. The results of turbidimetric titrations of this kind are shown by open circles in Fig. 8. It determines the solubility boundary which separates the area of homogeneous solutions from the phase-separation area, where the copolymers coagulate. The gel phase formed contains solvent that is richer in THF than the surrounding liquid.

The triangles in Fig. 8 indicate the eluent composition that eluted the SMMA samples from the C_8 column 5, cf., Fig. 7. Here and in the turbidimetric titrations, n-hexane was used as a hydrocarbon non-solvent. The triangles are close to curve c, thus indicating that the elution is due to precipitation and redissolution.

From the overlap of the curves in Fig. 7 it is concluded that the separation of the admixed specimens is not possible. On the other hand, rather good chromatograms of SMMA mixtures have been obtained using normal gradients of isooctane and THF (+ 10% methanol) on a silica column[17]. The elution characteristics of one of these separations (Fig. 2 in ref. 17) is represented by curve a in Fig. 8. It is obvious that the elution occurred at a THF concentration distinctly above the solubility boundary. The separation took place within the solution area, i.e., under the influence of retention by adsorption. What is remarkable is the parallelism between the retention characteristic a and the solubility characteristic c.

The curve b shows the eluent composition at the position of the peaks from SEC fraction 4, cf., Fig. 1. This gradient elution was performed on a silica column having an obviously lower activity than that of column 2. Nevertheless, the elution of the copolymer components required a higher concentration of THF than needed in the experiments with the reversed-phase columns. Other experiments with silica
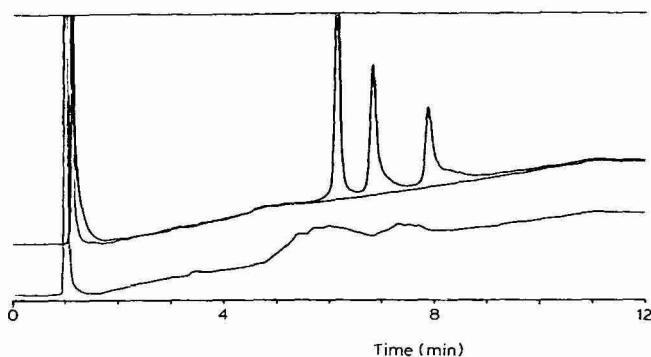
Fig. 9. Upper curve, gradient elution of SMMA mixture C (2.0 μg VI + 3.3 μg IV + 5.8 μg in V_0 = 9 μl) on silica (column 7). First peak is SMMA VI. The lower curve was obtained on C_{18} column 6. Gradient No. 04/85 was used in each case.

columns yielded elution characteristics in between the limits given by the curves a and c in Fig. 8, see also ref. 17.

The drawback of the SMMA investigations reported so far was that they had been performed at different places with different equipment and different brands of eluents. In order to come to a definite conclusion, we eluted the three SMMA samples II, IV and VI and their mixture C from the reversed-phase C_{18} column 6, employing the normal-phase gradient 04/85, comprising isooctane and THF. There was retention, but no resolution.

Immediately after that experiment, the mixture C was investigated under exactly the same conditions but on the silica column 7. Fig. 9 shows the rather good separation obtained. It also shows the elution curve of the mixture C on the C_{18} column. Obviously, the retention is longer on the silica than on the C_{18} column.

The THF concentration at the position of the first statistical moment of the broad elution curves obtained after separate investigation of the SMMA II, IV and VI on the C_{18} column is indicated in Fig. 8 by full circles. They are slightly below the solubility borderline, which was measured by turbidimetric titration with n-hexane. The difference can be explained by the higher temperature of the elution experiment (50°C instead of 20°C in the turbidimetric titration) and might be influenced also by the use of isooctane in the HPLC experiments.

The influence of the column packing material on separation in the elution of SMMA copolymers was observed independently also in gradient systems of cyclohexane and THF[18]. Silica columns have also been employed by Danielewicz and Kubin[19].

CONCLUSIONS

The gradient elution of SAN copolymers in general and the elution of SMMA copolymers on a reversed-phase column are determined by solubility phenomena. With the SMMA specimens, polar column packings cause additional retention which, although small, is essential for the separation by composition of these copolymers.

From a chromatographic point of view, a normal-phase gradient requires a normal-phase column for efficient separation. Thus, the behaviour of the SMMA copolymers is straightforward.

Taking into account the narrow solubility window of polymers on the other hand, the strong influence of the thermodynamic quality of the eluent is quite obvious. Further investigations with additional copolymer systems will reveal whether the behaviour observed with the SANs represents the rule or belongs to the exceptions.

At any rate, it is worthwhile to note that chromatographic cross-fractionation is possible with SMMA copolymers as well as with SANs —independent of the rather remarkable differences in retention mechanisms. This gives hope that coupled-column chromatography can generally be used for very much needed analyses of synthetic copolymers.

ACKNOWLEDGEMENT

REFERENCES

1 A. V. Topčiev, A. D. Litmanovič and V. Ja. Štern, *Dokl. Akad. Nauk SSSR*, 147 (1962) 1389.
2 E. L. Johnson, R. Gloor and R. E. Majors, *J. Chromatogr.*, 149 (1978) 571.
3 H. Inagaki and T. Tanaka, *Pure Appl. Chem.*, 54 (1982) 309.
4 T. Tanaka, M. Omoto, N. Donkai and H. Inagaki, *J. Macromol. Sci., Phys.*, B 17 (1980) 211.
5 B. G. Belenkii and E. S. Gankina, *J. Chromatogr.*, 141 (1977) 13.
6 S. Teramachi, A. Hasegawa and S. Yoshida, *Macromolecules*, 16 (1983) 542.
7 M. Hoffmann and H. Urban, *Makromol. Chem.*, 178 (1977) 2683.
8 G. Glöckner, V. Albrecht and F. Francuskiewicz, *Angew. Makromol. Chem.*, 127 (1984) 153.
9 G. Glöckner, V. Albrecht, F. Francuskiewicz and D. Ilchmann, *Angew. Makromol. Chem.*, 130 (1985) 41.
10 G. Glöckner and R. Koningsveld, *Makromol. Chem., Rapid Commun.*, 4 (1983) 529.
11 G. Glöckner, J. H. M. van den Berg, N. L. J. Meijerink and Th. G. Scholte, in L. A. Kleintjens and P. J. Lemstra (Editors), *Integration of Fundamental Polymer Science and Technology*, Elsevier, Barking, 1986, Ch. 2, p. 85.
12 G. Glöckner and D. Ilchmann, *Acta Polym.*, 35 (1984) 508.
13 G. Glöckner and J. H. M. van den Berg, *Chromatographia*, 19 (1984) 55.
14 G. Glöckner, H. Kroschwitz and Ch. Meissner, *Acta Polym.*, 33 (1982) 614.
15 G. Glöckner, *Trends Anal. Chem.*, 4 (1985) 214.
16 G. Glöckner, *Pure Appl. Chem.*, 55 (1983) 1553.
17 G. Glöckner and J. H. M. van den Berg, *J. Chromatogr.*, 352 (1986) 511.
18 S. Teramachi, personal communication, 1984.
19 M. Danielewicz and M. Kubin, *J. Appl. Polym. Sci.*, 26 (1981) 951.
20 G. Glöckner and D. Ilchmann, 1983, unpublished results.
21 E. Claus, *Diploma project*, Dresden University of Technology, 1984.

CHROMSYMP. 1031

USE OF PATTERN-RECOGNITION TECHNIQUES TO ANALYZE CHROMATOGRAPHIC DATA

MOSES E. COHEN*

Department of Mathematics, California State University, Fresno, CA 93740 (U.S.A.)

DONNA L. HUDSON

Section on Medical Information Science, University of California, San Francisco, CA (U.S.A.)

LEWIS T. MANN

Veterans Administration Medical Center and University of California, San Francisco, CA (U.S.A.)

JACK VAN DEN BOGAERDE

Veterans Administration Medical Center, San Francisco, CA (U.S.A.)

and

NORMAN GITLIN

Veterans Administration Medical Center and University of California, San Francisco, CA (U.S.A.)

SUMMARY

A pattern-recognition technique has been established using a new class or orthogonal polynomials, developed by Cohen. The method is based on a supervised learning approach, and allows classification of data into two or more categories. In this paper, the usefulness of the method in the analysis of chromatographic data is illustrated by its application to the diagnosis of bacterial infection of patients with liver disorders by use of chromatograms obtained from ascitic fluid withdrawn from the patients.

INTRODUCTION

Decision-making algorithms, often denoted expert systems, have been designed which utilize different approaches to automated reasoning[1,2]. These include statistical discrimination techniques[3–6], and decision analysis utilizing methods of pattern recognition[7–11].

Work in pattern recognition of chromatographic data has been done by Albano *et al.*[12], and Wold and Johansson [13], using the SIMCA method. The SIMCA method involves fitting a hyperplane to each class. The method has been applied in various areas, including obtaining chromatographic profiles of human brain tissues[13], classification of fungi[14], and classification of human cancer cells[15]. Unlike the SIMCA method, the techniques described in this paper do not rely on the restrictive properties of hyperplanes in n-dimensional space, but rather permit the fitting of non-linear surfaces to each category using non-statistical methods. A pattern-recognition technique has been developed based on a new class of Cohen orthogonal

polynomials which can be used to classify diverse types of data. The method utilizes a supervised learning approach, consisting of a number of phases: feature extraction, iterative development of a separating hypersurface, and testing of the resulting hypersurface for accuracy. The method is applicable to the analysis of chromatographic data where combinations of either the occurrence of a peak at certain retention times or the magnitude of the peaks is of importance in classifying the chromatogram into two or more categories. The method will be illustrated as applied to the analysis of chromatograms obtained from the analysis of ascitic fluid of patients with liver disorders.

In the study described here, chromatographic analysis is used to analyze ascitic fluid, a substance which accumulates in the abdomen of patients with liver disorders. Under some circumstances, patients sometimes develop a life-threatening disorder, known as spontaneous bacterial peritonitis (SBP)[17]. The objective of the procedure described here is to use the chromatographic data to determine at an early stage if a patient has SBP.

In the first phases —feature extraction— parameters are identified which may be useful in separating data into categories. In the case of the ascitic fluid, the objective was to divide the samples into two catagories: those from patients with SBP, and those from patients without SBP, by analyzing the pattern of organic acids which occurred in the patients with liver disorders for which prompt diagnosis is crucial. Peaks were identified by establishing time intervals, denoted buckets, which consisted of the most likely occurrence of a peak $\pm$ a fixed interval adjustment. There were 47 possible peaks present, which were treated both qualitatively as the presence or absence of a peak at a designated time, and quantitatively as the area under each peak. Thus, there were 94 possible features.

Available data of known classification were divided into two groups: a training set and a test set. The training set was then used, in conjunction with the orthogonal function, to obtain weighting factors for each feature. The data set contained 46 samples, of which 26 were positive for SBP. A training set of 12 was selected, with 6 positives. A separating hypersurface was then obtained.

METHODOLOGY

A sample of ascites fluid was withdrawn by paracentesis from the abdomen of a patient, usually in the course of his treatment. The ascitic fluid was routinely cultured to ascertain the presence of infection, and if positive, the identity of the pathogen. A portion of the ascites fluid was frozen for future study and served as the source of the samples analyzed in this study.

Prior to attempting to determine the organic acid profile of a particular sample using high-performance liquid chromatography (HPLC), it was necessary to isolate the acids from other potentially interfering constituents typically present in ascitic fluid. The following extraction procedure was developed for this project:

To 1.0 ml of sample was added 0.2 ml of saturated K_2HPO_4 to achieve a slightly basic pH and the resulting solution thoroughly mixed with 3 ml of an organic solvent consisting of *tert.*-butyl ether–isopropyl alcohol (95:5). Following centrifugation, the overlying organic layer containing many of the interfering constituents was suctioned off and discarded. The pH of the aqueous phase was then lowered by

the addition of 0.2 ml of 9 M sulfuric acid and the undissociated organic acids extracted by thorough agitation into 5.0 ml of the tert.-butyl ether–isopropyl alcohol solvent. Following centrifugation to enhance complete separation of the two phases, 4.5 ml of the overlying organic layer was pipetted off and retained; the remainder, as well as the aqueous phase, were discarded; 2.0 ml of 0.1 M sodium hydroxide was added to the organic phase and the organic acids back-extracted into the aqueous phase via thorough mixing. Following centrifugation, the overlying organic acids in the aqueous phase, the water was removed via freeze-drying under vacuum. Finally, an aqueous solution of the organic acids was reconstituted by dissolving the freeze-dried residue in 0.5 ml of water and 0.1 ml of 1 M sulfuric acid. A water blank was simultaneously carried through the extraction procedure so that any artifacts introduced by the extraction could subsequently be identified and eliminated from consideration.

Separation of the organic acids in the extracted and reconstituted sample of ascites fluid was performed with HPLC, primarily via the ion-exclusion mode, on a 220 × 4.6 mm Brownlee Labs. column, packed with Polypore H, a 10-μm, macroporous styrene–divinylbenzene resin. The column was maintained at a uniform temperature of 39°C. The mobile phase or eluent consisted of 0.01 M sulfuric acid, prepared from deionized water, deaerated and filtered through a 0.45-μm filter before use. Eluent was delivered to the column by a Consta Metric III metering pump from Laboratory Data Control at a rate of 0.6 ml/min. Samples were introduced with a 50-μl syringe, via a Rheodyne injection valve, into a 20-μl loop in the eluent flow. Effluent from the HPLC column passed into the flow cell of a Laboratory Data Control Spectro Monitor III spectrophotometer, where the organic acids were detected in the UV at the carboxyl absorption band of 210 nm. Detector output was recorded on a Spectra-Physics SP4270 chromatography integrator, which subsequently analyzed the individual organic acid peaks for retention time and area. The water blank was also subjected to HPLC and the areas of the peaks that appeared were subtracted from the areas of the corresponding peaks in the sample chromatogram.

It was presumed that an organic acid could be identified by the retention time of its chromatographic peak. Individual standard solutions of known concentrations of biologically important short-chained mono-, di- and tri-protic organic acids were prepared and the retention time of each determined by HPLC under the aforementioned experimental conditions. Retention times for the following organic acids were identified in this manner: oxalic, oxaloacetic, citric, isocitric, ketoglutaric, tartaric, pyruvic, ascorbic, malic, succinic, lactic, 3-hydroxybutyric, formic, glutaric, acetic, fumaric, propionic, isobutyric, n-butyric, 3-methylbutyric, 2-methylbutyric, valeric and caproic acids.

Ascitic fluid was analyzed by the above method. In addition, some of the fluid was cultured for the presence of bacteria for 72 h. Chromatographic analysis and pattern recognition took approximately 3 h.

Although the automatically integrated chromatogram contained continuous analog data, two aspects of these time series data are of significance: (1) the area under each peak; (2) the elution time of each peak. In each chromatogram as many as 47 separate areas and elution times may be present. Thus there are potentially 94 distinct elements which are of significance for analysis of the chromatogram.

Initially, the area under each peak and the elution time of that peak were manually entered for each chromatogram into a data base program on the VAX 11/750 computer. This method is time-consuming and error-prone. Hence, an automated system was established. In this system, an analog to digital converter was connected to the chromatograph, which then sampled the analog data at fixed time intervals, and transmitted all data to an IBM PC microcomputer. Each chromatogram required approximately 1 h to run. The data were then compressed on the IBM PC, and were transmitted via a hardwire connection to the VAX 11/750, where numerical integration was performed prior to the transfer of the data to the data base described above. The correct classification was then entered for each case from results of the bacteriological examination.

Once the data base on the VAX was completed by one of the above methods, pattern classification was begun. The objective in this case was to obtain a two-category classification: Class 1, patients with SBP; Class 2, patients without SBP. Only a subset of the 94 mentioned above will prove useful in obtaining the correct classification.

The pattern recognition algorithm utilized a non-statistical supervised learning approach. The data obtained from the above procedure were divided into two groups, the training set and the test set; the training set was used to obtain a separating hypersurface. An iterative classification method was used which incorporated the potential function approach to the generation of decision surfaces. The potential function is defined by:

$$P(\bar{x},\bar{y}) = \sum_{i=1}^{\infty} \lambda_i^2 \, f_i(\bar{x}) \, f_i(\bar{y}) \tag{1}$$

where $f_i(\bar{x})$, $f_i(\bar{y})$, $i = 1,2,\ldots$ are orthonormal functions, $\bar{x},\bar{y}$ are n-dimensional vectors, and λ_i, $i = 1,2,\ldots$ are real numbers. The decision surface is adjusted iteratively according to:

$$D_{k+1}(\bar{x}) = D_k(\bar{x}) + r_{k+1} \, P(\bar{x},\bar{x}_{k+1}) \tag{2}$$

where $P(\bar{x},\bar{x}_{k+1})$ is the potential function from eqn. 1, and

$$r_{k+1} = \begin{array}{l} 1 \text{ for } \bar{x}_{k+1} \in \omega_1 \text{ and } P_k(\bar{x}_{k+1}) < 0 \\ -1 \text{ for } \bar{x}_{k+1} \in \omega_2 \text{ and } P_k(\bar{x}_{k+1}) > 0 \\ 0 \text{ otherwise} \end{array} \tag{3}$$

where ω_1 represents class i, $i = 1,2$. $P_0(\bar{x})$ is assumed to be zero, and

$$P_1(\bar{x}) = \begin{array}{l} P_0(\bar{x}) + P(\bar{x},\bar{x}_1) = \quad P(\bar{x},\bar{x}_1) \text{ if } \bar{x}_1 \in \omega_1 \\ \\ P_0(\bar{x}) - P(\bar{x},\bar{x}_1) = -P(\bar{x},\bar{x}_1) \text{ if } \bar{x}_1 \in \omega_2 \end{array} \tag{4}$$

$D(\bar{x}) = 0$ at the completion of the iterative procedure provides the separating hy-

persurface in the two category case. A new class of orthogonal Cohen functions was used as the potential functions. Two special cases of this general class are considered: $f_n(x)$ and $g_n^{\lambda,\xi}(x)$, where λ and ξ are arbitrary real numbers. These functions are defined by their recurrence relations:

$$f_0(x) = 1 \qquad f_1(x) = 2 - 3x$$
$$(1 - 2^n)f_n(x) - x(1 + 2^n)f_{n-1}(x^2)$$
$$+ (1 + 2^{n-1})f_{n-1}(x) + x(2^{n-1} - 1)f_{n-2}(x^2) = 0 \quad n \geqslant 2 \tag{5}$$

$$g_0^{\lambda,\xi}(x) = 1 \qquad g_1^{\lambda,\xi}(x) = \lambda - (\lambda + 1)x$$

$$\left[\frac{\xi^n - 1}{\xi - 1}\right] g_n^{\lambda,\xi}(x) + x\left[\lambda + \frac{\xi^{n-1}}{\xi - 1}\right] g_{n-1}^{\frac{\lambda+2,\xi}{\xi}}(x^\xi) - \tag{6}$$

$$\left[\lambda + \frac{\xi^{n-1} - 1}{\xi - 1}\right] g_{n-1}^{\lambda,\xi}(x) - x\left[\frac{\xi^{n-1} - 1}{\xi - 1}\right] g_{n-2}^{\frac{\lambda+2,\xi}{\xi}}(x^\xi) = 0 \quad n \geqslant 2$$

These new polynomials were compared with the standard Jacobi classical polynomial, which is defined by the recurrence relation:

$$P_0^{a,b}(x) = 1 \qquad P_1^{a,b}(x) = \tfrac{1}{2}[a - b + (a + b + 2)x]$$
$$2n(n + a + b)(2n + a + b - 2)P_n^{a,b}(x) \tag{7}$$
$$- (2n + a + b - 1)[(2n + a + b - 2)(2n + a + b)x + a^2 - b^2]P_{n-1}^{a,b}(x)$$
$$- 2(n + a - 1)(n + b - 1)(2n + a + b)P_{n-2}^{a,b}(x) = 0 \quad n \geqslant 2$$

The orthogonal relationships for these three polynomials are:

$$\int_0^1 x\, f_n(x)\, f_m(x)\mathrm{d}x = 0 \qquad\qquad m \neq n$$
$$= 1/2^{n+1} \qquad\qquad m = n \tag{8}$$

$$\int_0^1 x^{\lambda - 1}\, g_n^{\lambda,\xi}(x)\, g_m^{\lambda,\xi}(x)\, \mathrm{d}x = 0 \qquad\qquad m \neq n$$
$$= 1/\lambda + 2[\xi^n - 1/\xi - 1] \quad m = n \tag{9}$$

$$\int_{-1}^1 (1 - x)^a(1 + x)^b\, P_n^{a,b}(x)\, P_m^{a,b}(x)\, \mathrm{d}x = 0 \qquad\qquad m \neq n$$
$$= k_n \qquad\qquad m = n \tag{10}$$

$$\text{where } k_n = \frac{2^{1 + a + b} \, \Gamma(1 + a + n) \, \Gamma(1 + b + n)}{n! \, (1 + a + b + 2n) \, \Gamma(1 + a + b + n)} \tag{11}$$

The above are functions of the one-dimensional variable, x. The orthogonality of these functions permits generation of functions of higher dimensions by the following scheme:

$$
\begin{aligned}
\theta_1(x_1, x_2, \ldots, x_n) &= \varphi_1(x_1)\varphi_1(x_2)\ldots\varphi_1(x_n) \\
\theta_2(x_1, x_2, \ldots, x_n) &= \varphi_1(x_1)\varphi_1(x_2)\ldots\varphi_2(x_n) \\
\theta_3(x_1, x_2, \ldots, x_n) &= \varphi_1(x_1)\varphi_1(x_2)\ldots\varphi_2(x_{n-1})\varphi_1(x_n)
\end{aligned}
$$

$$\tag{12}$$

$$\theta_{n+1}(x_1, x_2, \ldots, x_n) = \varphi_2(x_1)\varphi_1(x_2)\ldots\varphi_1(x_n)$$

where φ_i, $i = 1, \ldots, n$ are the orthogonal functions defined above. It should be noted that in the strict sense, orthonormality is required, rather than orthogonality. An orthogonal function has the property:

$$
\int_a^b w(x)F_n(x)F_m(x) \, dx = 0 \qquad m \ne n
$$

$$\tag{13}$$

$$
= C \qquad m = n
$$

where C is a constant. Orthonormality requires that $C = 1$. Since the resulting decision surfaces are compared with zero, the equations can be multiplied by the normalizing constant, C, without affecting the comparison.

Five variables were used as features: the standardized lactic acid peak area and the presence or absence of peaks of four selected elution times. The identity of the peaks was unknown. A training set of 12 was used, including 6 positive samples and 6 negative samples. The algorithm was run using three polynomials: $f_n(x)$, $g_n^{0.5,2}(x)$, and $P_n^{0,\frac{1}{2}}(x)$. An additional standard discriminant analysis was performed on the same data using the Biomedical Data Processing (BMDP) statistical package[6].

RESULTS

A separating hypersurface was obtained by using the above method. A sample equation, obtained for $g_n^{0.5,2}(x)$ is given below:

$$
\begin{aligned}
D_g = {} & -3.0 - 3.8x_1 - 1.2x_2 + 1.4x_3 + 3.9x_4 + 2.9x_5 + 1.1x_1x_2 + \\
& + 0.9x_1x_3 + 4.6x_1x_4 + 0.5x_1x_5 + 0.2x_2x_3 + 5.6x_2x_4 - \\
& 1.2x_2x_5 - 3.2x_3x_4 - 1.1x_3x_5 + 1.2x_4x_5
\end{aligned}
\tag{14}
$$

These separating hypersurfaces were then used to classify the samples in the test set.

TABLE I

NUMBER OF MISCLASSIFIED SAMPLES

	$f_n(x)^*$	$g_n^{0.5,2}(x)^{**}$	$P_n^{\frac{1}{2},\frac{1}{2}}(x)^{***}$	Discriminant analysis§
Class 1 (+)	4	3	2	7
Class 2 (−)	1	1	3	0
Overall	5	4	5	7

* Special case 1 of Cohen polynomial.
** Special case 2 of Cohen polynomial.
*** Special case of Jacobi polynomial.
§ Run using BMDP statistical package.

In all, 46 samples were analyzed, 26 of which were positive for SBP. The results are summarized in Table I.

It should be noted that, once the classification algorithm has been run to obtain the separating hypersurfaces, classification of new samples can be made by direct substitution into the separating hypersurface equation. In the above analysis, the resulting classification provides a strictly categoric variable. However, the results obtained from substitution into the hypersurface equations can be interpreted in another way. A numerical value is obtained. Since the separation occurs at $D(\bar{x}) = 0$, the absolute value of the results can be interpreted as a degree of membership in that category: the larger the absolute value, the more certain the classification.

Work is continuing on this application as additional patient data become available. The work described can be extended in two directions. The pattern recognition technique is applicable not only to SBP data but to any analysis in which chromatograms are obtained. In addition, by modifying the knowledge representation and feature extraction phase, the pattern recognition method can be applied to any classification problem and has, in fact, been used in a number of applications[16-18] including diagnosis of SBP by a method which does not involve chromatograms[19,20].

REFERENCES

1 E. A. Patrick, *Syst., Man, Cybern. Rev.*, 6 (1977) 4.
2 E. H. Shortliffe, B. G. Buchanan and E. A. Feigenbaum, *Proc. IEEE*, 67 (1079) 1207.
3 P. Armitage and E. A. Gehan, *Int. J. Cancer*, 13 (1974) 16.
4 M. Ben-Bassat, R. W. Carlson, V. K. Puri, M. K. Davenport, J. A. Shriver, M. Latif, R. Smith, L. D. Portigal, E. H. Lipnick and M. H. Weil, *IEEE Trans. Pattern Anal. Machine Intell.*, PAMI-2 (1980) 1481.
5 M. Ben-Bassat, D. B. Campbell, A. R. MacNeil and M. H. Weil, *IEEE Trans. Pattern Anal. Machine Intell.*, PAMI-5 (1983) 225.
6 W. J. Dixon (Editor), *BMDP Statistical Software*, University of California Press, Berkeley, 1983, p. 519, p. 537.
7 L. N. Kanal, *IEEE Trans. Inform. Theory*, 6 (1974) 697.
8 E. A. Patrick, *Systm. Man, Cybern. Rev.*, 6 (1977) 4.
9 E. A. Patrick, F. Stelmock, L. Shen, *IEEE Trans. Systems, Man, Cybernetics*, SMC4 (1974) 1.
10 D. Coomans, D. L. Massart, I. Broeckaert and A. Tassin, *Anal. Chim. Acta*, 133 (1981) 215.
11 D. Coomans, I. Broeckaert and D. L. Massart, *Anal. Chim. Acta*, 134 (1982) 139.
12 C. Albano, W. Dunn, U. Edland, E. Johansson, B. Norden, M. Sjöström and S. Wold, *Anal. Chim. Acta*, 103 (1978) 429.

13 S. Wold and E. Johansson, *Anal. Chim. Acta*, 133 (1981) 251.

14 G. Blomquist, E. Johansson, B. Söderström and S. Wold, *J. Chromatogr.*, 173 (1979) 19.

15 E. Jellum, I. Bjørnson, R. Nesbakken, E. Johansson and S. Wold, *J. Chromatogr.*, 217 (1981) 231.

16 M. E. Cohen, D. L. Hudson and P. C. Deedwania, *Use of Pattern Recognition Techniques to Classify Exercise Testing Data, Park City, UT, September 1984*, IEEE, New York, 1984.

17 M. E. Cohen, D. L. Hudson, P. C. Deedwania and N. Gitlin, *Pattern Recognition Using New Orthogonal Functions to Classify Medical Data, Proc., Microcomputers in Medicine, New York, 1984*, ISMM, New York, 1984.

18 M. E. Cohen and D. L. Hudson in M. Gupta (Editor), *Approximate Reasoning in Expert Systems*, North-Holland, 1985, p. 435.

19 M. E. Cohen, D. L. Hudson and N. Gitlin, *Pattern Classification Using a New Orthogonal Function for Recognition of SBP, Proc., American Association of Medical Systems and Informatics, San Francisco, May, 1984*, IEEE, New York, 1984.

20 D. L. Hudson, M. E. Cohen and N. Gitlin, *Pattern Classification of Patients with Spontaneous Bacterial Peritonitis Using New Orthogonal Functions with Extensions to Higher Dimensions, Proc., Symposium on Computer Applications in Medical Care, Washington, DC, November, 1984*, IEEE, New York, 1984.

CHROMSYMP. 958

SIMULTANEOUS OPTIMIZATION OF REAGENT CONCENTRATION AND pH IN REVERSED-PHASE ION-PAIRING CHROMATOGRAPHY

HUGO A. H. BILLIET*, JOHAN VUIK, JOOST K. STRASTERS and LEO DE GALAN

Laboratorium voor Analytische Scheikunde, TH-Delft, De Vries van Heystplantsoen 2, 2628 RZ Delft (The Netherlands)

SUMMARY

The procedure developed earlier by the authors for simultaneous two-parameter optimization in reversed-phase liquid chromatography has been adapted to ion-pair chromatography. From the many parameters controling reversed-phase ion-pair chromatography, the mobile phase concentration of the ion-pair reagent and the pH exert the largest effect on selectivity.

Initial chromatograms are chosen to cover the parameter space such that a good initial estimate of the optimum can be obtained. The true retention behaviour is approximated iteratively, and the optimum is located in a few additional chromatograms. The procedure can be followed through appropriate visualization of the results obtained in each step in the iterative procedure.

Two samples were subjected to the procedure, one containing only anions, the other containing cations, anions, and neutral molecules. The ion-pair reagents were sodium octylsulfonate and tetrabutylammonium bromide. A citrate buffer was used to control the pH between 2.5 and 6.

INTRODUCTION

The mobile phase composition in reversed-phase ion-pair (RP-IP) chromatography is often complex. In addition to the ion-pair reagent, buffers, neutral salts, and organic solvents can be used. The theoretical dependence of the capacity factor on the pK_a values of the solutes and the pH of the buffer, the counterion concentration, the mobile phase concentration of the ion-pair reagent, and the concentration of ion-pair reagent in the stationary phase has been studied in numerous papers by various authors[1–6]. Systematic studies on the influence of various parameters on the retention behaviour have been performed by Bartha and co-workers[7–11]. Such studies provide the key to systematic ion-pair optimization. In a previous study[12], we have described the application of an iterative regression procedure, developed by Drouen and co-workers[13–15], to the optimization of the ion-pair reagent concentration only. The present study describes an extension of the same procedure to the simultaneous optimization of two parameters. Alternative computer-aided procedures have been described by Goldberg *et al.*[16] and Lindberg *et al.*[17]. To select the two most appro-

priate parameters, the influence of various parameters in ion-pair chromatography will be briefly reviewed.

The type of ion-pair reagent of the desired charge (either cation or anion) is, of course, sample-dependent and best selected on the basis of practical considerations, such as availability, solubility, purity, and stability. Hydrophobicity (chain length) seems important, but Bartha *et al.*[10] have shown that chain length is not a useful parameter to optimize. With increasing chain length of the ion-pair reagent less concentrated solutions are needed to reach the same coverage of the stationary phase. However, too long a chain makes it difficult to remove the ion-pair reagent from the column.

Studies by Bartha *et al.* and others[1-11] have shown that with increasing concentration of the ion-pair reagent, solute retention initially increases, but then levels off at a certain concentration, after which there is no further gain in selectivity.

The pH of the mobile phase directly influences the ionization of the solutes and of the ion-pair reagent and thus constitutes the second important parameter in ion-pair optimization. The choice of the buffer is dictated by its solubility in the mobile phase. Inorganic phosphate buffers have often been used for their wide pH ranges. However, organic buffers, like citric acid–citrate, are more soluble in mobile phases rich in organic solvents. Citric acid–citrate buffers have an even larger pH range than phosphate buffers.

The cations introduced with the buffer contribute to the total ionic strength of the mobile phase. A neutral salt can be added to keep the counter-ion concentration constant. Control of the counter-ion concentration results in the above-mentioned chain length independence and in a more linear relationship between $\log k$ and $\log P_m$ (the ion-pair concentration in the mobile phase)[9,10]. The salt is chosen for its solubility and non-corrosive properties.

In ion-pair chromatography, the addition of an organic modifier influences the overall retention in two ways: increased elution power towards the solutes as in ordinary reversed-phase chromatography and decreased adsorption of ion-pair reagent on the stationary phase[7,10]. Consequently, the concentration of organic solvent is a convenient parameter for controlling the retention of the last-eluted peak, but too high a solvent content must be avoided. The type of the organic solvent selected offers specificity as in reversed-phase liquid chromatography (LC)[18]. As a stationary phase, C_{18}-modified silica is preferred, because it accepts more ion-pair reagent per surface area than silicas modified with shorter chains. On the basis of these considerations it was decided to direct the simultaneous optimization of two parameters to the ion-pair reagent concentration and the pH of the mobile phase.

EXPERIMENTAL

Instrumentation

The liquid chromatograph consisted of a Waters (Millipore, Waters Chromatography Division, Milford, MA, U.S.A.) M6000A pump, a Rheodyne (Rheodyne, Cotati, CA, U.S.A.) 7125 sample injector with a 20-μl loop, a Waters RCM-100 radial compression unit, containing a Nova-Pak C_{18} column (10 cm $\times$ 8 mm from Waters) and a Waters M440 UV detector with a 254-nm filter.

The optimization program was developed in FORTRAN 77 on a Waters 880

data management system, equipped with 512 kbyte memory, a dual diskette drive (2 × 400 kbyte), integral 10-mbyte Winchester disk drive, extended bit-map graphics with colour monitor, a letter printer LA 100 (all from Digital, Maynard, MA, U.S.A.) and a Hewlett-Packard (Hewlett-Packard, San Diego, CA, U.S.A.) HP7470A graphics plotter.

Chemicals

Methanol was obtained from Rathburn Chemicals (Walkerburn, U.K.). Sodium bromide and citric acid monohydrate were "Baker Analyzed" reagents from J. T. Baker (Deventer, The Netherlands). Tetrabutylammonium bromide and anhydrous sodium octanesulphonate, were from Janssen Chimica (Beerse, Belgium). The solutes used were of the highest quality available.

Mobile phases

The composition of the five mobile phases used in the initial phase of the optimization of two different samples is presented in Table I. Between consecutive experiments the column was washed with a mobile phase containing the citrate buffer having the pH of the next experiment, but without the ion-pair reagent and the sodium bromide. The methanol concentration was increased (and decreased in the same way) by steps of 25% up to a maximum of 75%. Each step took 15 min. Finally, the column was equilibrated to the next mobile phase for at least 15 min. The total time needed to wash and equilibrate the column for the new mobile phase was 2 h. The detector base line was recorded to decide when washing and equilibration was completed. In all cases, the pH was adjusted to within 0.05 pH units in the aqueous solution. After that, methanol was added to the desired concentration.

TABLE I

PREPARATION OF BUFFERS WITH CONSTANT IONIC STRENGTH AND STARTING MOBILE PHASES

pH	Citric acid (g/l)	NaOH (g/l)	NaBr (g/l)
2.50	5.25	0.244	9.29
4.25	5.25	1.360	6.22
6.00	5.25	2.560	—

To prepare the five initial mobile phases, the following amounts of sodium octylsulphonate (Na-Oct) and NaBr were added to the buffers (mobile phase contains 5% methanol).

Mobile phase	log P_m* (mmol)	Na-Oct (g/l)	NaBr (g/l)	log $(P_m + 1)$** (mmol)	TBA (g/l)	NaBr (g/l)
pH = 2.50/6.00	0	0.216	7.10	0	0	0.926
pH = 4.25	0.923	1.812	6.34	0.5	0.696	0.704
pH = 2.50/6.00	1.845	15.140	—	1	2.902	—

    * P_m = mobile phase concentration of ion-pair reagent.
   ** $P_m + 1$, to be able to take the zero ion-pair concentration.
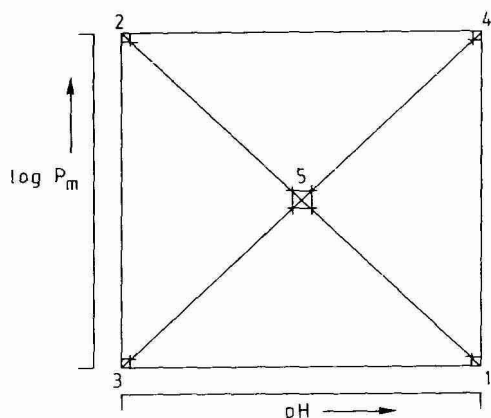
Fig. 1. Location of the five initial mobile phase compositions used to start the optimization procedure.

Software

Existing software for quaternary optimization in reversed-phase LC has been adapted in such a way that the parameter space can be calculated and presented over a square instead of a triangle[15]. Instead of calculating with 100 steps (1% resolution) over the range of each parameter, 30 steps (3.3%) were taken to reduce the computing time from 20 to 2 min. A further increase of the step size reduces the accuracy of the results while the gain in computing speed is marginal. The graphic presentation includes iso-response contour plots, pseudo-isometric 3D-plots of the response surfaces, and a simple indication of the data points and their confidence ranges in the parameter space.

RESULTS AND DISCUSSION

For an unambiguous description of the rectangular parameter space five initial mobile phase compositions were chosen as shown in Fig. 1 (ref. 19). In the present procedure the boundaries of the parameter space are set by the operator on the basis of previous experience. From the retention data of the corresponding chromatograms the complete retention behaviour and, hence, any desired optimization criterion can be calculated over the entire parameter space, and an optimum value can be predicted. In the next chromatogram the prediction is tested indirectly, because it has been shown previously that the use of a shifted mobile phase composition improves the efficiency of the procedure[14]. After each new data point, the calculation of the response surface of the optimization criterion is repeated, and the prediction of the optimum is updated. After a few such iterations the global optimum is found and the procedure stops[14].

It should be realized that the basis of the procedure is the calculation of retention surfaces. As in previous publications[15], the retention surface of a solute is calculated by linear interpolation between measured data points. For the present study, an approximately linear relationship can be safely assumed to exist between $\log k$ and $\log P_m$[12], but the relationship between $\log k$ and pH will usually be S-shaped. As has been shown previously, however, such S-shapes can be readily de-
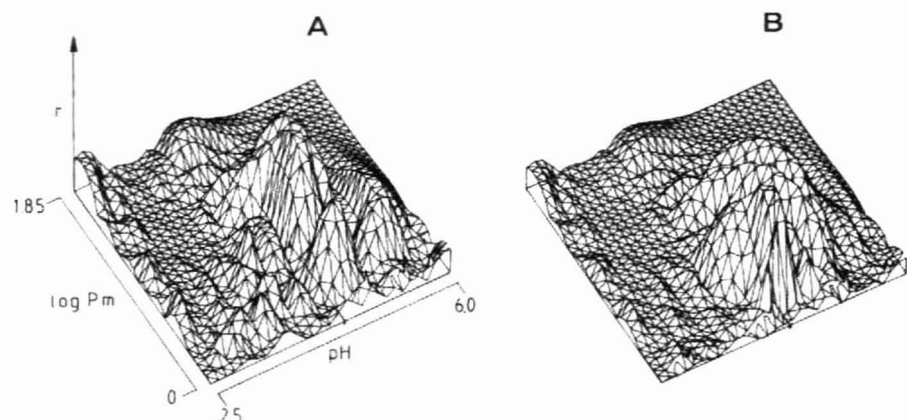
Fig. 2. (A) Representation in a 3D-plot of the criterion value (r) over the parameter space calculated from the five starting chromatograms of sample 1. (B) Representation of the final 3D-plot of the criterion value (r) for sample 1. A total of 10 chromatograms were used.

scribed by linear segments[19]. The procedure will now be illustrated by the optimization of two typical samples.

The first sample contained acidic, basic, and neutral solutes. The sodium octylsulphonate concentration ran from 1 to 70 mmol/l and the pH from 2.50 to 6.00. The optimization criterion used was the relative resolution product[13], which aims at an even spreading of the solutes over the chromatogram. Fig. 2A presents the 3D-plot, which shows that the predicted optimum is situated in an area with high values over a relatively broad range. This is desirable, as it is difficult to prepare the pH of the mobile phases with a precision better than 0.05 units. The program calculates the next mobile phase composition, and the procedure is repeated. Table II presents the composition of the successive, predicted "optimum" mobile phases used to refine the response surface. Obviously, the composition moves around a relatively small region,
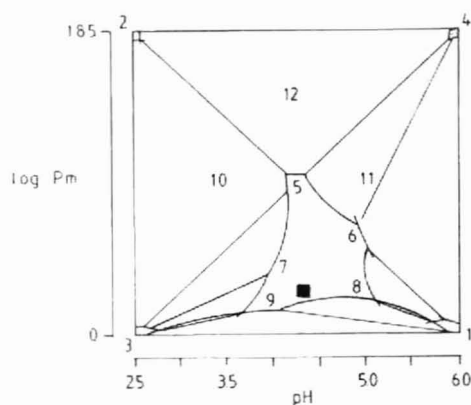
Fig. 3. Overview of the parameter space with indication where chromatograms were taken during the optimization procedure. ■ indicates the optimum. The shaded area represents the parameter space where a preset accuracy has been obtained.
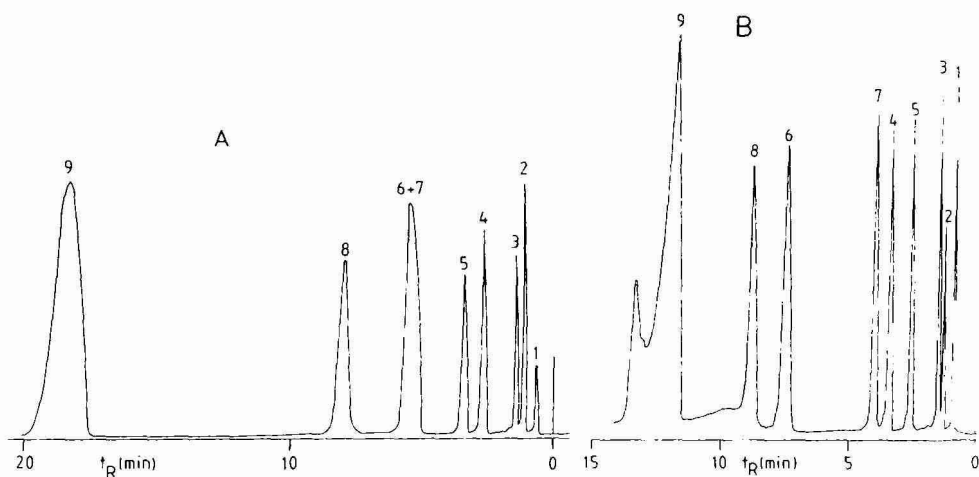
Fig. 4. (A) Chromatogram of sample 1, obtained with the first predicted optimum. Solutes: 1 = 2,4-dinitrobenzenesulphonic acid, 2 = L-DOPA, 3 = tyrosine, 4 = 3,4-dihydroxyphenylacetic acid, 5 = nor-adrenaline, 6 = 5-hydroxyindole-3-acetic acid, 7 = adrenaline, 8 = phenol, 9 = 3-hydroxytyramine. (B) Chromatogram obtained at the optimal mobile phase concentration (see Table II for conditions).

TABLE II

OPTIMIZATION OF SAMPLE 1

Ion-pair reagent is sodium octylsulphonate.

Chromatogram	Composition		Criterion Rel. Res. Prod.*
	pH	log P_m	
1	6.0	0	0.096
2	2.5	1.85	0.132
3	2.5	0	0.002
4	6.0	1.85	0.000
5	4.25	0.93	0.124

	Predicted optimum			Shifted composition		Criterion	
	pH	log P_m	Crit.	pH	log P_m	Predicted	Real
6	4.46	0.73	0.457	4.87	0.60	0.004	0.382
7	4.69	0.49	0.543	4.13	0.41	0.381	0.444
8	4.23	0.37	0.663	4.81	0.26	0.367	0.198
9	4.23	0.31	0.720	3.91	0.16	0.127	0.098
Opt	4.35	0.24	0.687				
Real optimum	4.35	0.24	0.372				

* Relative resolution product (see ref. 14).

as illustrated in Fig. 3, and the procedure comes to a halt after four more chromato-grams. As is clear from Fig. 3, a large area of the parameter space remains un-searched, but a few additional chromatograms taken in "open" areas (data points 10, 11 and 12 in Fig. 3) did not change the location of the global optimum. The final 3D-plot is presented in Fig. 2B. The gradual improvement of the description of the retention surfaces can be judged from a comparison between the criterion values predicted and measured for the shifted composition (the "optimum" composition is not measured until the procedure is completed). The initially poor agreement is al-ready greatly improved in the next iteration and remains acceptable in the following steps.

Fig. 4 presents two chromatograms. The one in Fig. 4A resulted after the first predicted optimum and was taken against the advice of the program, which con-sidered the information at this point insufficient. Indeed, solutes 6 and 7 were poorly resolved. The second chromatogram in Fig. 4B is the final result after four more iterations. The complexity of the separation can be judged from the many peak re-versals. Clearly, the solute peaks are more evenly spread and better separated. Indeed, the criterion value has improved from 0.02 to 0.37. Also, the analysis time is reduced from 19 min to 14 min. However, this is unintentional, because the criterion does not aim for minimum analysis time. As can be seen from Table II, the criterion value observed in the final chromatogram of Fig. 4B (r = 0.37) is significantly lower than the value of 0.697 predicted by the procedure after run Opt (indicated in Table II). The reason is that the product of resolution of adjacent peak pairs is very sensitive to minor shifts in the position of ill-resolved peaks, e.g., solutes 2 and 3 in Fig. 4B.

The second sample contained twelve acidic and neutral compounds. Tetra-butylammonium bromide was chosen as the ion-pair reagent. The concentration ran from 0 to 9 mmol/l, and the pH from 2.5 to 6.0. These boundaries were again chosen from chromatographic experience. To demonstrate the versatility of the procedure, the optimization criterion in this example was the minimal resolution of the critical peak pair (R_s min.).
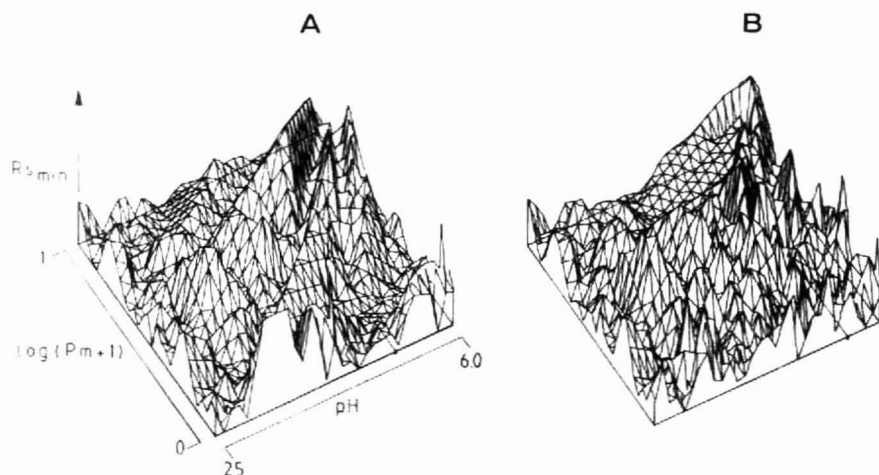
Fig. 5. Representation in a 3D-plot of the criterion value (R_s min.) over the parameter space calculated (A) after five starting chromatograms and (B) at the optimum for sample 2.
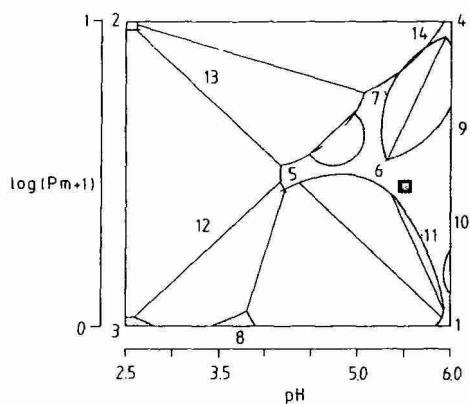
Fig. 6. Overview of measured chromatograms for sample 2 (see also Fig. 3). ■ indicates the optimum. The shaded area represents the confidence range.

The response surfaced calculated from the five initial chromatograms (Fig. 5A) predicted a highest value for $R_{s\ min}$ of 1.4, but due to many cross-overs of solute retention the surface was highly irregular and showed many secondary maxima of potentially similar importance. Probably, the surface was poorly defined at this early stage of the procedure, and the prediction should be judged with caution. Still, even for this complex sample only five additional chromatograms were needed for the

TABLE III

OPTIMIZATION OF SAMPLE 2

Ion-pair reagent is tetrabutylammonium bromide.

Chromatogram	Composition		Criterion $R_{s\ min}$
	pH	log $(P_m + 1)$	
1	6.0	0	0.4
2	2.5	1	0.6
3	2.5	0	0.3
4	6.0	1	0.1
5	4.25	0.5	0.0

	Predicted optimum			Shifted composition		Criterion	
	pH	log $(P_m + 1)$	Crit.	pH	log $(P_m + 1)$	Predicted	Real
6	5.16	0.50	1.4	5.23	0.5	0.9	0.5
7	5.27	0.76	1.4	5.16	0.76	1.2	0.4
8	3.42	0.0	1.2	3.75	0.00	0.3	0.0
9	5.97	0.73	1.2	6.00	0.64	0.6	0.2
10	5.85	0.40	1.3	6.00	0.35	0.1	0.2
11	5.85	0.30	1.3	5.74	0.28	0.8	0.9
Opt	5.50	0.46	1.2				
Real optimum	5.50	0.46	0.9				

Fig. 7. Chromatograms of sample 2. (A) First optimum after five initial runs. Solutes: 1 = 3,4,5-trihydroxybenzoic acid, 2 = phenylalanine, 3 = p-aminobenzoic acid, 4 = 3,4-dihydroxybenzoic acid, 5 = p-hydroxybenzoic acid, 6 = 4-hydroxy-3-methoxybenzoic acid, 7 = m-hydroxybenzoic acid, 8 = 3,4-dihydroxycinnamic acid, 9 = benzoic acid, 10 = phthalic acid, 11 = chlorogenic acid, 12 = DL-cathechine dihydrate. (B) Final chromatogram at the optimal mobile phase composition.

procedure to come to a halt. The successive mobile phase compositions are presented in Table III and their location in the parameter space in Fig. 6. In comparison to Fig. 3, a somewhat broader range of mobile phase compositions is covered, and the jump from composition 7 to composition 8 indicates the presence of an important secondary maximum. Nevertheless, the advice of the procedure to stop after data point 11 was correct, because additional chromatograms taken at compositions 12–14 did not change the final optimum. Fig. 5B presents the final 3D-plot, and Fig. 7 shows chromatograms taken for the first optimum (Fig. 7A) composition predicted on the basis of the five initial chromatograms ($R_{s\ min}$ equal to 0.5) and for the global optimum taken after six additional chromatograms ($R_{s\ min}$ equal to 0.90) (Fig. 7B). All twelve solutes in the sample are well separated.

CONCLUSIONS

The feasibility of simultaneous optimization of two parameters with the iterative regression design has been clearly demonstrated. The efficiency of the procedure, requiring only about ten chromatograms, is important in ion-pair optimization, because a fair amount of time is needed to change from one mobile phase composition to the next one. Because it is difficult to fine-tune the pH of the mobile phase, optimization criteria that produce response surfaces with very sharp maxima can be better avoided. In the present study, the ion-pair reagent concentration and the pH were selected as the most promising optimization parameters. However, organic solvent concentration could also have been chosen[13,18] and the type of solvent is ex-

pected to yield the same specificity as in ordinary RPLC. Computer calculation time has been brought back to acceptable proportions, certainly for a two-parameter optimization. In this study, the boundaries of the parameter space were selected from chromatographic experience. Efforts are now underway to derive the boundaries from well-planned preliminary experiments.

ACKNOWLEDGEMENT

REFERENCES

1 Cs. Horváth, W. Melander and I. Molnár, *Anal. Chem.*, 49 (1977) 142, 2295.
2 J. H. Knox and R. A. Hartwick, *J. Chromatogr.*, 204 (1981) 3.
3 C. P. Terwey-Groen, S. Heemstra and J. C. Kraak, *J. Chromatogr.*, 161 (1978) 69.
4 B. A. Bidlingmeyer, *J. Chromatogr. Sci.*, 18 (1980) 525.
5 R. S. Deelder and J. H. M. van den Berg, *J. Chromatogr.*, 218 (1981) 327.
6 B. L. Karger, J. N. LePage and N. Tanaka, in Cs. Horváth (Editor), *High-Performance Liquid Chromatography*, Vol. 1, Academic Press, New York, 1980, p. 113.
7 A. Bartha and Gy. Vigh, *J. Chromatogr.*, 260 (1983) 337.
8 A. Bartha and Gy. Vigh, *J. Chromatogr.*, 265 (1983) 171.
9 A. Bartha, H. A. H. Billiet, L. de Galan and Gy. Vigh, *J. Chromatogr.*, 291 (1984) 91.
10 A. Bartha, Gy. Vigh, H. A. H. Billiet and L. de Galan, *J. Chromatogr.*, 303 (1984) 29.
11 A. Bartha, Gy. Vigh, H. A. H. Billiet and L. de Galan, *Chromatographia*, 20 (1985) 587.
12 H. A. H. Billiet, A. C. J. H. Drouen and L. de Galan, *J. Chromatogr.*, 316 (1984) 231.
13 P. J. Schoenmakers, A. C. J. H. Drouen, H. A. H. Billiet and L. de Galan, *Chromatographia*, 15 (1982) 688.
14 A. C. J. H. Drouen, H. A. H. Billiet, P. J. Schoenmakers and L. de Galan, *Chromatographia*, 16 (1982) 48.
15 A. C. J. H. Drouen, H. A. H. Billiet and L. de Galan, *J. Chromatogr.*, 352 (1986) 127.
16 A. P. Goldberg, E. Nowakowska, P. E. Antle and L. R. Snyder, *J. Chromatogr.*, 316 (1984) 241.
17 W. Lindberg, E. Johansson and K. Johansson, *J. Chromatogr.*, 211 (1981) 201.
18 P. J. Schoenmakers, H. A. H. Billiet and L. de Galan, *J. Chromatogr.*, 218 (1981) 261.
19 P. R. Haddad, A. C. J. H. Drouen, H. A. H. Billiet and L. de Galan, *J. Chromatogr.*, 282 (1983) 71.

CHROMSYMP. 940

BAND-SPACING IN REVERSED-PHASE HIGH-PERFORMANCE LIQUID CHROMATOGRAPHY AS A FUNCTION OF SOLVENT STRENGTH

A SIMPLE AND FAST ALTERNATIVE TO SOLVENT OPTIMIZATION FOR METHOD DEVELOPMENT

M. A. QUARRY and R. L. GROB

Department of Chemistry, Villanova University, Villanova, PA 19085 (U.S.A.)

L. R. SNYDER* and J. W. DOLAN

LC Resources Inc., 1933 Adele Place, San Jose, CA 95125 (U.S.A.)

and

M. P. RIGNEY

Department of Chemistry, University of Minnesota, Minneapolis, MN 55455 (U.S.A.)

SUMMARY

Numerous reports have described the use of solvent optimization for isocratic reversed-phase high-performance liquid chromatography method development. Solvent optimization involves the use of different solvents (usually methanol, acetonitrile and tetrahydrofuran) to control band-spacing for maximum resolution of the sample. Here, we examine an alternative approach, based on variation of the concentration of organic solvent in the mobile phase (solvent strength). This procedure is less powerful than classical solvent optimization, but it nevertheless possesses a significant ability to effect changes in band-spacing. It is also much more easily carried out. Many samples do not require solvent optimization, and in these cases, a change in solvent strength may be the more practical approach.

The retention data required for solvent-strength optimization are most conveniently collected by using two initial gradient runs. The application of gradient retention data for developing a final isocratic separation is facilitated by the use of commercial software. The advantages and limitations of gradient-retention data for this purpose are examined.

INTRODUCTION

A major part of method development in high-performance liquid chromatography (HPLC) consists of achieving satisfactory resolution of the sample. The basic equation for resolution, R_s, in isocratic HPLC[1],

$$R_s = (1/4) (\alpha - 1) N^{0.5} [k'/(1 + k')] \qquad (1)$$

tells us that separation is affected by solvent strength (capacity factor k'), separation factor α, and column plate number N. Usually method development begins with adjustment of the mobile phase solvent strength [percent water in reversed-phase (RP) HPLC] to achieve adequate values of k', followed by change in conditions to optimize band-spacing (values of α for adjacent bands). Finally, an increase in N can be obtained by varying "column conditions": column length, particle size and flow-rate[2]. Conditions for satisfactory values of k' and N are usually not difficult to find, so that the main challenge is in optimizing α values.

Several studies have been reported for RP-HPLC, that show large changes in band-spacing as a result of varying the organic solvent(s) used in the mobile phase[3-8]. This has led to a more or less standard approach to mobile phase optimization for isocratic RP-HPLC: mapping sample resolution as a function of the composition of mobile phases that are prepared from mixtures of methanol, acetonitrile, tetrahydrofuran (THF) and water[6]. The result has been accurately described as "automated method development"[8]. However, such an approach often requires a large number of experimental runs to adequately map resolution as a function of mobile-phase composition; e.g., seven runs for the sample and for each sample component. Specialized software is also needed to get the most out of this approach.

An alternative is to make use of some other change in separation conditions to alter band-spacing; e.g., bonded-phase or column type[9,10], temperature[11], or solvent strength (mobile phase water content)[5,12]. Gant et al.[13] examined the combined effect of changes in solvent strength and temperature, so as to maintain analysis time approximately constant (see also the similar studies of Melander et al.[14]). In this paper we examine the variation of solvent strength as a means of changing band spacing and optimizing retention. Here and elsewhere[15] we also describe an alternative approach to optimizing band-spacing, based on initial gradient runs plus variations of solvent strength. A procedure based on the same principle has been described for the gradient-elution separation of peptide samples[16].

EXPERIMENTAL

Steroid separations

Equipment. The HPLC system was a DuPont 8800 liquid chromatograph (DuPont, Wilmington, DE, U.S.A.) equipped with a Model 860 fixed-wavelength detector and heated column compartment. Gradient simulations and calculations were carried out with DryLab™ 45 software from LC Resources Inc. (San Jose, CA, U.S.A.), using an IBM XT personal computer.

Reagents. Solvents were HPLC-grade acetonitrile and THF (J. T. Baker, Phillipsburg, NJ, U.S.A.). A Milli-Q system with Organex-Q cartridge (Millipore, Bedford, MA, U.S.A.) was used for water purification.

Samples. Steroid samples were obtained from Roussel Corp. (New York, NY, U.S.A.) and were of pharmaceutical grade.

Nitroaromatic separations

Equipment. An IBM (Danbury, CT, U.S.A.) Model 9533 HPLC system was used; columns were placed in a closed column compartment and operated at ambient temperature. An IBM Model 9522 fixed-wavelength UV detector was used at 254

nm. Data were collected with an IBM Model 9000 data system with CAP 1.4 software.

Reagents. HPLC-grade methanol was purchased from Fisher Scientific (Pittsburgh, PA, U.S.A.) and water was purified in a Nanopure II purification unit (Barnstead Co., Boston, MA, U.S.A.). Before use, all solvents were filtered through a 0.45-μm filter and vacuum-degassed; continuous helium sparging was used to maintain degassed solvents air-free during HPLC operation.

Samples. All nitroaromatic samples were of reagent grade or better, obtained from J. T. Baker and City Chemical Corp. (New York, NY, U.S.A.).

Software. The DryLab 45 software used in this work is available from LC Resources Inc., 1933 Adele Place, San Jose, CA 95125, U.S.A.

RESULTS AND DISCUSSION

Band spacing and solvent strength

In RP-HPLC, retention can usually be described by the approximate (empirical) relationship

$$\log k' = \log k_w - S\varphi \tag{2}$$

where φ is the volume fraction of organic solvent in the mobile phase, k_w is the (extrapolated) value of k' for water as mobile phase ($\varphi = 0$), and S is a constant characteristic of the given compound. Eqn. 2 is normally adequately accurate over the k' range of usual interest ($1 < k' < 10$). An example of the validity of eqn. 2 is shown in Fig. 1, where retention data are plotted *vs.* φ for a series of compounds
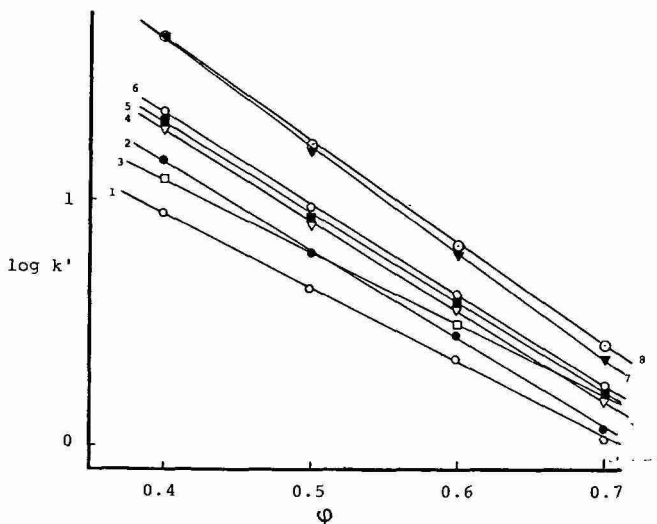
Fig. 1. Plots of log k' *vs.* volume fraction of organic solvent (φ) for a mixture of nitroaromatics. See Table III for details.
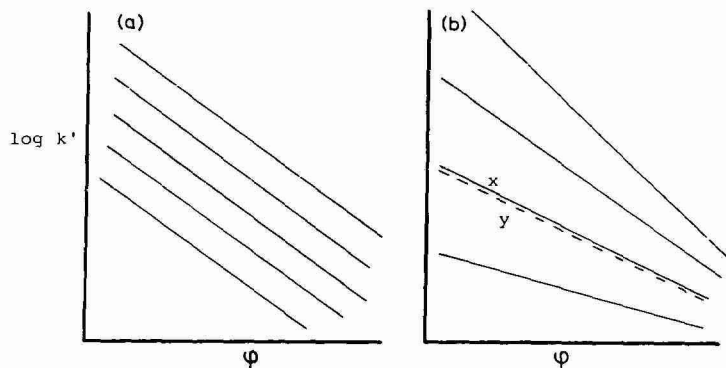
Fig. 2. Hypothetical plots of log k' vs. φ for related solutes, where variation in φ does not improve the separation of closely adjacent bands. (a) All S values equal. (b) S values increase with solute retention; x and y refer to bands that overlap.

(methanol–water, C_8 column). For each of these eight solutes, the data points fall reasonably close to a straight line*.

When the slopes S of two solutes are equal (parallel plots of log k' vs. φ), the separation factor α for the two compounds is not a function of solvent strength (value of φ). This is the case for compounds 5 and 6 in Fig. 1, so that their relative band-spacing cannot be altered by changes in φ. In the case of bands 2 and 3 of Fig. 1, on the other hand, the S values differ, and a change in φ leads to a change in relative retention. This in turn means that the resolution of these two bands will vary markedly as solvent strength φ is varied; e.g., $R_s = 0$ at $\varphi = 0.52$ (methanol–water, 52:48).

Our ability to improve band spacing by changes in φ depends on the S values of the sample compounds. There are two cases where a change in φ will not change band spacing: (a) when all the solute S values are equal (or nearly so), as in Fig. 2a; and (b) when there is a strong correlation of solute S values with corresponding k' values, as in Fig. 2b. Note in Fig. 2b that a decrease in φ for this case can improve separation by increasing α values for all adjacent solute-pairs. However, if two bands are essentially unresolved at one value of φ (e.g.., bands x and y of Fig. 2b) they will be unresolved at other values of φ. Because closely adjacent (overlapping) bands present the major challenge in method development, S values as in Fig. 2b will generally preclude any real improvement in band spacing by varying φ.

It is known[18] that values of S generally increase with the molecular size of solutes. Therefore, if two compounds differ significantly in molecular weight and are unresolved for a given value of φ, a change in φ should result in their resolution. The further dependence of S on other aspects of solute structure is still unclear. The present study was undertaken, in part, to clarify this question.

Studies of Schoenmakers et al. Schoenmakers et al.[5] reported S values for 32 small-molecule solutes of varied structure. The main conclusions drawn in their paper with regard to S values as a function of the solute were as follows:

(1) For methanol as organic solvent, values of S correlate strongly with log k_w (correlation coefficient, $r = 0.98$), as in Fig. 2b.

---

* The following discussion is also applicable for cases where these plots have a slight curvature[17].

(2) For THF as organic solvent, there is a weak correlation between S and log k_w ($r = 0.76$).

(3) For acetonitrile as organic solvent, there is no significant correlation between S and log k_w ($r = -0.06$).

These results would lead us to conclude that acetonitrile–water mobile phases will give significant changes in band spacing as φ is varied, while methanol–water mobile phases will show little change in band-spacing as a function of φ (THF–water mobile phases are intermediate). However, the actual situation is more complicated.

We have carried out a detailed examination of values of S vs. solute structure (using the raw data from ref. 5). As noted above, variations in S that are a function of sample retention (as in Fig. 2b) are of little value in changing band-spacing (for the case of $\alpha \approx 1.00$). Therefore, we first eliminated contributions to S that were retention-dependent. The correlations between S and retention, reported by Schoenmakers et al.[5], are as follows (base-10 logarithms, rather than the natural logarithms reported in ref. 5):

$$\text{(Methanol)} \quad S = 0.99 + 0.34 \log k_w \tag{3}$$

$$\text{(THF)} \quad S = 1.88 + 0.34 \log k_w \tag{4}$$

$$\text{(Acetonitrile)} \ S = 2.55 \tag{5}$$

The retention-independent contribution to S can be defined as the experimental S value minus the value calculated from eqns. 3, 4 or 5, respectively. These residual ΔS values then determine the potential change in band spacing that might result when φ is varied, for a band pair that is unresolved for some value of φ. That is, if two compounds have different values of ΔS for a given organic solvent, then a change in φ should yield values of $\alpha \neq 1.00$ for some value of φ.

An examination of ΔS values, determined from the data in ref. 5, shows many apparent regularities, and it appears that values of ΔS correlate strongly with the functionality of the solute. This is illustrated in Table I for four solute classes with methanol as solvent: alkylbenzenes, alkylphenols, phenylalkanols, and dialkyl phthalates. In this case, ΔS values for alkylbenzenes are about 0.5 units smaller than are ΔS values for dialkyl phthalates having similar retention (similar k' values). Differences in ΔS of this magnitude can lead to useful changes in band spacing when φ is varied (for compounds having similar retention)*.

Table II summarizes data, as in Table I, for other solutes and mobile phases from ref. 5. Here, average values of ΔS are reported for solutes of similar functionality, along with the variation (1 S.D.) in this quantity. These results are useful for anticipating when band-spacing changes will result from variation in φ. Thus, large differences in ΔS values for different solutes and a given organic solvent suggest the use of that solvent for band-spacing optimization via changing φ. On this basis, THF

---

* It should be noted that the correlations of eqns. 3–5 are empirical, as is the approximate constancy of S values for solutes of similar functionality. We also do not mean to imply that "retention-dependent" and "retention-independent" contributions to S reflect different retention processes or "mechanisms". Our discussion here is purely functional and is aimed only at the practical question of how separation will change as mobile phase composition is varied by changing φ.

TABLE I

SIMILARITY OF S VALUES FOR SOLUTES OF SIMILAR FUNCTIONALITY WITH METHANOL WATER AS THE MOBILE PHASE

Based on experimental S values in ref. 5. ΔS values were calculated as experimental S value minus value of eqn. 3.

Compound	ΔS	Compound	ΔS
Alkylbenzenes		*Alkylphenols*	
Benzene	−0.28	Phenol	0.06
Toluene	−0.22	o-Cresol	0.01
Ethylbenzene	−0.17	2,4-Dimethylphenol	−0.03
		Quinolone	0.03
		m-Nitrophenol	0.03
Average	−0.23 ± 0.05 (1 S.D.)		0.02 ± 0.03
Phenylalkanols		*Dialkyl phthalates*	
Benzyl alcohol	0.09	Dimethyl phthalate	0.40
1-Phenylethanol	0.08	Diethyl phthalate	0.26
2-Phenylpropanol	0.07		
3-Phenylpropanol	0.06		
Average	0.07 ± 0.01		0.33 ± 0.10

and acetonitrile appear somewhat more promising than methanol, but considerable band-spacing control should be possible with methanol as well. This is illustrated in the example of Fig. 1 (methanol–water mobile phase), where several changes in band spacing are seen as φ is varied.

TABLE II

VARIATION IN S VALUES WITH SOLUTE TYPE AND MOBILE PHASE

Data from ref. 5 treated as in Table I.

Solute type	n	ΔS^*		
		Methanol	THF	Acetonitrile
Alkylanilines	3	−0.1 ± 0.1	−0.4 ± 0.1	−0.4 ± 0.2
Alkylbenzenes	3	−0.2 ± 0.0	−0.3 ± 0.0	−0.2 ± 0.2
Chlorobenzene	1	−0.2	−0.2	−0.1
Benzaldehyde, phenyl ketones	2	0.0 ± 0.1	−0.1 ± 0.1	−0.2 ± 0.1
Phenylalkyl ethers	2	−0.2**	−0.2 ± 0.0	−0.1 ± 0.1
Polyaromatic hydrocarbons	2	0.2 ± 0.1	0.0 ± 0.0	−0.1 ± 0.2
Biphenyl	1	−0.1	−0.1	0.1
Benzonitrile	1	0.1	−0.1	−0.2
Nitrobenzenes	2	0.2 ± 0.0	0.0 ± 0.0	0.0 ± 0.1
Alkyl phthalates	2	0.3 ± 0.1	0.3 ± 0.0	0.2 ± 0.0
Phenylalkanols	4	0.1 ± 0.0	0.2 ± 0.2	0.4 ± 0.1

* Values for mobile phases containing indicated organic solvents.
** One obviously incorrect value discarded.
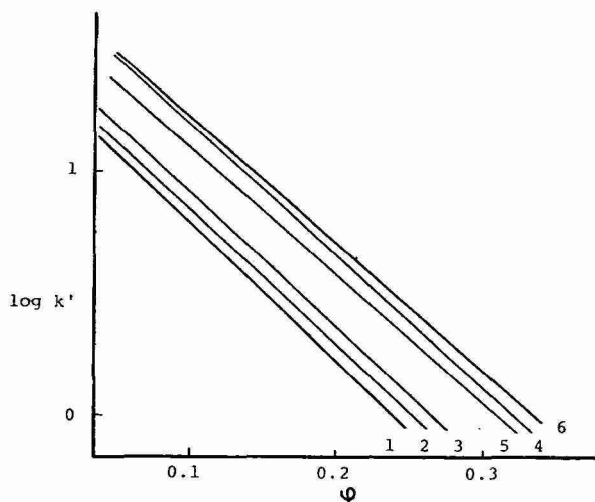
Fig. 3. Plots of log k' vs. φ for steroid mixture. See Table VI for details.

The data of Table II can also be used to suggest useful differences in ΔS for a given sample. The sample in Fig. 1 is a mixture of nitroaromatics plus benzene, separated with methanol–water mobile phases. Benzene (Table II) is in the alkylbenzene group, with $\Delta S = -0.2$. Nitrobenzenes have $\Delta S = +0.2$ for this mobile phase. Therefore the S value for benzene should be about 0.4 units smaller than for adjacent nitroaromatics in this sample. Compound 3 in Fig. 1 is benzene, and its S value (slope of log k' vs. φ) is seen to be significantly lower than surrounding solutes (nitrobenzene derivatives), as predicted from the difference in ΔS values. Note also that the S values of adjacent nitroaromatics in Fig. 1 (all bands except No. 3) are fairly similar, as suggested by the data in Table II. However, even for the nitroaromatics we see that isomeric compounds 7 and 8 are unresolved when the value of φ is low enough ($\varphi = 0.4$), reflecting a difference in their S-values.

Compounds of similar molecular weight and functionality

Molecules having similar size and functionality are expected to have similar S values. This is, in fact, the case, as the retention data in Fig. 3 illustrate. Here, plots of log k' vs. φ are shown for six steroids discussed in a following section. The molecular weights of these compounds fall within a $\pm 5\%$ range, and the functional groups are hydroxyls and carbonyls for each compound. It is seen that the slopes of these plots in Fig. 3 are all similar, with no change in band position as φ is varied. However, it would be a mistake to conclude that φ variation cannot be useful for this sample, as we will shortly see.

Use of gradient elution to optimize solvent strength and band-spacing for corresponding isocratic separations

We believe that the use of gradient elution for initial method development is preferable to the use of corresponding isocratic elution for several reasons:

(1) For unknown samples, a gradient experiment is more likely to reveal bands that might otherwise be lost in the solvent front (eluted at column dead-time, t_0) or

TABLE III

RETENTION DATA FOR NITROAROMATIC MIXTURE

Conditions: two 8 × 0.4 cm, 5-μm Reliance[§] cartridges* in series; methanol–water mixtures as mobile phase; flow-rate, 0.7 ml/min; temperature, 25°C. Compounds: 1 = nitrobenzene; 2 = 2,6-dinitroluene; 3 = benzene; 4 = 2-nitrotoluene; 5 = 4-nitrotoluene; 6 = 3-nitrotoluene; 7 = 2-nitro-1,3-xylene; 8 = 4-nitro-1,3-xylene. Column dead-time t_0 = 1.84 min; gradient dwell-time t_D = 8.14 min.

Solute	Retention time (min)						
	Gradient runs**			Isocratic runs[§]			
	20 min	40 min	80 min	40%	50%	60%	70%
1	22.77	31.47	44.26	18.30	9.84	5.95	3.77
2	23.76***	34.02	50.80	28.48	13.12***	7.01	4.01
3	23.76***	33.17	47.08	24.05	13.12***	7.64	4.62***
4	24.48	35.42	53.80	37.58	16.52	8.40	4.62***
5	24.66	35.79	54.50	40.06	17.58	8.87	4.83
6	24.90	36.25	55.41	43.84	19.08	9.48	5.08
7	25.80	38.45	60.73	88.00	31.16	12.82	5.99
8	26.08	38.87	61.28	88.00	32.51	13.88	6.55

  * DuPont.
 ** For different gradient times t_G.
*** Overlapping bands.
  § For different percentages methanol in methanol–water mobile phases.

disappear as late-eluted bands; gradient elution is also more likely to provide initial separation of bands that are clustered at the front of the chromatogram.

(2) Only two gradient experiments are required to define completely the separation characteristics of a sample with a broad k' range (for a given combination of mobile phase solvents); several isocratic runs would typically be required to obtain the same information.

(3) Some samples require gradient elution for effective separation, others can be resolved isocratically; gradient elution provides information that can be used for either type of sample.

We will illustrate this approach for the nitrocompounds in Fig. 1.

Relative accuracy of isocratic data predicted from gradient data. Any two isocratic experiments, carried out with different values of φ, can be used to determine values of S and k_w from eqn. 1. This then allows prediction of retention for any value of φ, using eqn. 1. We have previously described[17] the similar derivation of S and k_w values from two gradient experiments with different gradient times, t_G, and have shown that reliable and precise values of k' vs. φ can also be obtained in this way. The present study permits a further examination of this approach, because the data in Table III allow us to compare values of S and log k_w derived from either isocratic or gradient experiments. This comparison is summarized in Table IV.

First, consider derived values of S and k_w. Table IV gives the best values of S and log k_w for each compound in Table III, as derived from best-fit curves to the isocratic data of Fig. 1. We have used various pairs of runs (isocratic and gradient) from Table III to derive corresponding values of S and log k_w for comparison with

TABLE IV

COMPARISON OF ISOCRATIC PARAMETERS S AND LOG k_w

Derived from either gradient or isocratic runs in Table III. Gradient run pairs: 20/40 min, 40/80 min and 20/80 min refer to different pairs of gradient runs (20/40 min refers to calculations from 20-min and 40-min runs). Isocratic run pairs: 40/60%, etc. refer to calculations for two isocratic runs with 40 and 60% methanol in water.

Solute (see Table III)	Value of parameter calculated in different ways*						
	Gradient run pairs			Isocratic run pairs			Best**
	20/40 min	40/80 min	20/80 min	40/60%	50/70%	40/70%	
	S-values						
1	3.20	2.90	3.05	3.01	3.09	3.10	3.10
2	3.77	3.62	3.70	3.56	3.58	3.63	3.58
3	2.99	2.73	2.86	2.92	3.04	3.01	2.95
4	3.73	3.75	3.74	3.68	3.61	3.70	3.67
5	3.74	3.73	3.73	3.68	3.61	3.69	3.68
6	3.72	3.73	3.72	3.70	3.63	3.71	3.72
7	4.20	4.30	4.25	4.47	4.25	4.39	4.20
8	4.03	4.11	4.07	4.27	4.07	4.21	4.03
Average error	0.08	0.07	0.06	0.06	0.05	0.04	–
Average change in k'****	2×	2×	4×	5×	5×	11×	–
	log k_w values						
1	2.21	2.09	2.14	2.16	2.18	2.19	2.19
2	2.25	2.13	2.18	2.25	2.31	2.29	2.26
3	2.67	2.60	2.63	2.59	2.58	2.61	2.59
4	2.77	2.78	2.78	2.76	2.71	2.77	2.76
5	2.81	2.80	2.80	2.79	2.74	2.84	2.85
6	2.84	2.84	2.84	2.84	2.79	2.84	2.85
7	3.30	3.36	3.34	3.46	3.33	3.43	3.33
8	3.24	3.29	3.26	3.38	3.26	3.35	3.27
Average error	0.03	0.04	0.04	0.04	0.03	0.03	–

* Isocratic parameters calculated from eqn. 2, using two runs of different methanol–water compositions.

** Parameters derived from best-fit curves in Fig. 1.

*** Average change in solute k' values for the two runs used to measure S.
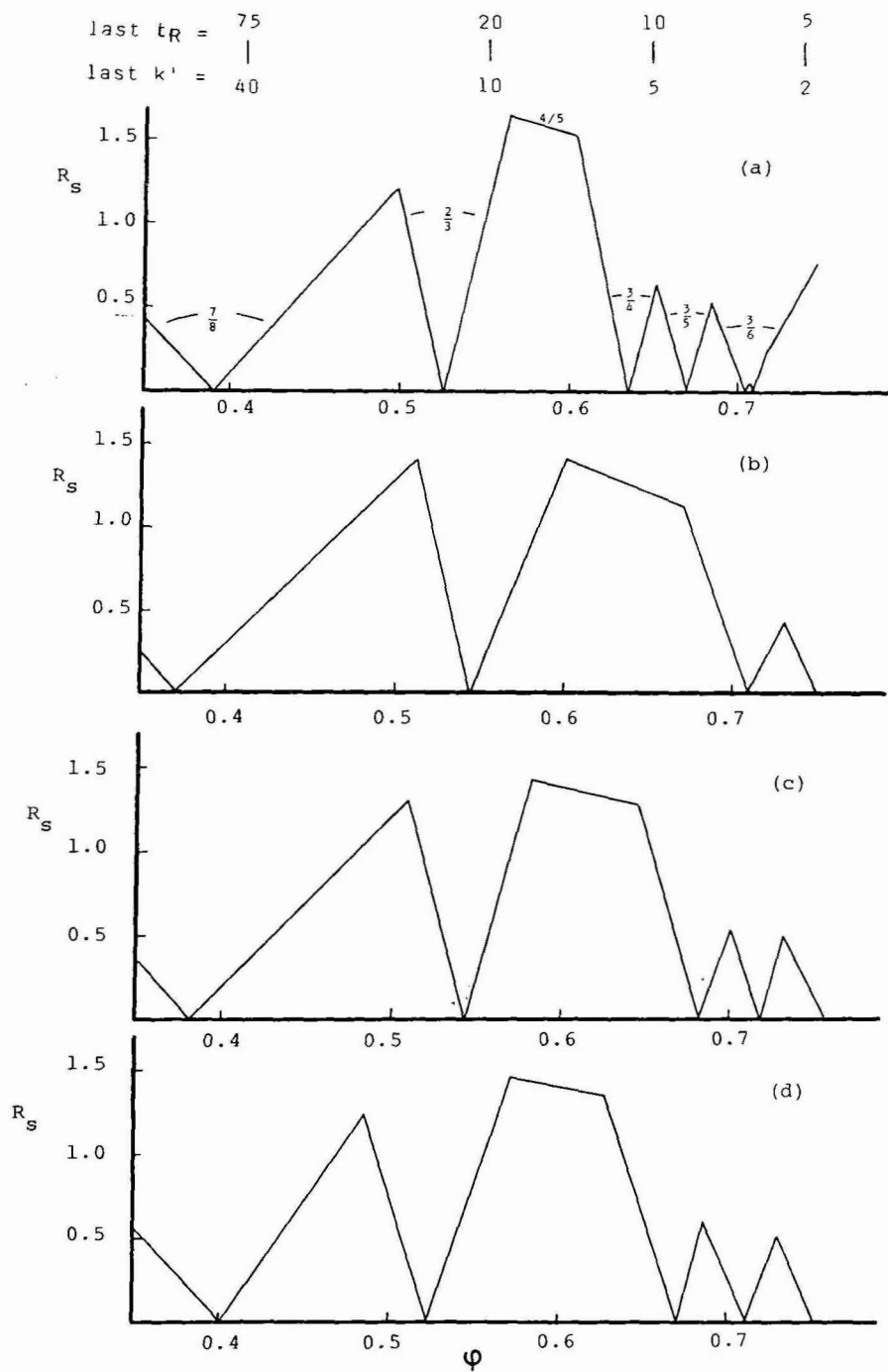
Fig. 4.
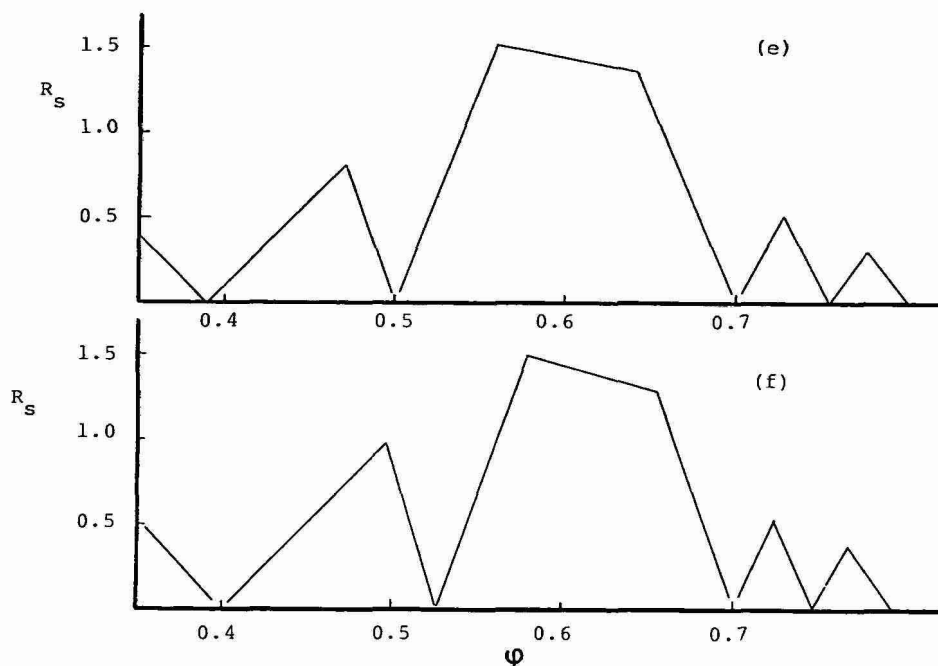
Fig. 4. Relative-resolution maps for the nitroaromatic sample in Table III and Fig. 1. Calculated for 10 000-plate column, using DryLab 45 software. (a) Derived from 20- and 40-min gradient runs; (b) 40- and 80-min gradient runs; (c) 20- and 80-min gradient runs; (d) isocratic runs with 40 and 60% methanol; (e) 50 and 70% methanol; (f) 40 and 70% methanol. t_R = Retention time in min.

these best values. Values of S are of primary interest, because they determine relative band-spacing as φ is varied. From Table IV we see that the errors in S are similar for both isocratic and gradient runs: 0.06–0.08 units for the gradient runs, and 0.04–0.06 units for the isocratic runs (*i.e.*, a 1–2% error in S). These errors should decrease when the two isocratic runs have more different values of φ, or when the ratio of t_G values for the gradient runs is larger[17], because in each case this corresponds to a larger change in k' between the two runs. When the average change in k' between the various pairs of runs (Table IV) is estimated, the error in S is seen to correlate well with this quantity. That is, the error in S is similar for both isocratic and gradient runs when the change in k' between the two runs is comparable. Also the error in S will decrease for larger ratios of the gradient elution time, or larger differences in percent organic solvent for two isocratic runs.

Errors in derived values of log k_w (Table IV) are also seen to be similar for either isocratic (± 0.03–0.04) or gradient (± 0.03–0.04) runs. Thus, when experimental conditions are comparable, gradient runs allow the prediction of isocratic data with an accuracy that is similar to that obtained by direct measurements of isocratic retention. That is, random experimental errors apparently have an equal effect on k' values measured either isocratically or by gradient elution[17,19,20].

Measuring resolution as a function of φ. The DryLab 45 program allows the user to determine relative resolution as a function of mobile phase composition (value

TABLE V

COMPARISON OF RESOLUTION-DIAGRAM PREDICTIONS BASED ON DIFFERENT GRADIENT AND ISOCRATIC RUNS

Application of DryLab 45 Program to data from Table III.

(a) Predictions of φ for $R_s = 0$

Basis*	Value of φ for overlap of indicated bands					Average error
	7/8	2/3	3/4	3/5	3/6	
Best**	35%	53%	69%	72%	82%	—
20/40 min	37	54	71	75	81	2
40/80 min	39	53	64	67	71	4
20/80 min	38	54	68	72	77	2
40/60%	40	52	67	71	75***	3
50/70%	39	50	70	75	80	2
40/70%	40	53	70	75	79	

(b) Predictions of φ and R_s for maximum resolution

Basis*	Values of φ and R_s (in parentheses) for indicated bands§					
	7/8, 2/3		2/3, 4/5		3/4, 3/5	
20/40 min	51%	(1.4)	60%	(1.4)	73%	(0.4)
40/80 min	50%	(1.2)	56%	(1.6)	65%	(0.6)
20/80 min	51%	(1.3)	58%	(1.4)	70%	(0.5)
40/60%	48%	(1.2)	57%	(1.4)	68%	(0.6)
50/70%	47%	(0.8)	56%	(1.5)	73%	(0.5)
40/70%	50%	(1.0)	58%	(1.5)	72%	(0.5)
Average	50%	(1.2)	58%	(1.5)	70%	(0.5)

  * 20/40, 40/80 and 20/80 refer to different pairs of gradient runs (20/40 refers to calculations from 20-min and 40-min runs); 40/60% refers to isocratic runs with 40% and 60% methanol in water, etc.
  ** Calculations from best-fit lines to all isocratic data; see Table IV.
  *** Isocratic predictions show bands 1/2 as the critical pair in this region of φ values (resolution for 1/2 and 3/6 are both small).
  § See Fig. 4a for R_s-maximum defined by 7/8, 2/3, etc.

of φ), beginning with data from either two gradient runs or two isocratic runs (Table III). Because only one separation variable (φ) is involved in resolution mapping, the results are conveniently represented by window diagrams[21]; i.e., plots of minimum α vs. φ. Even more useful are corresponding relative-resolution maps (RRMs): plots of R_s for a 10 000-plate column vs. φ. Relative resolution is defined here as:

$$\text{relative } R_s = (1/4) (\alpha - 1) (10\ 000)^{0.5} [k'/(1 + k')]$$
$$= 25 (\alpha - 1) [k'/(1 + k')] \tag{6}$$

The DryLab 45 program provides isocratic relative-resolution maps for each sample.

A RRM should be distinguished from a map of R_s vs. φ. The RRM is based on two experimental gradient (or isocratic) runs and assumes a column plate number of $N = 10\,000$ for all bands, whereas a plot of R_s vs. φ is based on data gathered from
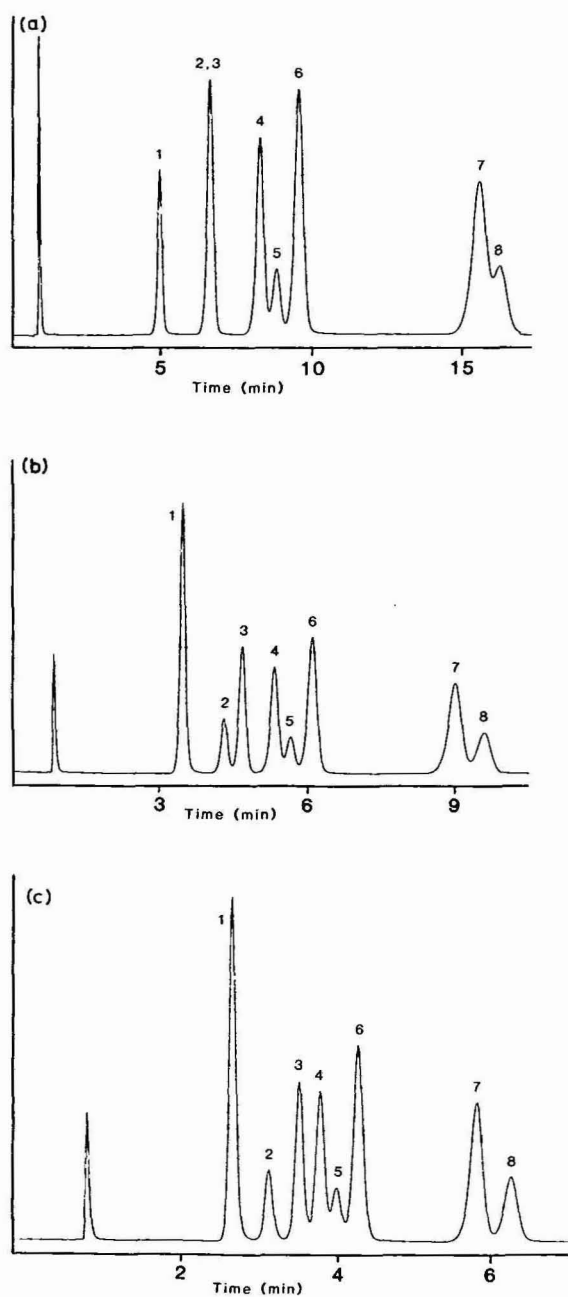
Fig. 5.
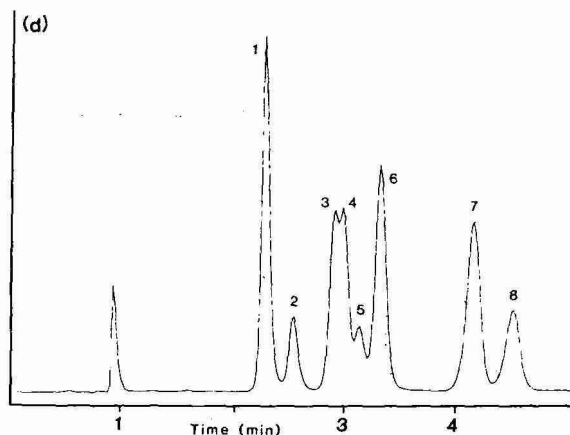
Fig. 5. Isocratic chromatograms of nitroaromatic mixture for different mobile phase compositions (values of φ). Column, two 8 × 0.4 cm, 5-μm Reliance C_8 cartridges in series; mobile phase, methanol–water; other conditions as in Table III. (a) methanol–water (54:46); (b) methanol–water (58:42); (c) methanol–water (61:39); (d) methanol–water (66:34).

a number of experimental isocratic runs in which N is measured for each band. The RRM is a very powerful tool, because it allows us to determine the resolution at one φ value *relative* to any other φ value, yet it only requires two experimental runs. Examples of RRMs for the present nitroaromatic sample are shown in Fig. 4, derived from various combinations of initial gradient or isocratic run pairs. It is seen that all of these plots are similar, reflecting the equivalent accuracy of DryLab 45 predictions, derived from either isocratic or gradient retention data. Table V presents further comparisons of the agreement between the various RRMs in Fig. 4. Mobile phases of minimum resolution (Table Va, unresolved bands) are predicted by the various RRMs with an average error of only ±3%. The accuracy of these predictions is somewhat better for the 20/80-min gradient runs, or isocratic runs with 40–70% methanol (because of a wider k' range). Likewise, predictions of mobile phases for maximum resolution are also in good agreement (Table Vb, ±1 to 2% for the major resolution maxima).

Any of these RRMs from Fig. 4 allow the selection of an optimum mobile phase composition. Because we have seen that the data from runs with larger differences in t_G or φ are somewhat more accurate, we will use Fig. 4c (20/80-min gradient runs) as an example. A broad optimum in relative resolution is seen in the region of 58–64% methanol, with maximum resolution occurring for methanol–water (58:42). Because this optimum is rather flat, a good choice of φ would be about 60% methanol. This provides for reasonable resolution (R_s = 1.3–1.4), even if small errors (±2%) in the methanol composition should occur for any reason. Selection of the absolute R_s maximum at 58% would lead to variations in R_s from 0.6 to 1.4 for similar errors in φ. Fig. 5 shows isocratic separations at several values of φ; the separations for φ = 58% (Fig. 5b) and φ = 61% methanol (Fig. 5c) show acceptable resolution, as predicted by Fig. 4.

The DryLab 45 program also tracks analysis time or k' range for the sample as a function of φ (see Fig. 4a). These data can be considered together with RRMs

TABLE VI

GRADIENT RETENTION DATA FOR THE STEROID SAMPLE IN FIG. 3

Column, 25 × 0.46 cm, 6-μm Zorbax C_8; methanol–water mobile phase, 2 ml/min; 35°C.

Solute		Gradient retention times (min)			S^*		$\log k_w^*$
		$t_G = 10$ min	$t_G = 20$ min	$t_G = 40$ min	20/40	10/20	20/40
1	Prednisone	4.18	6.03	8.70	5.67	5.69	1.92 1.93
2	Cortisone	4.30	6.24	9.07	5.53	5.60	1.95 1.96
3	Hydrocortisol	4.45	6.52	9.61	5.47	5.62	2.00 2.04
4	Dexamethasone	5.05	7.67	11.80	5.33	5.52	2.25 2.31
5	Corticosterone	4.97	7.47	11.34	5.13	5.33	2.14 2.20
6	Cortixolone	5.17	7.85	12.07	5.07	5.30	2.21 2.29

* Values derived from two gradient runs of varying t_G; 10/20 refers to a 10-min and 20-min gradient.

in arriving at the final preferred separation conditions. When the mobile phase composition has been thus optimized by computer simulation (DryLab 45), column dimensions, flow-rate, and particle size[2] can also be optimized by computer simulation, using the DryLab program. This is further described in ref. 15.

   Resolution of a steroid sample. The six-component sample of Fig. 3 was also tested by DryLab 45 computer simulation. The retention data from three initial gradient runs are summarized in Table VI, along with derived values of S and log k_w. Comparison of values of S and log k_w, derived from different pairs of gradient runs (20/40 or 40/80 min), shows agreement comparable to that seen in Table IV. That is, the data of Table VI provide a further illustration of the accuracy of DryLab 45 in predictions of isocratic separation *vs.* φ. Fig. 6a shows the corresponding RRM for this six-component steroid sample, calculated from both the 20/40 and 40/80 min gradient runs of Table VI. Predictions of resolution *vs.* φ are similar enough for selecting the optimum mobile phase composition: 32.5% organic solvent, with R_s
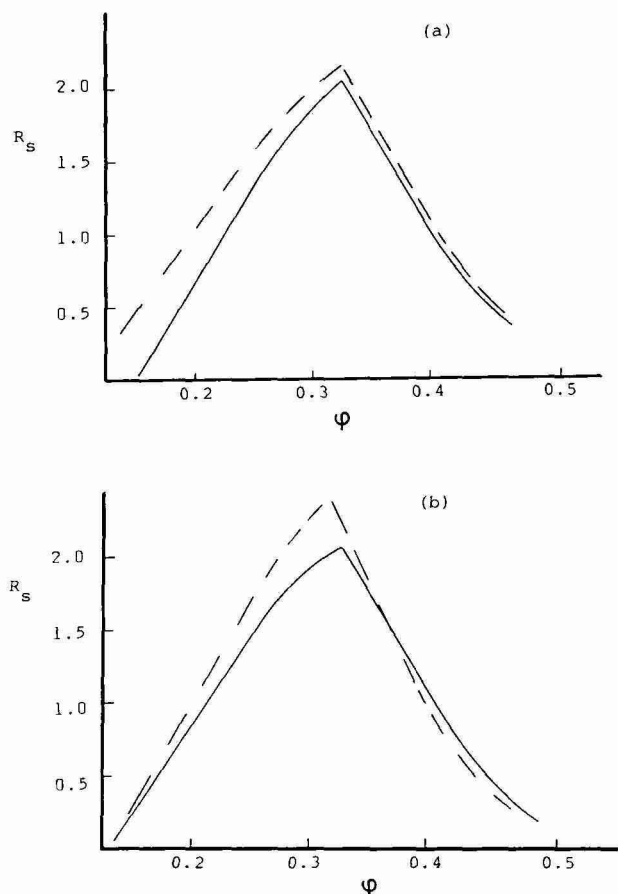
Fig. 6. Relative-resolution maps for steroid sample in Table VI and Fig. 3. (a) ———, 20/40-min runs; — — —, 40/80-min runs; (b) ———, 20/80-min runs; — — —, same as (a) except 10% error in V_D assumed (V_D = 6.25 ml; correct value, 5.75 ml).

= 2.0–2.1 for N = 10 000. Note that the use of other mobile phase compositions can result in significantly inferior separations in this case. Thus, even samples having components that are quite similar in molecular size and functionality can often benefit from φ optimization.

Maximizing the accuracy of gradient/isocratic predictions

Previous work summarized in ref. 17 has dealt with the steps that must be taken in order to obtain adequately reliable isocratic retention data from gradient runs. The present paper shows (with these precautions) that gradient-derived data can be as reliable as actual isocratic measurements. All the examples shown here are for small-molecule samples, with molecular weights less than 500. Larger molecules, such as proteins and synthetic polymers, require additional care for accurate gradient/isocratic conversions[17], but several studies have now shown that this procedure works equally well for high-molecular-weight compounds[17,22–25].

Measuring the dwell-volume of the HPLC system. Previously[22] we have suggested that the system dwell-volume V_D (volume from the gradient mixer to the column inlet) be measured from linear gradients, carried out without a column in the system. Some workers regard this as inconvenient. There is a possible alternative, which is facilitated by the DryLab 45 software. First, carry out two gradient runs, then use DryLab 45 to predict isocratic retention as a function of φ. Next an isocratic separation is performed that is predicted to yield convenient values of k' and analysis time. When the correct value of V_D is assumed, the isocratic retention data should agree best with the DryLab 45 predictions from the two gradient runs.

An error in V_D can result in significant errors in predicted isocratic retention. However, the effect on the resulting RRM is often less serious. This is illustrated in Fig. 6b, where the predictions based on the correct V_D value of 5.75 ml (solid line) are compared with predictions (broken line) based on a V_D value that is 10% larger. Work on the further analysis of possible errors related to imprecise V_D values and other sources is in progress.

CONCLUSIONS

The variation of solvent strength (percent water in the mobile phases for RP-HPLC) can lead to significant changes in band-spacing for many samples. This means that such samples can be adequately resolved by mapping resolution as a function of solvent strength. Method development based on this approach will generally be much faster than alternatives where different mobile phase solvents are investigated (solvent optimization), or where different HPLC columns are tried. This approach appears particularly promising in the case of samples having components that differ in molecular weight or functionality. However, even compounds of similar molecular size and chemical nature show useful changes in band-spacing as solvent strength is varied.

The use of solvent-strength optimization is facilitated by the use of initial gradient elution experiments at the beginning of method development. If two gradient runs are carried out in which only the gradient time is varied (*e.g.*, 20 and 60 min), the resulting retention data can be used to predict retention as a function of mobile phase composition (percent water) in corresponding isocratic separations (same sam-

ple and column). These predictions are most conveniently (and rapidly) carried out by computer simulations, using the DryLab 45 software package from LC Resources.

When the present approach is combined with computer simulation for optimizing column dimensions, particle size, and flow-rate (using DryLab 1–3 software), a very fast and powerful procedure for HPLC method development results. With only three or four actual laboratory experiments, plus perhaps half an hour of simulations using a personal computer, most samples should yield acceptable resolution for the purpose at hand. Method development carried out in this way is applicable to unknown samples, as well as samples with known components.

REFERENCES

1 L. R. Snyder and J. J. Kirkland, *Introduction to Modern Liquid Chromatography*, Wiley-Interscience, New York, 2nd ed., 1979.
2 L. R. Snyder and P. E. Antle, *LC, Liq. Chromatogr. HPLC Mag.*, 3 (1985) 98.
3 S. R. Bakalyar, R. McIlwrick and E. Roggendorf, *J. Chromatogr.*, 142 (1977) 353.
4 N. Tanaka, H. Goodell and B. L. Karger, *J. Chromatogr.*, 158 (1978) 233.
5 P. J. Schoenmakers, H. A. H. Billiet and L. de Galan, *J. Chromatogr.*, 185 (1979) 179.
6 J. L. Glajch, J. J. Kirkland, K. M. Squire and J. M. Minor, *J. Chromatogr.*, 199 (1980) 57.
7 P. J. Schoenmakers, H. A. H. Billiet and L. de Galan, *J. Chromatogr.*, 218 (1981) 261.
8 J. C. Berridge, *Techniques for the Automated Optimization of HPLC Separations*, Wiley-Interscience, New York, 1985.
9 P. E. Antle, A. P. Goldberg and L. R. Snyder, *J. Chromatogr.*, 321 (1985) 1.
10 P. E. Antle and L. R. Snyder, *LC, Liq. Chromatogr. HPLC Mag.*, 2 (1984) 840.
11 D. E. Henderson and D. J. O'Connor, *Adv. Chromatogr.*, 23 (1984) 65.
12 A. F. Poile and R. D. Conlon, presented at *8th International Symposium on Column Liquid Chromatography, New York, May 20–25, 1984.*
13 J. R. Gant, J. W. Dolan and L. R. Snyder, *J. Chromatogr.*, 185 (1979) 153.
14 W. R. Melander, B.-K. Chen and Cs. Horváth, *J. Chromatogr.*, 318 (1985) 1.
15 L. R. Snyder, J. W. Dolan and M. Rigney, *LC, Liq. Chromatogr. HPLC Mag.*, 4 (1986) 921.
16 J. L. Glajch, M. A. Quarry, J. F. Vasta and L. R. Snyder, *Anal. Chem.*, 58 (1986) 280.
17 M. A. Quarry, R. L. Grob and L. R. Snyder, *Anal. Chem.*, 58 (1986) 907.
18 X. Geng and F. E. Regnier, *J. Chromatogr.*, 332 (1985) 147.
19 M. A. Quarry, R. L. Grob and L. R. Snyder, *J. Chromatogr.*, 285 (1984) 1.
20 M. A. Quarry, R. L. Grob and L. R. Snyder, *J. Chromatogr.*, 285 (1984) 19.
21 R. J. Laub and J. H. Purnell, *J. Chromatogr.*, 112 (1975) 71.
22 M. A. Stadalius, H. S. Gold and L. R. Snyder, *J. Chromatogr.*, 296 (1984) 31.
23 E. S. Parente and D. B. Wetlaufer, *J. Chromatogr.*, 355 (1986) 29.
24 R. W. Stout, S. I. Sivakoff, R. D. Ricker and L. R. Snyder, *J. Chromatogr.*, 353 (1986) 439.
25 M. G. Kunitani, D. J. Johnson and L. R. Snyder, *J. Chromatogr.*, 371 (1986) 313.

CHROMSYMP. 1067

SUBNANOLITER LASER-BASED REFRACTIVE INDEX DETECTOR FOR 0.25-mm I.D. MICROBORE LIQUID CHROMATOGRAPHY

REVERSED-PHASE SEPARATION OF NANOGRAM AMOUNTS OF SUGARS

DARRYL J. BORNHOP*, THOMAS G. NOLAN** and NORMAN J. DOVICHI*,*

Department of Chemistry, University of Wyoming, Laramie, WY 82071 (U.S.A.)

SUMMARY

A simple, inexpensive, small-volume refractive index detector has been applied to the separation of nanogram amounts of sugars by capillary column high-performance liquid chromatography.

INTRODUCTION

The incorporation of lasers as light sources in spectroscopic instrumentation has produced spectacular improvements in detection limits. These improvements arise from several unique properties of laser radiation. In particular, the high spatial coherence of the laser beam facilitates study of small volume samples; laser beams may be focused to very small spots without loss of power to produce excellent detection limits[1-3]. Capillary liquid chromatography offers several important advantages compared with conventional chromatographic instrumentation. Particularly important advantages include low solvent consumption and excellent mass sensitivity[4,5]. The latter advantage is of value when small amounts of rare and expensive analytes must be determined.

However, the small volume of capillary columns introduces severe constraints upon the system dead-volume. In particular, the major limitation in capillary liquid chromatographic performance appears to be detector technology[4-6]. It is very difficult to miniaturize conventional detector instrumentation without compromising the detector performance. Subnanoliter detectors have been developed based upon fluorescence, absorbance, light scatter, and electrochemistry[7-16]. However, no universal detector has been developed for capillary chromatography. A universal detector provides an analytical signal for all analytes. The typical example in conventional chro-

matography is the refractive index (RI) detector. The RI detector is often listed as the second or third most popular detector for conventional liquid chromatography.

Unfortunately, there are no subnanoliter RI detectors available. A very sensitive RI detector has been reported which utilizes a Fabry-Perot interferometer to measure directly the change in optical path length induced by a change in solute concentration[17]. However, the volume of this instrument appears to approach 1 ml, far too large for capillary liquid chromatography. A second, less sensitive, RI detector has been developed which is based upon a miniaturized Fresnel prism and has a volume of 1 μl[18]. The instrument uses a focused laser beam to probe the cuvette; detection limits of $\Delta RI = 2.0 \cdot 10^{-7}$ are reported.

We will describe a subnanoliter RI detector for capillary liquid chromatography. This detector is a miniaturized version of a previously described instrument[19]. A tightly focused laser beam passes slightly off-axis through a fused-silica capillary tube, filled with analyte. The beam profile is distorted upon passage through the tubing, producing a somewhat elliptically shaped beam. This beam profile changes shape with a change in RI of the analyte. A small area photodiode is located at a relatively sharp light–dark boundary on the beam profile. As the RI of the analyte changes, the beam profile changes, producing a change in intensity at the photodiode. The resulting current change produced by the photodiode is linearly related to the RI of the analyte over several orders of magnitude in RI change.

Use of a tightly focused beam and a small I.D. capillary tube can result in a very low detector volume. For example, a 10-μm spot-size laser beam within a 100-μm I.D. capillary defines a cylindrical probe volume of 30 pl. Of course, the dead-volume of the detector is not limited by the probed volume of the laser beam, but instead, is limited by the size of the tubing. For a detection region located immediately downstream from the column end frit, peak spreading is likely to extend down the tube by a length given by the tube radius. A 100-μm diameter cuvette will have a dead volume of approximately 0.4 nl. Smaller diameter capillary tubing will produce a corresponding decrease in detector volume.

EXPERIMENTAL

The laser-based, small-volume, RI detector is similar to one described before[19]. Fig. 1 presents an experimental diagram. A low-power, linearly polarized beam at 632.8 nm is provided by a helium–neon laser (Melles Griot, Irvine, CA, U.S.A.). A linear polarizer is located in the optical train and rotated to maximize the transmitted intensity. A quarter-wave plate is placed after the polarizer and rotated to eliminate any retroreflected light from reaching the laser cavity. These retroreflections primarily originate from the focusing lens and sample cuvette, described below. It also is necessary to tilt each of the polarizing elements slightly to prevent retroreflections from their surfaces from reaching the laser cavity. A microscope cover slip is used to direct *ca.* 5% of the laser light to a reference photodetector, described below. A piece of frosted glass is located before the reference photodetector. Translation of the frosted glass allows convenient balancing of the intensity of light reaching the signal and reference photodetectors.

The main portion of the beam is focused with a 16-mm focal-length microscope objective into the sample cuvette. The objective is mounted rigidly in space. The
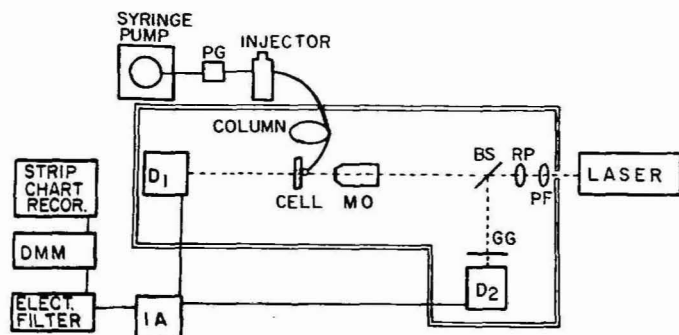
Fig. 1. Experimental diagram of the laser-based, small-volume RI detector. PG = pressure gauge; PF = polarizing filter; RP = quarter-wave retardation plate; BS = beam splitter; MO = microscope objective; D1 and D2 = identical photodiodes; IA = instrumentation amplifier; elect. filter, 1-Hz low pass electronic filter; DMM = digital multimeter. The optical system is enclosed in a box denoted by the double-line figure.

sample cuvette consists of a 100-μm I.D. × 245-μm O.D. fused-silica capillary tube (Polymicro Technologies, Phoenix, AZ, U.S.A.) with a thin polyimide coating. This capillary fits inside a 250-μm I.D. × 400-μm O.D. fused-silica tubing (Polymicro Technologies) which has had the polyimide coating removed. The sample cuvette is tilted slightly from vertical. The larger tubing is the chromatographic column and the smaller tubing holds the column end frit in place. The cuvette is located on a three axis translation stage to provide convenient alignment with respect to the laser beam.

The laser beam is allowed to propogate *ca.* 15 cm to a small area (1 mm²) photodiode located on a single translation stage. The photodiode may be translated perpendicular to the plane formed by the laser beam and sample cuvette to a region where the laser beam profile undergoes a large change with a change in RI of analyte. The signal and reference photodiodes are identical Model SD 041-11-11-011 silicon photodiodes (Silicon Detector, Newbury Park, CA, U.S.A.). The output of the diode is conditioned with a current-to-voltage converter, consisting of a JFET operational amplifier, LF 351, wired with a 1-MΩ feedback resistor in parallel with a 47 pF capacitor. The outputs of the signal and reference photodiodes are subtracted using a Model AD 524 instrumentation amplifier (Analog Devices, Norwood, MA, U.S.A.). A low pass electronic filter (Ithaco, Ithaca, NY, U.S.A.) with a 1-Hz cut-off is employed to smooth the signal. The chromatogram is displayed on a strip-chart recorder. The injection mark is obtained by shifting the range scale on the recorder coincident with the injection. The injection itself produces no perturbation in the chromatogram.

Alignment

Alignment of the sample cuvette and signal detector with respect to the laser beam is important for achieving good sensitivity and detection limit. First, the vertical position of the cuvette is adjusted so that the laser beam traverses the cuvette a small distance below the chromatographic column end frit. Next, the cuvette is moved along the beam path to locate the sample at the beam waist, about 5 mm from the lens. Last, the cuvette is moved perpendicularly to the beam path so that the center

of the cuvette is about 0.1 mm from the beam axis. This alignment produces an elliptically shaped beam profile at the detector plane. The signal photodiode is placed at the sharp boundary between the main beam and the first adjoining dark fringe.

Chromatographic system

The chromatographic system consists of a Model 314 high-pressure syringe pump (Isco, Lincoln, NE, U.S.A.), a Model 2D430 pressure gauge (Alltech, Chicago, IL, U.S.A.), a 100-μl Model EC14W air actuated injection valve (Valco, Houston, TX, U.S.A.), and a locally prepared reversed-phase capillary liquid chromatography column. The column preparation is similar to that published elsewhere[5,14,20,21]. A 0.6-m long piece of 250-μm I.D. fused silica is used for the column. The polyimide coating is removed from the bottom 5 cm with a cool flame. A short piece of 100-μm I.D. × 245-μm O.D. fused-silica tubing is inserted in the chromatography column exit and used to hold a thin PTFE frit in place (Fig. 2). The frit is located at the top of the region which has been stripped of polyimide, and the region below is the detector cuvette. A small drop of high temperature epoxy is placed at the bottom of the 250-μm column to hold the 100-μm I.D. tubing in place.

The reversed-phase column is prepared from 5-μm diameter C_{18} spheres (Supelco, Bellefonte, PA, U.S.A.). A slurry of the packing material is prepared in chloroform–methanol (80:20) at a 1:7 (w:v) ratio of stationary phase to slurry solvent. The high-pressure packing pump (Shandon) is filled with methanol. After filling the empty column, the well sonicated slurry is placed in a 700-μl volume reservoir, connected to the column and packed initially at low pressure (1000 p.s.i.). The pressure is slowly raised to 5500 p.s.i. and held at that pressure for *ca.* 2 h. A valve is closed between the column and the pump, and the column pressure is allowed to drop to atmospheric conditions. About ten column volumes of water are next passed through the column to help stabilize the bed[22].
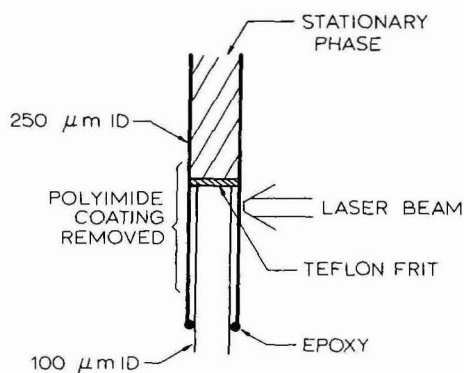
Fig. 2. Detail of cuvette and column exit. The upper tube is a piece of 250-μm I.D. fused-silica tubing which forms the chromatography column. The frit is a thin section of porous Teflon. The polyimide coating of the chromatography column is removed below the frit. A sort section of 245-μm O.D. × 100-μm I.D. tubing is inserted in the chromatography column and holds the column end frit in place. A small bead of epoxy glue holds the cuvette assembly in place.

Reagents

All chemicals are reagent grade or better. Stock sugar solutions are prepared in water. The chromatographic mobile phase is water with a very small amount of acetonitrile (see below). A typical flow-rates is 1.3 μl/min.

RESULTS AND DISCUSSION

Although not ideal, reversed-phase chromatography on C_{18} columns may be employed for the chromatographic determination of simple sugars. Fig. 3 presents a chromatogram of 667 ng of glucose, 707 ng of sucrose, and 845 ng of raffinose. The chromatographic efficiency is fair, about 4500 plates or 7500 plates/m. Other work utilizing the same detector and column but another separation suggests that detector dead volume does not limit the chromatographic resolution. These sugars are base line resolved; however, an attempt to separate several additional sugars on this column failed. Work is continuing in this laboratory to prepare an NH_2 capillary column for additional separation efficiency of complex mixtures of sugars. Note, the last (inverted) peak in the chromatogram is associated with the solvent used to prepare the solutions and occurs whenever water is injected into the system. Presumably, a small, residual amount of acetonitrile from a previous chromatographic experiment remained in the syringe pump to contaminate the solvent used in this experiment. Injection of pure water yields a small change in RI and a corresponding negative peak in the chromatogram.

A roughly ten-fold dilution of the sugar solution was injected onto the column (Fig. 4) and the sensitivity of the recorder was increased. The detection limit, three standard deviations above the background, is estimated from the peak-to-peak noise in the chromatogram[23]. For the sugars it is about 40–50 ng injected, about half the amount injected in this chromatogram. A 1-s low pass filter was employed in this chromatogram; since the peak elution time is about 30 s, a much longer time constant on the detection electronics could be employed with a corresponding improvement in detection limit.
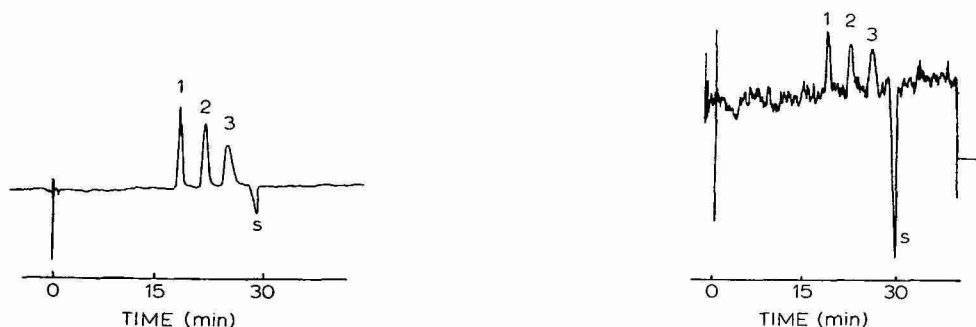
Fig. 3. Chromatogram of sugars. Peaks: 1 = 667 ng of glucose, 2 = 707 ng of sucrose, 3 = 845 ng of raffinose.

Fig. 4. Chromatogram of dilute sugars. Peaks: 1 = 83 ng of glucose, 2 = 88 ng of sucrose, 3 = 106 ng of raffinose. This injected amount is approximately twice the detection limit.

Of course, the sugars which elute from the column are more dilute than the injected sample; it is of interest to seprate the chromatographic performance from the detector performance. Assuming a Gaussian peak and estimating the standard deviation of the peak as 0.42 times the full width at half maximum yields a standard deviation of about 0.8 μl and a peak analyte concentration at the detection limit of about $2 \cdot 10^{-5}$ g/ml. At the detection limit, a RI change of about $2.8 \cdot 10^{-6}$ is produced at the maximum of the sucrose peak. This value is three times larger than the detection limit reported in our earlier work. The larger detection limit probably is a result of the much more narrow cuvette capillary employed in the present work. Narrow capillary columns are more sensitive to both vibrations and temperature changes. The latter effect is due to the small heat capacity of very narrow capillary columns.

Detection limits for the amount of analyte injected into the column fall in the mid-nanogram region for the sugars employed in this separation. However, much less material is present in the detection volume. With a 0.4-nl detection volume, only $8 \cdot 10^{-12}$ g is present at the detection limit whereas $6 \cdot 10^{-13}$ g is present within the 30-pl volume probed by the laser. These very small numbers are a direct result of the small volume detector employed in this experiment. Calibration curves were prepared for the three sugars. The linearity, $r > 0.999$, extended over a factor of 35 in mass injected from the detection limit to about 1.3 μg injected. A negative curvature was observed at higher concentrations. This deviation from linearity appears not to be due to the detector, but instead, due to overloading of the chromatographic column. Future work will explore the ultimate dynamic range of the detector.

It is important to comment upon the simplicity and cost of this instrument. Only one alignment step is critical—positioning of the cuvette perpendicular to the laser beam —and once the desired far-field beam profile is observed, realignment is very rapid. The laser employed is one of the least expensive and most reliable lasers on the market. Any low-power helium–neon laser may be employed, although a polarized laser should give a more stable signal. The optical components individually cost less than US$ 100, and are available from a number of vendors. The cost for the entire detector, minus the optical table, is about US$ 1200, half of the total being the cost of the strip chart recorder!

ACKNOWLEDGEMENTS

REFERENCES

1 T. Hirschfeld, *Appl. Opt.*, 15 (1976) 2965.
2 C. Radzewicz, P. Glowczewski and J. Kraninski, *App. Phys.*, 17 (1978) 423.
3 E. K. Gustafson and R. L. Byer, *Opt. Lett.*, 9 (1984) 220.
4 M. Novotny, *Anal. Chem.*, 53 (1981) 1294A.
5 J. C. Gluckman, A. Hirose, V. L. McGuffin and M. Novotny, *Chromatographia*, 17 (1983) 303.

6 H. Poppe, *Anal. Chim. Acta*, 145 (1983) 17.
7 G. J. Diebold and R. N. Zare, *Science*, 196 (1977) 1439.
8 L. W. Hersshberger, J. B. Callis and G. D. Christian, *Anal. Chem.*, 51 (1979) 1444.
9 S. Folestad, L. Johnson, B. Josefsson and B. Galle, *Anal. Chem.*, 54 (1982) 925.
10 N. J. Dovichi, J. C. Martin, J. H. Jett and R. A. Keller, *Science*, 219 (1983) 845.
11 J. W. Jorgenson and E. J. Guthrie, *J. Chromatogr.*, 255 (1983) 335.
12 N. J. Dovichi, T. G. Nolan and W. A. Weimer, *Anal. Chem.*, 56 (1984) 1700.
13 T. G. Nolan, W. A. Weimer and N. J. Dovichi, *Anal. Chem.*, 56 (1984) 1704.
14 T. G. Nolan, D. J. Bornhop and N. J. Dovichi, *J. Chromatogr.*, 384 (1987) 189.
15 F. Zarrin and N. J. Dovichi, *Anal. Chem.*, 57 (1985) 1826.
16 R. L. St. Claire and J. W. Jorgenson, *J. Chromatogr. Sci.*, 23 (1986) 186.
17 S. D. Woodruff and E. S. Yeung, *Anal. Chem.*, 56 (1982) 1174.
18 S. A. Wilson and E. S. Yeung, *Anal. Chem.*, 57 (1985) 2611.
19 D. J. Bornhop and N. J. Dovichi, *Anal. Chem.*, 58 (1986) 504.
20 D. C. Shelly, J. C. Gluckman and M. Novotny, *Anal. Chem.*, 56 (1984) 2990.
21 T. G. Nolan and N. J. Dovichi, in preparation.
22 M. Konishi, Y. Mori and T. Amano, *Anal. Chem.*, 57 (1985) 2235.
23 J. E. Knoll, *J. Chromatogr. Sci.*, 23 (1985) 422.

CHROMSYMP. 1068

CROSSED-BEAM THERMAL-LENS DETECTION FOR 0.25-mm DIAMETER MICROBORE LIQUID CHROMATOGRAPHY

SEPARATION OF 2,4-DINITROPHENYLHYDRAZONES

THOMAS G. NOLAN*, DARRYL J. BORNHOP** and NORMAN J. DOVICHI**,*

Department of Chemistry, University of Wyoming, Laramie, WY 82071 (U.S.A.)

SUMMARY

The crossed-beam thermal-lens detector is applied to capillary liquid chromatography for the separation of picomole amounts of 2,4-dinitrophenylhydrazones. A relatively inexpensive instrument is described, which utilizes a 3-mW helium–cadmium pump laser and a low-power helium–neon probe laser. Detection limits of 120 fmol of acetone (injected) are obtained.

INTRODUCTION

The incorporation of lasers as light sources in optical methods of analysis has produced spectacular improvements in detection limits. These improvements arise from several unique properties of laser light. In particular, the high spatial coherence of continuous wave laser beams facilitates the study of small-volume analytes. For example, tightly focused laser beams have been used to probe subnanoliter to subpicoliter volumes by fluorescence[1-3], light scatter[4-6], and absorbance[7-9]. Unfortunately, the limited wavelength selection available from inexpensive lasers and the limited spectral information produced by electronic transitions of fluid-phase molecules results in limited qualitative information about the analyte. The nature of the analyte may be discerned in favorable cases by chromogenic reaction. However, highly specific chromogenic reactions are not available for most analytes. Instead, chromatographic separation and retention are used to provide qualitative information about the analyte.

Capillary liquid chromatography is a powerful method for the separation of complex mixtures. Two primary advantages of capillary chromatography compared with conventional chromatography are decreased solvent consumption and improved mass detection limits. The latter property is important when analyzing small amounts

---

of rare or expensive analytes. However, to obtain good performance from capillary chromatography, it is necessary to reduce the dead-volume to a minimum. Unfortunately, only a limited number of detector technologies exist for capillary chromatography[10-12]; it is often difficult to miniaturize conventional detectors to the required low volume without concomitant loss of sensitivity. It is not surprising that the combination of capillary liquid chromatography with laser-based detection is attractive[11]. The high sensitivity and low probed volume of the laser techniques compliments the high separation efficiency and low dead volume requirements of capillary liquid chromatography.

In this paper, we describe a low-volume, high-sensitivity absorbance detector based upon the crossed-beam thermal-lens for 0.25-mm I.D. slurry-packed capillary liquid chromatography. The detector has been utilized before for amino acid determination with a commercial 1-mm I.D. chromatography column[12]. Detection limits of subpicomole quantities of amino acids injected into the column were reported. Presumably, combination of this detector with capillary liquid chromatography should produce improved detection limits. In the crossed-beam thermal-lens technique, two laser beam are crossed within a weakly absorbing sample[7-9]. Absorbance of light from a tightly focused and modulated pump beam produces a time-varying temperature rise within the sample. The resulting refractive index perturbation within the sample acts to defocus periodically the probe beam. A simple, small-area photodiode, centered in the probe beam profile, is used to measure the beam defocusing. A lock-in amplifier acts as a phase-sensitive amplifier to demodulate the crossed-beam thermal-lens signal. This thermo-optical technique has a property important for small-volume absorbance determinations: the signal is generated *only* at the intersection region of the two beams and is independent of path-length. Small-volume samples may be probed simply by using tightly focused laser beams.

Like other thermo-optical techniques, the sensitivity of the crossed-beam thermal-lens increases linearly with pump-laser power[13]. Furthermore, the sensitivity is inversely proportional to the pump beam spot size; as the pump beam is more tightly focused, both the sensitivity and spatial resolution of the technique improve. It is not surprising that the crossed-beam thermal-lens produces excellent mass detection sensitivity. For example, detection limits corresponding to 120 iron atoms as the 1,10-phenanthroline complex have been observed with the crossed-beam thermal-lens in a 0.2-pl probe volume[9]. These detection limits were achieved with a modest power pump laser, 100 mW at 514.5 nm, and a water–methanol solvent.

EXPERIMENTAL

The chromatographic system is constructed from a Model 314 high-pressure syringe pump (Isco, Lincoln, NE, U.S.A.), a 60-nl Model EC14W air-actuated injection valve (Valco, Houston, TX, U.S.A.), and a 40 cm × 0.25 mm I.D. fused-silica capillary column. The chromatographic stationary phase consist of 5-μm diameter C_{18} particles (Supelco, Bellefonte, PA, U.S.A.). The column is packed with a chloroform–methanol (80:20) slurry at 5000 p.s.i.[14-17]. The mobile phase flow-rate is 2 μl/min. The detector cuvette is an 80-μm I.D. square-bore glass-capillary tube (Wale, Hellertown, PA, U.S.A.) which has been glued into the end of the column and holds the column end-frit in place.
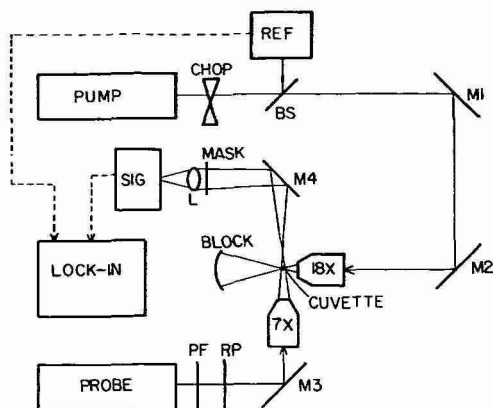
Fig. 1. Block diagram of the crossed-beam thermal lens detector. PUMP, helium–cadminum pump laser; CHOP, mechanical chopper; BS, beam splitter; M1–M4, mirrors; 18 × , microscope objective; CUVETTE, 80-μm square-bore capillary tube; BLOCK, beam block, PROBE, helium–neon probe laser; PF, polarization filter; RP, quarter-wave retardation plate; 7 × , microscope objective; MASK, mask formed by two razor blades; L, one inch focal lenth lens; SIG, signal detector; REF, reference detector; LOCK-IN, lock-in amplifier.

The block diagram of the crossed-beam thermal-lens instrument is presented in Fig. 1. The optical system is constructed on a Model KST-48 4 ft. × 8 ft. optical table (Newport, Fountain Valley, CA, U.S.A.). The pump laser beam is provided by a Liconix (Sunnyvale, CA, U.S.A.) model 4210B helium–cadmium laser, which delivers to the sample a linearly polarized, 3-mW beam at modulated in a symmetric square wave by a variable-frequency chopper at 128 Hz. A microscope cover slip is used to divert a small portion of the laser beam to a reference detector, described below. The transmitted beam is reflected from two mirrors and focused into the detector cuvette with a 10-mm focal length (18 ×) microscope objective. After transmission of the pump beam through the sample, it is absorbed by a metal beam stop. The probe beam is provided by a 5-mW He–Ne helium–neon laser (Melles Griot, Irvine, CA, U.S.A.) at 632.8 nm. A dichroic polarization filter and a quarter-wave plate are used to reduce retroreflected light reaching the probe laser cavity. This retroreflected light can produce a significant amount of intensity noise in the probe beam. After passage through the polarization components of the optical train, the probe beam is reflected from one mirror and focused before the sample with a stationary 22-mm focal length microscope objective. The transmitted probe beam is reflected from a mirror and centered upon a 1-mm slit constructed from two razor blades. The slit is oriented in the plane of the two laser beams and acts as a spatial filter to average spatial noise in the probe beam profile while simultaneously acting as a limiting aperture for the thermal-lens signal. The transmitted light is collected with a large diameter lens and focused onto a photodiode. Any defocusing of the probe beam produced by the heated sample is translated into a change in optical power at the detector.

It is important to note that all optical components are held with massive fixtures and precision micrometer-driven translation stages. In our instrument, the

probe-beam path is fixed in space. The sample cuvette is glued to a piece of aluminum stock so that the cuvette windows are perpendicular to the pump- and probe-beam paths. The cuvette is positioned with a three-axis translation stage and located past the probe beam waist so that the cuvette does not vignette the beam. The pump-beam lens, mounted on a three-axis translation stage, and the two mirrors allow great freedom in the location of the pump beam waist. Typically, the pump beam is focused in the center of the cuvette. Small adjustments in the pump beam position are performed while a high-concentration peak is eluted from the chromatographic column. With high efficiency columns and quickly eluted peaks, this adjustment requires nimble fingers.

The reference and signal detectors are identical 1-mm^2 silicon photodiodes (Silicon Detector, Newbury Park, CA, U.S.A.). The photodiode signal is conditioned with a current-to-voltage converter constructed from a FL 351 JFET operational amplifier wired with a 1-MΩ feedback resistor in parallel with a 470-pf capacitor. The crossed-beam thermal-lens signal is demodulated with a Model 393 lock-in amplifier (Ithaco, Ithaca, NY, U.S.A.) operating in the amplitude mode and with a 4-s time constant. The amplitude mode eliminates any phase noise produced by temperature or flow-rate fluctuations. The chromatograms are displayed on a strip-chart recorder.

Reagents

2,4-Dinitrophenylhydrazine was from Aldrich, as were the six ketones: acetone, methyl ethyl ketone, cyclohexanone, *tert.*-butyl methyl ketone, adamantanone, and 4-methyl benzophenone. Acetonitrile was from Alltech; all other chemicals were reagent grade or better. The chromatographic mobile phase was acetonitrile–water (3:1). 2,4-Dinitrophenylhydrazone crystals were prepared following a standard recipe[18,19]. The samples were recrystalized from ethanol and dried. Sample solutions were prepared in acetonitrile.

RESULTS AND DISCUSSION

Flowing samples resent as particular challenge to thermo-optical instruments[20–23]. Flow acts to translate heat downstream from the pump beam, decreasing the strength of the thermo-optical element. However, some of the decrease in signal may be counteracted by translating the pump beam upstream from the probe beam[22]; heat flows downstream to the probe laser, increasing the thermal-lens signal. Furthermore, flow acts as a heat-loss mechanism, in addition to thermal diffusion. The thermal-lens signal exhibits a faster approach to steady state in flowing samples compared to static samples; higher modulation frequencies may be employed in flowing systems to decrease low frequency noise in the measurement. However, to optimize the instrument, low linear flow-rates are desirable.

In this manuscript we present preliminary results of the crossed-beam thermal-lens for detection in packed 0.25-mm I.D. capillary chromatography columns. In particular, separation of 2,4-dinitrophenylhydrazine derivatives of ketones was chosen as a model. This derivatization reagent is commonly employed for identification of carbonyl compounds and forms dark-red derivatives. These derivatives have modest molar absorptivity at the helium–cadmium laser 442-nm line, 2500–5000

1 mol^{-1} cm^{-1}. The absorbance maximum of these derivatives is located around 360 nm where the molar absorptivity is about 20000 l mol^{-1} cm^{-1}.

We employ a helium–cadmium laser operating at 442 nm. This laser is relatively inexpensive and relyable and is quite simple to operate. However, the 442-nm wavelength is not ideally suited for this analysis; the 325-nm line would better match the absorbance maximum. On the other hand, the reduced power available at 325 nm coupled with greater solvent absorbance should limit the crossed-beam thermal-lens performance.

For the separation of 2,4-dinitrophenylhydrazones, conventional chromatographic instrumentation has previously been used[18]. Little modification of this separation scheme is required for capillary liquid chromatography. Fig. 2 presents a chromatogram of a mixture of six derivatized ketones. The concentration of each ketone was 5.0 · 10^{-5} M. At an injection volume of 60 nl, only 3 pmol of each ketone was injected. For acetone, 180 pg was injected. The variation in response for these compounds appears to reflect variations in molar absorptivity at the 442-nm helium–cadmium laser wavelength. Detection limits, three standard deviations above background[24], were near 120 fmol for acetone and 600 fmol for adamantanone, injected on-column. Of course, much less material is present within the detection volume: assuming a 2-pl probe volume, at the detection limit *ca.* 3 · 10^{-19} mol or 1.5 · 10^{-17} g of acetone is present at the peak maximum. Clearly, the crossed-beam thermal-lens is well designed for absorbance detection in small volume chromatography. Actually, the detector volume is much greater than the probed volume in this instrument. It appears that open tubular liquid chromatography will be required to utilize fully the small volume detection capabilities of the crossed-beam thermal-lens.
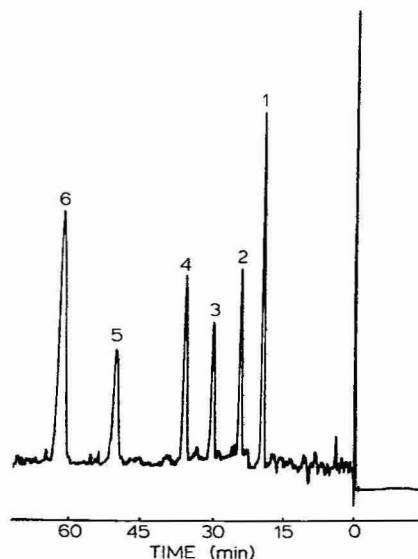
Fig. 2. Chromatogram of 2,4-dinitrophenylhydrazine derivatives of six ketones. Peaks: 1 = acetone, 2 = methyl ethyl ketone, 3 = cyclohexanone, 4 = *tert.*-butyl methyl ketone, 5 = adamantanone derivative, 6 = 4-methylbenzophenone. An amount of 3 pmol of each compound are injected. Note that the injection mark is obtained by momentarily blocking the probe beam; no transient signal is observed coincident with the injection.

Other thermo-optical techniques have been applied to liquid chromatographic detection[12,25-33]. For example, absorbance detection limits of 500 fg of rug dye were reported with a 1-mm I.D. chromatographic column using the coaxial pump-probe thermal lens[33]. However, that analysis required a high-power argon ion laser, 1.25 W, as the pump beam and tested an analyte with very high absorptivity. The high cost of the argon ion laser required in the pump-probe thermal lens will undoubtedly discourage frequent application. More importantly, the relatively large detection volume of that instrument (8 μl) precludes application for 0.25-mm I.D. capillary liquid chromatography.

It is worth emphasizing that very low-power lasers were employed in our instrument; the pump and probe lasers produced 3 and 5 mW, respectively. Since the sensitivity of thermo-optical techniques scales linearly with pump laser power, the low-pump laser power employed in our crossed-beam instrument produces a factor of 400 lower sensitivity than would be produced by a pump laser of the same power as employed in the coaxial pump-probe thermal lens instrument. Of course, detection limits for the two instruments are similar. The improvement in performance of the crossed-beam thermal lens over the coaxial pump-probe thermal-lens is based upon the path length independence property of the crossed-beam instrument. No penalty is paid for small path-length measurements.

Furthermore, it should be noted that the crossed-beam instrument employs relatively inexpensive lasers. The crossed-beam thermal-lens detector could be duplicated minus the optical table, for less than US$ 6000, comparable to the cost of the remainder of the chromatographic system. Although some optical experience is required for the initial alignment of the system, alignment after a change of column takes only *ca.* 5 min.

ACKNOWLEDGEMENT

REFERENCES

1 G. J. Diebold and R. N. Zare, *Science*, 196 (1977) 1439.
2 L. W. Hershberger, J. B. Callis and G. D. Christian, *Anal. Chem.*, 53 (1981) 2110.
3 N. J. Dovichi, J. C. Martin, J. H. Jett and R. A. Keller, *Science*, 219 (1983) 845.
4 P. J. Crosland-Taylor, *Nature*, 171 (1953) 37.
5 M. Hercher, W. Mueller and H. M. Shapiro, *J. Histochem. Cytochem.*, 27 (1979) 350.
6 F. Zarrin and N. J. Dovichi, *Anal. Chem.*, 57 (1985) 1826.
7 N. J. Dovichi, T. G. Nolan and W. A. Weimer, *Anal. Chem.*, 56 (1984) 1700.
8 T. G. Nolan, W. A. Weimer and N. J. Dovichi, *Anal. Chem.*, 56 (1984) 1704.
9 T. G. Nolan and N. J. Dovichi, *IEEE Circuits and Devices Magazine*, 2 (1986) 54.
10 L. A. Knecht, E. J. Guthrie and J. W. Jorgenson, *Anal. Chem.*, 56 (1984) 497.
11 J. C. Gluckman, D. C. Shelly and M. V. Novotny, *Anal. Chem.*, 57 (1985) 1546.

12 T. G. Nolan, B. K. Hart and N. J. Dovichi, *Anal. Chem.*, 57 (1985) 2703.
13 N. J. Dovichi, *CRC Crit. Rev. Anal. Chem.*, in press.
14 J. C. Gluckman, A. Hirose, V. L. McGuffin and M. Novotny, *Chromatographia*, 17 (1983) 303.
15 D. C. Shelly, J. C. Gluckman and M. Novotny, *Anal. Chem.*, 56 (1984) 2990.
16 D. J. Bornhop, T. G. Nolan and N. J. Dovichi, *J. Chromatogr.*, 384 (1987) 181.
17 T. G. Nolan and N. J. Dovichi, in preparation.
18 R. L. Shriner, R. C. Fuson and D. Y. Curtin, *The Systematic Identification of Organic Compounds*, Wiley, New York, 4th ed., 1956, p. 219.
19 L. J. Papa and L. P. Turner, *J. Chromatogr. Sci.*, 10 (1972) 747.
20 N. J. Dovichi and J. M. Harris, *Anal. Chem.*, 53 (1981) 689.
21 W. A. Weimer and N. J. Dovichi, *App. Opt.*, 24 (1985) 2981.
22 W. A. Weimer and N. J. Dovichi, *App. Spectrosc.*, 39 (1985) 1009.
23 W. A. Weimer and N. J. Dovichi, *Anal. Chem.*, 57 (1985) 2436.
24 J. E. Knoll, *J. Chromatogr. Sci.*, 23 (1985) 422.
25 R. A. Leach and J. M. Harris, *J. Chromatogr.*, 218 (1981) 15.
26 C. E. Buffet and M. D. Morris, *Anal. Chem.*, 54 (1982) 1824.
27 S. D. Woodruff and E. S. Yeung, *Anal. Chem.*, 54 (1982) 1174.
28 C. E. Buffet and M. D. Morris, *Anal. Chem.*, 55 (1983) 376.
29 T.-K. J. Pang and M. D. Morris, *Anal. Chem.*, 56 (1984) 1467.
30 M. J. Sepaniac, J. D. Vargo, C. N. Kettler and M. P. Maskarinec, *Anal. Chem.*, 56 (1984) 1252.
31 T.-K. J. Pang and M. D. Morris, *Appl. Spectrosc.*, 39 (1985) 90.
32 Y. Yang, S. C. Hall and M. S. De La Crus, *Anal. Chem.*, 58 (1986) 758.
33 T. W. Collette, N. J. Parekh, J. H. Griffin, L. A. Carreira and L. B. Rogers, *Appl. Spectro.*, 40 (1986) 164.

CHROMSYMP. 934

COUNTER-CURRENT CHROMATOGRAPHY

APPLICATIONS TO THE SEPARATION OF BIOPOLYMERS, ORGANELLES AND CELLS USING EITHER AQUEOUS–ORGANIC OR AQUEOUS–AQUEOUS PHASE SYSTEMS

IAN A. SUTHERLAND and DEBORAH HEYWOOD-WADDINGTON

National Institute for Medical Research, Mill Hill, London NW7 1AA (U.K.)

and

YOICHIRO ITO*

National Heart, Lung, and Blood Institute, Laboratory of Technical Development, Bethesda, MD 20892 (U.S.A.)

SUMMARY

Counter-current chromatography is a form of liquid–liquid chromatography which uses low-speed centrifugation to hold one phase of an immiscible liquid pair stationary while the other is eluted through it.

Two types of countercurrent chromatography are described: one suitable for preparative/analytical separation with aqueous–organic phase systems and the other for analytic fractionations using aqueous–aqueous phase systems.

Applications of both processes are described, ranging from the purification of antibiotics, pesticides, and peptides to the fractionation of whole cells.

INTRODUCTION

Counter-current chromatography can be considered either as liquid–liquid chromatography without a solid support or as a continuous form of liquid–liquid extraction. Since it was first introduced in the 1970s, the process has been through a number of development phases which have improved its design and efficiency. With few exceptions, all the schemes involve continuous coils of PTFE tubing, rotating in some form of planetary motion without rotating seals. The process is now being used for the analytical/preparative separation and purification of a wide range of natural products and soluble biopolymers with aqueous–organic phase systems and for analytical fractionations of membranes and organelles with double aqueous phase systems.

There are two essential requirements for successful countercurrent chromatography: the retention of one of the phases in the coil and adequate mass transfer of sample constituents, as the other mobile phase passes through and mixes with the retained phase. Successful retention is largely a function of the physical properties

of the phase systems and interactions with the walls of the coils. Mass transfer depends on effective mixing, which is determined by hydrodynamic factors.

This paper reviews the latest counter–current chromatography techniques used for separations with both aqueous–organic and aqueous–aqueous phase systems.

COUNTER-CURRENT CHROMATOGRAPHY WITH AQUEOUS–ORGANIC PHASE SYSTEMS

All advanced forms of counter-current chromatography require some form of enhanced gravity to hold one phase of an immiscible liquid pair stationary while the other is eluted through it. Mixing takes place either by synchronous rotation of the

Uniform Acceleration Field
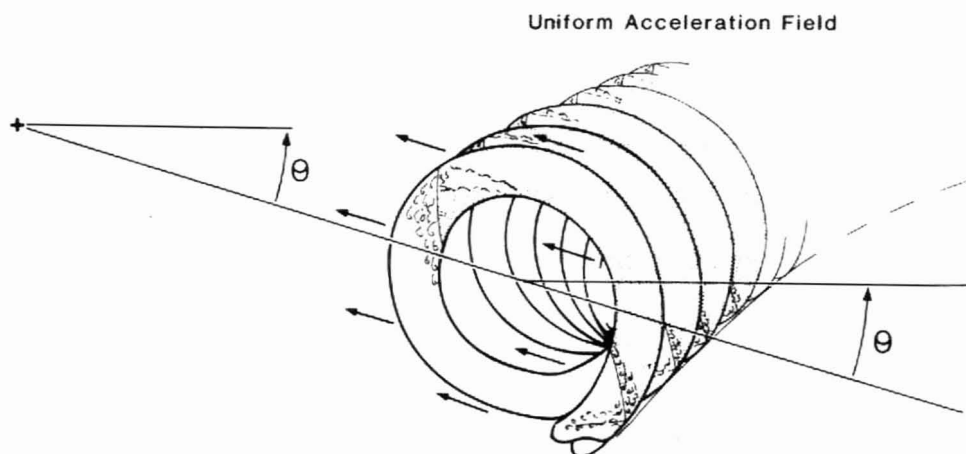
Fig. 1. Synchronous coil planet centrifuge—cascade mixing.

Fluctuating Acceleration Field
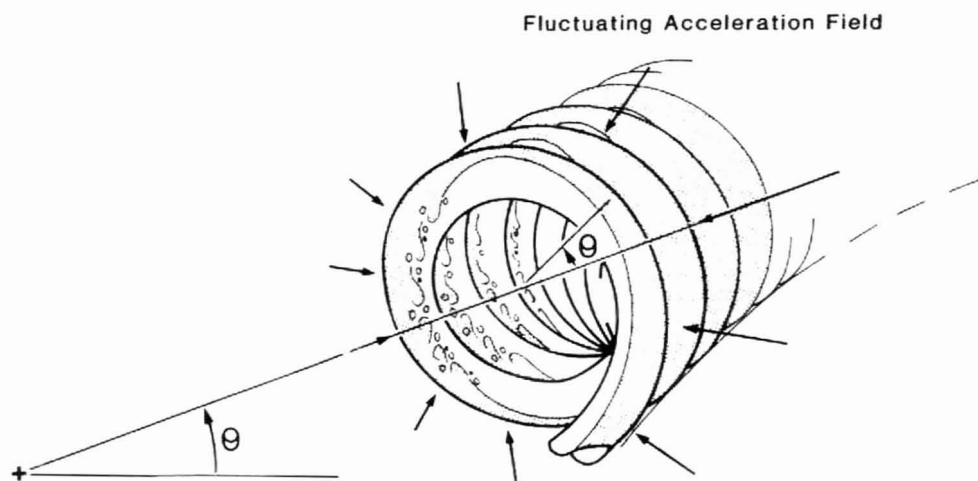
Fig. 2. Epicyclic coil planet centrifuge—wave mixing.

coils, which mixes the phases in a cascade fashion (Fig. 1) or by the relative stability of two layers of flow, as determined by a fluctuating force field (Fig. 2).

Up to the end of the 1970s the mixing methods were mainly of the synchronous variety[1-9]. Geometrical constraints limited retention to less than 50%, and the high mixing rates of these coil planet centrifuges, while enhancing resolution, were rather sensitive to carry-over and loss of the stationary phase. The process was therefore limited to analytical-scale, high resolution separations, biased towards the high-interfacial-tension range of phase systems.

By the late 1970s Ito had developed a new form of coil rotation (the epicyclic coil plant centrifuge), which fundamentally changed the mixing concept within each coil (Fig. 2). Instead of a succession of cascades, mixing was achieved between two thin layers of liquids in such a way that zones of mixing and settling travelled along the tubing coincident with areas of low and high force fields, set up by the epicyclic motion of the coils[10-12].

The time between successive mixing and settling cycles is typically between 50 and 100 ms, and the phase systems have to be able to respond to these fast changes without emulsification. Consequently, this particular scheme is limited to use with aqueous–organic phase systems where these physical properties at enhanced gravitational fields of between 100 and 200 g are such that these response times can be achieved.

The prime benefits of this new motion are:

(1) increased retention of stationary phase (up to 90%);

(2) faster flow-rates with minimal loss of retention;

(3) greater stability, allowing use of a wider range of lower interfacial tension phase systems;

(4) greater capacity, the sequence of phase mixing and settling is independent of tubing size and can therefore be scaled up;

(5) simplicity and ease of manufacture.

Description of motion

The motion of the epicyclic coil planet centrifuge is shown schematically in Fig. 3. Its major advantage is that the planetary mechanism is simple and can be mounted in a bench centrifuge.

The coil is mounted circumferentially around a drum, attached to gear "B" (Fig. 3a) such that the locus of the point "P" on the periphery of the coil prescribes a cardioid. This produces an acceleration vector that varies in both magnitude and direction, as shown in Fig. 3b[12]. The position of coils on the drum is defined by the β value (where $\beta = r/R$).

Liquids can be passed to and from the rotating coils without the use of rotating seals, provided the input/output tubes are passed through the center line of the centrifuge at "O" (Fig. 3a), and then turn through 180 degrees, reentering the planetary system along its center line at point "C".

The coils are initially filled with the intended stationary phase. Mobile phase is then pumped in, while the coils are rotating. Operation proceeds in a similar way to a standard chromatography process, the sample being injected with the mobile phase and eluted into a fraction collector.

(a)
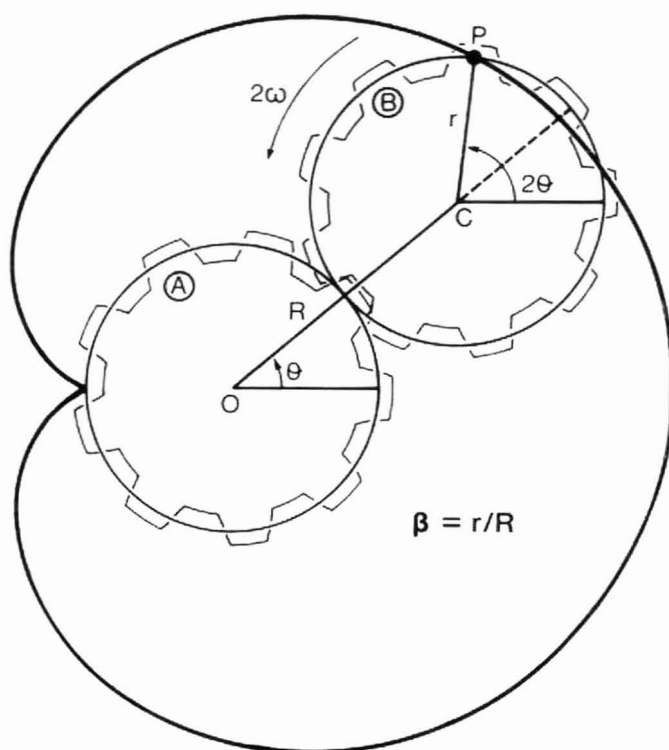
(b)
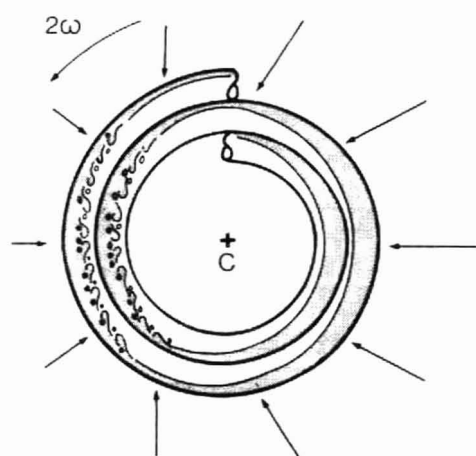
Fig. 3. The principle of motion showing (a) the cardioid locus of a point "P" and (b) the effect on the phase system of a fluctuating force field.

Applications

Using aqueous–organic phase systems, an example of the recent improvement in both resolution and throughput in countercurrent chromatography can be given for the work on purifying polyene macrolide antibiotics[13,14], where a separation of candicidin on an early synchronous coil planet centrifuge is compared with the same separation on the epicyclic coil planet centrifuge (Fig. 4a and b). Similar resolution
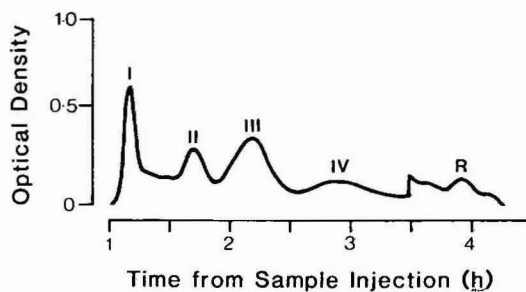
(a) Synchronous Coil Planet Centrifuge
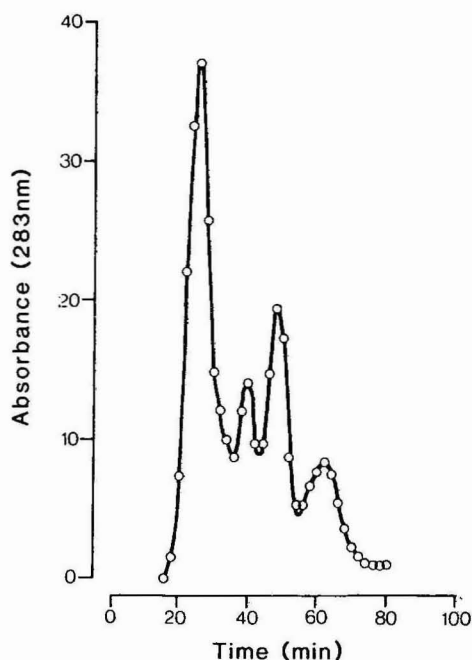
(b) Epicyclic Coil Planet Centrifuge

Fig. 4. The fractionation of candicidin, a polyene antibiotic on (a) the synchronous coil planet centrifuge and (b) the epicyclic coil planet centrifuge. Conditions: (a) Solvent, chloroform–methanol–water (4:4:3); sample size, 0.3 ml; concentration, 1.0 mg/ml; speed, 500 rpm; flow, 60 ml/h; retention, 40%; column capacity, 110 ml. (b) Solvent, chloroform–methanol–water (4:4:3); sample size, 100 mg; concentration, 10 mg/ml; speed, 800 rpm; flow, 240 ml/h; retention, 57%; column capacity, 285 ml.

is achieved in a fraction of the time and with greater throughput by means of the new form of rotation.

Recently, the capability of the present method has been further demonstrated in separation and purification for broad spectrum of samples which include many other antibiotics[15,16], steroids[17], pesticides[18,19], and herbicides[20], plant hormones[21], pigment[22], tannins[23], DNP-amino acids[24,25], a variety of biologically active peptides[25–28], etc.

While preliminary studies[29,30] have shown that, in principle, scale-up is possible, the widespread application of the technique and full industrial scale-up will only be achieved if the basic factors affecting both resolution and throughput are more clearly understood. The studies of Ito and Conway on a wide range of phase systems in the epicyclic coil planet centrifuge[31] have identified viscosity as being an important factor determining which phase is retained in the coil. Nevertheless, studies on the hydrodynamics of the phase systems have been limited[32–34], and the fundamental reasons governing the retention of one phase in preference to the other are still not understood[30].

COUNTER-CURRENT CHROMATOGRAPHY WITH DOUBLE AQUEOUS-PHASE SYSTEMS

Principle

When certain polymers are mixed with water, two immiscible aqueous phases can be formed that can, with suitable additives, provide a hospitable medium for cells or organelles[35,36]. Unfortunately, these aqueous-phase systems have an increased viscosity, lower density difference, and considerably reduced interfacial tension, when compared to aqueous/organic phase systems. This makes them unsuitable for use in the conventional, high-resolution coils just described, due to their long mixing/settling cycle times. However, this does not preclude their use with counter-current chromatography on an analytical scale. Special torodial coils can be mounted perpendicular to the force field. A mixing scheme similar to the one in Fig. 1 is used, except that the coils are fixed relative to the acceleration vector, and cascade mixing is produced simply by one phase flowing relative to the other[37].

Coils can be wound around the drum of an epicyclic coil planet centrifuge[38] or, alternatively, mounted circumferentially on a rotating disc (Fig. 5). The coil is initially filled with one of the phases. The plate is rotated at 1000 rpm while the other phase is pumped in. As the phases mix, centrifugal force ensures that the lighter and heavier phases are retained in the inner and outer halves of each coil unit, respectively. The pumped phase progressively displaces the other phase from the coils until an equilibrium is established. Continuous pumping of the mobile phase sets up a series of cascades (much like waterfalls) through the retained segments of the other phase in each coil unit.

The sample is injected with the mobile phase, using a conventional liquid chromatography sample loop, and undergoes a series of mixing and settling steps before it is eventually eluted into the fraction collector. Sample components partitioned toward the mobile phase will be eluted early, while components favoring the stationary phase or interface will be retained. As there is no solid support, either phase can be used as the mobile phase or even a mixture of the two. Adding a small proportion of the stationary phase in the mixture in the above example would accelerate the
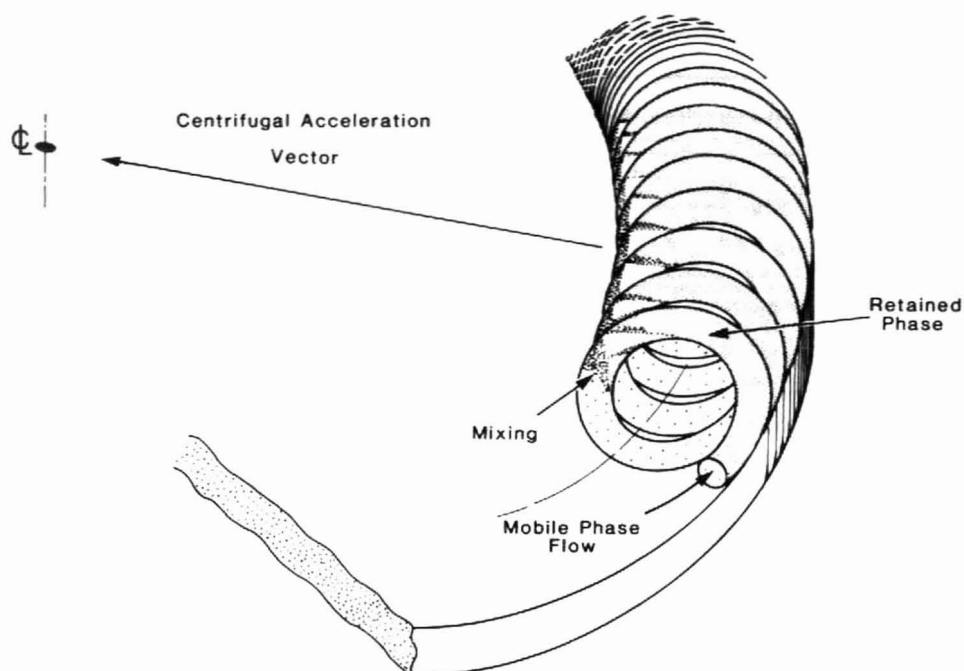
Fig. 5. Schematic diagram of the torodial coil rotor.

elution of all the retained components and clear the coil system for another sample loading.

Applications using double aqueous-phase systems

    Rat liver homogenates. Both the toroidal coil and epicyclic coil planet centrifuges have been used for subcellular particle fractionations. For example, rat liver homogenate has been successfully fractionated on both machines, using a phase system containing 3.3% (w/w) dextran T 500, 5.4% PEG 6000, 10 mM sodium phosphate–phosphoric acid buffer (pH 7.4), 0.26 M sucrose, 0.05 mM Na$_2$EDTA, and 1 mM ethanol[38].

    Sample preparation and enzyme assay procedures are outlined in detail by Heywood-Waddington *et al.*[39] and Sutherland *et al.*[37]. Fractionations in either machine are qualitatively similar, the plasma membrane being eluted early, lysosomes shortly afterwards, and endoplasmic reticulum spread over possibly three fractions. Heywood-Waddington *et al.*[39] used rat liver homogenate in a standard fractionation for studying a number of operating parameters, such as rotational speed, flow-rate, coil geometry, and sample loading. The process was shown not to be critical, and small changes in these parameters did not significantly affect the order of elution or resolution of the process, provided certain boundary conditions were met.

    Torpedo membranes. Torpedo electroplax membranes, enriched in nicotinic cholinergic receptor sites have been successfully purified by Flanagan *et al.*[40] by affinity partitioning techniques with phase systems operating near the critical point.

Flanagan *et al.*[40] have elegantly demonstrated the power of linking affinity partition with counter-current chromatography and supports his case by performing a complementary study with thin-layer counter-current distribution techniques. He has also made major contributions by defining the procedures for operating the toroidal coil near the critical point, and examining the effects of sample loading. He found that it was essential to pump an emulsion of upper and lower phases (approximately in the ratio 10:1) to effect any elution of material at all, unlike in the phase system used for the rat liver fractionation, where it was optional. He also concluded that sample loading was limited not by the process but by the ability to obtain a sufficiently concentrated sample.

Bacterial cells. Bacterial cells are approximately 1 μm in diameter, and their separation presents a borderline choice between the toroidal coil centrifuge or the non-synchronous coil planet centrifuge[41]. While these cells have been successfully separated on the toroidal coil planet centrifuge[42], the non-synchronous centrifuge was used in the following examples, on the purification of different strains of *Escherichia coli* and the separation of *Salmonella typhimurium* cells.

The partition behavior for two different strains of *E. coli* in a PEG–dextran
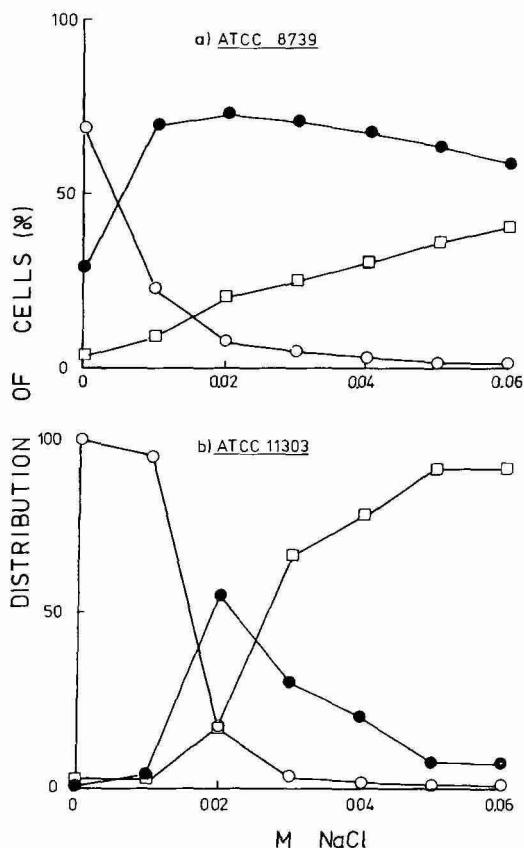
Fig. 6. The distribution of two different strains of *E. coli* in a two-phase polymer system. (○) In upper phase; (●) at interface; (□) in lower phase.

phase system is illustrated in Fig. 6 for various sodium chloride concentrations. The basic phase system used consisted of 5% (w/w) dextran 500, 4% (w/w) PEG 6000, and 0.01 M potassium phosphate (pH 6.9). Both strains were partitioned towards the upper phase at zero sodium chloride concentration. As the sodium chloride concentration increased, *E. coli* I started to partition predominantly toward the interface at a concentration greater than 0.005 M, while *E. coli* II exhibited the same behavior above a sodium chloride concentration of 0.015 M.

A 200-coil column of 1-mm I.D. PTFE tubing was used. It was initially filled with the heavier phase, and the centrifuge was set to rotate at 750 rpm with a coil rotation of 5.25 rpm. The flow-rate was 14 ml/h.

The *E. coli* cells of Fig. 6a, injected with the mobile phase, were eluted at the solvent front when no sodium chloride was present, but were retained in the column when a sodium chloride concentration of 0.06 M was used. This signified that a gradient separation was feasible. The column was then filled with the heavier phase at 0.02 M sodium chloride concentration. A mixture of the two *E. coli* strains (Fig. 6) was injected with the mobile phase. In order to produce a sodium chloride gradient (0.02–0.00 M), the mobile upper phase was made up with zero sodium chloride concentration and fed via a 5-ml continuously stirred mixing chamber (initially filled
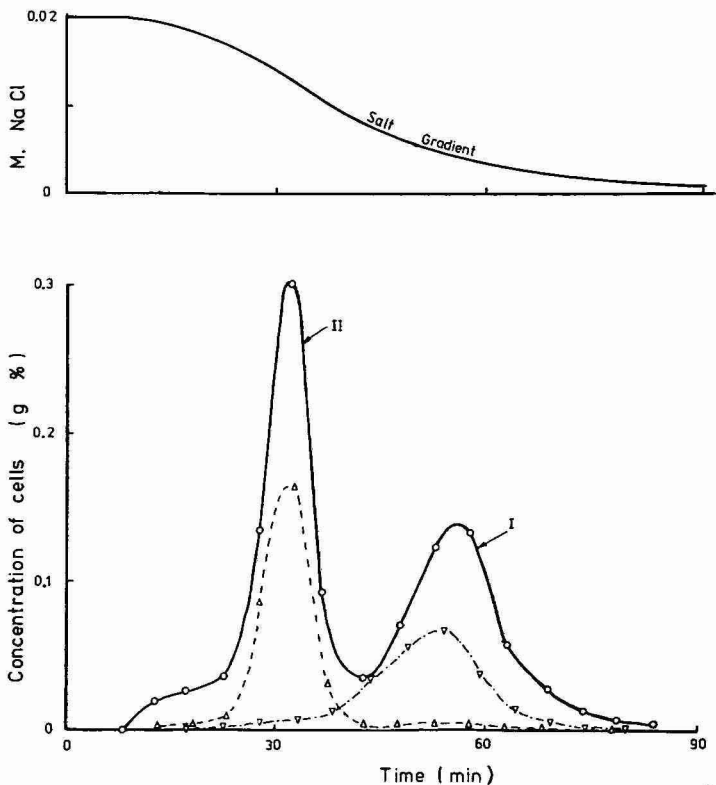
Fig. 7. A gradient separation of a mixture of two strains of *E. coli* cells by use of the non-synchronous coil planet centrifuge. Phase system, 5% PEG, 4% dextran. I = ATCC 8739; II = ATCC 11303. (O) Mixture of I and II; (∇) re-run of I; (△) rerun of II.

with upper phase containing 0.02 M sodium chloride concentration) before being pumped into the column.

The cells were eluted in two populations (Fig. 7). The most concentrated fractions from each peak were collected and rerun separately with up to 93% reproducibility in both cases. Earlier runs with the individual pure *E. coli* strains produced single peaks at the expected positions. Separations were repeated and found to be reproducible.

Counter-current chromatography on the non-synchronous coil planet centrifuge without rotating seals[43] was used to separate cells of *Salmonella typhimurium*, which have identical surfaces except for the proportion of lipopolysaccharide (LPS) molecules with long *versus* short polysaccharide chains[44].

Human erythrocytes. Sutherland and Ito have demonstrated that the non-synchronous coil planet centrifuge could be used for larger cells by separating different species of red blood cells[41]. They demonstrated that cells of varying size could be separated on the basis of their partition behaviour and were not affected by sedimentation. These cell separations were achieved under operating conditions similar to the ones previously described, except that the process was stopped before elution, and the coil contents were pumped out. When the process was extended beyond elution, peaks would spread out, possibly due to sedimentation effects in the outlet tubing.

Other research workers[45] have reported difficulties in reproducing these results, partly due to discrepancies in phase-system composition, and partly due to the fact that this is a non-elution process. Clearly, if these barriers were overcome, a promising new cell separation process could emerge.

CONCLUSIONS

Counter-current chromatography is easy to use, has a wide range of applications and is suited to automation. But its major asset is low cost and high sample recovery rates. The absence of a solid support minimizes adsorption problems and allows one set of coils to be used with a variety of different phase systems.

Counter-current chromatography with aqueous–organic phase systems has the potential of becoming a preparative-scale alternative to high-performance liquid chromatography for the separation of peptides and antibiotics. The principle of phase mixing and settling in the epicyclic coil planet centrifuge has the potential for further scale-up, once fundamental aspects concerning the hydrodynamics are understood.

The counter-current chromatographic techniques used for aqueous–organic phase systems cannot be applied directly for use with polymer phase systems, due to their high viscosity and low density difference. Consequently, its application has so far been restricted to analytical methods with toroidally wound coils that enhance retention of these viscous phases.

Counter-current chromatography is an emerging technique which is far from optimized. Phase system requirements are only beginning to be understood. One way for the technology to move forward is for new biocompatible phase systems to be identified with physical properties more suited for use with counter-current chromatography.

REFERENCES

1 Y. Ito, I. Aoki, K. Nunogaki, E. Kimura and Y. Nunogaki, *Anal. Chem.*, 41 (1969) 1579.
2 Y. Ito and R. L. Bowman, *Anal. Chem.*, 43 (1971) 69A.
3 Y. Ito and R. L. Bowman, *Science*, 173 (1971) 420.
4 R. E. Hurst and Y. Ito, *Clin. Chem.*, 18 (1972) 814.
5 Y. Ito, R. L. Bowman and F. W. Noble, *Anal. Biochem.*, 49 (1972) 1.
6 Y. Ito and R. L. Bowman, *J. Chromatogr. Sci.*, 11 (1973) 284.
7 Y. Ito and R. L. Bowman, *Science*, 182 (1973) 391.
8 Y. Ito, R. E. Hurst, R. L. Bowman and E. K. Achter, *Sep. Purif. Methods*, 3 (1974) 133.
9 Y. Ito and R. L. Bowman, *Anal. Biochem.*, 65 (1975) 310.
10 Y. Ito and R. L. Bowman, *Anal. Biochem.*, 82 (1977) 63.
11 Y. Ito and R. L. Bowman, *J. Chromatogr.*, 147 (1978) 221.
12 Y. Ito, *J. Chromatogr.*, 188 (1980) 33.
13 I. A. Sutherland and J. E. E. Sharpe, *J. Chromatogr.*, 122 (1976) 333.
14 J. W. Lightbown, P. Newland, I. A. Sutherland and J. W. A. Dymond, *Proc. Anal., Div. Chem. Soc.*, 14 (1977) 34.
15 G. M. Bril, J. B. McAlpine and J. E. Hochlowski, *J. Liq. Chromatogr.*, 8 (1985) 2259.
16 D. G. Martin, S. A. Mizsak and W. C. Krueger, *J. Antibiot.* (1985), 746.
17 R. G. Williams, *Pittsburgh Conference and Exposition on Analytical Chemistry and Applied Spectroscopy*, 1985, No. 300.
18 Y. W. Lee and C. E. Cook, *J. Liq. Chromatogr.*, 8 (1985) 2253.
19 J. M. Ruth, Y. Ito, N. B. Mandava and V. P. Flanagan, *J. Liq. Chromatogr.*, 8 (1985) 2239.
20 N. B. Mandava, Y. Ito and J. M. Ruth, *J. Liq. Chromatogr.*, 8 (1985) 2221.
21 N. B. Mandava and Y. Ito, *J. Liq. Chromatogr.*, 7 (1984) 303.
22 H. M. Fales, L. K. Pannell, E. A. Sokoloski and P. Carmeci, *Anal. Chem.*, 57 (1985) 376.
23 L. J. Putman and L. G. Butler, *J. Chromatogr.*, 318 (1985) 85.
24 Y. Ito, *J. Chromatogr.*, 214 (1981) 122.
25 Y. Ito, J. Sandlin and W. G. Bowers, *J. Chromatogr.*, 244 (1982) 247.
26 M. Knight, Y. Ito, A. M. Kask, C. A. Tamminga and T. N. Chase, *J. Liq. Chromatogr.*, 7 (1984) 2525.
27 M. Knight, Y. Ito, P. Peters and C. diBello, *J. Liq. Chromatogr.*, 8 (1985) 2281.
28 M. Knight, Y. Ito, J. L. Sandlin and A. M. Kask, *J. Liq. Chromatogr.*, 9 (1986) 791.
29 J. L. Sandlin and Y. Ito, *J. Liq. Chromatogr.*, 7 (1984) 323.
30 J. L. Sandlin and Y. Ito, *J. Liq. Chromatogr.*, 8 (1985) 2153.
31 Y. Ito and W. D. Conway, *J. Chromatogr.*, 301 (1984) 405.
32 W. D. Conway and Y. Ito, *Abstracts Pittsburgh Conference on Analytical Chemistry and Applied Spectroscopy, Atlantic City, NJ, March 1984*, Paper No. 472.
33 I. A. Sutherland and D. Heywood-Waddington, *Abstracts Pittsburgh Conference on Analytical Chemistry and Applied Spectroscopy, New Orleans, LA, February 1985*, Paper No. 302.
34 I. A. Sutherland, S. Jones and D. Heywood-Waddington, *Abstracts Pittsburgh Conference on Analytical CHemistry and Applied Spectroscopy, Atlantic City, NJ, March 1986*, Paper No. 1045.
35 P. Å. Albertsson, *Partition of Cell Particles and Macromolecules*, Wiley-Interscience, New York, 1986.
36 H. Walter, D. E. Brooks and D. Fisher (Editors), *Partitioning in Aqueous Two-Phase Systems: Theory, Methods, Uses and Application to Biotechnology*, Academic Press, 1986.
37 I. A. Sutherland, D. Heywood-Waddington and T. J. Peters, *J. Liq. Chromatogr.*, 7 (1984) 363.
38 I. A. Sutherland, D. Heywood-Waddington and T. J. Peters, *J. Liq. Chromatogr.*, 12 (1985) 2315.
39 D. Heywood-Waddington, I. A. Sutherland, W. B. Morris and T. J. Peters., *Biochem. J.*, 217 (1984) 751.
40 S. D. Flanagan, G. Johansson, B. Yost, Y. Ito and I. A. Sutherland, *J. Liq. Chromatogr.*, 7 (1984) 385.
41 I. A. Sutherland and Y. Ito, *Anal. Biochem.*, 108 (1980) 367.
42 I. A. Sutherland and Y. Ito, *J. High Resolut. Chromatogr. Chromatogr. Commun*, 3 (1978) 171.
43 Y. Ito, G. T. Bramblett, R. Bhatnagar, M. Huberman, L. Leive, L. M. Cullinane and W. Groves, *Sep. Sci. Technol.*, 18 (1983) 33.
44 L. Leive, L. M. Cullinane, G. Bramblett and Y. Ito, *J. Liq. Chromatogr.*, 7 (1984) 403.
45 J. M. Harris, M. G. Case, R. S. Snyder and A. A. Chenault, *J. Liq. Chromatogr.*, 7 (1984) 419.

CHROMSYMP. 1056

MICELLAR LIQUID CHROMATOGRAPHY FOR THE ANALYSIS OF NUCLEOSIDES AND BASES

YONG-NAM KIM and PHYLLIS R. BROWN*

Department of Chemistry, University of Rhode Island, Kingston, RI 02881 (U.S.A.)

SUMMARY

A new high-performance liquid chromatographic method for the analysis of nucleosides and bases was developed in which a micellar mobile phase is used. Separation was achieved on a polyvinyl alcohol (PVA) column by isocratic elution with micellar sodium dodecyl sulfate (SDS) as the mobile phase. The retention behavior of the nucleosides and bases was significantly different from that obtained by reversed-phase chromatography. Effect of pH, temperature, and concentration of SDS and the counter ion (Na^+) on retention behavior were investigated. With the PVA column, the best conditions for an isocratic separation were 0.01 M SDS (pH 3.4) and a flow-rate of 2 ml/min at ambient temperature. Mechanisms for the retention of the nucleosides and bases on the PVA column with a micellar mobile phase were proposed and an application of the separation was demonstrated by the analysis of human serum.

INTRODUCTION

In 1980 Armstrong and Henry[1] proposed the use of an aqueous micellar solution as a selective mobile phase in reversed-phase liquid chromatography (RPLC). This method has been used in various practical applications[2–23].

For the analysis of physiological samples containing the biologically important nucleosides and bases, high-performance liquid chromatography (HPLC) is most useful[24–32]. Most of published methods for HPLC of nucleic acid constituents involve RPLC on silica-based columns with hydroorganic mobile phases; however, it is difficult to retain some of the pyrimidines and several important compounds may not be resolved. In addition, for gradient elution, the column must be re-equilibrated, which is time-consuming.

Recently, separations of nucleosides and bases on porous polyvinyl alcohol (PVA) columns with several different buffer and salt solutions[33,34] and on a poly(styrene–divinylbenzene) (PRP-1) column with a hydroorganic mobile phase[35] have been reported. Because of relatively long retention times and poor resolution, improvements in these methods were sought. Thus, we explored the potential of micellar liquid chromatography for the separation of nucleosides and bases on a PVA column.

EXPERIMENTAL

Apparatus

A Waters M 6000A pump (Waters Assoc., Milford, MA, U.S.A.) equipped with a Rheodyne 7125 injector (50 μl) (Berkeley, CA, U.S.A.) connected to a Waters 440 dual-wavelength detector was used. The column used was a 9-μm Asahipak GS 320H PVA column (25 cm × 7.6 mm I.D.) (Asahi Chemical Industry, Kawasaki, Japan). A Hamilton cartridge guard column (Hamilton, Reno, NV, U.S.A.) was used for protecting the analytical column. The column was placed in a constant-temperature column compartment (DuPont Instruments, Wilmington, DE, U.S.A.). Chromatograms were recorded on an Omniscribe strip chart recorder (Houston Instruments, Austin, TX, U.S.A.).

Reagents

Nucleosides and bases were obtained from Sigma (St. Louis, MO, U.S.A.). Stock solutions were prepared in double-distilled. deionized water, and the pH was adjusted to 7.3 with phosphate buffer. All stock solutions were stored at $-20°$C. Electrophoresis-grade sodium dodecyl sulfate (SDS) was obtained from Bio-Rad (Richmond, CA, U.S.A.) and was used as received.

Procedure

Mobile phases were prepared by adding the appropriate amount of SDS to distilled water. The pH values of the solutions were adjusted with phosphate buffer, and the solutions were filtered through 0.45-μm Nylon 66 membrane filters (Rainin Instruments, Ridgefield, NJ, U.S.A.). The separations were performed isocratically at a flow-rate of 2 ml/min at ambient temperature. Blood from a healthy volunteer was collected and centrifuged immediately. The serum was passed through a membrane cone (Amicon, Lexington, MA, U.S.A.) at 750 g for 15 min and stored at $-20°$C. Peaks were identified by previously published methods[24]. Quantitation was carried out for uridine, uric acid, xanthine, and guanosine by comparing peak heights obtained from runs on serum samples with those from runs on sets of standards. Linearity of response to each compound was obtained.

RESULTS

The retention behavior of the following nucleosides and bases was investigated: uric acid (UA), uracil (Ura), thymine (Thy), hypoxanthine (Hyp), xanthine (Xan), adenine (Ade), cytosine (Cyt), uridine (Urd), inosine (Ino), thymidine (Thd), guanosine (Guo), and adenosine (Ado). These purines and pyridines were chosen, because they are important in biological studies. The capacity factors, k', were measured as a function of the pH, the concentration of SDS, the concentration of counter ion, and the temperature.

Chromatography

Fig. 1 shows the isocratic elution profiles of nucleosides, bases, and a mixture of both classes of compounds on the PVA column when a mobile phase at pH 3.4, containing 0.01 M SDS, is used. Most of the hydroxylated purines and pyrimidines
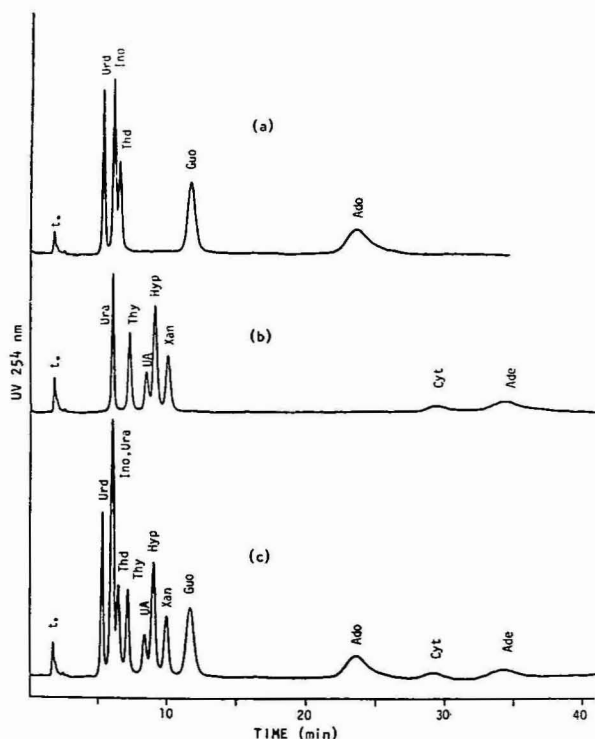
Fig. 1. Isocratic elution profiles of (a) nucleosides, (b) bases, and (c) a mixture of nucleosides and bases. Column, 9-μm Asahipak GS 320H; mobile phase, 0.01 M SDS (pH 3.4); flow-rate, 2 ml/min; sample concentration, 2 · 10^{-5} M each; injection volume, 10 μl; sensitivity, 0.01 a.u.f.s.; temperature, ambient.

were well resolved in 12 min. Only Cyt, Ade, and Ado, compounds with amino functional groups, had longer retention times and significant band-broadening. Thus, this separation could be very useful in studies where a rapid analysis of the hydroxylated purine bases, Hyp, Xan, and UA, is needed.

Good reproducibility of retention of nucleosides and bases was observed, as can be seen in Table I. Although poor peak asymmetry is usually observed in RPLC on silica-based columns with a micellar mobile phase, we found peak asymmetry of 1.05 for Thy and 0.92 for Guo with the PVA column.

Effect of pH

The elution behaviour of nucleosides and bases on the PVA column by micellar liquid chromatography is quite different from that on RPLC silica-based columns eluted with a hydroorganic mobile phase[24-32]. With the RPLC method, the k' values of the purine bases (Hyp, Xan) were higher than those of the pyrimidine bases (Ura, Thy) in the pH range of 3.4–6, and the nucleosides had greater retention than their respective bases. However, with our method, the k' values of the purines were lower than those of the pyrimidines, and the k' values of the nucleosides (Ado, Thd, Ino, Urd) were lower than those of their respective bases (Ade, Thy, Hyp, Ura). In ad-

dition, the pyrimidine base Cyt, which is eluted near the void volume in RPLC, was strongly retained.

The elution of Ura, Thy, Urd, Ino and Thd was influenced only slightly by changes in pH from 2 to 7 (Fig. 2). On the other hand, there was a significant increase in retention at pH 3.4 for compounds possessing an amino group on the purine or pyrimidine ring (Ade, Ado, Guo, Cyt). This retention behavior is in contrast to that obtained by Yasukawa et al.[34] who used a phosphate buffer on a PVA column in the pH range of 3–7. They found a decrease in retention at low pH and explained that the decrease was a result of a weakening in the hydrophobic interaction of the protonated purine or pyrimidine ring moiety with the gel matrix. However, the increase in retention of Ade, Ado, Guo and Cyt at pH 3.4 that we observed can best be explained by electrostatic attraction of the protonated ring moiety with the negatively charged stationary phase. At pH 3.4, nucleosides and bases with an amino group are positively charged[37–39]. Since negatively charged sites are produced by adsorption of the anionic surfactant monomers on the surface of the PVA stationary phase, these negatively charged sites can cause the positively charged ring moiety to be retained longer than other species. Therefore, the PVA stationary phase in the presence of SDS can act as a cation exchanger. A possible retention model of the electrostatic attraction between the positively charged solute and a negatively charged stationary phase site is shown in Fig. 3.

Effect of SDS concentration

The concentration of SDS in the mobile phase at pH 3.4 affected the retention mainly of Ade, Ado, Guo and Cyt, which have an amino group on the ring. The k' values of these compounds decreased greatly as the concentration of SDS increased (Fig. 4). This increase in retention can be explained by the formation of anionic micelles of the excess SDS molecules in solution; thus, there is electrostatic attraction of the positively charged ring moiety to the increased number of anionic micelles in the mobile phase. The positively charged rings compete effectively with the counter

TABLE I

REPRODUCIBILITY OF RETENTION OF NUCLEOSIDES AND BASES

All conditions as in Fig. 1. $n = 10$.

Compound	k'	S.D.	C.V. (%)
Urd	2.12	0.00882	0.416
Ino	2.54	0.0129	0.508
Ura	2.54	0.0129	0.508
Thd	2.82	0.00882	0.313
Thy	3.24	0.0137	0.423
UA	4.00	0.0149	0.373
Hyp	4.27	0.0176	0.412
Xan	4.92	0.0180	0.366
Guo	5.77	0.0191	0.331
Ado	12.5	0.0943	0.754
Cyt	15.8	0.111	0.703
Ade	18.6	0.115	0.618

ions (Na$^+$) in the mobile phase to pair up with the micelles. In essence, since only a limited number of SDS molecules can be adsorbed on the stationary phase, there are a large number of non-adsorbed, free micelles in the mobile phase. As the SDS concentration increases, the positively charged ring moieties are attracted to the large number of available negatively charged micelles in the mobile phase.

When $1/k'$ values were plotted against SDS concentrations, a linear relationship was observed for the bases Cyt and Ade (Fig. 5). Although the relationship was not linear for the nucleosides with an amino group (Guo, Ado), both plots of $1/k'$ values against SDS concentrations had positive slopes. This relationship suggests that at pH 3.4 electrostatic attraction is the dominant effect in the retention of purine or pyrimidine compounds containing an amino group.

Effect of counter-ion concentration

By plotting the increase in sodium chloride concentration against k', the effect of counter-ion concentration is indicated (Fig. 6). Increased counter-ion concentration caused sharply decreased k' values of the bases Ade and Cyt and the nucleoside
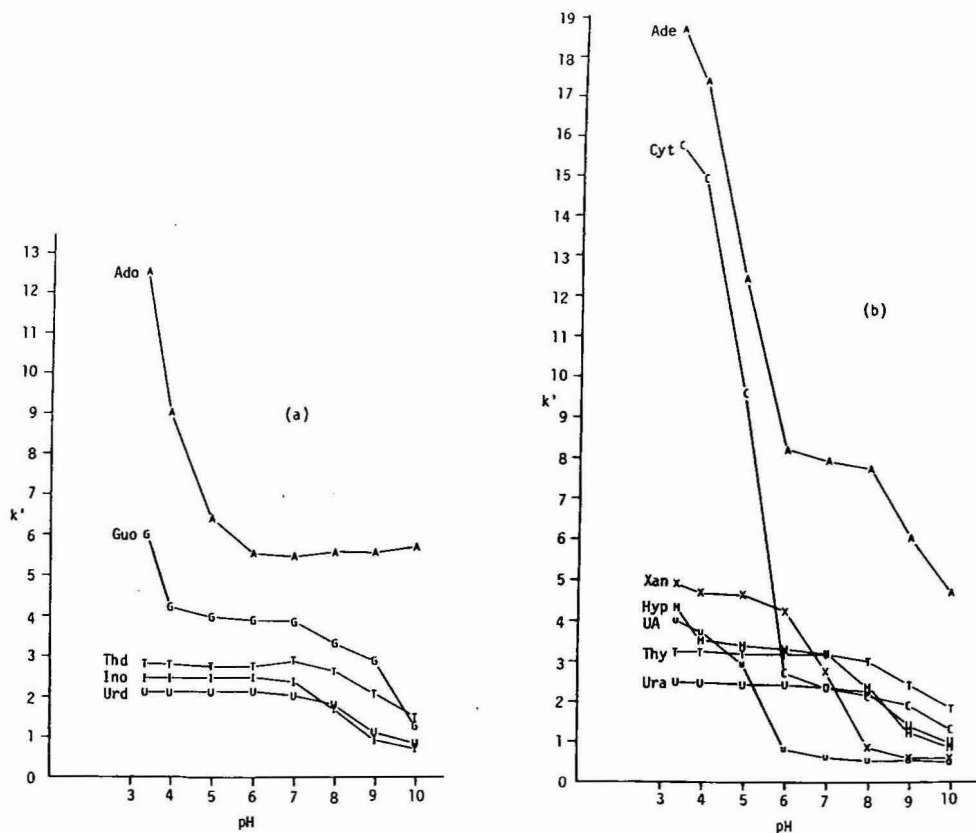
Fig. 2. Effect of pH on the capacity factors of (a) nucleosides and (b) bases. Column, 9-μm Asahipak GS 320H; mobile phase, 0.01 M SDS; flow-rate, 2 ml/min; temperature, ambient. Each point represents the average of three determinations.
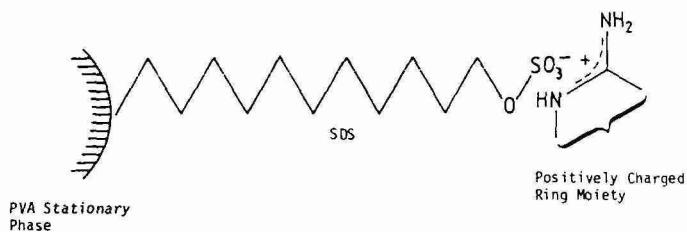
Fig. 3. Proposed electrostatic attraction of the protonated ring moiety with the negatively charged stationary phase.

Ado. At low concentrations (up to 0.01 M), the k' values of Hyp, Xan, UA, and Guo decreased moderately. However, the degree of reduction in retention with increasing counter-ion concentration was smaller than that with increasing SDS concentration. In addition, the elution order of Guo and Hyp changed with increasing counter-ion concentration.
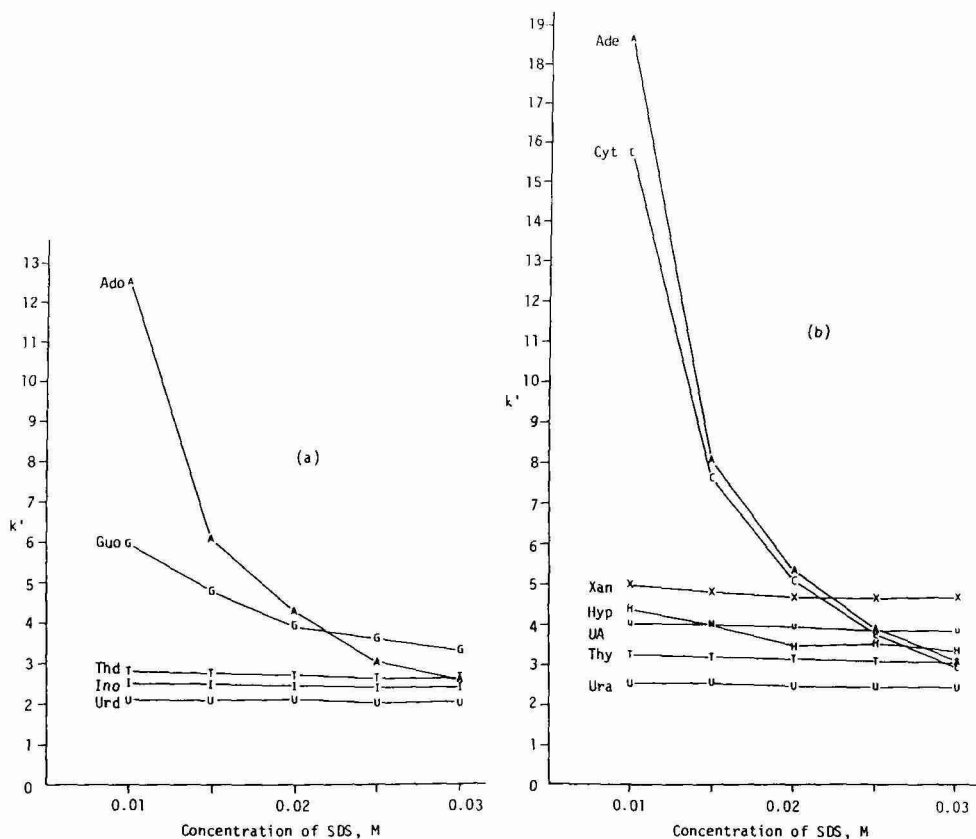
Fig. 4. Effect of SDS concentration on the capacity factors of (a) nucleosides and (b) bases. Mobile phase, aqueous SDS (pH 3.4). Other chromatographic conditions are the same as in Fig. 2. Each point represents the average of three determinations.

When capacity factors were plotted against the reciprocal of the concentration of counter ion, no linearity was observed, indicating that both electrostatic attraction and hydrophobic interaction mechanisms were operative. In addition, as the concentration of counter ion, *i.e.*, ionic strength, increases, there is a salting-out effect. The solute is then less soluble in the mobile phase, and thus the hydrophobicity of the solute is increased.

Effect of temperature

A van 't Hoff plot was constructed over a temperature range of 25–55°C with a mobile phase of 0.01 *M* SDS at pH 3.4 (Fig. 7). Linear relationships were observed for all nucleosides and bases over the full temperature range. However, the slopes of Cyt and Ade were opposite to the slopes of the bases which did not contain an amino group. In addition, the retention enthalpies, ΔH_r, for Ado and Ade from the van 't Hoff plot were -0.2 and $+0.5$ kcal/mol, respectively. These results indicate that a different retention-controlling mechanism is operative in the retention of the bases containing an amino group.
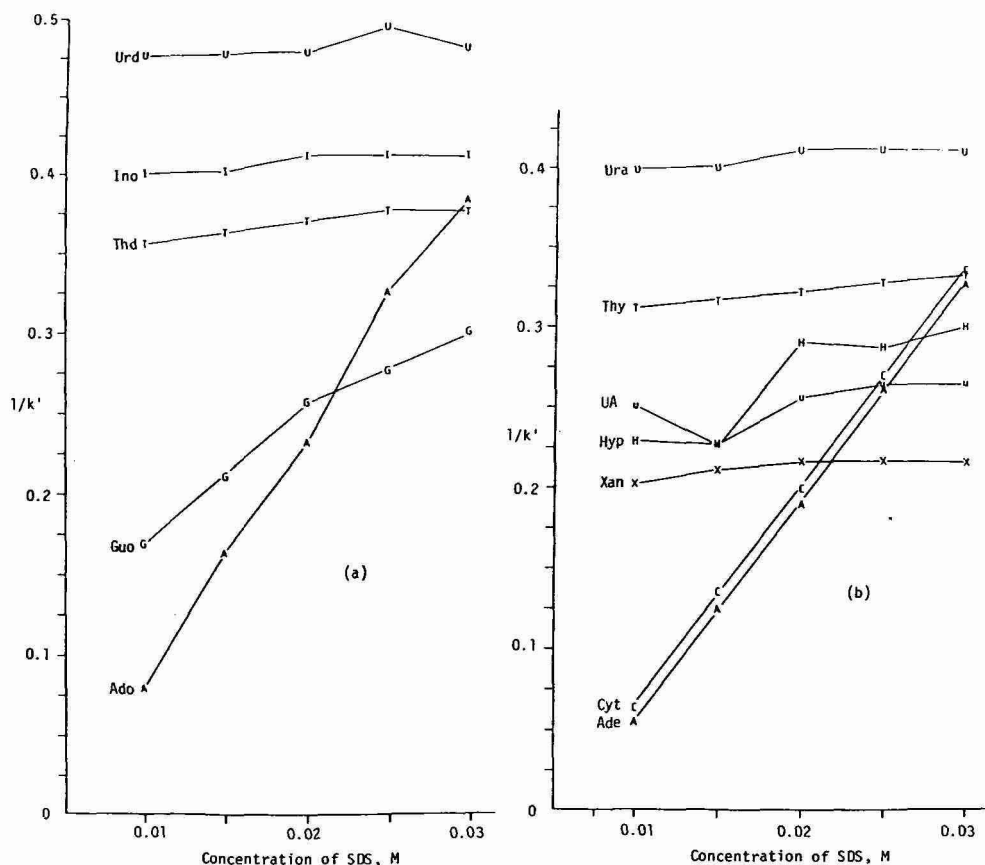
Fig. 5. A plot of SDS concentration against the reciprocal of the capacity factors of (a) nucleosides and (b) bases. All chromatographic conditions are the same as in Fig. 4. Each point represents the average of three determinations.
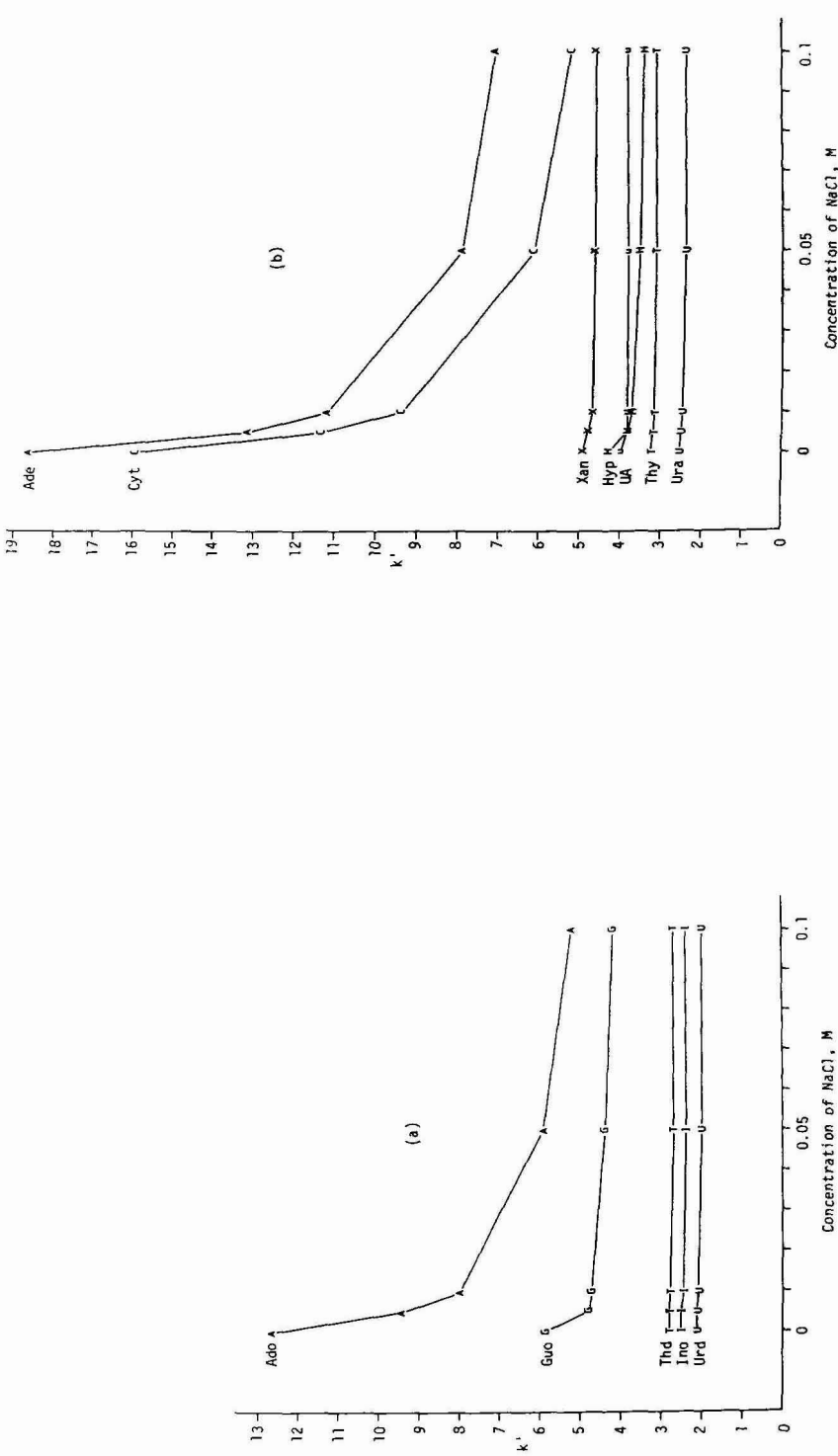
Fig. 6. Effect of counter-ion concentration on the capacity factors of (a) nucleosides and (b) bases. Concentrations of sodium chloride, 0.005, 0.01, 0.05 and 0.1 *M*; mobile phase, 0.01 *M* SDS (pH 3.4); flow-rate, 2 ml/min; temperature, ambient. Each point represents the average of three determinations.
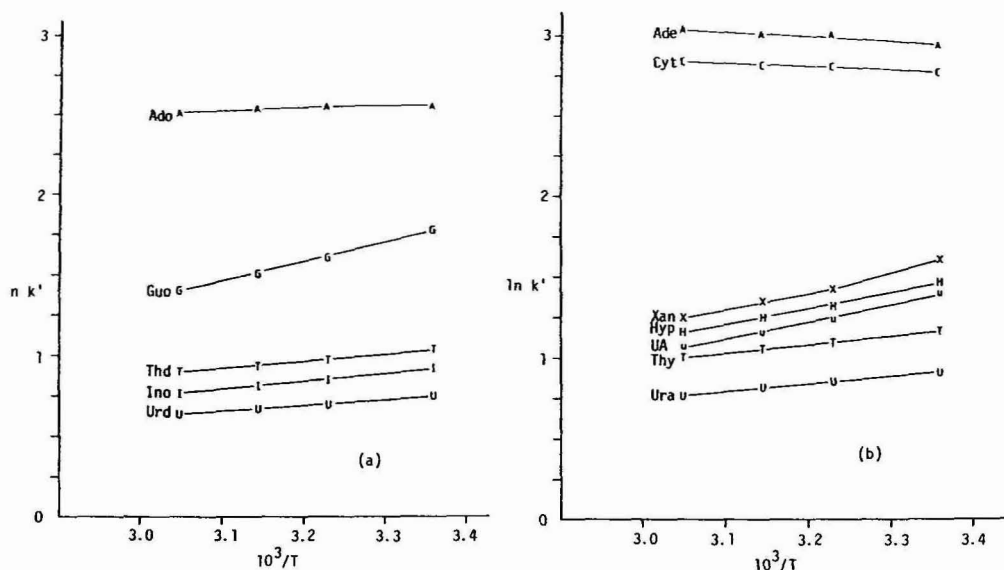
Fig. 7. Van 't Hoff plots of the capacity factors of (a) nucleosides and (b) bases. Temperature, 25, 37, 45 and 55°C; mobile phase, 0.01 M SDS (pH 3.4); flow-rate, 2 ml/min. Each point represents the average of three determinations.

Mechanisms of retention

Since the PVA stationary phase contains hydrophilic sites(hydroxyl groups) and hydrophobic sites (polymer matrix), it is expected that the polar head groups of SDS monomers would be adsorbed on hydrophilic sites, whereas, the hydrophobic tails of SDS monomers would be adsorbed on hydrophobic sites. As a result of our investigation of the effects of an SDS mobile phase with different types of stationary phases[36], it appears that the PVA stationary phase adsorbs the SDS monomers in two ways, i.e., by hydrophilic adsorption and hydrophobic adsorption; thus, the retention behavior of nucleosides and bases on the PVA column can be controlled by hydrophobic interaction in combination with electrostatic attraction. A schematic model of hydrophobic interaction and electrostatic attraction between solutes and the modified PVA stationary phase is shown in Fig. 8.
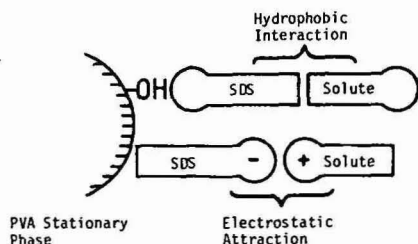
Fig. 8. A schematic model of hydrophobic interaction and electrostatic attraction between solutes and the modified PVA stationary phase.

Functional groups of purines and pyrimidines play an important role in hydrophobic interaction and electrostatic attraction. Since non-ionized bases are more hydrophobic than their respective nucleosides, which contain ribosyl or deoxyribosyl rings with several hydroxyl groups, these bases interact more with hydrophobic sites on the modified PVA stationary phase. As a result, nucleosides are eluted earlier than their respective bases (Figs. 1 and 2). Higher k' values of purine bases compared to those of the pyrimidine bases are also due to the hydrophobic interaction of the purines with the stationary phase. The additional ring in purine bases contributes to increased hydrophobicity and gives purines longer retention times than pyrimidines. The effect of hydrophobic interaction can also be observed in the elution of Ura and Thy, which have similar structures. However, Thy has a methyl group at C-5, which makes it more hydrophobic; thus, Thy is retained longer than Ura. As was discussed in the previous sections, electrostatic attraction takes place and mainly controls retention when positively charged purines and pyrimidines containing an amino group interact with the negatively charged sites on the modified PVA stationary phase.

DISCUSSION

Most of the published separations of nucleosides and bases have been achieved by RPLC on silica-based columns. In order to determine whether our micellar method was useful for the analysis of nucleosides and bases in biological matrices, the low-molecular-weight, UV-absorbing constituents of human serum were separated on the PVA column by isocratic elution with 0.01 M SDS at different pH values (Fig. 9).

Optimum separation was achieved at pH 3.4. In contrast to the RPLC gradient method, there were no interferences from tyrosine, phenylalanine, and creatinine. In addition, Urd, Hyp, and Xan, which usually overlap, and Ino and Guo, which are eluted very close together in RPLC, are well separated by the micellar method. Under the stated conditions, Ino and Ura are unresolved, and the UA peak can interfere
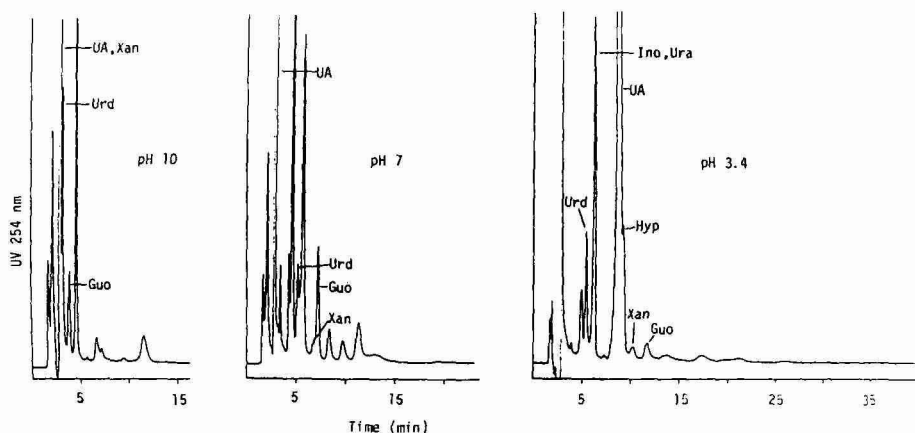
Fig. 9. Isocratic elution profiles of human serum at different pH values. Injection volume, 30 μl. Other chromatographic conditions are the same as in Fig. 1.

TABLE II

QUANTITATION AND DETECTION LIMITS OF SELECTED NUCLEOSIDES AND BASES

$n = 4$.

Compound	Concentration ($\mu mole/l$)	S.D.	C.V. (%)	Literature value ($\mu mole/l$)	Detection limits* ($\mu mole/l$)
Urd	8.35	0.161	1.93	0.95–8[24,40]	0.2
Guo	3.19	0.0424	1.33	0–1.98[24]	0.8
UA	202	5.10	2.52	155–429[24]	0.6
Xan	2.71	0.117	4.32	0.54–4.70[24]	0.8

* Detection sensitivity 0.005 a.u.f.s. (signal-to-noise ratio = 2).

with the Hyp peak if a large amount of UA is present. However, these peaks can be separated by adjustments in mobile phase, even though the separation was not designed for the resolution of these two compounds.

Quantitation and detection limits of Urd, Guo, UA, and Xan in human serum were investigated. The results are summarized in Table II. The values for serum constituents are in good agreement with those obtained by RPLC methods reported in the literature.

CONCLUSIONS

Micellar liquid chromatography on a PVA column was found to be quite selective and useful for the separation of some of the important nucleosides and bases found in biological matrices, especially, purines and pyrimidines which contain keto groups. The isocratic elution gave adequate separation of these compounds, compared to gradient elution with hydroorganic mobile phases. The main advantage of the method is that rapid separation of the major purines and pyrimidines containing keto groups can be obtained isocratically; thus, equilibration after each separation is unnecessary. In addition, different selectivities are found for the various nucleosides and bases; compounds that are not well separated by RPLC can be readily resolved by this method. Thus, this method can be used in conjunction with RPLC in the identification of peaks. Since it can also be optimized for any selected nuceloside or base and/or a group of these compounds, micellar liquid chromatography on a PVA column can be very useful for monitoring abnormalities in purine and pyrimidine metabolism as well as therapeutically important nucleoside and base analogues in biological fluids.

REFERENCES

1 D. W. Armstrong and S. J. Henry, *J. Liq. Chromatogr.*, 3 (1980) 657.
2 D. W. Armstrong and F. Nome, *Anal. Chem.*, 53 (1981) 1662.
3 D. W. Armstrong, W. L. Hinze, K. H. Bui and H. N. Singh, *Anal. Lett.*, 14 (1981) 1659.
4 R. Weinberger, P. Yarmchuck and L. J. Cline Love, *Anal. Chem.*, 54 (1982) 1552.
5 P. Yarmchuck, R. Weinberger, R. F. Hirsch and L. J. Cline Love, *Anal. Chem.*, 54 (1982) 2233.
6 J. G. Dorsey, M. T. De Echegaray and J. S. Landy, *Anal. Chem.*, 55 (1983) 924.
7 D. W. Armstrong and G. Y. Stine, *J. Am. Chem. Soc.*, 105 (1983) 6220.
8 E. Pramauro and E. Pelizzetti, *Anal. Chim. Acta*, 154 (1983) 153.
9 D. W. Armstrong and G. Y. Stine, *Anal. Chem.*, 55 (1983) 2317.
10 P. Yarmchuck, R. Weinberger, R. F. Hirsch and L. J. C. Love, *J. Chromatogr.*, 283 (1984) 47.
11 J. G. Dorsey, M. G. Khaledi, J. S. Landy and J.-L. Lin, *J. Chromatogr.*, 316 (1984) 183.
12 R. A. Barford and B. J. Sliwinski, *Anal. Chem.*, 56 (1984) 1554.
13 M. Arunyanart and L. J. Cline Love, *Anal. Chem.*, 56 (1984) 1557.
14 G. F. Kirkbright and F. G. P. Mullins, *Analyst (London)*, 109 (1984) 493.
15 F. G. P. Mullins and G. F. Kirkbright, *Analyst (London)*, 109 (1984) 1217.
16 J. S. Landy and J. G. Dorsey, *J. Chromatogr. Sci.*, 22 (1984) 68.
17 J. A. Singleton and H. E. Pattee, *J. Am. Oil Chem. Soc.*, 62 (1985) 739.
18 F. J. Deluccia, M. Arunyanart and L. J. Cline Love, *Anal. Chem.*, 57 (1985) 1564.
19 M. G. Khaledi and J. G. Dorsey, *Anal. Chem.*, 57 (1985) 2190.
20 F. J. Deluccia, M. Arunyanart, P. Yarmchuk, R. Weinberger and L. J. Cline Love, *LC, Liq. Chromatogr. HPLC Mag.*, 3 (1985) 794.
21 M. Arunyanart and L. J. Cline Love, *J. Chromatogr.*, 342 (1985) 293.
22 M. F. Borgerding and W. L. Hinze, *Anal. Chem.*, 57 (1985) 2183.
23 M. Arunyanart and L. J. Cline Love, *Anal. Chem.*, 57 (1985) 2837.
24 R. A. Hartwick, A. M. Krstulovic and P. R. Brown, *J. Chromatogr.*, 186 (1979) 659.
25 A. McBurney and T. Gibson, *Clin. Chim. Acta*, 102 (1980) 19.
26 R. J. Simmonds and R. A. Harkness, *J. Chromatogr.*, 226 (1981) 369.
27 R. P. Agarwal, P. P. Major and D. W. Kufe, *J. Chromatogr.*, 231 (1982) 418.
28 P. R. Brown, *Cancer Invest.*, 1 (1983) 527.
29 P. R. Brown (Editor), *HPLC in Nucleic Acid Research*, Marcel Dekker, New York, 1984.
30 M. J. Bennett and K. H. Carpenter, *Ann. Clin. Biochem.*, 21 (1984) 131.
31 K. Nakano, K. Shindo, T. Yasaka and H. Yamamoto, *J. Chromatogr.*, 332 (1985) 127.
32 R. Boulieu, C. Bory and C. Gonnet, *J. Chromatogr.*, 339 (1985) 380.
33 H. Wada, H. Ozaki, K. Makino and T. Takeuchi, *Anal. Lett.*, 16 (1983) 1537.
34 K. Yasukawa, M. Kasai, Y. Yanagihara and K. Noguchi, *Nucleic Acids Res.*, 12 (1984) 109.
35 D. P. Lee and J. H. Kindsvater, *Anal. Chem.*, 52 (1980) 2425.
36 Y. N. Kim and P. R. Brown, manuscript in preparation.
37 R. M. Izatt, J. J. Christensen and J. H. Rytting, *Chem. Rev.*, 71 (1971) 439.
38 J. S. Kwiatkowski and B. Pullman, *Adv. Heterocycl. Chem.*, 18 (1975) 199.
39 R. P. Panzica, University of Rhode Island, personal communication, 1986.
40 A. Leyva, C. J. van Groeningen, I. Kraal, H. Gall, G. J. Peters, J. Lankelma and H. M. Pinedo, *Cancer Res.*, 44 (1984) 5928.

CHROMSYMP. 974

SOLVATOCHROMIC SOLVENT POLARITY MEASUREMENTS AND SELECTIVITY IN REVERSED-PHASE LIQUID CHROMATOGRAPHY

BRUCE P. JOHNSON*, MORTEZA G. KHALEDI** and JOHN G. DORSEY*

Department of Chemistry, University of Florida, Gainesville, FL 32611 (U.S.A.)

SUMMARY

The $E_T(30)$ polarity values of binary acetonitrile–water and methanol–water mobile phases, used in reversed-phase liquid chromatography, were measured and compared with methylene selectivity (α_{CH_2}) for both traditional siliceous bonded phases and for a polystyrene–divinylbenzene resin reversed-phase material. The variation in methylene selectivity for both was found to correlate best with percent organic solvent in methanol–water mixtures, while the $E_T(30)$ polarity provided the best correlation in acetonitrile–water mixtures. The polymeric resin column was found to provide higher methylene selectivity than the siliceous bonded phase at all concentrations of organic solvent.

INTRODUCTION

The description of methylene selectivity in reversed-phase liquid chromatography (RPLC) has traditionally been more difficult than that of retention. In a sense, the methylene selectivity (α_{CH_2}) is quite similar to the retention of normal alkanes, since it is based on the measurement of the capacity factors for a homologous series. It has also been referred to as the "hydrophobic selectivity", or "non-specific selectivity", owing to the large hydrophobicity of the methylene group. Methylene selectivity serves as a convenient measure of elution strength. Thus, knowledge of this for a given system is quite useful, since the mobile phase strength can be held constant for different modifiers, while the selectivity of other interactions is exploited to maximize the separation between two or more solutes.

From an energetic standpoint, log α_{CH_2}, is directly related to the change in the free energy of transfer, caused by adding or subtracting a methylene group to a molecule, by the following equation

$$\log \alpha_{CH_2} = -\Delta\Delta G \tag{1}$$

_____ __

* Present address: Eastman-Kodak Company, Eastman Chemicals Division, Kingsport, TN 37662, U.S.A.
** Present address: Department of Chemistry, University of New Orleans, New Orleans, LA 70148, U.S.A.

Of course, eqn. 1 applies to any form of selectivity; any two solutes that possess different free energies of transfer will be differentially retained. Methylene selectivity is thus only one aspect of chromatographic separations. In terms of research on retention mechanisms, there are at least two distinct advantages to the study of chromatographic selectivity.

First, it can be seen that log α values are not affected by the phase ratio of the column. Different phase ratios lead to changes in capacity factors (k'). These phase ratios are a function of the bonded-group chain length, the degree of surface coverage, the pore structure of the original silica, as well as the manner in which the column was packed. Thus, drawing conclusions about the variation in k' for different columns is hindered by the number of variables to be considered. Since the methylene selectivity (or any selectivity, for that matter) is not affected by the phase ratio, any differences seen between columns are due to actual differences in the nature of the bonded-phase structure. Moreover, the log α_{CH_2} values are generally independent of the specific column used, so that all C_{18}-type bonded phases will exhibit similar behavior, implying that only the most fundamental aspects of the retention process are being probed.

A second advantage, obtained only in the study of methylene selectivity, is that of lack of sensitivity to the presence of residual silanols on the bonded-phase surface. Residual silanols lead to anomalous retention behavior of many solutes which possess highly polar and/or hydrogen-bond donor–acceptor groups. While the individual solutes which comprise the homologous series may be susceptible to these effects, the change in k' caused by additional methylene groups will still be measurable, and largely unaffected by specific interactions with the stationary phase.

Many papers have been published in regard to methylene selectivity. For example, Karger et al.[1] reported a linear relationship between log α_{CH_2} and percent methanol for a C_{18} column, while the behavior of acetonitrile–water mixtures was found to be more complex. This behavior was ascribed to the differing natures of the two modifiers, in that methanol is a proton acceptor–donor, which leads to less disruption in the overall solvent mixture structure as the concentration is varied. The structure of acetonitrile–water mixtures is of much greater complexity, since acetonitrile does not associate with water to any extent in comparison with methanol.

Colin et al.[2] carried out an extensive investigation of methylene selectivity, in which a total of seven binary and one ternary systems were explored. These measurements were then used to derive an eluotropic scale of solvent strength. These new values were found to correlate quite well with Snyder's eluotropic values for RPLC solvents[2,3].

It is also worth noting here that homologous series have been used in the determination of dead volumes[4]. In essence, this method involves the adjustment of the elution times for an unretained species (t_0) used to calculate k' values, such that the highest correlation is obtained in a plot of log k' versus carbon number for the homologous series when the "true" t_0 is reached.

We have previously reported on correlation between chromatographic retention and empirical solvent polarity measurements[5]. A total of 332 retention data sets (of log k' versus percent organic solvent) were examined, and, in general, a linear relationship was found between log k' and the $E_T(30)$ polarity for the same solvent mixture. That is, plots of log k' versus $E_T(30)$ polarity were generally found to be

better descriptors of chromatographic retention than the more commonly used plots of log k' *versus* percent organic solvent. For the 332 retention data sets, the average squared correlation coefficients for log k' *versus* percent organic solvent or $E_T(30)$ polarity were 0.9783 and 0.9910, respectively. The $E_T(30)$ solvent polarity measure used is a single-parameter probe that is sensitive to dipole interactions as well as hydrogen-bond donating and accepting interactions. The analytical uses of this probe and the synthetic procedure have recently been reported[6]. For the sake of clarity, we will refer to the polarity value as $E_T(30)$ and the probe molecule itself as ET-30.

In the experiments described herein, the methylene selectivity was evaluated for a C_{18} bonded-phase column (Ultrasphere ODS), and a styrene–divinylbenzene (polymeric; Hamilton PRP-1) reversed-phase column, with methanol and acetonitrile as the organic solvent. Also, a large body of methylene selectivity data has been extracted from the literature, either directly from tabulated log α_{CH_2} values, or calculated from the slope of log k' *versus* carbon number. Here we report correlations between methylene selectivity, percent organic solvent, mole fraction organic solvent, and $E_T(30)$ polarity.

EXPERIMENTAL

Retention measurements (other than those reported in the literature), were obtained with a Spectra-Physics (San Jose, CA, U.S.A.) SP8700 ternary proportioning LC system. Columns used were an Altex (San Ramon, CA, U.S.A.) Ultrasphere ODS (5 μm particle size) and a Hamilton (Reno, NV, U.S.A.) PRP-1 (10 μm) and both were 15 cm $\times$ 4.6 mm I.D. Test solutes were obtained from Aldrich (Milwaukee, WI, U.S.A.) and Eastman-Kodak (Rochester, NY, U.S.A.). Sample introduction was achieved with either an Altex Model 210 injector, equipped with a 5-μl sample loop, or a Rheodyne (Cotati, CA, U.S.A.) Model 7125 injector, equipped with a 20-μl sample loop. Flow-rates were either 1.0 or 2.0 ml/min. The column was thermostated at 40 $\pm$ 0.1°C with a Haake (Saddle Brook, NJ, U.S.A.) Model D1 water bath. HPLC-grade methanol and acetonitrile (Fisher Scientific, Fair Lawn, NJ, U.S.A.) were used as received. Water was first purified with a Barnstead (Boston, MA, U.S.A.) Nanopure system and then irradiated with UV light in a Photronix (Medway, MA, U.S.A.) Model 816 HPLC reservoir for at least 24 h. The water was then filtered through a 0.45-μm nylon-66 membrane filter (Rainin Instruments, Woburn, MA, U.S.A.) prior to use. A fixed-wavelength, 254-nm, Beckman Model 153 UV detector (Altex) was used.

The t_0 values were evaluated with injections of the pure organic solvent (either methanol or acetonitrile). For the Hamilton PRP-1 column, this proved to be difficult at low organic solvent concentrations due to actual retention of the acetonitrile or methanol. Other supposedly unretained solutes (such as urea and uracil) exhibited similar behavior. Therefore, as t_0, obtained from injections of pure organic solvent, the t_0 at 60% organic solvent concentration was used, since at this concentration the retention time reached a minimum in each of the two solvent systems.

Simple linear regression calculations were performed with the "Curve Fitter" program (Interactive Microware, State College, PA, U.S.A.), run on an Apple (Cupertino, CA, U.S.A.) II Plus 48K microcomputer. The program was modified to allow calculation of 95% confidence intervals for slope and y-intercept values. This

program was also used to interpolate $E_T(30)$ values for solvent compositions that had not been measured (*e.g.*, methanol–water, 45:55).

The sensitivity of the probe and the measurement of the polarity values have been described previously[5]. $E_T(30)$ energy values can be converted to kJ/mole by multiplying the value in kcal/mole by 4.184.

RESULTS

Ultrasphere ODS column

The methylene selectivity was measured by using the homologous series of benzene, toluene, ethylbenzene and *n*-butylbenzene. In Figs. 1 and 2, the results of experiments with the Ultrasphere ODS column are shown for methanol–water mixtures. The selectivity data are plotted in two ways: percent organic solvent (Fig. 1) and $E_T(30)$ polarity (Fig. 2). For methanol as an organic modifier, methylene selectivity decreases in a linear manner as the percentage of organic modifier is increased ($r^2 = 0.9972$ for a straight-line fit of the data in Fig. 1). The squared correlation coefficient does decrease to 0.9884 in Fig. 2 (*versus* $E_T(30)$ polarity), though this may be due in part to an increase in scatter; it is likely that the $E_T(30)$ values have contributed some extra variance to the linear regression. The regression line drawn through the data in Fig. 2 is given by

$$\log \alpha_{CH_2} = -4.82 \pm 0.37 + 0.08817 \pm 0.0065 \cdot E_T(30) \qquad (2)$$

$$(n = 5, s = 0.0107)$$

In Figs. 3 and 4, the methylene selectivity results for acetonitrile–water mixtures are plotted with respect to percent acetonitrile, and $E_T(30)$ polarity, respectively. As shown in Fig. 3, for percent organic solvent, the methylene selectivity varies in a non-linear manner; r^2 for a straight line regression is 0.9655. Plotting with respect to the $E_T(30)$ polarity (Fig. 4) yields the best linear correlation ($r^2 = 0.9919$). The regression equation for the line in Fig. 4 is given by

$$\log \alpha_{CH_2} = -3.24 \pm 0.16 + 0.06116 \pm 0.0028 \cdot E_T(30) \qquad (3)$$
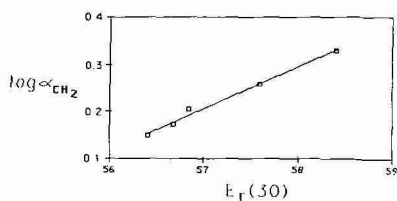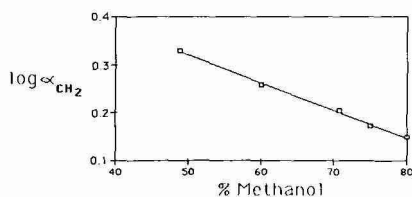
$$(n = 6, s = 0.0068)$$

Fig. 1. Chromatographic selectivity measurements as a function of percent methanol. Ultrasphere ODS column, 150 × 4.6 mm; 5 μl injection volume; flow-rate 1.0 ml/min. Alkylbenzenes used as the homologous series.

Fig. 2. Chromatographic selectivity measurements as a function of $E_T(30)$ polarity of methanol–water mixtures. For conditions, see Fig. 1.
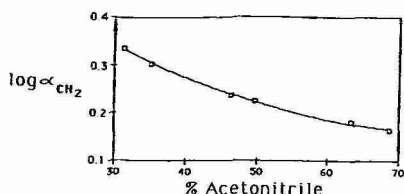
Fig. 3. Chromatographic selectivity measurements as a function of percent acetonitrile. For conditions, see Fig. 1.
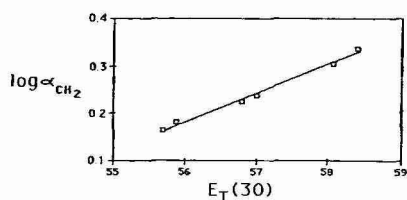
Fig. 4. Chromatographic selectivity measurements as a function of $E_T(30)$ polarity of acetonitrile–water mixtures. For conditions, see Fig. 1.

The ratio of the two slopes found in eqns. 2 and 3 is 1.44. That is, selectivity in the methanol–water system is more affected by overall changes in mobile phase polarity than with acetonitrile as the organic solvent. It should also be noted that the value of this ratio is the same as that found for slopes of log k' versus $E_T(30)$, as we have previously reported[5]. This is not surprising, considering the effect of solvation of the stationary phase alkyl chains by the organic solvent. Acetonitrile has been shown to solvate the stationary phase to a much greater extent than methanol[7], so that in the methanol–water system, changes in overall mobile phase polarity have more effect on retention or selectivity, since the stationary phase polarity is not changing significantly. The two lines defined by eqns. 2 and 3 intersect at an $E_T(30)$ value of 58.5 kcal/mole. This corresponds to approximate organic solvent concentrations of 45 and 28% for methanol and acetonitrile, respectively. That is, at these concentrations the methylene selectivity would be equivalent in the two systems. This also means that, except at this one intersection point, iso-$E_T(30)$ polarity values would not correspond to equivalent methylene selectivity in the two systems.

Literature data

A wealth of methylene selectivity data have been published in the literature by various workers[1,2,8-11]. In some cases, the $\log\alpha_{CH_2}$ values have been tabulated (with respect to percent organic solvent), while in other cases the α_{CH_2} values can be calculated from the reported k' values for a homologous series. Linear regression was carried out for data reported in these six references.

The results of the various correlations with all data sets discussed are shown in Table I. Squared correlation coefficients are reported for each of the three comparisons (*vs.* percent organic solvent, *vs.* mole fraction and *vs.* $E_T(30)$ polarity). This provides a way in which the general trends of the data may be viewed. In Fig. 5 the results of Table I are shown graphically. Squared correlation coefficients for log α_{CH_2} *versus* percent organic solvent are plotted with respect to those found for log α_{CH_2} *versus* $E_T(30)$ polarity. The line drawn through Fig. 5 corresponds to "iso-r^2" values. That is, all points would fall along this line if all correlation coefficients were equivalent for the two comparisons. Thus, a point appearing above the line denotes a better correlation when the log α_{CH_2} data are plotted with respect to percent organic solvent. Of the eleven data sets, in seven cases the correlation is clearly equal to or better than the "*vs.* $E_T(30)$ polarity" comparisons.

There are a number of conclusions that can be reached regarding the data in

TABLE I

SQUARED CORRELATION COEFFICIENTS (r^2) FOR LOG α_{CH_2} DATA WITH RESPECT TO PERCENT ORGANIC SOLVENT, MOLE FRACTION ORGANIC SOLVENT AND $E_T(30)$ POLARITY

Ref.	Organic solvent	n^*	Concentration range (%)	r^2 versus		
				Percent organic solvent	Mole fraction organic solvent	$E_T(30)$ polarity
This work	Methanol	5	50–80	0.9972	0.9897	0.9884
This work	Acetonitrile	6	32–68	0.9655	0.9173	0.9919
1	Methanol	13	0–100	0.9943	0.9337	0.9655
1	Acetonitrile	8	5–80	0.9186	0.7777	0.9921
10	Methanol	7	40–100	0.9945	0.9501	0.9858
11	Methanol	6	10–100	0.9903	0.9488	0.9902
11	Acetonitrile	7	10–80	0.9102	0.8032	0.9859
2	Methanol	11	0–100	0.9923	0.9592	0.9486
2	Acetonitrile	9	0–80	0.9492	0.8829	0.9776
8	Methanol	10	55–100	0.9983	0.9738	0.9936
9	Acetonitrile	6	20–70	0.9855	0.9684	0.9439

* n is the number of individual α values used for the correlations.

Table I. One interesting pattern that is apparent is that for every data reference where the methylene selectivity was measured with both organic modifiers, the correlation coefficients for "vs. percent organic solvent" and "vs. $E_T(30)$" mirror each other. That is, in methanol–water mixtures, the methylene selectivity varies most closely with the percent organic solvent, while in the acetonitrile–water system, $E_T(30)$ polarity values yield the highest correlation. In contrast to the excellent correlation seen between log k' and $E_T(30)$ polarity[5], here there is a clear-cut distinction between the two organic modifiers.

Of course, the variation with respect to percent organic solvent is also quite complex, especially with acetonitrile–water mixtures. Colin et al.[2] found that, except for methanol–water mixtures, every system studied exhibited a non-liner variation in log α_{CH_2} with respect to percent organic solvent.

Hamilton PRP-1 column

While RPLC is typically performed with chemically bonded silica, there are
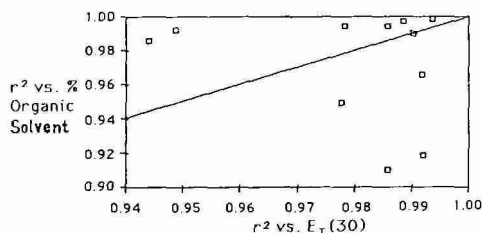
Fig. 5. Comparison between r^2 values for plotting methylene selectivity data with respect to either percent organic solvent or $E_T(30)$ polarity.

other materials that may serve as suitable stationary phases. In recent years, a number of polymeric reversed-phase columns have become commercially available. Polymer-based RPLC columns offer a number of potential advantages over their more traditional counterparts. Unlike silica-based columns, polymeric columns are stable to pH levels of 1–13 and high concentrations of buffer salts, with no degradation in performance.

Another aspect of these columns that can be of use is their preferential retention of aromatic compounds. Apparently, the presence of aromatic moieties on the stationary phase leads to preferential retention of aromatic solutes, leading to a different chromatographic selectivity than that observed with silica-based RPLC columns.

A final advantage is the lack of any silanol groups whatsoever. The presence of these groups on the surface of conventional bonded phases can be a problem in the chromatography of highly polar solutes, which will, in effect, be retained by a dual adsorption–partitioning mechanism. Thus, polymeric columns are, by virtue of their composition, entirely free of these troublesome residual silanols.

The experiments carried out with a Hamilton PRP-1 column involved measuring the methylene selectivity over 0–100% methanol and 0–80% acetonitrile. Owing to the high retentivity of the polymer matrix with respect to aromatic compounds, it was found that the homologous series of alkylbenzenes is unsuitable at low concentrations of organic solvent (*i.e.*, less than 60%). Therefore, nitroalkanes (nitromethane through nitrohexane) were used to measure log α_{CH_2} values, and were found to be usable over the entire range of organic solvent concentrations.

Since the polymeric column has a preferential retentivity toward aromatic compounds, it was necessary to insure that the use of a different homologous series would not significantly affect the measurement of log α_{CH_2}. Both nitroalkanes and alkylbenzenes were used to measure selectivity values at three different concentrations of each of the two organic solvents. Concentrations were so chosen that the alkylbenzenes could still be used to measure the methylene selectively (> 60% organic solvent). The results of these comparisons are found in Table II, and are plotted in Fig. 6. The slope of the line drawn through the data was 1.02 ± 0.17, with a *y*-intercept of −0.005 ± 0.04. Based on these results, it does not appear that the measurement of

TABLE II

COMPARISON OF LOG α_{CH_2} VALUES AS MEASURED BY NITROALKANES AND ALKYLBENZENES

Hamilton PRP-1 column.

Mobile phase	log α_{CH_2}	
	Alkylbenzenes	Nitroalkanes
Acetonitrile–water (50:50)	0.2167	0.2274
Acetonitrile–water (65:35)	0.1667	0.1645
Acetonitrile–water (80:20)	0.1328	0.1288
Methanol–water (70:30)	0.3215	0.3130
Methanol–water (80:20)	0.2425	0.2361
Methanol–water (90:10)	0.1677	0.1727
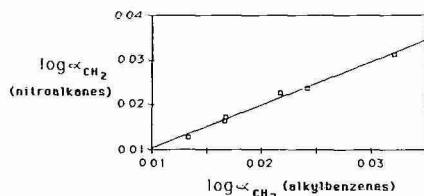
Fig. 6. Comparison between methylene selectivity results obtained with either 1-nitroalkanes or alkylbenzenes as the homologous series. Hamilton PRP-1 (polymeric) column 150 × 4.6 mm; 20 μl injection volume; flow-rate 1.0 ml/min.

methylene selectivity is significantly biased by the homologous series used to measure it, and is consistent with results previously published for conventional bonded phases[2].

One distinct disadvantage of the use of nitroalkanes is their generally low absorption of light in the UV region. For example, the molar absorptivity of nitromethane is only $18.6 \, l \, mol^{-1} \, cm^{-1}$ in ethanol, with a λ_{max} of 271 nm. Nevertheless, it was found that by increasing the concentration of nitroalkanes in the injected standards to approximately 5 mg/ml (20 μl sample volume; 100 μg injected), a 254-nm UV detector could still be used for the nitroalkanes. The peak shapes did not appear to be distorted by the large amount of injected solute; this may be a reflection of the nature of the polymeric stationary phase, since a higher load level should (in theory) be tolerated.

The results of the mesurements of α_{CH_2} for methanol–water mixtures appear in Figs. 7 and 8. Fig. 7 shows that the methylene selectivity decreases in a highly linear fashion as the percent methanol is increased. The regression line corresponds to

$$\log \alpha_{CH_2} = -5.24 \pm 0.34 + 0.0970 \pm 0.0058 \cdot E_T(30) \tag{4}$$

$$(n = 11, s = 0.0468)$$

Plotting with respect to the $E_T(30)$ polarity (Fig. 8) results in curvature, though at higher $E_T(30)$ polarities (lower methanol concentrations) the dependence is nearly linear.

The results for the same measurements with acetonitrile as the organic solvent
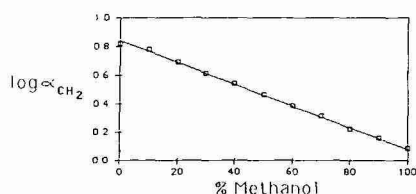
Fig. 7. Chromatographic selectivity measurements as a function of percent methanol. Nitroalkanes used as the homologous series. For conditions, see Fig. 6.
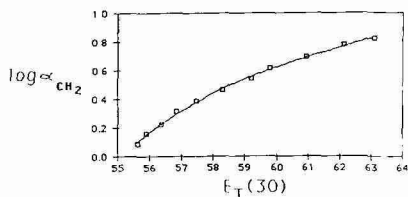
Fig. 8. Chromatographic selectivity measurements as a function of $E_T(30)$ polarity of methanol–water mixtures. For conditions, see Fig. 7.
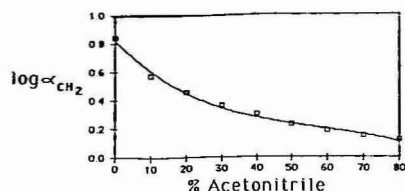
Fig. 9. Chromatographic selectivity measurements as a function of percent acetonitrile. For conditions, see Fig. 7.
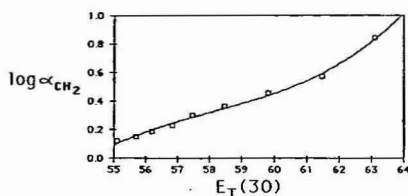
Fig. 10. Chromatographic selectivity measurements as a function of $E_T(30)$ polarity of acetonitrile–water mixtures. For conditions, see Fig. 7.

appear in Figs. 9 and 10. Here, the curve shapes are distinctly different from those seen with methanol. Instead of linearity *versus* percent organic solvent, strong curvature is seen (Fig. 9); this behavior in the two organic solvents is quite similar to that seen with standard bonded-phase columns[1,2]. The change in log α_{CH_2} is most pronounced at low concentrations of organic solvent. In Fig. 10, the selectivity increases in a nearly linear manner with respect to $E_T(30)$, with strong curvature seen at high $E_T(30)$ polarity values (low acetonitrile concentration). If the data in Fig. 10 are fitted to a straight-line model, the resultant regression line is given by

$$\log \alpha_{CH_2} = -4.58 \pm 0.31 + 0.0847 \pm 0.0053 \cdot E_T(30) \tag{5}$$

$(n = 9, s = 0.0411)$.

Correlation coefficients for the three comparisons discussed herein appear in Table III.

The ratio of slopes of eqns. 4 and 5 is 1.15. As discussed previously, the ratio of the slopes of eqns. 2 and 3 (α_{CH_2} for methanol and acetonitrile with the C_{18} column) is 1.44. That these ratios are different is further evidence that these slope ratios are a measurement of stationary phase solvation effects. The difference in the solvation structure between methanol and acetonitrile is less for the polymeric resin column than for the traditional C_{18} column. These ratios may prove useful for characterizing

TABLE III

CORRELATIONS BETWEEN LOG α_{CH_2} AND PERCENT ORGANIC SOLVENT, MOLE FRACTION ORGANIC SOLVENT OR $E_T(30)$ POLARITY FOR A HAMILTON PRP-1 POLYMERIC COLUMN

Organic solvent	n^*	Concentration range (%)	r^2 versus		
			Percent organic solvent	Mole fraction organic solvent	$E_T(30)$ polarity
Methanol	11	0–100	0.9989	0.9498	0.9692
Acetonitrile	9	10–90	0.8816	0.7352	0.9731

* n is the number of individual α values used for the correlations.

reversed-phase columns. We are further investigating these values for different mobile phases and columns.

At 100% organic solvent concentration, the log α_{CH_2} values are 0.0850 and 0.0754 for methanol and acetonitrile, respectively. This is as one might expect, owing to the greater "strength" of acetonitrile as a modifier in RPLC. Lastly, it should be noted that log α_{CH_2} values for this column are significantly higher at a given organic solvent concentration than that of the Ultrasphere ODS bonded phase-column. This shows that the polymeric surface is even more "hydrophobic" than the bonded phases, since the free energy of transfer of a methylene group is larger.

CONCLUSIONS

The variation in methylene selectivity for both traditional bonded phases as well as a polymeric column was found to correlate best with percent organic solvent in methanol–water mixtures, while the $E_T(30)$ polarity variation provided the best correlation in acetonitrile–water mixtures. Also, the polymeric column was found to provide higher methylene selectivity at all concentrations of organic solvent. Thus, this type of column appears to have great utility in the separation of molecules of very similar structure.

ACKNOWLEDGEMENTS

REFERENCES

1 B. L. Karger, J. R. Gant, A. Hartkopf and P. H. Weiner, *J. Chromatogr.*, 128 (1976) 65–78.
2 H. Colin, G. Guiochon, Z. Yun, J. C. Diez-Masa and P. Jandera, *J. Chromatogr. Sci.*, 21 (1983) 179–184.
3 L. R. Snyder, *Principles of Adsorption Chromatography*, Marcel Dekker, New York, 1968.
4 G. E. Berendsen, P. J. Schoenmakers, L. de Galan, G. Vigh, Z. Varga-Puchony and J. Inczedy, *J. Liq. Chromatogr.*, 3 (1980) 1669–1686.
5 B. P. Johnson, M. G. Khaledi and J. G. Dorsey, *Anal. Chem.*, 58 (1986) 2354–2365.
6 B. P. Johnson, B. Gabrielsen, M. Matulenko, J. G. Dorsey and C. Reichardt, *Anal. Lett.*, 19 (1986) 939–962.
7 R. M. McCormick and B. L. Karger, *Anal. Chem.*, 52 (1980) 2249–2257.
8 P. Dufek, *J. Chromatogr.*, 299 (1984) 109–117.
9 T. Hanai and J. Hubert, *J. Liq. Chromatogr.*, 8 (1985) 2463–2473.
10 S. Petrović, S. Lomić and I. Šefer, *J. Chromatogr.*, 348 (1985) 49–65.
11 P. J. Schoenmakers, H. A. H. Billiet and L. de Galan, *J. Chromatogr.*, 218 (1981) 261–284.

CHROMSYMP. 1005

VOID-COLUMN LIQUID CHROMATOGRAPHIC REACTOR STUDIES TO DETERMINE REACTION RATES IN MOBILE AND STATIONARY PHASES

ALEXANDER H. T. CHU and STANLEY H. LANGER*

Department of Chemical Engineering, University of Wisconsin-Madison, Madison, WI 53706 (U.S.A.)

SUMMARY

A liquid chromatographic reactor system was modified to incorporate a void column, connected between two packed octadecylsilane columns. By varying the void-column volume and the eluent flow-rate, reactant retention times in both the mobile and stationary phases can be decoupled, facilitating the simultaneous measurement of rate constants in both phases. The knowledge of mobile phase rates is of special significance, since this makes it possible to evaluate reaction rates in the stationary phase for a variety of columns. From these phase rates it is possible to obtain information about phase compositions and possibly retention mechanisms. The pseudo-first order base-catalyzed esterification reactions of tetrachloroterephthaloyl chloride were studied in the void-column liquid chromatographic reactor for comparison with earlier studies. Kinetic measurements in the methanol eluent in both the void and packed sections were comparable with those obtained from a batch reactor, indicating no significant external or internal mass transfer effects under moderate operating conditions. The stationary phase kinetic data obtained here support the previous generalized model in which solute molecules interact with both the associated methanol pseudo-layer and the octadecylsilane moieties.

INTRODUCTION

In previous studies[1,2] two conclusions were drawn from experiments on the organic base-catalyzed tetrachloroterephthaloyl chloride (TCTPCl$_2$) esterification reactions in an octadecylsilane bonded liquid-chromatographic (LC) reactor system, operated with a methanol mobile phase. These were: (1) mass transfer effects on reaction kinetic measurements were negligible; and (2) the reaction rate measurements for reaction in the mobile and stationary phases support a generalized assumption of a stationary phase consisting of hydrocarbon ligands with associated methanol molecules. To explore the homogeneous composition assumption in the mobile phase further and to check the experimental accuracy of the stationary phase rate determination, additional studies were made here on determining the on-column rate constants simultaneously in both phases. In the operation of ordinary chromatographic reactors only an apparent or composite rate constant can be obtained by varying the flow-rate of the mobile phase, if a reaction occurs at comparable rates

in both phases. This is because the residence time ratio, t_m/t_s, is dependent on the intrinsic phase ratio of the volumes occupied by the mobile (m) phase and the stationary (s) phase (f_m/f_s) only. Because reaction rates in bonded stationary phases offer considerable promise for understanding retention mechanisms, methods for decoupling and evaluating these rate constants independently are of special interest. Varying the length of an empty column before an analytical chromatographic reactor is an alternative to changing the column phase ratio[3], but the formation of product inside this empty tube must be considered. Varying the loading of the stationary phase is another[4], but this is difficult to implement quantitatively with chemically-bonded LC systems. Here, use of a single void column between two chromatographic reactor columns was selected for study as a means for conveniently obtaining kinetic data in both phases. The single void-column LC reactor appears to be an attractive technique for further development when data on reaction kinetics in the mobile-phase solvent are unavailable or inconvenient to obtain with conventional reactor techniques (*e.g.* reactants of insufficient purity). For slow reactions, incorporation of the void column into the array can also extend the range of rate-constant measurements due to increasing reactant retention in the system; this is especially attractive because of the limited diffusion occurring with LC as compared to gas chromatography (GC).

Void columns of stainless-steel (ss) tubing of varying lengths and diameters were placed between two high-performance liquid chromatography (HPLC) packed columns, so that product peaks from reaction in the void would then be superimposed upon the eluted product wave. These peaks originate in the void column where reaction continues to proceed in the absence of separation. The area of the void peak is proportional to the reaction rate and the volume of the void column[3]. This approach is also attractive for the separation and isolation of any desired product that is formed continuously in the void-column section of the chromatographic reactor array.

Generally, band-broadening in a well packed efficient micro-particular LC column (5–10 μm particle size) has no significant effect on first-order reaction kinetic measurements, while mass-transfer resistances for slow reactions should not be of concern[1,2,5]. Efficiency can be improved by raising the temperature[6], since the rates of most processes will increase while mobile phase viscosity decreases.

EXPERIMENTAL CONSIDERATIONS AND DESIGN

A schematic diagram of the experimental apparatus is shown in Fig. 1. Detailed information on the packed Altex Ultrasphere ODS columns and associated instruments and hardware (including Waters 6000A pump, Perkin-Elmer LC55 UV–VIS detector, and Spectra-Physics SP4000 data processor) for our LC reactor system are described elsewhere[1]. Several void columns made of ss 316 tubing were available (Alltech Assoc., Deerfield, IL, U.S.A.), all of 1/16 in. O.D.: 30 ft. × 0.01 in. I.D., 50 ft. × 0.01 in. I.D., 100 ft. × 0.01 in. I.D., 30 ft. × 0.02 in. I.D., 50 ft. × 0.02 in. I.D., and 30 ft. × 0.03 in. I.D. The choice of column dimensions depends on two requirements which are:

(1) production of a maximum conversion in the void volume for accurate response measurements;

(2) minimization of the effect of dispersion in the void column.
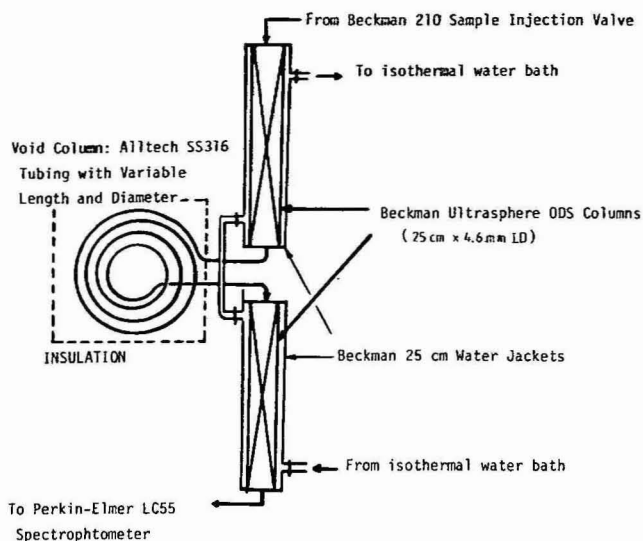
Fig. 1. The design of the single void-column LC reactor. The void column is placed between two Ultrasphere ODS columns, which are encased with water jackets to maintain constant temperature. They are connected in series. (See ref. 1 for description of other related chromatographic equipment.)

The dispersion effect for this proposed single void-column LC reactor assembly has been examined experimentally. Dispersion in tubes of larger inner diameter (*e.g.*, 30 ft. × 0.03 in. I.D.) was serious, because laminar or convective dispersion is more pronounced in tubes with large diameters; on the other hand, use of tubings of lesser diameter (*e.g.*, 30 ft. × 0.01 in. I.D.) did result in insufficient conversion for adequate void-peak response, particularly at relatively fast flow-rates, where there was limited residence time in the void column. Although first order kinetic measurements should not be affected by dispersion good peak resolution is still important for accurate chromatogram interpretation (see Fig. 5). The end and wall effects in chromatographic and empty columns should be minimized, since they can be detrimental to the performance of LC systems[7,8]. Coq *et al.*[5] have found that the variance of band-broadening due to trans-column effects between columns with different inner diameters is proportional to the square of the packed column diameter and the square of the ratio of the diameter of connecting empty tubing and column diameter. The permeability and thickness of the porous frits in the column ends and the mobile phase flow-rate can further contribute to this variance. The spreading, resulting from velocity variations associated with end effects, can be several hundred times higher than that due to velocity inequalities due to laminar flow or convective dispersion in a packed bed[9,10]. We found from the preliminary tests that void columns of both 100 ft. × 0.01 in. I.D. and 50 ft. × 0.02 in. I.D. gave reasonable chromatograms, suitable for analysis (*cf.* Figs. 3 and 4) in the operating flow range between 0.10 and 0.90 ml/min.

The connections between the empty tubing and the packed columns were made with low-dead-volume (LDV) female Swagelok nuts (Beckman Instruments, Berkeley, CA, U.S.A.) to minimize further resolution loss. The analytical columns were

two (Beckman) 5-μm Ultrasphere ODS reversed-phase columns (dimension 25 cm × 0.46 cm I.D.) encased by Beckman water jackets to provide reaction temperature control. The void column was well insulated or immersed in the isothermal water-bath to minimize temperature fluctuations. Other equipment, reagents, and experimental methods employed in this LC reactor system have been described earlier[1,2].

Choice of reaction

The reaction choice must match the situation. Since the void peak is super-imposed on the eluted product wave, the reaction should be relatively selective with respect to product formation in order to minimize problems in interpretation of reactor chromatograms. Secondly, the reaction rate should be fast enough to produce a significant amount of response for product formed in the void zone. Finally, all the participating species should be resolved in the chromatographic column to minimize any interference and to facilitate the required measurement of peak areas. Here, we have chosen tetrachloroterephthaloyl chloride ($TCTPCl_2$), R, as reactant because of familiarity with its reactions[1,11]. With organic bases (pyridine or 4-picoline) in methanol, monoquaternary ammonium salts are formed initially.
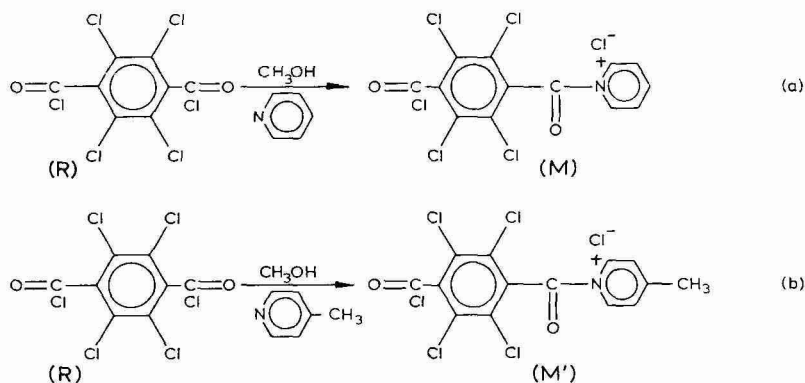
The initial intermediate products have been identified earlier as quaternary pyridinium (M) or picolinium chloride (M') salts[11]. Chromatogram peaks are identified and resolved (see Figs. 2–5). Areas for reactant, added inert standard, and product formed in the void section can all be measured for subsequent kinetic analysis.

Reaction samples and solvents

The reaction sample solution contained 0.0004 M of $TCTPCl_2$ reactant, 0.25 M of tetrahydrofuran with 0.017 M of 1-phenyloctane inert standard in methanol in all of our experiments. The initial peak ratio of reactant to inert standard measured at 0.9 ml/min methanol was 1.58 ± 0.03. The flow-rate of the mobile phase was varied in a random fashion at 0.1, 0.2, 0.3, 0.6, and 0.9 ml/min. At least four replicate runs were conducted for each flow-rate to provide good experimental data structure for regression analysis. The mobile-phase solvent contained 0.25 M tetrahydrofuran in methanol, the base catalyst concentration being varied as follows:

(1) 4-picoline 0.00615 M at 25°C;
(2) 4-picoline 0.00615 M at 35°C;
(3) pyridine 0.00745 M at 25°C;
(4) pyridine 0.00745 M at 35°C.

An experimental design, incorporating features of the four series of experiments above was performed; each containing three separate void-column features: (a) without void (a typical LC reactor), (b) with void column 100 ft. × 0.01 in. I.D. (V_{void} = 1.7 ± 0.1 ml), and (c) with void column 50 ft. × 0.02 in. I.D. (V_{void} = 3.7 ± 0.1 ml).

REACTION KINETIC DATA ANALYSIS

The kinetic analysis for the void-column LC reactor was performed using measured peak areas for reactant, inert standard, and product formed in the void column. Both, linearized and non-linear, rate expressions were used to determine reaction kinetics in both the stationary and mobile phases simultaneously; the rate constants evaluated from these different rate expressions can be cross-checked to insure accurate determination of rate constants in each phase.

Linearized rate expression

For any designated void column, connected between two packed chromatographic columns, the ratio of $(t_m + t_{void})/t_s$ is invariant, where subscripts "m" and "s" for time (t) indicate reactant residence periods in the mobile and stationary phases, respectively; t_{void} is time in the void column. This experimental feature can be incorporated into a generalized LC reactor treatment, where the total mobile-phase retention time then is $t_m + t_{void}$. The chromatographic area ratio of reactant to inert standard, A_R/A_I, is equal to (see ref. 1 for detailed derivation)

$$\ln\left(\frac{A_R}{A_I}\right) = \ln\left(\frac{A_R}{A_I}\right)_{t=0} - k_{app}t_R \tag{1}$$

where the apparent reaction rate constant, k_{app}, applies to the total reactant retention time in the system, t_R (eqn. 2). By employing different void column sizes in LC reactor arrays, $(t_m + t_{void})/t_s$ ratios can be varied to provide independent measurement of rate constants in both phases. Then

$$k_{app} = k_s\left(\frac{t_s}{t_R}\right) + k_m\left(\frac{t_m + t_v}{t_R}\right) \tag{2}$$

or

$$k_{app} = k_s\left(\frac{t_s}{t_R}\right) + k_m\left(\frac{t_m}{t_R}\right)\left(\frac{t_m + t_v}{t_m}\right) \tag{3}$$

where t_m or mobile volume can be determined separately, *e.g.* by use of the homologous series method[2,12]. By plotting k_{app} against the total retention time ratio, $(t_m + t_v)/t_R$ or $(t_m + t_v)/t_m$, following eqns. 2 and 3, the rate constants in the mobile and the stationary phases, k_m and k_s, can be obtained directly from the slope and the intercept of the linear plot. This linearized method is advantageous, because it can provide direct visual display on the trend of kinetic measurements. If a first-order reaction is involved, the plot should be linear, and any poor fit of experimental data can be reviewed. This treatment also is free of any need for nonlinear regression software in a computer. Nevertheless, the rate constant measurement is of limited accuracy, since the best-fit straight line with limited data points (*i.e.*, LC reactor, 100 ft. × 0.01 in. I.D., and 50 ft. × 0.02 in. I.D. each give a single value in the plot, as illustrated in Fig. 8 below) is subject to errors. The error structure for the original experimental data is also changed upon linearization[13,14].

Non-linear rate expressions

For first-order reactions in the void-columns LC reactor, the output reactant peak area follows an exponential decay[1,3]:

$$\frac{A_R}{A_I} = \left(\frac{A_R}{A_I}\right)_{t=0} \exp(-k_{m,v}t_v - k_{m,c}t_m - k_s t_s) \tag{4}$$

where $k_{m,v}$ and $k_{m,c}$ represent the mobile phase rate constant in the void and packed sections, respectively. A discrimination between these two parameters is important because it is desirable to examine the effects of flow pattern or velocity profile on the rate constant measurement.

The first order rate constant in the void section, $k_{m,v}$, can be evaluated separately from the area ratio of void peak to inert standard peak, A_v/A_I:

$$\frac{A_v}{A_I} = \left(\frac{S_R}{S_P}\right)\left(\frac{A_R}{A_I}\right)_{t=0} [1 - \exp(-k_{m,v}t_v)] \tag{5}$$

where S_R/S_P is the ratio of the detector sensitivity factor for reactant and product.

By obtaining A_R/A_I ratios with varying retention times, t_v, t_m, and t_s, through altering void column size and eluent flow-rate (0.1–0.9 ml/min), the initial reactant/inert peak area ratio($t = 0$) and the rate constant in each phase ($k_{m,v}$, $k_{m,c}$ and k_s) can be estimated using nonlinear regression with eqn. 4 (a four-parameter model). Other simplified (three-parameter) models are available when any known value of these parameters is introduced into the equation. The error structure assumed to be independently distributed[15] is not changed, and more accurate estimates can be obtained with a total of more than 100 data points regressed simultaneously.

A complementary model based on the total product area formed at the system outlet (including the void peak), $A_p + A_v$, is also available for analysis[16]:

$$\frac{A_p + A_v}{A_I} = C_1 - C_2 \exp(-k_{m,v}t_v - k_{m,c}t_m - k_s t_s) \tag{6}$$

where C_1 and C_2 are empirical constants, as discussed elsewhere[17]. However, since the reaction chromatogram for base-catalyzed reaction of TCTPCl$_2$ does not show a resolved pyridinium or 4-picolinium chloride product peak for interpretation because of void-peak formation confounded with other side-products, this rate expression is not recommended for use in evaluating kinetic parameters.

RESULTS AND DISCUSSION

Pyridine (0.00745 M) at 35°C

Three series of reaction chromatograms at various flow-rates are shown: Fig. 2 for an LC reactor without the void column, Fig. 3 for the void-column LC reactor with a 100 ft. × 0.01 in. I.D. void column, and Fig. 4 for the LC reactor with 50 ft. × 0.02 in. I.D. void column. In these chromatograms, the decrease of the reactant peak with the increase of the void volume and the retention time can be easily perceived. The chromatogram can be divided into three parts: void, product, and reactant using the procedures described earlier[3,16,18]. A typical chromatogram interpretation with a 100 ft. × 0.01 in. I.D. void column is illustrated in Fig. 5. All peak areas were measured using a planimeter as well as area counts from the data processing unit. The reactant/inert peak area ratios were plotted against the total reactant retention times on a semi-logarithmic scale for both the 100 ft. × 0.01 in. I.D. void-column LC reactor (Fig. 6) and the 50 ft. × 0.02 in. I.D. void-column LC reactor (Fig. 7). Good linearity was observed for both chromatographic reactor systems (correlation coefficient $r = 0.965$ and 0.990) with good estimates of the initial reactant/inert standard area ratio (1.47 to 1.58). The k_{app} values were obtained from the slopes estimated by linear regression; they were then plotted against two different
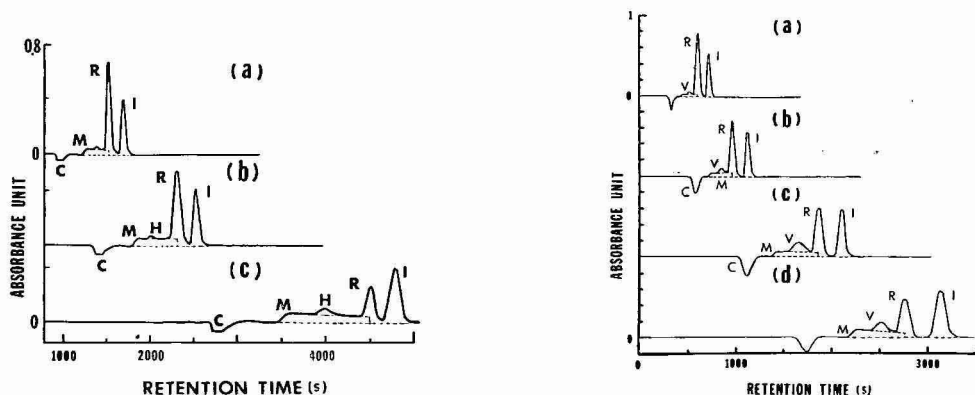
Fig. 2. Typical set of reaction chromatograms for the LC reactor without the void column. Mobile phase: 0.0075 M pyridine–0.123 M THF in methanol at 35°C. R = Reactant (TCTPCl$_2$), I = inert standard (1-phenylheptane), M = product (pyridinium, Cl-TCTP), H = Half methyl ester (methyl, Cl-TCTP), C = catalyst (pyridine) vacancy peak. (See text for formulae.) Flow-rate: (a) 0.32 ml/min; (b) 0.21 ml/min; (c) 0.11 ml/min. (See ref. 11 for reactions.)

Fig. 3. Typical set of chromatograms for the LC reactor with 100 ft. × 0.01 in. I.D. void column. Mobile phase: 0.0075 M pyridine–0.123 M THF in methanol at 35°C. R = Reactant (TCTPCl$_2$), I = inert standard (1-phenyloctane), M = product (pyridinium, Cl-TCTP), C = catalyst (pyridine) vacancy peak, V = product (pyridinium, Cl-TCTP) formed in the void volume. Flow-rate: (a) 0.95 ml/min; (b) 0.63 ml/min; (c) 0.32 ml/min; (d) 0.21 ml/min.
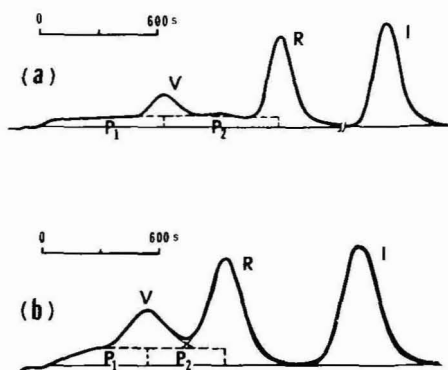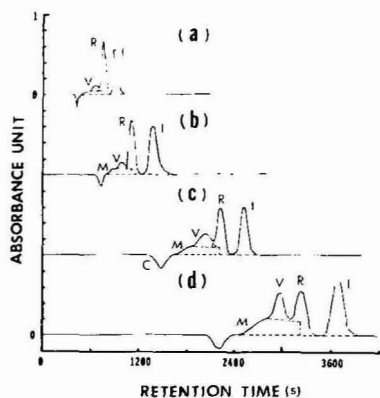
Fig. 4. Typical set of chromatograms for the LC reactor with 50 ft. × 0.02 in. I.D. void column. Mobile phase: 0.0075 M pyridine–0.123 M THF in methanol at 35°C. R = Reactant (TCTPCl$_2$), I = Inert standard (1-phenyloctane), M = product (pyridinium, Cl-TCTP), V = product (pyridinium salt) formed in the void section, C = catalyst (pyridine) vacancy peak. Flow-rate: (a) 0.95 ml/min; (b) 0.63 ml/min; (c) 0.32 ml/min; (d) 0.21 ml/min.

Fig. 5. Reaction chromatogram interpretation for the single void-column LC reactor. (a) with 100 ft. × 0.01 in. I.D. void column at 0.21 ml/min; (b) with 50 ft. × 0.02 in. I.D. void column at 0.32 ml/min. Mobile phase: 0.0075 M pyridine–0.123 M THF in methanol at 35°C. V = Product (pyridinium, Cl-TCTP) peak formed in the void section, P$_1$, P$_2$ = product M (pyridinium, Cl-TCTP) formed in the first and second packed columns, respectively. R = Reactant (TCTPCl$_2$), I = inert standard (1-phenylheptane).

retention ratios, $(t_m + t_v/t_R$ and $(t_m + t_v)/t_m$, on the basis of reactant retention volumes at 8.4 ml (Fig. 8a and b). The rate constants with one standard deviation, k_m and k_s, were also estimated using linear least-squares in the MINITAB statistical package[19]. Excellent linearity (t = 0.997 and 0.998) was found for both methods, indicating that simple first-order reaction kinetics are followed in the void-column chromatographic system. The agreement of rate estimates using different retention
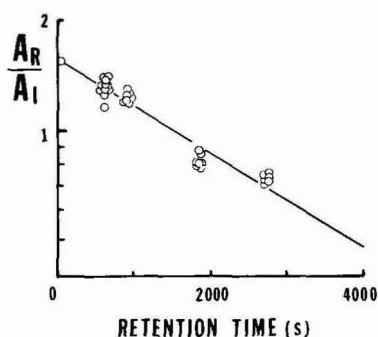
Fig. 6. Inert standard method plot of area ratio A_R/A_I versus reactant retention time, t_R, for the void-column LC reactor with 50 ft. × 0.02 in. I.D. void column at 35°C. Catalyst: 0.0075 M pyridine in methanol. A_R/A_I = ln(1.581 ± 0.058) – (0.0003058 ± 0.00001185)t_R by linear regression, using eqn. 1.
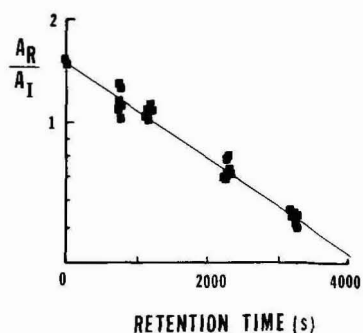
Fig. 7. Inert standard method plot of area ratio A_R/A_I versus reactant retention time t_R for the void-column LC reactor with 50 ft. × 0.02 in. I.D. void column at 35°C. Catalyst: 0.0075 M pyridine in methanol. A_R/A_I = ln(1.467 ± 0.053) – (0.0003105 ± 0.0000078)t_R by linear regression, using eqn. 1.
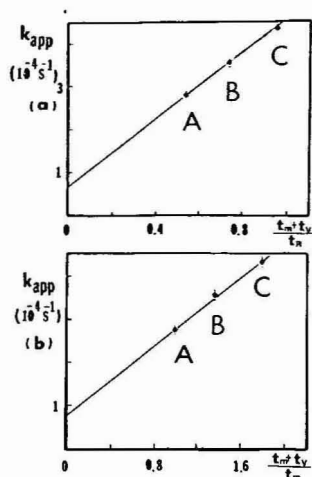
Fig. 8. Linear plot of apparent rate constant, k_{app}, versus retention time ratio (a) $(t_m + t_v)/t_R$ and (b) $(t_m + t_v)/t_m$ for the void-column LC reactor. Reaction: the first-step of 0.0075 M pyridine-catalyzed esterification of $TCTPCl_2$ at 35°C (reaction a). Here, points A, B and C correspond to the apparent rate constant values, obtained from the LC reactor without the void column, the void-column LC reactor with 100 ft. × 0.01 in. I.D. void column (Fig. 6), and the reactor with 50 ft. × 0.02 in. I.D. void column (Fig. 7), respectively. (See eqns. 2 and 3.)

ratios (see eqns. 2 and 3) suggests little effect from retention data measurements. The mobile phase rate constants $[k_m = (3.83 \pm 0.23) \cdot 10^{-4}$ or $(3.74 \pm 0.28) \cdot 10^{-4}$ $s^{-1}]$ were quite comparable to data obtained from a complete mixed batch reactor $[(3.80 \pm 0.15) \cdot 10^{-4} \; s^{-1}]$. This supports the earlier assumption that the mobile-phase composition is homogeneous. The axial dispersion effect, which might be significant in LC columns[2,20], apparently does not affect the kinetic measurements for first-order reactions. Furthermore, it validates the LC reactor approach for evaluation reaction kinetics in the mobile phase solvent.

A separate nonlinear least-squares analysis with 134 data points was conducted, using eqn. 4, and the results are summarized in Table I. The nonlinear regression routine LS which used a modified Newton–Gauss method was employed for parameter estimation[21]. Examination of the results showed that rate estimates in both mobile and the stationary phases were quite comparable to the predicted or experimental values, the correlation between k_m and k_s was decoupled (coefficient = -0.88316), and the residuals were randomly distributed around the model-predicted values. If we assume that the rate constant in the packed section is known ($3.8 \cdot 10^{-4}$ s^{-1}), the rate estimate in the void column $[k_{m,v} = (4.10 \pm 0.66) \cdot 10^{-4} \; s^{-1}]$ was in fair agreement with the batch reactor value $[k_{m,c} = (3.80 \pm 0.15) \cdot 10^{-4} \; s^{-1}]$. The discrepancy might arise from the effect of velocity profiles in the void section. It has been established that for first-order reactions conversion is smaller in a laminar-flow reactor than in a plug-flow (packed-bed) reactor[22]. For the flow-rates (0.1–0.9 ml/min) used here, a laminar flow is developed in the void column; thus, it is reasonable to obtain an overestimated rate constant $(k_{m,v})$ in the void section, assuming the same conversion.

Although relatively large errors were associated with the estimates, it is per-

TABLE 1

COMPARISON OF METHANOL–THF MOBILE PHASE RATE CONSTANTS IN THE VOID AND THE PACKED COLUMNS OF THE LC REACTOR FOR THE 0.0075 M PYRIDINE-CATALYZED REACTION OF TCTPCl$_2$ AT 35°C

RSS = residual sum of squares.

A_{RO}/A_f*	k_m (void)** $(10^{-4}\,s^{-1})$	k_m (packed)** $(10^{-4}\,s^{-1})$	k_s (column)*** $(10^{-4}\,s^{-1})$	Corr. matrix	RSS
1.524 ± 0.032§	4.021 ± 0.587		1.209 ± 0.833	$\begin{matrix} 1 & & \\ 0.35033 & 1 & \\ 0.01285 & -0.90038 & 1 \end{matrix}$	0.64238
1.524 ± 0.032§§		3.975 ± 0.536	1.254 ± 0.757	$\begin{matrix} 1 & & \\ 0.36392 & 1 & \\ 0.02936 & -0.88316 & 1 \end{matrix}$	0.63314
1.526 ± 0.033§§§	4.096 ± 0.659	3.80	1.473 ± 0.357	$\begin{matrix} 1 & & \\ 0.39234 & 1 & \\ 0.70313 & -0.08850 & 1 \end{matrix}$	0.64118
1.58†	3.709 ± 0.157	–	–	–	0.5180

   * Experimental measurement is 1.58 ± 1.62.
  ** From completely mixing batch reactor study, $k_m = (3.80 ± 0.15) \cdot 10^{-4}\,s^{-1}$.
 *** Predicted rate constants for stationary phase models I and II are $(2.38 ± 0.43) \cdot 10^{-4}\,s^{-1}$ and $(0.75 ± 0.24) \cdot 10^{-4}\,s^{-1}$ respectively; see ref. 1 for detailed calculations and discussion.
   § Estimated with $V_m + V_{void} = 8.1$ ml using A_R/A_f measurements (eqn. 4).
  §§ Estimated with $V_m + V_{void} = 8.3$ ml using A_R/A_f measurements (eqn. 4).
 §§§ Substituted with a "known" value of the mobile phase constant to decouple k_s and $k_{m,void}$ (eqn. 4).
   † Estimated using A_v/A_f measurements (eqn. 5).

TABLE II

COMPARISON OF METHANOL–THF MOBILE PHASE RATE CONSTANTS IN THE VOID AND THE PACKED COLUMNS OF THE LC REACTOR FOR THE 0.0075 M PYRIDINE-CATALYZED REACTION OF TCTPCl$_2$ AT 25°C

A_{RO}/A_I [*]	k_m (void)[**] (10^{-4} s^{-1})	k_m (packed)[**] (10^{-4} s^{-1})	k_s (column)[***] (10^{-4} s^{-1})	Corr. matrix	RSS
1.510 ± 0.027[§]	2.194 ± 0.624	2.194 ± 0.387	0.316 ± 0.495	1 0.47641 1 −0.14754 −0.91193 1	0.36349
1.509 ± 0.026[§§]		2.110 ± 0.355	0.460 ± 0.437	1 0.48530 1 −0.11817 −0.89098 1	0.36516
1.512 ± 0.029[§§§]	2.194 ± 0.624	1.853 ± 3.963	0.752 ± 4.528	1 0.54277 1 −0.28323 −0.74855 1 0.31298 0.75008 −0.99904 1	0.36230
1.511 ± 0.027[†]	2.159 ± 0.412	2.15	0.414 ± 0.198	1 0.51993 1 0.71389 0.07745 1	0.36237
1.511 ± 0.025[†]	2.15	2.035 ± 2.615	0.545 ± 2.981	1 0.21833 1 −0.16678 −0.99781 1	0.36237

[*] Experimental measurement in 1.58–1.60.

[**] From completely mixing batch reactor study, $k_m = (2.15 ± 0.09) \cdot 10^{-4}$ s^{-1}.

[***] Predicted rate constants for stationary phase models I and II are $(1.54 ± 0.28) \cdot 10^{-4}$ s^{-1} and $(0.43 ± 0.15) \cdot 10^{-4}$ s^{-1} respectively.

[§] Estimated with the column dead volume, V_m = 4.5 ml, using a three-parameter model (eqn. 4).

[§§] Estimated with the column dead volume, V_m = 4.6 ml, using a three-parameter model (eqn. 4).

[§§§] Obtained from the A_R/A_I measurements (eqn. 4) with a four-parameter model.

[†] Substituted with a "known" value of the mobile-phase rate constant, k_m.

tinent to find that k_s and $k_{m,void}$ were completely decoupled (coefficient = -0.0885). A separate estimation, using the A_v/A_1 data (eqn. 5), also showed good consistency for the rate constant in the void section [$(3.71 \pm 0.16) \cdot 10^{-4} \, \text{s}^{-1}$]. The independently determined rate estimates in the stationary phase [$k_s = (1.21 \pm 0.83) \cdot 10^{-4}$ or $(1.25 \pm 0.76) \cdot 10^{-4} \, \text{s}^{-1}$] support the concept of a composite stationary phase, operative between models I and II but favoring model II, as discussed in a previous paper[1]. Here model I refers to the stationary phase model, proposed by Knox and Pryde[23], where solute molecules interact with the associated methanol pseudo-layer only, while model II refers to a generalized stationary phase model, composed of methanol molecules associated with octadecylsilane ligands, as proposed by Yonker et al.[24].

Pyridine (0.00745 M) at 25°C

The linear plots of A_R/A_1 versus t_R for the first step of the TCTPCl$_2$ reaction with 0.00745 M pyridine catalyst in tetrahydrofuran (THF)–methanol (2:98) at 25°C were obtained in a similar manner for the single void-column LC reactor with both a 100 ft. × 0.01 in. void column and a 50 ft. × 0.02 in. I.D. void column. These plots manifest good linearity and agreement with initial experimental values. The calculated apparent rate constants, obtained from eqn. 1, were then plotted against two retention time ratios, $(t_m + t_v)/t_R$ and $(t_m + t_v)/t_m$, to evaluate the rate constants k_m and k_s, respectively, using eqns. 2 and 3. Relatively large errors were associated with the stationary phase estimates [$k_s = (0.76 \pm 1.38) \cdot 10^{-4}$ or $(0.78 \pm 1.41) \cdot 10^{-4} \, \text{s}^{-1}$] because of the more scattered k_{app} values associated with the low conversion for this slow reaction. Nevertheless, the estimates still show fair agreement with the predicted value from the idealized dispersion [$k_{s,II} = (0.43 \pm 0.15 \cdot 10^{-4} \, \text{s}^{-1}$] compared with that of Knox and Pryde [$k_{s,I} = (1.54 \pm 0.28) \cdot 10^{-4} \, \text{s}^{-1}$]. Since the mobile phase rate values [$k_m = (2.07 \pm 0.88) \cdot 10^{-4}$ or $(2.06 \pm 0.90) \cdot 10^{-4} \, \text{s}^{-1}$] are comparable with the value obtained from a well-mixed batch reactor [$(2.15 \pm 0.09) \cdot 10^{-4} \, \text{s}^{-1}$], it appears that there are little or no external (diffusion from the bulk liquid in the interstices to the particle surface) or internal (pore diffusion) mass transfer limitations. This is because the reaction rates studied here are relatively slow, so that the effect of reactant diffusion is not significant in the measurement[2].

The results from the nonlinear regression analysis are summarized in Table II. The calculated rate constants in both phases agree with the expected values but less error is associated with the stationary phase estimate. This is because a total of 110 data from three void-column experiments were regressed simultaneously to decouple as well as estimate the rate parameters in the two-phase chromatographic system. The effect of a variation of dead volume measurement, V_m, on the kinetic studies was also tested; while an error of 0.1 ml in $V_m = 4.5$ ml produces only a *ca.* 4% error in the mobile phase rate constant, it can cause about 30% uncertainty in the stationary phase value. When the decoupling role of the void column was removed by using a "known" value ($2.15 \cdot 10^{-4} \, \text{s}^{-1}$) for $k_{m,void}$, highly correlated but less accurate rate estimates were obtained (coefficient = -0.99781); when the mobile phase rate constant from a batch study ($k_{m,c} = 2.15 \cdot 10^{-4} \, \text{s}^{-1}$) was directly substituted into the treatment based on eqn. 4, the estimates of $k_{m,void}$ and k_s were completely decoupled (coefficient = 0.07745). This demonstrates the realization of the original objective of decoupling rate constants with the introduction of an independently varied void-column size.

4-Picoline (0.00615 M) at 35°c

The apparent rate constants obtained from the linear plots of $\ln(A_R/A_I)$ *versus* t_R (Figs. 9 and 10) were again plotted against two retention time ratios to evaluate rate constants in both phases (Fig. 11a and b). Linearity ($r = 1.000$) was observed for both cases. It is worth noting again that the dead-volume estimate does have a significant effect on the rate-constant measurements. For the 50 ft. × 0.02 in. I.D. void-column LC reactor in both figures, the dashed and solid lines represent the linear plots with $V_m + V_{void} = 8.3$ and 8.1 ml, respectively. An error of 0.2 ml can change the mobile phase estimates from $(7.77 \pm 0.06) \cdot 10^{-4}$ or $(7.74 \pm 0.20) \cdot 10^{-4}$ to $(8.13 \pm 0.14) \cdot 10^{-4}$ or $(8.14 \pm 0.01) \cdot 10^{-4}$ s^{-1}, and the stationary phase values from $(1.61 \pm 0.10) \cdot 10^{-4}$ or $(1.71 \pm 0.35) \cdot 10^{-4}$ to $(1.12 \pm 0.24) \cdot 10^{-4}$ or 1.16 $\pm 0.01) \cdot 10^{-4}$ s^{-1}. Thus, kinetic studies utilizing the LC reactor require not only accurate area measurements but also accurate determination of reactant retention data and dead-volume.

As before, a nonlinear regression with 120 A_R/A_I data was conducted using eqn. 4. The estimated rate parameters in the mobile phase were comparable with the batch reactor values (Table III), while the stationary-phase rates were in agreement with those predicted from the modified model of Burke *et al.*[24] rather than that of Knox and Pryde[23]. This discrimination between the stationary phase models is achieved through the measurements. To check for any possible systematic errors during experiments, the reproducibility of the apparent rate constant was further examined. The k_{app} value without the void column, obtained from this work [$(4.99 \pm 0.07) \cdot 10^{-4}$ s^{-1}], was compared with that measured by Bolme and Langer[25] [$(4.95 \pm 0.24) \cdot 10^{-4}$ s^{-1}], who used a different sample preparation procedure, different initial ratio of reactant to inert standard, and a different data analysis method [to correct for large accumulation of undesired (4-methoxycarbonyl-2,3,5,6-tetrachloro-
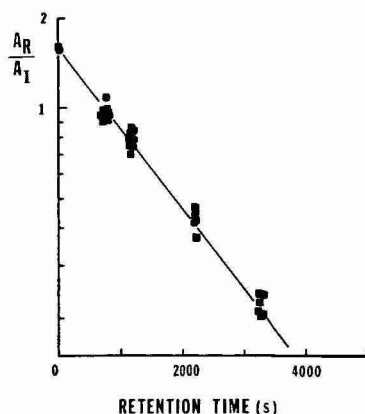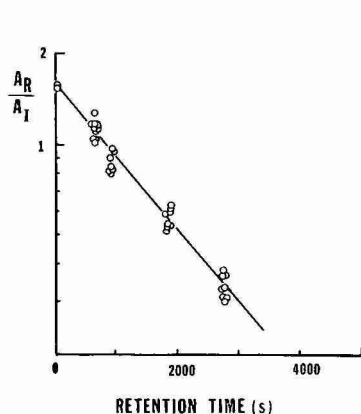
Fig. 9. Inert standard method plot of area ratio A_R/A_I *versus* reactant retention time, t_R, for the void-column LC reactor with 100 ft. × 0.01 in. I.D. void column at 35°C. Catalyst: 0.00615 M 4-picoline in methanol. $A_R/A_I = \ln(1.551 \pm 0.054) - (0.000556 \pm 0.0000098)t_R$ by linear regression, using eqn. 1.

Fig. 10. Inert standard method plot of area ratio A_R/A_I *versus* reactant retention time, t_R, for the void-column LC reactor with 50 ft. × 0.02 in. I.D. void column at 35°C. Catalyst: 0.00615 M 4-picoline in methanol. $A_R/A_I = \ln(1.518 \pm 0.051) - (0.000600 \pm 0.0000088)t_R$ by linear regression, using eqn. 1.

TABLE III

ESTIMATION OF METHANOL–THF MOBILE PHASE RATE CONSTANTS IN THE VOID AND THE PACKED COLUMNS OF THE LC REACTOR FOR THE 0.00615 M 4-PICOLINE-CATALYZED REACTION OF TCTPCl$_2$ AT 35°C

A_{RO}/A_I [*]	k_m (void) [**] (10^{-4} s^{-1})	k_m (packed) [**] (10^{-4} s^{-1})	k_s (column) [***] (10^{-4} s^{-1})	Corr. matrix			RSS
1.496 ± 0.032[§]		7.706 ± 0.616	1.215 ± 1.047	1			0.25504
				0.17889	1		
				0.27002	−0.86633	1	
1.496 ± 0.033[§§]		8.080 ± 0.677	0.720 ± 1.135	1			0.24966
				0.13837	1		
				0.26826	−0.89015	1	
1.496 ± 0.033	7.812 ± 0.700	7.26	1.713 ± 0.553	1			0.26025
				0.22034	1		
				0.75560	−0.26608	1	
1.489 ± 0.034	7.26	8.028 ± 5.330	0.884 ± 6.912	1			0.26565
				−0.33680	1		
				0.39957	−0.99694	1	

* Experimental measurement is 1.58–1.67.
** From completely mixing batch reactor study, $k_m = (7.26 \pm 0.06) \cdot 10^{-4}$ s^{-1}.
*** Predicted rate constants for stationary phase models I and II are $(3.97 \pm 0.45) \cdot 10^{-4}$ s^{-1} and $(1.25 \pm 0.25) \cdot 10^{-4}$ s^{-1} respectively.
§ With $V_m + V_{void} = 8.1$ ml from A_R/A_I measurements (eqn. 4).
§§ With $V_m + V_{void} = 8.3$ ml from A_R/A_I measurements (eqn. 4).

TABLE IV

ESTIMATION OF METHANOL–THF MOBILE PHASE RATE CONSTANTS IN THE VOID AND THE PACKED COLUMNS OF THE LC REACTOR FOR THE 0.00615 M 4-PICOLINE-CATALYZED REACTION OF TCTPCl$_2$ AT 25°C

A_{RO}/A_I *	k_m (void)** ($10^{-4}\,s^{-1}$)	k_m (packed)** ($10^{-4}\,s^{-1}$)	k_s (column)*** ($10^{-4}\,s^{-1}$)	Corr. matrix	RRS
$1.401 \pm 0.264^§$	3.670 ± 0.777		1.442 ± 1.095	1 0.3108 1 −0.0477 0.9069 1	0.29020
$1.400 \pm 0.0372^§$	4.00	3.677 ± 0.758	1.057 ± 0.469	1 0.3644 1 0.6903 −0.1763 1	0.29016
$1.40^§$	4.00	3.675 ± 0.701	1.055 ± 0.338	1 −0.6350 1	0.29016
$1.590 \pm 2.388^{§§}$	3.386 ± 5.594	–	–	1 −0.99950 1	0.00976
$1.40^{§§}$	3.898 ± 0.204	–	–	1	0.00978

* Experimental measurement is 1.45 ± 0.05.

** From completely mixing batch reactor study, $k_m = (4.03 \pm 0.06) \cdot 10^{-4}\,s^{-1}$.

*** Predicted rate constants for stationary phase models I and II are $(3.24 \pm 0.52) \cdot 10^{-4}\,s^{-1}$ and $(0.90 \pm 0.27) \cdot 10^{-4}\,s^{-1}$ respectively.

§ Values obtained from the A_R/A_I measurements (eqn. 4).

§§ Values from the A_v/A_I measurements (eqn. 5).
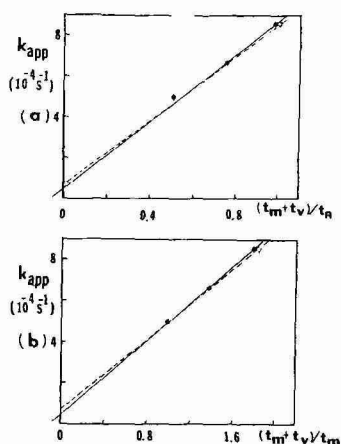
Fig. 11. Linear plot of apparent rate constant, k_{app}, *versus* retention time ratio (a) $(t_m + t_v)/t_R$ and (b) $(t_m + t_v)/t_m$ for the void-column LC reactor. Reaction: the first-step of 0.00615 M 4-picoline-catalyzed esterification of TCTPCl$_2$ at 35°C. The dashed and solid lines represent the linear plots with $V_m + V_{void}$ = 8.3 and 8.1 ml, respectively. (See text for detailed discussion.)

benzoyl chloride) half ester intermediate]. The agreement between these two values, measured three years apart, reflects the consistency and reproducibility of the LC reactor experimental results under carefully controlled conditions.

4-Picoline (0.00615 M) at 25°C

The linearized method (eqn. 1) was used again to evaluate the apparent rate constants for both the 100 ft. × 0.01 in. I.D. void-column LC reactor and the 50 ft. × 0.02 in. I.D. void-column LC reactor. Despite data scattering for the large void column at low flow-rates because of dispersion effects, good linearity was still observed for both cases (r = 0.987 and 0.985). This is because the first-order rate constant would be independent of reactant concentration variation due to moderate flow dispersion (dilution) along the chromatographic column. The rate constants in both phases were measured from the linear plots to estimate reaction kinetics in both phases. Use of two different retention ratios assures consistent rate estimates, free of measurement error, in retention data. The estimated mobile phase kinetics [(k_m = (3.66 ± 0.33) · 10^{-4} or (3.61 ± 0.38) · 10^{-4} s^{-1}] agree within the experimental error with the batch reactor value [(4.03 ± 0.06) · 10^{-4} s^{-1}), while those in the stationary phase suggest a generalized model involving both the methanol pseudo-layer and the octadecylsilanes [$k_{s,n}$ = (0.90 ± 0.27) · 10^{-4} s^{-1}]. Results from the nonlinear models of eqns. 4 and 5 with 80 data points all drew the same conclusions regarding the "homogeneous continuum" assumption in the mobile phase and the generalized-partition stationary phase mechanism (Table IV).

Generally speaking, the single void-column LC reactor appears to be a suitable method for studying the on-line two-phase reaction kinetics simultaneously. By simply varying the void-column size and the eluent flow-rate, reactant residence times in two phases can be changed because of the incorporation of retention variation in the void column of the void-column LC reactor array; thus, rate constants in each phase can be measured independently.

The reaction technique illustrated here can be utilized as a diagnostic method for detecting any void zone in chromatographic columns[26]; from the shape of the reaction product curve in the chromatograms substantial information can be obtained about the homogeneity of the column packing. Knowledge of the first-order mobile and stationary phase rate constants and a detectable void peak also make it possible to estimate void-zone volumes[3].

APPENDIX

Temperature inhomogeneity effect on reaction kinetic measurement in LC reactors

For the analytical-scale chromatographic reactor with small pulsed injection of reactant solution, isothermal conditions have been assumed for the whole reactor system. For GC reactors, this temperature homogeneity assumption is valid, except for extremely exothermic or endothermic reactions. However, LC columns of moderate lengths are usually operated at pressure dropss up to several thousand pounds per square inch to obtain reasonable flow-rates through the 5–10 μm microparticle-packed columns. Under such conditions, internal heat generation, due to irreversible viscous dissipation, can result in non-uniform temperature distribution in the column[27,28].

For our LC reactor, where the radial dependence of temperature (T) is not of major concern, it would be of interest to know the magnitude of a maximum possible temperature increase due to the viscous dissipation[29–31]. For methanol flow-rates ranging from 0.1 to 0.9 ml/min,

(a) At 0.9 ml/min methanol with pressure drop (Δp) about 2000 p.s.i.,

$$\Delta T_{max} = \frac{u_0(\Delta p/L)R^2}{4k_c} = \frac{\dfrac{F}{\pi}(\Delta p/L)}{4k_c}, \qquad k_{c,methanol} = 0.0004 \text{ cal/cm s } ^\circ\text{C} \tag{A1}$$

where u_0 is the linear velocity of the mobile phase solvent, L is the column length, R is the column internal radius and F is the mobile phase flow-rate; therefore

$$\Delta T_{max} = \frac{0.90 \text{ ml/min} \left(\dfrac{2000 \text{ p.s.i.}}{14.7 \text{ p.s.i.}} \cdot 1033.3 \text{ g}_f \text{ cm/50 cm} \right)}{\pi \cdot 4 \cdot 0.0004 \cdot 60 \text{ cal/cm min } ^\circ\text{C}}$$
$$= 0.084 \cdot 10^5 \text{ g}_f \text{ cm } \frac{^\circ\text{C}}{\text{cal}} \tag{A2}$$
$$= 0.084 \text{ kg}_f \text{ m} \cdot 23.44 \frac{\text{cal} \quad ^\circ\text{C}}{\text{kg}_f \text{ m cal}} \simeq 2^\circ\text{C}$$

The average temperature increase will be around 1°C. For activation energies of base-catalyzed reactions studied here, $E_a = 10\,500$ cal/mol, thus only 6% error in rate constant measurements will be incurred due to viscous heat generation at 0.9 ml/min flow-rate.

(b) At 0.1 ml/min methanol with pressure drop about 500 p.s.i., the same

treatment can be applied to obtain $\Delta T_{max} = 0.08°C$ or $\Delta T_{average} = 0.04°C$. Thus, only 0.25% error will be introduced into rate-constant estimates.

The calculation above shows that the influence of the viscous heat effect should not be significant, since the flow-rate range here is limited to below 0.9 ml/min to achieve appreciable residence time for the relatively slow reactions. Therefore, for the analytical physicochemical application purpose, the chromatographic system can be assumed to be isothermal, as outlined in the ideal chromatographic reactor treatment[32]. However, precautions would be appropriate when high flow-rates with small particle sizes are employed.

ACKNOWLEDGEMENT

REFERENCES

1 A. H. T. Chu and S. H. Langer, *Anal. Chem.*, 57 (1985) 2197.
2 A. H. T. Chu and S. H. Langer, *Anal. Chem.*, 58 (1986) 1617.
3 J. E. Patton and S. H. Langer, *Anal. Chem.*, 42 (1970) 1449.
4 S. H. Langer, H. R. Melton, T. D. Griffith and J. Coca, *J. Chromatogr.*, 122 (1976) 487.
5 B. Coq, G. Cretier, J. L. Rocca and R. Kastner, *J. Chromatogr.*, 178 (1979) 41.
6 K. Tsuji and J. F. Goetz, *J. Chromatogr.*, 157 (1978) 185.
7 J. H. Knox, G. R. Laird and P. A. Raven, *J. Chromatogr.*, 122 (1976) 129.
8 J. J. Kirkland, W. W. Yau, H. J. Stoklosa and C. H. Dilks, Jr., *J. Chromatogr. Sci.*, 15 (1977) 303.
9 J. C. Giddings, *Dynamics of Chromatography*, Marcel Dekker, New York, 1965.
10 C. Horvath and H.-J. Lin, *J. Chromatogr.*, 126 (1976) 401.
11 S. H. Langer, A. H. T. Chu, M. W. Bolme, M. S. Turner and G. R. Quinting, *J. Chem. Res.*, Synop., (1985) 342.
12 A. M. Krstulovic, H. Colin and G. Guiochon, *Anal. Chem.*, 54 (1982) 2438.
13 R. J. Cvetanovic and D. L. Singleton, *Int. J. Chem. Kinet.*, 9 (1977) 481.
14 R. J. Cvetanovic, D. L. Singleton and G. Paraskevopoulos, *J. Phys. Chem.*, 83 (1979) 50.
15 G. E. P. Box, W. G. Hunter and J. S. Hunter, *Statistics for Experimenters: An Introduction to Design, Data Analysis, and Model Building*, Wiley, New York, 1978.
16 S. H. Langer and T. D. Griffith, *J. Phys. Chem.*, 82 (1978) 1327.
17 T. D. Griffith, A. H.-T. Chu and S. H. Langer, *J. Chem. Eng.*, submitted for publication.
18 S. H. Langer and J. Y. Yurchak, *153rd National Meeting of the ACS, Miami Beach, Fl*, American Chemical Society, Washington, DC, No. R46, 1967.
19 T. A. Ryan, Jr., B. L. Joiner and B. F. Ryan, *MINITAB: Student Handbook*, Duxbury Press, MA. Boston, 1976.
20 B. L. Karger, M. Martin and G. Guiochon, *Anal. Chem.*, 46 (1983) 1640.
21 W. E. Stewart and J. P. Sørensen, *LS: Nonlinear Regression Routine*, Engineering Computing Laboratory, University of Wisconsin-Madison, Madison, WI, 1971.
22 K. G. Denbigh and J. C. R. Turner, *Chemical Reactor Theory*, Cambridge University Press, London, New York, 2nd ed., 1971, pp. 90–95.
23 J. H. Knox and A. Pryde, *J. Chromatogr.*, 112 (1975) 171.
24 C. R. Yonker, T. A. Zwier and M. F. Burke, *J. Chromatogr.*, 241 (1982) 257; 269.
25 M. W. Bolme and S. H. Langer, *J. Phys. Chem.*, 87 (1983) 3363.
26 S. H. Langer, J. Y. Yurchak and C. M. Shaughnessy, *Anal. Chem.*, 40 (1968) 1747.
27 R. Endele, I. Halász and K. Unger, *J. Chromatogr.*, 99 (1974) 377.
28 M. Martin, C. Eon and G. Guiochon, *J. Chromatogr.*, 99 (1974) 357.
29 H.-J. Lin and Cs. Horváth, *Chem. Eng. Sci.*, 36 (1981) 47.
30 H. Poppe, J. C. Kraak, J. F. K. Huber and J. H. M. van den Berg, *Chromatographia*, 14 (1981) 515.
31 H. Poppe and J. C. Kraak, *J. Chromatogr.*, 282 (1983) 399.
32 S. H. Langer and J. E. Patton, in J. H. Purnell (Editor), *New Developments in Gas Chromatography*, Wiley, New York, 1973, pp. 293–373.

CHROMSYMP. 1033

FACTORS CONTROLLING THE SEPARATION OF AMINO ACIDS IN ISOCRATIC REVERSED-PHASE LIQUID CHROMATOGRAPHY

SHULAMIT LEVIN and ELI GRUSHKA*

Department of Inorganic and Analytical Chemistry, The Hebrew University, Jerusalem (Israel)

SUMMARY

Amino acids can be separated with a simple isocratic liquid chromatographic system in which no pre- or post-column derivatization of the amino acids is needed. Copper ions and alkylsulphonate additives are used to effect both the selectivity and the retention of the solutes. The effect of several operating conditions on the performance of the system was examined, especially the nature and concentration of the alkylsulphonate, the concentration of copper ions, the ionic strength of the buffer and temperature. Guidelines are given for optimization of the separation. The deleterious effects of system peaks and means of overcoming them are discussed.

INTRODUCTION

We recently described a method for the separation of amino acids[1] in which the mobile phase was an aqueous acetate buffer containing alkylsulphonate and copper(II) acetate. A reversed-phase column and UV detection were used. The two major features of the method are that elution is isocratic and that it is unnecessary to derivatize the amino acids. The chromatographic equipment is readily assembled, highly reproducible and inexpensive.

The rationale behind the choice of the mobile phase constituents has been described in detail[1]. However, for the sake of completeness, it should be mentioned here that copper ions were added to control the detection and retention of the amino acids, and the alkylsulphonate was added to retard the early eluting solutes. Some of the technical problems related to this particular chromatographic system and the influence of the chromatographic parameters on the retentions and selectivities of several representative amino acids were also discussed[1].

This work intends to illustrate the usefulness of this chromatographic system by examining the influence of some chromatographic parameters on the chromatogram, rather than on the behaviour of individual solutes, as was done previously[1]. The effects of varying parameters such as the alkylsulphonate chain length and concentration, Cu^{2+} concentration, ionic strength and temperature were studied. These parameters affect the retention and resolution considerably.

EXPERIMENTAL

As the experimental setup was described in detail previously[1], only a brief description is given here.

Materials

The mobile phase was prepared by dissolving the appropriate amounts of a given alkylsulphonate and copper(II) acetate in an acetate buffer (pH 5.6). All the alkylsulphonates and amino acids were purchased from Sigma (St. Louis, MO, U.S.A.).

Instrumentation

The chromatographic system consisted of a Perkin-Elmer (Norwalk, CT, U.S.A.) Series 4 liquid chromatograph, a Rheodyne (Cotati, CA, U.S.A.) injection valve and a Perkin-Elmer 85B variable-wavelength spectrophotometric detector. The column temperature was maintained with the aid of a thermostated water-bath. All the chromatographic analyses were carried out using a Merck (Darmstadt, F.R.G.) LiChrosorb RP-18 cartridge (250 × 4 mm I.D.).

Procedures

The flow-rate of the mobile phase was 2 ml/min. Detection was carried out at 235 nm. The concentrations of the injected amino acids were 2.4–10 nmole, depending on the elution time of the solutes.

RESULTS AND DISCUSSION

Effect of chain length of the alkylsulphonate

It was shown previously that the retention of the amino acids, at a given sulphonate concentration, increases as the length of the alkyl portion of the sulphonate is increased[1]. This is to be expected, as the retention processes here are identical with those in a more conventional ion-pair system[2]. Hence the same number of amino acids can be separated in roughly the same time by using different concentrations of
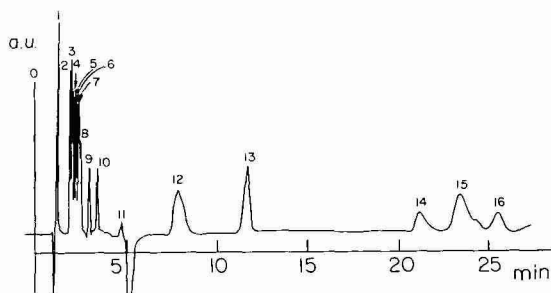
Fig. 1. Separation of amino acids with pentanesulphonate. Mobile phase, 10 mM acetate buffer–0.5 mM copper(II) acetate–5 mM pentanesulphonate. Detection, 235 nm, 0.32 a.u.f.s.; amino acid concentrations, 0.5–1 mM; flow-rate, 2 ml/min; temperature, 30°C. Peaks: 1 = Asp + Glu; 2 = Gly; 3 = Ser; 4 = Asn; 5 = Ala; 6 = Gln; 7 = Hyp; 8 = Thr; 9 = His; 10 = αAbu; 11 = Pro; 12 = Val + Nvl + Lys; 13 = Met; 14 = Arg; 15 = Tyr + Ile; 16 = Leu.

Fig. 2. Separation of amino acids with hexanesulphonate. Mobile phase, 10 mM acetate buffer–0.5 mM copper(II) acetate–5 mM hexanesulphonate. Other conditions as in Fig. 1. Peaks: 1 = Asp; 2 = Glu; 3 = Gly; 4 = Ser; 5 = Asn; 6 = Ala; 7 = Gln; 8 = Thr; 9 = Hyp; 10 = αAbu; 11 = His; 12 = Pro; 13 = Val; 14 = Nvl; 15 = Met; 16 = Lys; 17 = Tyr; 18 = Ile; 19 = Leu; 20 = Arg.

the various alkylsulphonates. For example, it was found that mobile phases containing either 0.8 mM heptanesulphonate, 4 mM hexanesulphonate or 10 mM pentanesulphonate in the mobile phase gave similar chromatograms. This finding is important in the optimization of the method.

In the previous study we investigated the use of C_6–C_8 sulphonates; this work extends the method to pentanesulphonate. Fig. 1 shows a chromatogram with 16 peaks, all eluted in less than 30 min. However, the early part of the chromatogram is crowded, 11 peaks being eluted in less than 5 min. Moreover, some of the peaks are actually due to mixtures of several amino acids. The use of hexanesulphonate can alleviate these difficulties, as shown in Fig. 2. The chromatographic conditions for Figs. 1 and 2 were identical, except for the chain length of the ion-pairing reagent. The resolution improved considerably with the introduction of the longer chain sulphonate, but the retention time also increased. For example, with pentanesulphonate in the mobile phase, leucine, which is the last solute in Fig. 1, was eluted in about 25 min whereas with hexanesulphonate in the mobile phase it was retained for over 50 min.

Effect of sulphonate concentration

The behaviour of some representative amino acids as a function of the sulphonate concentration was examined previously[1]. Studies in which hexanesulpho-

Fig. 3. Effect of Cu^{2+} and sulphonate concentration on the separation of amino acids. Mobile phase, 10 mM acetate buffer–0.25 mM copper(II) acetate–5 mM hexanesulphonate. Other conditions as in Fig. 1. Peaks: 1 = Asp + Glu; 2 = Gly; 3 = Ser; 4 = Asn + Ala; 5 = Gln; 6 = Thr; 7 = Hyp; 8 = system peak D; 9 = αAbu; 10 = His; 11 = Pro; 12 = Val + Nvl; 13 = Met; 14 = Lys; 15 = Tyr; 16 = Ile; 17 = Leu; 18 = Arg.

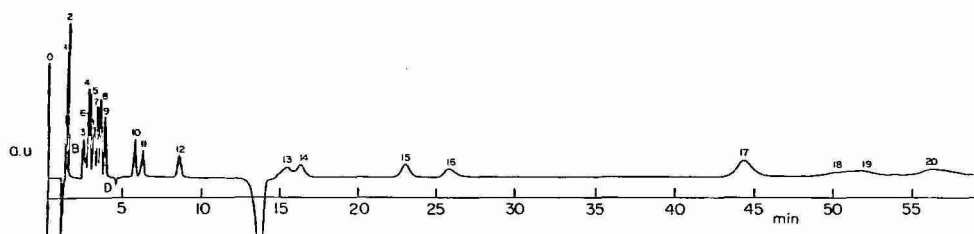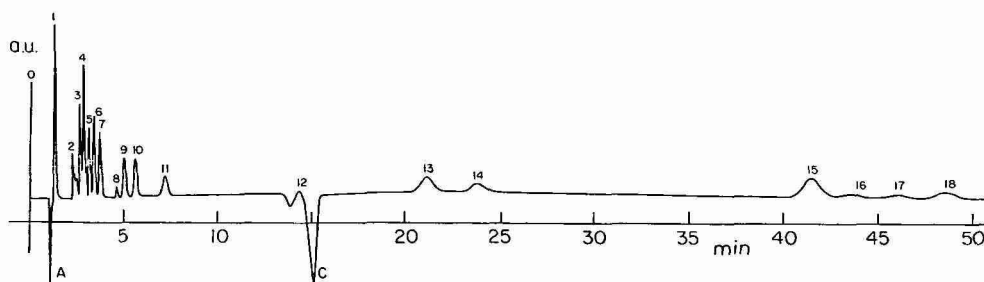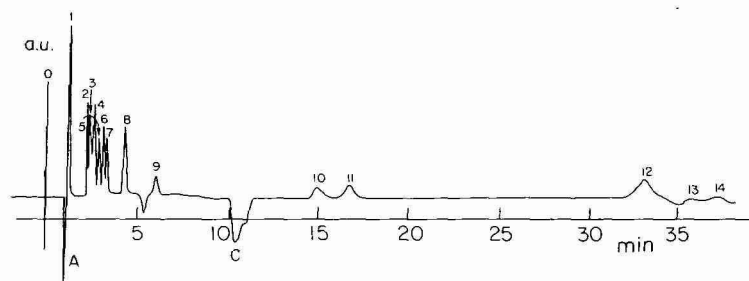Fig. 4. Effect of sulphonate concentration on the separation of amino acids. Mobile phase, 10 mM acetate buffer–0.25 mM copper(II) acetate–2.5 mM hexanesulphonate. Other conditions as in Fig. 1. Peaks: 1 = Asp + Glu; 2 = Gly + Ser; 3 = Asn; 4 = Ala; 5 = Gln; 6 = Thr; 7 = Hyp; 8 = αAbu + His; 9 = Pro; 10 = Lys; 11 = Met; 12 = Tyr + Arg; 13 = Ile; 14 = Leu.

nate, heptanesulphonate and octanesulphonate were used as mobile phase additives showed similar patterns of solute behaviour. As the sulphonate concentration increased, so did the retention of the test solutes. This is further demonstrated in Figs. 3 and 4. In these two instances, the same concentration (and pH) of acetate buffer and of copper ions were used, viz., 10 mM and 0.25 mM, respectively. However, in the first instance the sulphonate concentration was 5 mM, whereas in the second it was 2.5 mM. The general increase in retention times and the improved resolutions are evident from Figs. 3. For example, the peaks due to αAbu and His are well resolved as peaks 9 and 10 in Fig. 3, but when the concentration of the sulphonate is halved (Fig. 4) they are eluted in single peak (peak 8).

Several other interesting features can be observed in Figs. 3 and 4. First, the Val and Nvl peaks are masked by a system peak (peak C) in both chromatograms. In Fig. 3 they are indicated as peak 12, whereas in Fig. 4, where they are completely overlapped by system peak C, they are not indicated. The increase in the retention times of the two amino acids and of the system peak, C, are fortuitously identical as the concentration of the sulphonate is increased from 2.5 to 5 mM. Second, the behaviour of the polar amino acids is strongly influenced by the concentration of the sulphonate. The resolution among the members of this group is better when higher concentrations of sulphonate are used. Finally, Arg is very sensitive to the sulphonate concentration[1]. It appears as the last-eluted solute when 5 mM sulphonate is used (peak 18 in Fig. 3, following the Leu and the Ile peaks). However, at a lower sulphonate concentration its retention is decreased, so that it precedes the Leu and Ile peaks, and merges with Tyr to yield peak 12 in Fig. 4.

All of the above observations can be explained in terms of the retention processes that occur in the column. It is assumed that the copper ions form a charged complex with the amino acids, which in turn forms an ion-pair complex with the alkylsulphonate. Hence the polarity of the amino acids determines the extent of interaction with the sulphonate, and therefore the retention in the column. Moreover, the basic amino acids, being positively charged under the conditions of the experiment, should interact very strongly with the negatively charged sulphonate. This was verified experimentally.
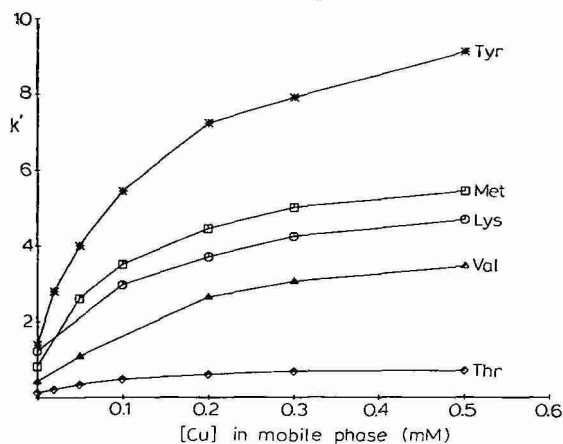
Fig. 5. Dependence of retention on Cu^{2+} concentration. Mobile phase, 0.1 M acetate buffer–5 mM heptanesulphonate with various concentrations of copper(II) acetate. Temperature, 30°C; flow-rate, 2 ml/min; concentration of amino acids, 0.4 mM.

Effect of copper concentration

The copper ions, having the unique ability of complexing amino acids, are essential to the method and the copper concentration in the mobile phase is a very important parameter. The retention of five representative amino acids as a function of the copper content in the mobile phase is illustrated in Fig. 5. The concentration of all the amino acids was 0.4 mM and that of copper in the mobile phase was varied from 0 to 0.5 mM. The acetate buffer and the concentration of the sulphonate were kept constant throughout this set of experiments.

In this range of concentrations, the resulting amino acid–copper complex is an equimolar complex. Hence in the experiments depicted in Fig. 5, when the copper concentration was increased the extent of formation of the copper–amino acids complex also increased. This, in turn, resulted in longer retention times up to a certain copper concentration, above which no further increase in the complex concentration and therefore no retention changes will be observed. This explains the saturation shape of the curves displayed in Fig. 5. These curves can be utilized to calculate the formation constants of the amino acid–Cu^{2+}–alkylsulphonate ternary complex using the methodology developed by Horváth et al.[3] and Grushka and Cohen[4]. The situation in the present instance is complicated by the fact that the sulphonate extracts copper ions into the stationary phase, making the mathematics more complicated. This point will be dealt with in a subsequent publication.

The effect of the copper concentration in the mobile phase on the whole chromatogram is shown in Figs. 2 and 3. Two cases are presented in which the buffer and the sulphonate concentrations were kept constant while the copper concentration was changed. In one instance 0.5 mM copper was used (Fig. 2) and in the other 0.25 mM copper was used (Fig. 3). An improvement in the resolution is obtained at the higher copper concentration, but the analysis time is increased. The improvement in resolution is most notable with the polar amino acids, as was observed in the study of the sulphonate concentration. An example is Asp and Glu. Whereas these two amino acids can be resolved at the higher concentration of copper (peaks 1 and 2 in

Fig. 2), no resolution is observed at the lower concentration (Fig. 3). Asn and Ala exhibit the same behaviour: they arc separated at the higher copper concentration (peaks 4 and 5 in Fig. 2), whereas at the lower copper concentration they are unresolved (peak 4 in Fig. 3). Val and Nvl are separated at the higher copper concentration and appear in the chromatogram following the system peak (indicated by C). However, at the lower copper concentration, Val and Nvl are eluted earlier, while the retention time of the system peak increases a slightly little. The result is overlapping of these peaks, and the solutes are masked by the intense system peak.

The copper ions have an additional role in addition to controlling the retention. *i.e.*, they aid in the detection by the virtue of the absorbance of the charge-transfer complex with the amino acid. In general, as the copper ion concentration is increased the detection limits improve. However, this improvement is counterbalanced by the fact that the increasing copper concentration also increases the retention. As the elution is isocratic, the peaks of the strongly retained solutes are very broad, and their detection limits are far poorer than those of the fast-eluted solutes. Typical detection limits for the less retained amino acids are around 10^{-5} M, whereas they are an order of magnitude higher for the strongly retained amino acids.

Effect of ionic strength

The retention of the amino acids in the present system also depends on the ionic strength. The behaviour of several representative amino acids as a function of ionic strength has been investigated previously[1]. It was shown that the retention times decreased sharply as the concentration of the acetate buffer increased up to 0.1 M. At higher buffer concentrations the changes in the retention times were much more moderate.

Figs. 4 and 6 show examples of the influence of the concentration of the acetate buffer on the chromatograms as a whole. Two cases are presented. The sulphonate and the copper concentrations were kept constant at 2.5 and 0.25 mM, respectively, in both instances. The chromatogram shown in Fig. 4 was obtained with a 10 mM acetate buffer, whereas for Fig. 6 a 25 mM acetate buffer was used. The first notable
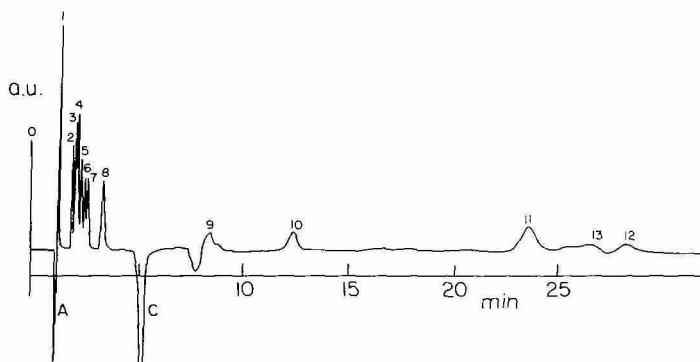
Fig. 6. Effect of ionic strength on the separation of amino acids. Mobile phase, 25 mM acetate buffer–0.25 mM copper(II) acetate–2.5 mM hexanesulphonate. Other conditions as in Fig. 1. Peaks: 1 = Asp + Glu; 2 = Gly; 3 = Ser; 4 = Gln + Asn; 5 = Ala; 6 = Thr; 7 = Hyp; 8 = αAbu + His; 9 = Lys + Val + Nvl; 10 = Met; 11 = Tyr; 12 = Leu; 13 Ile + Arg.
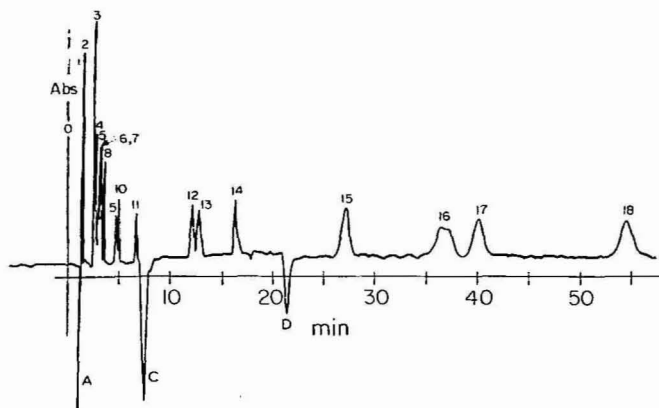
Fig. 7. Chromatogram obtained at 40°C. Mobile phase, 10 mM acetate buffer–0.4 mM copper(II) acetate–0.8 mM heptanesulfonate. Other conditions as in Fig. 1. Peaks: 1 = Asp; 2 = Glu; 3 = Gly + Ser; 4 = Asn; 5 = Gln; 6 = Thr; 7 = Ala; 8 = Thr; 9 = αAbu; 10 = His; 11 = Pro; 12 = Val; 13 = Nvl; 14 = Met; 15 = Tyr; 16 = Ile; 17 = Leu; 18 = Arg.

feature is the interference of the system peaks, which is more serious at the higher buffer concentration. As some of the system peaks appear in the middle range of the chromatogram, they may mask some amino acids such as Pro, Lys, Val and Nvl. For example, the Pro and Lys peaks (peaks 9 and 10, respectively, in Fig. 4) are absent from Fig. 6, being completely masked by the adjacent system peaks. As mentioned before, the Val and Nvl peaks are masked in both instances.

The general trend of the data shows a non-selective decrease in retention with increasing ionic strength. The resolution is relatively independent of the ionic strength, especially at buffer concentrations higher than 0.1 M. The different number of separable solutes is a result of the interference of the system peaks rather than changes in the retention times of the solutes.

Effect of temperature

The influence of temperature on the retention of the amino acids in the present system was briefly examined previously[1]. The general trend observed was a selective
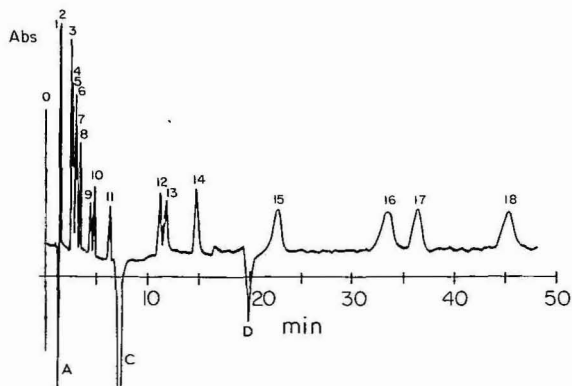
Fig. 8. Chromatogram obtained at 45°C. Conditions and peaks as in Fig. 7.
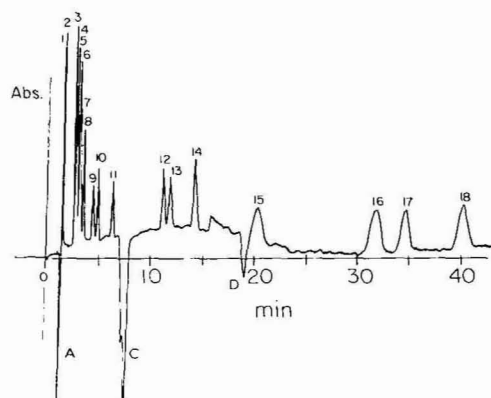
Fig. 9. Chromatogram obtained at 48°C. Conditions and peaks as in Fig. 7.

decrease in the retention times of the amino acids when the temperature was increased. The effect of temperature changes on the whole chromatogram is shown in Figs. 7–9. An identical mixture of amino acids was chromatographed in three systems, each containing 10 mM acetate buffer. 0.8 mM heptanesulphonate and 0.4 mM copper(II) acetate, but at different temperatures. Although the temperature range studied covered only 8°C, the system is sensitive enough to demonstrate a relatively large effect. The general trend is as expected, a decrease in retention times as the temperature is increased. The analysis time for the separation of 18 peaks decreased from 60 min at 40°C to about 40 min at 48°C. However, this is a small enough temperature range so that the selectivities, and hence the resolutions, do not change appreciably. Therefore, temperature can be an important parameter in the optimization of the separation of amino acids. An important effect of temperature on the chromatographic baseline is exhibited in these figures. At higher temperatures the baseline instability is marked, which results in poorer detection limits, partly offsetting the gain in the analysis times.

The problem of the system peaks

The solutes were injected into the column as solutions in pure water. This gave rise to four system peaks in the present system, in addition to peaks due to the solutes. The system peaks are present in all chromatograms, but are best seen in Figs. 7–9, where three of them (A, C and D) are clearly observed. The origins and the processes leading to the formation of these system peaks are discussed elsewhere[5]. They were found to be due to sodium, copper(II) and sulphonate ions, respectively. The fourth system peak (which is present but not visible in the chromatograms shown here) is probably related to the acetate. Using the terminology of ref. 5, it will be called system peak B. Peaks A, C and D are usually negative, whereas peak B is positive in the concentration range of solutes and mobile phase additives employed in this separation system.

Although the information conveyed by the system peaks is extremely useful, they can interfere with the chemical analysis. Of the four system peaks in the present study, peak A is eluted before all the solutes. In fact, it can be employed as the void volume marker. Peak B is usually small and is eluted with the polar amino acids

group. These two system peaks are fairly insensitive to changes in the experimental conditions and therefore do not interfere seriously with the identification or the determination of the amino acids. On the other hand, peak C, which is attributed to the copper ions, is very sensitive to changes in the chromatographic parameters and to the sample concentration. It may appear as an intensely negative peak and, as it may overlap with solute peaks, the latter can be completely masked. System peak D is related to the presence of the sulphonate ions. Although when hexanesulphonate is used peak D is not much influenced by the solute concentration, it may be sufficiently negative to mask adjacent solutes effectively.

The solution to this interference problem lies in an understanding of the nature of these peaks and the reasons for their specific behaviour[5]. When the interference is due to the copper peak (peak C), the sample should contain sufficient copper ions, roughly similr to the total concentration of the injected amino acids. This will compensate for the vacancy of the copper(II) in the sample zone. When peak D causes the difficulties, the solution is even simpler. The sulphonate should be present in the injected sample at roughly the same concentration as in the mobile phase. The old adage of liquid chromatography that the sample should be dissolved in, and diluted with, the mobile phase is particularly true for the system described here. In fact, it was found that frequently the sample had to be enriched with respect to some of the mobile phase components. This was essential in order to counteract the possibly severe local equilibrium disturbances due to the strong interactions between the solutes and the mobile phase components.

CONCLUSION

Not all the 20 or so natural amino acids can be separated in one chromatographic run with the system described here. However, frequently a smaller subset of this group of amino acids needs to be separated. As the "fine tuning" of the selectivity of this system is easy and direct, it is simple to choose suitable conditions for any particular group of amino acids. When a mixture of hydrophobic and basic amino acids needs to be separated, the ionic strength of the mobile phase and the column temperature should be raised, whereas the concentrations of copper and sulphonate should be lowered. On the other hand, when the mixture contains mostly polar, acidic or small amino acids, the above changes should be reversed.

There are several other attractive features of the method. As elution is isocratic and pre- or post-column derivatization of the amino acids is not required, the chromatographic setup is simple and is readily constructed. It includes the minimum number of components essential for an HPLC system: one reservoir, a simple pump, a conventional RP-18 column (40 000 plates/m is sufficient) and a UV detector capable of operating at 235 nm. The equilibration time of the column is short. The linearity of the quantitative determination is excellent, provided that the sample is injected at the appropriate concentrations range[1]. However, several precautions must be taken in order to overcome some practical problems related to the use of copper(II) ions in the mobile phase. These are detailed in our previous paper[1].

REFERENCES

1 S. Levin and E. Grushka, *Anal. Chem.*, 57 (1985) 1830.
2 J. Knox and R. A. Hartwick, *J. Chromatogr.*, 204 (1981) 3.
3 Cs. Horváth, W. Melander and A. Nahum, *J. Chromatogr.*, 186 (1979) 371.
4 E. Grushka and A. S. Cohen, *J. Chromatogr.*, 353 (1986) 389.
5 S. Levin and E. Grushka, *Anal. Chem.*, 58 (1986) 1602.

CHROMSYMP. 1006

RETENTION REPRODUCIBILITY OF THIAZIDE DIURETICS AND RELATED DRUGS IN REVERSED-PHASE HIGH-PERFORMANCE LIQUID CHROMATOGRAPHY

ROGER M. SMITH*, GRACE A. MURILLA* and TONY G. HURDLEY

Department of Chemistry, Loughborough University of Technology, Loughborough, Leicestershire, LE11 3TU (U.K.)

and

RICHARD GILL and ANTHONY C. MOFFAT**

Central Research Establishment, Home Office Forensic Science Service, Aldermaston, Reading, Berkshire RG7 4PN (U.K.)

SUMMARY

A method has been developed for the separation of thiazide diuretics and a number of related drugs by high-performance liquid chromatography on an ODS-Hypersil column with acetonitrile–1% aqueous acetic acid as the eluent. The effects caused by changes in the separation conditions on the reproducibility and robustness of alternative methods for recording retentions (including capacity factors, retention indices based on the alkyl aryl ketone scale, and relative capacity factors compared to a thiazide standard) have been examined. The results confirm that good interlaboratory reproducibility will only be achieved when operators control the temperature of the column and use the same brand of column packing material. The retentions should be recorded using a relative method, as these were found to be virtually independent of minor variations in the eluent composition.

INTRODUCTION

The retention time of a compound in high-performance liquid chromatography (HPLC), during a single analytical determination, is usually very consistent, and a close correspondence is obtained between analytes and standards. However, retention properties are susceptible to even small changes in the chromatographic conditions, such as the proportion of the organic component, the pH or ionic strength of the eluent, or the temperature of the column. They are also very sensitive to the brand of column packing material used, even if such materials are nominally equivalent, and retentions can even differ with different batches of the same brand. As a conse-

---

* Present address: Government Chemist Department, P.O. Box 20753, Nairobi, Kenya.
** Present address: Home Office Forensic Science Laboratory, Hinchingbrooke Park, Huntingdon, Cambridge PE18 8NP, U.K.

quence, it is difficult to identify samples by comparisons with results from other laboratories or to build up compilations of retention values in libraries or databases. Each laboratory must, instead, calibrate each analytical system using a full set of standard compounds, or use interlaboratory databases for preliminary comparisons, followed by a direct calibration with a limited number of credible compounds for each unknown.

As part of a series of studies aimed at improving the reproducibility of retention values in HPLC so that values obtained in one laboratory can be used in another, a number of drug separations of forensic interest have been examined. This work has included detailed studies on the influence of the eluent composition, operating conditions, and the nature of the stationary phase on the retentions of barbiturates[1,2] and local anaesthetic drugs[3]. The purpose of this approach was to identify the factors that need to be closely controlled in order to obtain consistent results and to compare different methods of recording retentions[1-4]. Experience with the various drug separations showed that, for reproducible results, the pH of the eluent and the temperature of the column need to be closely controlled and, if possible, a single batch of the stationary phase (and certainly the same brand of packing material) should be used.

The most robust results were obtained when the retentions were recorded as relative values, either as retention indices compared to the alkyl aryl ketones or as relative retention times or relative capacity factors compared to a related standard. Conventionally, capacity factors $[k' = (t_R - t_0)/t_0]$ have been used to record retentions in HPLC but their calculation is very dependent on the value measurement for the column void volume (t_0). As yet there is no standard method for this measurement and, although numerous different techniques have been proposed, these often give different values on the same column[5]. In practice, individual laboratories may use different techniques, while in many reports the method used is not stated. However, even small absolute changes in this value can cause large changes in the calculated values of k' from the same measured retention times.

Although Kováts retention indices, based on the n-alkanes have been widely used in gas–liquid chromatography (GLC) to define retentions, so far, similar concepts have not gained wide acceptance in HPLC. The first proposals were made by Baker and Ma[6], who suggested that the alkan-2-ones could be used as the basis of a scale. However, these compounds have only a weak ultraviolet absorption, and Smith[7] suggested that the homologous alkyl aryl ketones would be more readily detected. In both cases, the standards showed a linear relationship between the number of carbon atoms and log k', and the retention indices of neutral sample compounds were virtually independent of the proportion of methanol–water in eluents over a wide range. The application of retention indices based on the alkyl aryl ketone scale has subsequently been extended by the selection of a set of column test compounds the indices of which can be used to characterise column differences and mobile-phase selectivities in a similar manner to the use of McReynolds constants in GLC[8-10]. The value of relative retention measurements was confirmed by an interlaboratory collaborative study of the separation of the barbiturates[11].

As all these drug separations used aqueous methanol as eluents, studies have recently been undertaken to confirm that the retention index concept is also generally valid with other modifiers of the mobile phase, such as acetonitrile or tetrahydro-

furan[12]. This work confirmed that there was a linear relationship between the log k' of the ketones and their carbon number. The variations of the retention indices of test compounds with different proportions of acetonitrile or tetrahydrofuran suggested that these systems might be less robust and show greater changes in retention indices with the composition of the mobile phase than with methanol.

Based on this work, the present paper examines in detail the application of a separation system in which a mobile phase containing acetonitrile is used for the separation of the thiazide diuretic drugs. Previously, a number of HPLC methods have been reported for the determination of individual thiazide diuretics because of their importance as widely used antihypertensive drugs. However, most of these methods have concentrated on the quantitative determination of a single or a small group of thiazides as known constituents in a biological fluid (e.g. hydrochlorothiazide)[13]. A few studies have examined the identification of the thiazides[14–16], and a more detailed study has recently been reported by De Croo et al.[17], who examined the effect of eluent composition, organic modifier, pH, and temperature on the capacity factors of a number of diuretic drugs. In a second paper, they examined the differences between C_2, C_8 and C_{18} alkyl-bonded stationary phases for this separation[18].

The present paper has adapted a mobile phase of acetonitrile–1% aqueous acetic acid, proposed by Tisdall et al.[15]. Our work included a detailed examination of the reproducibility of the method and of the robustness of different approaches to recording retentions.

EXPERIMENTAL

Chemicals and eluents

Reference samples of alkyl aryl ketones (acetophenone, propiophenone, butyrophenone, and valerophenone) and column test compounds (toluene, nitrobenzene, 2-phenylethanol, N-methylaniline and p-cresol) were of laboratory reagent grade from a range of different suppliers. Acetonitrile was of HPLC grade (Fisons Scientific Apparatus, Loughborough, U.K.) and acetic acid was AnalaR grade (BDH Chemicals, Poole, U.K.).

The thiazide diuretic drugs and related compounds (Table I) were from the reference collection at the Central Research Establishment, Home Office Forensic Science Service. They were made up as solutions in acetonitrile (50–100 mg/l). The following HPLC column packing materials were used: ODS-Hypersil, 5 μm, batches 10/1229 and 6/868 (Shandon Southern, Runcorn, U.K.), ODS-Zorbax (Du Pont, Wilmington, DE, U.S.A.), ODS-Techsil 5 C18, 5 μm, and ODS-Techsphere, 5 μm, (HPLC Technology, Macclesfield, U.K.), Lichrosorb RP-18 (Merck, Darmstadt, F.R.G.), Nucleosil 5 C_{18}, 5 μm, (Machery-Nagel, Duren, F.R.G.). Columns (100 × 5 mm, Shandon Southern) were prepared by slurry packing.

Routine HPLC method[19]

The separations were carried out using a M6000 pump (Waters Chromatography Division, Milford, MA, U.S.A.) and a CE272 Spectrophotometric detector (Cecil Instruments, Cambridge, U.K.), operated at 271 nm. The samples (10 μl), dissolved in acetonitrile, were injected using a 7125 valve (Rheodyne, Cotati, CA,

TABLE I

THIAZIDE DIURETICS AND RELATED DRUGS USED IN THE STUDY

Compound number	Compound	Structure	X	R^1	R^2
Thiazide diuretics			CF_3	H	$CH_2C_6H_5$
1	Bendrofluazide		Cl	H	$CH_2SCH_2C_6H_5$
2	Benzthiazide				(3,4-dehydro)
3	Chlorothiazide		Cl	H	H(3,4-dehydro)
4	Cyclopenthiazide		Cl	H	$CH_2C_5H_9$
5	Cyclothiazide		Cl	H	Norborn-5-en-2-yl
6	Hydrochlorothiazide		Cl	H	H
7	Hydroflumethiazide		CF_3	H	H
8	Methyclothiazide		Cl	CH_3	CH_2Cl
9	Polythiazide		Cl	CH_3	$CH_2SCH_2CF_3$
10	Trichlormethiazide		Cl	H	$CHCl_2$

Non-thiazide diuretic drugs

11   Chlorthalidone

12   Clopamide

13   Clorexolone

14   Mefruside

15   Metolazone

16   Quinethazone

U.S.A.), fitted with a 20-μl loop, into an ODS-Hypersil column (batch 10/1229) (160 × 5 mm I.D.) at ambient temperature. The column was eluted with acetonitrile–1% aqueous acetic acid (30:70, v/v) at 2 ml/min.

Reproducibility studies

Reproducibility studies of the HPLC separation were carried out using a 4010 pump (Pye Unicam, Cambridge, U.K.) and 153 fixed-wavelength detector (Altex Scientific, Beckman Instruments, San Ramon, CA, U.S.A.), set at 254 nm. The samples (10 μl) were injected using a Rheodyne 7125 valve into an ODS-Hypersil column (batch 10/1229) (100 × 5 mm I.D.), encased in a water jacket at 30°C. The column was eluted with acetonitrile–1% aqueous acetic acid (35:65, v/v) at 2 ml/min, which had been passed through a precolumn, containing silica, placed between the pump and injection valve. The column void volume was determined by using an aqueous solution of sodium nitrate (12.16 mg/ml). The chromatographic peaks were recorded using a C-R3A integrator (Shimadzu, Tokyo, Japan).

Calculations

The retention times were determined in triplicate, and the mean values were reported. Retention indices were determined as described previously using a least-squares correlation between the logarithm of the capacity factors for the alkyl aryl ketones and their carbon numbers[7]. The retention indices are based on *RI*(ketones) = number of carbon atoms × 100. Relative capacity factors were calculated relative to polythiazide.

RESULTS AND DISCUSSION

As part of a process of rationalisation of HPLC methods within U.K. Forensic Science Laboratories, ODS-Hypersil has been selected as the standard reversed-phase column packing material to facilitate the transfer of methods and data between laboratories. A common batch of this packing material is supplied to each laboratory. The present study therefore commenced with the conversion of the method proposed by Tisdall et al.[15], for a μBondapak C$_{18}$ column, to an ODS-Hypersil column.

Development of the eluent system

In their work, Tisdall et al.[15] showed that all the commonly used diuretics could be separated on a μBondapak C$_{18}$ column using acetonitrile–1% aqueous acetic acid (either 8:92 or 35:65) eluents. The former, weaker eluent was primarily required to separate chlorothiazide and hydrochlorothiazide from interfering components in biological fluids and was not studied in the present work.

When the second eluent, acetonitrile–1% aqueous acetic acid (35:65) was used to separate a series of thiazide diuretics and related compounds (Table I) on the ODS-Hypersil column, the order of elution was very similar to that reported[15], except that in this case polythiazide was eluted just before bendrofluazide whereas the reverse order had been obtained on the μBondapak C$_{18}$ column. Most of the analytes gave good peak shapes. Multiple peaks were obtained from cyclothiazide, but only the two major peaks have been noted in this report. Similar multiple peaks were also found by Tisdall et al.[15] and De Croo et al.[17] and were ascribed to the presence of

isomers. Metolazone, quinethazone, and trichlormethiazide slowly decomposed on standing in the mobile phase, and after a few days, additional peaks were observed. Therefore, fresh samples had to be prepared at frequent intervals.

It was found that isocratic eluents with acetonitrile contents in the range 30-40% gave satisfactory results for typical thiazides. From these results, acetonitrile-1% aqueous acetic acid (30:70, v/v) was selected for routine use[19], as this gave sufficient retention of the early-eluted components without unduly prolonging the assay. Typical values of the capacity factors for the thiazide diuretics and related compounds were determined at ambient temperature (Table II)[19]. Fig. 1 shows the separation of eight compounds on a 16-cm column, demonstrating the good peak shapes.

Retention reproducibility

As part of the series of studies[1-3] aimed at assessing the factors that influence reproducibility of drug separations of forensic interest, a more detailed examination was then carried out under carefully controlled conditions to investigate the retention properties of the diuretic drugs. In order to identify any factors that need to be closely controlled in the separation of the diuretic drugs, it was necessary to determine the magnitude of any effects arising from small changes in the operating conditions or eluent composition. An eluent of acetonitrile-1% aqueous acetic acid (35:65)[15], with a 10-cm column, maintained at 30°C, was selected for this work and each of the variables was altered in turn.

TABLE II

CAPACITY FACTORS AND RELATIVE CAPACITY FACTORS OF THIAZIDE DIURETICS AND RELATED DRUGS

ODS Hypersil column (160 × 5 mm); eluent, acetonitrile-1% aqueous acetic acid (30:70); ambient temperature.

Compound	Capacity factor	Relative capacity factor × 100
Thiazide diuretics		
Chlorothiazide	0.54	3.5
Hydrochlorothiazide	0.70	4.6
Hydroflumethiazide	1.30	8.6
Trichlormethiazide	3.10	20.5
Methyclothiazide	3.82	25.3
Benzthiazide	9.32	61.8
Cyclothiazide 1	10.78	71.4
Cyclothiazide 2	11.91	78.9
Polythiazide	15.09	100.0
Bendrofluazide	15.35	101.7
Cyclopenthiazide	16.45	109.0
Non-thiazide diuretic drugs		
Quinethazone	0.67	4.4
Chlorthalidone	1.28	8.5
Metolazone	4.89	32.4
Clorexolone	7.26	48.1
Mefruside	8.67	57.4
Clopamide	4.01	26.6
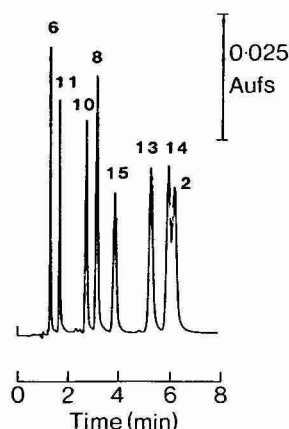
Fig. 1. Separation of diuretic drugs on ODS-Hypersil (160 × 5 mm). Eluent, acetonitrile–1% aqueous acetic acid (30:60) at 2 ml/min; ambient temperature; detection at 271 nm. Peaks correspond to Table I.

The study also set out to compare whether alternative methods to capacity factors for recording retention values might be more robust and less susceptible to the variations in conditions. One of the problems with the use of capacity factors for identifications is their susceptibility to small differences in the eluent composition and the value of the column void volume. In their paper, De Croo *et al.*[17] examined a number of alternative systems for the determination of t_0 for this assay and selected the use of ^2H_2O–acetonitrile as a marker but this requires a refractive-index detector for detection. They found that different concentrations of sodium nitrate gave dif-

TABLE III

CAPACITY FACTORS OF ALKYL ARYL KETONES AND COLUMN TEST COMPOUNDS

ODS Hypersil column (100 × 5 mm); temperature, 30°C; eluent acetonitrile–1% aqueous acetic acid (35:65).

Compound	Capacity factor	Retention index	Retention index, acetonitrile–buffer, pH 7 (30:70)*
Retention index standards			
Acetophenone	2.76	800	800
Propiophenone	6.00	900	900
Butyrophenone	11.89	1000	1000
Valerophenone	24.13	1100	1100
Column test compounds			
N-Methylaniline	0.75	615	828
2-Phenylethanol	1.45	706	713
p-Cresol	2.30	771	776
Nitrobenzene	4.68	870	869
Methylbenzoate	5.51	888	886
Toluene	12.72	1009	996

* Comparison with retention indices obtained in an earlier study for a similar eluent[12].

Fig. 2. Effect of the proportion of acetonitrile on (a) capacity factors, (b) retention indices and (c) relative capacity factors of selected thiazide diuretics and related drugs. Numbers correspond to Table I.

ferent values, but if a dilute solution of fixed concentration is used (as in the present study) the void volume values will be reproducible.

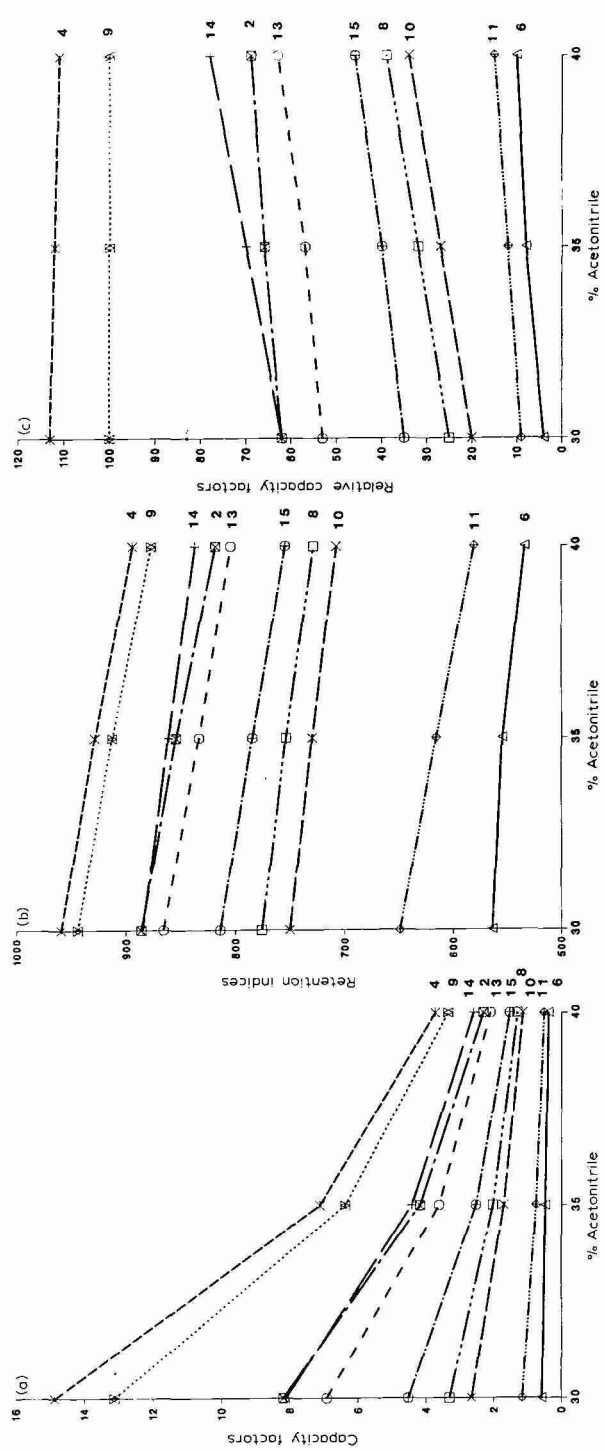*Separation selectivity*

The alkyl aryl ketones (acetophenone–valerophenone) and the column test compounds (toluene, nitrobenzene, *p*-cresol, 2-phenylethanol, and N-methylaniline) were chromatographed with acetonitrile–1% aqueous acetic acid (35:65), and the capacity factors and retention indices were calculated (Table III). With the exception of N-methylaniline, which would be protonated in acetic acid, the indices of the column test compounds were very similar to those measured previously on the same column when acetonitrile–phosphate buffer, pH 7 (30:70) is used as the eluent[12]. The changes in pH and buffer components, therefore, appear to have little effect on the overall selectivity of the separation system. The retention indices for the column test compounds were also determined in all of the present studies but are usually not

TABLE IV

EFFECT OF THE PROPORTION OF ACETONITRILE IN THE MOBILE PHASE ON THE CA-PACITY FACTORS, RETENTION INDICES, AND RELATIVE CAPACITY FACTORS OF THIA-ZIDE DIURETICS AND RELATED DRUGS

ODS Hpersil column (100 × 5 mm); temperature, 30°C. Relative capacity factors calculated relative to polythiazide.

Compound	Capacity factor			Retention index			Relative capacity factor × 100		
	Acetonitrile (%)			Acetonitrile (%)			Acetonitrile (%)		
	30	35	40	30	35	40	30	35	40
Thiazide diuretics									
Chlorothiazide	0.47	0.40	0.32	539	527	508	3.6	6.3	9.6
Hydrochlorothiazide	0.58	0.49	0.38	564	555	534	4.4	7.3	11.3
Hydroflumethiazide	1.13	0.85	0.63	645	632	615	8.6	13.3	18.8
Trichlormethiazide	2.66	1.72	1.14	750	730	708	20.3	26.9	34.0
Methyclothiazide	3.31	2.04	1.30	776	754	729	25.2	31.9	38.8
Benzthiazide	8.19	4.19	2.31	886	855	819	62.4	65.6	69.0
Cyclothiazide 1	9.38	4.78	2.85	903	873	852	71.4	74.8	85.1
Cyclothiazide 2	10.28	5.21	3.52	914	885	886	78.3	81.5	105.1
Polythiazide	13.13	6.39	3.35	944	913	878	100.0	100.0	100.0
Bendrofluazide	13.53	6.60	3.45	948	918	883	103.0	103.3	103.0
Cyclopenthiazide	14.87	7.13	3.73	959	929	895	113.3	111.6	111.3
Non-thiazide diuretic drugs									
Quinethazone	0.61	0.46	0.35	570	546	522	4.6	7.2	10.4
Chlorthalidone	1.16	0.76	0.51	649	616	581	8.8	11.9	15.2
Metolazone	4.52	2.54	1.53	814	785	755	34.4	39.8	45.7
Clorexolone	6.92	3.63	2.10	866	834	805	52.7	56.8	62.7
Mefruside	8.11	4.43	2.60	885	862	838	61.8	69.3	77.6
Clopamide	4.34	3.64	2.64	809	835	841	33.1	57.0	78.8
Column void volume (ml)	1.02	0.98	0.94						

reported, as they were unaffected by the changes in operating conditions or eluent composition.

Effect of proportion of acetonitrile

The separation of the thiazide and related diuretics were then examined using different proportions of acetonitrile in the eluent (30–40%). Over this range, there were considerable changes in the capacity factors of both the alkyl aryl ketones and the diuretic drugs (Table IV, Fig. 2a). A comparison of the results for acetonitrile-1% aqueous acetic acid (30:70) in Table IV with those obtained in the initial work (Table II) emphasises the problems of interlaboratory reproducibility. Both sets of capacity factors were determined on columns packed with the same batch of packing material, but the studies were carried out in different laboratories with different HPLC systems, column sizes, and temperatures.

For each eluent composition, the logarithmic relationship between the capacity factors of the alkyl aryl ketones and their carbon numbers was linear (Fig. 3) and the slope decreased as the proportion of acetonitrile increased (Table V). Based on these values, the retention indices of the diuretic drugs were calculated (Table IV, Fig. 2b). These showed some changes with eluent composition, but the effects were much smaller than for the capacity factors. Previously, De Croo *et al.*[17] found that the capacity factors of the diuretic drugs behaved similarly as the proportion of
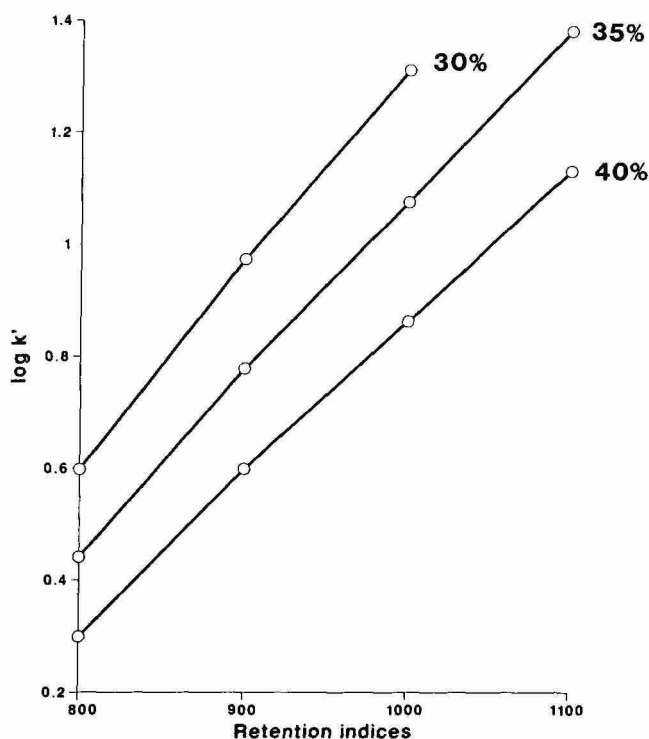

Fig. 3. Comparison of capacity factors of alkyl aryl ketones compared to their retention indices in different proportions of acetonitrile.

TABLE V

RELATIONSHIP BETWEEN THE LOGARITHM OF CAPACITY FACTORS AND NUMBER OF CARBON ATOMS FOR ALKYL ARYL KETONES IN DIFFERENT PROPORTIONS OF ACETONITRILE

Amount acetonitrile in eluent (%)	Correlation coefficient	Slope ($\times 10^3$)	Intercept
30	0.9995	3.56	-2.25
35	0.9996	3.11	-2.04
40	0.9996	2.75	-1.89

acetonitrile changed, with the exception of chlorthalidone. In the present study, clopamide appeared to be anomalous, as its retention index increased with the proportion of acetonitrile, whereas the retention indices for all the other compounds decreased. This probably reflects the fact that clopamide, which is basic, will be protonated under the separation conditions and thus will interact with the stationary phase in a way different from that of the other compounds.

In the earlier study on the barbiturates, relative retention times and relative capacity factors (compared to a barbiturate standard) were found to be even more robust than retention indices as a method of recording retentions[11]. It appeared that, because of the close structural similarities of the barbiturates, they would all interact in similar way with the column. If a barbiturate was selected as the internal standard, it would therefore compensate for any changes in the specific interactions in the separation. In the present study, the relative capacity factors were calculated using polythiazide as a standard (Table IV, Fig. 2c). This compound was chosen, because it has a relatively long retention, and would be less susceptible to errors in the measurement of the column void volume or in retention times. For some of the diuretics, such as benzofluazide and cyclopenthiazide, this method compensated well for the changing proportion of acetonitrile in the eluent, but for many of the other diuretics the relative capacity factors varied considerably. Even if different diuretic drugs had been considered as the standard compound, it is clear that none of them would have been able to compensate for the behaviour of all the other drugs. The same problem would have also been encountered if relative retention times had been examined, although they usually have the advantage that they can often be reported directly by many integrators.

These significant changes in the retention indices and relative capacity factors on changing the composition of acetonitrile were not unexpected, as in the preliminary experiments the retentions of the column test compounds varied considerably in this composition range[12]. However, both relative retention methods showed much smaller changes than the capacity factors. Close control over the composition of acetonitrile is therefore likely to be necessary to obtain good interlaboratory reproducibility, much more so than in the separations of the barbiturates[1] or local anaesthetics[3].

Effect of proportion of acetic acid and the pH

A series of separations were carried out in which the proportion of acetic acid

was altered from 0.7 to 1.5% (Table VI). The capacity factors and retention indices of all the compounds were virtually unaffected, except for clopamide, which showed a k' value of 4.11 at both 0.7 and 1.5% acetic acid, higher than previously measured on the same column for an eluent with 1% acetic acid ($k' = 3.64$). However, reinvestigation of the 1% acetic acid eluent also gave $k' = 4.11$. Presumably this drug must have an unusual interaction with the column or the surface properties of the packing material appear to have altered during these experiments with different concentrations of acetic acid.

Altering the proportion of acetic acid would also have had a minor effect on the pH of the eluent. However, the thiazides are weak acids (pK_a 8–10)[20] and would not be ionised in this eluent and should therefore be unaffected. In their study, De Croo et al.[17] found that there was no effect on the retentions of the thiazides over the range pH 3–7, but the retentions of some of the non-thiazides altered markedly. To determine whether pH was a critical factor in the present study, the pH of the aqueous solution (normally pH 2.62) was deliberately altered to pH 3.5 with sodium hydroxide or to pH 2.5 with hydrochloric acid, before the acetonitrile was added. With the exception of clopamide (pH 2.5, $RI = 849$ and pH 3.5, $RI = 706$), both the capacity factors and retention indices of all the drugs were unaffected by these

TABLE VI

EFFECT OF THE PROPORTION OF ACETIC ACID ON THE CAPACITY FACTORS OF THIAZIDE DIURETICS AND RELATED DRUGS

ODS Hypersil column (100 × 5 mm); eluent, acetonitrile–aqueous acetic acid (35:65); temperature, 30°C.

Compound	Amount acetic acid in eluent (%)		
	0.7	1.0	1.5
Thiazide diuretics			
Chlorothiazide	0.38	0.40	0.37
Hydrochlorothiazide	0.47	0.49	0.46
Hydroflumethiazide	0.82	0.85	0.82
Trichlormethiazide	1.68	1.72	1.67
Methyclothiazide	1.99	2.04	1.99
Benzthiazide	4.07	4.19	4.12
Cyclothiazide 1	4.64	4.78	4.69
Cyclothiazide 2	5.06	5.21	5.11
Polythiazide	6.22	6.39	6.24
Bendrofluazide	6.42	6.60	6.45
Cyclopenthiazide	6.92	7.13	7.04
Non-thiazide diuretic drugs			
Quinethazone	0.47	0.46	0.54
Chlorthalidone	0.71	0.76	0.72
Metolazone	2.46	2.54	2.50
Clorexolone	3.51	3.63	3.63
Mefruside	4.30	4.43	4.37
Clopamide	4.10	3.64*	4.11
Column void volume (ml)	0.98	0.98	0.98

* On repeating separation with 1.0% acetic acid $k' = 4.11$ (see Discussion).

changes. The proportion of acetic acid and the pH are clearly not critical factors in this assay, except for the basic diuretic, clopamide.

Effect of temperature

The temperature of the column was altered from 10–40°C, and the capacity factors, retention indices, and relative capacity factors of the drugs and column test compounds were calculated (Table VII). All compounds showed a marked decrease in their capacity factors with increasing temperature and an increase in efficiency, *e.g.* polythiazide $N = 554$ at 10°C and $N = 2128$ at 40°C. In a similar study over the range 25–50°C, De Croo *et al.*[17] found that the thiazide drugs gave a linear relationship between their capacity factors and the reciprocal of the absolute temperature (Van 't Hoff plots).

The retention indices showed much smaller variations and, over a limited temperature range, would be effectively constant. The relative capacity factors changed to different extents, depending on the compound. These results again confirm the advantages of relative retention values over direct measurements. If the columns are nominally controlled at the same temperature in different laboratories, any small differences in temperature which may occur are unlikely to have a significant effect on relative capacity factors or retention indices but might still have a marked effect on absolute capacity factors.

On comparing the results from the initial study at ambient temperature (Table II) with the values at 30°C for the same composition (Table IV), both the capacity factors and relative capacity factors were found to differ, confirming that, for identification purposes, temperature control is important for this HPLC separation.

Reproducibility of repeated measurements

The separations under the standard conditions [acetonitrile–1% aqueous acetic acid (35:65)] with the same column and equipment were repeated daily for four days, using fresh preparations of eluent, and were compared with the initial chromatogram to test the reproducibility. The mean values, standard deviations (S.D.), and coefficients of variance (C.V.) for the capacity factors and retention indices were calculated (Table VIII). For almost all the samples, the results from the different runs were very close with variations similar to those obtained in earlier drug separation studies[1,3], showing that high reproducibility can be obtained if the conditions are carefully controlled. However, the capacity factors of clopamide and quinethazone had changed since the first analysis. Although the repeated separations on successive days gave consistent values these were markedly different from the first measurement. Apparently during the study with different pH eluents the nature of the column surface had been altered.

Effect of the stationary phase

Differences in the retentions of compounds on nominally equivalent stationary phases, such as ODS-silicas, are probably the greatest source of differences between separations reported in the literature. Major differences in the properties of bonded-phase columns can occur, even if they are coated with the same alkyl chains, because different manufacturers use different silicas and different bonding methods. Furthermore, batch-to-batch variations in the efficiency of the bonding reactions and capping

TABLE VII

EFFECT OF TEMPERATURE ON THE CAPACITY FACTORS, RETENTION INDICES, AND RELATIVE CAPACITY FACTORS OF ALKYL ARYL KETONES, COLUMN TEST COMPOUNDS, THIAZIDE DIURETICS, AND RELATED DRUGS

ODS Hypersil column (100 × 5 mm); eluent, acetonitrile–1% aqueous acetic acid (35:65).

Compound	Capacity factor				Retention index				Relative capacity factor × 100			
	Temperature (°C)				Temperature (°C)				Temperature (°C)			
	10	20	30	40	10	20	30	40	10	20	30	40
Retention index standards												
Acetophenone	3.67	3.37	2.76	2.50								
Propiophenone	8.26	7.57	6.00	5.32								
Butyrophenone	17.05	15.56	11.89	10.39								
Valerophenone	36.71	33.21	24.13	20.76								
Column test compounds												
2-Phenylethanol	1.73	1.69	1.45	1.35	699	706	706	709				
p-Cresol	3.20	2.89	2.30	2.04	780	777	771	768				
Nitrobenzene	6.90	6.04	4.68	4.00	880	875	870	864				
Methyl benzoate	7.35	6.72	5.31	4.70	889	889	888	887				
Toluene	18.49	16.69	12.72	11.00	1009	1008	1009	1009				

Thiazide diuretics

Chlorothiazide	0.65	0.52	0.40	0.32	571	551	527	504	5.3	5.3	5.3	6.3	6.4
Hydrochlorothiazide	0.80	0.64	0.49	0.40	598	578	555	536	6.5	6.5	6.5	7.7	8.0
Hydroflumethiazide	1.47	1.15	0.85	0.68	678	656	632	611	12.0	11.6	11.6	13.3	13.6
Trichlormethiazide	3.02	2.41	1.72	1.38	772	753	730	712	24.6	24.3	24.3	26.9	27.5
Methyclothiazide	3.61	2.89	2.04	1.64	796	777	754	737	29.4	29.2	29.2	31.9	32.7
Benzthiazide	7.71	6.26	4.19	3.34	895	879	855	838	62.8	63.2	63.2	65.6	66.5
Cyclothiazide 1	8.39	7.01	4.78	3.88	906	894	873	859	68.4	70.8	70.8	74.8	77.3
Cyclothiazide 2	9.37	7.75	5.21	4.20	920	907	885	871	76.4	78.3	78.3	81.5	83.7
Polythiazide	12.27	9.90	6.39	5.02	956	940	913	896	100.0	100.0	100.0	100.0	100.0
Bendrofluazide	12.29	10.29	6.60	5.14	963	945	918	899	105.8	103.9	103.9	103.3	102.4
Cyclopenthiazide	12.82	10.70	7.13	5.73	961	950	929	915	104.5	108.1	108.1	111.6	114.1

Non-thiazide diuretic drugs

Quinethazone	0.61	0.55	0.46	0.40	563	558	546	536	5.0	5.6	5.6	7.2	8.0
Chlorthalidone	1.04	0.94	0.76	0.66	633	629	616	607	8.5	9.5	9.5	11.9	13.1
Metolazone	3.78	3.37	2.54	2.20	802	797	785	779	30.8	34.0	34.0	39.8	43.8
Clorexolone	4.48	4.66	3.63	3.29	835	840	834	836	36.5	47.1	47.1	56.8	65.5
Mefruside	6.73	5.98	4.43	3.80	877	893	862	856	54.8	60.4	60.4	69.3	75.7
Clopamide	5.51	4.40	3.64	3.11	851	833	835	828	44.9	44.4	44.4	57.0	61.9
Column void volume (ml)	0.98	0.98	0.98	0.98									

TABLE VIII

REPRODUCIBILITY OF THE CAPACITY FACTORS AND RETENTION INDICES OF THIAZIDE DIURETICS AND RELATED DRUGS

ODS Hypersil column (100 × 5 mm); eluent, acetonitrile–1% aqueous acetic acid (35:65); temperature, 30°C. Based on five separate determinations on different days on the same systems with fresh eluent.

Compound	Capacity factor			Retention index		
	Mean	S.D.	C.V. (%)	Mean	S.D.	C.V. (%)
Thiazide diuretics						
Chlorothiazide	0.40	0.01	2.5	526	2.8	0.53
Hydrochlorothiazide	0.48	0.01	2.1	552	1.8	0.33
Hydroflumethiazide	0.83	0.01	1.2	630	1.3	0.21
Trichlormethiazide	1.68	0.02	1.2	729	1.1	0.15
Methyclothiazide	2.00	0.03	1.5	753	1.3	0.17
Benzthiazide	4.07	0.08	2.0	853	1.8	0.21
Cyclothiazide 1	4.65	0.09	1.9	871	1.1	0.13
Cyclothiazide 2	5.06	0.10	2.0	883	1.2	0.14
Polythiazide	6.19	0.14	2.3	911	1.2	0.13
Bendrofluazide	6.41	0.14	2.2	916	1.2	0.13
Cyclopenthiazide	6.92	0.16	2.3	927	1.5	0.16
Non-thiazide diuretic drugs						
Quinethazone*	0.57	0.01	1.8	578	3.0	0.52
Chlorthalidone	0.74	0.02	2.7	613	2.3	0.38
Metolazone	2.48	0.04	1.6	783	1.5	0.19
Chlorexolone	3.54	0.06	1.7	833	1.1	0.13
Mefruside	4.32	0.08	1.9	861	1.1	0.13
Clopamide*	4.73	0.10	2.1	874	4.0	0.46

    * Based on four measurements on consecutive days. Fifth value measured on same column two weeks earlier; quinethazone, $k' = 0.46$, $RI = 546$; clopamide, $k' = 3.64$, $RI = 835$.

steps by a single manufacturer are also significant. Even larger changes are found, if different alkyl bonded groups are used. De Croo *et al.*[18] compared the retentions of RP-2, RP-8, and RP-18 Lichrosorb and found that, although the thiazides gave fairly similar results, large differences were seen for the non-thiazide diuretic drugs.

    The separation of the drugs was therefore repeated, using a range of different ODS-silica packing materials. Two different batches of ODS-Hypersil were also included in the comparison. In the study of the separation of barbiturates, negligible differences were found between batches of this packing material[2], and virtually identical results were also obtained in this study (Table IX). However, considerable variations in the capacity factors were observed for both the diuretic drugs and the column test compounds on the other brands of packing material.

    The retention indices were calculated for each column, but the results have a greater spread than would be useful for identification purposes (Table X). The ODS-Zorbax column gave particularly unusual results with much smaller retention indices that the other columns. This effect was reflected also by the column test compounds on this column, particularly the low retention index value for *p*-cresol. Similar results with this column material were previously noted in column comparison studies[9].

TABLE IX

EFFECT OF ODS-SILICA COLUMN PACKING MATERIAL ON THE CAPACITY FACTORS OF ALKYL ARYL KETONES, COLUMN TEST COMPOUNDS, THIAZIDE DIURETICS, AND RELATED DRUGS

Columns, 100 × 5 mm; eluent, acetonitrile–1% aqueous acetic acid (35:65); temperature, 30°C. Columns: H1, ODS-Hypersil Batch 10/1229; H2, ODS-Hypersil Batch 6/868; Z, ODS-Zorbax; T, Techsil 5 C18; TS; Techsphere ODS; L, Lichrosorb RP 18; N, Nucleosil 5 C18.

| Compound | Capacity factor | | | | | | | Mean | S.D. |
| | Column material | | | | | | | | |
	H1	H2	Z	T	TS	L	N		
Retention index standards									
Acetophenone	2.76	2.78	5.11	2.67	3.58	3.57	3.80	3.47	0.86
Propiophenone	6.00	5.94	11.07	5.51	7.84	7.56	8.02	7.42	1.90
Butyrophenone	11.89	11.68	22.18	10.42	15.66	14.65	15.50	14.57	3.93
Valerophenone	24.13	23.67	45.86	20.33	32.17	29.34	30.83	29.48	8.40
Column test compounds									
2-Phenylethanol	1.45	1.50	2.34	1.40	1.74	1.91	1.93	1.75	0.34
p-Cresol	2.30	2.36	3.32	2.13	2.78	2.94	3.03	2.69	0.44
Nitrobenzene	4.68	4.66	8.18	4.51	6.08	6.00	6.54	5.81	1.33
Methyl benzoate	5.31	5.22	9.92	4.95	6.97	6.81	7.20	6.63	1.72
Toluene	12.72	11.81	23.65	10.71	17.37	15.63	16.19	15.44	4.37
Thiazide diuretics									
Chlorothiazide	0.40	0.43	0.41	0.38	0.43	0.48	0.52	0.44	0.05
Hydrochlorothiazide	0.49	0.53	0.53	0.46	0.52	0.60	0.64	0.54	0.06
Hydroflumethiazide	0.85	0.91	1.00	0.83	0.96	1.05	1.16	0.97	0.12
Trichlormethiazide	1.72	1.90	2.17	1.67	1.97	2.14	2.41	2.00	0.26
Methyclothiazide	2.04	2.27	2.63	2.00	2.33	2.55	2.87	2.38	0.32
Benthiazide	4.19	4.72	5.40	3.88	4.75	5.17	5.72	4.83	0.65
Cyclothiazide 1	4.78	5.38	6.17	4.31	5.39	6.29*	6.36	5.40	0.79
Cyclothiazide 2	5.21	5.82	6.74	4.64	5.88	6.29*	6.87	5.92	0.80
Polythiazide	6.39	7.04	8.59	5.91	7.44	7.75	8.81	7.42	1.07
Bendrofluazide	6.60	7.26	9.08	6.03	7.81	7.98	8.99	7.68	1.14
Cyclopenthiazide	7.13	7.91	9.08	6.16	8.04	8.49	9.14	7.99	1.07
Non-thiazide diuretic drugs									
Quinethazone	0.46	0.46	0.48	0.44	0.48	0.55	0.59	0.49	0.05
Chlorthalidone	0.76	0.84	0.80	0.71	0.79	0.92	0.99	0.83	0.10
Metolazone	2.54	2.80	3.16	2.32	2.81	3.09	3.35	2.87	0.36
Chlorexolone	3.63	4.03	4.58	3.13	3.93	4.34	4.54	4.03	0.52
Mefruside	4.43	4.80	6.07	3.98	5.16	5.30	5.82	5.08	0.74
Clopamide	3.64	3.21	6.12	1.41	4.43	3.04	1.68	3.36	1.61
Column void volume	0.98	1.10	0.82	1.12	0.88	1.10	1.10		

* Only one peak observed on this column.

When the relative capacity factors of the thiazide drugs were calculated, they gave better correlations between the different columns and virtually compensated for the unusual behaviour of ODS-Zorbax (Table XI). This is in contrast to the earlier comparisons when relative capacity factors did not compensate for differences in the mobile phase or the temperature. Irrespective of the method of recording retentions,

TABLE X

EFFECT OF ODS-SILICA COLUMN PACKING MATERIAL ON THE RETENTION INDICES OF COLUMN TEST COMPOUNDS, THIAZIDE DIURETICS, AND RELATED DRUGS

Separation conditions and columns as Table IX.

Compound	Retention index							Mean	S.D.
	Column material								
	H1	H2	Z	T	TS	L	N		
Column test compounds									
2-Phenylethanol	706	707	690	701	698	708	699	701	6.4
p-Cresol	771	771	739	763	762	769	764	763	11.1
Nitrobenzene	870	868	862	875	870	872	875	870	4.5
Methyl benzoate	888	884	889	889	889	890	889	888	1.9
Toluene	1009	1001	1008	1003	1014	1009	1006	1007	4.3
Thiazide diuretics									
Chlorothiazide	527	529	451	506	506	510	511	506	25.9
Hydrochlorothiazide	555	559	486	535	532	542	540	536	24.0
Hydroflumethiazide	632	636	574	623	616	622	626	618	20.7
Trichloromethiazide	730	741	680	727	715	724	732	721	19.8
Methyclothiazide	754	766	706	754	738	749	756	746	19.6
Benzthiazide	855	870	805	852	836	850	856	846	20.8
Cyclothiazide 1	873	889	824	868	853	878	871	865	21.1
Cyclothiazide 2	885	900	836	879	865	878	882	875	20.1
Polythiazide	913	927	869	915	897	908	918	907	19.0
Bendrofluazide	918	931	877	918	904	912	921	912	17.4
Cyclopenthiazide	929	944	877	921	908	921	923	918	20.9
Non-thiazide diuretic drugs									
Quinethazone	546	539	473	529	521	529	528	524	23.7
Chlorthalidone	616	625	543	600	589	603	603	597	26.5
Metolazone	785	796	732	776	764	776	779	773	20.3
Chlorexolone	834	848	783	821	810	825	823	821	20.3
Mefruside	862	873	821	856	847	854	858	853	16.2
Clopamide	835	815	822	702	826	774	679	779	63.8

clopamide showed major differences between the various columns, presumably reflecting its partial ionisation and different interaction.

CONCLUSIONS

Clearly, the use of the present HPLC system for the identification of the diuretic drugs requires certain aspects of the experimental conditions to be closely defined, if good interlaboratory reproducibility is to be obtained. In particular, the proportion of acetonitrile in the mobile phase, the column temperature, and the brand of column packing material are important. A common brand of packing material should be adopted for interlaboratory comparisons. However, the pH and the exact proportion of acetic acid in the aqueous component are not critical, except for a few non-thiazide analytes.

TABLE XI

EFFECT OF ODS-SILICA COLUMN PACKING MATERIAL ON THE RELATIVE CAPACITY FACTORS OF THIAZIDE DIURETICS AND RELATED DRUGS

Separation conditions and columns as Table IX.

Column	Relative capacity factor × 100							Mean	S.D.
	Column material								
	H1	H2	Z	T	TS	L	N		
Thiazide diuretics									
Chlorothiazide	6.2	6.1	4.8	6.4	5.8	6.2	5.9	5.9	0.6
Hydrochlorothiazide	7.7	7.5	6.2	7.8	7.0	7.7	7.3	7.3	0.6
Hydroflumethiazide	13.3	12.9	11.6	14.0	12.9	13.6	13.2	13.1	0.7
Trichlormethiazide	26.9	27.0	26.3	28.3	26.5	27.6	27.4	27.0	0.9
Methyclothiazide	31.9	32.2	30.6	33.8	31.2	32.9	32.6	32.2	1.0
Benzthiazide	65.6	67.0	62.8	65.6	63.8	66.7	64.9	65.2	1.5
Cyclothiazide 1	74.8	76.4	71.8	72.9	72.4	81.2	72.2	74.5	3.3
Cyclothiazide 2	81.5	82.7	78.5	78.5	79.0	81.2	78.0	79.9	1.8
Bendrofluazide	103.3	103.1	105.7	102.0	105.0	103.0	102.0	103.5	1.4
Cyclopenthiazide	111.6	112.4	105.7	104.2	108.1	109.6	103.8	107.9	3.5
Non-thiazide diuretic drugs									
Quinethazone	7.2	6.5	5.6	7.4	6.4	7.1	6.7	6.7	0.6
Chlorthalidone	11.9	11.9	9.3	12.0	10.6	11.9	11.2	11.3	1.0
Metolazone	39.7	39.8	36.8	39.3	37.8	39.9	38.0	38.7	1.2
Clorexolone	56.8	57.2	53.3	52.9	52.8	56.0	51.5	54.4	2.3
Mefruside	69.3	68.2	70.7	67.3	69.4	68.4	66.1	68.5	1.5
Clopamide	57.0	45.6	71.1	23.9	59.5	39.2	19.1	45.1	19.1

It is important to use a relative retention method, such as relative retention times, relative capacity factors, or retention indices to record the results, but there is no clear advantage of one method over the other, as none of the diuretic drugs appear to be ideal as a standard. Relative capacity factors appear to have an advantage when different column materials are being used, although significant differences are still present, which would reduce the reliability of any identification. Retention indices have the advantage that a common scale can be used for different HPLC systems, and in our study the method proved to be virtually as robust as relative capacity factors.

ACKNOWLEDGEMENTS

REFERENCES

1 R. M. Smith, T. G. Hurdley, R. Gill and A. C. Moffat, *Chromatographia*, 19 (1984) 401.
2 R. M. Smith, T. G. Hurdley, R. Gill and A. C. Moffat, *Chromatographia*, 19 (1984) 407.

 3 R. M. Smith, T. G. Hurdley, R. Gill and A. C. Moffat, *J. Chromatogr.*, 355 (1986) 75.
 4 R. M. Smith, T. G. Hurdley, R. Gill and A. C. Moffat, *LC, GC, Mag. Liq. Gas Chromatogr.*, 4 (1986) 314.
 5 A. M. Krstulovic, H. Colin and G. Guiochon, *Anal. Chem.*, 54 (1982) 2438.
 6 J. K. Baker and C.-Y. Ma, *J. Chromatogr.*, 169 (1979) 107.
 7 R. M. Smith, *J. Chromatogr.*, 236 (1982) 313.
 8 R. M. Smith, *J. Chromatogr.*, 236 (1982) 321.
 9 R. M. Smith, *Anal. Chem.*, 56 (1984) 256.
10 R. M. Smith, *J. Chromatogr.*, 324 (1985) 243.
11 R. Gill, A. C. Moffat, R. M. Smith, and T. G. Hurdley, *J. Chromatogr. Sci.*, 24 (1986) 153.
12 R. M. Smith, G. A. Murilla and C. M. Burr, *J. Chromatogr.*, in press.
13 S. J. Soldin, E. Hach, A. Pollard and A. G. Logan, *Therapeutic Drug Monitor*, 1 (1979) 399.
14 R. E. Moskalyk, R. A. Locock, L. G. Chatten, A. M. Veltman and M. F. Bielech, *J. Pharm. Sci.*, 64 (1975) 1406.
15 P. A. Tisdall, T. P. Moyer and J. P. Anhalt, *Clin. Chem.*, 26 (1980) 702.
16 P. P. Koopmans, Y. Tan, C. A. M. Van Ginneken and F. W. J. Gribnau, *J. Chromatogr.*, 307 (1984) 445.
17 F. De Croo, W. Van den Bossche and P. De Moerloose, *J. Chromatogr.*, 325 (1985) 395.
18 F. De Croo, W. Van den Bossche and P. De Moerloose, *J. Chromatogr.*, 349 (1985) 301.
19 A. C. Moffat, J. V. Jackson, M. S. Moss and B. Widdop (Editors), *Clarke's Isolation and Identification of Drugs*, The Pharmaceutical Press, London, 1986.
20 A. Albert and E. P. Serjeant, *The Determination of Ionisation Constants*, Chapman and Hall, London, 3rd ed., 1984.

CHROMSYMP. 986

EFFECT OF ENTHALPY ON RETENTION IN REVERSED-PHASE LIQUID CHROMATOGRAPHY

Y. ARAI, M. HIRUKAWA and T. HANAI*

Gasukuro Kogyo Inc., 237 2 Sayamagahara, Iruma 358 (Japan)

SUMMARY

Retention in reversed-phase liquid chromatography has been found to be related to the Van der Waals volume, pi-energy and hydrogen-bonding energy effects. However, higher-molecular-weight compounds were retained more strongly than expected. In order to investigate this effect more fully, the retention times of phenols were measured on an octadecyl-bonded silica gel in acidic acetonitrile–water mixtures at different temperatures. The enthalpies of phenols were then calculated from their log k' values. The magnitude of the enthalpy effect increases with increasing molecular size, but the polarity of the molecule is the predominant factor in the enthalpy effect.

INTRODUCTION

Octadecyl-bonded silica gels are a most popular packing material in liquid chromatography. In particular, these packings are used in aqueous-phase liquid chromatography for separating a variety of polar and non-polar compounds, but the retention mechanism involved is not well understood. Retention times in reversed-phase liquid chromatography have been discussed in conjunction with physico-chemical parameters, namely the Van der Waals volume, pi-energy and hydrogen-bonding energy effects[1–3]. However, the predicted retention times of higher-molecular-weight compounds were less than the observed retention times. An increase in the number of methylene units in alkylbenzenes did not significantly affect the pi-energy effect on their retention, but the enthalpy effect increased dramatically[4]. This means that an hydrophobic compound can be adsorbed directly onto an octadecyl-bonded silica gel. The value of the enthalpy effect of a methylene unit in alkylbenzenes was calculated to be 500 cal/mol[4]. Enthalpy effects were also measured for the retention of phenols on an octadecyl-bonded silica gel in acidic acetonitrile–water mixtures.

EXPERIMENTAL

The liquid chromatograph used consisted of an ERC Model 3510 degasser (ERMA Optical Works, Tokyo, Japan), a CCPD pump (Toyo Soda, Tokyo, Japan), a Model 7161 injector (Rheodyne, Cotati, CA, U.S.A.), a Model SE11 refractometer

TABLE I

PHYSICAL PARAMETERS AND THE LOGARITHMS OF THE CAPACITY FACTORS FOR PHENOLS

For experimental conditions see Fig. 1.

Compound	VWV*	log k' at $1/T \cdot 10^{-5}$							Energy** effect (kcal/mol)	$-\Delta H$ (kcal/mol)
		309.6	314.5	319.5	324.7	330.0	335.6	341.3		
1 Phenol	53.88	−0.2752	−0.2591	−0.2384	−0.2059	−0.1903	−0.1617	−0.1272	7.883	1.980
2 2-Methylphenol	65.03	−0.1327	−0.1140	−0.0892	−0.0661	−0.0424	−0.0208	−0.0125	8.259	1.683
3 4-Methylphenol	65.03	−0.1718	−0.1538	−0.1312	−0.1054	−0.0820	−0.0627	−0.0270	8.704	1.910
4 2,3-Dimethylphenol	76.18	−0.0313	−0.0130	0.0125	0.0346	0.0581	0.0829	0.1130	9.116	1.926
5 2,4-Dimethylphenol	76.18	−0.0204	0.0058	0.0263	0.0456	0.0708	0.0933	0.1241	–	1.872
6 2,5-Dimethylphenol	76.18	−0.0191	0.0003	0.0191	0.0489	0.0674	0.0922	0.1220	9.013	1.880
7 2,6-Dimethylphenol	76.18	0.0183	0.0427	0.0624	0.0866	0.1078	0.1440	0.1607	8.524	1.941
8 3,4-Dimethylphenol	76.18	−0.0868	−0.0681	−0.0436	−0.0176	0.0025	0.0265	0.0561	9.762	1.906
9 3,5-Dimethylphenol	76.18	−0.0650	−0.0373	−0.0172	0.0052	0.0260	0.0660	0.0820	9.489	1.889
10 2,3,5-Trimethylphenol	87.33	0.0842	0.1035	0.1244	0.1547	0.1797	0.1968	0.2294	9.851	1.947
11 2,3,6-Trimethylphenol	87.33	0.1266	0.1463	0.1693	0.1962	0.2171	0.2416	0.2721	9.360	1.940
12 2,4,6-Trimethylphenol	87.33	0.1422	0.1606	0.1819	0.2113	0.2553	0.2525	0.2837	9.175	1.898
13 2,3,5,6-Tetramethylphenol	98.48	0.2937	0.3140	0.3356	0.3655	0.3888	0.4081	0.4404	10.126	1.960
14 2-Ethylphenol	75.26	−0.0006	0.0230	0.0462	0.0659	0.0900	0.1108	0.1444	9.192	1.877
15 3-Ethylphenol	75.26	−0.0561	−0.0315	−0.0087	0.0098	0.0341	0.0541	0.0866	–	1.838
16 4-Ethylphenol	75.26	−0.0553	−0.0281	−0.0094	0.0152	0.0386	0.0620	0.0880	9.122	1.886
17 2-Chlorophenol	63.03	−0.1191	−0.0990	−0.0757	−0.0559	−0.0345	−0.0080	0.0111	8.017	1.899
18 3-Chlorophenol	63.03	−0.0915	−0.0686	−0.0435	−0.0183	0.0050	0.0315	0.0538	7.647	2.118
19 4-Chlorophenol	63.03	−0.1035	−0.0853	−0.0626	−0.0391	−0.0044	0.0145	0.0352	7.884	2.085
20 2,3-Dichlorophenol	72.51	0.0144	0.0366	0.0610	0.0816	0.1045	0.1428	0.1512	8.225	2.061

21	2,4-Dichlorophenol	72.51	0.0625	0.0851	0.1074	0.1455	0.1555	0.1807	0.2016	7.673	2.029
22	2,5-Dichlorophenol	72.51	0.0551	0.0725	0.0960	0.1208	0.1416	0.1699	0.1936	8.004	2.031
23	2,6-Dichlorophenol	72.51	0.0447	0.0643	0.0869	0.1101	0.1313	0.1683	0.1794	7.829	2.032
24	3,4-Dichlorophenol	72.51	0.0525	0.0715	0.0976	0.1220	0.1464	0.1748	0.1971	7.830	2.133
25	3,5-Dichlorophenol	72.51	0.1331	0.1586	0.1859	0.2093	0.2346	0.2717	0.2797	7.204	2.209
26	2,3,4-Trichlorophenol	81.99	0.1803	0.1993	0.2235	0.2494	0.2731	0.2992	0.3215	7.943	2.083
27	2,3,5-Trichlorophenol	81.99	0.3663	0.3932	0.4215	0.4477	0.4743	0.5077	0.5282	8.226	2.374
28	2,3,6-Trichlorophenol	81.99	0.1924	0.2125	0.2372	0.2613	0.2853	0.3129	0.3349	7.989	2.093
29	2,4,5-Trichlorophenol	81.99	0.2271	0.2474	0.2735	0.2993	0.3224	0.3505	0.3744	8.083	2.157
30	3,4,5-Trichlorophenol	81.99	0.2418	0.2663	0.2931	0.3207	0.3457	0.3816	0.3990	7.411	2.335
31	2,3,4,5-Tetrachlorophenol	91.47	0.5336	0.5627	0.5929	0.6195	0.6481	0.6813	0.7024	7.489	2.470
32	2,3,5,6-Tetrachlorophenol	91.47	0.3936	0.4156	0.4428	0.4682	0.4947	0.5233	0.5470	7.335	2.251
33	Pentachlorophenol	100.95	0.5349	0.5626	0.5922	0.6205	0.6484	0.6776	0.7024	7.434	2.439
34	3-Bromophenol	66.48	-0.0484	-0.0303	-0.0062	0.0190	0.0376	0.0679	0.0909	7.966	2.039
35	4-Bromophenol	66.48	-0.0611	-0.0434	-0.0186	0.0050	0.0261	0.0541	0.0769	8.199	2.024
36	2,4-Dibromophenol	79.08	0.1478	0.1659	0.1901	0.2150	0.2357	0.2631	0.2854	7.854	2.021
	Void volume (ml)		1.488	1.485	1.481	1.470	1.463	1.443	1.432		

* Van der Waals volume calculated by Bondi's method[5].

** Energy effect from ref. 3.

(Shodex, Tokyo, Japan), an ERC Model 8710 ultraviolet detector (ERMA Optical Works) and a Model CR3A integrator (Shimadzu, Kyoto, Japan). An IBM PC-5510 computer was used for the calculations. Deionized water was purified further in a Model Pureline still (Yamato Sci. Co., Tokyo, Japan).

Acetonitrile was of high-performance liquid chromatography (HPLC) grade (Kishida Kagaku Co., Tokyo, Japan). The other reagents were mainly supplied by Tokyo Chem. Ind. Co. (Tokyo, Japan), and are listed in Table I with their physical parameters. The octadecyl-bonded silica gel column was an ERC 1000 (10 cm × 6 mm I.D.) from ERMA Optical Works, packed with Hypersil ODS, and it was thermostatted in a water-bath. The eluent was acetonitrile–0.05 M aqueous phosphoric acid (pH 2.016).

RESULTS AND DISCUSSION

The capacity factors measured in 70% aqueous acetonitrile with 0.05 M phosphoric acid at different temperatures are listed in Table I. The isomer effect on the retention of alkylphenols is weak, but it is not negligible in the case of chlorophenols. Halogenated phenols were retained more strongly than alkylphenols, and halogenated benzenes more than alkylbenzenes. The relationship between the log k' values, measured at 30°C, and the Van der Waals volumes is shown in Fig. 1.
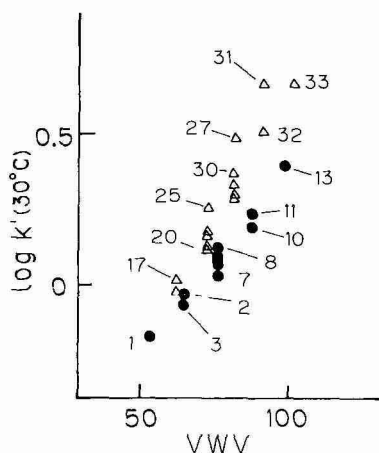
Fig. 1. Relationship between the Van der Waals volumes and log k' for phenols in reversed-phase liquid chromatography. Column: ERC 1000, packed in a 10 cm × 6.0 mm I.D. stainless-steel tube. Eluent: 70% aqueous acetonitrile, containing 0.05 M phosphoric acid. Column temperature: 30°C. Numbers beside symbols are the same as in Table I. ●, Methylphenols; △, chlorophenols.

The enthalpy of a solute can be calculated from the following equations and the capacity factors measured at different temperatures:

$$\Delta G = \Delta H - T\Delta S$$
$$\Delta G = -RT \ln K$$
$$k' = \varphi K$$

Therefore, $\ln k' = -\Delta H/RT + \Delta S/R + \ln \varphi$, where G is the free energy, H is the enthalpy, T is the absolute temperature, S is the entropy, R is the gas constant, K is the partition coefficient and k' is the capacity factor. The phase ratio, $\ln \varphi$, is approximately zero in this system, therefore, this equation can be rewritten as:

$$\ln k' = -\Delta H/RT + \Delta S/R$$

The slope of a plot $\log k'$ *vs.* $1/T$ of gives the calculated enthalpy for each compound, which is listed in Table I. The correlation coefficient is 0.996 ($n = 37$), the enthalpy effect of methylphenols being about 1.910 kcal/mol. No large difference in the magnitude of the effect was found among the isomers of this group, as shown in Fig. 2.
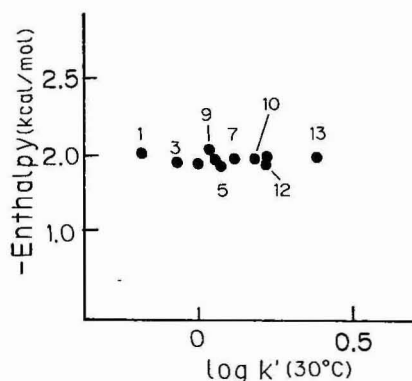
Fig. 2. Relationship between the enthalpy, $-\Delta H$, and $\log k'$ values for methylphenols on an ERC 1000 column, eluted with acetonitrile–0.05 M aqueous phosphoric acid. Numbers beside symbols are the same as in Table I.

The difference in the enthalpy effect between toluene and monomethyl-substituted phenols is about 200 cal/mol, and that between ethylbenzenes and monoethyl-substituted phenols is about 100 cal/mol. The energy effect for the retention of alkylphenols, however, varies from 7.883 kcal/mol for phenol to 10.126 kcal/mol for 2,3,5,6-tetramethylphenol. This means that the retention of alkylphenols is mainly due to pi- and hydrogen-bonding energy effects and not to the enthalpy effect.
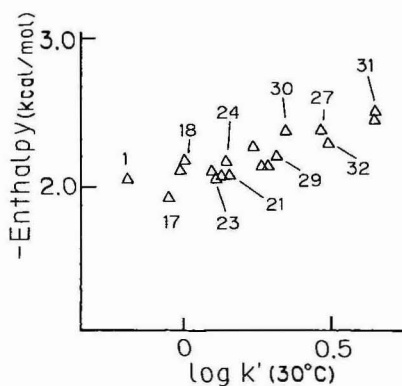
Fig. 3. Relationship between the enthalpy, $-\Delta H$, and $\log k'$ values for chlorophenols. Details as in Fig. 2.

The difference in the enthalpy effect between chlorobenzene and monochlorophenols is the same as in the case of alkylphenols, but the effect increases slightly for polychloro-substituted phenols. Differences among isomers were observed, as shown in Fig. 3.

The energy effect of *ortho*-substituted halogenated phenols is less than that of the corresponding *meta* and *para* compounds, but it is still greater than their enthalpy effect. This result indicates that the predominant factors in the retention of phenols in this system are the pi- and hydrogen-bonding energy effects, not the enthalpy effect. Thus, polar compounds may not be directly adsorbed onto the surface of an octadecyl-bonded silica gel under the above experimental conditions, and the retention of phenols can be described by the following equation

$$\log k' = \log k' \text{ (VWV)} - \log k' \text{ (pi)} - \log k' \text{ (OH)}$$

where VWV is the Van der Waals volume of the solute, pi is the pi-energy effect of the phenyl group in phenols and OH is the hydrogen-bonding energy effect of the hydroxy group in phenols[6].

REFERENCES

1 T. Hanai and J. Hubert, *J. Chromatogr.*, 290 (1984) 197.
2 T. Hanai and J. Hubert, *J. Chromatogr.*, 291 (1984) 81.
3 T. Hanai and J. Hubert, *J. Chromatogr.*, 302 (1984) 89.
4 T. Hanai, A. Jukurogi and J. Hubert, *Chromatographia*, 19 (1984) 266.
5 A. Biondi, *J. Phys. Chem.*, 68 (1964) 441.
6 T. Hanai, *J. Chromatogr.*, 332 (1985) 189.

CHROMSYMP. 948

SIGNIFICANCE AND ESTIMATION OF CHROMATOGRAPHIC PARAMETERS

A. M. LENHOFF

Department of Chemical Engineering, University of Delaware, Newark, DE 19716 (U.S.A.)

SUMMARY

An analytical solution to the equations providing a mechanistic description of linear chromatography is used to examine the predicted effects of different parameters. The mechanisms accounted for are convection, axial dispersion, mass transfer to and within the particles, and sorption–desorption kinetics. Intraparticle rate limitations, *i.e.*, slow intraparticle diffusion and sorption kinetics, are found to produce similar chromatographic results, making it difficult to distinguish their effects. In both cases the resulting peaks are symmetric, in contrast to the pronounced tailing which is shown to arise from secondary sorption.

Calculation of plate heights from the model results indicates that moment determinations are susceptible to appreciable error; estimation of mechanistic parameters should therefore be performed using the time-domain results. The utility of several limiting approximations is demonstrated using both direct comparison with the analytical solution as well as order-of-magnitude estimates of the characteristic times of the different processes in the column.

INTRODUCTION

The mechanisms underlying chromatography in packed columns are well understood qualitatively and have been extensively investigated quantitatively as well. Nevertheless, a theoretical description adequate for detailed analysis in the time domain has not yet been applied to chromatography in a systematic fashion. The usual framework of theoretical plates not only lacks a realistic physical basis, but also lumps all the information present in a chromatographic peak into a relatively small number of quantities representing its most important characteristics, namely the peak area (zeroth moment), retention time (first moment) and peak width (second moment). A preferred approach is one based on the thermodynamic, transport and kinetic processes occurring in the column, the mechanisms of which are reasonably well understood. Such treatments have, of course, been used before, but generally with the results expressed in terms of the moments[1,2] or related to the usual theoretical plates analysis[3]. In this paper use is made of the complete analytical time-domain solutions to the describing equations to elucidate the effects of the parameters of greatest interest and to ascertain under which conditions limiting approximations

to the full analysis provide sufficient accuracy. In addition, implications of measurement errors in experimental application of the theoretical plates method are examined.

Strong motivation for this study comes from the existing and potential uses of liquid chromatography (LC) for preparative and process scale separations in, for example, the pharmaceutical industry. Here the frequent operation under mass overloading adds the additional complicating feature of non-linear sorption isotherms to the obvious problem of scale, and techniques appropriate for determination of optimal operating conditions in analytical chromatography lose their utility. While we intend to extend our study to the non-linear situation, this paper is restricted to linear chromatography.

THEORETICAL BASIS

Problem statement

The phenomena considered to be of importance in column LC are axial convection, convective dispersion ("eddy diffusion"), mass transfer to the particle surface and within the particle and sorption–desorption kinetics. The corresponding describing equations have appeared in various previous studies (e.g., refs. 2 and 3) with small differences in some details, particularly in the boundary conditions. They are simply solute continuity equations for the mobile phase (c_m) and stationary phase (pores, c_s, and surface, c_a) concentrations, expressed as functions of time, t, axial position, z, and intraparticle radial position, r:

mobile phase

$$\frac{\partial c_m}{\partial t} + u \frac{\partial c_m}{\partial z} = \mathscr{D}_m \frac{\partial^2 c_m}{\partial z^2} - \frac{3(1 - \varepsilon)}{\varepsilon} \frac{k_m}{R} (c_m - K c_s |_{r = R})$$

intraparticle

$$\varepsilon_i \frac{\partial c_s}{\partial t} = \mathscr{D}_s \frac{1}{r^2} \frac{\partial}{\partial r} r^2 \frac{\partial c_s}{\partial r} - k S_v (c_s - \alpha' c_a)$$

surface

$$\frac{\partial c_a}{\partial t} = k(c_s - \alpha' c_a)$$

with boundary conditions:

mobile phase

$$u c_m - \mathscr{D}_m \frac{\partial c_m}{\partial z} = 0 \quad \text{at} \quad z = 0$$

$$\frac{\partial c_m}{\partial z} = 0 \quad \text{at} \quad z = L$$

particle

$$\frac{\partial c_s}{\partial r} = 0 \quad \text{at} \quad r = 0$$

$$\mathcal{D}_s \frac{\partial c_s}{\partial r} = k_m(c_m - Kc_s) \quad \text{at} \quad r = R$$

and initial conditions

$$c_m = c_0 L\delta(z), \, c_s = c_a = 0 \quad \text{at} \quad t = 0$$

where u = mean interstitial mobile phase velocity; $\mathcal{D}_m$ = axial dispersion coefficient (includes "eddy diffusion"); ε = column void fraction; k_m = external mass transfer coefficient (mobile phase to particle surface); R = particle radius = $d_p/2$; K = size-exclusion distribution coefficient; ε_i = particle porosity; D_s = intraparticle effective diffusivity; k = sorption rate constant; L = column length; S_v = specific surface area available for sorption; α' = sorption partition coefficient.

The axial boundary conditions are those of Danckwerts[4], which preclude diffusive transport across the boundaries of the column. Under typical chromatographic conditions axial transport is overwhelmingly convective, and the use of alternative boundary conditions makes little difference to the final outcome.

The problem statement is scaled relative to appropriate characteristic quantities in such a way that the concentrations $\Theta_m = c_m/c_0$, $\Theta_s = c_s/c_0$, and $\Theta_a = c_a S_v/c_0$ are functions of dimensionless time $\tau = tu/L$ and position $\zeta = z/L$ and $\eta = r/R$, as well as the following dimensionless parameters:

$$\nu = \frac{d_p u}{\mathcal{D}} = \text{Péclet number (reduced velocity)};$$

$$\delta = \frac{d_p}{L} = \text{particle size–column length ratio};$$

$$E_m = \frac{\mathcal{D}_m}{\mathcal{D}} = \text{scaled dispersion coefficient};$$

$$E_s = \frac{\mathcal{D}_s}{\mathcal{D}} = \text{scaled intraparticle effective diffusivity};$$

$$\text{Sh} = \frac{k_m d_p}{\mathcal{D}} = \text{Sherwood number};$$

$$D = \frac{k \, S_v \, d_p}{u} = \text{Damköhler number};$$

$$\alpha = \frac{\alpha'}{S_v} = \text{scaled sorption partition coefficient}.$$

The significance of these parameters and their importance in the analysis will be discussed later.

Analytical solution

The scaled equations and boundary and initial conditions, which are not shown here, can be solved in either of two ways. The first, using separation of variables, leads to an eigenfunction expansion which is not, however, amenable to numerical evaluation, because of the very large value of $v\delta/E_m$ typical of column chromatography. The alternative approach makes use of the solution in Laplace transform domain, with inversion accomplished by contour integration in the complex plane. This method, used by Rosen[5] with a simplified model of chromatography, has been applied by Rasmuson[6] to computing breakthrough curves using essentially the same model as that given above. The resulting solution for effluent mobile phase concentration is

$$\Theta_m(\tau)\,|_{\zeta=1} = \frac{1}{\pi}\int_0^\infty \mathcal{R}(\bar{\Theta}_m(i\omega)\,|_{\zeta=1}\,e^{i\omega\tau})\,d\omega$$

where the overbar denotes the Laplace transform, and $\mathcal{R}$ denotes the real part. $\bar{\Theta}_m\,|_{\zeta=1}$ is given by

$$\bar{\Theta}_m(s)\,|_{\zeta=1} = \frac{be^{\bar{v}m_2}}{m_1^2 - m_2^2 e^{-\bar{v}b}}$$

where

$$m_{1,2} = \frac{1}{2}(1 \pm b)$$

$$\bar{v} = \frac{v}{\delta E_m}$$

$$b = \sqrt{1 - 4\psi/\bar{v}^2}$$

$$\psi = -s\bar{v} - \frac{6(1-\varepsilon)\text{Sh}}{\varepsilon\delta^2 E_m}\,\frac{w\coth w - 1}{\text{Sh}K/2E_s + w\coth w - 1}$$

$$w^2 = \frac{\delta vs}{4E_s}\left(\varepsilon_i + \frac{D}{s + D\alpha}\right)$$

This solution, which can be implemented numerically, forms the basis for the rest of the work described here. The solution in Laplace transform domain can, however, also be used to obtain the moments of the elution curve, from which the retention time, t_R, and the reduced plate height, h, can be found:

$$t_R = \frac{L}{u}\left[1 + \frac{1-\varepsilon}{\varepsilon K}\left(\varepsilon_i + \frac{1}{\alpha}\right)\right]$$

$$h = \frac{2E_m}{v} + \left[\left(\frac{v}{30E_s} + \frac{v}{3K\text{Sh}}\right)\left(\varepsilon_i + \frac{1}{\alpha}\right)^2 + \frac{2}{D\alpha^2}\right]\frac{(1-\varepsilon)}{\varepsilon K}\left(\frac{L}{ut_R}\right)^2$$

The expression for t_R contains three terms: the quantity 1 represents the mobile phase residence time, the term in ε_i the (intraparticle) pore residence time and that in α the contribution of the sorbed fraction. The observed value of the distrtibution ratio k' is therefore given by

$$1 + k' = \frac{1 + \dfrac{1 - \varepsilon}{\varepsilon K}\left(\varepsilon_i + \dfrac{1}{\alpha}\right)}{1 + \dfrac{1 - \varepsilon}{\varepsilon K}\varepsilon_i}$$

The expression for the reduced plate height neglects terms in $e^{-\bar{v}}$; it is based on the expressions given by Kučera[2] and differs only slightly from that given by Horváth and Lin[3]. The four terms represent the contributions of axial dispersion, external mass transfer, intraparticle diffusion and sorption–desorption kinetics respectively to band broadening. While the relative contributions of these effects can be evaluated from the equation, similar conclusions and much insight can be obtained by examining the relative characteristic times for the different processes. This is discussed in the next section.

Orders of magnitude and characteristic time scales

Much can be learned and understood about chromatography from order-of-magnitude arguments, which can be invaluable in the planning and interpretation of both modelling and experiment. These concepts are successfully used, for example, by Giddings[7] in formulating his plate height equations.

The most natural basis for a preliminary analysis is the set of time scales characterizing the system and the processes to which it is subjected. For the present description of LC these are: convection, $t_{conv} = d_p/u$; external mass transfer, t_{MT} d_p/k_m; intraparticle diffusion, $t_{diff} = d_p^2 /\mathcal{D}_s$; sorption, $t_{sorp} = 1/kS_v$;

These characteristic times arise naturally, and their ratios form the dimensionless parameters already introduced. For example, $t_{diff}/t_{conv} = v/E_s$, $t_{diff}/t_{MT} = Sh/E_s$ and $t_{conv}/t_{sorp} = D$. Since system behaviour depends on the relative speeds of the different processes, it may be characterised in terms of these dimensionless parameters. One example of this is well known to all chromatographers: the minimum reduced plate height occurs at a Péclet number (reduced velocity) between 1 and 10, where the flow-rate through the column is more or less comparable in speed to the rate of solute transport inside the particle, the latter usually being rate-limiting in chromatography

A generalisation of this observation follows from consideration of the mechanisms of band broadening and the framework within which they are described, but it is important to distinguish between the lateral transport mechanisms and axial dispersion. Lateral transport contributes to band broadening only as a result of its interaction with axial convection, and an evaluation of the magnitude of the contribution can come only from a consideration of this interaction. Therefore, appreciable band broadening will be observed if lateral transport is much slower than axial convection, a comparison which is made directly in the respective ratios of characteristic times: $t_{MT}/t_{conv} = v/Sh$, $t_{diff}/t_{conv} = v/E_s$ and $t_{sorp}/t_{conv} = 1/D$. Substantial band broadening is to be expected if any one of these ratios is much larger than unity. It is also

worth noting that these three lateral transport processes take place in series, so they will be dominated by any one which may be significantly slower than the other two. This forms the basis of one way for developing simpler, more efficient limiting approximations later in this paper.

Axial dispersion or eddy diffusion is accounted for by an explicit axial transport term into which all mobile phase dispersive effects are lumped; these generally originate in convective non-uniformities resulting from the geometry of and the hydrodynamics in the packed bed. Band broadening can occur by axial dispersion or by the essentially parallel mechanism resulting from the coupling of slow lateral transport with axial convection. The respective increases l in peak width during time period t_{conv} may be estimated as $l_{disp} \approx \sqrt{\mathcal{D}_m d_p/u}$ and $l_{lat} \approx u t_{lat}$, where t_{lat} is a characteristic lateral transport time. Since the faster of two parallel processes is dominant (*cf.* the serial steps in lateral transport), band broadening will be dominated by axial dispersion if $l_{disp}/l_{lat} \gg 1$, and *vice versa*. This criterion may be rearranged to give $\mathcal{D}_m d_p/u^3 t_{lat}^2 \gg 1$ which becomes, for instance, $Sh^2 E_m/v^3 \gg 1$, $E_m E_s^2/v^3 \gg 1$ or $D^2 E_m/v \gg 1$ if lateral transport is limited by external mass transfer, intraparticle diffusion or sorption, respectively.

When certain geometric or thermodynamic parameters take on extreme values, they may affect the time constants, so that the discussion above requires slight modifications. For example, very small values of α' (strong binding) do not affect sorption rates, but imply that desorption is slow. This clearly has an effect on the rate of lateral transport and consequently on band broadening, and is important in, for example, affinity chromatography. In this case the appropriate ratio of characteristic times changes from $1/D$ to $1/D\alpha$. The combination of the ratios of time constants with the thermodynamic and geometric parameters leads to terms such as those in the equation describing the reduced plate height; a comparison of the plate height and order-of-magnitude analyses demonstrates that they lead to the same conclusions regarding the limiting processes in chromatography.

RESULTS AND DISCUSSION

Parameter values

The dimensionless parameters can be divided into two categories for the purpose of selecting suitable base values. The kinetic quantities v, E_s and D have all been assigned base values of unity, the rationale for this selection becoming apparent when the discussion above of characteristic times is taken into account: the parameters have been chosen so as to make the rates of the different processes of approximately equal orders of magnitude, *i.e.*, no single transport step is rate-limiting. E_m, describing axial dispersion, and Sh, describing external mass transfer, are also kinetic parameters. The extensive studies of these two effects make it possible to depend with sufficient confidence on literature correlations to estimate appropriate parameter values. The equation of Hiby[8] has been used for describing axial dispersion

$$E_m = \frac{\mathcal{D}_m}{\mathcal{D}} = 0.67 + \frac{0.65v}{1 + 7v^{1/2}}$$

and that of Pfeffer[9] for external mass transfer

$$\text{Sh} = \frac{k_m d_p}{\mathscr{D}} = \mathscr{A} v^{1/3} \qquad A \approx 1$$

The second class of parameters conveys geometric and thermodynamic information. Realistic values are $\varepsilon = 0.35$, $\varepsilon_i = 0.3$, $K = 1$, $\alpha = 0.5$ and $\delta = 0.0001$, leading to a k' value of 3.39. Note that $K = 1$ implies that there is no size-exclusion effect.

It is, of course, possible to examine the system response throughout the parameter space. Instead, the emphasis here will be on the two mechanisms which are probably least understood, yet most often prove to be limiting in modern LC: intraparticle diffusion and sorption–desorption kinetics. That intraparticle diffusion is often limiting is apparent from the common situation, mentioned earlier, where the minimum reduced plate height is at a Péclet number of approximately order unity. Sorption–desorption kinetics have been studied less extensively, but the results of Horváth and Lin[3] suggest that they may be limiting in reversed-phase chromatography, while the strong binding associated with affinity systems makes desorption limiting there in the absence of solvent changes.

Time-domain calculations

Figs. 1 and 2 show the effects of the two parameters of greatest importance to the present discussion, namely E_s and D; dimensionless concentration is shown as a function of dimensionless time, *i.e.*, scaled relative to the extraparticle residence time L/u. The base case, for the parameters given above, gives a relatively narrow, sym-
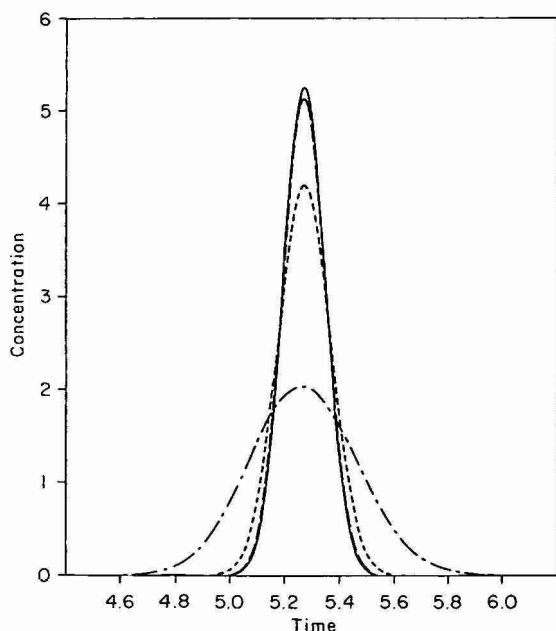
Fig. 1. Effect of intraparticle diffusivity on chromatography. Diffusivity ratio: (––) = 1; (– –) = 0.1; (- - -) = 0.01; (- · -) = 0.001.
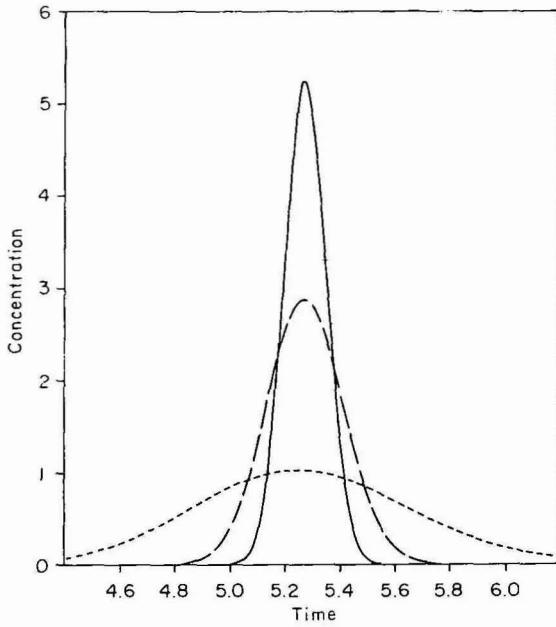
Fig. 2. Effect of sorption kinetics on chromatography. (—) $D = 1$; (– –) $D = 0.1$; (- - -) $D = 0.01$.

metric peak, as expected with convection and all the processes contributing to band broadening approximately equally rapid. As either E_s or D decreases, *i.e.*, as resistance to lateral transport increases, the peak becomes broader, again as expected: the
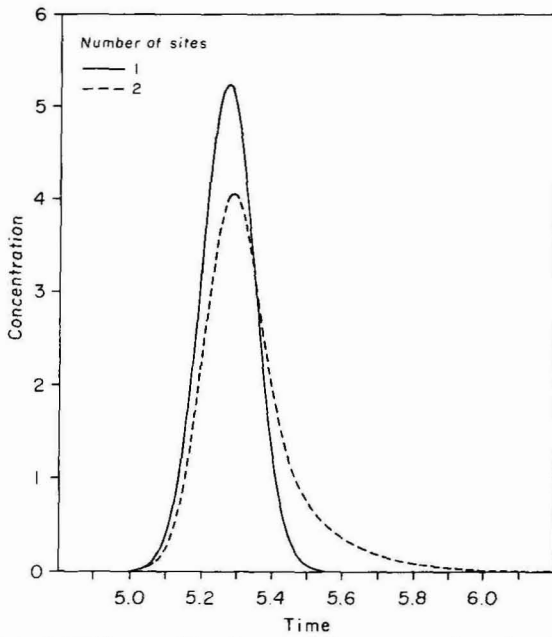
Fig. 3. Tailing resulting from sorption on secondary sites. (—) One site; (- - -) two sites.

ratios $t_{\text{diff}}/t_{\text{conv}} = v/E_s$ and $t_{\text{sorp}}/t_{\text{conv}} = 1/D$, respectively, become significantly greater than unity. A similar quantitative prediction of when appreciable band broadening increases will result from the various components of the lateral transport resistance can be obtained from the reduced plate height equation.

The similarity of the results for intraparticle diffusion and sorption limitations indicates that these two effects can not be distinguished by operating, for example, at different flow-rates: either particle size or sorption chemistry must be manipulated. It is particularly notable that peak symmetry does not appear to be lost in the range of parameters discussed here. Other results not shown do display some asymmetry when lateral transport resistance is high; this occurs at higher k' values (> 10), but the peaks are so broad as to be uncharacteristic of the asymmetric peaks often observed in, for example, reversed-phase systems. This suggests that slow sorption kinetics cannot alone account for appreciable asymmetry in chromatographic peaks, as is sometimes suggested[10]. Other suspected causes of asymmetry[10] include extra-column effects and sorption on secondary sites. It is possible to modify the model used here to test the second of these, by adding a second class of sorption sites characterised by different values of D and α, i.e., by different sorption kinetics and thermodynamics. The analytical solution can be obtained by a straightforward extension of the approach used for the single-site model. Fig. 3 shows the effect of adding secondary sites to the base case given by the values in above; the parameters associated with the secondary sorption are $D_2 = 3 \cdot 10^{-5}$ and $\alpha_2 = 30$. Because of the appearance of the specific surface area S_v in both these dimensionless parameters, the physical significance of this pair of values cannot be determined unambiguously. For example, both weak, slow binding on a large number of sites (large α', S_v; small k) as well as strong, fast binding on a small number of sites (small α', S_v; large k) are compatible with the (D, α) pair given, although the latter situation is what would be expected to apply to secondary sorption.

The effect of the secondary sites is primarily to add a tail to the peak, with the result being in qualitative agreement with what is often observed experimentally in, for example, reversed-phase chromatography. While the value of t_R determined from the peak value is not affected appreciably by the tail, the actual mean residence time is about 5.33 (cf. the different values of mean, median and mode of a skewed statistical distribution). The tail similarly affects the second moment more than is reflected by, for example, the peak width at half peak height. In the two-site situation, the values of t_R and h obtained from the moments are, strictly speaking, more representative of the full peak, but since the tail may contain relatively little material, the crude values based on peak height and width may often be adequate.

Moments of elution peaks

The usual approach to analysing linear chromatography involves determining a reduced plate height h from the response time and shape of the chromatographic peak. The variation of h with the reduced velocity or Péclet number v can provide information on the rate-limiting mechanism and on how well the column is packed, by use of the Van Deemter or Knox equation. The information provided by any peak is, however, reduced in this way to two quantities, viz. t_R and h, and even the multiple runs required for the h vs. v plot do not fully compensate for this lumping of information. In the case of skewed peaks, for example, t_R and h can still be calculated,

but the peak skewness is not reflected in either quantity; the third moment is required for this. On the other hand, the full analytical solution in the time domain conveys much more complete information regarding the peak in that it permits use of each point in the chromatographic profile.

Despite the disadvantages of the plate height approach, it continues to be used, and it is therefore important to be aware of possible sources of difficulty. Several studies of the susceptibility to error of moment and plate height calculations have been performed[11-15]; effects examined include extra-column effects, noise, baseline drift, tail truncation and peak skewness. In all these studies, however, it was impossible to relate the empirically observed shape of the chromatographic peak, whether simulated or actually measured experimentally, to mechanistically relevant parameters. The usual way of doing this in chromatography is by analysing h vs. v plots. but no previous studies seem to have generated these from purely mechanistic models solved in the time domain. It has therefore not been possible to separate the effects of errors in experimental measurements from errors in data processing. In what follows, then, the effects of data processing errors on h vs. v curves generated from exact analytical time-domain solutions will be examined.

The situation to be studied is the relatively simple one based on the parameters given previously, except that the the diffusivity ratio, E_s is taken to have the value 0.1. As is clear from Fig. 1, the resulting chromatographic peak is narrow and symmetric, and one would expect relatively few problems in applying moments to this system. Fig. 4 shows the dependence of h on v predicted by the exact plate height equation, as well as the values at some selected values of v found from the moments
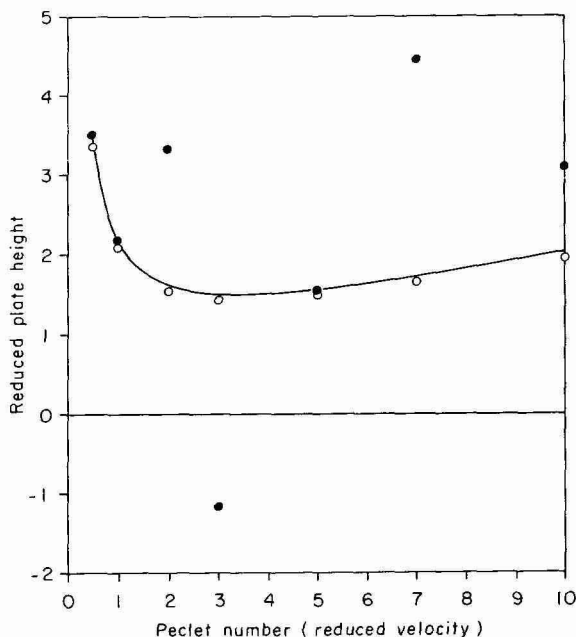
Fig. 4. Effects of integration error on computed value of reduced plate height. (—) Predicted by exact plate height equation; (●) 0.1% accuracy; (○); truncation at 2% of peak.

of the analytical time-domain solution evaluated by numerical integration. If the integration is performed accurately, agreement between the two methods is excellent. However, Fig. 4 also shows the effect of inaccurate integration. The solid circles denote points determined by integrating with an upper bound on integration error of 0.1%, using an adaptive quadrature package[16]. The extremely large errors are a consequence of the relationship between the plate height and the moments: h is proportional to $\mu_2 - \mu_1^2$, where μ_n ($n = 1, 2$) is the nth moment about the origin of the normalised chromatogram. Since the difference between μ_2 and μ_1^2 is typically small, small errors in integration can be significant, as is clearly demonstrated by the results. In principle, less accurate integration can, of course, give rise to still larger errors, but these are often masked by the correlation among the errors in the moments if, for example, trapezoidal integration is used.

The other possible source of error examined here is that of tail truncation, which has been examined previously[12,15]. The results obtained by truncating at 2% of peak height, shown by the open circles in Fig. 4, indicate a systematically slightly low value of h. The relatively small magnitude of the error is a consequence of the absence of a significant tail in the peak considered, but the effect is much more severe when tailing is appreciable. Correlation among the errors in the three moments also reduces the discrepancy in h.

It may thus be concluded, as have others previously, that calculations of plate heights from the moments are susceptible to appreciable errors. Use of peak width measurements appears from other studies to be, if anything, even less reliable. It is particularly difficult to estimate mechanistic parameters from plate height determinations, and use of the full time-domain results with the matching model solution is the preferred approach.

Limiting approximations

Matching experimental results to the analytical solution in the time domain requires the latter to be computed efficiently and accurately. For this purpose it is useful to consider approximate descriptions of the chromatographic process valid for certain limiting ranges of parameter values, since the solutions are typically more computationally efficient while still acceptably accurate. Four such cases are considered here.

The first approximation[17] involves lumping intraparticle diffusion into a mass transfer term. Solute concentration within the particle is assumed to be uniform, and solute influx across the external surface is given by $k_{int}(c_{s|R} - c_s)$, where k_{int} is an internal mass transfer coefficient usually assumed to be given by $B\mathscr{D}_s/d_p$, where B is a constant between 0.5 and 2.5. This approximation would be expected to be reasonable when intraparticle diffusion is rapid, *i.e.*, when t_{diff} is not large relative to the other two lateral transport times (t_{MT} and t_{sorp}) or to the convection time t_{conv}. This is borne out by detailed calculations, of which Fig. 5 is representative: the lumped mass transfer description is accurate for $E_s = 1$ but not for $E_s = 0.001$.

An approximation which is very often valid is that which assumes sorption kinetics to be fast relative to the other lateral transport steps; in the limit, sorption equilibrium may be assumed to apply within the particle ($c_s = \alpha'c_a$), corresponding to an infinite Damköhler number D. The effect of increasing Damköhler number is shown in Fig. 6, from which it is apparent that for values of D as small as 10 the
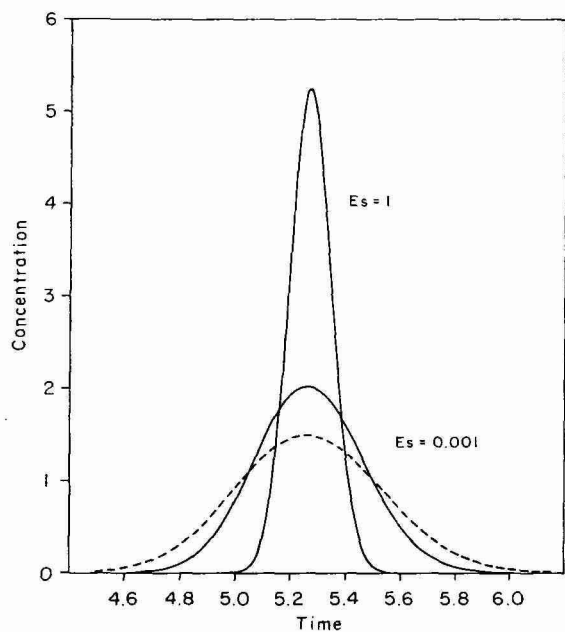
Fig. 5. Effect on model accuracy of lumping intraparticle diffusion. (—) Distributed mass transfer; (- - -) lumped mass transfer.
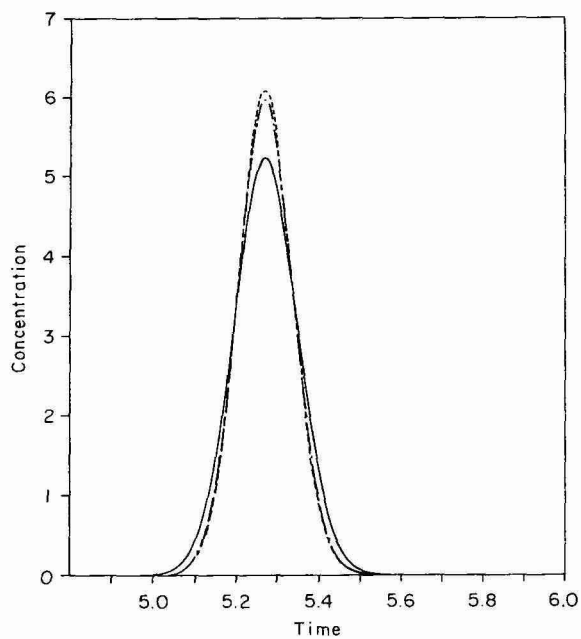
Fig. 6. Limiting approximation for instantaneous sorption and desorption. (—) $D = 1$; (- · -) $D = 10$; (- - -) $D = \infty$.
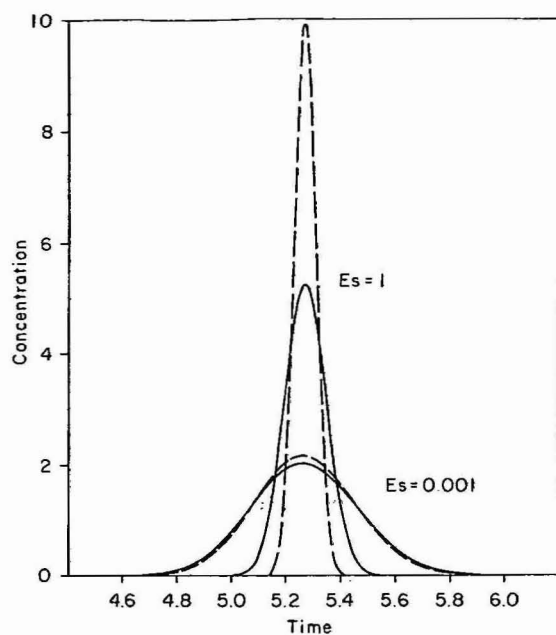
Fig. 7. Effect of neglecting axial dispersion. (—) With axial dispersion; (- - -) without axial dispersion.
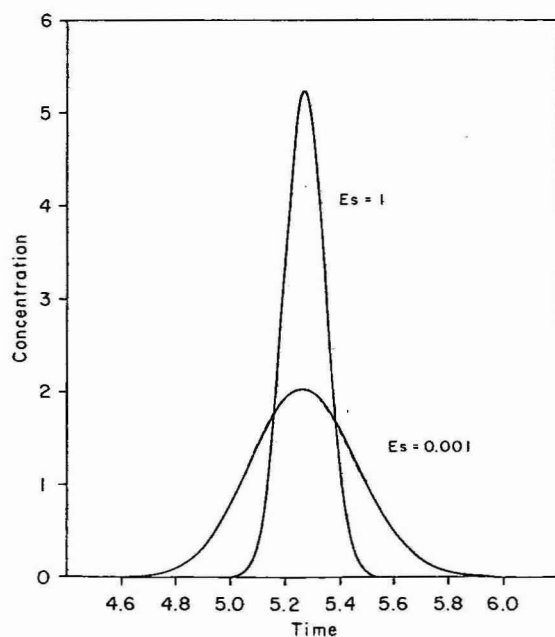
Fig. 8. Effect of lumping all band broadening mechanisms into single-phase effective dispersion coefficient. (—) Exact solution; (- - -) approximate solution.

assumption of equilibrium is reasonable. This is in agreement with the predictions of the order-of-magnitude analysis.

The neglect of axial dispersion may be reasonable if its contribution to band broadening is much smaller than that of the interaction between convection and lateral transport. Fig. 7 shows situations where this does and does not apply, with the intraparticle diffusivity being the manipulated parameter. Clearly at the lower value of E_s lateral transport is slow enough to cause enough band broadening to dominate the axial dispersive contribution. Again the order-of-magnitude analysis is in accord with this result.

Finally, an approximate solution can be developed on the basis of the observed symmetry of the chromatographic peaks over a wide range of parameter values. This symmetry suggests that the interaction between lateral transport and axial convection can be described in terms of an effective axial dispersion coefficient, $\mathscr{D}_{eff}$, in single-phase dispersed plug flow at an effective velocity, u_{eff}. The velocity is found from the solute mean residence time given by the first moment, μ_1, while $\mathscr{D}_{eff}$ can be found explicitly using the equation for reduced plate height h: $\mathscr{D}_{eff} = d_p u_{eff} h/2$. The concentration profile can then be calculated using either the short column asymptotic result[18] or the long column Gaussian result; the differences are small for normal chromatographic situations. As shown in Fig. 8, the agreement between the approximate and exact solutions is excellent over a wide range of values of E_s; similar results are observed when other parameters are varied.

CONCLUSIONS

The availability of the full analytical solution allows testing of several assumptions and procedures commonly used in linear chromatography. As has been shown, for example, slow lateral transport, whether diffusive or sorptive in origin, does not usually cause peak skewness. Secondary sorption, on the other hand, indeed appears to be a plausible cause of peak skewness. Other causes, not considered here, arise from extra-column effects such as dispersion in feeder tubes.

The use of moments to determine plate heights is susceptible to appreciable integration errors. In practice, this problem may be ameliorated to some extent by correlations among the errors in the three moments, but the use of plate heights remains a risky procedure. It would be much safer to perform parameter estimation using the full chromatographic peak in the time domain, thereby allowing a much more rigorous use of experimental data. For this purpose the modified single-phase dispersed plug flow model is accurate and efficient for chromatographic systems described by the model used here. It should be emphasised, however, that extra-column effects should be accounted for in the modelling process, since they can contribute to band broadening. For instance, for the parameter values given earlier it is possible to have reduced plate heights as low as about 1. Such low values are inconsistent with normal experimental observations, and extra-column effects are largely responsible.

Finally, it should be noted again that the plate height approach loses all validity in the non-linear region one would expect to encounter in many preparative situations. The full time-domain description would be needed here, and the procedures discussed here for linear chromatography may provide a basic framework which can be extended to non-linear systems.

REFERENCES

1 M. Kubin, *Collect. Czech. Chem. Comm.*, 30 (1965) 2900.
2 E. Kučera, *J. Chromatogr.*, 19 (1965) 237.
3 Cs. Horváth and H.-J. Lin, *J. Chromatogr.*, 149 (1978) 43.
4 P. V. Danckwerts, *Chem. Eng. Sci.*, 2 (1953) 1.
5 J. B. Rosen, *J. Chem. Phys.*, 20 (1952) 387.
6 A. Rasmuson, *AIChE J.*, 27 (1981) 1032.
7 J. C. Giddings, *Dynamics of Chromatography. Part I: Principles and Theory*, Marcel Dekker, New York, 1965.
8 J. W. Hiby, in *Proc. Symp. Interactions between Fluids and Particles*, Inst. Chem. Eng., London, 1962, p. 312.
9 R. Pfeffer, *Ind. Eng. Chem. Fundam.*, 3 (1964) 380.
10 L. R. Snyder and J. J. Kirkland, *Introduction to Modern Liquid Chromatography*, Wiley, New York, 2nd ed., 1979.
11 R. L. Curl and M. L. McMillan, *AIChE J.*, 12 (1966) 819.
12 S. N. Chesler and S. P. Cram, *Anal. Chem.*, 43 (1971) 1922.
13 R. E. Pauls and L. B. Rogers, *Sep. Sci.*, 12 (1977) 395.
14 D. J. Anderson and R. R. Walters, *J. Chromatogr. Sci.*, 22 (1984) 353.
15 J. J. Kirkland, W. W. Yau, H. J. Stokosa and C. H. Dilks, *J. Chromatogr. Sci.*, 15 (1977) 303.
16 P. C. Lewellen, *Comput. Phys. Commun.*, 27 (1982) 167.
17 E. Glueckauf and J. I. Coates, *J. Chem. Soc.*, 1947 (1947) 1315.
18 H. Brenner, *Chem. Eng. Sci.*, 17 (1962) 229.

CHROMSYMP. 1018

SYSTEMATIC ERRORS IN THE MEASUREMENT OF PEAK AREA AND PEAK HEIGHT FOR OVERLAPPING PEAKS

JOE P. FOLEY

Department of Chemistry, Louisiana State University, Baton Rouge, LA 70803-1804 (U.S.A.)

SUMMARY

Errors in the algorithms commonly employed by integrators and data systems for the measurement of peak areas and peak heights of overlapped peaks are re-evaluated for cases where one or both peaks is stailed. The errors due only to peak tailing (area ratio = 1) can be greater than 50% for peak area measurement by the perpendicular-drop algorithm; errors in peak height can be greater than 40%. Errors due to a combination of peak tailing and differences in peak size can exceed 200% for peak area and 80% for peak height. An empirical area equation, when used in conjunction with normal integration procedures, permits the accurate ($< \pm 4\%$) quantitation of overlapping peaks, provided that the valley between the peaks is less than 45%.

INTRODUCTION

Gas and liquid chromatography are powerful methods for the quantitative analysis of multi-component mixtures. Unfortunately, as the number of components in a mixture increases, the probability that all components will be baseline resolved drops precipitously[1,2]. Inevitably at least some of the partially resolved peaks will be of interest to the analyst. Thus, the quantitation of overlapping peaks is an important issue.

The quantitation of chromatographic peaks requires the measurement of either peak height or peak area. While the manual or electronic measurement of peak heights and peak areas for baseline-resolved peaks is straightforward and accurate, the same measurement for partially resolved peaks is neither, due to the distortion caused by peak overlap. Although peak deconvolution methods have been developed[3–7], the approach used by nearly all electronic integrators and most data systems (and the only approach available when manual measurements are made) is to approximate the peak areas and peak heights of overlapped peaks by measurements made directly from the overlapping chromatogram. For peak areas, the perpendicular-drop and tangent-skimming methods are used on overlapping peaks with comparable and disproportionate areas, respectively. For peak height, the apparent peak height is used in all cases.

The accuracy of these integrator–data system approximations for overlapping

peaks has been evaluated extensively[8–10]. It was found that peak height could be measured much more accurately than peak area for a given resolution and peak area ratio. Many refinements have been proposed, particularly for peak area measurements[8], including the use of correction factors based on calculated errors[11,12].

Unfortunately, although these overlapping peaks approximations have been evaluated in detail, previous researchers have assumed symmetric (Gaussian) peak profiles for the component peaks. However, it is clear from the chromatographic literature that many overlapping peak profiles frequently consist of asymmetric (tailed) chromatographic peaks. Our goals in the present study are (1) to re-evaluate the accuracy of these popular approximations for the measurement of peak area and peak height for overlapping peaks when one or both peaks are tailed; and (2) to investigate alternative approaches for the quantitation of overlapping peaks that do not require deconvolution. Because our emphasis is on the effect of peak asymmetry on overlapping peaks and not on the effect of relative peak size, which has already been extensively discussed (for overlapping Gaussian peaks)[9,10], we limited our studies to overlapping peaks with area ratios of 4 or less. Thus our present study does not include a re-evaluation of the tangent skimming method, since this method is inappropriate under these circumstances.

EXPERIMENTAL

Computations. An Apple Macintosh computer programmed in BASIC was used for all calculations.

Symmetric and asymmetric (tailed) peak models. Symmetric chromatographic peaks were generated using a normalized Gaussian function G(t),

$$G(t) = A/\sigma_G(2\pi)^{\frac{1}{2}}] \exp[-(t-t_G)^2/2\sigma_G^2] \qquad (1)$$

where A is the peak area, t_G is the retention time, and σ_G is the standard deviation of the peak. Tailed chromatographic peaks were generated using a normalized exponentially modified Gaussian function EMG(t). The EMG function results from the convolution of a Gaussian function and an exponential decay function and can be expressed in a variety of ways[13–15]. The specific form we used was

$$EMG(t) = A/\tau \exp[1/2(\sigma_G/\tau)^2 - (t-t_G)/\tau] \int_{-\infty}^{z} \exp(-y^2/2)/(2\pi)^{\frac{1}{2}}dy \qquad (2)$$

where A is the peak area, t_G and σ_G are the retention time and standard deviation of the Gaussian function respectively, τ is the time constant from the exponential decay function, and $z = (t-t_G)/\sigma_G - \sigma_G/\tau$. The integral in eqn. 2 was evaluated as previously described[16]. Note that the ratio τ/σ_G is a fundamental measure of peak symmetry. As τ/σ_G increases, the tailing of the chromatographic peak increases. As τ/σ_G approaches 0, the resulting peak approaches that of a Gaussian.

Peak overlap simulations. A pair of overlapping peaks was simulated by adding the functions representing the individual chromatographic peaks. Four combinations

of overlapping peaks (symmetric–symmetric, tailed–tailed, tailed–symmetric, and symmetric–tailed) were examined for five area ratios (0.25, 0.5, 1, 2, and 4), five τ/σ_G ratios (0.5, 1, 2, 3, and 4), and several values of resolution, resulting in over 600 pairs of overlapping peaks. Resolution was defined conventionally as $\Delta t_G/4$ (variance)$^{\frac{1}{2}}$, where $\Delta t_G = t_{G,2} - t_{G,1}$ and σ_G^2 and $\sigma_G^2 + \tau^2$ are the variance of a Gaussian and an EMG peak, respectively. A constant Gaussian contribution to the total variance (fixed value of σ_G) was assumed for both peaks in every peak combination, although the EMG–EMG peak combinations were also examined from the point of view of constant total variance. Resolution values of 1.75, 1.5, 1.25, 1.125, 1, 0.875, 0.625, 0.5, 0.375, and 0.25 were used in generating the data for this study. Although the resolution parameter proved useful in generating the data, it was found to be inadequate in describing peak overlap in cases where one or both peaks is tailed (see Results and discussion).

Measurement of peak parameters. A search algorithm for the measurement of the retention time, peak height, and width and asymmetry of an isolated peak at any peak height fraction[16] was modified to measure the pertinent parameters of overlapping peaks (see Fig. 2). in simulating the perpendicular-drop algorithm, peak areas were calculated by summation from the valley to the appropriate baseline. This is the method most commonly employed by chromatographic integrators and/or data systems.

RESULTS AND DISCUSSION

Preliminary considerations

Peak modeling. The Gaussian and the exponentially modified Gaussian (EMG) functions were used as models for symmetric and asymmetric (tailed) chromatographic peaks. Four combinations of overlapping peaks, described below, were examined in our evaluation of the perpendicular-drop and apparent-peak-height methods for peak area and peak height measurement.

(1) Symmetric peak–symmetric peak. Neither peak is subject to asymmetric band-broadening processes. This combination has been the only one examined in nearly all prior studies of overlapping peaks.

(2) Tailed peak–tailed peak. Both peaks are subject to asymmetric band-broadening processes. This is most likely to be observed when extra-column effects (which affect closely eluted peaks similarly) cannot be eliminated, although it could also be observed if both peaks participated in an irreversible retention mechanism.

(3) Tailed peak–symmetric peak. Only the first peak is subject to an asymmetric band-broadening process. This could occur when an additional, irreversible (slow) retention mechanism is operative for one of the peaks.

(4) Symmetric peak–tailed peak. Same as 3, except that the tailed peak is eluted last.

To perform the simulations, values for the variances of the overlapping peaks must be assumed. We assumed a constant symmetric variance (σ_G^2) for both peaks of the overlapped pair; this is consistent with the scenarios described above. Thus for Gaussian peaks the total variance (σ_G^2) was fixed, whereas for the EMG peaks the total variance ($\sigma_G^2 + \tau^2$) increased as the asymmetry ratio (τ/σ_G) was increased.

The generation of overlapping peaks is illustrated in Fig. 1. Isolated symmetric
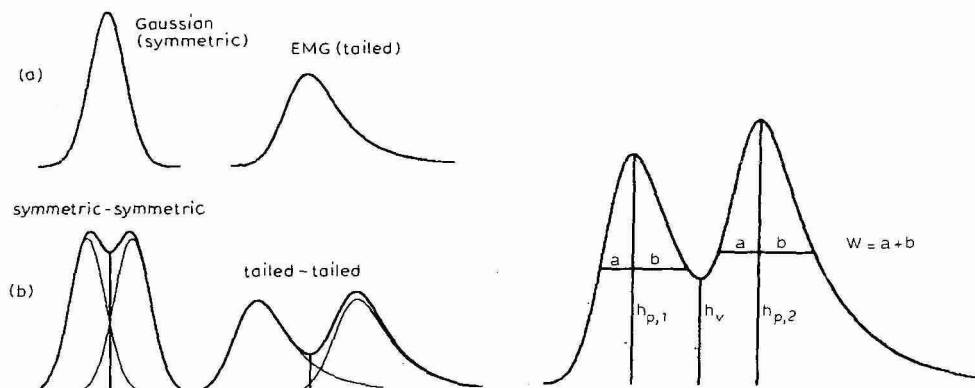
Fig. 1. Overlapping peak simulations. Individual Gaussian and exponentially modified Gaussian (EMG) functions in Fig. 1a were offset and added to produce the symmetric peak–symmetric peak, tailed peak–tailed peak combinations shown in Fig. 1b, as well as the tailed peak–symmetric peak and tailed peak–symmetric peak combinations that are not shown.

Fig. 2. Graphical parameters of overlapping peaks, shown here for two tailed (EMG) peaks of equal area with an asymmetry ratio (τ/σ_G) of 2. The relative valley is defined as the ratio of h_v/h_p, and is conveniently expressed as a percentage. The width, W, and asymmetry factor, b/a, are shown at the peak height fraction, $\alpha = 0.5$.

(Gaussian) and tailed (EMG, $\tau/\sigma_G = 2$) peaks of unit area in Fig. 1a are merged with identical peaks to produce the symmetric–symmetric and tailed–tailed overlapping peak combinations in Fig. 1b. The resolution, R_s, defined as $\Delta t_R/4\sigma^2$ [where σ^2 is the total variance (second statistical moment)], was 0.625 for both pairs of overlapping peaks.

    Measures of peak overlap. Fig. 1b illustrates the inadequacy of the present definition of resolution to describe the overlap of real chromatographic peaks. As noted long ago by Kirkland *et al.*[17], the "apparent resolution" is better for the tailed peaks than for the symmetric peaks. This paradox can be explained in terms of the greater error in peak height and peak area estimation for the tailed peak pair which we discuss in detail shortly.

    Given the inadequacy of the resolution parameter to describe peak overlap, we decided to employ an empirical parameter, the relative valley, as illustrated in Fig. 2. We define the relative valley as the ratio of the height of the valley, h_v, to the apparent height of the peak in question, h_p. We will frequently report it as a percentage, *i.e.*, % (relative) valley = $h_v/h_p \times 100$. Note that, unless the apparent peak heights are the same for two peaks of an overlapping peak pair ($h_{p,1} = h_{p,2}$), the relative valleys for the two peaks will not be the same. Finally, although the relative valley is empirical, it is an unambiguous parameter, one that is easily measured in practice.

Errors in peak area and peak height measurements

    General comments. The results of our study show that errors in the perpendicular-drop and apparent peak height methods for the measurement of peak area and peak height of overlapping peaks are due primarily to two distinguishable effects,

one resulting from a difference in the relative size (areas) of the two peaks that overlap, the other resulting from the asymmetry of one or both peaks of the over-lapped pair. We shall denote these effects as *size effects* and *asymmetry effects*, re-spectively. Whereas the error in peak area will be negative for one peak and positive for the other, the error in peak height will be positive for both peaks. Obviously the error in either parameter becomes larger as the degree of peak overlap (relative valley) increases.

Size effects. We examined the errors in peak height and peak area measurement as a function of the relative areas of overlapping symmetric (Gaussian) peaks (and the degree of peak overlap). Because size effects have already been thoroughly dis-cussed[9,10], we only summarize the results for purposes of comparison with the asym-metry effects.

For all degrees of peak overlap (relative valley), errors in peak height are much smaller than corresponding errors in peak area. Errors in peak height are negligible, in fact, whenever the valley is less than 50%. For a given degree of peak overlap, errors in peak area are much more dependent on the area ratio than errors in peak height. The relative error in peak area and peak height was larger for the smaller of the overlapping peaks. Finally, the maximum errors due to size effects for peaks with an area ratio of four and a perceptible valley were −28% for peak area and +7.5% for peak height (for the smaller peak in both cases).

Asymmetry effects. We examined the errors in peak height and peak area mea-surement as a function of the asymmetry (tailing) of one or both of the overlapping peaks, *i.e.*, by examining tailed peak–tailed peak, tailed peak–symmetric peak, and symmetric peak–tailed peak combinations for peaks of equal size. Except for a recent reference to peak height[18], asymmetry effects have been completely ignored.

Since we assumed a constant symmetric variance (σ_G^2) for all peaks, tailed peaks of unit area are shorter than corresponding symmetric peaks, as shown in Fig. 1a. It was thus impossible to produce overlapping peaks of equal area *and* equal peak height for the tailed peak–symmetric peak and symmetric peak–tailed peak combi-nations. Because area is more easily fixed for EMG peaks (see eqn. 2), our studies used peaks of equal area.

(1) Tailed peak–tailed peak combinations. An example of the asymmetry effect is given in Fig. 3 for the tailed peak–tailed peak peak combination with $\tau/\sigma_G = 3$. Individual peaks were lightly traced, whereas the composite peak is shown with a
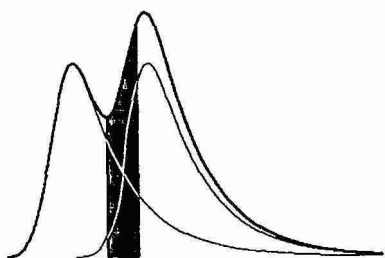
Fig. 3. Illustration of the asymmetry effect for the tailed peak/tailed peak combination, shown here for two overlapped EMG peaks of equal area with an asymmetry ratio (τ/σ_G) of 3. Shaded area represents the error of the perpendicular-drop algorithm for peak area. The errors in peak area are −34% and +34% for the first and second peaks; the errors in peak height are 0.03% and 26%.
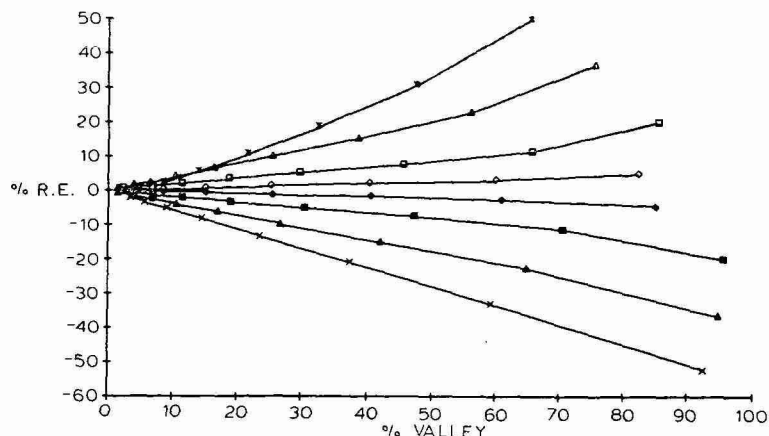
Fig. 4. Summary of asymmetry effects on peak area for two overlapping, tailed peaks of equal area. Filled symbols indicate results for the first peak, open symbols represent the second peak. Values for $\tau \sigma_G$ (asymmetry ratio): 0.5 (○), 1 (□), 2 (△), and 4 (×).

bold tracing. The shaded area represents the error of the perpendicular-drop algorithm, *i.e.,* the amount by which the area of the first peak is underestimated and by which the area of the second peak is overestimated. The shaded area represents a substantial portion (34%) of the total area. Also, in contrast to the size effect, the asymmetry effect on peak *height* is significant (+26%), although only for the second peak.

Asymmetry effects for the tailed peak–tailed peak combinations are summarized in Figs. 4 and 5 for peak area and peak height for $\tau/\sigma_G = 0.5$, 1, 2, and 4. As expected, the greatest errors in peak area occurred for the peak combinations with $\tau/\sigma_G = 4$ (the greatest tailing). The maximum observed errors were -52% and $+50\%$ for the first and second peaks. (Slight differences are attributed to truncation errors in the integration of the second peak.) For peak height, the greatest errors for
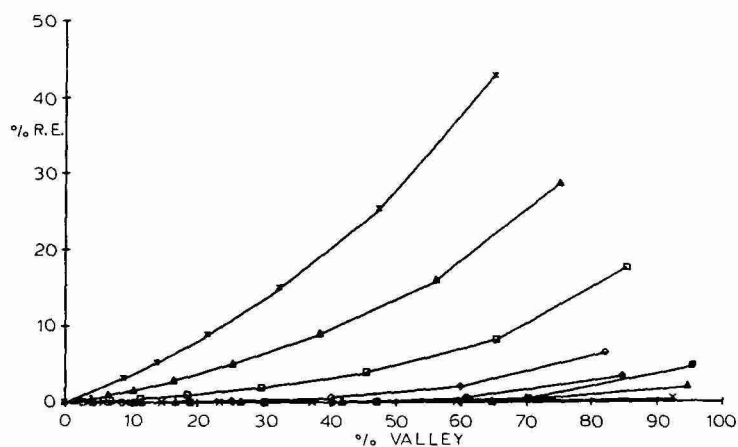
Fig. 5. Summary of asymmetry effects on peak height for two overlapping, tailed peaks of equal area. Conditions as in Fig. 4.

the first peak ($+5\%$) occurred for peak combinations with moderate tailing ($\tau/\sigma_G = 1$) whereas the greatest errors for the second peak $+40\%$) occurred for the combination with maximum tailing.

(2) Tailed peak–symmetric peak combinations. The asymmetry effects for this combination were slightly larger for peak area and moderately lower for peak height than for the tailed peak–tailed peak combination above, although the general pattern remained the same. For this reason no figures are included for these data, although they will be made available as supplementary material. The maximum errors in peak area were -58% and $+56\%$ for the first and second peaks. For peak height, the largest errors were $+5\%$ for the first peak (at $\tau/\sigma_G = 0.5$) and $+20\%$ for the second peak (at $\tau/\sigma_G = 4$). The difference between the asymmetry effects for the tailed peak–tailed peak and tailed peak–symmetric peak combinations is attributed to the fact that, although the first and second peaks were of equal area for both combinations, the first peak was shorter in the tailed peak–symmetric peak combination.

(3) Symmetric peak–tailed peak combinations. The results for the case where only the second peak is tailed were different from the results of the two previous combinations. Errors in peak area were much lower ($\pm12\%$), and the area of the first peak was *over*estimated instead of *under*estimated as in the previous combinations (and vice versa for the second peak). Errors in peak height were comparable for the first and second peaks (a maximum of $+8\%$), and fell between the errors observed for the first and second peaks in previous combinations. Finally, errors in both peak area and peak height were much less dependent on the asymmetry of the second peak.

The difference between the asymmetry effects for the symmetric peak–tailed peak combination and the first two combinations was not unexpected. By definition the leading edge of a tailed (EMG) peak more closely resembles a Gausian peak than the trailing edge. Since the leading edge of the EMG peak is the part that overlaps with the Gaussian in the symmetric peak–tailed peak combination, we expect the asymmetry effects to be much less pronounced. The effects we do observe are attributed to the somewhat smaller slope of the leading edge of the EMG peak due to the larger variance. We could predict similar results for two partially resolved Gaussian peaks, the second of which had a larger variance.

In summary, the most serious errors in peak area and peak height resulting from asymmetry effects occurred when the first peak was tailed. These errors, which have previously been ignored, sometimes exceeded 50%. When only the second peak was tailed, the errors were less than 15%.

Combined size–asymmetry effects

The combined effects of size and asymmetry were studied by examining the overlapping peak combinations tailed peak–tailed peak, tailed peak–symmetric peak, and symmetric peak–tailed peak for peaks with area ratios of 0.25:1, 0.5:1, 1:0.5, and 1:0.25. For reasons of brevity, we will not consider all combinations in detail. Data and charts are available upon request.

For peak area, in general, the errors induced by the combined size–asymmetry effects were additive, and thus substantially larger than for the separate effects, although occasionally a fortuitous cancellation of error was observed. (A cancellation of error is possible, since both effects produced positive and negative errors.) For
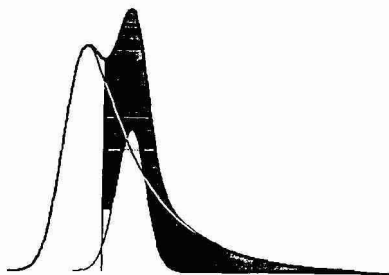
Fig. 6. Illustration of the combined effects of size and asymmetry on the measurement of peak area and peak height. Relative peak area (tailed peak: symmetric peak) = 4:1. Shaded area represents the error of the perpendicular-drop algorithm for peak area. The errors in peak area are −54% and +208% for the tailed and symmetric peaks respectively; errors in peak height are +0.5% and +86.0, respectively.

peak height, since errors due to size and asymmetry are always positive, no cancellation of error is possible. In general, errors in peak height due to combined effects were additive, but since size effects are several times smaller than asymmetry effects, the errors in peak height due to combined effects were only marginally larger than errors due to asymmetry effects alone.

The largest errors observed for both parameters resulted from the overlap of a large highly tailed peak with a small, symmetric peak, as shown in Fig. 6 for peaks with an area ratio of four-to-one. As in Fig. 3, the shaded area represents the error of the perpendicular-drop algorithm, *i.e.*, the amount by which the area of the tailed peak is underestimated and by which the area of the symmetric peak is overestimated. For the tailed and symmetric peaks in Fig. 6 the errors in peak area were −54% and +208%; errors in peak height were +0.5% and +86%.

Improving the accuracy of quantitation

The above discussion shows that, due to symmetry effects which have previously been ignored, the systematic errors of current integrator-based methods for peak area and peak height measurement on overlapping peaks are much larger than previously estimated. This is particularly true for partially resolved peaks of nearly equal area, for which errors in the perpendicular-drop algorithm have formerly been assumed to be negligible.

The best way to eliminate quantitative errors caused by overlapping peaks is to eliminate the overlap, *i.e.*, change the chromatographic conditions so that the peaks of interest are baseline-resolved. Because this cannot always be done in practice, it is thus desirable to consider what improvements in quantitation are possible wihtout an improvement in the separation.

Empirical area equation. Since the errors in peak height and peak area measurement for overlapping peaks are a direct result of the distortion caused by the overlap, a logical approach would be to use or develop a quantitative method, based on measurements in regions of minimum distortion. In our studies, we observed much less distortion for the first peak than the second, as evidenced by the generally insignificant errors in peak height for the first peak.

We recently developed[19] a set of empirical equations for the calculation of
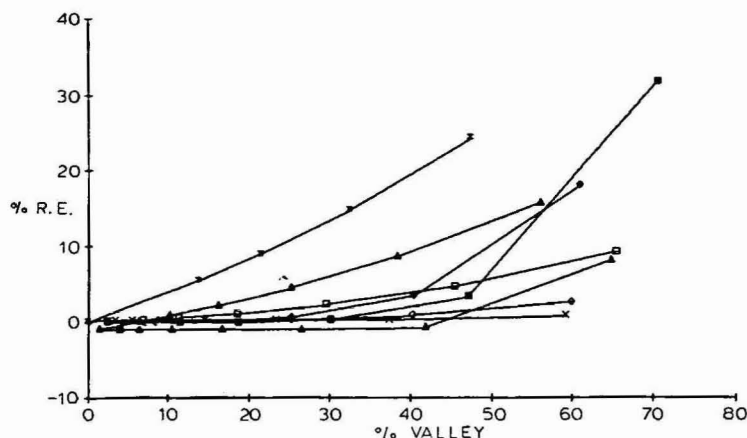
Fig. 7. Summary of asymmetry effects on eqn. 3, $A = 1.64 h_p W_{0.75} (b/a)^{+0.717}$, for two overlapping tailed peaks of equal area. Conditions as in Fig. 4.

peak area for symmetric (Gaussian) and tailed (EMG) peaks. These equations were obtained by fitting plots of A_{true}/A_G vs. the asymmetry factor (b/a), where A_G is the area calculated using a Gaussian equation. Although these equations were originally developed for peak modeling studies, one of them proved useful for the present study. The equation is

$$A = 1.64 h_p W_{0.75} (b/a)^{0.717} \qquad (3)$$

where A is the peak area, h_p is the peak height, and $W_{0.75}$ and b/a are the peak width and asymmetry measured at 75% of the peak height, respectively. The bias of eqn. 3 is less than $\pm 1\%$ for well-resolved symmetric (Gaussian) and tailed (EMG) peaks from $\tau/\sigma_G = 0$ to 4.2. The expected precision of eqn. 3, calculated via error propagation, is $\pm 1\%$, assuming a precision of $\pm 0.5\%$, $\pm 0.5\%$, and $\pm 1\%$ for h_p, $W_{0.75}$, and b/a.

The accuracy of eqn. 3 for overlapping peaks is shown in Fig. 7 for the tailed peak–tailed peak peak combination. For peak overlap (valleys) up to 45%, errors were less than $\pm 4\%$ for both the first and the second peaks, except in the cases of extreme tailing $(\tau/\sigma_G = 3, 4)$. In these instances, the relative errors were large for the second peak but less than $\pm 1\%$ for the first peak.

Eqn. 3 was comparably accurate for the remaining tailed peak–tailed peak combinations and for all the tailed peak–symmetric peak combinations. Errors for the first peak never exceeded $\pm 4\%$; errors for the second peak were large, as in Fig. 7, for cases of extreme tailing $(\tau/\sigma_G = 3, 4)$.

For the symmetric peak–tailed peak combinations, eqn. 3 was more accurate for the second peak than for the first. In addition, the errors were nearly independent of the degree of tailing. For valleys up to 50%, errors were less than $\pm 2\%$ for the second (tailed) peak regardless of asymmetry. For the first (symmetric) peak, errors ranged from $+5$ to $+20\%$.

Although we did not examine peak combinations with area ratios outside the

range of 1:4 to 4:1, we can safely assume that, for the *larger* peak of an overlapped pair, eqn. 3 wil be more accurate than stated above (provided the valley limits are not exceeded), because the distortion of the larger peak of an overlapped pair for peak combinations outside the range of 1:4 to 4:1 will be less than for combinations within this range.

To summarize, for overlapping peaks with area ratios between 1:4 and 4:1, the empirical area equation, eqn. 3, is accurate to within ±4% for the first peak of tailed peak–tailed peak or tailed peak–symmetric peak combinations, provided that the valley between peaks is less than 45%. For the symmetric peak–tailed peak combination, eqn. 3 is accurate to within ±2% for the second peak, if the valley is less than 50%. For overlapping peaks with area ratios outside the range of 1:4 and 4:1, eqn. 3 will be somewhat more accurate, but only for the larger peak of the overlapped pair.

Combined area equation–integrator approach. By itself, eqn. 3 facilitates the accurate ($< \pm 4\%$) quantitation of only *one* peak of an overlapped pair. However, if an integrator is used to measure the total area of the two overlapping peaks, the area of the other peak can be accurately determined by subtraction, *i.e.*,

$$A_{\text{other}} = A_T - A_{\text{eq}} \qquad (4)$$

where A_T is the total area provided accurately by the integrator, A_{eq} is the area of the peak for which eqn. 3 is accurate, and A_{other} is the area of the other peak.

The accuracy and precision by which A_{other} can be measured is, of course, related to the accuracy and precision by which A_T and A_{eq} can be measured. Assuming (1) A_T can be measured with much greater accuracy and precision than A_{eq}; and (2) neglibible covariances, the relative error (R.E.) and relative standard deviation (R.S.D.) of A_{other} are given by

$$\text{R.E. } (A_{\text{other}}) = - [A_{\text{ratio}} \text{ R.E. } (A_{\text{eq}})] \qquad (5)$$

$$\text{R.S.D. } (A_{\text{other}}) = A_{\text{ratio}} \text{ R.S.D. } (A_{\text{eq}}) \qquad (6)$$

where $A_{\text{ratio}} = A_{\text{eq}}/A_{\text{other}}$. Thus, the accuracy and precision of the indirectly measured

TABLE I

RELATIVE ERROR IN PEAK HEIGHT AND PEAK AREA MEASUREMENT FOR A LARGE, TAILED PEAK, OVERLAPPED WITH A SMALL, SYMMETRIC PEAK*

Parameter	Relative error (%)	
	Tailed peak	Symmetric peak
Peak height	0.0	+ 45.6
Peak area (perpendicular-drop)	− 31.1	+ 117.3
Peak area, eqns. 3 and 4	+ 0.4	− 1.6

* Tailed (EMG) peak with $\tau/\sigma_G = 4$ and area = 1. Symmetric (Gaussian) peak with area = 0.25. Valley between the peaks is 54% relative to the tailed peak (60% relative to the symmetric peak).

peak depends directly on the accuracy and precision of the area equation and on the area ratio of the overlapping peaks. For $0.25 < A_{ratio} < 1$, the relative accuracy and precision of A_{other} will be better than for A_{eq} (the accuracy of A_{eq} was not confirmed for $A_{ratio} < 0.25$). For $A_{ratio} > 1$, the accuracy and precision of A_{other} will be worse. Assuming R.E. (A_{eq}) = R.S.D. (A_{eq}) = $\pm 1\%$, A_{ratio} can be no higher than 10:1 for acceptable ($\pm 10\%$) accuracy and precision of A_{other}.

As described above, the combined equation–integration method for peak area measurement of overlapping peaks (eqns. 3 and 4) is appropriate for $0.25 < A_{ratio} < 10$. Although limited to pairs of peaks with area ratios in this range, this method can easily be implemented on programmable integrators and data systems and will improve the accuracy of area quantitation substantially in these cases. An example of the superior accuracy of the combined area equation–integration method for peak quantitation (eqns. 3 and 4) over common integrator–data system methods for peak height and peak area is shown in Table I for a highly tailed peak (τ/σ_G = 4, area = 1) overlapped with a symmetric peak (area = 0.25). The peak combination is the same as illustrated in Fig. 6, exept that the peak overlap was somewhat less (valleys of 54% and 60% for the tailed and symmetric peaks).

Correction factors. The true value, T, for peak area or peak height, is related to the observed value, O, by the relative error, R.E. = $(O - T)/T$. Solving this equation in terms of T yields

$$T = O/(\text{R.E.} + 1) \tag{7}$$

We can regard $1/(\text{R.E.} + 1)$ in eqn. 7 as a correction factor (C.F.) and write

$$T = O \times \text{C.F.} \tag{8}$$

Correction factors can be interpolated manually or by computer from a previously generated look up table. Alternatively, if a sufficiently accurate functional relationship can be obtained, these correction factors can be calculated on-line using a computer.

When *only* the size effect is considered (Gaussian peak shapes are assumed), it is possible to calculate accurate correction factors as a function of only two variables: area ratio and degree of peak overlap (resolution, R_s), i.e.,

$$\text{C.F.} = f[A_{ratio}, \text{ peak overlap } (R_s)] \tag{9}$$

Correction factors based only on size effects have been calculated previously for peak areas[11,12]. However, as we have shown in this report, asymmetry effects on the quantitation of overlapping peaks are frequently as important or more important than size effects. Thus, size-effect-only "correction factors" are generally inaccurate.

Unfortunately, the incorporation of peak asymmetry into the correction factor, as shown in eqn. 10, makes the calculation and use of correction factors difficult if not impossible.

$$CF = f[A_{ratio}, \text{ type of combination, peak overlap } (\neq R_s), \text{ peak asymmetry}] \tag{10}$$

First, for a given set of area ratios the number of overlapping peak combinations has

increased from one (symmetric–symmetric) to four (symmetric–symmetric, tailed–tailed, tailed–symmetric, and symmetric–tailed). Since each combination requires a pair of correction factors (one for each peak of the overlapped pair), eight sets of correction factors are now required instead of two. Second, an empirical measure of peak overlap must be used, since the fundamental resolution parameter, R_s, can no longer be visually estimated (except by comparison with standard drawings for the hundreds of possible combinations, which is clearly impractical). Finally, the dimensionality of each set of correction factors is increased from two to four. If correction factors are to be *interpolated* from tabulated values, a four-dimensional table will be required instead of a two-dimensional table for each set of correction factors. If correction factors are to be *calculated,* an accurate relationship for eqn. 10 must be deduced, presumably by multivariate regression. (Our efforts in obtaining a satisfactory empirical relationship for eqn. 10 were unsuccessful.)

Other discussion

Implications for preparative liquid chromatography. Because asymmetry effects have previously been ignored, peak purity has probably been overestimated for overlapping tailed peaks. In particular, if the valley is used as the cutpoint for peak fractions of overlapping peaks, the second compound will be highly contaminated with the first. To ensure the purity of the second peak, the cutpoint should be made more conservatively, *i.e.,* considerably later than the valley between the peaks.

Errors due to overlap of more than two peaks. Although we did not perform a simulation involving a *series* of overlapping peaks, the trends observed for overlapping *pairs* of peaks enables us to make the following predictions for a series of peaks, assuming that (1) the tailing is approximately the same for all peaks; (2) the peak areas are within a factor of 4 for neighboring peaks; and (3) all neighboring peaks have valleys between them.

For the first peak of a series, the error in peak height wil be negligible, as will the error in peak area calculated using eqn. 3, if the valley is less than 45%. In contrast, the error in peak area, as determined by the perpendicular-drop algorithm, wil be large, especially if the peaks are highly tailed. For interior peaks, errors in peak height are expected to be significant, due to peak distortion from both sides. Errors in peak area resulting from use of eqn. 3 will be also be substantial. On the other hand, errors in the perpendicular-drop algorithm for peak area may or may not be significant. Asymmetry effects are expected to cancel, whereas size effects may be somewhat enhanced if the middle peak is smaller than its neighbors. Finally, for the last peak in a series of partially resolved tailed peaks, we expect all three measurements (peak height, peak area via perpendicular-drop, and peak area via eqn. 3) to be inaccurate. Note that an approach analogous to eqn. 4 (eqn. 11 below) will not work, because $A_{interior}$, the area of the interior peaks, cannot always be determined with sufficient accuracy.

$$A_{last} = A_T - A_{first} - A_{interior} \qquad (11)$$

CONCLUSIONS

Because peak asymmetry (tailing) has previously been ignored, the accuracy

of the integrator-based measurement of peak area and peak height has been substantially overestimated for overlapping peaks. For peaks of comparable size, errors in the perpendicular-drop algorithm for peak area, which were formerly assumed to be negligible, can be greater than 50%. Errors in peak height, also frequently assumed to be negligible, can be greater than 40%. The combination of asymmetry effects and differences in relative peak size can lead to errors in peak height that exceed 80% and errors in peak area that exceed 200%. Baseline or near-baseline resolution is therefore essential for the accurate quantitation of overlapping peaks when common integrator–data system methods are used and one or both peaks is tailed. Alternatively, the combined use of an empirical area equation and normal integration procedures (eqns. 3 and 4) allows accurate quantitation ($< \pm 4\%$) for overlapping peaks, provided that the valley between the peaks is less than 45%. The use of correction factors does not appear to be a viable approach whenever one or both overlapping peaks is tailed.

SUPPLEMENTARY MATERIAL

Data and charts for all the overlapping peak combinations described are available upon request.

REFERENCES

1 J. M. Davis and J. C. Giddings, *Anal. Chem.*, 57 (1985) 2168–2177.
2 J. M. Davis and J. C. Giddings, *Anal. Chem.*, 57 (1985) 2178–2182.
3 R. F. Lacey, *Anal. Chem.*, 58 (1986) 1404–1410.
4 S. D. Frans, M. L. McConnel and J. M. Harris, *Anal. Chem.*, 57 (1985) 1552–1559.
5 R. A. Vaidya and R. D. Hester, *J. Chromatogr.*, 287 (1984) 231–244.
6 R. A. Vaidya and R. D. Hester, *J. Chromatogr.*, 333 (1985) 152–155.
7 A. W. Westerberg, *Anal. Chem.*, 41 (1969) 1770–1777.
8 J. A. Perry, *Introduction to Analytical Gas Chromatography*, Marcel Dekker, New York, 1981, pp. 361–385.
9 L. R. Snyder and J. J. Kirkland, *Introduction to Modern Liquid Chromatography*, Wiley, New York, 2nd ed., 1979, pp. 38–48, 556–559.
10 L. R. Snyder, *J. Chromatogr. Sci.*, 10 (1972) 200–212.
11 J. Novák, K. Petrović and S. Wičar, *J. Chromatogr.*, 55 (1971) 221–229.
12 E. Proksch, H. Bruneder and V. Granzner, *J. Chromatogr. Sci.*, 7 (1969) 473–483.
13 D. Hanggi and P. W. Carr, *Anal. Chem.*, 57 (1985) 2394–2395.
14 R. Delley, *Chromatographia*, 18 (1984) 374–382.
15 R. Delley, *Anal. Chem.*, 57 (1985) 388.
16 J. P. Foley and J. G. Dorsey, *J. Chromatogr. Sci.*, 22 (1984) 40–46.
17 J. J. Kirkland, W. W. Yau, H. J. Stoklosa and C. H. Dilks, Jr., *J. Chromatogr. Sci.*, 15 (1977) 303–316.
18 D. A. Dezaro, T. R. Floyd, T. V. Raglione and R. A. Hartwick, *Chromatogr. Forum*, 1 (1986) 34–37.
19 J. P. Foley, *Anal. Chem.*, submitted for publication.

CHROMSYMP. 1042

STUDY OF THE RETENTION MECHANISMS FOR BASIC COMPOUNDS ON SILICA UNDER "PSEUDO-REVERSED-PHASE" CONDITIONS

G. B. COX* and R. W. STOUT

Biomedical Products Department, DuPont Company, Building 100, Glasgow Site, Wilmington, DE 19898 (U.S.A.)

SUMMARY

The performance characteristics of a set of nitrogenous bases were studied on a number of silicas using aqueous organic mobile phases. The retention characteristics were complex functions of the organic solvent and buffer concentrations as well as pH. The retention mechanisms were shown to be a combination of ion-exchange and interaction with siloxane and silanol groups over the entire range of concentration of organic solvent. The differences in retention on silica were due largely to the differences in ion-exchange strength of the silanol groups and the surface concentration of the siloxane bridges. The same solutes were studied on a range of C_8-bonded phases of varying surface coverage, where the same interactions were observed as seen on silica with the addition of reversed-phase interactions. The unexpected relation between capacity factor and bonded-phase coverage was explained by interaction of the several retention mechanisms involved. The retention of small proteins on pure silica was also related to its ion-exchange strength. The performance of the silicas was related to that of the bonded-phase packings prepared from them, the retention of the proteins again being related to the ion-exchange characteristics.

INTRODUCTION

The analysis of bases by high-performance liquid chromatography (HPLC), especially under reversed-phase conditions, is characterised by long and variable retention times, poor efficiency of separation and excessive peak tailing. Many strategies have been used in attempts to control these effects, the most popular being ion-pair chromatography and the so-called ion-suppression chromatography. Whilst these are successful in many cases, a few problems remain. Some of these can be eliminated by the use of alternative modifiers, such as triethylammonium salts[1], which are thought to act as competitors for the "active sites" that cause the chromatographic problems. In all cases the problem is usually assigned to some form of interaction with unbonded silanol groups which remain on the silica surface. It has been demonstrated that at least a part of this interaction is ionic in nature, the silica surface of a C_{18} packing acting as a weak cation-exchanger for aromatic bases over a very wide range of organic solvent concentrations[2,3]. In order to study the phe-

nomena involved in such interactions between bases and silanol groups it is clearly necessary to begin with a study of the interactions in which pure silica is used in order to remove any variability in results due to small differences in bonded-phase coverage resulting from variability in the synthesis or from hydrolysis of the bonded-phase under the test conditions.

The first report on chromatography of bases on pure silica packings under conditions related to reversed-phase systems was by Jane[4], who performed the analysis of basic drugs of abuse in methanol-rich aqueous ammonium nitrate at high pH. Other researchers[5-7] have described similar systems. A more thorough study of the use of these aqueous eluents with silica as well as with octadecylsilyl-bonded phases for the chromatography of bases at methanol compositions above 50% has been reported by Sugden et al.[8]. This group concluded that ion-exchange mechanisms were less important than other interactions between protonated species and silanol groups and ion-pair interactions. Since this time, Flanagan and Jane[9] have reported on the chromatography of basic amines and quaternary ammonium compounds on silica, mostly at high organic solvent concentration. Although ion-exchange mechanisms were postulated, a few observations were made which could not be reconciled with them. Very recently, work which extends these studies to a wider range of solvent compositions and to alumina was reported[10].

To date, little work has been reported which relates the chromatographic to the physical properties of silicas. It is known that silicas prepared by different routes do possess different properties[11]. Data on retention of diethylaniline in unbuffered systems[11] and of basic peptides[12] have been presented, although these investigations were carried out on bonded phases and no chromatographic data for the pure silicas were obtained.

The work reported in this paper attempts to address a number of questions. The mechanisms of retention of basic compounds on silica were shown to be more complex than merely ion exchange. The influence of increasing surface coverage of bonded phase on the separations were found to be unexpected and increasingly complex. Differences between different silicas were shown to be due largely to different ion-exchange capacities and/or strengths and were reflected in the performance of bonded-phase packings which were prepared from the silicas for the separation of proteins.

THEORETICAL

The surface of silica is not simple[13]. Although only two types of group exist on the surface (the silanols and the siloxane bridges), there are many and complex interrelationships. Silanol groups are known to be either isolated or hydrogen bonded. The majority are weakly acidic, although a small (currently undefined) proportion is strongly acidic and is ionised even at low pH[11]. In addition to single silanol groups, there is an appreciable proportion of geminal silanols. It is believed that these are among the first to react with bonded-phase reagents[11], although how they are distributed between the different types of silanols is not known. The siloxane bridges are frequently assumed to be inactive or to contribute to the retention by some "hydrophobic" chromatographic mechanism[14]. Little is known about these groups other than that they are formed by dehydration of silica and that they can be rehydrated

to generate silanol groups under suitable conditions. Since silica is characterised as a "living polymer"[13] it is not unreasonable to suppose that the silanols and siloxane groups exist in some kind of slow equilibrium. Against this background, it is not surprising that the chromatography performed on silica-based materials is not always reproducible or explicable, especially when the compounds being separated interact with the silica surface as well as with a chemically bonded phase.

Since the major interaction which is likely to occur with the silanol groups is ion exchange, it is useful to consider aspects of the ion-exchange equilibrium. For cation exchange (which is involved here) the ion-exchange process can be represented as [15]
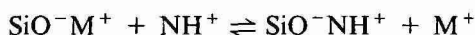
$$SiO^-M^+ + NH^+ \rightleftharpoons SiO^-NH^+ + M^+$$

The ion-exchange equilibrium constant K_{ix} is given by

$$K_{ix} = [SiO^-NH^+][M^+]/[SiO^-M^+][NH^+]$$

If the solute is ionogenic, the pH of the system controls the concentration of the cation through its ionisation constant K_a. If one assumes that only the charged form of the solute is present in the stationary phase, then the distribution coefficient, D_{ix}, for the process can be derived. This turns out to be

$$D_{ix} = \frac{[SiO^-NH^+]}{[NH^+] + [N]} = K_{ix} \cdot \frac{[SiO^-M^+]}{[M^+]} \cdot \frac{1}{1 + \dfrac{K_a}{[H^+]}}$$

Thus, the distribution coefficient is, to a first approximation, related to the ion-exchange equilibrium constant and to the number of accessible ionised silanol groups (which also depends upon the pH and the pK_a of the silica surface). It is also related to the inverse of the concentration of counter-ions in solution. Thus, a plot of capacity factor (k'), which is directly related to the distribution coefficient, against the inverse of counter-ion concentration should be a straight-line graph, passing through the origin (assuming that no other retention mechanism exists), with a slope proportional to the ion-exchange equilibrium constant and the number of ionised silanol groups on the silica surface. The presence of other retention mechanisms not related to ionic processes will result in an intercept on the k' axis which corresponds to an "infinite" competing-ion concentration.

Interacting retention mechanism

The majority of HPLC experiments are performed under conditions where it is hoped that essentially only one retention mechanism predominates. In this case, it is relatively simple to understand how retention is affected by changes in mobile phase composition, parameters relating to the packing material and the nature of the solute. In addition, it is frequently possible to predict k' and selectivity from a knowledge of the structure of the solutes[16]. The situation becomes more complex when several mechanisms of retention come into play. It is quite unreasonable to assume that a solute molecule is retained by only one interaction at any one time —indeed, chiral separations, which require a three-point contact with the surface, would be

impossible under such a circumstance[17]. Thus, a polar molecule could be retained by a reversed-phase and a silanol interaction at the same time, acting on different parts of the molecule. If it is assumed that each individual interaction acts only on a specific part of the molecule, independently of the presence (or absence) of other interactions, then the total energy of interaction would be the sum of the individual energies of interaction.

Since the distribution coefficients are related to the free energy of the system by the relation

$$\Delta G = - RT \ln K$$

the overall distribution coefficient arising from the interacting retention mechanism would be equal to the product of the individual coefficients. For a retention equilibrium with distribution coefficient K_i, there is a phase ratio (φ_i) associated with it which depends upon the packing material and the mobile phase. In the case of a single retention mechanism this phase ratio is simply the ratio of the stationary and mobile phase volumes appropriate to that mechanism. If several mechanisms exist, the individual phase ratio will be a function of the number of sites on the packing material which interact with the solute within that equilibrium. If two or more retention mechanisms interact, there is an associated phase ratio which reflects the number of groups on the surface in a suitable configuration for such interaction. This ratio defines the extent of the interaction. Since the volume of the mobile phase in the column is not a function of the retention mechanism, the critical parameter in the phase ratio is the stationary phase volume for each interacting mechanism. This is simply seen as a parameter which relates to the frequency of occurrence of the interacting groups on the surface of the packing in a configuration close enough to allow concurrent interactions with one solute molecule.

In the case of uniform random distributions of the interactive sites on a packing material, the maximum distribution coefficient due to the interacting mechanisms should be observed when the concentrations of the sites are equal. If the sites are not uniformly distributed on the surface, e.g., as has been postulated for reversed-phase chromatography where "rifle stacks" of bonded-phase molecules are thought to occur in the predominantly aqueous environment[18], then the interacting mechanisms would be more likely to occur in localised areas. In this example this would be around the edge of the "stacks" where both the bonded phase and the silica surface are easily accessible. For these interacting retention mechanisms the associated stationary phase volume must be a function of the product of the individual phase volumes.

These stationary phase volumes are difficult to assign, even in the case of a single retention mechanism, especially where there is some uncertainty concerning the actual mechanism of a retention process. Several proposals have been made in an attempt to solve this problem[19]; of these perhaps the most useful is to view the phase ratio as the ratio of molecules participating in the retention in the stationary phase to the total number of molecules in the mobile phase. This avoids the difficulty of having to cope with combinations of surface areas and volumes and, consequently, the derivation of distribution coefficients which have the dimension of reciprocal length.

The foregoing arguments imply that, if more than one retention mechanism

is involved, the observed capacity factor is determined not only by the sum of the products of the individual distribution coefficients and their phase ratios but also by the addition of the products of interacting distribution coefficients (K_i) and phase ratios (φ_i).

$$k' = K_1\varphi_1 + K_2\varphi_2 + \cdots + K_i\varphi_i + K_1K_2\varphi_1\varphi_2 + \cdots + K_iK_j\varphi_i\varphi_j + \\ + \cdots + K_1K_2K_3 \cdots K_i\varphi_1\varphi_2\varphi_3 \cdots \varphi_i$$

One way of studying these processes is to modify the individual phase ratios by changing the surface coverage of a bonded-phase packing and observing the retention changes in an otherwise fixed system. A number of papers describing such experiments have appeared[20-22], although the intention of their authors was not necessarily to study this question. One universal observation has been that the plots of k' against surface coverage or percent carbon of the bonded-phase for the ostensibly reversed-phase systems studied were not linear, as would be predicted from a single reversed-phase mechanism, although this aspect has not been addressed. The data can be rationalised by the presence of interacting mechanisms. In this case, the phase ratios for the various processes would be related to the surface coverage of the bonded phase: reversed-phase processes relating to the bonded phase would obviously show direct proportionality, whilst mechanisms involving the silica surface would be related to a function of the original silica surface area less that covered by the bonded-phase. Hence, k' in such a case would not be related linearly to the surface coverage, as would be expected for a "pure" reversed-phase mechanism, but would be a quadratic or higher power function of the surface coverage (depending on the number of interacting mechanisms), resulting in non-linear plots of k' against bonded-phase coverage.

EXPERIMENTAL

Instrumentation
    A DuPont (Wilmington, DE, U.S.A.) 8800 "Sentinel" fully automated HPLC system with as DuPont spectrophotometric detector and a Hewlett-Packard (Avondale, PA, U.S.A.) 1090A HPLC system fitted with a filter photometric detector were used throughout this work. A Nelson Analytical (Cupertino, CA, U.S.A.) data system based upon a Hewlett-Packard 200 series computer, modified in house to give theoretical plate height and skew data, was used.

Columns
    Stainless-steel columns (15 cm × 4.6 mm I.D.) were packed by proprietary procedures using a slurry method.

Mobile phases
    Mobile phases were mixed dynamically from phosphate buffers (made from appropriate mixtures of mono- and dibasic sodium phosphate and orthophosphoric acid to achieve the desired pH at the required sodium ion concentration) and methanol for the amine studies. Protein separations were performed using a gradient from 0.01% aqueous trifluoroacetic acid to 60% aq. acetonitrile containing 0.01% trifluoroacetic acid in 40 min.

Flow-rates were 2 ml/min for the amine studies and 1 ml/min for the proteins. All separations were performed at ambient temperature.

Materials

HPLC-grade solvents were obtained from J. T. Baker (Phillipsburg, NJ. U.S.A.). Protein standards were obtained from Sigma. Other chemical reagents were purchased from Fisher Scientific (Fairlawn, NJ, U.S.A.).

Packing materials

Silicas used in this study were experimental DuPont Process Grade silica, approximately 10 μm particle diameter and either 260 m^2/g surface area with 90 Å pore diameter (Type S) or 170 m^2/g surface area with 120 Å pore diameter (Type L).

Bonded-phase packings were synthesised by a minor modification of the method of Kinkel and Unger[23] using octyldimethylchlorosilane. Those materials which were capped after bonding were similarly treated with trimethylchlorosilane. Materials of restricted surface coverage were prepared by limiting the quantity of octyldimethylchlorosilane in the reaction mixture to the molar proportion, calculated from the desired coverage and the surface area of the silica. These packings were not capped.

RESULTS AND DISCUSSION

The solutes chosen for this study were intended to exemplify the different types of basic compound which may be expected to interact with silica surfaces. These were thiamine (a quaternary ammonium compound) morphine (a basic tertiary amine) and caffeine (which is not basic and is generally assumed to be "well-behaved" in reversed-phase systems).

Initial experiments were performed using a Type S silica. The effect of changing the methanol concentration in 0.05 M phosphate at pH 4.6 on the capacity factors of the three solutes is shown in Fig. 1. The U-shaped graphs for thiamine and morphine are typical of separations on silica. Curves of similar shape have been seen in the separation of crown ethers[14] as well as basic amino compounds[8-10]. The shape has generally been ascribed to hydrophobic interactions at low organic solvent concentrations and to changes in protonation[9] or to changes in counter-ion solvation[10] at high organic solvent concentration.

Because of the way in which the mobile phase was mixed and the assumed ion-exchange mechanism, at least part of the change was believed to be due to a dilution of the buffer by the addition of methanol. This was addressed by performing the same experiment with concentrations of between 0.2 and 0.01 M phosphate and plotting k' values against the inverse of the calculated concentration of sodium ion in the mobile phase at various methanol concentrations. All of these plots (see Fig. 2) are linear, indicating that the mechanism is indeed ionic, and show a positive intercept on the k' axis. Ion-exchange theory[15] predicts that for a pure ion-exchange mechanism the plot of k' against inverse competing-ion concentration should give straight lines passing through the origin of the plot, the slope being proportional to the ion-exchange equilibrium constant and the ion-exchange capacity of the packing. An interesting point to note is the change of the slope of the plots with changes in
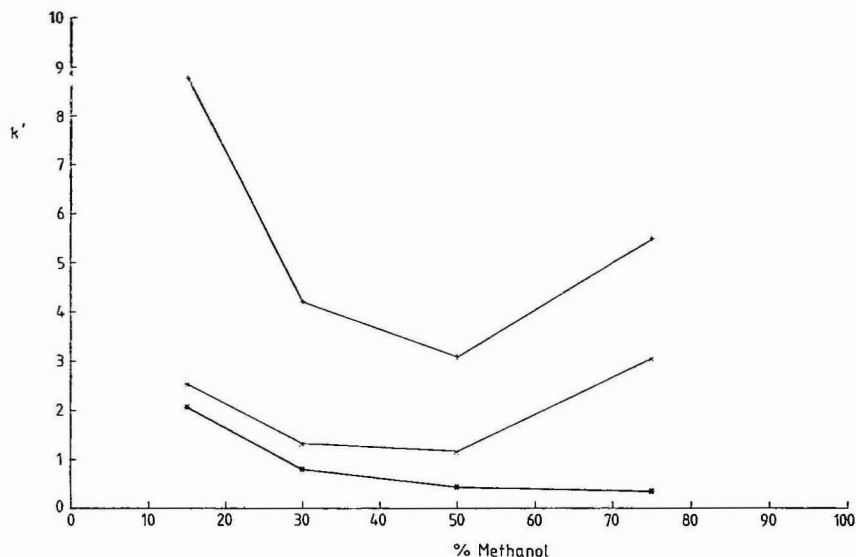
Fig. 1. Plot of k' against methanol concentration. Type S silica, mobile phase made from mixtures of methanol with 0.05 M sodium phosphate buffer (pH 4.6). + = Thiamine; * = caffeine; × = morphine.

methanol concentration. The initial increase in methanol concentration from 15 to 50% results in a decrease in slope. At higher methanol concentrations the slope of the plot increases. An experiment to measure the pH of the solutions at the methanol concentrations employed showed that the pH (uncorrected for changes in electrode performance with change in methanol concentration) increased with added methanol, reaching a value of 6.4 at 75%. This means that the silica surface is increasingly ionised at high methanol concentration, and this is probably the cause of the in-
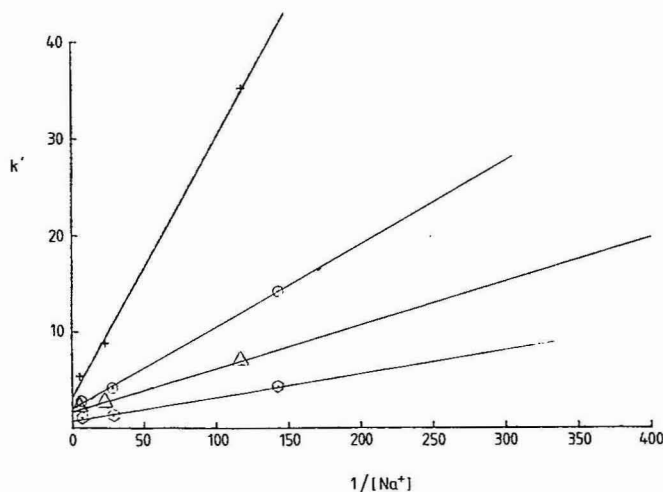
Fig. 2. Plot of k' against inverse buffer concentration. Type S silica, mobile phase 15 and 30% methanol in phosphate buffer (pH 4.6). + = Thiamine, 15% methanol; △ = thiamine, 30% methanol; ○ = morphine, 15% methanol; ○ = morphine, 30% methanol.

creased retention of thiamine and morphine. Since the pH of the solution slowly increases with methanol concentration, at low methanol concentrations the pH of the solution is not appreciably affected by the addition of methanol and it is reasonable to suppose the number of ionised silanol groups on the silica surface does not appreciably increase. Thus, the decrease in slope with low methanol concentration appears to be a result of change in the ion-exchange equilibrium constant. The reduction in retention with added organic solvent concentration under ion-exchange conditions has been noted in the past[24].

The positive intercept of the plot of k' *versus* inverse competing-ion concentration can be taken as evidence for additional retention mechanism(s) which exist at "infinite" buffer concentration, *i.e.* not influenced by the concentration of the ions in solution and therefore not ionic in nature. A plot of k', measured at infinite buffer concentration, against methanol concentration (see Fig. 3) has the same form as the other plots. Since in this case the ion-exchange effects are eliminated, this plot must arise from the other mechanisms which exist. Possible changes in solute ionisation which could influence the retention of morphine may be discounted due to the similarity in behaviour of morphine and thiamine which as a quaternary salt is fully ionised under these conditions. Additionally, the pH of the mobile phase is at all times well below the pK of morphine and so changes in the level of ionisation are expected to be minimal. At low methanol concentrations, the plot follows the expected form of a reversed-phase separation, whilst at high concentrations the k' values increase. This increase is probably due to non-ionic interactions of the solutes with silanol groups, in some form of normal-phase or adsorption mode. Evidence for such a mechanism was seen in the chromatography of crown ethers[14]. In contrast, at first sight, caffeine shows no evidence of ionic interactions or adsorption and
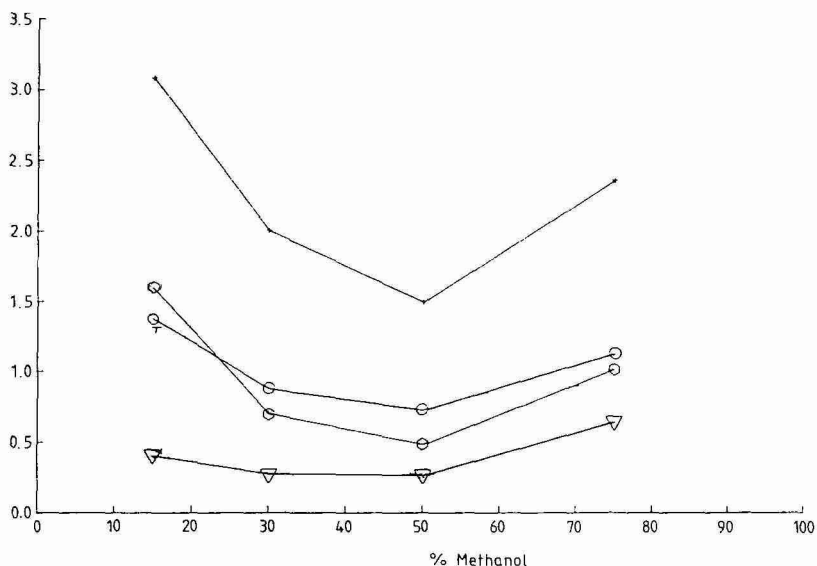
Fig. 3. Plot of k' against methanol concentration at "infinite" buffer concentration (pH 4.6). $+$ = Thiamine, Type S silica; $\bigcirc$ = morphine, Type S silica; $\bigcirc$ = thiamine, rehydroxylated Type L silica; ∇ = morphine, rehydroxylated Type L silica.

appears to behave as if the only retention mechanism involved were reversed-phase partition. Its behaviour is entirely consistent with such a mechanism in that the retention increases with increasing buffer concentration, corresponding to expected salting-out effects.

In order to investigate reversed-phase separations on silica further, an experiment was carried out on the same silica column measuring the retention of toluene and uracil as a function of methanol concentration. Toluene was expected to show a reversed-phase type of behaviour as has been observed for butylbenzene[14], whilst uracil was originally chosen as a dead-volume marker. Fig. 4 shows the plot of capacity factors of uracil and toluene against methanol concentration observed in this experiment. Toluene clearly shows a close approximation to the expected relationship between log k' and methanol concentration. The data for caffeine (not shown) plotted as log k' vs. percent methanol does not show such a clear linearity. A curvature relative to the plot obtained for toluene suggests strongly that some adsorption at high methanol concentration does take place. Uracil clearly does not function as an unretained marker in this system (unlike its behaviour on fully bonded and capped reversed-phase packings) and shows a U-shaped plot similar to the other bases. Since, in this case, the mobile phase was unbuffered, the increase in retention at high methanol concentrations is probably due to adsorption.

The plots of k' vs. methanol concentration at other pH values show increased retention as the pH increases, corresponding to the expected increase in the number of ionised silanol groups on the silica surface. Over the pH range studied (2.1 to 7.0) this increase was exponential for thiamine, an observation similar to that of Lingeman et al.[10]. The plots of k' against the inverse of buffer concentration were linear at these other pH values, although the slopes and intercepts differ. The values of slopes and intercepts are reported in Table I. The slopes of the plots are clearly increased between pH 2.1 and 4.6, reflecting increased ionisation of the silica, even though this range is well below the pK of silica and reflects the inhomogeneity of the
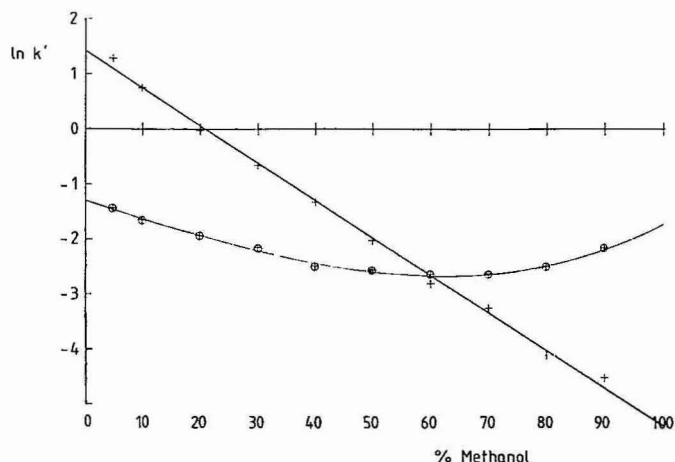
Fig. 4. Plot of ln k' of toluene and uracil against methanol concentration. Type S silica. Mobile phase, methanol–water mixtures. + = Toluene; O = uracil.

TABLE I

SLOPES AND INTERCEPTS OF k' vs. 1/[BUFFER] PLOTS: TYPE S SILICA

pH	Methanol concen- tration (%)	Thiamine		Caffeine		Morphine	
		Slope	Intercept	Slope	Intercept	Slope	Intercept
2.1	15.0	0.00975	1.28	−0.0002	1.19	0.00474	1.12
4.6	15.0	0.271	3.09			0.0453	1.59
	30.0	0.0845	2.00			0.0247	0.70
	50.0	0.0448	1.49			0.0197	0.48
	75.0					0.0263	1.01
7.0	15.0	2.03	8.12	0.0153	0.73	1.152	6.43

surface. The intercepts, too, are larger, although by a much smaller factor. As expected, the slopes increase markedly between pH 4.6 and 7, due to the enhanced ionisation. The data for caffeine show an interesting feature in that at pH 7 there is a change in mechanism. Some ion-exchange character is introduced since the slope of the plot changes to a positive (although extremely small) value.

In addition to the silica used for the above data, two Type L silicas, known to have differing degrees of surface rehydroxylation, were examined. The first ("packing a") was a material which had been heat-treated at excessive temperature before rehydroxylation by a standard acid treatment and the second ("packing b") was a silica prepared by the procedure of Köhler and Kirkland[25]. A plot of k' against 1/buffer concentration for thiamine and morphine is shown in Fig. 5. Data for the slopes and intercepts of these packings are shown in Table II. It is of interest to observe that
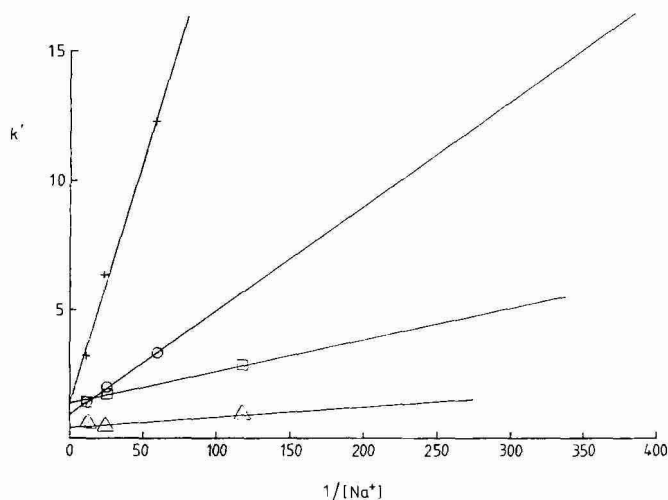
Fig. 5. Plot of k' against 1/buffer concentration. Type L silicas. + = Thiamine, packing a; ○ = morphine, packing a; □ = thiamine, packing b; △ = morphine, packing b.

TABLE II

SLOPES AND INTERCEPTS OF k' vs. 1/[BUFFER] PLOTS: TYPE L SILICAS

Methanol concentration		Thiamine		Morphine	
Silica	(%)	Slope	Intercept	Slope	Intercept
a	15	0.186	1.390	0.040	0.931
	30	0.064	1.156	0.020	0.447
	50	0.035	0.805	0.016	0.262
	75	0.036	0.922	0.021	0.434
b	15	0.014	1.368	0.004	0.397
	30	0.007	0.869	0.003	0.272
	50	0.005	0.716	0.003	0.255
	75	0.007	1.121	0.004	0.641

the two silicas have essentially the same intercept on the k' axis and markedly different slopes for thiamine. Morphine, however, displays a smaller intercept as well as a similarly reduced slope. Thus, the conclusion can be drawn that the major difference between these silicas is simply the ion-exchange character of the materials. This agrees well with the hypothesis that the surface treatment modifies the silanols in such a way as to increase the number of hydrogen-bonded (less acidic) silanols at the expense of the more acidic, free groups. At the same time, it appears that the other mechanisms of retention for thiamine are essentially the same for the two silicas. Caffeine, however, is retained to a much smaller extent on the rehydroxylated silica, as is morphine at "infinite" buffer concentration. Since at this pH the retention is not influenced by ion-exchange, it appears that the sites of interaction of caffeine with the surface are decreased in number or strength by the treatment. This implies that caffeine is retained either by interaction with the strongly ionised surface silanols or by siloxane bridges which are converted to silanols by the rehydroxylation process. Interaction with the silanol groups would explain the slightly reduced retention of caffeine at pH values above 4.8 (see Table I) in that the majority of silanols begin to ionise above this value. The form of such an interaction is not so easy to deduce.

A hydrogen-bonding interaction would be expected to decrease with increasing water concentration. The alternative is that the number of siloxane bridges which are postulated to sorb by hydrophobic interaction may be reduced by the rehydroxylation. This reduction would therefore lead to lower retention of caffeine, although this mechanism does not explain the reduced k' at high pH, since it should remain invariant. In order to elucidate this further, the "pseudo-reversed-phase" retention of toluene on silica was studied further. In this experiment toluene was chromatographed with a range of methanol concentrations at two different pH values (2.1 and 7.0). The capacity factors under the two sets of conditions were identical, proving that the retention is invariant with changes in ionisation of the surface. A second experiment was carried out in which retention of toluene was compared on two silicas, one prepared by the standard technique and the other by a rehydroxylation procedure analogous to that of Köhler and Kirkland. In this case, the retention of
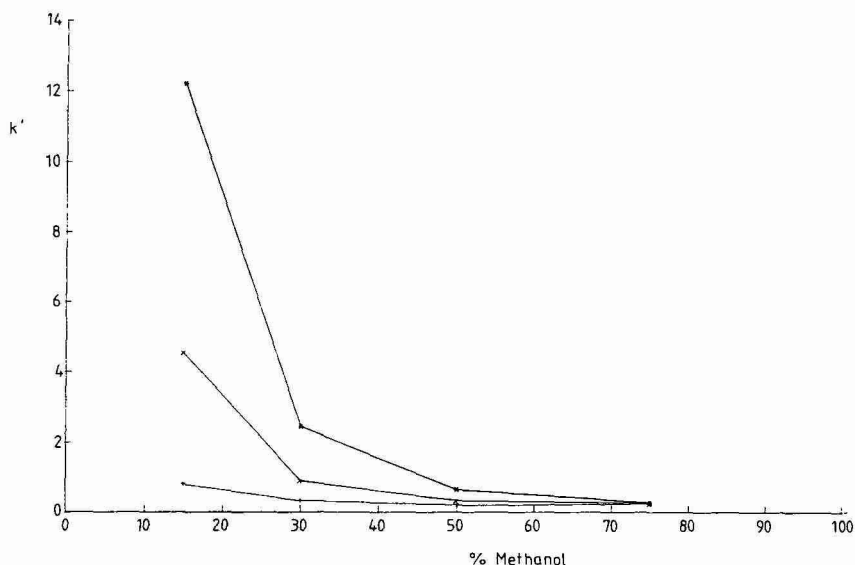
Fig. 6. Plot of k' against methanol concentration. Fully covered C_8-bonded phase. All other conditions as Fig. 1. $+$ = Thiamine; $*$ = caffeine; $\times$ = morphine.

toluene was very markedly reduced on the rehydroxylated silica, indicating that retention occurred on the surface siloxane bridges, the number of which were reduced by the process. This implies that the retention of caffeine and, in part, that of morphine also occurs by interaction with the siloxane groups.

Preparation of a C_8 bonded-phase with high surface coverage (3.37 μmoles/m^2) from the Type S silica changes its performance in the chromatography of the test solutes dramatically. This is illustrated in Fig. 6. The retention of caffeine at 15% methanol in 0.05 M phosphate buffer was increased relative to silica while thiamine and morphine were retained to a much smaller extent. This may be attributed to reversed-phase interactions of caffeine and reduction of the ion-exchange retention of basic compounds by virtual elimination of ionic silanols through bonding or steric masking with the bulky bonded-phase molecules. Morphine is retained more than thiamine by virtue of reversed-phase interactions, although in this case the relative participation of siloxane and C_8 interactions is not clear. A more interesting result is observed when the transition between silica and a bonded phase with maximum coverage is investigated. A range of C_8 phases was prepared from the Type S silica with a wide range of surface coverage. Their properties are reported in Table III. The capacity factors and plate counts for thiamine, caffeine and morphine were determined for 15, 30, 50 and 75% methanol in 0.05 M phosphate buffer. Fig. 7 shows a plot of k' against surface coverage (α_{exp}) at 15% methanol. It is clear that these curves do not fit the plots of log k' against percent carbon which have been reported for packings at low values of surface coverage[20–22]. Most of these data were collected from C_{18}-bonded phases which had surface coverage values of less than 1.6 μmoles/m^2. Since, according to the idealised mechanism of reversed-phase chromatography, the capacity factor should be related directly to the bonded-phase coverage

TABLE III

PROPERTIES OF C$_8$-BONDED-PHASE PACKINGS

Designation	Carbon (%)	α_{exp} (μmoles/m^2)
1	0.00	0.00
2	2.37	0.78
3	3.49	1.17
4	4.78	1.63
5	5.47	1.89
6	6.90	2.43
7	7.61	2.71
8	8.25	2.97
9	9.19	3.36

through the phase ratio (assuming the reversed-phase distribution coefficient remains constant throughout the range of coverage), it is hard to see why the plots should turn out to be logarithmic, especially over a wide range of coverage. The shape of the curves was unexpected, and clearly mechanisms other than reversed-phase partition are operating on the bonded-phase packings. It is noteworthy that at low surface coverages (< 1.6 μmoles/m^2) the plots follow the same general form as those reported earlier. It is at the higher values of coverage where the assumed log function no longer applies. Fig. 8 shows data on the efficiency, as measured by the number of theoretical plates for the three test solutes. Since all of these columns showed between 5000 and 6000 theoretical plates for toluene, chromatography of the solutes is clearly
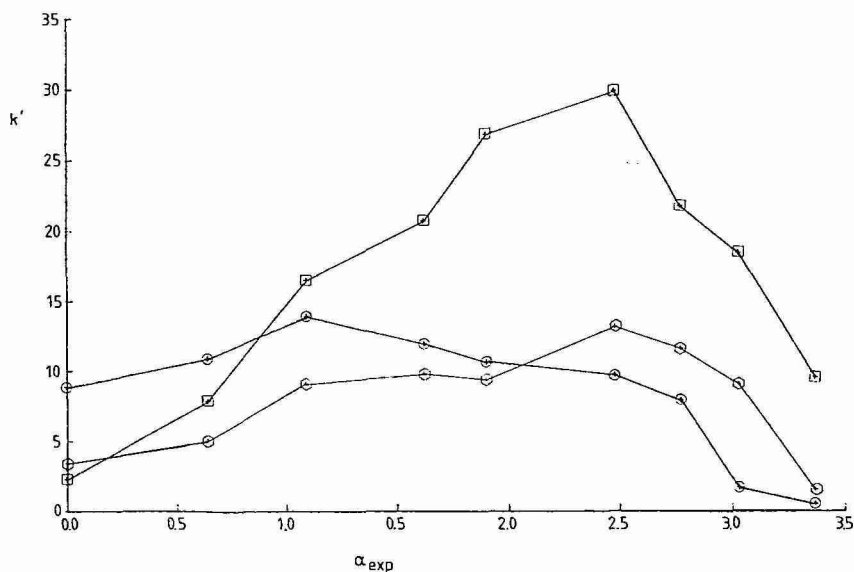
Fig. 7. Plot of k' against surface coverage (α_{exp}). Type S silica; mobile phase, 15% methanol in 0.05 M phosphate buffer (pH 4.6). ○ = Thiamine; □ = caffeine; ○ = morphine.
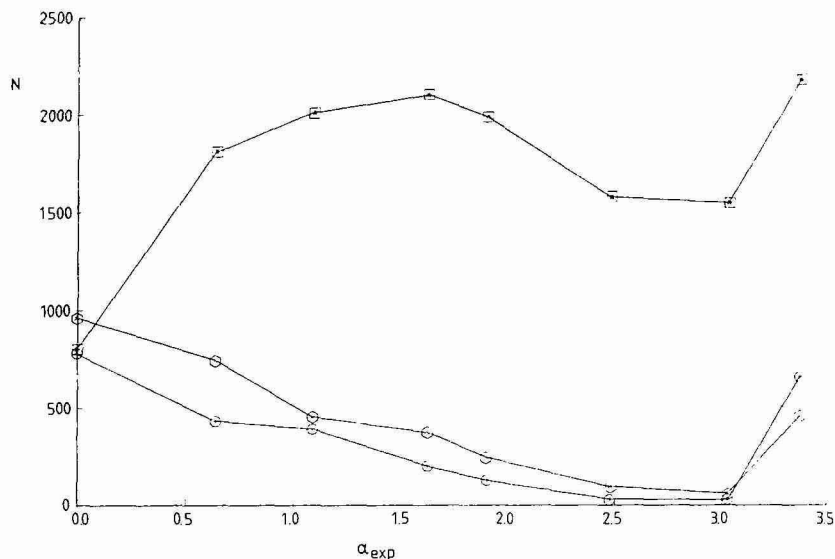
Fig. 8. Plot of plate number (N) against surface coverage. All other conditions as in Fig. 7.

not optimal, the maximum number of plates being only a little over 2000 for caffeine and the minimum number being below 100 for thiamine. It is also significant that the minima in the efficiency plots coincide with the maxima in the retention plots. This suggests that the maxima in the plots of k' are due to interaction of retention mechanisms which severely reduce the desorption rates and thereby increase the plate heights. From the silica data it is clear that cation exchange is the major retention mechanism for thiamine. This view is supported by plots of k' against inverse sodium concentration for a C_8-bonded-phase silica with 1.63 μmoles/m^2 loading (Fig. 9). The plots for thiamine and morphine are consistent with the proposed ion-exchange
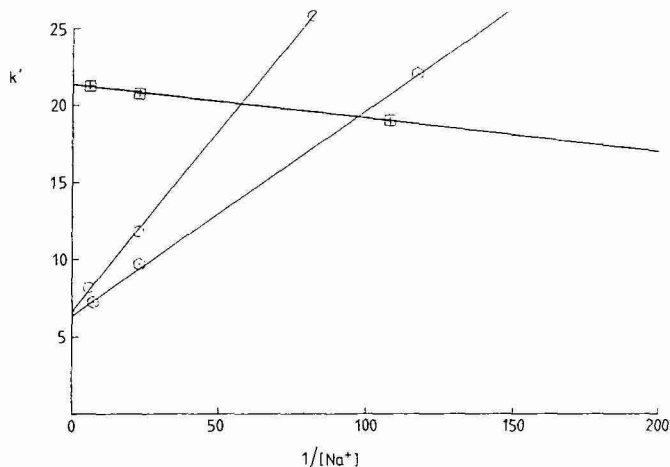
Fig. 9. Plot of k' against 1/buffer concentration on a partially bonded C_8 packing. Mobile phase, 15% methanol in phosphate buffer (pH 4.6). $\bigcirc$ = Thiamine; $\square$ = caffeine; $\bigcirc$ = morphine.

mechanism, whilst that for caffeine shows a slope of the opposite sign (indicating salting out), as has been seen for separations on silica. The retention at "infinite" sodium concentration shows that there are additional mechanisms for all three test substances, one of which appears to be a hydrophobic type, occurring at low methanol concentrations and the other being possibly an adsorption (or silanophilic) type which is measurable at higher methanol concentrations. The plots of log k' against methanol concentration (Fig. 10) show clearly the marked curvatures which suggest this. Thiamine does not appear to have a particularly great affinity for the hydrocarbon chain of the bonded-phase packing, according to the very low retention on a fully bonded material. Thus, any addition to the interacting retention mechanisms arising from the traditional reversed-phase interaction is at best small. This lack of reversed-phase character for thiamine is also shown at other mobile phase pH values. At higher methanol concentrations any contribution by reversed-phase or hydrophobic interactions would be expected to be minimal. At 75% methanol the plot of k' against α_{exp} for thiamine is simplified and follows more closely a straight line, as shown in Fig. 11, suggesting that hydrophobic processes which are largely eliminated at high methanol concentrations are small but important for thiamine. Although these do not immediately appear to be related to the bonded phase, they cannot result from interaction with the silica surface, since changing the number of siloxane bridges does not particularly influence the retention of thiamine on silica as seen from the intercepts of the k' vs. 1/[buffer] plots. Morphine shows a little higher retention on the bonded-phase packing and thus it may be concluded that reversed-phase interaction with the bonded phase is more important for this compound. This is further borne out by its performance at higher pH. When chromatographed on a C_8-bonded phase in a mobile phase prepared from pH 7 buffer (Fig. 12), the retention
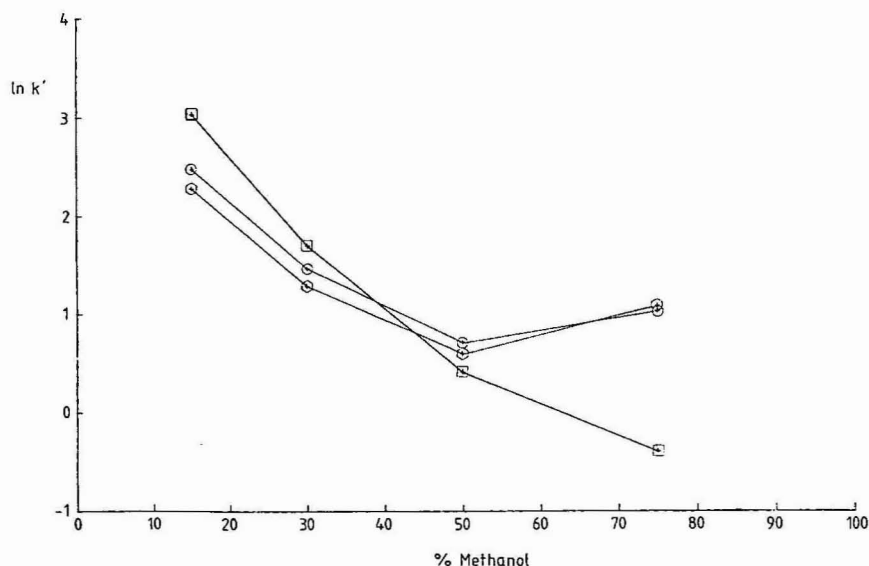
Fig. 10. Plot of log k' against methanol concentration for a partially bonded C_8 packing. Other conditions as in Fig. 1. O = Thiamine; □ = caffeine; O = morphine.

Fig. 11. Plot of k' of thiamine against surface coverage at 75% methanol. Other conditions as in Fig. 7.

of morphine increases dramatically to exceed that of caffeine. This presumably is due to changes in the extent of ionisation of morphine, despite the fact that the pH of the system is below the pK of morphine. Thiamine, in contrast, does not show this effect, indicating that ion-exchange processes are not important here. Thus, each of the test solutes displays a different variety of mechanisms. Thiamine is retained main-ly by ion-exchange processes throughout the range of bonded-phase coverage from silica to C_8. In addition, there is evidence for a silanol interaction at high methanol
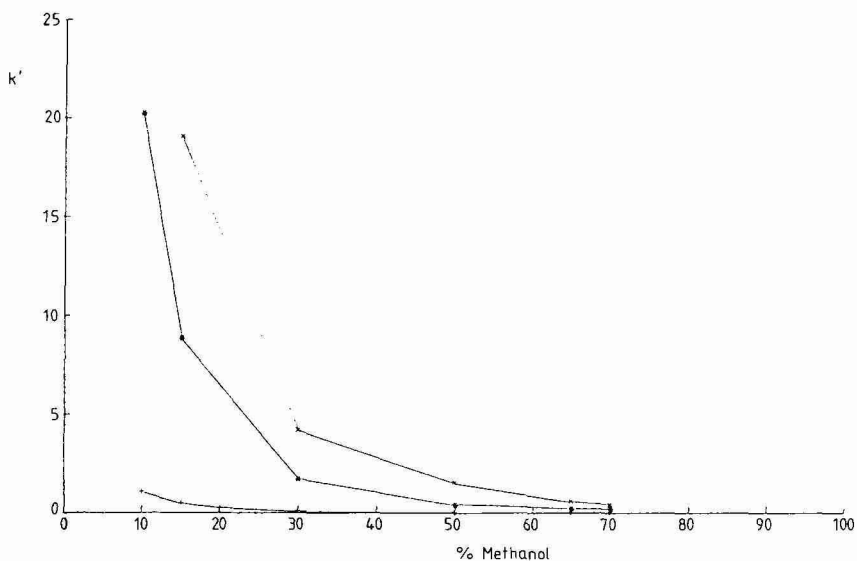
Fig. 12. Plot of k' against methanol concentration at pH 7. C_8-Bonded phase; other conditions as in Fig. 1. + = Thiamine; * = caffeine; × = morphine.

concentrations, minimal hydrophobic interaction with the silica and a little interaction with the bonded phase. For each of the two main processes it appears that the surface with which thiamine interacts is that of the silica and only that small part of the retention which is governed by the reversed-phase process is directly related to the concentration of bonded phase. Hence, the retention of this compound is largely a function of the freely accessible silanol groups on the surface. If the bonded-phase molecules are randomly distributed over the silica surface during the bonding process, then the decrease in accessible silanol concentration should be linearly related to the increase in bonded-phase coverage. This implies that the curvature of the k' vs. surface coverage plot is not due to non-linear changes of the concentration of the silanol groups and must therefore be caused by the proposed interaction of retention mechanisms. It is not possible to explain the shape of this and the plots for morphine and caffeine by summation of capacity factors or distribution coefficients. Only functions of higher order than unity can fit the curves. This means that several mechanisms must interact in this system. The case for morphine is very similar, except for the greater reversed-phase character in the retention mechanism. This is reflected in the movement of the maximum in the k' vs. surface coverage plot to higher coverages relative to thiamine. The plots for all solutes at higher methanol concentrations also show shifts in the maximum, in this case to lower values of coverage, which is expected from the decrease in reversed-phase retention. Caffeine behaves differently in that ion exchange is relatively unimportant in its retention relative to reversed-phase interactions. This is clear from its greater retention as surface coverage of the C_8 phase increases. The decrease in retention at high values of coverage is clear evidence for a coupling of retention mechanisms, since this should not occur if only reversed-phase interaction with the bonded phase were important. In order to ensure that these observations were not an artifact of the bonded phase, a number of simple compounds were tested under reversed-phase conditions using the set of columns with a range of surface coverage. The k' vs. coverage plots are shown in Fig. 13. Toluene shows essentially a straight-line plot under these conditions, suggesting that for a pure reversed-phase separation the k' value is, as is expected, linearly related to the bonded-phase coverage. Other, simple molecules show less than linear plots which again can be taken as evidence for additional retention mechanisms, especially as the curvature increases with the polarity of the molecule. Similar effects can be seen in the data of Hennion et al.[20], Miller et al.[21] and Kaliszan et al.[22] at the lower surface coverages they employed. It is interesting to note that the curves relating k' and surface coverage for most of these solutes have essentially the same shape and can be approximated by a polynomial which is third-order in surface coverage. Work in progress in our laboratories in this area will form the basis of a forthcoming paper.

Protein retention studies

Following the discovery that silicas prepared by different procedures and rehydroxylation processes show different ion-exchange characteristics it was thought that even on well-bonded reversed-phase silicas these ion-exchange properties may remain in evidence for separations. Accordingly, a range of proteins were chromatographed on C_8-bonded-phase columns, prepared from normally synthesised silica, the silica which displayed highly ionic character (reported above) and from silica prepared by procedures analogous to those of Köhler and Kirkland[25]. A 0.1% tri-

TABLE IV

RETENTION TIMES (t_R), PEAK WIDTHS (w_b) AND PEAK SKEW VALUES FOR PROTEIN STANDARDS ON C_8 COLUMNS PREPARED FROM SILICAS OF DIFFERING SLOPES

ND = Not determined.

Slope of k' vs. $1/[\ ]$	Bovine insulin			Lysozyme			Ribonuclease A			Cytochrome c		
	t_R (min)	w_b (min)	Skew	t_R (min)	w_b (min)	Skew	t_R (min)	w_b (min)	Skew	t_R (min)	w_b (min)	Skew
0.014	27.8	0.42	1.19	32.8	1.15	1.28	26.8	0.75	0.78	30.7	0.93	1.34
0.081	28.6	0.62	1.72	33.9	1.91	1.86	27.2	0.99	1.57	31.5	1.63	1.93
0.101	32.1	1.73	1.94	41.4	5.85	1.39	31.4	2.68	1.56	37.9	2.14	ND
0.186	35.8	2.03	1.85	*	–	–	*	–	–	*	–	–

* Peak not eluted under these chromatographic conditions.
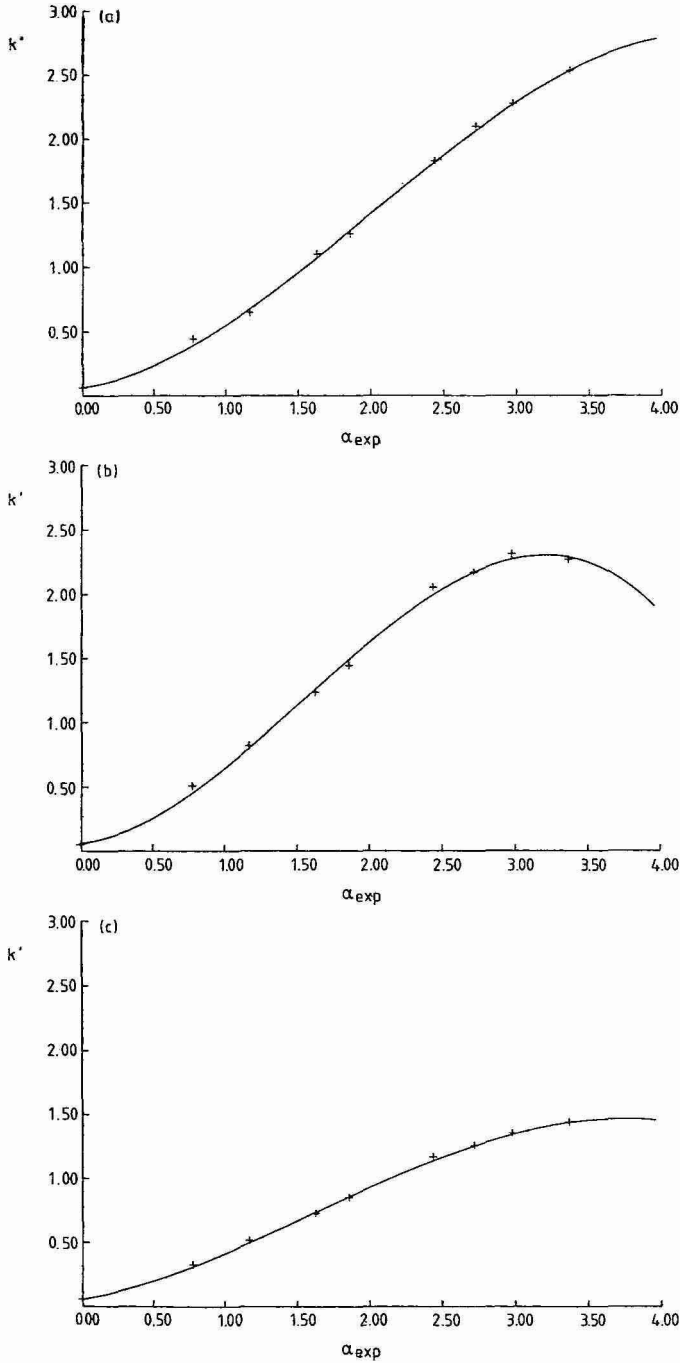
Fig. 13. Plots of k' against surface coverage for non-basic solutes. Mobile phase, 70% aq. methanol. (a) Toluene; (b) allyl phthalate; (c) anisole.

fluoroacetic acid-containing acetonitrile–water gradient was chosen in order to achieve elution under relatively low ionic strength conditions, which was expected to show the maximum effect of the underlying silica properties. Table IV shows the retention times, baseline peak widths (measured in minutes) and peak skew of four protein standards under a standard set of gradient conditions. Fig. 14 shows the retention times of insulin plotted against the value of the slope of the k' *versus* 1/buffer concentration plots, derived above for these and other silicas. The other parameters shown in Table IV follow similar trends. It is, therefore, clear that silicas with higher slope values give rise to bonded-phase packings with poor elution properties for the proteins. In these cases, and probably in the case of certain basic small molecules, the ionic character of the silica is important when mobile phases of low ionic strength are employed. In order to study the performance of the silicas for protein separations further, columns packed with silica were tested with insulin under the same conditions. A much wider range of retention was seen in comparison with the bonded-phase packings which suggested that the difference in the underlying silica retention was modifying the retention on the derived bonded-phase materials. The plot of retention time against slope of the k' *vs.* 1/buffer concentration plots is shown in Fig. 15. Again, a direct relation between retention time and slope was seen, those materials which had the smaller slopes also showing shorter elution times. These data are shown as a plot of retention time against slope in Fig. 15 and demonstrate the importance of the ion-exchange process on the retention. There is hence a clear influence of the ion-exchange character of the silica on the chromatography of peptides and proteins on bonded-phases. In order to obtain more reproducible packing materials, the ion-exchange effects should be minimised. This can be done by the use of high-ionic-strength buffers or by modification of the silica. It has been suggested that rehydroxylation techniques can enhance the recovery of certain peptides and proteins from bonded-phase silicas[11]. The data here show that there are links between the hydroxylation process and the ion-exchange character of the silica and between the ion-exchange character and the chromatographic behaviour of some
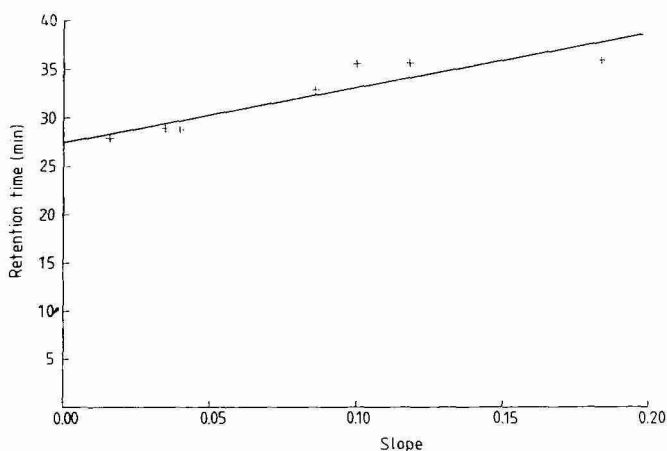
Fig. 14. Plot of insulin retention time on C_8-bonded phase packings against slope of the k' *vs.* 1/[buffer] curves for the silicas. For gradient conditions see text.
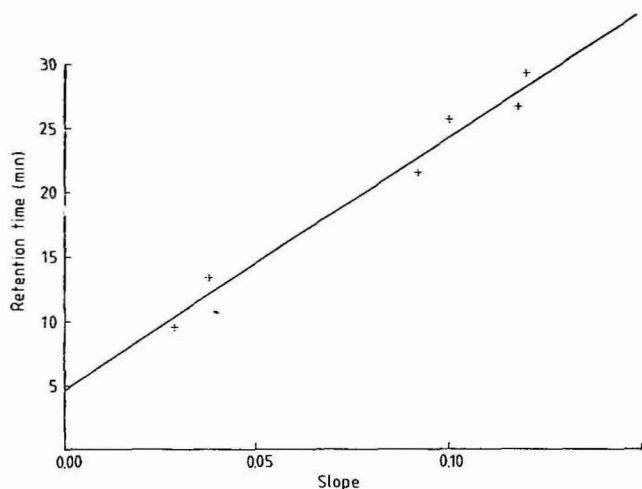
Fig. 15. Plot of insulin retention time on silicas against slope of the k' vs. 1/[buffer] curves. For gradient conditions see text.

proteins on the derived bonded-phase packing. Other, as yet unknown, parameters are certainly also involved in influencing the retention behaviour of proteins on silica-based packings, but it is evident that ion-exchange effects are an important modifier of the hydrophobic effects normally considered to determine their retention.

CONCLUSIONS

We have investigated the mechanisms of retention of basic compounds on silica and C_8 reversed-phase packings. These were shown to be mainly ion exchange for compounds ionised under the conditions of elution, and hydrophobic interaction for non-ionised materials. Separate hydrophobic interactions were seen with bonded-phase molecules and with the silica surface. Evidence was obtained which showed that these interactions were with the siloxane bridges and not the silanol groups. Study of the retention of the test solutes on a range of packings with differing bonded-phase coverages additionally gave strong evidence for the interaction between separation mechanisms. Silicas prepared by different routes were shown to have different ion-exchange properties and these were demonstrated to be important in the chromatography of proteins on bonded phases.

ACKNOWLEDGEMENT

REFERENCES

1 J. E. Rivier, *J. Liq. Chromatogr.*, 1 (1978) 343.
2 E. Papp and Gy. Vigh, *J. Chromatogr.*, 259 (1983) 49.
3 E. Papp and Gy. Vigh, *J. Chromatogr.*, 282(1983) 59.
4 I. Jane, *J. Chromatogr.*, 111 (1975) 227.
5 B. B. Wheals, *J. Chromatogr.*, 187 (1980) 65.
6 B. A. Bidlingmeyer, J. K. Del Rios and J. Korpi, *Anal. Chem.*, 54 (1982) 442.
7 H. Richardson and B. A. Bidlingmeyer, *J. Pharm. Sci.*, 73 (1984) 1480.
8 K. Sugden, G. B. Cox and C. R. Loscombe, *J. Chromatogr.*, 149 (1978) 377.
9 R. J. Flanagan and I. Jane, *J. Chromatogr.*, 323 (1985) 173.
10 H. Lingeman, H. A. van Munster, J. H. Beynen, W. J. M. Underberg and A. Hulshoff, *J. Chromatogr.*, 352 (1986) 261.
11 J. Köhler, D. B. Chase, R. D. Farlee, A. J. Vega and J. J. Kirkland, *J. Chromatogr.*, 352 (1986) 275.
12 J. Glajch, J. J. Kirkland and J. Köhler, *J. Chromatogr.*, 384 (1987) 81.
13 R. K. Iler, *The Chemistry of Silica*, Wiley, New York, 1979.
14 K. E. Bij, Cs. Horváth, W. R. Melander and A. Nahum, *J. Chromatogr.*, 203 (1981) 65.
15 J. C. Kraak, in C. F. Simpson (Editor), *Techniques in Liquid Chromatography*, Wiley Heyden, 1982, p. 304.
16 P. Jandera, *J. Chromatogr.*, 352 (1986) 91.
17 W. H. Pirkle, M. H. Hyun and B. Bank, *J. Chromatogr.*, 316 (1984) 585.
18 C. H. Lochmüller and D. R. Wilder, *J. Chromatogr. Sci.*, 17 (1979) 574.
19 P. Jandera, H. Colin and G. Guiochon, *Anal. Chem.*, 54 (1982) 435.
20 M. C. Hennion, C. Picard and M. Caude, *J. Chromatogr.*, 166 (1978) 21.
21 M. L. Miller, R. W. Linton, S. G. Bush and J. W. Jorgenson, *Anal. Chem.*, 56 (1984) 2204.
22 R. Kaliszan, K. Osmialowski, S. A. Tomellini, S.-H. Hsu, S. D. Fazio and R. A. Hartwick, *J. Chromatogr.*, 352 (1986) 141.
23 J. N. Kinkel and K. K. Unger, *J. Chromatogr.*, 316 (1984) 193.
24 G. B. Cox, C. R. Loscombe, M. J. Slucutt, K. Sugden and J. A. Upfield, *J. Chromatogr.*, 117 (1976) 269.
25 J. Köhler and J. J. Kirkland, *J. Chromatogr.*, 385 (1987) 125.

CHROMSYMP. 1048

INFLUENCE OF THE ACCURACY OF THE EXTRA-COLUMN PEAK-WIDTH DETERMINATION ON THE VERIFICATION OF THEORETICAL PLATE-HEIGHT EQUATIONS*

JOSEF F. K. HUBER* and ANDREAS RIZZI

Institute of Analytical Chemistry, University of Vienna, Waehringerstrasse 38, A-1090 Vienna (Austria)

SUMMARY

The influence of extra-column peak-width contributions on the experimentally observed reduced theoretical plate height is discussed for high-performance liquid chromatographic systems as a function of the reduced flow velocity (Peclet number) and the capacity factor on the basis of model calculations. This allows an estimation of the minimum accuracy of the extra-column peak width, which is necessary for a detailed discussion of the in-column peak-broadening mechanism. The estimated minimum accuracy is compared with typical statistical and systematic errors, associated with the usual methods of measuring extra-column peak widths.

INTRODUCTION

Discussions of a comprehensive theory of chromatographic peak dispersion in column chromatography have been stimulated again by a number of recently published papers[1–5]. The influence of the capacity factor on the contributions to peak variance caused by the mass transfer in the flowing fluid and in the fixed bed is still a subject of controversy[1,3,6–10]. It seems that one reason for this is the inaccurate experimental determination of the peak width resulting exclusively from the chromatographic process in the column. This contribution is masked by other contributions to the peak width from outside the column. Each theoretical model is based on the assumption that this extra-column contribution to the peak width is known exactly, or that the error in determining it does not significantly affect the results. The validity of these assumptions and its implications for the accuracy of the model form the subject of the following discussion.

First, the systematic divergence between the measured peak width generated by the total chromatographic system and the peak width created by the column is investigated. Only the column contribution is the result of the kinetics of the chromatographic process and is therefore subject to theoretical interpretation[1,6–12]. The

---

* Dedicated to Professor A. Neckel on the occasion of his 60th birthday.

superposition of different contributions to the peak variance is investigated by means of model calculations, using a set of reasonable and typical values for the peak-broadening parameters[10]. The results of these calculations permit an estimation of the maximum allowable error in the determination of the extra-column contribution to the peak width and specify those ranges of capacity factor and particle size values where the relative extra-column contribution to the total peak width becomes insignificant. Such experimental conditions should be used, if possible, for the experimental verification of theoretical models.

For small particle sizes and small capacity factors, the extra-column contribution to the peak width will not be negligible, and a highly accurate determination of this contribution is required in order to correct for it[13,14]. Unfortunately, all methods described so far are subject to appreciable statistical or systematic errors. The systematic error involved in estimating the extra-column contribution by use of the linear extrapolation method[15-18] is demonstrated by model calculations, and the approximate magnitude of the extra-column band broadening in typical chromatographic systems is reviewed.

THEORETICAL

The basic equation which relates the output variances of a system, σ^2, with the variances of its N subsystems, σ_n^2, is given by

$$\sigma^2 = \sum_n^N \sigma_n^2 \tag{1}$$

where n is the number of the subsystem. This can be used in chromatography[19] to divide the total peak variance, σ_i^2, into two contributions: one, $\sigma_{c,i}^2$, resulting from the chromatographic column and the second, σ_{ex}^2, from all the other parts of the system, such as the injection device, connections, capillaries and detector cell:

$$\sigma_i^2 = \sigma_{c,i}^2 + \sigma_{ex}^2 \tag{2}$$

In this equation the subscript i denotes the analyte, indicating that the in-column peak broadening depends on data specific to a particular compound, i.e., the diffusion coefficient and the capacity factor. The influence of the different diffusion coefficients of solutes on the extra-column contribution, σ_{ex}^2, is neglected. The peak standard deviation, σ_i, can be measured as the half-peak-width at 0.607 of the peak height for pure Gaussian-type peaks, or, in the more general case and as required when measuring without a column, as the square root of the second moment of the peak.

The column variance, $\sigma_{c,i}^2$, given in volume units is related to the retention volume, V_{Ri}, of the compound, i, by the fundamental equation

$$\sigma_{c,i}^2 = \frac{H_i}{L} \cdot V_{Ri}^2 \tag{3}$$

where H_i is the theoretical plate height of the column for the compound i and L is the length of the column. Substitution of eqn. 3 into eqn. 2 leads to

$$\sigma_i^2 = \frac{H_i}{L} \cdot V_{Ri}^2 + \sigma_{ex}^2$$

$$= \frac{H_i}{L} \cdot V_{Ro}^2 (1 + \kappa_i)^2 + \sigma_{ex}^2 \tag{4}$$

where κ_i is the capacity factor of component i and V_{Ro} is the retention volume of an unretained substance. One of the two contributions to the total variance depends on the square of the retention volume, V_{Ri}, the other is independent of it. The retention-dependent contribution depends also on the theoretical plate height, H_i.

The theory of the chromatographic process[1,6-12] shows that H_i is a function of the average flow velocity, v, the mean particle diameter, $\bar{d}_p$, of the fixed bed, the capacity factor, κ_i, and the diffusion coefficients, D_{mi} and D_{pi}, of the solute in the mobile phase, m, and the particles, p, of the fixed bed and of a number of geometry factors specific to the particles and the bed. Introducing dimensionless variables

$$h_i = H_i / \bar{d}_p \tag{5a}$$

$$v_i = v \, \bar{d}_p / D_{mi} \tag{5b}$$

where v_i is the reduced flow velocity, in chemical engineering the Peclet number (Pe). The theoretical plate-height equation of Huber[7,10] is

$$h_i = \frac{a_1}{v_i} + \frac{a_2}{1 + a_3 v_i^{-\frac{1}{2}}} + a_4 \, v_i^{\frac{1}{3}} \left(\frac{\kappa_i^*}{1 + \kappa_i^*}\right)^2 + a_5 \, v_i \cdot \frac{\kappa_i^*}{(1 + \kappa_i^*)^2} \tag{6a}$$

or

$$h_i = h_{di} + h_{ci} + h_{fi} + h_{bi} \tag{6b}$$

The subscripts d, c, f and b indicate the contributions associated with various dispersion processes: mixing due to axial diffusion, convective mixing, mass exchange in the flowing fluid and mass exchange in the fixed bed (including the contributions from the stagnant mobile phase and the stationary phase). The factors, a_1-a_5, are constants for a given column, depending on the geometry of the particles and of the packing; κ_i^* is defined as the mass distribution coefficient between the fixed bed, b, and the flowing fluid, f

$$\kappa_i^* = \frac{\varepsilon_m}{\varepsilon_f} (\kappa_i + 1) - 1 \tag{7}$$

where κ_i is the mass distribution coefficient (capacity factor) between the stationary phase, s, and the mobile phase, m, ε_m is the fraction of the column volume occupied by the mobile phase and ε_f is the fraction occupied by the flowing part of the mobile phase.

If the geometry factors, a_1-a_5, in eqn. 6a are known, h_i can be calculated for various flow velocities, particle diameters, diffusion coefficients and mass distribution

coefficients. Huber *et al.*[10] investigated silica-packed columns and determined the geometry factors by non-linear regression analysis of experimental σ_i^2 data, minimizing an appropriate least-squares function:

$$F = \sum_m \sum_i \left(\frac{h_{i,m}^{exp} - h_{i,m}^{calc}}{h_{i,m}^{exp}}\right)^2 \tag{8}$$

Here, the index i represents the solutes and m the experiments made for a solute i. In a given experiment, h_i^{exp} describes the experimentally found column band broadening, evaluated by means of eqn. 9 after measuring σ_i^{exp}, σ_{ex} and V_{Ri}:

$$h_i = \frac{(\sigma_i^{exp})^2 - \sigma_{ex}^2}{V_{Ri}^2} \cdot \frac{L}{\overline{d_p}} \tag{9}$$

h_i^{calc} is estimated by use of eqn. 6a.

Considering the influence of the capacity factor on the value of h_i, Huber *et al.*[10] found for silica packings a significant dependence of h_i on κ_i, higher capacity factors resulting in higher values of h_i. Consideration of these results leads to the conclusion that eqn. 4 cannot give a linear dependence of σ_i^2 on V_{Ri}^2, because both V_{Ri} and H_i are functions of κ_i. This means that a linear regression analysis, performed on σ_i^2 vs. V_{Ri}^2 data, will give an intercept which is not exactly identical to σ_{ex}^2. Since H_i is also a function of D_{mi}, sometimes this effect may also mask the correlation of σ_i^2 with V_{Ri}^2.

The geometry factors determined by Huber *et al.*[10] show that the contribution h_{bi} is relatively small for the flow velocities and particle sizes used in practice. For a correct differentiation of the various h contributions in eqn. 6 and the estimation of their magnitude, especially of the two mass-exchange contributions, h_{fi} and h_{bi}, it is necessary to know the experimental value, h_i, with great accuracy. Eqn. 9 shows that the accuracy of h_i depends strongly on the accuracy of σ_{ex}. The error, Δh_i, in h_i which results purely from the error, $\Delta\sigma_{ex}$, in σ_{ex}, is given by eqn. 10a:

$$\Delta h_i = -2 \frac{\sigma_{ex}\Delta\sigma_{ex}}{V_{Ri}^2} \cdot \frac{L}{\overline{d_p}} \tag{10a}$$

$$\Delta\sigma_{ex} = -\frac{\overline{d_p} V_{Ri}^2}{2 L} \cdot \frac{\Delta h_i}{\sigma_{ex}} \tag{10b}$$

Eqn. 10b gives the minimum accuracy in σ_{ex} which is necessary to keep the error in the reduced plate height below a desired level, Δh_i. If, for instance, the error, Δh_i, in the reduced theoretical plate height is required to be less than half of one of the four contributions to h_i, the maximum allowable error, $\Delta\sigma_{ex}^{max}$, in the determination of the extra-column peak width, at a given value of σ_{ex}, is obtained from eqn. 10b and given by the expression

$$\Delta\sigma_{ex}^{max} = \frac{1}{4} \cdot \frac{\sigma_{ki}^2}{\sigma_{ex}} \tag{11}$$

where k refers to the subscripts d, c, f, b in eqn. 6b and σ_{ki}^2 is correlated to h_{ki} by analogy with eqn. 3.

At a constant error $\Delta\sigma_{ex}$, one can calculate the maximum allowable extra-column peak width, σ_{ex}^{max}, which just gives the desired accuracy for a given peak-broadening contribution:

$$\sigma_{ex}^{max} = \frac{1}{4} \cdot \frac{\sigma_{ki}^2}{\Delta\sigma_{ex}} \tag{12}$$

RESULTS AND DISCUSSION

Effect of the extra-column peak-width contribution on the h(v) curve

The strategy of model calculations was chosen to discuss the influence of the extra-column peak-width contribution on the accuracy of the theoretical plate-height determination. First, the distortion of a "true" $h_i(v_i)$ curve by an assumed extra-column contribution, σ_{ex}, is investigated for different capacity factors and for different particle diameters. In this approach a calculated $h_i(v_i)$ curve is assumed to be the "true" curve: the equation of Huber[6,7] (eqn. 6a) is used to describe the dependence of h_i on the reduced flow velocity, v_i, and on the capacity factor, κ_i. For the geometry constants, a_1-a_5, the following values obtained for a well packed silica column[10] were used: $a_1 = 2.90$, $a_2 = 1.30$, $a_3 = 7.60$, $a_4 = 0.92$ and $a_5 = 0.10$. The apparent values, h_i', are now estimated by including also the assumed extra-column contributions to the peak width, σ_{ex}^2. Three different assumptions, listed in Table I, have been made for σ_{ex}. These give σ_{ex} as a function of the flow-rate. Fig. 1 shows the influence of the different assumed σ_{ex} values on the $h_i'(v_i)$ curves for two different capacity factors. Fig. 1a deals with a small particle size ($\bar{d}_p = 5 \ \mu m$), Fig. 1b with a large particle size ($\bar{d}_p = 35 \ \mu m$). A marked influence of σ_{ex}^2 on h_i' is seen for small particles and for small capacity factors. The influence is much less pronounced for high capacity factors. In Fig. 1a the superposition of the extra-column variance produces a crossing of the h_i' curves corresponding to different capacity factors. In practice, this indicates appreciable extra-column contributions to the peak width. Such an effect is not observed with large particles.

From these calculations two important conclusions follow immediately: first,

TABLE I

ASSUMED VALUES FOR THE EXTRA-COLUMN PEAK WIDTH, σ_{ex} (μl), AS A FUNCTION OF THE FLOW-RATE

These data are used in the calculations shown in Fig. 1. A flow-rate of 1.0 ml/min corresponds to a reduced velocity of about 4.5 for a column of 4 mm I.D. and 5-μm particles. D_{mi} is assumed to be $3.7 \cdot 10^{-5} \ cm^2/s$.

Assumption	Flow-rate (ml/min)					
	0.5	1.0	1.5	2.0	2.5	3.0
1	5	5	5	5	5	5
2	5	10	15	20	25	30
3	8	16	24	32	40	48
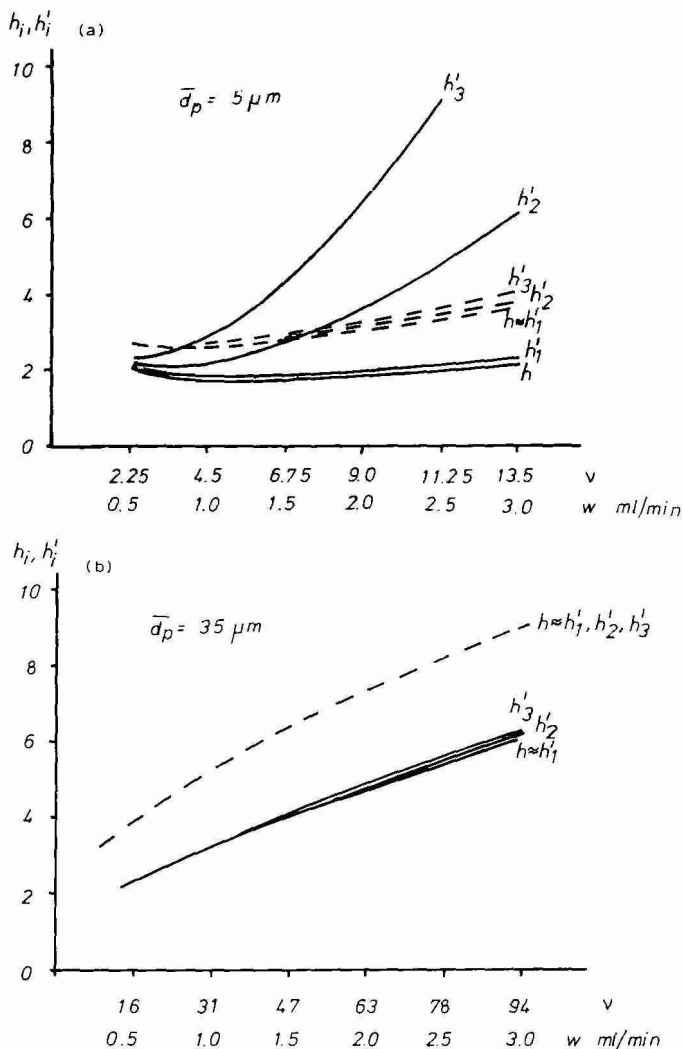
Fig. 1. Influences of the particle diameter and the solute capacity factor on the relative effect of the extra-column peak-width contribution to the h_i' vs. v_i curves. Particle size: (a) small ($\bar{d}_p = 5$ μm) and (b) large ($\bar{d}_p = 35$ μm). Capacity factors: small, $\kappa_i = 0.2$ (——); large, $\kappa_i = 5.0$ (--------). The h_i curves are calculated according to eqn. 6a by using the geometry factors $a_1 = 2.90$, $a_2 = 1.30$, $a_3 = 7.60$, $a_4 = 0.92$, $a_5 = 0.10^{10}$. The "apparent" curves, h_1', h_2', h_3', are obtained by superposition of the assumed extra-column band-broadening contributions of Table I on the corresponding h_i curves. The indices 1, 2, 3, refer to the various assumptions in Table I. Column data: 250 mm $\times$ 4 mm I.D., ε_m 0.8, ε_f 0.4; D_{mi} 3.7 $\cdot$ 10^{-5} cm^2/s. w = flow-rate corresponding with v.

investigations on the influence of the capacity factor on the theoretical plate height should be performed with large particles, whenever possible, in order to avoid significant interference by the σ_{ex}^2 contribution and inadequate corrections. However, as a consequence, measurements near the minimum of the $h_i'(v_i)$ curve require very small flow velocities. Secondly, the influence of σ_{ex}^2 can be significantly reduced, even

for small particles, by using solutes with large capacity factors. However, it must be kept in mind that the functions $\left(\dfrac{\kappa_i^*}{1+\kappa_i^*}\right)^2$ and $\dfrac{\kappa_i^*}{(1+\kappa_i^*)^2}$ associated with the two mass-exchange terms vary slightly at high capacity factors. Hence the determination or verification of the different κ- dependence of these two terms should be done at small capacity factors.

Estimation of minimum accuracy of σ_{ex}^2

Based on calculations of h_i by means of the geometry factors a_1–a_5, given before[10], the minimum accuracy of the extra-column variance, σ_{ex}^2, is evaluated, which is needed to avoid a significant interference with the small contributions to h_i, e.g., the contribution h_{bi} in eqn. 6. An accurate quantitation of h_{bi} together with h_{fi} is important for estimating correctly the influence of the capacity factor, κ_i, on the $h_i(\nu_i)$ function. Eqn. 11 gives the maximum allowable error, $\Delta\sigma_{ex}^{max}$, in the extra-column peak width, producing an error in a particular contribution to h_i, which is just half of this contribution. It is seen from eqn. 10b that at small values of σ_{ex} a greater maximum allowable error, $\Delta\sigma_{ex}^{max}$, in its determination is allowed to achieve a constant error, Δh_i, in the theoretical plate height. This is of some importance, because the errors, $\Delta\sigma_{ex}$, (and difficulties) in the experimental determination of the extra-column peak width, σ_{ex}, increase at high flow-rates, as does the peak width itself.

Let us assume that the error, Δh_i, should be smaller than half of the mass-exchange term, h_{bi}, in the fixed bed, which has been recognized, at least for silica columns[10], to be very small at moderate values of the reduced flow velocity, ν_i. With this assumption, Fig. 2 gives the maximum allowable error, $\Delta\sigma_{ex}^{max}$, as a function of the magnitude of the extra-column band width, σ_{ex}, for various reduced flow velocities. The contribution, h_{bi}, is calculated from eqn. 6a using the value $a_5 = 0.10$ given before[10].

Table II gives the maximum acceptable extra-column peak width, σ_{ex}^{max}, at various flow-rates, obtained by eqn. 12, assuming various constant errors, $\Delta\sigma_{ex}$, i.e., 3 and 10% relative error and 1 μl absolute error. In Table III these data are compared with typical values for σ_{ex}, measured in various chromatographic systems. It is seen that an accurate determination of the minor contributions to h_i requires that the extra-column peak width be smaller than the values usually obtained by using standard equipment.

Accuracy of the experimental determination of the extra-column peak width

In the discussion of the maximum acceptable error in the extra-column peak width, the possibilities of its accurate experimental determination must be considered critically. Several methods have been proposed for this purpose.

(i) Determination of the column contribution to the overall variance by varying the column length. Extrapolation to zero length gives the extra-column variance. This method requires columns of exactly the same dispersion per unit length, which cannot be assumed *a priori*. Variation of the column length by coupling of columns for which the peak dispersion characteristics have been determined previously may be an acceptable approach, providing no additional contributions are introduced by the connections between the columns. At the present time, no experimental values are available concerning the accuracy and precision of this method.
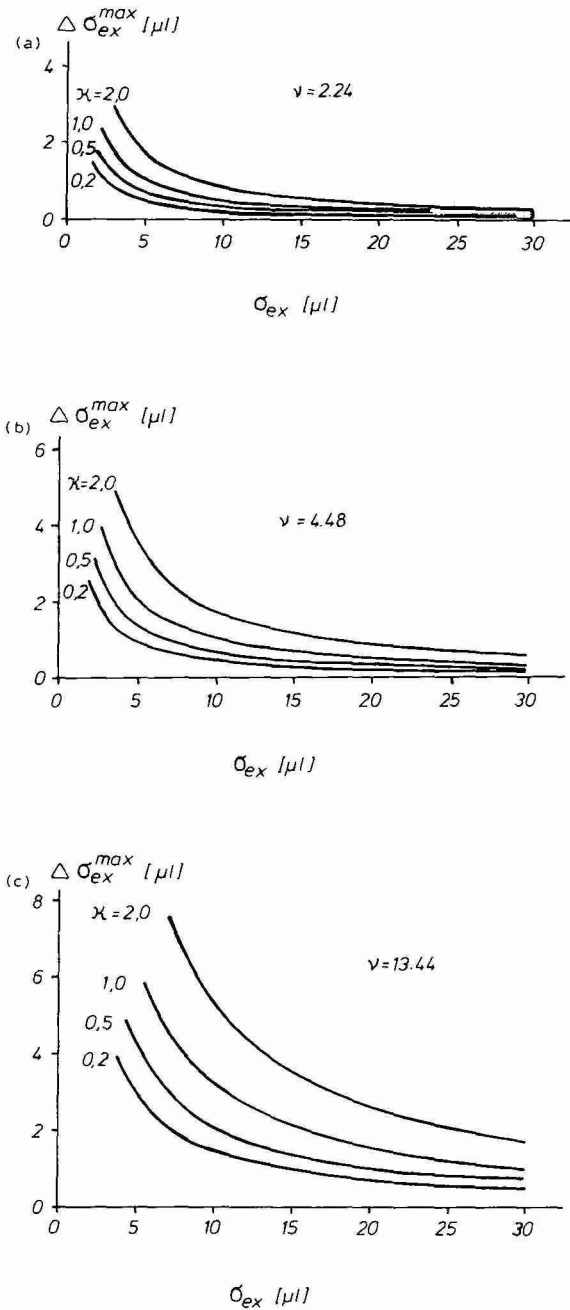
Fig. 2. Maximum allowable error, $\Delta\sigma_{ex}^{max}$ (μl), in the extra-column peak width as a function of the extra-column peak-width contribution, σ_{ex}, at various capacity factors, κ, and reduced flow velocities, v. The maximum allowable error is defined in this context as the error which allows the estimation of h_i with an accuracy and precision better than half of the contribution h_{bi} in the fixed bed. Column data as in Fig. 1 except 5-μm particles and $v = 2.24$ (a), 4.48 (b) and 13.44 (c).

TABLE II

MAXIMUM ALLOWABLE EXTRA-COLUMN PEAK WIDTH, σ_{ex}^{max} (μl), FOR DIFFERENT VALUES OF THE ERROR, $\Delta\sigma_{ex}$, IN ITS DETERMINATION

The maximum allowable error is defined as the value which permits the estimation of h_i with an accuracy and precision equal to half of the contribution h_{bi}, where h_{bi} is calculated from eqn. 6a by use of the geometry factor $a_5 = 0.10$. Column data: 250 mm × 4 mm I.D., 5-μm particles, ε_m 0.8, ε_f 0.4; D_{mi} 3.7 · 10^{-5} cm^2/s.

v_i	κ_i	$\Delta\sigma_{ex}$		
		+3%	+10%	+1 μl
2.25	0.2	9.0	5.1	2.4
	0.5	11.0	6.0	3.6
	1.0	13.3	7.3	5.3
4.50	0.2	13.0	7.1	5.1
	0.5	15.3	8.4	7.0
	1.0	18.8	10.3	10.6
6.75	0.2	15.9	8.7	7.6
	0.5	18.8	10.3	10.6
	1.0	23.1	12.7	16.0
13.5	0.2	22.3	12.2	14.8
	0.5	26.6	14.6	21.2
	1.0	32.7	17.9	31.9

TABLE III

APPROXIMATE EXPERIMENTAL EXTRA-COLUMN PEAK WIDTH, σ_{ex} (μl), REPORTED FOR TYPICAL CHROMATOGRAPHIC SYSTEMS EQUIPPED WITH SPECTROPHOTOMETRIC DETECTORS

Flow-rate (ml/min)	Reference				
	*	17	18	13	14
0.2			8–15		
0.5	12–17	7.5		7.5	2.5–15
1.0	17–22				5–22
1.2		9.7		9.0	
1.5	22–27				
2.4		13.3		9.9	
3.0	32–45			10.0	
Detector cell volume (μl)	8	4	8	4.5	1–4.5
Injection volume (μl)	10	16	1	1	0.5
Eluent constituents (volume ratio)	Heptane	Water–acetonitrile (3:2)	Water–methanol (1:1)	Water–acetonitrile (3:2)	

* Present measurements on a commercially available standard system without optimization.
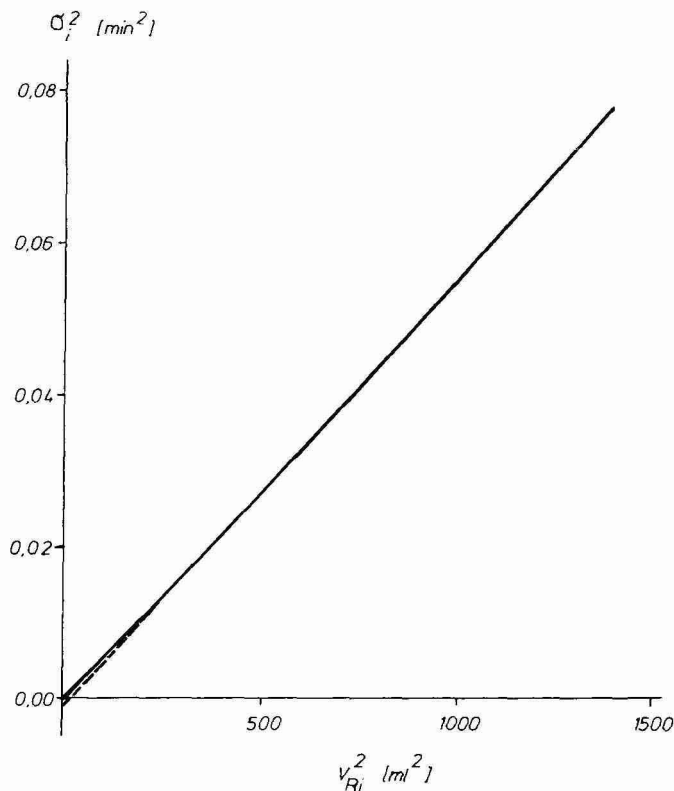
Fig. 3. Example of a σ_i^2 versus V_{Ri}^2 plot. The broken line represents the linear extrapolation from high V_{Ri}^2 values to zero retention volume. The data are calculated from eqn. 6a by using the geometry factors in Fig. 1. Column data as in Fig. 1 except 5-μm particles and $v = 4.5$.

(ii) Measuring the band broadening in a system consisting of an injector, connectors and detector but without the column[13]. In this method the chromatographic system without the column must be simulated exactly, and this is quite difficult in practice. Due to the reduction of the flow resistance, the flow conditions and the streaming profiles are not exactly the same. An inaccuracy in σ_{ex} of at least 5% is expected although the measurements can be carried out with a precision of about 2%[13].

(iii) A linear regression of the total peak variance, σ_i^2, and the square of the retention volume, V_{Ri}^2. The intercept of this straight line can be used as an approximate measure of the extra-column peak variance, σ_{ex}^2 (refs. 15–18). This approach neglects the fact that the theoretical plate height, H_i, depends on the capacity factor, κ_i, and on the diffusion coefficient, D_{mi}, of the solutes. The slope, H_i/L, of the $\sigma_i^2(V_{Ri}^2)$ function will therefore not be constant, unless accidentally in cases where the influences of the capacity factor and of diffusion coefficient compensate each other. Since h_i depends appreciably on κ_i (refs. 6, 7, 9 and 10), this strategy produces regression σ_{ex}^2 results (intercepts) that cannot be assumed to be a good approximation for σ_{ex}^2. This is illustrated by the model calculations shown in Fig. 3: h_i values are cal-

TABLE IV

EXTRA-COLUMN PEAK-WIDTH CONTRIBUTION, σ_{ex}, OBTAINED FROM THE INTERCEPT OF THE $\sigma^2(V_{Ri}^2)$ REGRESSION LINE

The capacity factors ranged from 0.2 to 10.0.

Flow-rate (ml/min)	ν	σ_{ex} (μl)	
		Assumed*	Extrapolated**
0.5	2.25	0	−15.3
1.0	4.5	0	−17.2
2.0	9.0	0	−20.8
3.0	13.5	0	−22.6

* Value chosen for the calculation of the σ^2/V_{Ri}^2 function.
** Estimated from eqn. 4, where H_i is calculated according to eqn. 6a using the geometry factors $a_1 = 2.90$, $a_2 = 1.30$, $a_3 = 7.60$, $a_4 = 0.92$, $a_5 = 0.10^{10}$. A constant diffusion coefficient was assumed for all solutes. Column data as in Table II.

culated for several solutes with equal diffusivity but different capacity factors, using the same geometry constants, a_1–a_5, as before[10] and applying the Huber equation[7]. The extra-column peak width, σ_{ex}, is assumed to be zero. The σ_i^2 values corresponding to the calculated h_i data are plotted *versus* V_{Ri}^2. A slightly concave curve is obtained in the usual working range. This implies that a linear regression of these data yields intercepts smaller than the true value of σ_{ex}^2. Table IV summarizes the error in determining the extra-column peak width by this linear regression method. The negative values indicate that the true extra-column peak broadening is underestimated by this procedure. The errors obtained by this model calculation (capacity factor ranges from 0.1 to 10) are appreciable. Although the obtained error may be smaller when using a smaller capacity factor range, it is clear that this method cannot fulfil the requirements of an accurate determination.

CONCLUSIONS

Model calculations have been used to illustrate the importance of accuracy and precision in the measurement of the extra-column peak width when the peak dispersion process in the column is investigated. Since the "true" $h_i(v_i)$ curve has to be recalculated from the measured, "apparent" curve, $h_i'(v_i)$, a certain error is introduced in the model when the extra-column peak width is not negligible or cannot be determined accurately and precisely. This problem is not so important when large particles are used and for solutes with large capacity factors, since the column peak-width contribution is large under these circumstances. Microparticulate columns, however, are superior in separation performance and large particles imply very low flow velocities when working near the theoretical plate-height minimum. For the investigation of the capacity factor dependence of the theoretical plate height, solutes with low capacity factors have to be used in order to be able to separate the effects of the two mass-exchange terms, h_{fi} and h_{bi}. Therefore it is essential to minimize the extra-column peak width contribution and to reduce the error in its determination.

The maximum error in the extra-column peak width was calculated which still allows determination of the smallest contribution to the theoretical plate height, without this value being significantly falsified. This error is dependent on the extra-column variance (which itself depends on the chromatographic equipment and the flow-rate) on the one hand and the column volume and the capacity factor on the other hand. When assuming typical extra-column variances measured and reported in the literature, their errors should be less than a few microlitres at column volumes of a few millilitres. Unfortunately, the systematic error in the experimental determination of the extra-column peak width was found to be of the same order of magnitude in most cases.

Thus, the accuracy or the precision of the experimental determination of the extra-column peak width contribution in chromatographic systems must be carefully checked whenever a verification of theoretical models of chromatographic processes is attempted. The approximate evaluation of this value from the intercept of a linear regression in a $\sigma_i^2(V_{Ri}^2)$ diagram is unsatisfactory in this context.

REFERENCES

1 J. H. Knox and H. P. Scott, *J. Chromatogr.*, 282 (1983) 297.
2 E. Katz, K. L. Ogan and R. P. W. Scott, *J. Chromatogr.*, 270 (1983) 51.
3 R. W. Stout, J. J. DeStefano and L. R. Snyder, *J. Chromatogr.*, 282 (1983) 263.
4 N. H. C. Cooke, B. G. Archer, K. Olsen and A. Berick, *Anal. Chem.*, 54 (1982) 2277.
5 J.-C. Chen and S. G. Weber, *Anal. Chem.*, 55 (1983) 127.
6 J. F. K. Huber, *J. Chromatogr. Sci.*, 7 (1969) 85.
7 J. F. K. Huber, *Ber. Bunsenges. Phys. Chem.*, 77 (1973) 179.
8 G. J. Kennedy and J. H. Knox, *J. Chromatogr. Sci.*, 10 (1972) 549.
9 Cs. Horváth and H.-J. Lin, *J. Chromatogr.*, 149 (1978) 43.
10 J. F. K. Huber, J. H. Quaadgras and A. Rizzi, in preparation.
11 J. C. Giddings, *Dynamics of Chromatography*, Marcel Dekker, New York, 1965.
12 E. Grushka, L. R. Snyder and J. H. Knox, *J. Chromatogr. Sci.*, 13 (1975) 25.
13 K.-P. Hupe, R. J. Jonker and G. Rozing, *J. Chromatogr.*, 285 (1984) 253.
14 K. W. Freebairn and J. H. Knox, *Chromatographia*, 19 (1984) 37.
15 J. F. K. Huber, unpublished results.
16 W. Kutner, J. Dębowski and W. Kemula, *J. Chromatogr.*, 218 (1981) 45.
17 H. H. Lauer and G. P. Rozing, *Chromatographia*, 14 (1981) 641.
18 W. Th. Kok, U. A. Th. Brinkman, R. W. Frei, H. B. Hanekamp, F. Nooitgedacht and H. Poppe, *J. Chromatogr.*, 237 (1982) 357.
19 J. C. Sternberg, *Adv. Chromatogr. (N.Y.)*, 2 (1966) 205.

CHROMSYMP. 999

MEASUREMENT OF LIPOPHILICITY BY HIGH-PERFORMANCE LIQUID CHROMATOGRAPHY

COMPARISON WITH CALCULATED LIPOPHILICITY VALUES

JULIE J. SABATKA*, DOUGLAS J. MINICK, THOMAS K. SHUMAKER, GORDON L. HODGSON Jr. and DAVID A. BRENT

Wellcome Research Laboratories, Burroughs Wellcome Co., Research Triangle Park, NC 27709 (U.S.A.)

SUMMARY

Reversed-phase high-performance liquid chromatography (HPLC) was used to measure the lipophilicities of a series of biphenyl acids and their non-acid precursors. Values obtained by HPLC for the precursors were as predicted from the calculated lipophilicity values. For the biphenyl acids, a systematic deviation in the correlation of calculated log P and log k' was observed (hydrogen-bond acceptors and non-hydrogen-bonding substituents described two separate lines in the correlaton). An explanation of these results is presented, based on steric effects which control the way the biphenyl acids interact with the stationary phase.

INTRODUCTION

Octanol–water partition coefficients (log P), as measured by the standard shake-flask method, are widely used in structure–activity studies. This method is time-consuming and limited by problems such as difficulty in measuring very high or low partitions, and variance in the results due to impurities, dissociation, decomposition, poor detectability, and emulsion formation. Despite these limitations, a large data base of measured values exists. In an effort to avoid the problems associated with the shake-flask method, calculation methods and chromatography have been used to measure lipophilicity. Chromatography avoids many of the problems and has the added advantage of being easily amenable to automation.

In this study, reversed-phase high-performance liquid chromatography (RP-HPLC) was used to measure the lipophilicities of a series of biphenyl acids (Table I) and their precursors (*p*-bromobenzene analogues containing substituents similar to those varied in the acid series, Table II). The goals of this study were: (i) to use the lipophilicity constants from HPLC and the calculated log P values independently to develop quantitative structure–activity relationships for the biphenyl acids and their precursors; (ii) to investigate the correlation between the HPLC constants and calculated log P values.

The first of these goals was unsuccessful. Neither HPLC nor calculated log P

TABLE I

BIPHENYL ACIDS: SUBSTITUENTS AND LIPOPHILICITY DATA
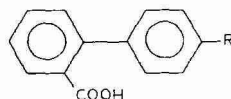
Compound number	Substituent	log k'	Calculated log P
1	H	0.397	3.773
2	Cl	1.04	4.506
3	Br	1.19	4.656
4	OCH_3	0.693	3.736
5	S(n-hexyl)	3.56	6.996
6	SO(n-butyl)	1.44	3.815
7	SO(n-hexyl)	2.31	4.873
8	$SO_2N(C_2H_5)_2$	1.5	4.071
9	$SO_2N(C_2H_5)(C_3H_7)$	2.083	4.6
10	$SO_2N(C_3H_7)_2$	2.34	5.129
11	SCF_3	1.88	5.46
12	CH_3	0.922	4.422
13	C_2H_5	1.35	4.951
14	Isopropyl	1.85	5.35
15	Butyl	2.46	6.009
16	tert.-Butyl	2.21	5.749
17	Phenyl	2.18	5.661
18	CF_3	1.42	4.69
19	CHO	0.522	3.195
20	COOH	−0.109	3.561
21	$CO_2C_3H_7$	2.132	4.853

values was useful for predicting the activity of this series (the structure–activity study will be published later). However, a correlation between HPLC lipophilicity constants, and log P values was found for both acids and precursors, and some interesting results emerged from these correlations.

EXPERIMENTAL

The distinguishing features of our HPLC method are the highly deactivated stationary phase (made by further deactivation of Corasil C_{18}) and the mobile phase of pH and ionic strength similar to blood (taking into account the organic solvent effect on the mobile phase pH)[1].

Apparatus

The HPLC equipment consisted of an autoinjector (Micromeretics, Norcross, GA, U.S.A.), two high-pressure pumps (Waters Model M-45) and a variable-wavelength UV detector (Water Model 450, Waters Chromatography Division of Millipore, Milford, MA, U.S.A.). The columns were made of 316 SS (5 × 0.46 cm I.D.).

TABLE II

BROMOBENZENE PRECURSORS: SUBSTITUENTS AND LIPOPHILICITY DATA

Br—⟨O⟩—R
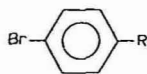
Compound number	Substituent	log k'	Calculated log P
1	H	0.881	3.005
2	F	0.96	3.148
3	Cl	1.32	3.718
4	Br	1.44	3.868
5	OCH_3	1.08	3.064
6	SCH_3	1.43	3.648
7	$SOCH_3$	−0.02	1.1414
8	$SO_2N(C_2H_5)_2$	0.825	3.258
9	$SO_2(C_2H_5)(C_3H_7)$	1.55	3.787
10	$SO_2N(C_3H_7)_2$	1.94	4.316
11	C_2H_5	1.78	4.183
12	C_6H_5	2.35	4.893
13	CF_3	1.51	3.888
14	$CO(CH_2)_3CH_3$	1.868	4.107
15	$CO(C_6H_5)$	1.75	4.159
16	$CO_2C_2H_5$	1.46	3.579

Materials

In all experiments, HPLC-grade methanol (Fisher Scientific, Pittsburgh, PA, U.S.A.), HPLC purified water (Hydro Services, Durham, NC, U.S.A.), and reagent-grade buffer salts (Mallinckrodt, Paris, KY, U.S.A.) were used.

Procedures

Columns were packed by a tap-fill procedure with highly deactivated stationary phase [made by further deactivation of Corasil C_{18} (Waters)][1]. Mobile phases were of pH and ionic strength similar to blood (taking into account the organic solvent effect on the mobile phase pH)[1].

For all experiments the flow-rate was 2 ml/min, detection was at 254 nm, and injection volumes were 10 μl. All mobile phases were filtered through 0.45 μm filters (Millipore, Bedford, MA, U.S.A.).

Capacity factors, k', were the average of three measurements. The retention of an injection of methanol was used to determine the void volume.

The mobile phase for the biphenyl acid series [methanol–buffer (1:4)] was prepared from 1.6123 g $NaH_2PO_4 \cdot H_2O$ and 11.7620 g $Na_2HPO_4 \cdot 7H_2O$. The phosphates were dissolved in 800 ml water, and 200 ml of methanol was added. The apparent pH of the resulting solution was 7.79. The calculated ionic strength was 0.15 molal. The mobile phase for the p-bromobenzene series [methanol–buffer (2:3)] was prepared from 1.6075 g $NaH_2PO_4 \cdot H_2O$ and 11.1945 g $Na_2HPO_4 \cdot 7H_2O$. The phosphates were dissolved in 600 ml water, and 400 ml methanol was added. The apparent pH of the mobile phase was 8.14, the calculated pH 7.40. The calculated ionic strength was 0.15 molal.
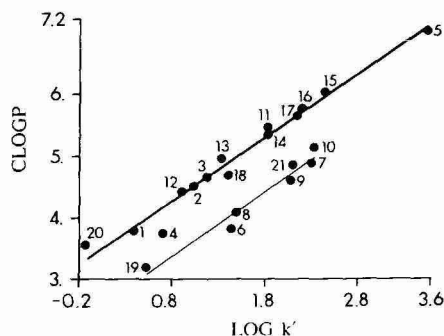
Fig. 1. Biphenyl acids: correlation of calculated log P (CLOGP) with log k' (LOG k'). Curve 1 (thin line) is the correlation of hydrogen-bond acceptors. Curve 2 (heavy line) is the correlation for non-hydrogen bonders. Regression data are in Table III.
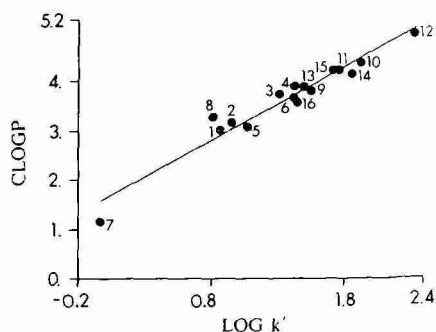
Fig. 2. *p*-Bromobenzene precursors: correlation of calculated log P (CLOGP) with log k' (LOG k'). Regression data are in Table III.

Calculated log P values were determined using the CLOG P program, Version 3.3. Structures were entered with the SMILES program (both Ponoma Medicinal Chemistry Project, Ponoma College, Claremont, CA, U.S.A.). Conformational analysis and energy minimization of the biphenyl acid structure model were carried out using Macro Model (Clark Still, Columbia University, New York, NY, U.S.A.).

RESULTS AND DISCUSSION

A comparison of the data plots for the biphenyl acids (Fig. 1) and their *p*-bromobenzene precursors (Fig. 2) shows a striking difference. While a single line described the correlation of log k' with log P for the *p*-bromobenzene series, two lines best described the same correlation for the acid series. For the biphenyl acids, there is a separation between hydrogen-bond acceptors (curve 1) and non-hydrogen-

TABLE III

LINEAR REGRESSION DATA FOR THE CORRELATIONS OF CALCULATED LOG P AND LOG k'

r = correlation coefficient; s = standard deviation; F = overall F test for the correlation, n = number of compounds.

Series	Calculated for log $P = a$ log $k' + b$					
	a	b	r	s	F	n
Biphenyl acids						
Curve 1	1.0386	2.5350	0.9800	0.1514	121.27	7
Curve 2	1.0194	3.434	0.9873	0.1606	464.45	14
Overall	0.9511	3.2538	0.8787	0.4499	64.38	21
p-Bromobenzene precursors						
Overall	1.4449	1.616	0.9695	0.2102	218.96	16

bonding substituents (curve 2). No hydrogen-bond donors were studied. Note that a dicarboxylic acid (Table I, compound 20) was included in the correlation. Under our chromatographic conditions, this compound is a dianion and should act as a hydrogen-bond acceptor. However, its log P was calculated for the neutral molecule. Lowering the calculated log P by four log units to correct for the anion substituent would place this point below the hydrogen-bond acceptor line. This result would be expected for a strong hydrogen-bond acceptor, such as an anion.

Table III gives the linear regression data for the correlations. In comparing the overall regression with the regression for fitting two lines to the data, the null hypothesis of equality of variances is tested by $F_0 = s_1^2/s_2^2$, where $s_1 \geqslant s_2$. F_0 has an F distribution with $n_1 - 1$ and $n_2 - 1$ degrees of freedom. The null hypothesis is rejected if $F_0 > F_{0.99} (V_1, V_2)$, where $F_{0.99} (V_1, V_2)$ is the appropriate critical value; i.e. prob$[F > F_{0.99} (V_1, V_2)] \leqslant 0.01$. Using this criterion, the fit of the individual curves is significantly better (to the 99% confidence level) than the fit of the overall correlation. When substituents similar to those used for the biphenyl acid series are para substituted on bromobenzene a significantly better fit results when a linear regression is used to fit all of the data to a single line, rather than two lines.

Several authors have reported systematic deviations in the correlation of HPLC data with log P. Unger et al.[2] have reported observing two lines in correlations comparing retention on an octanol-coated C_{18} column with an octanol-saturated aqueous mobile phase with the retention on a C_{18} column with a methanol–water mobile phase. The compounds studied were tuberin [N-(β-styryl)formamide] analogues. The substituents could be divided into non-hydrogen-bonding and hydrogen-bonding [i.e. SO_2PH, OCH_3, $N(CH_3)_2$] groups. As with our data, the hydrogen-bonding compounds (all hydrogen-bond acceptors) appeared more lipophilic by HPLC than by log P. However, Unger et al. found that a single line described the correlation of measured log P with retention data obtained on the octanol-coated C_{18} system. Therefore, one would expect two lines in correlations of log P with HPLC data from the methanol–water system.

Haky and Young[3] reported a second line for a series of phenolic calibration standards when they were compared to non-phenolic compounds. These compounds (which are strong hydrogen-bond donors) were predicted to be less lipophilic by HPLC than by log P. Haky and Young[3] and Davis[4] explain this deviation by hydrogen bonding with octanol. Yamagami et al.[5] showed the same sort of deviations for phenolic compounds and related this to the relative basicity of the methanol compared to octanol. Addition of tetrahydrofuran (THF) (a stronger base than methanol) to the mobile phase eliminates the deviation of the phenols by increasing their retention. Yamagami et al.[5] attribute this effect to the stronger hydrogen-bond acceptor properties of THF and the higher concentration of THF in the stationary phase[6]. While the first effect alone would tend to increase the solvation of the solute in the mobile phase and thus decrease retention, the increased possibility of such interactions with the THF in the stationary phase leads to longer retention.

Leo et al.[7] demonstrated that correlations between partition coefficients measured in apolar solvents versus water and those measured in octanol versus water were best described by dividing solutes into classes according to hydrogen-bonding characteristics. They found that strong hydrogen-bond donors were "minus deviants" and hydrogen-bond acceptors were "plus deviants". Examination of our data

and that of Unger *et al.*[2] suggests that hydrogen-bond acceptors may be further separated into groups (one for substituents like OCH_3, O-*tert.*-butyl etc. and another for SO_2CH_3, SO-*n*-butyl etc.), according to the strength of the interaction. This is supported by published data on hydrogen-bond acceptor strength[9].

While systematic deviations are reported for hydrogen-bond donors and acceptors as compared to non-hydrogen-bonding substituents, our data show this sort of selectivity for the biphenyl acids but not for the *p*-bromobenzene compounds. Differences in selectivities between these solute classes can be explained by differences in the effects of induction on the hydrogen-bond accepting capabilities of the substituents. The two functionalities [4-bromo compared to 4-(2-carboxyphenyl)], create different electronic environments for the substituents. In the *p*-bromobenzenes, induction would decrease the electron density of the substituents, and therefore decrease the hydrogen-bond accepting capabilities, making one line for all compounds more likely. This electronic effect could be the cause of the lack of selectivity for the *p*-bromobenzenes. By contrast, the narrow range of pK_a values and the lack of correlation of pK_a with sigma values (Table IV) indicate that there are no major inductive effects for the biphenyl acids; therefore, induction cannot be the cause of the two lines observed in the correlation.

The size and shape of molecules also contribute to the type of interaction which occurs with the stationary-phase surface, and could explain the differences in selectivity observed between the biphenyl acids and the *p*-bromobenzene compounds. Lochmuller *et al.*[8] have reported that a bonded phase of chain length greater than C_{12} is required to solvate a molecule the size of benzene in the stationary phase. The larger size of the biphenyl acids may restrict complete solvation of these molecules by the stationary phase, allowing the hydrogen-bond acceptor substituents to participate in the retention in a way different from that of the apolar substituents. The

TABLE IV

COMPARISON OF pK_a VALUES AND SIGMA *PARA* VALUES FOR THE BIPHENYL ACIDS

Substituent	Sigma* para	pK_a**
OCH_3	−0.27	3.50
CH_3	−0.17	3.78
C_2H_5	−0.15	3.94
Cl	0.23	3.29
Br	0.23	3.65
CO-*n*-butyl	0.48***	3.45
COC_6H_5	0.43	3.30
COOH	0.45	2.30, 4.68
CF_3	0.54	3.83
$SO_2N(C_3H_5)_2$	0.57§	3.69
$SO_2N(C_3H_7)_2$	0.57§	4.26

  *   From ref. 10.
 **   Measured in our laboratory.
***   Value for COC_2H_5.
  §   Values for SO_2NH_2.
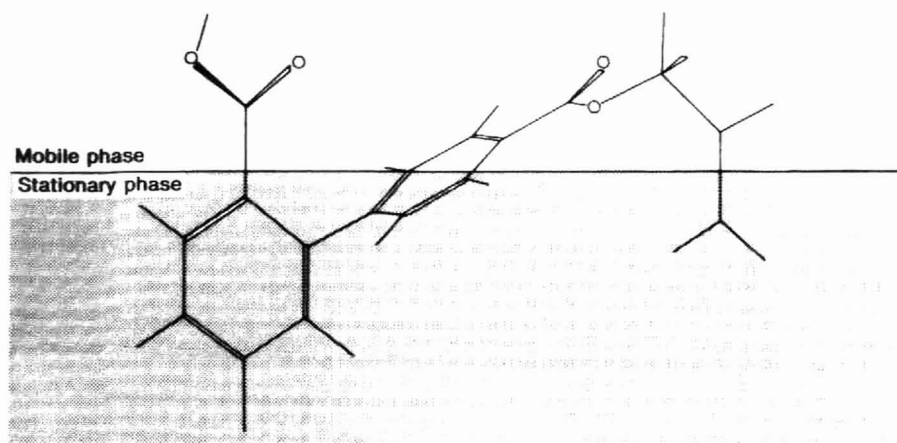
Fig. 3. An energy-minimized conformation of a biphenyl acid interacting with the stationary phase (substituent, CO_2-n-propyl).

smaller p-bromobenzene compounds would be completely solvated by the stationary phase, allowing no differentiation between hydrogen-bonding and non-hydrogen-bonding substituents. The ability of the stationary phase to solvate one class of solutes completely and not another, due to size restrictions, may account for the selectivity differences observed for this HPLC system.

Perhaps more significantly, the shape of the biphenyl acids (Fig. 3 shows an energy-minimized conformation of the molecule) driven by the position of the carboxylate, better explains why hydrogen-bond acceptors were differentiated in the correlation for the biphenyl acids and not for the p-bromobenzenes. The biphenyl acids contain a carboxylic acid group that is anionic under these HPLC conditions. Solvation of this group by methanol and water molecules would force this portion of the molecule to remain in contact with the mobile phase. This in turn, places the hydrogen-bond acceptors substituted on the other ring in a position to accept hydrogen-bonding interaction with methanol molecules coating the surface of the stationary phase (see Fig. 3 for a representation of this orientation in the stationary phase). This interaction would be absent from biphenyl acids with apolar substituents, and would explain the longer retention for the hydrogen-bond acceptors.

CONCLUSION

These results show that correlating lipophilicities measured by HPLC with octanol–water partition coefficients may not be straightforward, for some structural types, because other effects (*e.g.* hydrogen bonding) also influence the data. Experiments are currently being performed to test the proposals advanced in this paper to explain the deviations of the correlation.

REFERENCES

1 D. A. Brent, J. J. Sabatka, D. J. Minick and D. W. Henry, *J. Med. Chem.*, 26 (1983) 1014.

2 S. H. Unger, J. R. Cook and J. S. Hollenberg, *J. Pharm. Sci.*, 67 (1978) 1364.
3 J. E. Haky and A. M. Young, *J. Liq. Chromatogr.*, 7 (1984) 675.
4 S. S. Davis, *J. Pharm. Pharmacol.*, 25 (1973) 982.
5 C. Yamagami, H. Takami, K. Yamamoto, K. Miyoshi and N. Takao, *Chem. Pharm. Bull.*, 32 (1984) 4994.
6 R. M. McCormick and B. L. Karger, *Anal. Chem.*, 52 (1980) 2249.
7 A. Leo, C. Hansch and D. Elkins, *Chem. Rev.*, 71 (1971) 525.
8 C. H. Lochmuller and D. R. Wilder, *J. Chromatogr. Sci.*, 17 (1979) 574.
9 R. W. Taft, D. Gurka, L. Joris, P. von R. Schleyer and J. W. Rakshys, *J. Am. Chem. Soc.*, 91 (1969) 4801.
10 C. Hansch and A. J. Leo, *Substituent Constants for Correlation Analysis in Chemistry and Biology*, John Wiley, New York, 1979.

CHROMSYMP. 1070

ON-LINE LOW-LEVEL RADIOMETRIC DETECTION OF [14C]REMOXI-PRIDE IN LIQUID CHROMATOGRAPHIC EFFLUENTS

APPLICATION TO URINE SAMPLES

A. C. VELTKAMP and H. A. DAS

E.C.N., Westerduinweg 3, 1755 LE Petten (The Netherlands)

and

R. W. FREI* and U. A. Th. BRINKMAN

Department of Analytical Chemistry, Free University, De Boelelaan 1083, 1081 HV Amsterdam (The Netherlands)

SUMMARY

A method for on-line radiometric detection in liquid chromatography (LC) is described that permits the detection of low levels of radioactivity in LC effluents by using solvent segmentation and storage of the segmented effluent in a capillary storage loop.

The object of the method is to make the flow-rate in the on-line radioactivity monitor (and hence the mean residence time in the monitor) independent of the separation process. Therefore, after storage of the complete chromatogram, the segmented effluent is led through the monitor at flow-rates that can be chosen according to the residence time desired for accurate and precise radioactivity determination. In this system, it is possible to use a flow-cell volume small enough to preserve the chromatographic integrity, while maintaining the possibility of increasing the counting time.

Tests have been performed on the reproducibility of ^{14}C detection and the influence of the flow-rate through the monitor on the standard deviation in ^{14}C peak area and, thus, on the detection limit, using ^{14}C-labelled remoxipride. As an application, analyses of urine samples for [14C]remoxipride and one of its potential metabolites are reported.

INTRODUCTION

The advantages of using radionuclide-labelled compounds in metabolism and trace recovery studies are well recognized. Detection is selective and sensitive, the sensitivity depending on the background level, counting efficiency and counting time of background and sample. For the determination of groups of structurally similar analytes, such as metabolites, degradation products and by-products, the coupling of liquid chromatographic (LC) techniques with radiometric detection has become

a promising approach[1]. The radioactivity monitoring of LC effluents can be performed by off-line or on-line techniques.

In off-line counting, the LC effluent is fractionated. After mixing with a suitable liquid scintillator, the fractions are counted in a liquid scintillation counter. Obviously this method has the advantage of a free choice of counting time, depending on the radioactivity level and the standard deviation desired. The major drawback is the time-consuming procedure, which can easily lead to erroneous results and difficulties with automation and data acquisition. Also, the resolution depends on the fraction size chosen. Further, the reproducibility of the fraction collection becomes problematic with eluents that contain low percentages of organic solvents[2].

Two alternatives have been developed that permit the on-line radioactivity determination in LC effluents.

(1) Heterogeneous counting, in which the effluent is led through a radioactivity monitor with a flow cell packed with solid scintillator material. In this method, problems such as pressure build-up across the cell may arise, which will lead to leakage. Moreover, for some applications, irreversible adsorption of compounds on the scintillator material occurs. With radiolabelled compounds, this will lead to an undefined increase in the background, which hampers accurate and precise low-level radioactivity detection. Further, the counting efficiency for ^{3}H is low ($< 1\%$)[3].

(2) Homogeneous counting, in which the effluent is continuously mixed with a liquid scintillator before passing through the radioactivity monitor. In this instance no pressure build-up occurs but, as with heterogeneous counting, the counting time depends on the flow-rate (F) in the monitor and the flow-cell volume (V) as it equals the mean residence time t_d in the monitor:

$$t_d = V/F \tag{1}$$

In optimization of on-line radioactivity detection, one should focus on the increase in counts/peak in the radiogram recorded, as calculated from

$$\text{Counts} = EBt_d \tag{2}$$

where E is the counting efficiency and B the amount of radioactivity injected (Bq). For low beta-emitters, such as ^{14}C or ^{35}S, E values of over 0.5 are normally obtained. Therefore, as mentioned by Reeve and Crozier[4], little gain in sensitivity can be expected by increasing it. In general, a lower but constant E value is to be preferred over a high but varying performance.

The counting time, t_d, can be increased via the flow-cell volume, V. However, this will lead to a decrease in resolution. As a rule of thumb, the flow-cell volume should be less than one third of the volume standard deviation of the peak of interest[5]. Hence one should increase t_d while keeping V sufficiently low.

In a previous study we showed the possibility of increasing t_d independent of the separation process (that is, independent of the flow-rate, F, used for the separation process and the addition of liquid scintillator) by using solvent segmentation of the LC effluent[6]. Segmentation helps to suppress band broadening in the relatively large flow-cell volume and connecting tubing of the on-line radioactivity detector, as first demonstrated by Bakay[7], who succesfully used a semi-solid acrylamide gel as the segmentor. In our approach, two radiograms can be recorded, direct or reverse.

In the direct mode, after UV detection the water-containing effluent is mixed with a water-immiscible liquid scintillator. This scintillator has three functions: as an extraction medium for low- to medium-polarity compounds from the effluent into the scintillator; as a detection medium for the extracted radiolabelled compounds; and to segment the LC effluent with water-immiscible organic solvent plugs, which suppresses band broadening of the effluent in the capillaries. As a result, a solvent-segmented flow pattern is obtained, which is led through the radioactivity monitor and the direct radiogram is recorded at the combined flow-rate of eluent and scintillator (typically 2.0 ml/min). After detection, this mixture is stored in a capillary storage loop.

In the reverse mode, after storage of the complete chromatogram it can be reintroduced into the radioactivity monitor at a flow-rate independent of the chromatographic conditions, and so, as with off-line counting, in the reverse radiogram the counting time, t_d, can be chosen to match the radioactivity level (as recorded in the direct chromatogram) and the desired sensitivity. Owing to the increase in t_d, an increase in peak area and, hence, an increase in sensitivity are obtained relative to the direct radiogram. Further, it would be possible to program the flow-rate for the reverse measurement according to the radioactivity distribution, as recorded in the direct run, and/or by programming regions of interest in the chromatogram. This will be dealt with in a subsequent paper. In our opinion, this approach is more versatile than the alternative of lowering the flow-rates of the eluent and scintillator during the separation. In the latter instance much time will be wasted for regions where no radioactivity elutess. Also, the possible gain in t_d will be limited, owing to band broadening in the column, connecting tubes and detectors at very low flow-rates.

To test this system, the determination of polar [¹⁴C]remoxipride, a recently developed antipsychotic agent[8–10], in human urine samples from volunteers who had been given a dose of [¹⁴C]remoxipride was performed. A pharmaceutical compound was chosen because most applications of radio-LC refer to pharmaceutical and biomedical research[1]. Further, we wanted to demonstrate the applicability of this technique to polar compounds, *i.e.*, compounds that are poorly extractable into the scintillator phase under the separation conditions used.

EXPERIMENTAL

Apparatus

A schematic diagram of the system is given in Fig. 1. The set-up consists of a Model 3B dual-head pump (Perkin-Elmer, Norwalk, CT, U.S.A.), a Model 7126 injector (Rheodyne, Cotati, CA, U.S.A.), used with a Rheodyne 7163 solenoid valve kit, a Uvikon 725 UV detector (Kontron, Zurich, Switzerland) and a Minipuls Model HP4 peristaltic pump (Gilson Medical Electronics, Villiers-le-Bel, France), used for adding aqueous sodium hydroxide to the effluent. The combined flows are mixed with the scintillator through a T-piece. The segmented flow then passes a Model 12611 eight-port switching valve (Valco, Houston, TX, U.S.A.) with an air activator and a Rheodyne 7163 valve kit. Following the extraction coil, the flow is led through the radioactivity monitor, which consists of a laboratory-built light-tight housing, an Isoflo flow cell (Nuclear Enterprises, Edingburgh, U.K.) with a geometric volume of
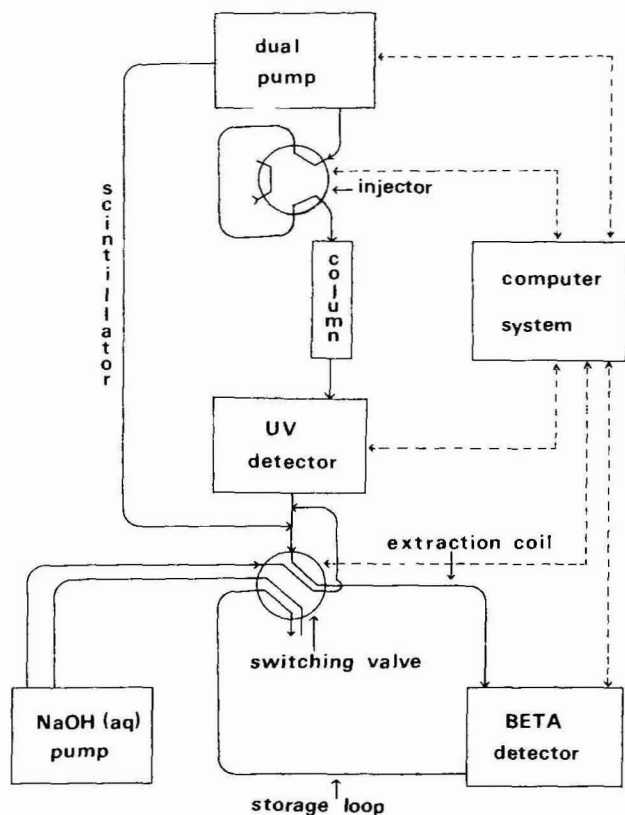
Fig. 1. Schematic diagram of LC equipment with on-line radioactivity monitor and extraction/storage system for the effluent.

63 μl, two Model 8575 photomultiplier (RCA, Harrison, NJ, U.S.A.), a Model 456 high-voltage power supply (Ortec, Oak Ridge, TN, U.S.A.), two PM bases (Ortec 265), two magnetic shieldings (Ortec 218), two scintillator pre-amplifiers (Ortec 113), two Model 2110 timing filter amplifiers (Canberra, Meriden, CT, U.S.A.), and two constant-fraction discriminators (Canberra 1428A). The segmented eluate is stored in a stainless-steel tube (50 m $\times$ 1/16 in. O.D. $\times$ 1.0 mm I.D.). The chromatographic apparatus is controlled with laboratory-devised software by a computer system consisting of a DATA-RAM LSI-11/2 computer with a DEC LSI-11/2 microprocessor under RT-11 (Digital Equipment, Maynard, MA, U.S.A.). A Model 862 interface (Nelson Analytical, Cupertino, CA, U.S.A.), a Model 910 terminal (Televideo, Sunnyvale, CA, U.S.A.), a Model MX-100 III printer (Epson, Nagano, Japan) and a laboratory-built coincidence counter/time interface are also used.

Modifications introduced during the investigation refer to alteration of the flow-rate range of the Perkin-Elmer dual-head LC pump and the extraction procedure of the LC effluent with the water-immiscible liquid scintillator:

(a) The lowest possible flow-rate of the Perkin-Elmer LC pump was changed electronically from 100 to 5 μl/min, thereby increasing the maximum residence time in the flow cell of the radioactivity monitor from 0.72 to 14.4 min.

(b) In order to increase the extractability of the compounds of interest into the scintillator phase, it was found necessary to increase the pH of the effluent to >9 before adding the scintillator. This was accomplished by post-column addition of an aqueous 1 M sodium hydroxide solution with a peristaltic pump. In the present set-up it is not possible to control the flow-rate of this pump externally by the computer system. However, by using the eight-port Valco switching valve it was possible to incorporate this pump in a recycling system. During the separation process (direct measurement), the sodium hydroxide solution is added to the effluent; during the reverse measurement, the solution automatically flows back into the aqueous sodium hydroxide reservoir.

(c) In contrast to previous work[6], the 2-μm in-line solvent filter, intended to increase the yield of analytes extracted into the scintillator, could not be used, because the combination of scintillator and sodium hydroxide solution led to irreversible salt formation on the filter and, thus, to high back-pressure and leakages. Fortunately, omitting the 2-μm filter did not adversely influence the extraction yield of the compound of interest.

Chemicals and standards

The chromatographic conditions were determined with Brownlee Cyano Spheri-5 cartridge columns (Brownlee Labs., Santa Clara, CA, U.S.A.), doubly distilled water, acetonitrile (HPLC grade) (Fisons, Loughborough, U.K.), acetic acid (Baker Analyzed reagent) (Baker, Deventer, The Netherlands) and tetra-n-butylammonium bromide (TBA) (HPLC grade) (Fisons). Ready Solv NA (Beckman, Fullerton, CA, U.S.A.) was used as a water-immiscible liquid scintillator.

For absolute activity determinations on standards, urine samples and injected samples, Instagel (United Technologies Packard, Warrenville, IL, U.S.A.) was used as a water-miscible scintillator.

Remoxipride, FLA 797 (a potential metabolite of remoxipride[11]), [¹⁴C]remoxipride (specific activity 1060 MBq/mmol, radiochemical purity 96.7%) and urine samples were gifts from ASTRA Alab (Södertälje, Sweden). Structural formulae of remoxipride and FLA 797 are given in Fig. 2.

All standards and stock solutions were kept at 4°C. Urine samples (taken 4–6 h after administration) were stored at -18°C. Two methods of sample treatment were used: enzymatic β-deglucuronidation was carried out by incubation of 1.0 ml of urine in 1.0 ml of 0.02 M acetate buffer (pH 4.5) containing 10 mg of Lipton
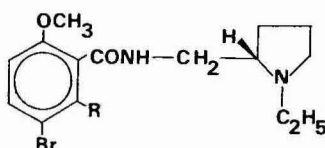
R:
remoxipride $-OCH_3$

FLA 797 $-OH$

Fig. 2. Structural formulae of remoxipride [R = OCH_3; (−)-form, as shown] and FLA 797 (R = OH; racemic mixture).

acetone powder Type I (Sigma, St. Louis, MO, U.S.A.) for 24 h at 37°C; acid hydrolysis was performed by heating 1.0 ml of urine in 1.0 ml of 12 M hydrochloric acid (Merck, Darmstadt, F.R.G.) at 100°C for 1 h. Both hydrolysates were extracted with chloroform (Baker Analyzed reagent) after adjustment of the pH with aqueous sodium hydroxide (Baker grade) to pH 11. The organic phase was separated and evaporized under a gentle stream of nitrogen. The residue was diluted in 200 μl of eluent and volumes of 23 μl were injected.

RESULTS AND DISCUSSION

LC of remoxipride and FLA 797

FLA 908, a phenolic isomer of FLA 797, has earlier been identified as a human remoxipride metabolite and the compound has also been determined in urine after enzymatic hydrolysis[12]. For this determination a liquid chromatographic system giving peak compression effects[13] was applied together with UV detection. In our procedure, ion-pair chromatography on a cyano-bonded column is used, which performs better than an RP-18 column. On the cyano-bonded column, the retention time of remoxipride was decreased from 21 to 3.6 min by the addition of 1.0 M TBA to the eluent. This may be due to a competition between the analyte and TBA for the residual silanol groups on the packing material. This hypothesis is supported by the fact that the more polar FLA 797 had a longer retention time than remoxipride.

Fig. 3 shows a chromatogram of remoxipride and FLA 797 with UV detection. Both peaks show tailing, as amine-containing (basic) pharmaceuticals often do.

Post-column addition of aqueous sodium hydroxide

Because of the small range of the beta particles emitted in the radioactive decay of ^{14}C (ref. 14), it is desirable that the ^{14}C-labelled compounds be in the scintillator phase in order to obtain an adequate counting efficiency. Therefore, in batch experiments, the influence of the pH of the eluent on the extraction of remoxipride and FLA 797 was tested, using *o*-xylene or dichloromethane as the extraction medium and UV detection.

At pH < 6, the extraction yield was <0.1% for both analytes. At pH 11.5, extraction was almost quantitative for both analytes, both in the presence and ab-
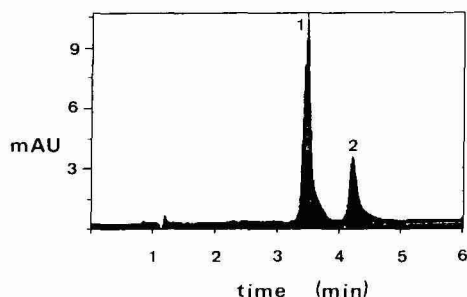
Fig. 3. Chromatogram of (1) remoxipride and (2) FLA 797 with UV detection. Sample, 6.87 · 10^{-5} M (1.58 nmol) remoxipride and 2.15 · 10^{-5} M (0.49 nmol) FLA 797 in 23 μl; column, Brownlee Cyano Spheri-5 (100 × 4.6 mm I.D.); eluent, acetonitrile–water–acetic acid (40:60:1, v/v/v) (pH 3.1) containing 1.0 mM TBA; flow-rate, 1.0 ml/min; detection, 233 nm.

sence of TBA. For remoxipride the pH effect is demonstrated in Fig. 4B and C. Fig. 4A shows the UV chromatogram for a 1.55 nmol (1640 Bq) injection of [¹⁴C]remoxipride. Fig. 4B and C show the corresponding radiograms (direct measurement) without and with post-column addition of sodium hydroxide, respectively. Both radiograms were smoothed by fast Fourier transform (FFT) filtering. The counting efficiencies (as calculated from eqn. 2) are 0.04 and 0.65, respectively.

Surprisingly, an additional advantage of the post-column increase in the pH is the more rapid formation of a clear segmentation pattern for the scintillator and effluent.

Linearity and reproducibility of UV and ¹⁴C detection

The linearity of the system for direct measurements was tested by varying the amounts of [¹⁴C]remoxipride and FLA 797 injected. For UV detection, the plots
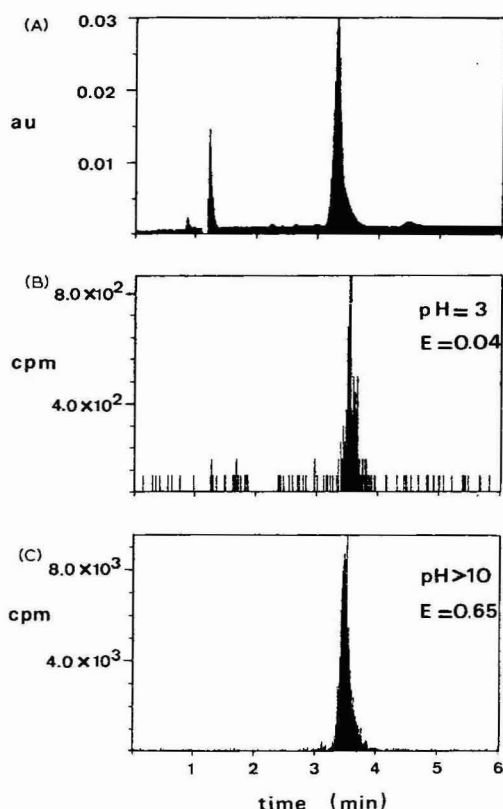
Fig. 4. UV chromatogram and direct radiograms for 1640 Bq (1.55 nmol) [¹⁴C]remoxipride injections without and with addition of aqueous sodium hydroxide to the eluate. For convenience, y values from the radiograms are normalized to cpm, according to cpm = $(60/ST) \times$ counts (ST = sampling time in seconds, counts = counts per sample). The radiograms are smoothed by FFT filtering. Liquid scintillator, Ready Solv NA (flow-rate = 1.0 ml/min). For chromatographic conditions, see Fig. 3. (A) UV chromatogram; (B) direct radiogram without addition of sodium hydroxide; ¹⁴C peak area equals 121 ± 12 counts; (C) direct radiogram with addition of sodium hydroxide (0.23 ml/min); ¹⁴C peak area equals 1671 ± 41 counts.

were linear over 2.5 orders of magnitude for remoxipride and FLA 797 ($r = 0.9999$, $n = 8$). At concentrations above $0.3 \cdot 10^{-3}$ M fronting of the peaks occurred. The reason for this is unknown. It could be attributed to overloading of the column and/or the presence of an insufficient excess of the ion-pair reagent relative to the analyte.

For radioactivity detection, the plot was linear over 1.5 orders of magnitude ($r = 0.9995$, $n = 20$). The upper limit was determined by the maximum concentration that could be prepared from the stock solution. It should be borne in mind that for radioactivity measurements, weighted regression analysis has to be performed because the statistical weights of the data vary appreciably[15].

To test the reproducibility, a sample of [^{14}C]remoxipride (4600 Bq, 4.34 nmol) was injected repeatedly ($n = 9$) with direct and reverse measuring times of 6.0 and 60.0 min, respectively. For UV detection, the mean peak area was 118.6 mAU · ml [relative standard deviation (R.S.D.) = 1.62%]. For ^{14}C detection, the mean peak areas were 4846 (R.S.D. = 2.07%) and 61 030 (R.S.D. = 1.77%) counts for direct and reverse measurements, respectively. From these figures it can be concluded that the reproducibility of ^{14}C detection almost equals that of UV detection.

It should be noted that, owing to the statistical nature of the radioactive decay, with known values for mean peak areas and number of measurements, the R.S.D. can be calculated for these areas[15]; values of 1.36% and 0.39% were found for the direct and reverse measurements, respectively. It is of interest to compare these expected R.S.D. values (*i.e.*, values calculated if the deviations were determined by the radioactive decay alone) with the experimental values. As expected for these high-activity injections, the experimental R.S.D. is determined by factors others than the radioactive decay, such as fluctuations in amount injected, counting efficiency or flow-rate through the radioactivity monitor.

With regard to the peak areas, the peak areas from the reverse measurements are about 12.6 times larger than those from the direct measurements, although t(rev.) is exactly ten times t(dir.). This can be attributed to differences in the flow-rates through the radioactivity monitor (0.195 and 2.17 ml/min, respectively) and differences in the effective cell volume of the monitor. The latter does not necessarily equal the geometric volume but is a function of the flow-rate (and hence the flow pattern) through the cell[16]. In this instance the values 62 and 72 μl apply to direct and reverse measurements, respectively.

Finally, from the ratios of peak areas for direct and reverse measurements it can be calculated that the ^{14}C counting efficiency is not adversely influenced by the storage process of the segmented effluent.

Influence of the reverse flow-rate on ^{14}C peak area

For the high-activity injections of [^{14}C]remoxipride it was concluded that the R.S.D. values of ^{14}C peak areas were determined mainly by the experimental conditions (*i.e.*, reproducibility of injection, flow-rate through the radioactivity monitor and counting efficiency). For low-activity injections, the R.S.D. of ^{14}C peak areas are expected to be determined largely by the statistical nature of the radioactive decay[17]. This is especially true for the direct measurements, where small peak areas are obtained, owing to the relatively short counting time.

For the determination of the relationship between ^{14}C peak areas, or their
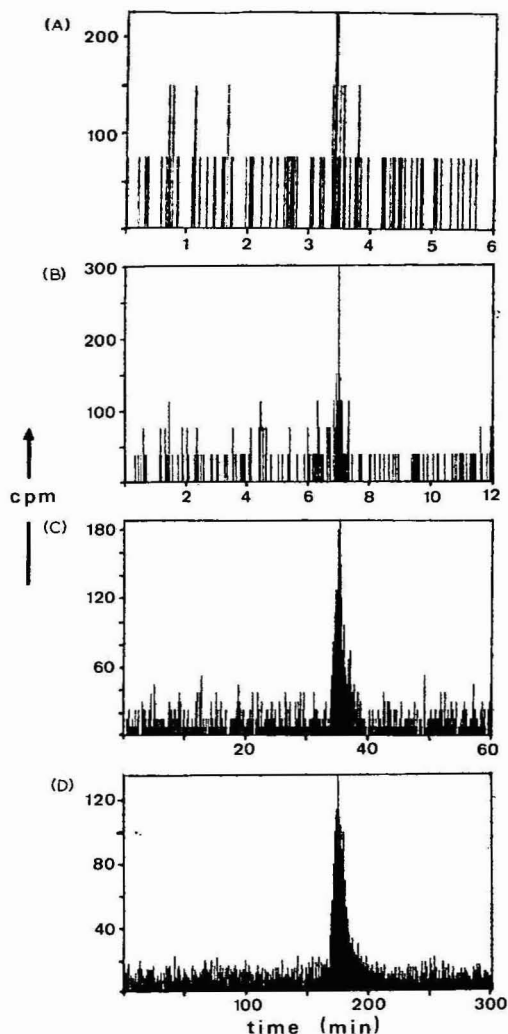
Fig. 5. Radiograms for 16 Bq (15 pmol) injections of [^{14}C]remoxipride as a function of the flow-rate (counting time) in the radioactivity monitor. For comparison, raw data (data not FFT filtered) are given. The y values are normalized to cpm. For chromatographic conditions, see Fig. 4C. (A) direct radiogram, $F(\text{dir.}) = 2.05$ ml/min ($t_d = 0.03$ min); (B) reverse radiogram, $F(\text{rev.}) = 1.00$ ml/min ($t_d = 0.06$ min); (C) radiogram, $F(\text{rev.}) = 0.20$ ml/min ($t_d = 0.37$ min); (D) radiogram, $F(\text{rev.}) = 37$ μl/min ($t_d = 2.02$ min).

R.S.D., and the flow-rate through the radioactivity monitor (and, thus, the counting time), repetitive injections of 16 Bq (15 pmol) of [^{14}C]remoxipride were made while varying the reverse flow-rate from 5 to 2060 μl/min.

As examples, Fig. 5B–D show some reverse radiograms obtained at different flow-rates. Fig. 5A gives the direct radiogram. For comparison, raw data, *i.e.*, data not FFT filtered, are given. The increase in ^{14}C peak area, *i.e.*, the decrease in the detection limit, is clearly seen.

A more quantitative way of demonstrating the influence of the reverse flow-
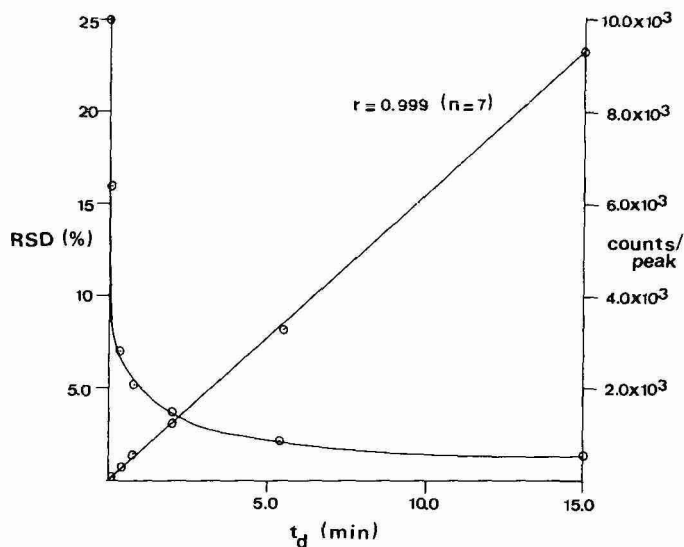
Fig. 6. Relative standard deviation of peak area as a function of the counting time and peak area as a function of the counting time for a 16 Bq (15 pmol) injections of [^{14}C]remoxipride. Data were taken from Fig. 5A–D and similar radiograms.

rate on the detection limit is to express the R.S.D. of the ^{14}C peak area as a function of the mean residence time, t_d, in the radioactivity monitor. This is illustrated in Fig. 6. Data were taken from the radiograms given in Fig. 5 and similar radiograms. The R.S.D. values were calculated according to:

$$\text{S.D.} = c_p + \left[\frac{(t_w)}{(t_b)} \cdot (c_b)^{1/2} \right]^{2 \quad 1/2} \tag{3}$$

$$\text{R.S.D.} = (\text{S.D.}/c_n) \cdot 100\% \tag{4}$$

where c_p = peak area (gross counts); c_n = peak area (net counts); c_b = background (counts recorded in time t_b); and t_w = peak width (s).

From Fig. 6, it is clear that there is a 5-fold increase in sensitivity on comparing the direct measurement (t_d = 0.03 min) with the reverse measurement (t_d = 0.73 min). Increasing t_d to 2.5 min yields only a small further gain in sensitivity (2-fold).

As is usual in radioactivity detection, the R.S.D. varies inversely with $(t_d)^{0.5}$, as can be verified from the data given in Fig. 6. Also, it is of interest to test the linearity of the peak area as a function of t_d. A correlation coefficient r = 0.9994 (n = 8) is calculated with weighted linear regression analysis. Deviations from the fitted line (see Fig. 6) can be ascribed to pumping inaccuracies at low flow-rates and the influence of flow-rate on the effective flow-cell volume mentioned above. Detailed experiments have shown that, for flow-rates below 15 μl/min, the pumping accuracy becomes problematic, although the reproducibility is satisfactory[18]. In other words, at low flow-rates the mean residence time, t_d, is still reproducible but is inaccurate.

Analysis of urine samples

As an application, some experiments were performed with human urine samples. The enzymatic or acid hydrolysis of the samples (see *Chemicals and standards*) did not adversely affect the percentage extraction of ^{14}C activity into the cloroform layer. From this, one may conclude that remoxipride and its metabolites are present in the samples in the free form. Consequently, samples of pH > 10 were extracted directly with chloroform.

An example is given in Fig. 7. The total activity injected was 20 Bq. The UV chromatogram is shown in Fig. 7A. The direct (t_d = 0.03 min) and reverse (t_d = 4.93 min) radiograms are shown in Fig. 7B and C, respectively. Fig. 7D shows the
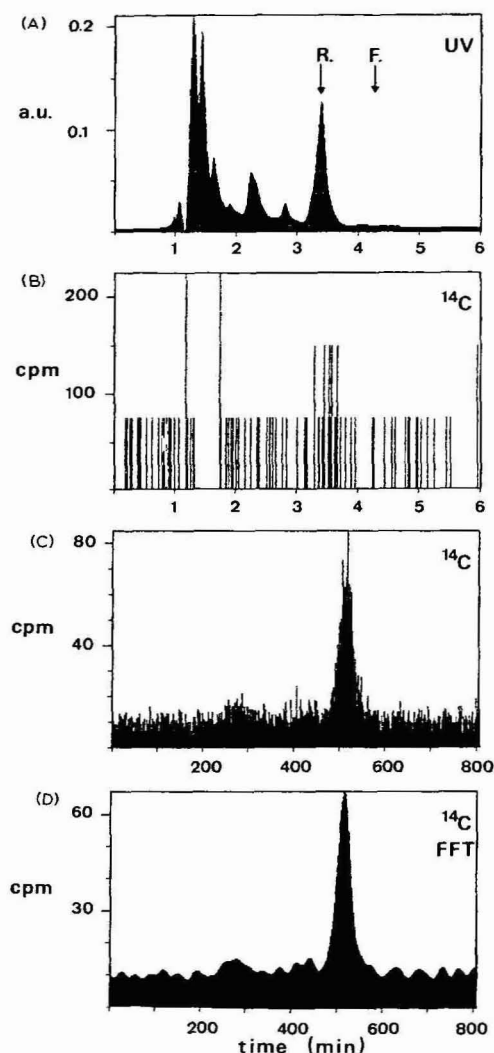
Fig. 7. (A) UV chromatogram and (B) direct and (C) reverse radiograms of a urine sample. (D) Reverse radiogram after smoothing the data by FFT filtering. The *y* values of the radiograms are normalized to cpm. For chromatographic conditions, see Fig. 4C.

reverse radiogram after smoothing the data by FFT filtering. The effect of flow-rate through the radioactivity detector is clearly seen. At $t_d = 1.5–2.0$ min some ^{14}C activity is present, which corresponds to $15 \pm 5\%$ of the [^{14}C]remoxipride peak area. From the ^{14}C detection limit it can be calculated that, in all samples, the amount of FLA 797 (if present) is less than 5% of the remoxipride dose given.

In most instances the peak shape for remoxipride is poor owing to overloading of the analytical column and/or the presence of an insufficient excess of the ion-pair reagent relative to the amount of remoxipride. This was caused by the relatively low specific activity of the [^{14}C]remoxipride dose given (prior to administration, [^{14}C]remoxipride of high specific activity was diluted about 650-fold with unlabelled remoxipride). As a result, the concentrations of remoxipride in the injected samples varied between 0.1 and 0.5 mM, with a low activity (10–50 Bq). In principle, this problem can be avoided by reducing the total dose while keeping the ^{14}C dose at the same level. In this way, a solution with a higher amount of ^{14}C activity can be prepared for injection, thereby minimizing the analysis time required for accurate and precise radioactivity determination.

CONCLUSIONS

A versatile and precise method has been developed for an on-line increase in the counting time in radio-LC. Segmentation of the LC effluent with a water-immiscible liquid scintillator permits the storage of the effluent with negligible peak broadening. Linear relationships between ^{14}C peak area and the mean residence time, t_d, and between the reciprocal of the R.S.D. of peak area and t_d were obtained.

Problems encountered during this study were (a) reduced accuracy of the pump at flow-rates of less than 15 μl/min and (b) owing to the very low specific activity of the [^{14}C]remoxipride dose administered to the volunteers it was not possible to prepare a more concentrated solution from the urine samples for injection. Therefore, long reverse measurements were necessary for accurate and precise radioactivity detection. This can be avoided by using as high as possible specific activities (not diluted with non-labelled remoxipride) for administration.

Experiments on another potential drug indicate that the present method can be used generally in metabolism studies on basic pharmaceuticals containing a tertiary amino group. The extractability of these compounds into the water-immiscible scintillator increases with increasing pH of the eluent.

For convenience, the post-column increase in the pH of the eluent can be accomplished by in-line generation of hydroxy anions on an anion-exchange column and eluent splitting, as described by Jansen *et al.*[19]. The obvious advantage is that the peristaltic pump can be omitted. In the future, this aspect will be explored, and also the possibility of post-column ion-pair extraction of basic pharmaceuticals with a suitable ion-pair reagent[20]. This reagent can be added to the eluate with a peristaltic pump, or it can be present in the eluent. In the latter instance, no extra pump would be needed.

A further improvement is the use of so-called "regions of interest". During the reverse measurement, only these regions in the stored effluent are transported through the radioactivity monitor at low flow-rates, the remainder being pumped through the monitor at a normal flow-rate. Hence the total analysis time is considerably shortened while long counting times in the regions of interest are maintained.

ACKNOWLEDGEMENT

REFERENCES

1 R. P. W. Scott, *Liquid Chromatography Detectors (Journal of Chromatography Library, Vol. 33)*, Elsevier, Amsterdam, 1986, p. 132.
2 R. F. Roberts and M. J. Fields, *J. Chromatogr.*, 342 (1985) 25–33.
3 N. G. L. Harding, Y. Farid, M. J. Stewart, J. Shepherd and D. Nicoll, *Chromatographia*, 15 (1982) 468–474.
4 D. L. Reeve and A. Crozier, *J. Chromatogr.*, 137 (1977) 271.
5 O. Oster and E. Ecker, *Chromatographia*, 3 (1970) 220.
6 H. J. van Nieuwkerk, H. A. Das, U. A. Th. Brinkman and R. W. Frei, *Chromatographia*, 19 (1984) 137–144.
7 B. Bakay, *Anal. Biochem.*, 63 (1975) 87–98.
8 L. Florvall and S. O. Ögren, *J. Med. Chem.*, 25 (1982) 1280–1286.
9 S. O. Ögren, H. Hall, C. Köhler, O. Magnusson, L. O. Lindbom, K. Ängeby and L. Florvall, *Eur. J. Pharmacol.*, 102 (1984) 459–474.
10 L. Lindström, G. Besev, G. Stening and E. Widerlov, *Psychopharmacology*, 86 (1985) 241–243.
11 T. de Paulis, Y. Kumar, L. Johnsson, L. Johansson, S. Rämsby, L. Florvall, H. Hall, K. Ängeby-Möller and S. O. Ögren, *J. Med. Chem.*, 28 (1985) 1263–1269.
12 L. B. Nilsson, B. Aryske, M. Widman and D. Westerlund, to be published.
13 L. B. Nilsson and D. Westerlund, *Anal. Chem.*, 57 (1985) 1835–1840.
14 L. N. Mackey, P. A. Rodriquez and F. B. Schroeder, *J. Chromatogr.*, 208 (1981) 1–8.
15 P. R. Bevington, *Data Reduction and Error Analysis for the Physical Sciences*, McGraw-Hill, New York, 1969.
16 H. J. van Nieuwkerk, H. A. Das, U. A. Th. Brinkman and R. W. Frei, *J. Radioanal. Nucl. Chem.*, 99 (1986) 423.
17 G. B. Sieswerda, H. Poppe and J. F. K. Huber, *Anal. Chim. Acta*, 78 (1975) 343–358.
18 A. C. Veltkamp and H. A. Das, unpublished results.
19 H. Jansen, C. J. M. Vermunt, U. A. Th. Brinkman and R. W. Frei, *J. Chromatogr.*, 366 (1986) 135–144.
20 C. van Buuren, J. F. Lawrence, U. A. Th. Brinkman and R. W. Frei, *Anal. Chem.*, 52 (1980) 700–704.

CHROMSYMP. 989

STRUCTURAL CLASSIFICATION OF FLAVONOIDS IN BEVERAGES BY LIQUID CHROMATOGRAPHY WITH ULTRAVIOLET–VISIBLE AND ELECTROCHEMICAL DETECTION

SUSAN M. LUNTE

The Procter and Gamble Company, Winton Hill Technical Center, Cincinnati, OH 45224 (U.S.A.)

SUMMARY

Liquid chromatography with both UV–VIS and electrochemical detection is used to structurally classify flavonoid compounds in wine and grape juice without isolation of the pure compound. Compounds are classified as flavonols, proanthocyanidins, or anthocyanidins, based on their absorption maxima. Catechol substituted compounds are identified using a dual electrode detector.

INTRODUCTION

Flavonoids are a large group of plant secondary metabolites based on the structure of 2-phenylbenzopyrone (Fig. 1). Thousands of flavonoids are known to exist in nature[1]. They differ from one another in the degree of unsaturation, the pattern of hydroxylation or methylation, and type of sugar attached. The most common flavonoids fall into three general classes: proanthocyanidins, flavonols, and anthocyanidins (Fig. 2).

Standards are not available for many of the flavonoids, making identification by direct comparison difficult. The traditional method for flavonoid identification is UV–VIS absorption spectroscopy following isolation by preparative chromatography[1–3]. Each class of flavonoid has unique spectral characteristics. Specific reagents are used in order to determine hydroxyl substitution. For example, orthohydroxylated (catechol) compounds exhibit a bathochromic shift in the presence of aluminum chloride[2].

Photodiode array detectors make it possible to obtain the spectrum of an unknown flavonoid during a single chromatographic run[4]. Flavonoids can be classified
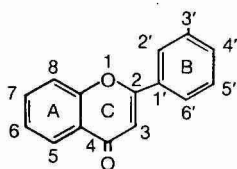
Fig. 1. 2-Phenylbenzopyrone: basic structure of flavonoids.
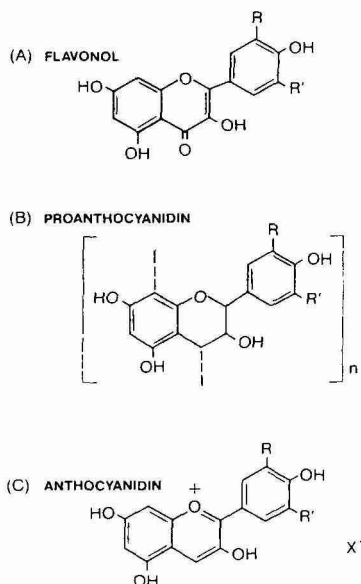
Fig. 2. Three types of flavonoids most commonly found in beverages: (A) flavonols, (B) proanthocyanidins, (C) anthocyanidins. R,R' = H, OH or OCH_3.

as proanthocyanidins, flavonols, or anthocyanidins without isolation of the pure compound, based on their absorption spectrum. However, it is difficult to determine the hydroxyl substitution of a flavonoid from the UV–VIS spectrum alone. Hostettmann et al.[4] have used a photodiode array detector with post-column mixing of shift reagents to determine the pattern of hydroxylation.

Liquid chromatography with electrochemical detection (LC–ED) has been used previously for the determination of phenolic compounds[5-9] in foods and beverages. Two electrodes in series can be used to enhance the selectivity for chemically reversible species such as catechols (Fig. 3)[10-15]. The ratio of the response of the downstream electrode to the upstream electrode is dependent on the electrochemical properties of the analyte[14]. In the case of phenols, the electrochemical behavior is directly related to the structure of the compound. Presented here is the combined use
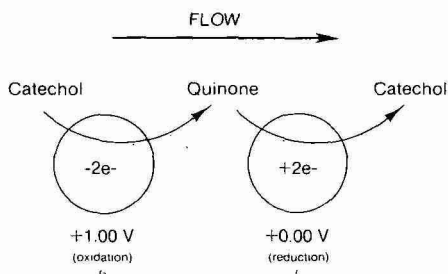
Fig. 3. Dual-electrode detection of catechol substituted compounds.

of a photodiode array detector and an electrochemical detector for the classification of flavonoids in beverage samples[16,17].

MATERIALS AND METHODS

Equipment

The liquid chromatographic system was a Varian Vista 5500 (Walnut Creek, CA, U.S.A.). Photodiode-array detection was accomplished with a LKB 2140 rapid spectral detector (Bromma, Sweden) which was interfaced to an IBM computer (Boca Raton, FL, U.S.A.). For single-wavelength detection a Kratos Spectroflow 773 UV–VIS variable-wavelength detector (Ramsey, NJ, U.S.A.) was used. Dual-electrode LC–ED experiments were performed with a Bioanalytical Systems LC-4B-17 amperometric detector (West Lafayette, IN, U.S.A.). Two glassy-carbon working electrodes were used, and all potentials are reported with reference to a Ag/AgCl reference electrode. Cyclic voltammetry experiments were performed with the BAS-100 electrochemical analyzer (Bioanalytical Systems).

Liquid chromatographic conditions

Flavonoids were separated by gradient elution. Solvent A was 0.05 M ammonium phosphate buffer at pH 2.5, solvent B was acetonitrile. The gradient was linear from 5 to 25% B over 50 min. The mobile phase was sparged with helium prior to and throughout the analysis to prevent bubble formation. The flow-rate was 1.5 ml/min. The Beckmann Altex C_{18} 5-μm column (25 cm $\times$ 4.6 mm I.D.) (Berkley, CA, U.S.A.), employed in all studies, was protected by a Brownlee C_{18} 5-μm pre-column (Santa Clara, CA, U.S.A.) and was thermostatted at 35°C. A 100-μl sample loop was used.

Chemicals

Chemicals were purchased from the following sources: catechin, epicatechin, quercetin, rutin, kaempferol were from Sigma (St. Louis, MO, U.S.A.); myricetin, myricitrin, kaempferol 3-rhamnosylglucoside, quercetin 3-arabinoside, kaempferol 7-neohesperidoside from Carl Roth (Karlsruhe, F.R.G.); orthophosphoric acid from E.M. Science (Cherry Hill, NJ, U.S.A.); ammonium hydroxide from J. T. Baker (Phillipsburg, NJ, U.S.A.). Procyanidins B-2, B-1, and C-1 were generous gifts from A. G. H. Lea (Long Ashton Research Station, Bristol, U.K.) and procyanidin B-4 was a kind gift from E. Haslam of the University of Sheffield (Sheffield, U.K.).

High-performance liquid chromatographic (HPLC) sample preparation

Ernest and Julio Gallo Burgundy and Welch's Grape Juice were used to illustrate this method. Flavonoids were separated from the phenolic acids using a C_{18} Sep-Pak cartridge (Waters Assoc., Milford, MA, U.S.A.). After applying 1 ml of beverage to the Sep-Pak cartridge, the sample was washed with 3 ml of water in order to remove sugars and organic acids. The phenolic acids were eluted with 1 ml of 1 M ammonium hydroxide and flavonoids were eluted with 1 ml of methanol. The resulting sample was diluted with an equal volume of mobile phase prior to injection. Untreated beverage samples were filtered through a 0.45-μm cellulose acetate filter prior to injection.

Cyclic voltammetry experiments

Cyclic voltammetry experiments were performed in a 0.05 M ammonium phosphate buffer (pH 2.5)–methanol (1:1, v/v) solution. Voltammograms were obtained at a scan-rate of 100 mV/s. Sample concentrations were approximately 1 mM. The three-electrode system consisted of a glassy-carbon working electrode, a Ag/AgCl reference electrode, and a platinum auxiliary electrode.

RESULTS

Electrochemical behavior of flavonoids

Cyclic voltammograms of quercetin 3-rutinoside (rutin) and kaempferol 3-rhamnosylglucoside are shown in Figs. 4 and 5. Rutin exhibits an anodic wave for the chemically reversible oxidation of the catechol moiety on the B ring to the quinone. On the reverse scan, a cathodic wave due to the reduction of this quinone is seen (Fig. 4). Kaempferol 3-rhamnosylglucoside, which is not chemically reversible, exhibits only an anodic wave for the oxidation of phenol to a radical species (Fig. 5). No cathodic wave is seen on the reverse scan for this compound, because the free radical reacts rapidly with solution components to give a product which is not electroactive. The oxidation of the 3',4',5'-trihydroxy derivative (myricetin) is also chemically irreversible.

Determination of collection efficiencies

The dual-electrode thin-layer detector cell was used in the series configuration, as illustrated in Fig. 3. The upstream electrode was operated at a potential of $+1.00$ V. At this potential all of the flavonoids studied are oxidized. The downstream electrode was operated at a potential negative enough to reduce the oxidation products produced at the upstream electrode. A potential of 0.00 V was chosen based on cyclic voltammetry experiments (Fig. 4) and selectivity considerations.

Collection efficiency, N_0, is defined as the fraction of upstream products which
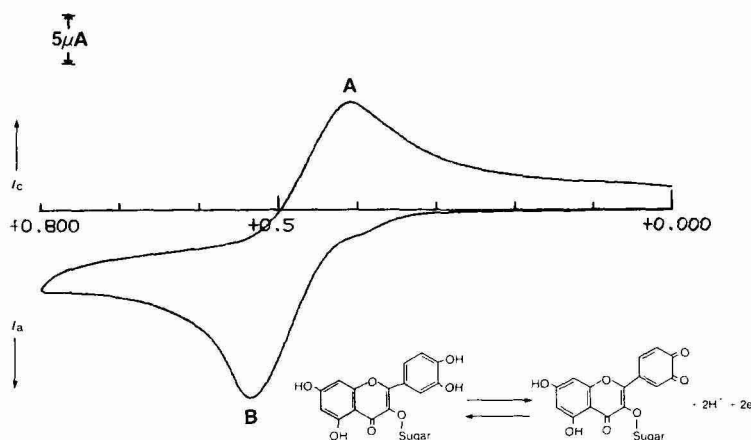
Fig. 4. Cyclic voltammogram of quercetin 3-rutinoside. (A) Oxidation to quinone; (B) reduction of quinone.
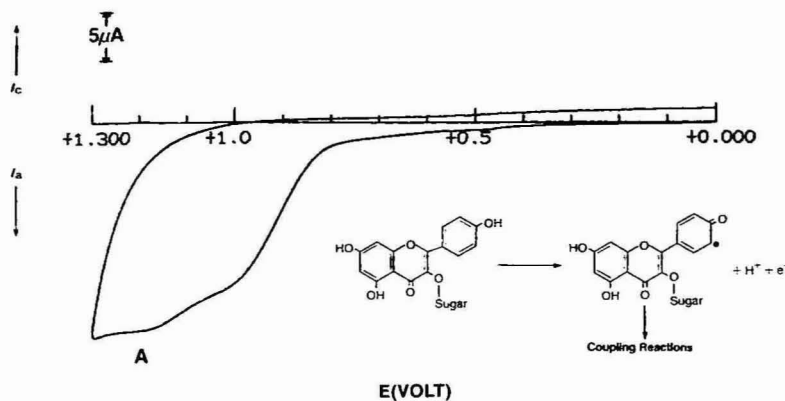
Fig. 5. Cyclic voltammogram of kaempferol 3-rhamnosylglucoside. (A) Oxidation to radical species.

are converted at the downstream electrode. It can be measured by taking the ratio of the current response at the upstream electrode to that at the downstream electrode[14]. Compounds which are chemically reversible, such as catechols and hydroquinones, exhibit high collection efficiencies. The compound produced by oxidation at the upstream electrode is stable and does not undergo further chemical reactions prior to its detection at the downstream electrode. In this case, the amount of product reaching the downstream electrode is entirely dependent on mass transport. The maximum collection efficiency attainable with this thin-layer cell design is 37% (ref. 14).

Compounds, like monophenols, that form chemically unstable products on oxidation exhibit low collection efficiencies. The product produced by oxidation at

TABLE I

COLLECTION EFFICIENCIES FOR SOME REPRESENTATIVE FLAVONOIDS

N_0 = Percent collection efficiency = (downstream/upstream) × 100. S.D. = Standard deviation of three trials.

Standard	N_0 (%)	S.D.
Myricetin 3-rhamnoside	7.4	0.5
Quercetin 3-arabinoside	32.5	1.3
Quercetin 3-rhamnoside	34.0	4.2
Quercetin 3-rutinoside	29.8	1.1
Quercetin	11.3	0.9
Kaempferol 3-rhamnosylglucoside	1.1	0.20
Kaempferol 7-neohesperidoside	2.8	0.40
Kaempferol	1.7	0.29
Myricetin	1.8	0.15
Catechin	12.1	1.0
Epicatechin	11.4	1.2
Procyanidin B-2	10.6	2.1
Procyanidin B-4	10.4	0.84
Procyanidin C-1	9.6	0.23
Procyanidin B-1	12.6	0.15
Pelargonidin	7.6	0.51

the upstream electrode is unstable and reacts to form a second compound which is not reducible. The decrease in magnitude of the collection efficiency is dependent on the decomposition rate of the reactive species. In the case of an extremely fast reaction, there will be no response at the downstream electrode[14].

The collection efficiency of a compound can provide information about the hydroxyl substitution of that compound. Table I gives the collection efficiencies for several different flavonoids. Quercetin glycosides show the highest degree of reversibility with collection efficiencies of approximately 30%. These compounds are all reversibly oxidized to quinones. The sugar-substituted quercetins exhibit higher collection efficiencies than their corresponding aglycones. The sugar moiety increases the hydrophilicity of the quinone produced at the upstream electrode, reducing the amount of adsorption on that electrode.

Catechins and procyanidins have collection efficiencies of *ca.* 10%. This is in the same range as quercetin aglycone. Quinones produced by the oxidation of these compounds are more hydrophobic than the corresponding glycosides and are adsorbed on the carbon electrode. Cyclic voltammetry experiments of aglycones show them to be less reversible than the corresponding glycosides. Procyanidin polymers have approximately the same collection efficiency values as the corresponding monomers.

Kaempferol, myricetin, pelargonidin, and their derivatives exhibit the lowest degree of chemical reversibility, with values of less than 8%. These flavonoids are mono- or trihydroxyphenols. Each is oxidized to an unstable radical species, which can react with solvent components.

Dual-electrode LC–ED of flavonoids
    The high collection efficiencies exhibited by catechol-substituted flavonoids can
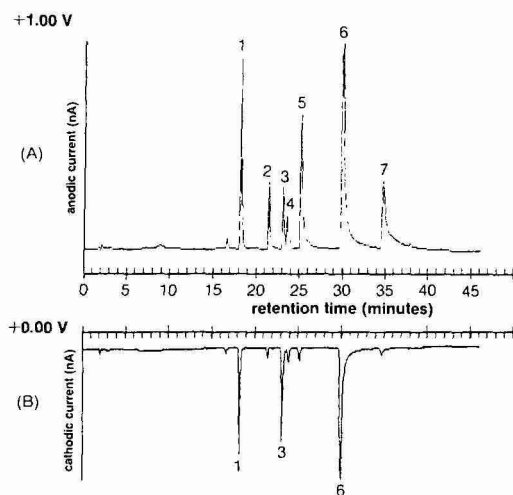
Fig. 6. Use of dual-electrode LC–ED to identify catechol substituted compounds. (A) Upstream electrode + 1.00 V *versus* Ag/AgCl (500 nA f.s.). (B) Downstream electrode + 0.00 V *versus* Ag/AgCl (125 nA f.s.). Identities: (1) epicatechin, (2) myricetin 3-rhamnoside, (3) quercetin 3-arabinoside, (4) kaempferol 7-neohesperidoside, (5) myricetin, (6) quercetin and (7) kaempferol.

be used in their identification. As an example, chromatograms of a mixture of epi-catechin, three flavonol glycosides, and three flavonol aglycones are shown in Fig. 6. The upstream electrode of the dual-electrode detector is operated at + 1.00 V. At this potential, all of the flavonoids present in the mixture are oxidized (Fig. 6A).

The response at the downstream electrode is shown in Fig. 6B. Only three compounds exhibit high collection efficiencies at the second electrode. Epicatechin, quercetin 3-rutinoside and quercetin are oxidized to quinones, which are reduced at the downstream electrode. Myricetin 3-rhamnoside, myricetin, and kaempferol produce unstable radical species upon oxidation, and show very little response at the downstream electrode.

Liquid chromatography with combined electrochemical and UV–VIS detection

As is apparent from the preceding section, the collection efficiencies can be used to obtain information regarding the hydroxylation pattern of flavonoids. When used in combination with a UV–VIS or photodiode-array detector, the structure of the parent flavonoid can be determined.

Liquid chromatography can be combined with UV–VIS detection and ED for the classification of flavonoids as follows. The flavonoids are divided into proantho-cyanidins, flavonols, and anthocyanidins, based on their absorption maxima. Proan-thocyanidins have one absorption maximum at 280 nm. Flavonols have maxima at both 280 and at 360 nm. Anthocyanidins are readily distinguishable by their absor-bance in the visible region around 525 nm[1–3,18–21]. Table II gives the ranges for the absorption maxima of proanthocyanidins, flavonols, and anthocyandins.

ED is used to distinguish the orthodihydroxylated flavonoids from the mono- and trihydroxy compounds. Catechol derivatives have high collection efficiencies (10–39%), while mono- and trihydroxylated flavonoids have very low collection ef-ficiencies (less than 10%). In general, the methoxylated derivatives exhibit lower col-lection efficiencies than their hydroxylated analogs[14]. In many cases, monophenols can be distinguished from trihydroxy compounds on the basis of their hydrophobic-ities, as inferred from relative retention times[18–25].

Grape juice analysis

As an example of the use of a photodiode-array detector in conjunction with an electrochemical detector, the analysis of a neutral extract of grape juice is shown in Figs. 7 and 8. Three flavonols were detected at 360 nm (Fig. 7). These three com-pounds were further classified on the basis of their electrochemical behavior. Fig. 8 shows the LC–ED chromatogram obtained for this sample. The response at the up-stream electrode is shown in Fig. 8A. Fig. 8B is the chromatogram obtained at the

TABLE II

ABSORPTION MAXIMA FOR FLAVONOID COMPOUNDS

Compound	Max (1) (nm)	Max (2) (nm)
Anthocyanidins	270–280	475–560
Flavonols	250–270	350–390
Proanthocyanidins	275–290	—
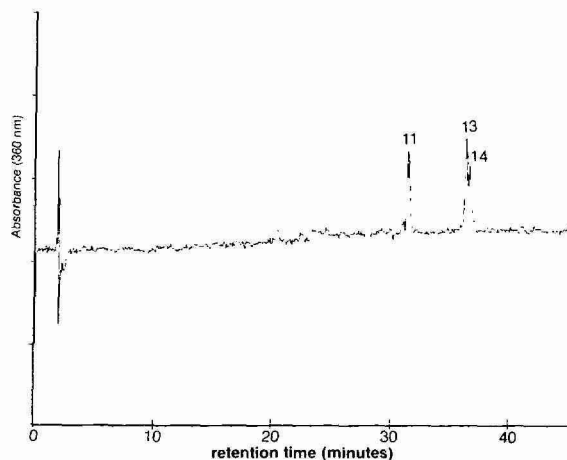
Fig. 7. Chromatogram of grape juice neutral extract at 360 nm.

downstream electrode. Based on spectral information and collection efficiency values, several flavonoids are identified in the grape juice sample. The spectrum obtained with the photodiode-array detector shows that peaks 11, 13 and 14 are flavonols. Peak 11 is a chemically irreversible flavonol glycoside. Based on the retention characteristics, it is probably a myricetin glycoside or a kaempferol diglycoside. Peaks 13 and 14 are quercetin glycosides with collection efficiencies of 26 and 25%, respectively.

Table III shows the data for several of the peaks present in the grape juice neutral extract. Peaks 3 and 8 are identified as catechin and epicatechin. They have collection efficiencies of about 10%, absorption maxima of 278 nm and are inseparable from standard compounds. Peaks 9 and 10 are procyanidins. They have absorption maxima of *ca.* 280 nm and collection efficiencies of *ca.* 10%.
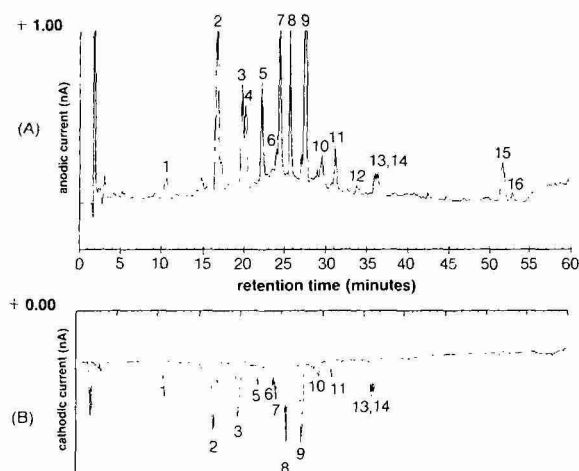
Fig. 8. Dual-electrode LC–ED chromatograms of grape juice neutral extract.

TABLE III

FLAVONOIDS IN GRAPE JUICE (SEE FIG. 8)

N_0 = Collection efficiency; t_R = retention time; ND = not detected.

Peak No.	t_R (min)	UV-Max (1) (nm)	UV-Max (2) (nm)	LC–ED N_0 (%)	Identity
1	10.69	ND		17.0	
2	16.77	276		5.2	Prodelphinidin
3	19.84	(280)		13.0	Catechin
4	20.26	313		1.4	
5	22.19	310		3.4	
6	24.03	280		16.5	Procyanidin
7	24.37	309	525	3.5	Anthocyanidin*
8	25.67	277		10.7	Epicatechin
9a	27.44	278		8.8	Procyanidin
9b	27.64	278		7.8	Procyanidin
10	29.63	280		10.2	Procyanidin
11	31.23	258	370	7.4	Myricetin glucoside
12	33.53	310	525	2.1	Anthocyanidin*
13	36.07	255	355	26.4	Quercetin glycoside
14	36.39	255	355	24.5	Quercetin glycoside
15	51.67	ND		1.1	
16	52.92	ND		0.9	

 * Delphinidin-p-coumaryl glycoside or methoxy derivative.
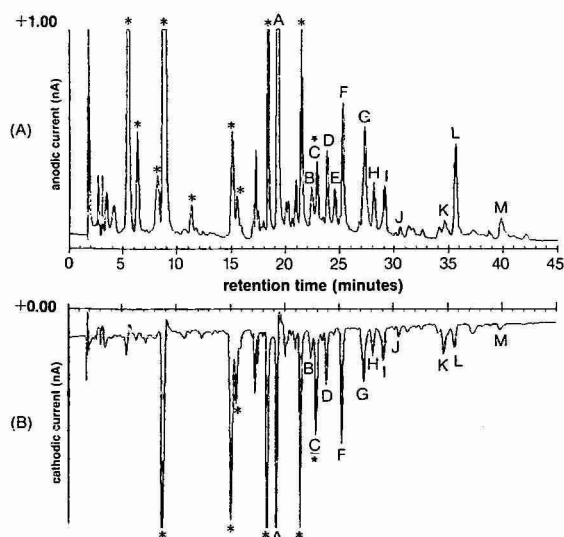
Fig. 9. Dual-electrode LC–ED chromatogram of wine sample.

Peaks 7 and 12 have two distinct absorption maxima. They are classified as anthocyanidins on the basis of their visible absorption at 525 nm. However, they have a second maximum at 310 with a UV spectrum identical with p-coumaric acid. Collection efficiencies for both compounds are very low, indicating a mono- or trihydroxylated compound.

Anthocyanidin-p-coumaryl glycosides have previously been reported to be present in wine and grape juice[20,21]. Based on spectral and electrochemical data, peaks 7 and 12 are most likely delphinidin or pelargonidin-p-coumaryl glycosides. The methoxy derivative, malvidin 3-p-coumaryl glycoside, is another possibility, since it should be less chemically reversible than the delphinidin derivative[14].

Peaks 4 and 5 are presently unidentified. These compounds have a maximum of ca. 310 nm and collection efficiencies of less than 2%. These data indicate that they may be esters and/or glycosides of coumaric acid.

Flavonoids in wine

Fig. 9 shows the LC–ED chromatogram of an untreated wine sample. The compounds marked with asterisks are phenolic acids. These compounds are removed during sample preparation by washing the Sep-Pak with 1 M ammonium hydroxide. The acids can be classified separately by a similar method[14,17]. Peaks K, L, and M have characteristic flavonol absorption spectra, with a maximum at 360 nm. A chromatogram of the wine sample at 360 nm is shown in Fig. 10A. The collection efficiencies for the three compounds K, L, and M are 33.3, 5, and 3.9%, respectively. K is a quercetin glycoside. Based on relative retention time, spectrum, and collection efficiency, L is classified as a kaempferol derivative and M appears to be a myricetin aglycone.

A chromatogram of the whole wine sample at 525 nm is shown in Fig. 10B. The peak labelled J absorbs at 525 and 310 nm and has a collection efficiency of 10%. It is probably a delphinidin or pelargonidin-p-coumaryl glycoside. Peaks labeled D, G, H, and I are classified by this method as procyanidins. Peak E is classified
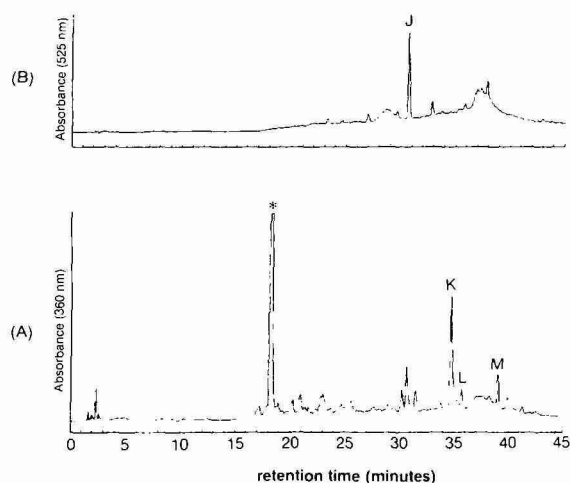
Fig. 10. (A) Chromatogram of a wine sample at 360 nm. (B) Same sample at 525 nm.

TABLE IV

FLAVONOIDS IN WINE (SEE FIG. 9)

Peak No.	t_R (min)	UV-Max (1) (nm)	UV-Max (2) (nm)	LC–ED N_0 (%)	Identity
A	19.44	280		13.4	Catechin
B	22.46	280		11.1	Procyanidin
C	23.00	280		33.0	Caffeic acid
D	23.93	280		10.4	Procyanidin
E	24.63	280		1.9	Prodelphinidin
F	25.37	280		15.9	Epicatechin
G	27.39	280		10.1	Procyanidin
H	28.22	280		12.8	Procyanidin
I	29.21	280		14.3	Procyanidin
J	30.59	310	525	10.0	Anthocyanidin*
K	34.70	280	360	31.0	Quercetin glycoside
L	35.75	280	360	3.7	Myricetin or kaempferol glycoside
M	39.93	280	360	3.9	Myricetin

* Delphinidin-*p*-coumaryl glycoside.

as a prodelphinidin. It is detected at 280 nm and has a low collection efficiency. A list of retention times, absorption maxima, collection efficiencies and tentative identifications for each of the peaks in Fig. 9 is given in Table IV.

CONCLUSIONS

The combination of a dual-electrode amperometric detector and a photodiode-array detector permits classification of complex mixtures of flavonoids on the basis of their conjugation pattern and hydroxyl substitution in a single chromatographic run without need for component isolation. If a photodiode array detector is not available, the same general scheme can be employed using a variable-wavelength detector. Chromatograms at 280, 360, and 525 nm are sufficient to classify the peaks as either proanthocyanidins, flavonols, or anthocyandins. The electrochemical detector can then be used to determine the degree and positions of hydroxylation.

ACKNOWLEDGEMENTS

REFERENCES

1 J. B. Harborne, T. J. Mabry and H. Mabry, *The Flavonoids*, Academic Press, New York, 1975, pp. 1–77.
2 K. R. Markham, *Techniques of Flavonoid Identification*, Academic Press, London, 1982.
3 J. B. Harborne, *Phytochemical Methods*, Chapman and Hall, New York, 1984, p. 37.
4 K. Hostettmann, B. Domon, D. Schaufelberger and M. Hostettmann, *J. Chromatogr.*, 283 (1984) 137.
5 G. Sonntag and K. Kral, *Fresenius Z. Anal. Chem.*, 309 (1981) 109.

 6 E. Frank, G. Kainz and G. Sonntag, *Ernaehrung*, 8 (1984) 195.
 7 D. A. Roston and P. T. Kissinger, *Anal. Chem.*, 53 (1981) 1695.
 8 T. M. Kenyhercz and P. T. Kissinger, *Lloydia*, 41 (1978) 130.
 9 L. C. Felice, W. P. King and P. T. Kissinger, *J. Agric. Food Chem.*, 24 (1976) 380.
10 D. A. Roston, R. E. Shoup and P. T. Kissinger, *Anal. Chem.*, 54 (1982) 1417A.
11 C. E. Lunte and P. T. Kissinger, *Anal. Chem.*, 57 (1985) 1541.
12 S. M. Lunte and P. T. Kissinger, *J. Chromatogr.*, 317 (1984) 579.
13 G. S. Mayer and R. E. Shoup, *J. Chromatogr.*, 255 (1983) 533.
14 D. A. Roston and P. T. Kissinger, *Anal. Chem.*, 54 (1982) 429.
15 L. A. Allison and R. E. Shoup, *Anal. Chem.*, 55 (1983) 8.
16 S. M. Lunte, in P. T. Kissinger (Editor), *1985 International Electroanalytical Symposium, Chicago, IL*, BAS Press, West Lafayette, IN, 1985, pp. 52–55.
17 S. M. Lunte, presented at the *ACS National Meeting, Chicago, IL, September, 1985*.
18 C. W. Nagel, *Cereal Chem.*, 62 (1985) 144.
19 K. Vande Casteele, H. Geiger, R. De Loose and C. F. Van Sumere, *J. Chromatogr.*, 259 (1983) 291.
20 J. Bakker and C. F. Timberlake, *J. Sci. Food Agric.*, 36 (1985) 1315.
21 M. Williams, G. Hrazdina, M. Wilkinson, J. Sweeny and G. Iacobucci, *J. Chromatogr.*, 155 (1978) 389.
22 A. G. H. Lea, *J. Chromatogr.*, 194 (1980) 62.
23 K. Vande Casteele, H. Geiger and C. F. Van Sumere, *J. Chromatogr.*, 240 (1982) 81.
24 M. H. Salagoity-Auguste and Alain Bertrand, *J. Sci. Food Agric.*, 35 (1984) 1241.
25 L. W. Wulf and C. W. Nagel, *J. Chromatogr.*, 116 (1976) 271.

CHROMSYMP. 995

CHEMICAL REDUCTION SYSTEM FOR THE DETECTION OF PHYLLOQUINONE (VITAMIN K₁) AND MENAQUINONES (VITAMIN K₂)

YACOOB HAROON* and DAVID S. BACON

Vitamin K Research Laboratory, USDA Human Nutrition Research Center on Aging at Tufts University, 711 Washington Street, Boston, MA 02111 (U.S.A.)

and

JAMES A. SADOWSKI

Vitamin K Research Laboratory and Nutrition Evaluation Laboratory, USDA Human Nutrition Research Center on Aging at Tufts University, 711 Washington Street, Boston, MA 02111 (U.S.A.)

SUMMARY

Both isocratic and gradient elution systems for fluorometric detection of K vitamins after post-column reduction with zinc metal to their hydroquinones are described. The reaction detection system for K vitamins (phylloquinone and menaquinones) in liquid chromatography is based on reduction of K vitamins to their corresponding hydroquinones with zinc metal in the presence of zinc ions. It was found that 95% of the injected quinones (K vitamins) could be reduced to their corresponding hydroquinones with zinc metal compared to 60% reduction for electrochemical detectors. Menaquinones could be detected down to 100 pg with relative ease during gradient elution.

INTRODUCTION

High-performance liquid chromatography (HPLC) has become a standard method for the analysis of vitamin K in a wide variety of biological samples[1–9]. A major drawback of previously developed methods has often been the inadequacy of the systems employed to detect selectively and sensitively the low physiological concentration of K vitamins. As a consequence, most assays for vitamin K require no less than two chromatographic steps to increase the selectivity of separating vitamin K from contaminants present in most biological lipid extracts. To increase the sensitivity for the detection of K vitamins in biological samples it is, moreover, necessary to process large sample volumes and gram quantities of food products[1,2,8,9].

Although these problems have to a certain extent been overcome by the recent introduction of an electrofluorometric assay for phylloquinone (K_1) which involves post-column electrochemical reduction of K_1 to vitamin K_1 hydroquinone[6], these methods suffer from incomplete reduction of the injected K vitamins[10]. In addition, the complete removal of oxygen is essential for both efficient electrochemical reduction and elimination of fluorescence quenching[6,10,11].

The purpose of this paper is to report on the development of a selective and sensitive chemical method which reduces 95% of the injected K_1 to its corresponding hydroquinone and thus eliminates the requirement for electrochemical reduction of K_1 prior to fluorescence detection. The method described also removes oxygen from the mobile phase to enhance fluorometric detection of K_1 hydroquinone.

EXPERIMENTAL

Chemicals

Synthetic phylloquinone (2-methyl-3-phytyl-1,4-napthoquinone; K_1) was obtained from a commercial source (Sigma, St. Louis, MO, U.S.A.). Menaquinones (MK 4–10) were gifts from M. J. Shearer (Guy's Hospital, London, U.K.). Phylloquinone 2,3-epoxide (K_1 epoxide) was synthesized as described previously[12]. HPLC-grade solvents were obtained from Burdick & Jackson (Muskegon, MI, U.S.A.).

HPLC

The liquid chromatograph consisted of either a Model 510 reciprocating pump (Waters Assoc., Milford, MA, U.S.A.) or a Perkin-Elmer (Norwalk, CT, U.S.A.) Model Series 3B pump which was connected to an autosampler (WISP, Waters) fitted with a C_{18} pre-column (30 × 4.6 mm I.D.; Rainin Instruments, Woburn, MA, U.S.A.). For pre-column reduction the electrochemical cell (Model 5100; Environmental Science Assoc., Bedford, MA, U.S.A.) or the zinc reducer column was inserted between the pre-column and the analytical column (C_8, Microsorb; 100 × 4.6 mm I.D.; Rainin). The analytical column was connected to a UV detector (Model LL-85B; Perkin-Elmer). For post-column reduction, the electrochemical cell or the zinc reducer column was placed between the analytical column (Hypersil ODS; 250 × 4.6 mm I.D.; Shandon Southern Products, Sewickly, PA, U.S.A.) and a fluorometer (Model 970 or Model 980; Kratos Analytical Instruments, Ramsey, NJ, U.S.A.).

Solid-phase reactor

High-purity 200-mesh zinc particles (Alfa Products, Danvers, MA, U.S.A.) were dry-packed into 20 × 3.9 mm I.D. stainless-steel columns, using 0.5-μm stainless-steel frits.

RESULTS AND DISCUSSION

General principles

The principle of the vitamin K reducer column is based on the earlier finding that 95% of the injected K_1 could be reduced to the corresponding hydroquinone (K_1H_2) when in contact with zinc metal in the presence of zinc ions[10].

$$Zn \rightarrow Zn^{2+} + 2e^- \tag{1}$$

$$2H^+ + 2e^- + K_1 \rightarrow K_1H_2 \tag{2}$$

$$\overline{Zn + 2H^+ + K_1 \rightarrow Zn^{2+} + K_1H_2} \tag{3}$$
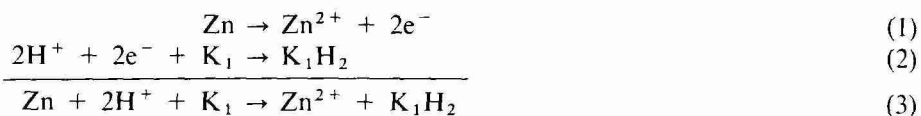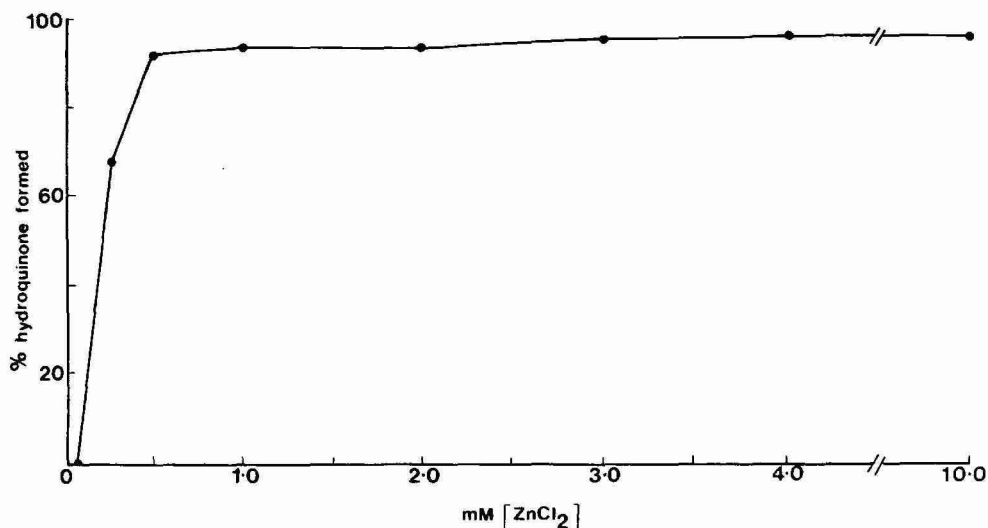
Fig. 1. Reduction efficiency for K_1 vs. zinc ion concentration. Column: Microsorb C_8; mobile phase, 95% methanol containing aqueous zinc chloride (pH 3.3); detection, 254 nm; flow-rate, 1.0 ml/min.

This finding was initially made while developing an electrofluorometric assay for K_1, which involved post-column electrochemical reduction of the quinone, followed by fluorometric detection of the generated hydroquinone. It was subsequently found that a similar reaction occurred when K_1 was allowed to react with zinc metal in the presence of zinc ions[10].

Selection of reaction conditions

In order to optimize the reaction conditions with respect to zinc ion concentration, a zinc reducer column was inserted between the analytical column and the injector, and the concentration of zinc chloride in a mobile phase of 95% aqueous methanol (pH 3.3) was varied. After separating the injected K_1 from the generated K_1H_2, it was found that as the concentration of zinc chloride was raised from 0.06 mM to 0.25 mM while maintaining the pH at 3.3, the reduction efficiency could be increased from 0 to 67% (Fig. 1). Maximum reduction (95%) was achieved between 1 and 10 mM zinc chloride. The maximum reduction efficiency remained constant as the pH of the mobile phase was varied between 2.1 and 4.5.

Flow-rate

The effect of decreasing the residence time of K_1 in the zinc reducer column as a function of K_1H_2 formation was examined by increasing the flow-rate from 0.5 to 2.0 ml/min. It was found that the reduction efficiency remained constant (95% K_1H_2 formed) with increasing flow-rate in this range.

Reductive efficiency

The efficiency of the zinc reducer column in reducing K_1 over a range of K_1 concentration was evaluated by injecting 5 ng to 2 μg K_1 "on-column". After separating K_1 from K_1H_2, it was found that within this range of concentrations, 95% of the injected quinone was consistently reduced to K_1H_2.
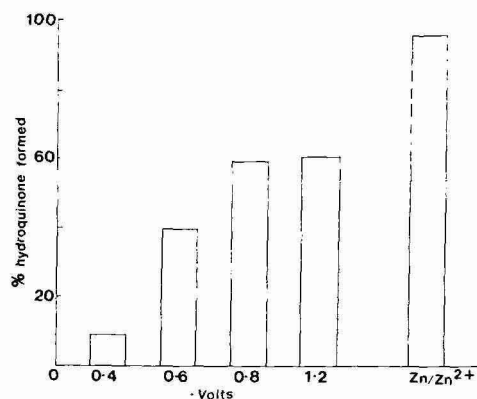
Fig. 2. Comparison of electrochemical and chemical reduction efficiencies for K_1. For conditions, see Fig. 1.

Comparison with electrochemical reduction

In order to compare the efficiencies of K_1 reduction between the zinc reducer column and previously developed electrochemical reduction methods[6,7], the zinc reducer column was replaced by a dual-electrode porous-graphite electrochemical cell. After separating K_1 from K_1H_2, it was found that at the peak plateau voltage (-0.8 V) for K_1, about 60% of the injected K_1 was reduced to K_1H_2 (Fig. 2). In analogous experiments with the zinc reducer column, 95% of K_1 was converted to K_1H_2 (Fig. 2). A possible reason for the incomplete electrochemical reduction of K_1 may be due to a coupled electrochemical reduction reaction preceding the reduction of K_1.

Electrode modification

In experiments in which the zinc column was inserted between the pump and the injector to scavenge oxygen[11] while K_1 was reduced electrochemically, it was found that the amount of hydroquinone generated (95%) remained constant as the
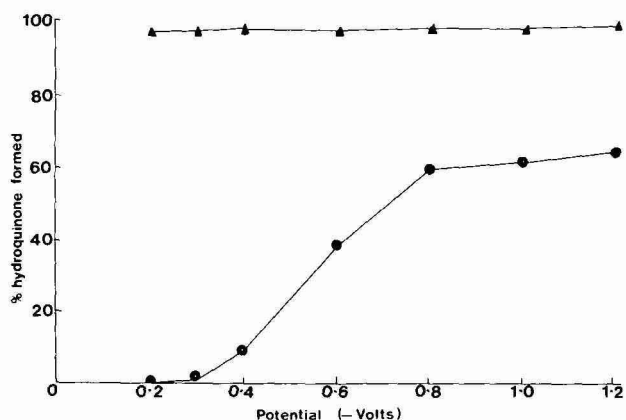
Fig. 3. Hydrodynamic voltammograms for K_1 after pre-column electrochemical reduction in the presence (▲—▲) and absence (●—●) of zinc metal. For conditions, see Fig. 1.
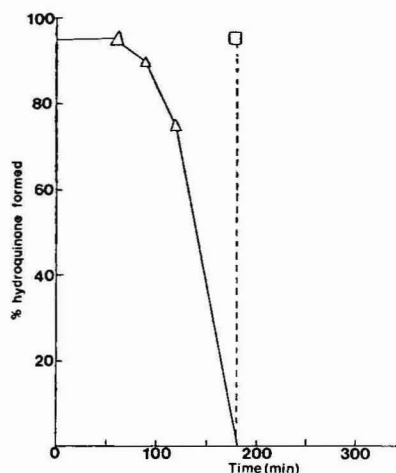
Fig. 4. Time-dependent loss of K_1 reduction at 0.00 V ($\triangle$--$\triangle$) and regeneration of reduction efficiency at -0.2 V (dashed line). For conditions, see Fig. 1.

reduction potential was changed from -0.2 to -1.2 V. These results were in contrast to the finding that in the absence of zinc, a peak plateau for K_1H_2 was reached at -0.8 V (Fig. 3). In later experiments, an observation was made which suggested that reduction was possible even if no potential is applied, though the reduction efficiency decreased over a period of several hours (Fig. 4). After the reduction efficiency had decreased to 0% K_1H_2 formation, it could be regenerated by applying a potential of -0.2 V (Fig. 4).

At potentials greater than -0.8 V zinc ions in the mobile phase may be reduced to zinc metal on the surface of the electrode, which then reacts with K_1, reducing it
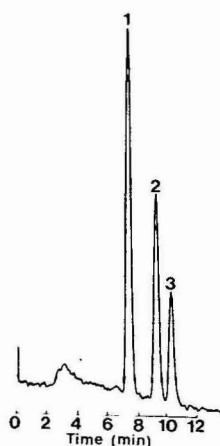
Fig. 5. Separation of vitamin K compounds by reversed-phase HPLC on Hypersil ODS. Mobile phase: 20% dichloromethane in methanol containing 10 mM zinc chloride and 0.1 M acetic acid–sodium acetate (pH 4.5); detection, 248 nm ex., 420 nm em.; flow-rate, 1.0 ml/min; peaks: 1 = K_1 epoxide (0.9 ng); 2 = K_1 (0.5 ng); 3 = K_1(I-H$_2$) (= K_1 with the 2',3' double bond hydrogenated) (0.25 ng).
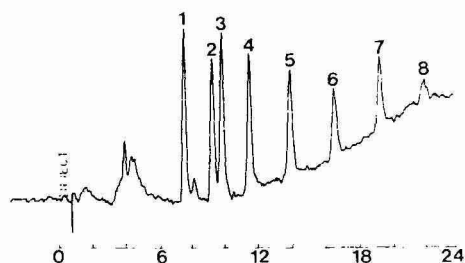
Fig. 6. Separation of vitamin K compounds (200 pg each) by reversed-phase HPLC on Hypersil ODS by gradient elution. Mobile phase A, 20% dichloromethane in methanol containing 10 mM zinc chloride; mobile phase B, 40% dichloromethane in methanol containing 10 mM zinc chloride and 0.1 M acetic acid–sodium acetate (pH 4.5); linear gradient 0 to 100% B in 20 min; detection, 248 nm ex., 420 nm em.; flow-rate, 1.0 ml/min; peaks: 1 = MK-4; 2 = MK-5; 3 = K$_1$; 4–8 = MK-6–MK-10.

and being oxidized to zinc ions (reaction 3) However, the precise nature of events leading to the reduction of K$_1$ at -0.2 V is not clear, as at this potential no reduction of zinc ions would take place. Reduction of K$_1$ at -0.2 V could be eliminated by applying a potential of $+0.9$ V.

Application of the zinc reducer column for post-column reduction of vitamin K compounds

The fluorometric detection of K$_1$ and related compounds after post-column reduction with zinc to their corresponding hydroquinones is shown in Fig. 5. Chromatography was performed on a reversed-phase column (Hypersil ODS) with a mobile phase consisting of 20% dichloromethane in methanol and containing 10 mM zinc chloride.

The major advantage of this mode of detection lies in the increased sensitivity that can be obtained for the detection of K$_1$ epoxide and K$_1$. The lower limits of detection for these compounds were found to be 25 pg compared to 500 pg for a UV

TABLE I

CAPACITY RATIOS (k') OF K VITAMINS BY REVERSED-PHASE HPLC AND ISOCRATIC ELUTION ON HYPERSIL ODS

Mobile phase 20% dichloromethane in methanol, containing 10 mM zinc chloride.

Compound	k'
MK-4	0.9
K$_1$ epoxide	1.2
MK-5	1.5
K$_1$	1.7
K$_1$(I-H$_2$)	2.0
MK-6	2.2
MK-7	3.3
MK-8	4.8
MK-9	7.1
MK-10	10.4

photometer, 100 pg for electrochemical detection, and 150 pg for chemical reduction[13,14]. In addition, the chromatographic system reported here overcame the solvent restrictions imposed during electrochemical reduction, which requires an eluent that can dissolve the supporting electrolyte. As a consequence, such methods rule out the use of the highly efficient reversed-phase systems, which require non-aqueous mobile phases for the separation of K vitamins[15,16].

The capacity ratios for MKs 4−10 and K$_1$ are shown in Table I. This separation was achieved with an isocratic mobile phase of 20% dichloromethane in methanol containing 10 mM zinc chloride (pH 4.7). A linear relationship between log of capacity factors for MKs 4−10 and the carbon number of the side-chain was observed.

A chromatogram obtained during gradient elution of 200 pg each of MKs 4−10 is shown in Fig. 6. The figure illustrates the use of high sensitivity gradient methods for the detection of sub-nanogram levels of MK. It was found that an increase in the dichloromethane content of the mobile phase to 40% during gradient elution caused considerable quenching of fluorescence and that 200 pg of MK-10 was barely detectable (Fig. 6). However, the systems described here constitutes a considerable enhancement in selectivity, sensitivity, and stability over electrochemical and chemical reduction methods for the detection of MKs having up to nine isoprenoid units.

REFERENCES

1 Y. Haroon, M. J. Shearer, S. Rahim, W. G. Gunn, G. McEnery and P. Barkhan, *J. Nutr.*, 112 (1982) 1105–1117.
2 M. J. Shearer, S. Rahim, P. Barkhan and L. Stimmeler, *Lancet*, ii (1982) 460–463.
3 Y. Haroon and P. V. Hauschka, *J. Lipid Res.*, 24 (1983) 481–484.
4 J. P. Hart, M. J. Shearer, P. J. McCarthy and S. Rahim, *Analyst (London)*, 109 (1984) 477–481.
5 U. Takani and J. W. Suttie, *Anal. Biochem.*, 133 (1983) 63–67.
6 J. P. Langenberg and U. R. Tjaden, *J. Chromatogr.*, 305 (1984) 61–72.
7 Y. Haroon, C. A. W. Schubert and P. V. Hauschka, *J. Chromatogr. Sci.*, 22 (1984) 89–93.
8 F. Zonta and B. Stancher, *J. Chromatogr.*, 329 (1985) 257–263.
9 S. A. Barnett, L. W. Frick and H. M. Baine, *Anal. Chem.*, 52 (1980) 610–614.
10 Y. Haroon, D. S. Bacon and J. A. Sadowski, *Biomed. Chromatogr.*, (1986) submitted for publication.
11 W. A. MacCrehan and W. E. May, *Anal. Chem.*, 56 (1984) 625–628.
12 L. F. Fieser, *J. Am. Chem. Soc.*, 61 (1939) 3467–3475.
13 M. J. Shearer, *Adv. Chromatogr. (N.Y.)*, 21 (1983) 243–301.
14 W. E. Lambert, A. P. DeLeenheer and M. F. Lefevere, *J. Chromatogr. Sci.*, 24 (1986) 76–79.
15 Y. Haroon, M. J. Shearer and P. Barkhan, *J. Chromatogr.*, 200 (1980) 293–299.
16 Y. Haroon, M. J. Shearer and P. Barkhan, *J. Chromatogr.*, 206 (1981) 333–348.

CHROMSYMP. 960

DETERMINATION OF MYCOTOXINS IN GRAIN BY HIGH-PERFORMANCE LIQUID CHROMATOGRAPHY AND THERMOSPRAY LIQUID CHROMATOGRAPHY–MASS SPECTROMETRY

EERO RAJAKYLÄ

Finnish Sugar Co. Ltd., Technical Center, SF-02460 Kantvik (Finland)

KATRI LAASASENAHO

University of Helsinki, Department of Analytical Chemistry, Vuorikatu 20, SF-00100 Helsinki (Finland)

and

PETER J. D. SAKKERS

Hewlett-Packard Nederland B.V., Startbaan 16, 1187 XR Amstelveen (The Netherlands)

SUMMARY

An high-performance liquid chromatographic method is described for determination of deoxynivalenol, patulin, diacetoxyscirpenol, HT-2-toxin, T-2-toxin, zearalenone and ochratoxin A using a reversed-phase column and a diode-array detector. The extraction and purification steps and optimum chromatographic conditions are described. Detection limits and recoveries from spiked wheat samples were investigated. The combination of the high-performance liquid chromatographic system described together with a modern thermospray quadrupole mass spectrometer is a very specific and sensitive method for analyzing a wide range of mycotoxins in biological samples.

INTRODUCTION
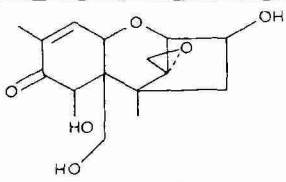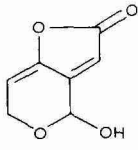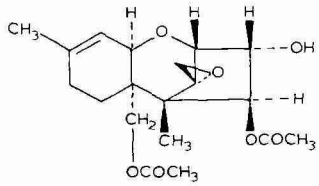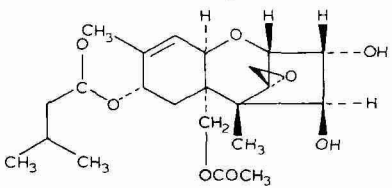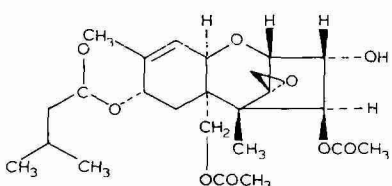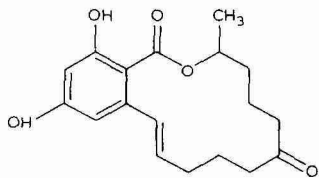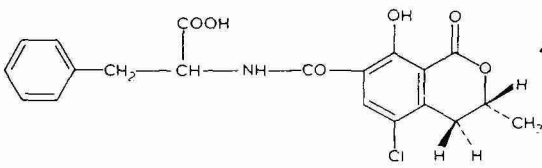
Mycotoxins are secondary metabolites of various fungal species. The study of these toxins has become of the utmost importance, because many of them contaminate foods, and in some countries constitute an important health hazard for human and animal populations. Increasing awareness of the hazards posed by fungal toxins in foodstuffs and feeds has led to the development of a plethora of methods for their purification and analysis.

There have been many attempts to identify and estimate mycotoxins using thin-layer chromatography[1-3], gas chromatography[4-10], gas chromatography–mass spectrometry[11-16], high-performance liquid chromatography (HPLC)[17-25], supercritical fluid chromatography–mass spectrometry (SFC–MS)[26] and thermospray HPLC–MS[27].

HPLC has become the fastest growing technique available to the analytical food laboratory. The most serious limitation at the present time is the sensitivity and specificity of the detectors and the poor response of many compounds to them. Sev-

TABLE I

SOME PHYSICOCHEMICAL DATA

Name	Structure	Molecular weight	$\lambda_{max.}$ (nm)
Deoxynivalenol (DON)		296.0	218 (ethanol)
Patulin		154.0	276 (ethanol)
Diacetoxyscirpenol (DAS)		366.4	No UV abs.
HT-2-toxin		484.3	No UV abs.
T-2-toxin		466.5	187 (cyclohexane)
Zearalenone		318.4	236 (ethanol) 274 316
Ochratoxin A		403.8	210 (methanol) 330

eral mycotoxins, for example, exhibit weak absorbance in the UV region (see Table I), and detection at 190 nm is severely hampered by the background absorption of other sample constituents or by organic solvents introduced during gradient elution. The method presented here overcomes many of these limitations. Following a preliminary acetonitrile extraction of a wheat sample, the extract is cleaned up before the separation of mycotoxins by HPLC on a reversed-phase column.

The mass spectrometer is a highly specific and sensitive detector and the introduction of the recently developed thermospray (TSP) interfacing technique[28] has permitted measurement of a wider range of organic compounds than previously. Voyksner et al.[27] successfully used this technique for the HPLC–MS analysis of some Fusarium mycotoxins.

The aim of the present investigation was to develop a fast, sensitive and reliable analytical method applicable to the detection of a wide range of mycotoxins.

EXPERIMENTAL

Equipment and materials

The experiments were carried out with a Model 5000 liquid chromatograph (Varian Aerograph, Walnut Creek, CA, U.S.A.) and an HP 1040A diode-array detection system (Hewlett-Packard, Waldbronn, F.R.G.). The stainless-steel columns, 150 mm × 4.6 mm I.D., were slurry packed in 2-propanol–acetone, using methanol as the pressurizing solvent, with the following modified 5-μm silicas: Vydac 201 HSB 5 reversed-phase (The Separation Group, Hesperia, CA, U.S.A.), Nucleosil 5 C_{18} (Macherey-Nagel, Düren, F.R.G.) and Spherisorb S 5 ODS-2, (Phase Separations, Queensferry, U.K.). Bond Elut NH_2 extraction columns were obtained from Analytichem International (Harbor City, CA, U.S.A.) and Acro LC13 HPLC sample filters from Gelman Sciences (Ann Arbor, MI, U.S.A.). The mycotoxins were obtained from Sigma (St. Louis, MO, U.S.A.) and acetonitrile, HPLC-grade, from Rathburn Chemicals (Walkerburn, U.K.).

The TSP apparatus consisted of an HP 5988A mass spectrometer and an HP thermospray interface. The HPLC system was an HP 1090A. The interface closely resembles the Vestal design with the important, additional features of a negative heat ramp for gradient elutions and a filament for electron-assisted ionization.

Preparation of standard solutions

The toxins are readily soluble in polar organic solvents, such as methanol and acetonitrile, but when the toxins were dissolved in water–acetonitrile instead of pure acetonitrile the peak shape of each toxin was much sharper. This increased the column efficiency significantly and decreased the detection limits. The standard mycotoxin solutions were prepared by first dissolving the toxins in acetonitrile and then adding water until the acetonitrile–water ratio was 3:4.

Sample preparation

A 20-g amount of finely ground wheat was extracted with 150 ml ACN on an automatic shaker for 120 min. The extract was filtered through a PTFE membrane (0.45 μm) and the residue was washed with 100 ml of acetonitrile. The combined filtrates were evaporated to dryness, and the residue was dissolved in 3 ml n-hexane.

This was extracted with three 2-ml portions of acetonitrile–water (3:4). The *n*-hexane layer was discarded. The pooled acetonitrile–water extracts were evaporated and the residue was dissolved in 1 ml acetonitrile–water. A 250-μl aliquot was filtered through an Acro LC13 0.45-μm membrane and analysed for patulin, zearalenone and ochratoxin A (step 1) using the described chromatographic system. The remaining extract was evaporated to dryness, and the residue was dissolved in *n*-hexane. This was transferred to a 3-ml Bond Elut NH$_2$ extraction column, and washed with 10 ml of *n*-hexane. The mycotoxins DON, DAS, HT-2 and T-2 were eluted from the column with 3 ml of ethanol–*n*-hexane (1:1). The eluate was evaporated, and the residue was dissolved in 750 μl of acetonitrile–water and membrane-filtered prior to chromatography (step 2).

RESULTS AND DISCUSSION

Optimization of HPLC conditions

The separation characteristics of DON, patulin, DAS, HT-2-toxin, T-2-toxin, zearalenone and ochratoxin A on several reversed-phase columns with water (pH 3, adjusted with phosphoric acid)–acetonitrile gradients as the mobile phase were investigated. These preliminary experiments indicated that the Vydac 201 HSB 5-μm reversed-phase material was superior in this application under these conditions. The resolution with the other column materials was often poor, *e.g.*, the Macherey-Nagel and Phase Separation materials did not resolve zearalenone and ochratoxin A although the other mycotoxins were quite well separated.

We observed that the pH very strongly influences the retention behaviour of
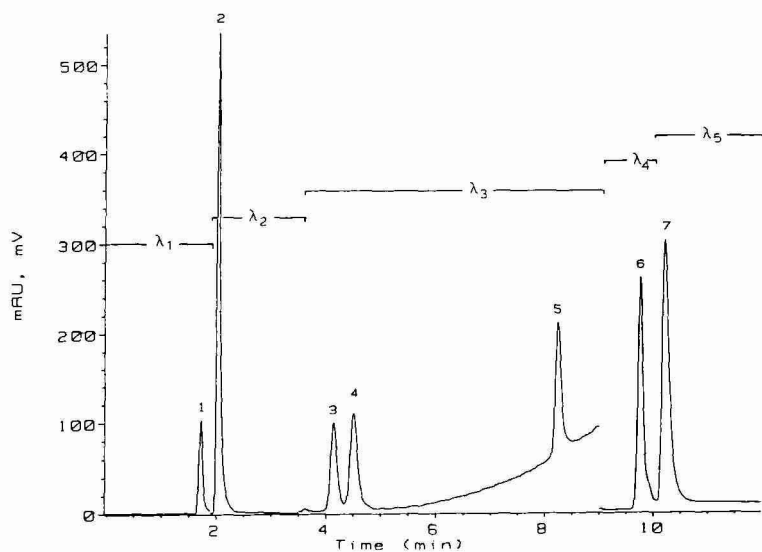
Fig. 1. Chromatogram of a mycotoxin standard (300–600 ng of each) under optimized conditions (see text). Wavelengths: λ_1 = 217, λ_2 = 275, λ_3 = 190, λ_4 = 237 and λ_5 = 210 nm. Peaks: 1 = deoxynivalenol (DON); 2 = patulin; 3 = diacetoxyscirpenol (DAS); 4 = HT-2-toxin; 5 = T-2-toxin; 6 = zearalenone; 7 = ochratoxin A.

ochratoxin A but has no significant effect on the retention times of the other my-
cotoxins. Also, the addition of ammonium acetate to the eluent system, which is
absolutely necessary for thermospray MS, has a very strong influence on the retention
of ochratoxin A. The column temperature was maintained at 35°C in order to stan-
dardize the conditions. Fig. 1 shows a typical chromatogram under optimized con-
ditions: Eluents: A, water (pH 3, phosphoric acid); B, acetonitrile; gradient from 40
to 70% B in 7 min, flow-rate 1 ml/min.

The absence of conjugated unsaturation in diacetoxyscirpenol (DAS), HT-2-
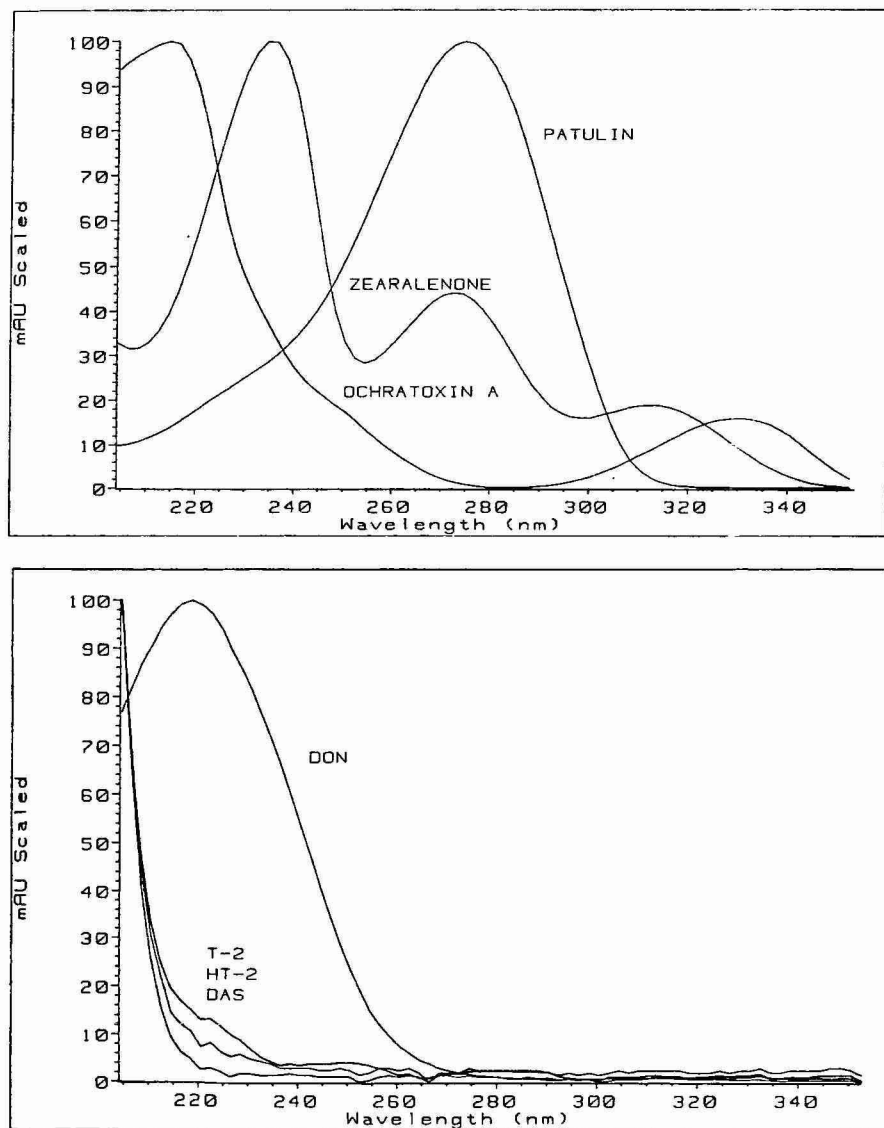
Fig. 2. The UV spectra of each toxin taken during chromatography of the standard (Fig. 1).
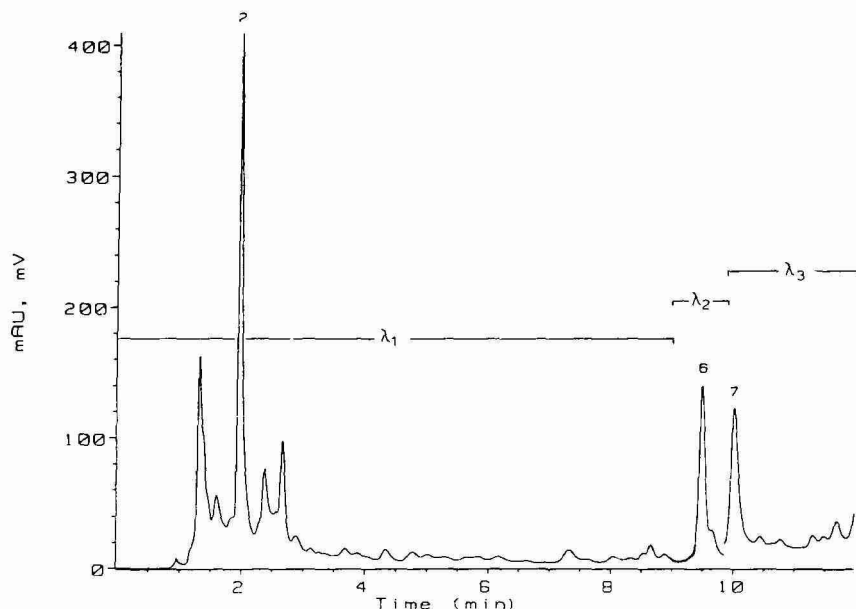
Fig. 3. Analysis of patulin (2, 314 ng), zearalenone (6, 375 ng) and ochratoxin A (7, 188 ng) in spiked wheat at wavelengths $\lambda_1 = 275$, $\lambda_2 = 237$ and $\lambda_3 = 210$ nm. Sample: preparation step 1.

toxin and T-2-toxin explains their weak UV absorbance and makes the analysis of these compounds very difficult. However, under the chromatographic conditions chosen, we were able to monitor the eluate for these compounds at 190 nm. DON, patulin, zearalenone and ochratoxin A were detected at 217, 275, 237 and 210 nm, respectively. The chromatograms for sample preparation steps 1 and 2 are shown in Figs. 3 and 4, respectively.
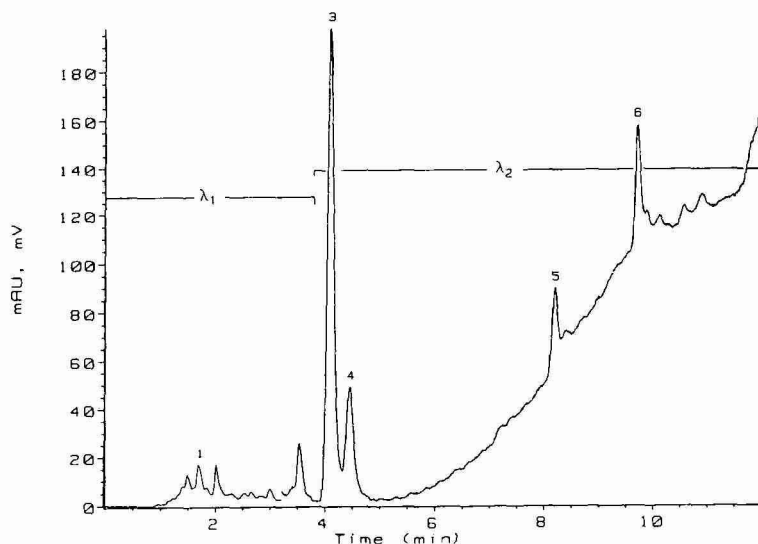
Fig. 4. Analysis of DON (1, 73 ng), DAS (3, 135 ng), HT-2-toxin (4, 353 ng) and T-2-toxin (5, 200 ng) in spiked wheat at wavelength $\lambda_1 = 217$, $\lambda_2 = 190$ nm. (step 2, see text). Peak 6 corresponds to zearalenone.

Linearity and detection limits

The relationships between the peak heights and concentration of each toxin were linear over the range 40–800 ng. The detection limits for the pure mycotoxins using the described chromatographic conditions varied from 1 to 20 ng per 10 μl, depending on the molar extinction coefficient of each compound. In real and in spiked wheat samples we were able to analyze reliably 50–200 ng per 10 μl of purified extract, representing a toxin concentration of 5–20 μg per 20 g of wheat.

Recoveries of mycotoxins from spiked wheat

Clean, mycotoxin-free, wheat samples were spiked with various amounts of mycotoxins and analyzed by the method described. The quantitative results are summarized in Table II. We have now extended this study to other grains, such as barley and rye and to animal feeds to determine whether our method has wider application. Poor results have been obtained in the case of the animal feeds.

Thermospray LC–MS analysis of mycotoxins

The operational temperatures at the tip of the probe and the source were held constant at 200 and 280°C respectively. The pressure in the analyzer was kept below $3 \cdot 10^{-6}$ Torr at a flow-rate of 1 ml/min. The mass spectrometer was optimized and calibrated with polypropylene glycol over the mass range 150–1000.

The samples were analyzed on the column mentioned earlier using water at pH 3 (acetic acid) and a gradient of 40–70% acetonitrile in 8 min. Spectra were measured with 0.001 and 0.05 mol ammonium acetate in the eluent. Fig. 5 shows the thermospray LC–MS reconstructed ion chromatogram of the standard mycotoxin sample. The retention time of ochratoxin A was very sensitive to the presence of ammonium acetate, whereas those of the other compounds were unaffected by it.

The spiked wheat sample (Fig. 5) gave results comparable to the standard with the exception of patulin. The background from the matrix limits the detection level of patulin, which has a relatively low mass ion (155, protonated molecular ion).

The mass spectra showed large differences depending on the concentration of ammonium acetate in the eluate. In thermospray LC–MS three competing ionization mechanisms are involved: the thermospray charge-transfer ionization, chemical ionization with plasma ions, which depend on the solvent composition and filament

TABLE II

RECOVERIES (%) OF MYCOTOXINS FROM SPIKED WHEAT SAMPLES

Toxin	Sample					Mean	R.S.D. (%)
	1	*2*	*3*	*4*	*5*		
DON	74	84	83	66	70	75.4	10.5
Patulin	76	81	83	75	77	78.4	4.5
DAS	88	91	83	90	85	87.4	3.8
HT-2	81	90	89	90	100	90.0	6.3
T-2	80	86	90	95	97	89.6	7.7
Zearalenone	65	68	82	60	79	70.8	13.1
Ochratoxin A	85	83	88	60	68	76.8	15.8
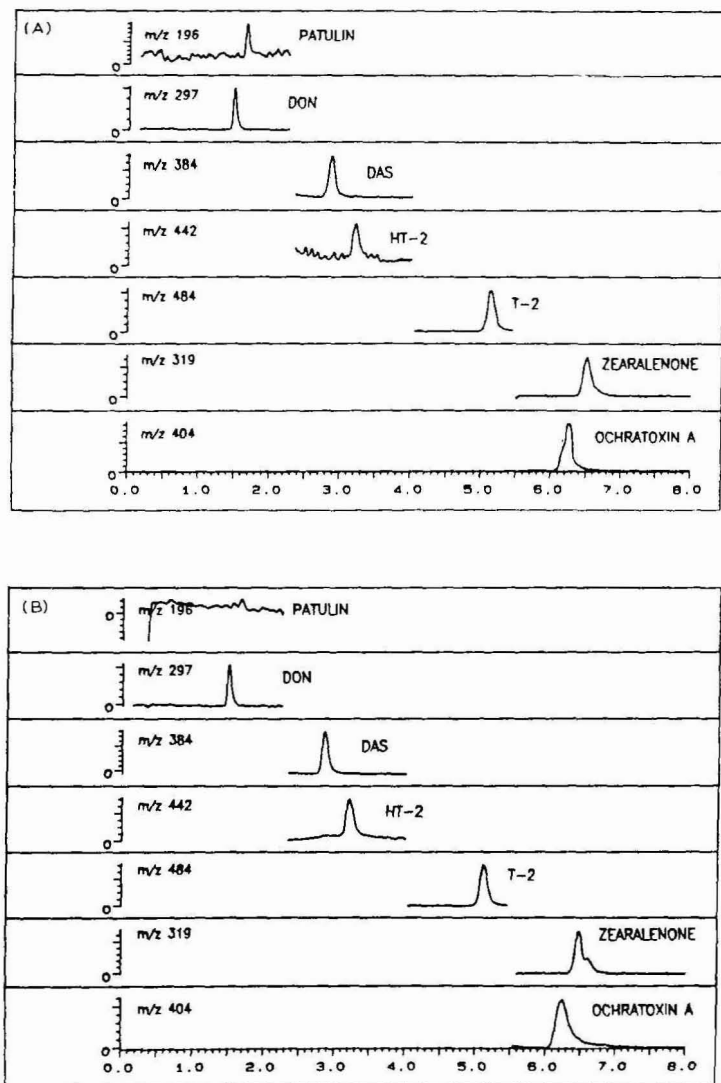
Fig. 5. The thermospray LC–MS reconstructed ion chromatograms of (A) a mycotoxin standard (30–60 ng of each) and (B) of wheat spiked with identical amounts of standard. Conditions as described in the text.

on/off mode and thermal ionization. It is not yet fully understood which one of these is dominant under any given conditions.

At very low ammonium acetate concentrations we can rule out the "thermospray ionization" which is the softest mechanism of the three. As the filament-on mode gave greater sensitivity, chemical ionization is the main mechanism. As a result, protonation and ammonium adduct formation occur, but there are also very specific fragmentation patterns for DAS, T-2-toxin and HT-2-toxin (Fig. 6). At higher ammonium acetate concentrations we noted an increase in sensitivity for all mycotoxins.

The spectra of DAS, T-2-toxin and HT-2-toxin showed a dominant $(M + NH_4^+)$ ion and no fragmentation. Fig. 7 compares the spectra of T-2-toxin under both conditions. Apparently the presence of an ester group favours the $(M + NH_4^+)$ formation,
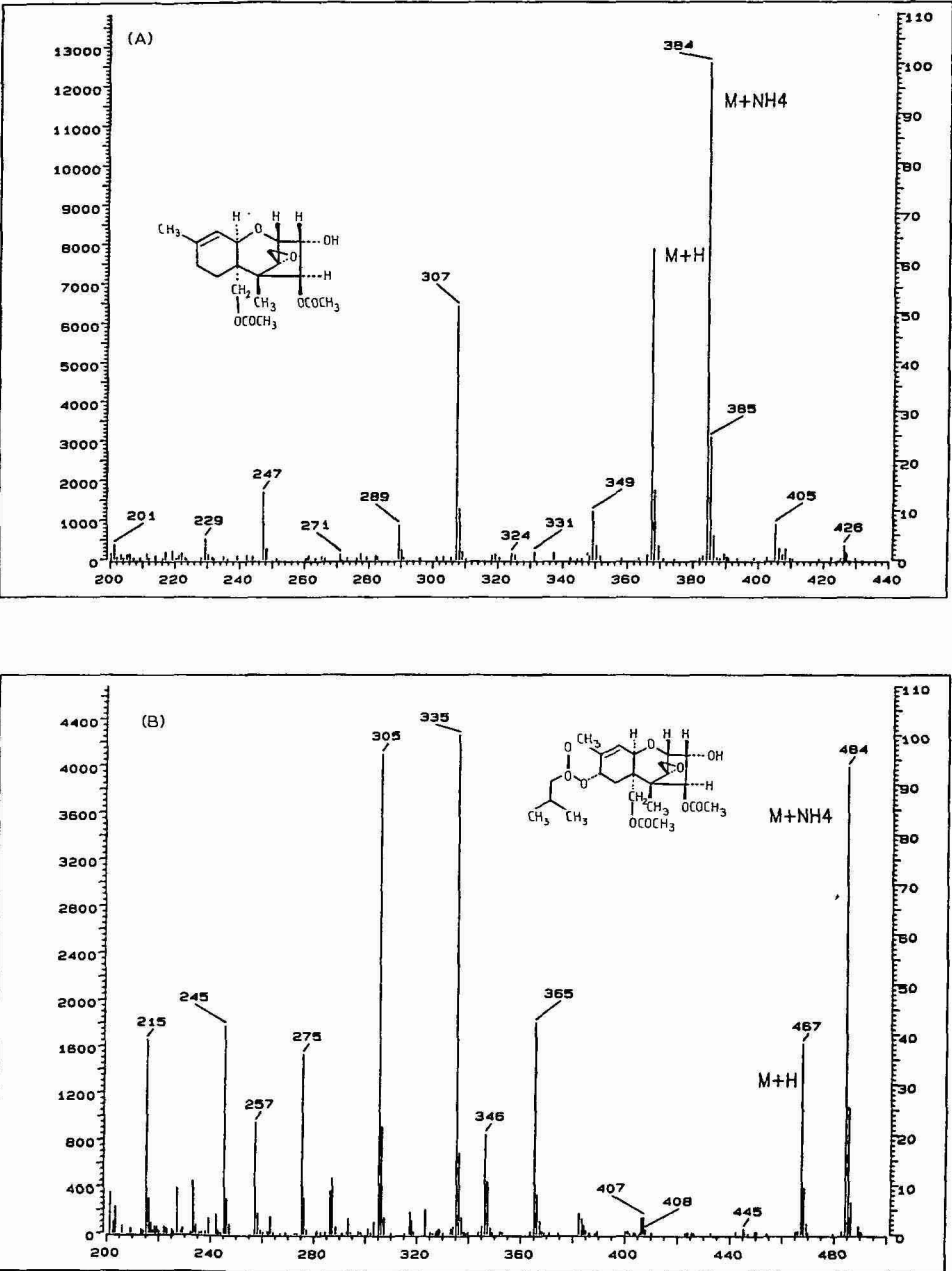
Fig. 6.
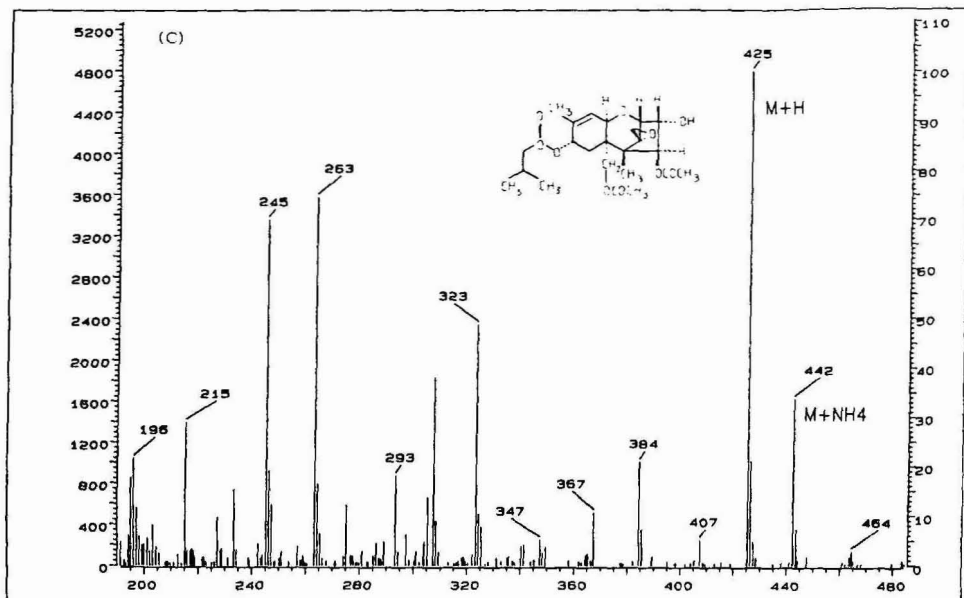
Fig. 6. The thermospray LC–MS positive ion spectra of (A) DAS, (B) T-2-toxin and (C) HT-2-toxin: filament on, 0.001 mol ammonium acetate.

rather than protonation by reaction with water. Evidence in support of this is provided by the observation of a much higher $(M + NH_4)$ adduction of T-2-toxin which contains one ester group more than the HT-2-toxin. The other compounds gave
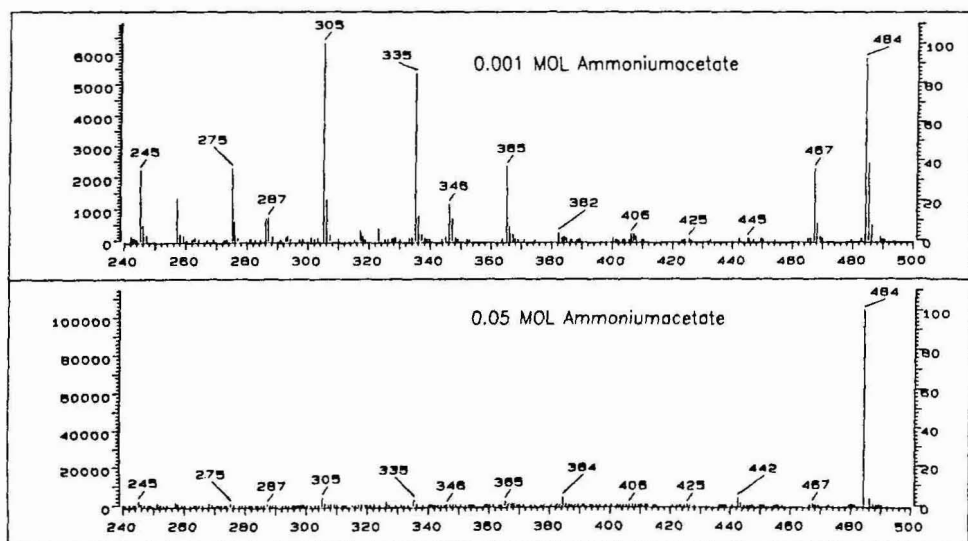
Fig. 7. Effect of the ammonium acetate concentration on the TSP LC–MS positive ion spectra of T-2-toxin.
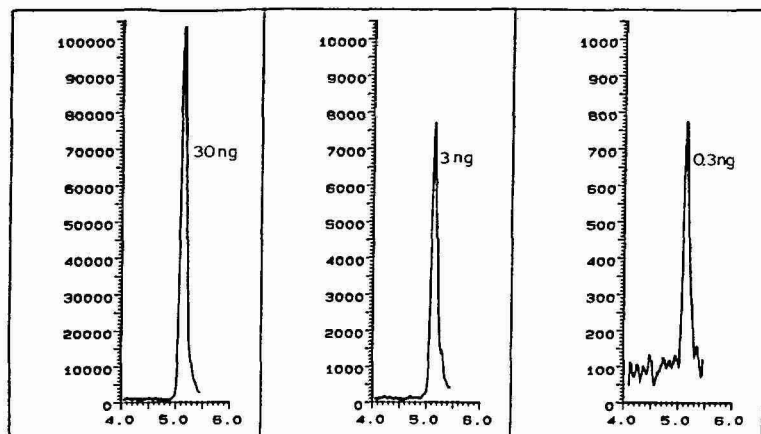
Fig. 8. Determination of the detection level of T-2-toxin.

simple spectra with protonated molecular ions and no fragmentation at both ammonium acetate concentrations.

In the LC–MS system, T-2-toxin gave the strongest response. Based on the results shown in Fig. 8, a signal-to-noise ratio (S/N) of 20 was obtained for 300 pg injected into the column. With a S/N of 5 the detection level was 75 pg. Detection levels for the other test compounds ranged from 100 pg to 1 ng. Relatively large injection volumes (20–30 μl) did not adversely affect the linearity of the detector response. It was therefore possible to measure mycotoxin concentrations ranging from 3 to 40 ppb (ng/g).

A sample of the residue from a rye-milling process (Ruismyllyn Jäte) was analyzed for T-2-toxin by the method described. Fig. 9 shows the results obtained with a 10-μl sample of the extract, compared with a 500-pg standard. A rough estimation gives a concentration of 30 pg/μl, equivalent to 1.5 μg/kg.
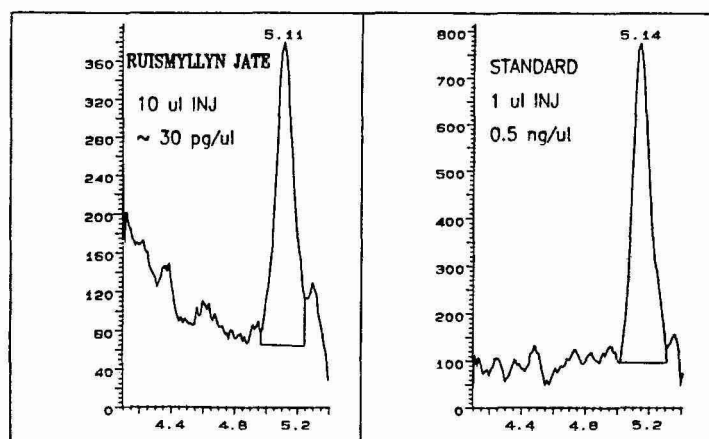
Fig. 9. Determination of T-2-toxin in the residue from a rye-milling process.

CONCLUSIONS

A novel HPLC method for the separation of mycotoxins has been described. The column, packed with Vydac 201 HSB 5-μm material, is stable, durable and superior to the other columns tested in this application under the specified conditions. The sample preparation is simple and the recoveries are acceptable. The most serious limitation of the method is the sensitivity of the available detectors.

Thermospray HPLC–MS, as demonstrated, shows great potential for the analysis of mycotoxins. By varying the electrolyte concentration, the analysis can be used for either qualitative or quantitative purposes. The additional ionization supplied by the filament at low concentrations of salt results in specific fragmentation patterns. At high salt concentration the sensitivity is increased by a factor of 5.

The sample preparation needed for the TSP–LC–MS determination of mycotoxins in grains and animal feeds is minimal (step 1) and background interference is negligible compared with UV detection.

ACKNOWLEDGEMENTS

REFERENCES

 1 S. Takitani, Y. Asabe, T. Kato, M. Suzuki and Y. Ueno, *J. Chromatogr.*, 172 (1979) 335.
 2 A. Sano, Y. Asabe, S. Takitani and Y. Ueno, *J. Chromatogr.*, 235 (1982) 257.
 3 M. W. Trucksess, S. Nesheim and R. Eppley, *J. Assoc. Off. Anal. Chem.*, 67 (1984) 40.
 4 P. M. Scott, P.-Y. Lau and S. R. Kanhere, *J. Assoc. Off. Anal. Chem.*, 64 (1981) 1364.
 5 B. G. Osborne and K. H. Willis, *J. Sci. Food Agric.*, 35 (1984) 579.
 6 T. Ilus, M.-L. Niku-Paavola and T.-M. Enari, *Eur. J. Appl. Microbiol. Biotechnol.*, 11 (1981) 244.
 7 C. O. Ikediobi, I. C. Hsu, J. R. Bamburg and F. M. Stron, *Anal. Biochem.*, 43 (1971) 327.
 8 H. Kamimura, M. Nishjima, R. Yasuda, K. Saito, A. Ibe, T. Nagayania, H. Ushiyama and Y. Nadi, *J. Assoc. Off. Anal. Chem.*, 64 (1981) 1067.
 9 T. R. Romer, T. M. Boling and J. L. MacDonald, *J. Assoc. Off. Anal. Chem.*, 61 (1978) 801.
10 C. E. Kientz and A. Verweij, *J. Chromatogr.*, 355 (1986) 229.
11 R. T. Rosen and J. D. Rosen, *Biomed. Mass. Spectrom.*, 9 (1982) 443.
12 C. J. Mirocha, R. A. Pawlosky, K. Chatterjee, S. Watson and W. Hayes, *J. Assoc. Off. Anal. Chem.*, 66 (1983) 1485.
13 E. Karppanen, A. Rizzo, S. Berg, E. Lindfors and R. Aho, *J. Agric. Sci. Finland*, 57 (1985) 195.
14 T. Krishnamurthy and E. W. Sarver, *J. Chromatogr.*, 355 (1986) 253.
15 J. D. Rosen, R. T. Rosen and T. G. Hartman, *J. Chromatogr.*, 355 (1986) 241.
16 R. Tiebach, W. Blaas, M. Kellert, S. Steinmeyer and R. Weber, *J. Chromatogr.*, 318 (1985) 103.
17 A. Visconti and A. Bottalico, *Chromatographia*, 17 (1983) 97.
18 R. Schmidt and K. Dose, *J. Anal. Toxicol.*, 8 (1984) 43.
19 R. Schmidt, E. Ziegenhagen and K. Dose, *J. Chromatogr.*, 212 (1981) 370.
20 G. M. Ware and C. W. Thorpe, *J. Assoc. Off. Anal. Chem.*, 61 (1978) 1058.
21 D. C. Hunt, A. T. Bourdon and N. T. Crosby, *J. Sci. Food Agric.*, 29 (1978) 245.
22 G. A. Bennett, O. L. Shotwell and W. F. Kwolek, *J. Assoc. Off. Anal. Chem.*, 68 (1985) 958.
23 T. Tanaka, A. Hasegawa, Y. Matsuki, U.-S. Lee and Y. Ueno, *J. Chromatogr.*, 328 (1985) 271.
24 K. C. Ehrlich and L. S. Lee, *J. Assoc. Off. Anal. Chem.*, 67 (1984) 963.
25 K. C. Ehrlich, L. S. Lee and A. Ciegler, *J. Liq. Chromatogr.*, 6 (1983) 833.
26 R. D. Schmith, H. R. Udseth and B. W. Wright, *J. Chromatogr. Sci.*, 23 (1985) 192.
27 R. D. Voyksner, W. M. Hagler, Jr., K. Tyczkowska and C. A. Haney, *J. High Resolut. Chromatogr. Chromatogr. Commun.*, 8 (1985) 119.
28 C. R. Blackley and M. L. Vestal, *Anal. Chem.*, 55 (1983) 75.

Author Index

PUBLICATION SCHEDULE FOR 1987

Journal of Chromatography and Journal of Chromatography, Biomedical Applications

MONTH	J	F	M	A	M	J	J	
Journal of Chromatography	384 385 386 387	388/1 388/2 389						The publication schedule for further issues will be published later.
Bibliography Section		412/1						
Cumulative Indexes, Vols. 351-400								
Biomedical Applications	413	414/1	414/2 415/1	415/2 416/1	416/2	417/1	417/2 418	

INFORMATION FOR AUTHORS

(Detailed *Instructions to Authors* were published in Vol. 362, No. 3, pp. 461–464. A free reprint can be obtained by application to the publisher: Elsevier Science Publishers B.V., P.O. Box 330, 1000 AH Amsterdam, The Netherlands.)

Types of Contributions. The following types of papers are published in the *Journal of Chromatography* and the section on *Biomedical Applications:* Regular research papers (Full-length papers), Short communications and Notes. Short communications are preliminary announcements of important new developments and will, whenever possible, be published with maximum speed. Notes are usually descriptions of short investigations and reflect the same quality of research as Full-length papers, but should preferably not exceed four printed pages. For review articles, see page 2 of cover under Submission of Papers.

Submission. Every paper must be accompanied by a letter from the senior author, stating that he is submitting the paper for publication in the *Journal of Chromatography.* Please do not send a letter signed by the director of the institute or the professor unless he is one of the authors.

Manuscripts. Manuscripts should be typed in double spacing on consecutively numbered pages of uniform size. The manuscript should be preceded by a sheet of manuscript paper carrying the title of the paper and the name and full postal address of the person to whom the proofs are to be sent. Authors of papers in French or German are requested to supply an English translation of the title of the paper. As a rule, papers should be divided into sections, headed by a caption (*e.g.,* Summary, Introduction, Experimental, Results, Discussion, etc.). All illustrations, photographs, tables, etc., should be on separate sheets.

Introduction. Every paper must have a concise introduction mentioning what has been done before on the topic described, and stating clearly what is new in the paper now submitted.

Summary. Full-length papers and Review articles should have a summary of 50–100 words which clearly and briefly indicates what is new, different and significant. In the case of French or German articles an additional summary in English, headed by an English translation of the title, should also be provided. (Short communications and Notes are published without a summary.)

Illustrations. The figures should be submitted in a form suitable for reproduction, drawn in Indian ink on drawing or tracing paper. Each illustration should have a legend, all the *legends* being typed (with double spacing) together on a *separate sheet.* If structures are given in the text, the original drawings should be supplied. Coloured illustrations are reproduced at the author's expense, the cost being determined by the number of pages and by the number of colours needed. The written permission of the author and publisher must be obtained for the use of any figure already published. Its source must be indicated in the legend.

References. References should be numbered in the order in which they are cited in the text, and listed in numerical sequence on a separate sheet at the end of the article. Please check a recent issue for the layout of the reference list. Abbreviations for the titles of journals should follow the system used by *Chemical Abstracts.* Articles not yet published should be given as "in press", "submitted for publication", "in preparation" or "personal communication".

Dispatch. Before sending the manuscript to the Editor please check that the envelope contains three copies of the paper complete with references, legends and figures. One of the sets of figures must be the originals suitable for direct reproduction. Please also ensure that permission to publish has been obtained from your institute.

Proofs. One set of proofs will be sent to the author to be carefully checked for printer's errors. Corrections must be restricted to instances in which the proof is at variance with the manuscript. "Extra corrections" will be inserted at the author's expense.

Reprints. Fifty reprints of Full-length papers, Short communications and Notes will be supplied free of charge. Additional reprints can be ordered by the authors. An order form containing price quotations will be sent to the authors together with the proofs of their article.

Advertisements. Advertisement rates are available from the publisher on request. The Editors of the journal accept no responsibility for the contents of the advertisements.

205b